LEABHARLANN CHOLÁISTE NA TRÍONÓIDE, BAILE ÁTHA CLIATH | TRINITY COLLEGE LIBRARY DUBLIN
Ollscoil Átha Cliath | The University of Dublin

Terms and Conditions of Use of Digitised Theses from Trinity College Library Dublin

Copyright statement

All material supplied by Trinity College Library is protected by copyright (under the Copyright and Related Rights Act, 2000 as amended) and other relevant Intellectual Property Rights. By accessing and using a Digitised Thesis from Trinity College Library you acknowledge that all Intellectual Property Rights in any Works supplied are the sole and exclusive property of the copyright and/or other IPR holder. Specific copyright holders may not be explicitly identified. Use of materials from other sources within a thesis should not be construed as a claim over them.

A non-exclusive, non-transferable licence is hereby granted to those using or reproducing, in whole or in part, the material for valid purposes, providing the copyright owners are acknowledged using the normal conventions. Where specific permission to use material is required, this is identified and such permission must be sought from the copyright holder or agency cited.

Liability statement

By using a Digitised Thesis, I accept that Trinity College Dublin bears no legal responsibility for the accuracy, legality or comprehensiveness of materials contained within the thesis, and that Trinity College Dublin accepts no liability for indirect, consequential, or incidental, damages or losses arising from use of the thesis for whatever reason. Information located in a thesis may be subject to specific use constraints, details of which may not be explicitly described. It is the responsibility of potential and actual users to be aware of such constraints and to abide by them. By making use of material from a digitised thesis, you accept these copyright and disclaimer provisions. Where it is brought to the attention of Trinity College Library that there may be a breach of copyright or other restraint, it is the policy to withdraw or take down access to a thesis while the issue is being resolved.

Access Agreement

By using a Digitised Thesis from Trinity College Library you are bound by the following Terms & Conditions. Please read them carefully.

I have read and I understand the following statement: All material supplied via a Digitised Thesis from Trinity College Library is protected by copyright and other intellectual property rights, and duplication or sale of all or part of any of a thesis is not permitted, except that material may be duplicated by you for your research use or for educational purposes in electronic or print form providing the copyright owners are acknowledged using the normal conventions. You must obtain permission for any other use. Electronic or print copies may not be offered, whether for sale or otherwise to anyone. This copy has been supplied on the understanding that it is copyright material and that no quotation from the thesis may be published without proper acknowledgement.

SLEEVED CONCRETE CYLINDERS

SUBJECT TO HARD IMPACT

by

Sarah J. Prichard

Thesis submitted to the University of Dublin, Trinity College,

for the Degree of Doctor of Philosophy

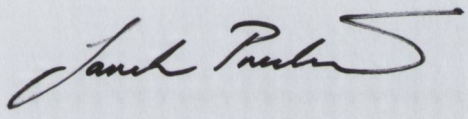
September 2000

TRINITY COLLEGE
15 DEC 2000
LIBRARY DUBLIN
Thesis
6023

DECLARATION

The author hereby declares that this thesis, in whole or in part, has not been submitted to any other university as an exercise for a degree. Except where reference has been given in the text, it is entirely the author's own work.

The author confirms that the Library may lend or copy this thesis upon request, for academic purposes.



Sarah. J. Prichard

September 2000

ABSTRACT

The purpose of this thesis is to determine the response of sleeved concrete cylinders to low velocity hard impact. Previous research has shown that, when concrete is uni-axially loaded and subject to the high strain rates associated with impact, it consistently exhibits a greater strength and stiffness than when statically loaded. Furthermore, other research has shown that when concrete is confined in two out of three mutually perpendicular directions its compressive strength in the third direction is considerably enhanced. This research combines these phenomena and studies the response of confined concrete to hard impact.

Impact tests were performed on cylinders of concrete (200 mm high and, typically 100 - 115 mm diameter) with different types of confinement, by dropping a solid steel impactor of weight 82.5 kg, at contact velocities between 3.2 m/s and 6.3 m/s. The main part of the experimental work examined confinement provided by steel sleeves (of varying thicknesses) and sleeves of aluminium and plastic. Similar impact tests on unconfined cylinders formed a reference series. Supplementary tests studied how cylinders, confined in a similar manner to those in the main test series, responded to static loads and the impact response of cylinders of both larger diameter and others where the confining sleeve was not supported at the base. The responses of the cylinders to impact loads were determined using a contact force loadcell integrated into the impactor, a base-plate loadcell placed beneath the cylinder and axial and lateral strain gauges attached along its length.

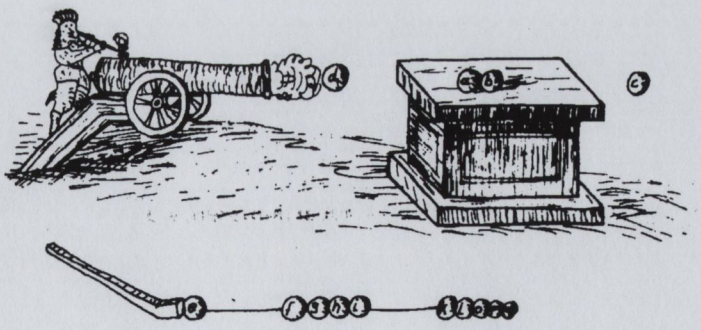
The results of the experiments are compared to three analytical studies which examine the effects that the confining sleeve has on the maximum contact force, the variation in the contact force over time using Hertz's law and the stress-strain relationship of the statically loaded and impacted cylinders. Each of the studies requires assumptions to be made regarding the response of the confined cylinders and result in good approximations for the behaviour of the composite. The models are particularly accurate in situations where the lateral dilation is sufficiently reduced to result in the confined concrete acting in an elastic manner. The analytical studies are complimented by a finite element analysis of the response of the composite cylinders to static and dynamic loads using the finite element programs ANSYS and DYNA3D. The models generated are intentionally simplified, as all the materials are assumed to be elastic but, nonetheless, facilitate an understanding of the load transfer mechanism from the loaded concrete core into the confining sleeve.

To the memory of my Father,

without whose inspiration this work would not have been started;

and to my Mother,

without whose encouragement this work could not have been finished.



Sketch by MARCUS MARCI (1639)

ACKNOWLEDGEMENTS

In the course of researching and writing this thesis I have received help from many people and I should like to take this opportunity to thank them. My work was carried out in the Department of Civil, Structural and Environmental Engineering, Trinity College Dublin. I am very grateful to the Trinity Foundation whose fellowship funded my studies for the last three years. My research was supervised by Professor S.H. Perry and I should like to thank him for his encouragement and help throughout - it has been truly immeasurable.

I would like also to thank my mentor, Dr. Roger West who has offered a guiding hand, a sound understanding of the finer elements of experimental and theoretical research and tongue in cheek criticism during my period as a research student in the Department.

This work could not have been completed without the help of the technical staff in the structural laboratory. I am indebted to George Jones in particular for, although initially he tried to persuade me not to study impact, he always found solutions for my more obscure problems and never ceased to laugh with me when things went awry. I should also like to thank our chief technician Chris O'Donovan and the technical staff who willingly and ably assisted me at all times - Eoin Dunne, Dave McAuley and Gerard McGranaghan.

Two colleagues, above all, have made some of the insurmountable problems of this research appear feasible. This research would never have been completed if Alan O'Connor had not re-invented the concept of a "half-day" and then never ceased to remind me of the importance of Newton's Laws. Toman MacGinley was my technical guru on the computer side of things - regardless of the problem, if it involved a computer - T. had a hand in sorting it out when things went wrong, as they so often did. I should also like to thank my colleagues in the Department, particularly Jim Robinson, Dermot O'Dwyer and Brian Broderick for their insights during the course of this work.

My heartfelt thanks go to my family, Bernadette, Ruth and David, who have supported me in so many ways during the years of soul searching it has taken to complete this thesis. Finally, I should like to thank some special friends and fellow sufferers, Catriona, Derek, Dawn, David, Eleanor, Geoff, Nicola, Treasa and above all Philip - who never failed to be amused by my fascination for smashing concrete.

TABLE OF CONTENTS

TITLE PAGE 1

DECLARATION 2

ABSTRACT 3

DEDICATION 4

ACKNOWLEDGEMENTS 5

TABLE OF CONTENTS 6

PRINCIPAL NOTATIONS 10

1. INTRODUCTION 12

1.1. THE IMPACT LOADING OF CONFINED CONCRETE 12
1.2. SCOPE OF THE CURRENT RESEARCH 16

2. THEORETICAL BACKGROUND TO IMPACT AND CONFINEMENT 18

2.1. HISTORICAL BACKGROUND 18
2.2. IMPACT CLASSIFICATION 21
2.3. PRINCIPLES OF IMPACT 25
2.3.1. Classical mechanics 25
2.3.2. The wave equations 27
2.4. ELASTIC STRESS WAVES AND THEIR PROPAGATION 30
2.4.1. Impact induced stress and strain 30
2.4.2. Stress waves in isotropic elastic media 31
2.4.3. Two dimensional longitudinal waves in bars 32
2.4.4. Coaxial collision of two bars 34
2.4.5. Reflection and superposition of waves 36
2.4.6. Exact theory of wave propagation 37
2.5. CONCRETE FILLED COMPOSITE COLUMNS 39
2.6. CONCLUSIONS 46

3. REVIEW OF PREVIOUS LITERATURE CONCERNING WORK ON CONCRETE SUBJECT TO IMPACT AND CONFINEMENT 47

3.1. INTRODUCTION 47
3.2. LOW VELOCITY IMPACT OF CONCRETE 50
3.2.1. Compressive strength enhancement with increasing strain rate 50
3.2.2. Contact force response of concrete subject to impact 54
3.2.3. Change in material properties with increases in strain rate 56

3.2.4. Failure patterns of concrete subject to impact 60
3.2.5. Stress-strain response of concrete subjected to increasing strain rates 63
3.2.6. Conclusions 66
3.3. CONCRETE CONFINEMENT 67
3.3.1. Experimental work on concrete confined by sleeves, spirals or hydraulically 67
3.3.2. Experimental work on confinement with confinement other than of steel 76
3.3.3. Theoretical work on confined concrete 77
3.4. DYNAMICALLY LOADED CONFINED CONCRETE 85
3.5. FINITE ELEMENT ANALYSIS OF CONFINED CONCRETE 89
3.6. CONCLUSIONS 94

4. DETAILS OF EXPERIMENTAL WORK AND TEST SPECIMENS 96

4.1. METHOD OF IMPACT LOADING 96
4.2. DETAILS OF TEST SPECIMENS 101
4.2.1. Geometry 101
4.2.2. Designation of test specimens 102
4.2.3. Properties of confining cylinders 103
4.2.4. Concrete properties and specimen production 105
4.2.5. Static test results 107
4.2.6. Cylinder instrumentation 108
4.3. MEASUREMENT OF CONTACT FORCE 110
4.4. STRESS MEASUREMENT 113
4.5. DATA ACQUISITION AND PROCESSING 119
4.6. TEST PROCEDURE 125

5. EXPERIMENTAL RESULTS FROM IMPACT TESTS 127

5.1. INTRODUCTION 127
5.2. CONTACT FORCE RESPONSE 130
5.2.1. Factorial analysis of maximum contact force results 138
5.2.2. Analysis of contact force results 144
5.3. BASE-PLATE FORCE AND STRESS RESPONSE 151
5.4. QUALITATIVE TEST RESULTS 164
5.5. STRESS-STRAIN RESPONSE 169
5.5.1. Strain gauge response 169
5.5.2. Plots of stress against strain for impacted cylinders 173
5.6. IMPACTOR REBOUND 183
5.7. ENERGY ABSORPTION DURING IMPACT 189
5.8. CONCRETE STRENGTH AFTER CONFINEMENT REMOVAL 191
5.9. RESULTS OF SUPPLEMENTARY TESTS 193
5.9.1. Static test results 193
5.9.2. Large diameter cylinder tests 198

5.9.3. Tests with reduced confinement at the base 203
5.9.4. Repeated impact tests 208
5.10. CONCLUSIONS FROM THE EXPERIMENTAL RESULTS 211

6. ANALYTICAL STUDY 215

6.1. INTRODUCTION 215
6.2. CONTACT FORCE PREDICTION 216
6.2.1. Theory 216
6.2.2. Comparison of predicted contact force with experimental results 220
6.3. HERTZ'S CONTACT LAW 224
6.3.1. Theory 224
6.3.2. Model 1 - A sine curve 228
6.3.3. Model 2 - A quasi-sine curve 230
6.3.4. Comparison between models 231
6.4. STRESS-STRAIN CURVES 238
6.4.1. Theory 238
6.4.2. Comparison of models with experimental stress-strain curves 241
6.5. CONCLUSIONS 251

7. FINITE ELEMENT ANALYSIS OF CONFINED CONCRETE 253

7.1. INTRODUCTION 253
7.2. STATIC ANALYSIS USING ANSYS 256
7.2.1. Theoretical background 256
7.2.2. Model creation - 2D 261
7.2.3. Results from ANSYS in 2-dimensions 265
7.2.3.1. Preliminary analysis 266
7.2.3.2. End restraint 271
7.2.3.3. Constant and linearly varying pressure loading 273
7.2.3.4. The effect of varying friction 273
7.2.3.5. Modelling of concrete with different types of confinement 275
7.2.4. Model creation - 3D 278
7.2.5. Results from ANSYS in 3 dimensions 280
7.3. WORK USING DYNA3D 283
7.3.1. Theoretical background 283
7.3.2. Model creation - 3D 287
7.3.3. Results from DYNA3D analysis 291
7.3.3.1. Preliminary analysis 291
7.3.3.2. Variation in contact velocity 301
7.3.3.3. Variation in the confining sleeve 303
7.4. COMPARISONS BETWEEN THE DIFFERENT MODEL TYPES 307
7.5. CONCLUSIONS 310

8. EXECUTIVE SUMMARY AND CONCLUSIONS **312**

8.1. EXECUTIVE SUMMARY 312

8.2. CONCLUSIONS 315

8.3. RECOMMENDATIONS FOR FURTHER WORK 319

REFERENCES **322**

APPENDIX 1 CONCRETE COMPOSITE COLUMNS - APPLICATION **331**

APPENDIX 2 MATERIAL PROPERTIES OF THE CONFINING SLEEVES **332**

APPENDIX 3.1 IMPACT RESPONSE OF UNCONFINED CONCRETE CYLINDERS **336**

APPENDIX 3.2 IMPACT RESPONSE OF SLEEVED CYLINDERS, 1.2 MM STEEL **340**

APPENDIX 3.3 IMPACT RESPONSE OF SLEEVED CYLINDERS, 3 MM STEEL **345**

APPENDIX 3.4 IMPACT RESPONSE OF SLEEVED CYLINDERS, 5 MM STEEL **353**

APPENDIX 3.5 IMPACT RESPONSE OF SLEEVED CYLINDERS, 6.5 MM STEEL **358**

APPENDIX 3.6 IMPACT RESPONSE OF SLEEVED CYLINDERS, 3.6 MM PLASTIC **363**

APPENDIX 3.7 IMPACT RESPONSE OF SLEEVED CYLINDERS, 3.25 MM ALUMINIUM **368**

APPENDIX 4.1 IMPACT RESPONSE OF LARGE DIAMETER SLEEVED CONCRETE CYLINDERS, STEEL, 3 MM THICK **373**

APPENDIX 4.2 IMPACT RESPONSE OF SLEEVED CONCRETE CYLINDERS, REDUCED LENGTH OF CONFINEMENT AT THE BASE **375**

APPENDIX 4.3 IMPACT RESPONSE OF SLEEVED CONCRETE CYLINDERS, REPEAT IMPACT TESTS **381**

APPENDIX 5 PROGRAM CODES USED IN FINITE ELEMENT ANALYSIS **384**

PRINCIPAL NOTATIONS

The following is a list of principal notations. All of the following are defined in the text where they are used and are solely listed here for clarity.

A	area	f_y	yield stress of steel
a	internal radius	g	acceleration due to gravity
a	major axis of ellipse	G	Shear modulus
{a}	vector of nodal degrees of freedom	h	height
b	external radius	I	impulse
b	minor axis of ellipse	[K]	global stiffness matrix
b	breadth of section	k_e	confinement effectiveness coeff.
c_0	speed of elastic wave propagation	KL	effective length of column
C_i	confinement index	k_1	effective mass
c_l	speed of longitudinal wave propagation	K, k_2	contact parameter
c_s	speed of shear or transverse wave propagation	l	length
D, d	diameter	M, m	mass
D_i	parameter controlling descent curve	p_0	effective pressure
e	coefficient of restitution	p_b	volumetric ratio
e	volume expansion	P	applied pressure
E	internal energy	r,θ,z	polar co-ordinates
E	Young's modulus	r	radius
E_{sec}	secant modulus	r_s	radius of gyration of steel tube
E_t	tangent modulus	s	pitch of spiral
F	applied force	t	thickness
{F}	vector of forces at nodes	t	time
f_c	strength of concrete	u,v,w	displacements
f_{cc}	confined strength of concrete	V	volume
f_{cu}, f_{c0}	unconfined strength of concrete	v	velocity
f_l	lateral stress	W	work
f_s	tensile strength of steel	W_{lm}	kinetic energy lost by impactor

x,y,z	Cartesian co-ordinates	A,B,C	constants
$\bar{y}$	mean value	f, g	constants

α	approach	ρ	density
α	concrete contribution factor	ρ_s	volumetric ratio reinforcement
Δ	Nyquist time between signals	σ	stress
δx	increment of x	σ_c	circumferential or hoop stress
ε	strain	σ_r	radial stress
ε_{01}	critical strain at peak stress	σ_t	tensile stress
ε_{cc}	strain in confined concrete	σ_z	longitudinal stress
ε_{cu}, ε_{c0}	strain in unconfined concrete	σ^2	variance
ε_u	ultimate concrete strain	θ	angle
ε_{vol}	volumetric strain	υ	Poisson's ratio
∇	Laplacian operator	τ	shear stress
λ	Lamé's constant		

1. INTRODUCTION

1.1. THE IMPACT LOADING OF CONFINED CONCRETE

Impact and blast loads have always existed in nature, ever since the first volcano erupted sending a shower of rocks and explosive gasses down onto the surrounding area. However, it was not until relatively recent millennia that man began to harness the destructive power of impact, starting with spears, rocks and catapults and then progressing to the bow and arrow. By biblical times, people protected themselves using hard, strong objects such as breastplates and armour, or energy absorbing materials, including hats made of layers of leather and wool, to resist the impact of arrows and stones. As the impact loads created by these weapons were comparatively minor and localised, little was done to protect early structures from these impact loads. Further developments in impact technology, including the advent of the cannon, capable of hurling explosively propelled solid metal balls, resulted in structures being strengthened considerably, as a series of well aimed cannon balls could reduce the wall of a castle to rubble within a relatively short time. However, until the twentieth century, buildings designed to resist impact loads were predominantly confined to the military sphere, as the probability of impact on a castle or bunker was considerably higher than on a civilian building, as each projectile was individually and 'accurately' aimed. With the advent of missiles, such as rockets, and high speed vehicles, for example aeroplanes, the scope for unpredictable impact has widened into civilian structures. Despite this, it would be impractical, not to mention extremely costly, to design all buildings to resist impact loads. Thus, of necessity, special attention is given to structures where the risk of impact is high or where structural failure as a result of impact, could result in consequences which are disproportional to the severity of the original impact. Examples of the latter would include accidental aircraft collision with nuclear power stations or objects being dropped on large sub-sea oil storage caissons.

Engineers worked throughout the twentieth century to solve many of the outstanding problems in the response of materials to various loading forms. This resulted in a vast amount of knowledge about how structures, and the materials of which they are constructed, respond to both static and quasi-static loading. However, many questions remain unanswered on how materials respond to the less familiar impact loading. Impact

occurs when a moving object, an impactor, suddenly and forcefully collides with another body, a target, which can either be moving or stationary. Under either static or quasi-static loading the stresses and strains which are induced in the structure have time to equilibrate during the period of loading. However, if a load is suddenly applied to a structure, and the duration of loading is short, relative to the time taken for the induced stress waves to be dissipated, then the properties which the material exhibits are quite different to those under static loading conditions. This "high strain rate loading" often occurs as the result of an impact or blast load. It characteristically results in a localised material response as there is insufficient time for the whole structure to resist the load. Figure 1.1 shows the different rates at which strain is applied (commonly known as the strain rate), and the type of loading with which they can be associated.

The design of buildings and structures to resist impact loads throughout the centuries was highly empirical. Although some have been subject to extensive impact loading, many of these structures still stand, bearing witness to the success of their empirical design for 'service' loads. However, recently the design of buildings has become more codified as attempts are being made to standardise construction, and to ensure that the great majority of concrete and steel buildings will withstand live, dead, wind and, in some situations, earthquake loading. Their cost driven construction, incorporating minimised factors of safety, means that they can usually resist the loads for which they are designed, but are rarely sufficiently strong to resist random impact loading. The consequences of their failure could be costly and environmentally harmful. Therefore, civil engineers have begun to study material responses to impact, in an attempt to develop an understanding of its effects and implications. The study of impact and blast loads did not begin in earnest until the middle of the twentieth century and was hindered because the response of materials and structures to these forms of loading is both difficult to measure and to model.

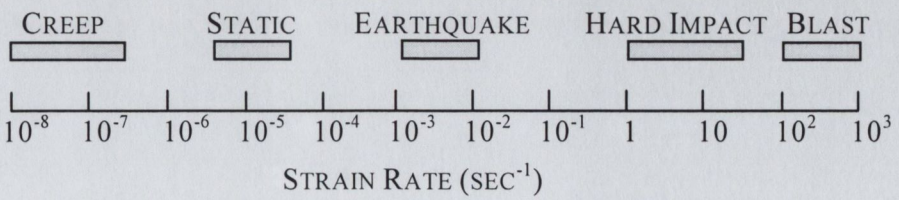


Figure 1.1 Magnitude of strain rates expected for different loading rates

(after Bischoff and Perry 1991)

Concrete has been used in construction for over two thousand years. However, it was only during the last century that its use became widespread and it has been employed as a reliable, resistant, easy to use, adaptable building material. It has become the market leader for a wide variety of structural projects, amongst which are some of the most vulnerable to impact loading. It is generally accepted that if concrete is loaded statically or quasi-statically then it behaves well in compression, but performs less well when subjected to tensile loads. The brittle, particulate nature of concrete results in it responding even less well when subjected to an impact load, which is a situation which can result in a localised material response. However, it is generally accepted that concrete, and many other materials, appear to exhibit an increase in its compressive strength as the strain rate is increased. A considerable amount of the research in the area of impact loading has involved work to quantify this increase in the compressive strength.

Researchers are now trying to ensure that cost effective conventional building elements will neither fail nor will suffer excessive damage, but will maintain structural integrity, in the event of an impact. Extensive research in the area of impact has, therefore, examined variables which might mitigate these effects, such as concrete strength; aggregates, admixtures and additives; energy absorbing 'fender' materials and a variety of reinforcing types.

One method which has been shown to enhance the response of concrete, and the structures built of concrete, to both impact and static loads is to maximise the benefits of confinement. It is well established that if a material, such as concrete, is confined in two out of three mutually perpendicular directions then the compressive strength in the third direction increases considerably. This is because cracks, which would have formed if the concrete was unconfined, are prevented from opening. In practice, partial confinement is usually provided to concrete using steel links, surrounding longitudinal steel reinforcement bars, which help to resist the outward dilation of the concrete when loaded axially. However, the effectiveness of the confinement provided can be increased if the longitudinal bars and links are replaced by hollow cylindrical sections into which the concrete is poured. These "concrete filled columns" provide confinement along the entire length of the section, and have the added advantage of acting as formwork for the concrete whilst it is poured. They also exhibit greater ductility, flexural stiffness and toughness than unconfined or even conventionally reinforced concrete, making them

extremely effective at resisting earthquake loading. These columns have the ability to carry high static loads, due to the interaction of the confining cylinder and the confined concrete, even when of seemingly small cross-sectional area and, as a result, they are becoming increasingly widely used in construction (as can be seen from Appendix 1). Confined concrete columns are extensively used where minimum dimensions are required, from bridge piers to internal columns in prime-rental office buildings. In addition, due to the ability of the confining cylinder to prevent outward dilation and resulting cracking in the concrete, this form of confinement is also suitable to resist impact loading, where the lateral dilation can result in the concrete cracking almost instantaneously.

The research in the area of the response of materials to impact began during the 1950s and the majority of the early work was experimental and often yielded qualitative results. This was due to the difficulty of measuring the transient responses which occur during impact event because of the very short time duration over which the impact occurs. However, developments in laboratory equipment have enabled researchers to acquire accurate data during the impact for in-depth post event analysis. The theoretical determination of the impact response of a material is a complicated process, due to the propagation and reflection of the induced stress waves, which requires considerable mathematical analysis. Work has also progressed considerably in the last twenty years in the area of predicting the response of concrete to impact, through the use of carefully verified constitutive relations or using computers to perform finite element or finite difference analysis of the response of materials and structures to impact loading. However, despite these advances, experimental results are still required to provide details of the material response which can then be used in the computational analysis. Furthermore, the results of all such predictions will always require careful calibration against actual measured impact responses.

1.2. SCOPE OF THE CURRENT RESEARCH

The main objective of the research work described in this thesis is concerned with an experimental evaluation of the response of confined concrete to hard impact. This includes an assessment of the increase in strength of the concrete composite element and of the stress-strain response of the composite when impacted. The work was undertaken with the intention of understanding better the composite's response to low velocity hard impact which had never previously been studied. The experimental results were then compared to analytical and finite element models in an attempt to better understand the way in which the loads were withstood by the composite cylinder.

The theory behind the impact loading of materials, especially concrete, is described in **Chapter 2**, starting with a brief history of its development. The classification of different forms of impact loading, details on how these loading forms are created, and the theory of stress wave propagation is developed. The theory of material confinement is also examined. The aim of this chapter is to provide the reader with background knowledge which would be required for an interpretation of the experimental results. It also includes a summary of different methods of loading and modes of failure which occur as a result of impact loading on civil engineering structures.

Chapter 3 includes a detailed survey of existing published work on the response of concrete to hard impact and on how the confinement affects the response of concrete when loaded. This includes a critical analysis of the previous work on the contact force response of concrete and on strength increases measured as a consequence of impact loading. It also considers the absorption of energy during an impact event and the effects which this has on the damage to the impacted material. The review of the existing literature includes an assessment of previous research work on the response of confined material to predominantly static loading. This chapter also reviews the limited work which has been undertaken, thus far, on the response of confined materials to dynamic loading. The chapter concludes with a discussion of recent work in the area of the finite element analysis of concrete when confined prior to loading and when subjected to low velocity hard impact.

The main focus of this thesis is on a series of impact tests undertaken on confined concrete cylinders subjected to low velocity hard impact in the Civil Engineering Laboratories of Trinity College Dublin. **Chapter 4** describes the experimental set up for the laboratory testing. It includes details on the development of the impact test rig, the impactor loadcell, which measures the contact force at the location of impact, and the thin plate loadcell, placed beneath the impacted cylinder to measure the stress at its base. The instrumentation used during the impact tests is also described in this chapter. The majority of tests involved cylinders which were confined using thin walled structural hollow sections of steel (of varying thickness), aluminium or PVC plastic pipe. The 200mm high sleeves were cut from structural sections and provided confinement and contained the concrete whilst it was being poured. Seven types of cylinder were tested, six of which were confined, and a seventh, unconfined group, formed a reference series. Other, more limited tests were undertaken which involved impacting larger diameter cylinders, cylinders which had a band of confinement cut away from near their bases which meant that their sleeves were not fully supported, and repeatedly impacting confined concrete cylinders. Some static tests were also undertaken for comparison purposes. The results of all of these tests are presented and discussed in **chapter 5**.

Chapter 6 provides an analytical insight into the response of confined concrete to hard impact and develops some of the existing theory in the area. This includes the development of a relationship to predict the maximum contact force, empirical work using Hertz's Law to model the contact force response over time and an examination of existing formula to predict the stress-strain response of statically loaded and impacted, confined and unconfined concrete. The findings are compared to the results generated by the experimental work. An extensive, if intentionally simplified, finite element study using commercially available packages is undertaken in **Chapter 7**. The work is split into two areas, namely a static analysis using ANSYS in 2- and 3-dimensions, and a 3-dimensional dynamic analysis using DYNA3D. The results are compared to the findings of the experimental work, and facilitate an understanding of the load transfer mechanism from the concrete core into the confining sleeve.

A summary of the work undertaken during the current research programme is given in **chapter 8**. This is followed by a series of conclusions and recommendations for future work in the area of the response of confined concrete to low velocity hard impact.

2. THEORETICAL BACKGROUND TO IMPACT AND CONFINEMENT

2.1. HISTORICAL BACKGROUND

The study of impact began over two thousand years ago when Aristotle (384-322 B.C.), in his *Problems of Mechanics,* described the falling of heavy bodies as "natural" motion and went on to develop a theory of impact. However, he assumed that heavier bodies fell faster to the ground than lighter ones, but was unable to prove or disprove his philosophy through experimentation as the ancient Greeks had no precise way of measuring either time or distance.

Aristotle's theories were not refuted until the mid seventeenth century, when Galileo (1564-1642) completed a series of experiments which showed that bodies fall at the same rate regardless of their mass. In his treatise *De Motu*, he analysed the mechanics of rigid bodies and established the classical laws of kinematics. He used these to prove that impact was the interaction between two or more bodies and to define the principle of inertia.

Four other seventeenth century scientists, Wallis, Wren, Huygens and Mariotte, were instrumental in the establishment of the principles behind the theory of impact. Wallis (1616-1703) began the process of making mechanics a mathematical science and distinguished between types of impact - perfectly hard, soft or elastic. In his book, *Mechanica, sive de Motu*, he proved the law of conservation of momentum in the case of impact. Wren (1632-1723) further developed this work and showed that the velocities before and after impact were equal. Hugyens (1629-1697) summarised his theoretical work on impact in *De Motu corporum ex percussion.* In this he stated that "if a body is at rest, and an equal body collides with it, after the impact the second body will be at rest and the first will have acquired the velocity that the other had before the impact". This was developed to state that, if the bodies are unequal in size, the relative velocity is that which counts. Another proposition stated that "if two bodies, moving in opposite directions, with velocities inversely proportional to their magnitudes, collide with each other, each one rebounds with the velocity it had before the impact". He went on to prove the law of conservation of energy for a perfectly elastic impact. Mariotte (1620-1684) published work

which contained the results of a considerable amount of experimental work which he completed on "perfectly elastic" and "perfectly soft" bodies.

Isaac Newton (1642-1727), in his *Principia*, defined the relations of classical mechanics, which became his three laws of motion. Specifically his third law, of action and reaction, was developed in both theory and practice to become Newton's Experimental Impact Law. This law states that the relative velocity before impact is proportional to the relative velocity after impact.

Euler (1707-1783), was the first person to complete a systematic analysis on the dynamics of particles. He developed the "Principle of Impulse" in which he stated that an impulse gives rise to an increase in momentum and defined the "Principle of Moments of Inertia". Hertz (1857-1894) worked on developing the quasi-static theory of waves travelling through bodies after impact and superseded many scientists' previous work with the theory of local contact deformations, derived through the theory of statics, which has been repeatedly applied to dynamic collision.

During the nineteenth century considerable work was completed on vibration as a result of impact. St Venant completed an analysis of one-dimensional impact for longitudinal and transverse vibrations. Pochhammer and Chree worked simultaneously and developed this into a three dimensional solution. They studied the impact of long rods and the waves travelling through them, concluding that there were trains of progressive simple harmonic waves of infinite duration travelling through isotropic cylinders of infinite length.

Both Rayleigh (1842-1919) and Love (1863-1940) studied surface waves travelling in layered media as a result of impact. Love advanced Rayleigh's rather limited theory for elastic surface waves, developing the theory behind polarisation and dispersion of primary and secondary surface waves. They also completed experiments to correct the existing theories of wave propagation for lateral inertia in longitudinal waves. Timoshenko, in the early years of the twentieth century, carried out experiments on the response of plates and shells to impact. He corrected the wave equation again, to include the effects of rotary inertia and shear.

Considerable research, starting in the 1930s and continuing even now, has been undertaken on elastic-plastic and plastic wave propagation theory. Researchers including Donnell, Taylor and Hawkyard have all contributed to our understanding of the response of materials to impulsive or elastic-plastic loading.

In the period since 1950 an extensive experimental programme has been undertaken internationally to find the actual response of materials to hard impact. This has been assisted greatly by the improvements in high speed instrumentation and sophisticated recording devices which, combined with developments in computing, have made the precise study of impact more realisable. Many of the more recent developments in the study of impact are outlined in the literature review in Chapter 3.

2.2. IMPACT CLASSIFICATION

It is well established that if a load is applied to a body made of concrete, at a strain rate considerably greater than if statically loaded, then the material reacts in a very different way to that anticipated from a knowledge of the effects of static loading. Under this loading regime, the analysis of the material and structural response is more complex than classical or Newtonian mechanics would have us believe, because of the importance of inertia forces and stress wave propagation.

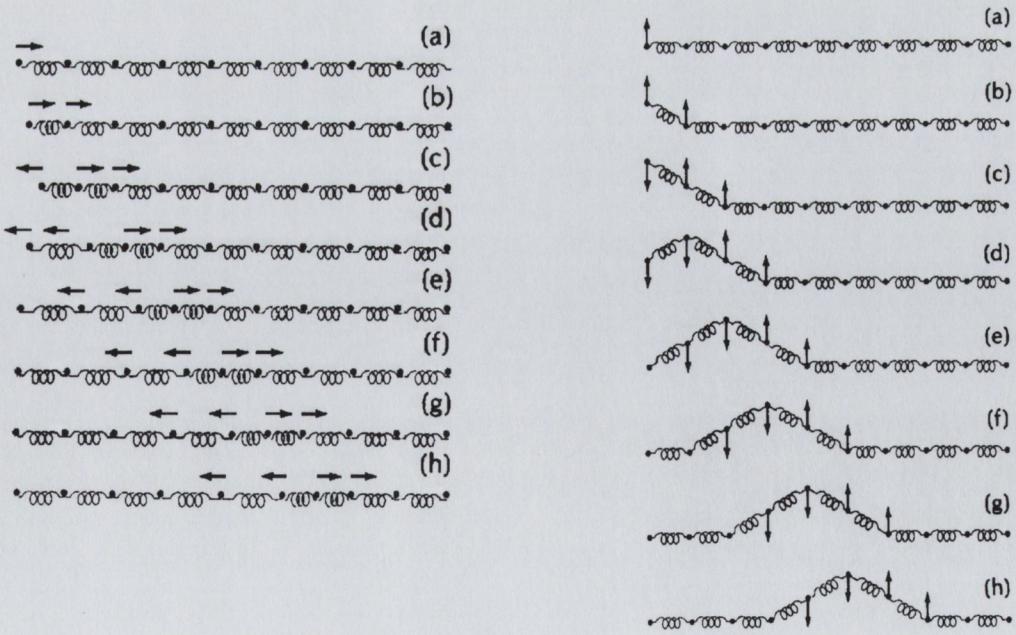
The phenomena of 'impulse' and 'impact' are closely linked. Impulse is generally massless involving the force of air, and is often associated with blast loading. If masses are involved, the resulting collision is an impact and the effects are inertial and proportional to the masses of the bodies.

Impact can be classified by an analysis of the velocity, shape and hardness of the impactor or by the ability of the impacted object to mitigate damage through energy absorption or change of shape. Impact velocities can range greatly, from high velocity, with speeds in excess of 100 m/s, to quite low velocities, with speeds of less than 25 m/s. High velocity impacts are often caused by ballistics or aircraft collisions and can only be simulated in the laboratory using a gas gun accelerator, an evacuated tube, or an explosive charge attached to the impactor. In contrast, low velocity impacts can occur if the impactor is dropped and falls under gravity, which could result, for example, from dislodged material falling as a result of an earthquake. It can be simulated in a laboratory using a dropped weight or, in the case of very low velocities, a notched bar or Charpy test (Goldsmith, 1964).

The loading rate in the case of impact is considerably higher than for static loading and the stresses and strains do not have time to equilibrate within the loading period (Eibl, 1982). If the kinetic energy of the impactor is absorbed through self deformation, then the impact is described as soft. However, if the impactor is sufficiently rigid for the majority of the kinetic energy to be transferred to the target, a hard impact results and can cause large deformations or damage to the target. The damage levels differ greatly depending on the object impacted but, in the case of a concrete slab, can include fragmentation, spalling or the formation of concrete plugs. This high energy transfer results in a large peak on the

graph of contact force against time, which has been illustrated experimentally by many researchers, including Perry *et al.* (1984).

The impact tends to induce high stresses and strains in the target structure at the point of contact, which can lead to localised material failure. If the forces are large enough, equilibrium is not maintained and the material loses its steady state conditions. Elastic stress waves, of magnitudes less than the strength of the material, travel away from the point of contact in an attempt to dissipate these high strains. The stress waves can either be longitudinal or transverse (shear) waves, and are illustrated in Figure 2.1. Longitudinal waves exist where the disturbance is parallel to the direction in which the waves are travelling and transverse waves are where the particles move at right angles to the direction in which the wave front propagates. The longitudinal and transverse stress waves can be compressive or tensile. When either type impinges on the surface of a solid, both types of wave form can be generated by reflection. If a compressive wave, where the wave moves in the same direction as the particles it vibrates, impinges on a surface, the resulting reflected wave will be tensile. If the magnitude of this wave is greater than the tensile strength of the material, for example the concrete or the aggregate within the concrete, then it will lead to tensile cracking and possibly to dislocation of fragments of the



Longitudinal wave movement Transverse wave movement

Figure 2.1 Transverse and longitudinal wave movement illustrated using springs (Ohanian, 1989)

material. If, even after the fracture, the magnitude of the wave is still greater than the tensile strength, multiple fractures will occur.

The loading rate directly affects the type of material response. Figure 2.2, a diagram created by Lindholm (1971) and modified by Zukas *et al* (1982), illustrates strain rates and the corresponding duration of loading at which inertia and stress wave propagation are perceived to become increasingly important. At strain rates in the range of 10^{-8} to 10^{-5} per second, creep is the main effect, and the material expands or contracts very slowly. The quasi-static range occurs between strain rates of 10^{-4} and 10^{-1} per second and, when the loading is uni-axial, the stress-strain curve is that which is obtained from standard constant strain rate tests in the laboratory. Although this type of curve is often thought of as a fundamental property of the material, it is actually only valid at the strain-rate at which the test is performed. As the strain rate increases, the material properties, including its stress-strain properties, change. At strains of over 10^3 per second, inertia and wave propagation become important. Depending on the brittleness or ductility of the material, shock waves can occur at strain rates over 10^5 sec^{-1}. Above this strain rate intensity thermodynamics and fluid dynamics become important in the material response.

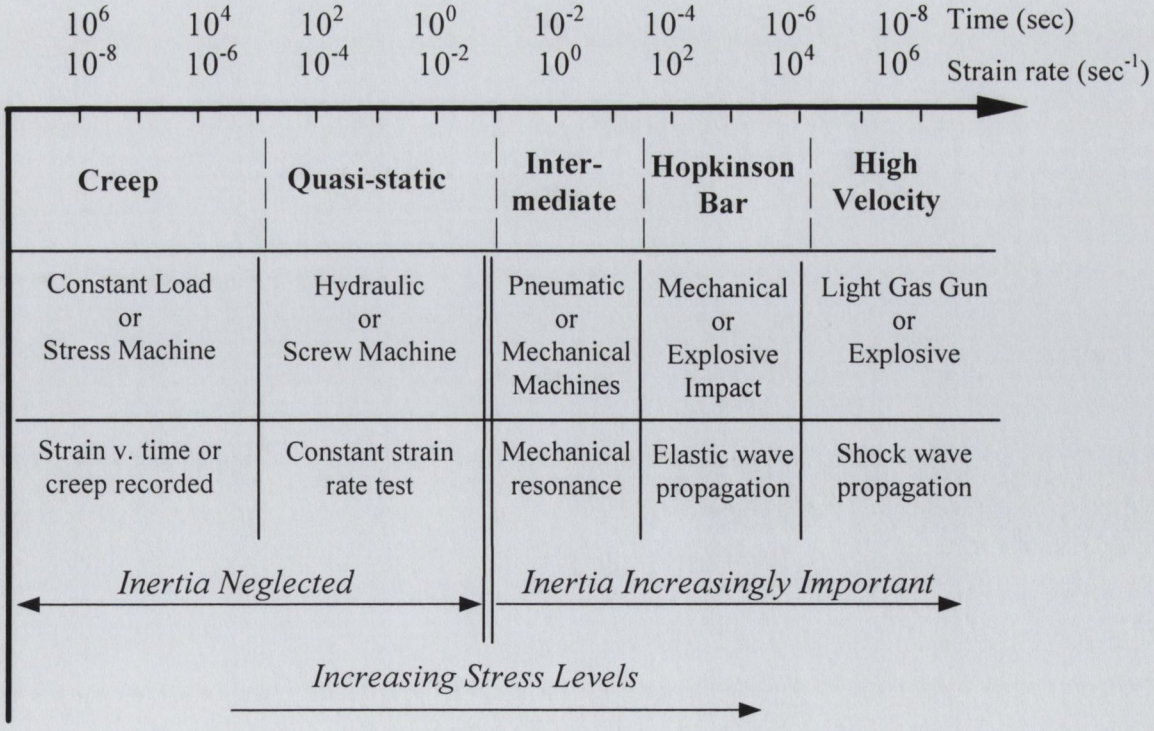


Figure 2.2 Dynamic aspects of testing (from Zukas *et al*, 1982, after Lindholm, 1971)

At lower rates of strain, a uni-axial tension or compression test is undertaken to determine the material response. If the speed of this test is increased it can be used to give a simple determination of the strain rate sensitivity of the material. A hydraulic or pneumatic machine allows strain rates of up to 100 per second, at the limit of the intermediate range, where inertia is just becoming important. These machines can also be used to rapidly accelerate a driving ram, creating a constant velocity for the duration of the test with a minimum of vibration. A drop weight apparatus is also commonly used as an effective method of creating strain rates in the intermediate range. This allows a heavy weight, possibly instrumented, to free-fall onto a target specimen and the resulting strains to be measured. However, this sudden impact can cause large amounts of vibrations and stress waves which can complicate the interpretation of the experimental data.

Many types of machine exist for the application of strains within the high strain rate category, one of which is a Split Hopkinson Pressure Bar. It allows the determination of dynamic stresses and strains and the displacement at the end of the bar. Other test apparatii include the Taylor Cylinder, an Expanding Ring, Dynamic shear tests and the Charpy impact or Dynamic bend tests on beams. These allow deformations under controlled conditions. Strain rates in excess of these, often generating shock waves, can only be produced in a laboratory using a gas gun accelerator attached to a mass, an explosive charge attached to the specimen, or an evacuated tube.

As illustrated in Figure 2.2, the strain rates and inertia effects must be considered in order to make a meaningful interpretation of experimental results. Furthermore, stress wave propagation and its measurement must be given careful attention to prevent misinterpretation of the results. Even if, as in the majority of cases, a loadcell is placed in series with the specimen, account must be taken of the finite time of propagation of the waves to this recording device. The interaction of different stress waves can be minimised if the longitudinal dimension of the specimen is kept to a minimum. However, sometimes in the case of an inhomogeneous material, for example concrete, this is not possible as other requirements, such as the need to obtain a meaningful representation of the material properties, are more critical. Therefore, account must be taken of the variation in stress along the length of the specimen.

2.3. PRINCIPLES OF IMPACT

This section is concerned with the principles underpinning the theory of impact. This is divided into main two areas - the fundamental principles of classical mechanics and the theory of the wave equation.

2.3.1. Classical mechanics

The fundamental theories of impact are based around three laws. These are the principles of conservation of mass, momentum and energy. The majority of the other principles relating to impact can be derived from these three laws, as can the equations governing stress and strain within the body.

The Principle of Conservation of Mass

This principle states that in a physical system, mass is conserved,

$$\int_V \rho dV = constant \tag{2.1}$$

where ρ is the density, that is the mass per unit volume, and V is the volume.

The Principle of Conservation of Momentum

This was derived from Newton's second law, which relates the force which a body experiences, F, to the mass of the body, m, and its acceleration, dv/dt, where v is the velocity and t is the time

$$F = m\frac{dv}{dt} \tag{2.2}$$

which can also be written as

$$F\,dt = m\,dv \tag{2.3}.$$

If both sides of this equation are integrated it results in the following,

$$\int_{t_1}^{t_2} F\,dt = \int_u^v m\,dv \tag{2.4}$$

where u is the velocity at time t_1 and v is the velocity at t_2. The principle of conservation of momentum, for a system of n masses, m_i, which are not subject to any external forces, states that

$$\sum_{i=1}^{n} m_i v_i = constant \tag{2.5}$$

Impulse (I) is defined as the product of the force, F, and the time, t, so that

$$I = \int F\, dt \tag{2.6}$$

and its units are Newton seconds. Impulse is also defined as a change in the momentum

$$I = m(v - u) \tag{2.7}$$

The Principle of Conservation of Energy

This principle states that the energy of a number of discrete masses (from 1 to j) before and after impact is constant, namely

$$\sum_j E_1 + \sum_j \frac{1}{2} m v_1^2 = \sum_j E_2 + \sum_j \frac{1}{2} m v_2^2 + W \tag{2.8}$$

where E is the internal energy stored within the body, W is the work done by the system, and v_1 and v_2 are the velocities prior to and after the impact.

Impact Stress in a Bar Loaded by a Uniform Weight

The greatest stress in a bar which is impacted by a rigid mass, falling under gravity, can by determined by assuming that all of the kinetic energy of the mass, prior to the impact, is absorbed as uniformly distributed strain energy in the bar after the impact. If M_1 is the mass of the body, v_0 is the velocity at impact and A_2, l_2, ρ_2 and E_2 describe the properties of the rod, then

$$A_2 l_2 \frac{\sigma^2}{2E_2} = \frac{1}{2} M_1 v_0^2 \tag{2.9}$$

Hence

$$\sigma^2 = \frac{M_1}{M_2} v_0^2 E_2 \rho_2 \tag{2.10}$$

2.3.2. The wave equations

The wave equations are a group of partial differential equations which are applicable to all types of wave and can be solved in a number of ways to suit the problem being analysed. An understanding of how stress waves, generated as a result of an collision, travel through a material is fundamental to the study of impact. Consider a straight, uniform, isotropic rod, subject to a modest, but rapidly applied force, which causes a disturbance to be propagated elastically through the bar. The behaviour of a small length of the rod, δx long and whose boundaries are at x and $x + \delta x$, with respect to a fixed origin is considered. Figure 2.3 shows the element, which has cross-sectional area A in its unstrained state. The strains and displacements are relatively small, and, according to Johnson (1972), the nominal compressive stress is $-\sigma$, (using the convention where stresses are positive if in tension). The net forces on the element cause it to accelerate so that the equation of motion can be written as

$$-\frac{\partial \sigma_0}{\partial x}\delta x A = A\rho\delta x\frac{\partial^2 u}{\partial t^2} \tag{2.11}$$

where u is the displacement and ρ is the density of the material. The negative sign applies because the compressive stress is in the direction of x decreasing. It follows that

$$\frac{\partial \sigma_0}{\partial x} = -\rho\frac{\partial^2 u}{\partial t^2} \tag{2.12}.$$

The strain, ε, in an element of length δx is $\partial u/\partial x$, which, if E is Young's modulus, assuming that the system remains linearly elastic, results in

$$-\frac{\sigma_0}{\partial u/\partial x} = E \tag{2.13}.$$

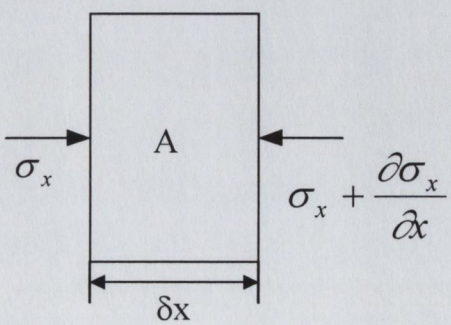


Figure 2.3 Free body diagram of element

If this equation is differentiated with respect to x then,

$$\frac{\partial \sigma_0}{\partial x} = -E\frac{\partial^2 u}{\partial x^2} \tag{2.14}$$

which can be substituted into equation (2.12), resulting in the following

$$\rho\frac{\partial^2 u}{\partial t^2} = E\frac{\partial^2 u}{\partial x^2} \tag{2.15}.$$

This can also be written as

$$c_0{}^2\frac{\partial^2 u}{\partial x^2} = \frac{\partial^2 u}{\partial t^2} \tag{2.16}$$

which is the one-dimensional wave equation. As will be shown, c_0 is the speed of elastic wave propagation through the unstressed bar. It is constant, independent of the stress wave frequency and of the initial velocity, but dependant on the material properties of the transmitting medium, and is defined by

$$c_0 = \sqrt{\frac{E}{\rho}} \tag{2.17}.$$

Equation (2.16) is a simple partial linear differential wave equation and its most general solution can be written thus,

$$u(x,t) = f(x - c_0 t) + g(x + c_0 t) \tag{2.18}$$

where f and g are arbitrary constants (which are not necessarily equal), consistent with the boundary conditions of the particular problem. The first term describes the wave propagation in the positive x-direction with velocity c_o, and the second term represents the wave propagation in the negative x-direction, with the same velocity c_o. When the material is fully compressed as a result of the stress wave, the particle moves in the same direction as the stress wave.

Using equation (2.18), the following can be deduced

$$\frac{\partial u}{\partial t} = -c_0\frac{\partial u}{\partial x} \quad \Rightarrow \quad \varepsilon = -\frac{v_0}{c_0} \tag{2.19}$$

$$\Rightarrow \quad \sigma = -E\frac{\partial u}{\partial x} = \rho c_0\frac{\partial u}{\partial t} = \rho c_0 v_0 \tag{2.20}$$

$$\Rightarrow \quad \sigma = v_0 \sqrt{E\rho} \tag{2.21}.$$

The speed of movement of a particle in the material at location x is $\partial u/\partial t$, which is denoted by v_0, and this velocity is proportional to the stress intensity in the bar, σ. The term $c_o\rho$ is called the mechanical or characteristic impedance of the material. This equation, relating stress to the particle velocity, is fundamental in the development of the theory of co-axial impact.

2.4. ELASTIC STRESS WAVES AND THEIR PROPAGATION

When a material is impacted by a hard object, travelling at a high velocity, stresses and strains are induced. If the rate of loading is sufficiently high, the stress and strain are not immediately dissipated and the material loses its equilibrium. A series of stress waves travelling at finite speeds through the medium, carry this loss of equilibrium through the body, away from the point of contact. Where the duration of impact is of the same order of magnitude as the natural period of vibration of the colliding object, the ratio of the energy associated with the vibration to the total energy becomes important. The vibration effects, therefore, cannot be neglected, and the simple law of linear momentum becomes less useful in interpreting the behaviour. This section considers the stresses and strains which are created and the propagation of the stress waves after the impact.

2.4.1. Impact induced stress and strain

The magnitude of the stress wave travelling longitudinally in a bar, given in equation (2.21), can also be derived from momentum considerations (Johnson 1972). Stress waves can either be compressive or tensile. If a wave, of speed c_0, is travelling through a bar, then, after a time t, the length of the zone compressed by the wave will be $c_0 t$. The bar is assumed to be initially stationary and, after the impact, it is assumed that the impacted face moves and maintains a constant velocity v_o, as can be seen in Figure 2.4. If the change in momentum is equated to the impulse generated by the impact, then

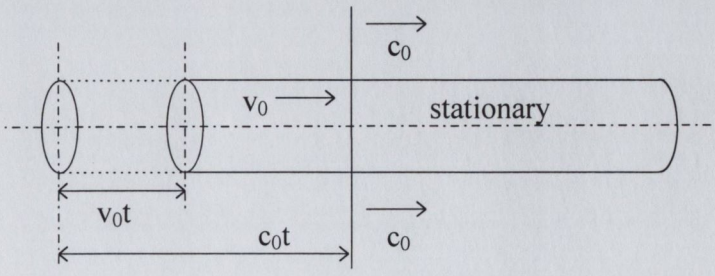


Figure 2.4 Wave propagation in a long bar

$$(A_0 c_0 t\rho)v_0 = (\sigma A_0)t \tag{2.22}$$

Hence,

$$\sigma = \rho c_0 v_0 \tag{2.23}$$

which is the one dimensional equation for the stress in a bar due to a compressive pulse.

2.4.2. Stress waves in isotropic elastic media

The one dimensional theory of stress wave propagation, detailed in section 2.4.1, can be extended to cover elastic wave motion in an isotropic medium which extends infinitely in all directions (Timoshenko and Goodier, 1970). The three dimensional equations of motion for a small element are obtained by combining the differential equations of displacement and the inertia forces and ignoring the body forces, thus

$$\begin{aligned}
(\lambda + G)\frac{\partial e}{\partial x} + G\nabla^2 u - \rho\frac{\partial^2 u}{\partial t^2} = 0 \\
(\lambda + G)\frac{\partial e}{\partial y} + G\nabla^2 v - \rho\frac{\partial^2 v}{\partial t^2} = 0 \\
(\lambda + G)\frac{\partial e}{\partial z} + G\nabla^2 w - \rho\frac{\partial^2 w}{\partial t^2} = 0
\end{aligned} \tag{2.24}$$

in which e is the volume expansion, u, v and w represent the displacements in the x, y and z directions, and the symbols can be explained by

$$\nabla^2 = \frac{\partial^2}{\partial^2 x} + \frac{\partial^2}{\partial^2 y} + \frac{\partial^2}{\partial^2 z} \qquad \text{Laplacian operator}$$

$$\lambda = \frac{\upsilon E}{(1+\upsilon)(1-2\upsilon)} \qquad \text{Lamé's constant}$$

$$G = \frac{E}{2(1+\upsilon)} \qquad \text{Shear modulus}$$

If the volume expansion, e, created by the wave is zero, then the deformation occurring is only as a result of shearing distortion and rotation, and equations (2.24) become

$$G\nabla^2 u - \rho\frac{\partial^2 u}{\partial t^2} = 0 \tag{2.25}$$

which describes an equivoluminal or distortion wave.

Timoshenko and Goodier explain that if the deformation produced by the waves does not cause any rotation of the body then an irrotational wave or wave of dilation results, which is described by

$$(\lambda + 2G)\nabla^2 e - \rho \frac{\partial^2 e}{\partial t^2} = 0 \qquad (2.26).$$

These two equations can be superimposed to describe wave propagation in an elastic medium and can be written as

$$\frac{\partial^2 e}{\partial t^2} = a^2 \nabla^2 e \qquad (2.27)$$

where

$$a = c_L = \sqrt{\frac{\lambda + 2G}{\rho}}$$

for waves of distortion, where c_L is the speed of a longitudinal wave,

or

$$a = c_S = \sqrt{\frac{G}{\rho}}$$

for waves of dilation, where c_S is the speed of a shear wave.

The following section will show that these two values of a describe the velocities of propagation of plane waves of dilatation and distortion.

2.4.3. Two dimensional longitudinal waves in bars

At a considerable distance from the centre of disturbance from where all stress waves propagate, the waves can be considered to be plane waves, of which there are two predominant types, namely, longitudinal, or distortion waves, and shear (transverse) waves, or dilational waves.

Longitudinal waves are induced when the disturbance is normal to the wave front. The propagation of a plane compressive longitudinal wave may be described mathematically. If ε_x and ε_y are equal but opposite transverse strains and σ_x and σ_y are the corresponding equal and opposite stresses, maintained on the lateral surfaces of the bar, then

$$E\varepsilon_y = \sigma_y - \upsilon(\sigma_y - \sigma_x) \qquad (2.28)$$

where υ is the Poisson's ratio for the material and, by symmetry, ε_y=ε_z and σ_y=σ_z. If the transverse strain, ε_y, is assumed to be zero, such that the body does not experience any transverse deformation and can assumed to be in a state of uni-axial strain, then

$$\sigma_y = -\frac{\upsilon\sigma_x}{(1-\upsilon)} \tag{2.29}$$

Furthermore, the strain in the x-direction can be written as

$$\frac{\partial u}{\partial x} = \varepsilon_x = \frac{-\sigma_x - 2\upsilon\sigma_y}{E} \tag{2.30}$$

If this is then substituted into equation (2.29)

$$\frac{\partial u}{\partial x} = -\sigma_x \frac{(1-\upsilon-2\upsilon^2)}{E(1-\upsilon)} \tag{2.31}$$

Hence,

$$\frac{\partial \sigma_x}{\partial x} = E\frac{(1-\upsilon)}{(1+\upsilon)(1-2\upsilon)} \cdot \frac{\partial^2 u}{\partial x^2} \tag{2.32}$$

When this is substituted into equation (2.12), it results in

$$\frac{\partial^2 u}{\partial t^2} = \frac{E}{\rho}\frac{(1-\upsilon)}{(1+\upsilon)(1-2\upsilon)} \cdot \frac{\partial^2 u}{\partial x^2} \tag{2.33}$$

The speed of the longitudinal dilatational wave is, therefore,

$$c_L = \sqrt{\frac{E}{\rho}\frac{(1-\upsilon)}{(1+\upsilon)(1-2\upsilon)}} \tag{2.34}$$

This can also be described using Lamé's constant and the shear modulus thus,

$$c_L = \sqrt{\frac{\lambda + 2G}{\rho}} \tag{2.35}$$

It can also be related to the speed of a longitudinal pulse in a free body (as previously derived),

$$\frac{c_L}{c_0} = \sqrt{\frac{(1-\upsilon)}{(1+\upsilon)(1-2\upsilon)}} \tag{2.36}$$

Shear waves occur when the material particles move in a plane at right angles to the direction in which the wave itself propagates and the speed of the transverse wave can also be found. The principal shear stresses, τ, are at a maximum and minimum on the planes at an angle of 45° to the applied stress because, on these planes, the tangential component is zero. The equation of motion of an element along these planes, at 45° to the direction of propagation of the wave along the principal tensile stress axis, is, therefore,

$$\rho A dx \frac{\partial^2 u}{\partial t^2} = A d\tau \tag{2.37}$$

Using the equation for the principal stresses in three directions, the shear strain ε_1 is

$$\varepsilon_1 = \frac{\partial u_1}{\partial x_1} = \frac{\tau(1+\upsilon)}{E} \tag{2.38}$$

and if equation (2.38) is substituted into equation (2.37)

$$\frac{\partial^2 u_1}{\partial t^2} = \frac{E}{\rho(1+\upsilon)} \cdot \frac{\partial^2 u_1}{\partial x_1^2} \tag{2.39}.$$

The speed of longitudinal wave propagation, where the element is not constrained from lateral dilation, can be written as

$$c' = \sqrt{\frac{E}{\rho(1+\upsilon)}} \tag{2.40}.$$

As this is at 45° to the direction of propagation of the wave, the speed of transverse or shear wave propagation, c_S, is $c' \times cos45$. Hence

$$c_S = \sqrt{\frac{E}{2\rho(1+\upsilon)}} = \sqrt{\frac{G}{\rho}} \tag{2.41}.$$

This can also be normalised by dividing it by the speed of longitudinal wave propagation

$$\frac{c_L}{c_S} = \sqrt{\frac{2(1-\upsilon)}{1-2\upsilon}} \tag{2.42}.$$

The ratio of the longitudinal velocities ranges from approximately 1.03 to 1.06 as Poisson's ratio varies between 0.15 and 0.33. In comparison, the ratio of the longitudinal wave velocity to the transverse wave velocity ranges from 1.56 to 1.99 for the same values of Poisson's ratio. When either a longitudinal or shear wave meets the surface of the solid in which it is travelling it generates both shear and longitudinal waves.

2.4.4. Coaxial collision of two bars

The stress intensity in a bar was used by Johnson (1972) to derive the equation for the stress induced when two bars of identical cross-sectional area, but unequal impedance (see section 2.3.2), collide co-axially, as in Figure 2.5. Prior to impact, the two bars are travelling in the same direction with velocities v_1 and v_2, where $v_1 < v_2$, and have different impedances (ρc). After impact, longitudinal compressive waves, of speeds c_1 and c_2, travel through the bars away from the interface. This interface, and the material engulfed

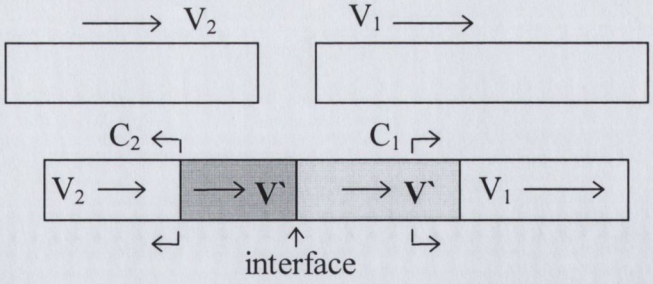


Figure 2.5 Coaxial impact of bars of identical cross-section

by both waves, will have a speed v'. As the action and reaction across the interface are equal and the cross-sectional areas are identical, the stress in each bar is the same.

The stress in a bar, travelling with initial velocity, v_1 is, therefore,

$$\sigma = \rho c_L .(v' - v_1) \tag{2.43}$$

from equation (2.23), where v_0 in the earlier equation is now understood to be the change in the particle speed, or the magnitude of the velocity discontinuity as a result of a wave travelling through the bar. Hence,

$$\sigma = \rho_2 c_2 (v_2 - v') = \rho_1 c_1 (v' - v_1) \tag{2.44}.$$

And,

$$v' = \frac{\rho_1 c_1 v_1 + \rho_2 c_2 v_2}{\rho_1 c_1 + \rho_2 c_2} \tag{2.45}$$

which means that the stress can be described by

$$\sigma = \frac{v_2 - v_1}{\frac{1}{\rho_1 c_1} + \frac{1}{\rho_2 c_2}} \tag{2.46}.$$

If the cross-sectional areas are not the same, then it is assumed that the forces at the location of impact are identical

$$A_1 \sigma_1 = A_2 \sigma_2 \tag{2.47}$$

and, in the same way as above, the stress can be found, thus

$$\sigma_1 = \frac{\rho_1 c_1 (v_2 - v_1)}{1 + \frac{\rho_1 c_1 A_1}{\rho_2 c_2 A_2}} \tag{2.48}.$$

A similar equation can be derived to find the stress in the second bar, σ_2.

2.4.5. Reflection and superposition of waves

When a wave travelling through an elastic media reaches a discontinuity, some of the waves are reflected and travel back through the first medium and some are refracted and travel into the next medium (Johnson, 1972). Discontinuities occur where there is a change in cross-sectional area or in the material properties and at free boundary interfaces. An example of such a discontinuity can be found in Figure 2.6 where there is a compressive stress wave, of intensity σ_I, travelling from left to right. At the interface, part of the wave is transmitted with amplitude σ_T, and part is reflected with amplitude, σ_R. At the interface the forces in both bars must be equal and the particle velocities must be continuous. Therefore,

$$A_1(\sigma_R + \sigma_I) = A_2\sigma_T \tag{2.49}$$

and

$$v_I - v_R = v_T \quad \text{or} \quad \sigma_I - \sigma_R = \sigma_T \tag{2.50}.$$

Using equation (2.23) the following expressions can be found for σ_R and σ_T in terms of σ_I

$$\sigma_T = \frac{2A_1\rho_2c_2}{A_1\rho_1c_1 + A_2\rho_2c_2}\sigma_I$$

$$\sigma_R = \frac{A_2\rho_2c_2 - A_1\rho_1c_1}{A_1\rho_1c_1 + A_2\rho_2c_2}\sigma_I \tag{2.51}.$$

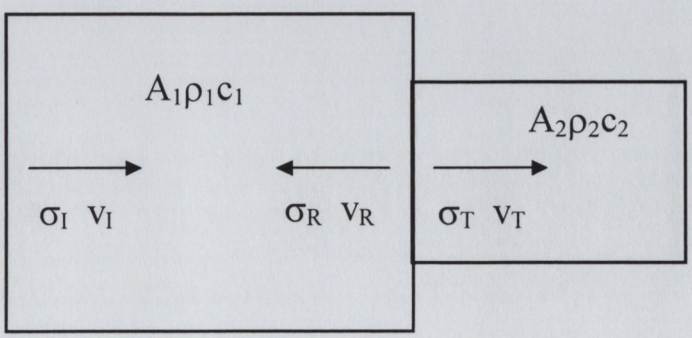


Figure 2.6 Wave reflection and transmission

2.4.6. Exact theory of wave propagation

The theory of wave propagation considered thus far has concerned body waves travelling through isotropic, homogeneous solid materials. No account has been taken of radial motion or of the boundary conditions associated with the propagation of these waves. This theory is, therefore, only valid for wavelengths which are large in comparison with the dimensions of the body through which they are travelling.

In the 1880s Rayleigh and Love examined the transverse radial motion of waves in an unbounded medium and showed that elastic waves can travel along the surface of a body. 'Rayleigh Waves' travel in 2-dimensions only, along the surface of the body at a velocity approximately half that of the distortional waves discussed above. Furthermore, these waves decrease exponentially in amplitude with the depth below the surface and the horizontal component of the wave front is not parallel to the direction of wave movement. Love investigated a shear surface wave which moves in the relatively shallow surface zone and found that these occurred most often when two media, with different properties, are in contact near to the surface of the body.

The vibration of waves in cylindrical bars was studied extensively by Pochhammer and Chree in the late nineteenth century, who found an 'exact' 3-dimensional, analytical solution to the problem of elastic stress waves travelling in bounded and unbounded media, where the velocity of propagation is dependant on the frequency of the wave. Although the problem is apparently quite simple, its solution is highly complicated. Pochhammer and Chree used the equations of wave motion in cylindrical co-ordinates and the expressions for sinusoidal waves propagating through a cylinder with various frequencies and subject to different modes of vibration, to find an infinite number of solutions for each of longitudinal, transverse and flexural waves (Timoshenko and Goodier, 1970). They concluded that the solution was only truly valid for cylinders with long lengths with respect to their radius, which allowed the end effects to be neglected and satisfied the requirement of zero shear stress at the end faces. Furthermore, the ratio of the bar radius to the wavelength must be less than 0.1 if the speed of longitudinal wave propagation, c_0, is to be predicted to within 1 %. The Pochhammer-Chree equations are very limited because of the rigorous end conditions which must be met in an attempt to generate realistic stresses and displacements and this makes the interpretation of impact problems, using these

equations, more difficult. Less rigorous theories, as described above, are used with simplified mathematical equations to find solutions to these impact problems and fortunately, as the pulse length increases, the differences between the exact and elementary theories become negligible.

The theories discussed in this section were originally generated for simple, elastic media in which waves were travelling. If the wave propagated is very intense, as in the case of high velocity impact, it is possible that the stress intensity will exceed the elastic limit of the material and cause it to behave non-linearly or plastically. Two waves will then propagate through the material - an elastic wave and a more intense plastic wave, which has a velocity of

$$c_P(\varepsilon) = \sqrt{\frac{\delta\sigma/\delta\varepsilon}{\rho}} \qquad (2.52).$$

This is similar to the wave velocity when elastic, except that Young's modulus is no longer linear but is a function of the stress and strain in the material (Kolsky, 1963). If the loading even more intense, and occurs over an extremely short duration, the material will exhibit fluid properties. No shear waves will be transmitted and the speed of the wave will be proportional to the bulk modulus of the material.

2.5. CONCRETE FILLED COMPOSITE COLUMNS

A concrete composite column is a compression member which may be either a concrete-encased structural section or a concrete filled tube. In the early twentieth century low strength concrete was placed around a steel section to enhance its fire protection. Initially, the presence of the concrete was ignored in the calculation of the column strength. However, designers soon realised that the encasing concrete increased the load carrying capacity of the composite section and that large savings could be made in steel costs if a higher quality concrete was used. Concrete was also placed inside the steel tube, which further enhanced the strength of the resulting composite. This withstood fire reasonably well as the encased concrete acted as a heat sink but the exposed steel still required fire protection. The design of these concrete filled columns was not governed in any detail by the various regulations until, in 1994, their design was incorporated into the new Eurocode 4, *Design of composite steel and concrete structures*, which presents the latest recommendations for composite column construction in static loading situations.

Concrete filled steel hollow sections have many advantages over conventional reinforced concrete columns. Firstly, they require little or no reinforcement and no formwork during construction as the hollow steel column encloses the concrete whilst it is being poured and secondly, the steel section provides bi-axial confinement to the concrete. Confinement is traditionally provided by longitudinal steel reinforcing bars with surrounding links, or more occasionally, by steel spirals. Both of these methods provide confinement to the concrete as the bars help resist both elongation and buckling when the concrete begins to dilate laterally when loaded axially. The concrete filled tubes have an additional advantage over conventional reinforcement in that the confinement which they provide is continuous along the entire length of the section and is not subject to the variations in the confining pressure associated with the steel in a conventional section.

However, composite columns can have certain disadvantages. Firstly, the connections between different elements can be difficult to effect because the solid, filled column provides no obvious method by which it can be attached to a horizontal beam, without the use of rigid precision bolts, which are extremely costly. Web and bottom flange cleats can be used to connect the beam and column but this only provides a semi-rigid connection as

some relative rotation is allowed between the two elements, yet provides a considerably cheaper solution (Narayanan, 1988). Secondly, the alkaline concrete which, after pouring, creates a humid environment within the confining tube can cause corrosion from the inside of the cylinder (Viest *et al*, 1997).

Experiments have consistently shown that, as would be expected, the composite element has greater ductility, flexural stiffness and toughness than unconfined, or even conventionally reinforced, concrete (Gardner and Jacobson, 1967). However, it is due to the ability of concrete filled columns to carry high loads, even when of small lateral dimensions, that they have become increasingly widely used, with the most prominent early use being the Almondsbury Motorway Interchange in 1965.

The way in which a composite column acts when laterally loaded can be examined through an axi-symmetric study of an internal pressure applied to a pipe, as the response of the confining cylinder is controlled by thin-shell or membrane action. The wall thickness is small compared to the radius of the cylinder and thus, has little resistance to bending.

If a thin walled cylinder has radius r and wall thickness t, and is subject to an internal pressure p, then the circumferential or hoop stress, σ_c, can be found as follows. Consider a section of the cylinder, of length L, and cut from the cylinder. The free body diagram of half of this element is shown in Figure 2.7. The originally internal effect of the hoop stress in the wall of the pipe, σ_c, is now shown as an external force on the free body (Nash, 1972). The horizontal components of the radial pressures cancel one another because of symmetry, and the vertical equilibrium equation is

$$\sum F_v = -2\sigma_c tL + \int_0^{\pi} prL(d\theta)\sin\theta = 0 \qquad (2.53).$$

When this is integrated, it results in the following relationship between the stress in the sleeve and the internal pressure

$$\sigma_c = \frac{pr}{t} \qquad (2.54).$$

This equation can be used to find the stress in the steel sleeve when subject to an internal pressure. This is caused by the lateral dilation of the concrete, resulting from longitudinal loading, and the Poisson's ratio effect, where it is assumed that the wall thickness of the pipe is small.

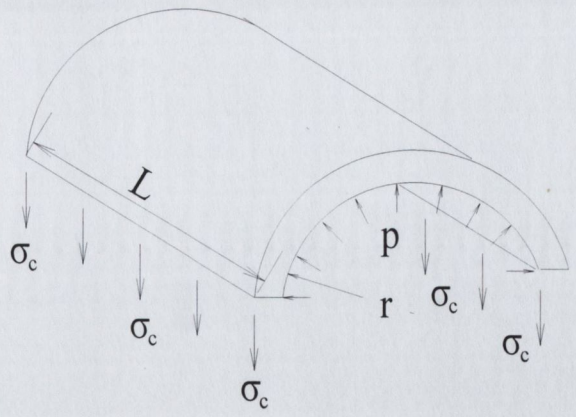


Figure 2.7 Free body diagram of stresses in an element of a confining tube

This theory remains valid if the thickness to radius ratio is less than 1:30, whereupon the theory for thin shells breaks down, as the radius of the shell changes considerably over its thickness and the strain across the section is not constant. These stresses, in the walls of a thick pipe, are considerably more complicated, but can be determined using equilibrium equations and are derived in all of the standard textbooks on stress analysis (see for example, Timoshenko and Goodier, 1970), so only the solutions will be given here. For a cylinder with internal radius, a, and external radius, b subjected to an internal pressure, p_i, the stresses can be determined at any particular radius, r, thus,

$$\sigma_c = \frac{a^2 p_i}{b^2 - a^2}\left(1 + \frac{b^2}{r^2}\right) \quad \text{circumferentially} \tag{2.55}$$

$$\sigma_r = \frac{a^2 p_i}{b^2 - a^2}\left(1 - \frac{b^2}{r^2}\right) \quad \text{radially} \tag{2.56}.$$

These equations show that σ_r is always a compressive stress and σ_c is always a tensile stress.

If only the concrete core of a composite element is concentrically loaded then the elastic behaviour can be determined using plane stress and plane strain theory. The values of radial, ε_r, circumferential, ε_θ, and longitudinal strain, ε_z, can be described in polar co-ordinates (as shown in Figure 2.8) in terms of the corresponding stress values, thus for the pipe

$$\varepsilon_{rp} = \frac{1}{E_p}(\sigma_r - \upsilon\sigma_\theta) \tag{2.57}$$

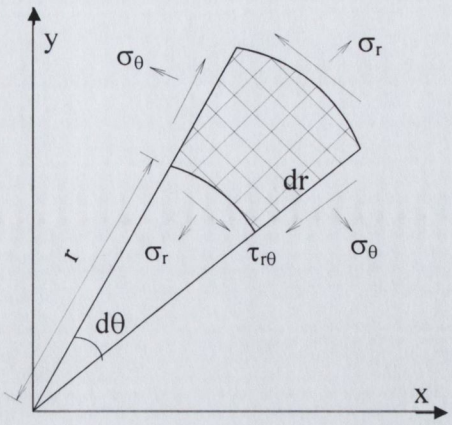


Figure 2.8 An element of the core or the sleeve showing the stresses in polar co-ordinates

$$\varepsilon_{\theta p} = \frac{1}{E_p}(\sigma_\theta - \upsilon\sigma_r) \tag{2. 58}$$

as there is no longitudinal stress applied to the pipe. However, the stress applied axially to the core is σ_z and results in the following relationships for the strains in the confined core.

$$\begin{aligned}
\varepsilon_{rc} &= \frac{1}{E}\left[\sigma_r - \upsilon(\sigma_\theta + \sigma_z)\right] \\
\varepsilon_{\theta c} &= \frac{1}{E}\left[\sigma_\theta - \upsilon(\sigma_r + \sigma_z)\right] \\
\varepsilon_{zc} &= \frac{1}{E}\left[\sigma_z - \upsilon(\sigma_\theta + \sigma_r)\right]
\end{aligned} \tag{2.59}.$$

The axially loaded concrete dilates laterally due to Poisson's ratio and causes an effective pressure at the interface between the core and the pipe. At the edge of the concrete core the radial and circumferential stresses are equal to the effective pressure, p_0. Similarly, the radial stress is equal to the effective pressure on the inner surface (radius a) and is zero on the outer surface (radius b). Hence, the stresses in the concrete core are

$$\sigma_r = \sigma_\theta = -p_0 \tag{2.60}$$

and using the thick pipe theory described above, the stresses at any radius r in the pipe can be determined, according to Kurt (1978) as

$$\sigma_r = -\frac{a^2 b^2}{b^2 - a^2}\frac{p_0}{r^2} + \frac{a^2 p_0}{b^2 - a^2} \tag{2.61}$$

$$\sigma_\theta = \frac{a^2 b^2}{b^2 - a^2}\frac{p_0}{r^2} + \frac{a^2 p_0}{b^2 - a^2} \qquad (2.62).$$

Equations (2.60) to (2.62) can be substituted into the equations for the strains in the pipe and the core. The circumferential strains at the core-pipe interface are equal and can, therefore, be equated to one another. The effective pressure can be determined using these equations and, for a thick pipe, is

$$P_0 = -\frac{\upsilon_c \sigma_z}{1 - \upsilon_c + \frac{E_c}{E_p}\left(\frac{b^2 + a^2}{b^2 - a^2} + \upsilon_p\right)} \qquad (2.63)$$

or, more simply for a thin pipe is

$$P_0 = -\frac{\upsilon_c \sigma_z}{1 - \upsilon_c + \frac{E_c}{E_p}\frac{D}{2t}} \qquad (2.64).$$

Equations (2.63) and (2.64) can be substituted into the equations above to determine the stresses in the pipe or the concrete core resulting from an axial load and an effective pressure caused by lateral dilation.

These equations become important in the determination of the structural behaviour of concentrically loaded concrete filled columns, which have a comparatively short length/diameter ratio. It was suggested by Sen *et al* (1972) that this should ideally be a value less than five. Furthermore, at this aspect ratio it can be assumed that the shear stresses in the column are zero, as the cylinder is usually long enough to ensure that plane sections will remain plane.

A short composite column, of length to diameter ratio less than two, is capable of taking its ultimate carrying capacity without local or overall buckling and allows the maximum design strengths to be developed in both the structural hollow cylinder and the concrete core. If both the concrete core and the confining cylinder are loaded axially, then the materials undergo the same increase in strain. Hence, the steel sleeve yields long before the concrete reaches its compressive strength, as is illustrated from the stress-strain diagram in Figure 2.9 (Narayanan, 1988). However, the concrete in the column pushes outward against the steel wall, offering support to the cylinder and preventing local buckling of the steel tube even after it has yielded. As the load is applied to the column,

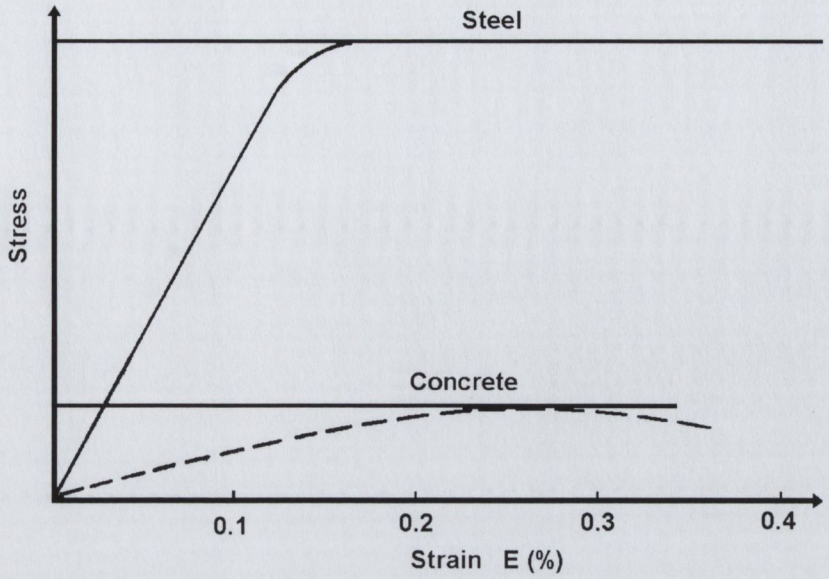


Figure 2.9 Stress-strain diagram for composite column (after Narayanan, 1988)

the axial load on the concrete core causes lateral dilation due to a Poisson's ratio effect. This dilation of the concrete causes an increase in the hoop stress in the confining tube, which reduces how much more stress can be achieved by the steel sleeve prior to yield. If the tube is short and cylindrical further enhancement in the strength of the concrete is experienced due to tri-axial confinement, which more than compensates for the reduction in the apparent strength of the steel. The ultimate squash load, N_u', is, therefore,

$$N_u' = A_s f_{sd}' + A_c f_{cd}' \tag{2.65}$$

where f_{sd}' is the reduced design strength of the steel and f_{cd}' is the enhanced design strength of concrete and A_s and A_c represent the cross-sectional areas of the two elements. This increase in the load carrying capacity is developed because the concrete is put into tri-axial confinement due to the presence of the confining steel section. The concrete contribution factor, α, is used to represent the proportion of the squash load taken by the concrete, and for cylindrical concrete filled columns is given by

$$\alpha' = \frac{A_c f_{cd}'}{N_u'} \tag{2. 66).}$$

The tri-axial confinement provided by the stiff steel sleeve increases the effective confinement of the core, when compared it an unconfined situation. However, if the length to diameter ratio is greater than three Viest *et al* (1997) suggest that the longitudinal stiffness of the steel shell is inadequate to resist inelastic buckling under compressive loads

and that the buckling capacity of the column should be determined without any increase in the concrete strength from lateral confinement.

If concrete is confined and prevented from expanding laterally, in two out of three mutually perpendicular directions then the ultimate compressive strength of the material in the third direction increases considerably (numerous papers which have shown this are well summarised in De Nicolo *et al*, 1997). This is because the concrete is unable to freely expand laterally and cracks, which would form in unconfined concrete under an axial load, are prevented from opening. It has been shown that the confining steel, which is in hoop tension, cannot buckle due to the outward dilation of the contained concrete and must yield prior to the concrete failing by crushing (for example see Shams and Saadeghvaziri, 1997). The lateral pressure can either be applied actively, where there is a lateral load on the concrete before it is loaded, or passively, where the lateral pressures are only mobilised when the confined concrete begins to dilate and generates an effective pressure between the core and the wall of the pipe. Considerable research has been undertaken to determine the deformational response of concrete when actively confined (Kotsovos and Pavlovic, 1995), but the deformational response of concrete confined passively by a steel tube, and where the lateral pressure is not equal throughout the period of loading, although less well documented, is considered in greater detail in chapter 3.

Hence, the axial loads are carried as a result of the interaction between the confining and the confined materials, transferred through an interface bond associated with friction at the interface. Virdi and Dowling (1980) suggested that this bond occurred due to the two types of imperfections in the confining steel, namely, surface roughness and shape variation. In certain cases where the limiting bond stress is likely to be exceeded, mechanical connectors may also be required.

2.6. CONCLUSIONS

This chapter provides background theory which will facilitate an understanding of the research undertaken and detailed in this thesis. The subject can be broken into two distinct areas - one concerning the response of materials and structures to low velocity hard impact and the other the use of a sleeve to provide confinement to concrete when axially loaded.

The impact theory is based on the assumption that the velocity is quite low, that the resulting material response will largely be elastic and will generate stress rather than shock waves in the impacted body. The chapter considers the history of the study of impact and then examines the fundamental theories governing the response of the body and of the elements within it. These theories range from simple classical mechanics to the details of wave propagation, transmission and reflection within an impacted body. The equations for the velocities of the various waves travelling away from the point of impact in an attempt to dissipate the high stresses generated as a result of the collision are also derived.

The confinement of concrete using a sleeve of a structural hollow section is also described. The study in this area, thus far, has solely been focused on the response of composite cylinders to axially applied static loads. The response of both thin and thick pipes to an applied internal pressure, using equilibrium equations, is summarised. Furthermore, the compatibility between the axially loaded concrete core and the unloaded confining pipe is also described. This allows the determination of the effective pressure at the interface and the stresses and strains on the cross-section of the confined element.

The focus of the current research is to combine these two theories and to subject a confined concrete cylinder to an axially applied impact load. The research will particularly consider the effects of impact on the composite and the way in which the load is transferred from the impacted core into the confining sleeve and along its length, predominantly using the theories outlined in this chapter.

3. REVIEW OF PREVIOUS LITERATURE CONCERNING WORK ON CONCRETE SUBJECT TO IMPACT AND CONFINEMENT

3.1. INTRODUCTION

Many materials used in the construction of buildings and structures, most particularly concrete, are sensitive to the rate of strain at which the load is applied. It is, therefore, critical that, prior to the design of buildings which may be subject to high rate loading, the engineer is familiar with the constitutive relationships and the failure criterion of the materials involved, in order to properly analyse the structure for the types of loading to which it will be subject. The strength, stiffness and ductility of materials can be affected by increases in the strain rate, particularly when these concern the several orders of magnitude between static and impact loading.

Many experimental investigations into the response of materials to impact have been undertaken and are well documented in the literature (Zukas *et al*, 1982). The mechanisms used to generate collisions between bodies (resulting in impacts which can be measured and assessed) include both simple and highly complicated drop weight test rigs creating impacts of low and moderate velocities, and compressed gas guns and explosives for generating impacts with higher velocities. The variables measured during impact tests have traditionally been quite restricted due to limitations in measurement equipment. However, due to significant improvements in high speed data acquisition, these can include

- the velocity, bulk motion, vibration and displacement of the impacting body
- contact phenomena - forces, deformation, penetration and perforation of the impacted body
- stress wave propagation effects in both the impactor and the target

which can all be coupled with a post-impact assessment of the modes of failure.

The response of homogeneous materials, such as steel, to impact is well established (Goldsmith, 1964). With increasing strain rates, steel exhibits enhancements in both its yield and ultimate strength, without appearing to change its modulus of elasticity. The relative increases in strength over the statically loaded values, with increasing strain rate are considerably less for high strength steels than for lower strength ones.

The impact response of concrete which is an inhomogeneous and brittle material, however, is less well understood. Considerable research within the last fifty years has been devoted to determining the impact response of uni-axially loaded concrete at ambient temperatures. Nonetheless, much more work must be undertaken before concrete's response to high strain rate loading, both uni-axially and multi-axially, is as well understood as its response to lower strain rates such as creep or static loads. Concrete is a heterogeneous material, with inherent micro-cracks, discontinuities and voids. The deformation of concrete occurs as a result of the propagation of these tensile micro-cracks in response to an applied load. When concrete is loaded rapidly the crack tips, which typically control its response to static loading or creep, have less time to form or to move within the period of loading and its response is quite different.

The beneficial effects of lateral confinement on the strength and deformational properties of concrete have been recognised since the early days of reinforced concrete construction. Work performed early last century chiefly concerned the strength enhancements which could be obtained using a closely spaced spiral of reinforcement to confine an enclosed core of concrete. The confining stress was mobilised by the lateral dilation of the confined concrete, under an axial stress, which was resisted by the reinforcement. As the reinforcement was closely spaced, it was considered that this force was applied uniformly to the concrete surface and could be described as uniform passive confinement.

The introduction in the 1950s of limit state design methods prompted investigations into the complete stress-strain behaviour of confined concrete. The initial studies predominately concerned confinement provided to the concrete by rectangular links. Although these links were used anyway to support the longitudinal steel bars in the design of columns and beams, their confining properties were not exploited initially because of a lack of experimental data. Similar to spirals, the confining stresses are mobilised by the passive reaction of the steel links to the dilation of the concrete. However, the confinement which they provide is not uniform because of their comparatively large spacing and their rectangular shape, which results in the confinement having a varying intensity over the internal perimeter.

Other work examined the effect of providing active confinement to the concrete which was achieved by imparting an initial tension to the confining steel spiral (Armstrong, 1983).

The active confinement provided was supplemented by the passive confinement generated by the spiral's resistance to the lateral dilation of the concrete. The active pressure could also be provided by axially loading the concrete and confining the concrete hydraulically using a tri-axial pressure chamber. However, care must be taken when loading to prevent the hydraulic fluid from penetrating the voids in the concrete and accelerating its fracture. This can result in an apparent decrease in strength, in a very similar manner to the effect of wetting concrete just prior to testing.

The research described in this thesis concerns the response of sleeved concrete to concentrically applied low velocity hard impact, where the sleeve of steel, aluminium or plastic provides a passive confining pressure to the axially loaded concrete. It is not the intention of the author to perform an exhaustive literature survey as some recent review papers already exist for both topics concerned (Bischoff and Perry, 1991; Shams and Saadeghvaziri, 1997), but rather to study the literature relevant to the current study.

The focus of the literature survey undertaken in this chapter is twofold. Firstly, it examines the response of concrete to compressive low velocity impact (or to tests with similar strain rates) from non-deforming hard missiles. The majority of the works consulted focus on the response of normal strength concrete to local deformations, such as cracking and fracture of the concrete. The literature survey concentrates on the strength enhancements, changes in material properties, energy absorption capacity and the stress-strain response of concrete under increased strain rates. The bulk of the research in this area occurred prior to the mid 1990s when the focus of the work changed from impact loads on concrete to those on new, composite materials and to the response of materials, including concrete, to high velocity impacts and explosions. The literature survey does not consider the global effects of flexure of the concrete or deformations including perforation, penetration or spalling, all of which are typically associated with beams or slabs subject to impact loads. Secondly, this chapter investigates the concentric loading of confined concrete cylinders and columns, and the enhancement in the strength and ductility of concrete when either passively or actively confined. It does not examine the extensive work completed on the response of confined concrete to eccentric loading or to the simultaneous application of an axial load and an end moment, as neither of these are pertinent to the types of loads applied in the current research.

3.2. LOW VELOCITY IMPACT OF CONCRETE

3.2.1. Compressive strength enhancement with increasing strain rate

Early tests on the impact strength of concrete involved dropping an un-instrumented weight onto a piece of concrete. The impact strength of the concrete was determined by the ability of the concrete to withstand a certain number of blows, or by determining the height at which a weight of a certain mass should be dropped to cause failure. The most important early work on the response of concrete to impact was undertaken by five researchers, namely Abrams (1917), Glanville (1938), Jones and Richart (1938), Evans (1942) and Watstein (1953). All concluded that the strength of concrete increases as the strain rate of the loading increases (Evans, 1942; Atchley and Furr, 1967).

Research undertaken by Green (1964) attempted to quantify the impact strength of concrete more accurately using a ballistic pendulum to impact concrete cubes. He defined his criterion for strength as the number of blows which the concrete could sustain until the hammer did not rebound. Even using this simple method, he found that concrete made with crushed aggregate had a greater impact strength than uncrushed aggregate, as the smooth surfaces of the uncrushed gravel did not allow a sufficient bond to be formed with the mortar. He concurred with previous researchers that, for ordinary Portland cement, the impact strength increased with an increase in the compressive strength. The curing conditions of the concrete were also found to be important in its response to impact as the cubes stored in air could resist a greater number of blows than water cured cubes because the internal stresses had time to redistribute whilst the concrete dried slowly.

Atchley and Furr presented results in 1967 on the strength of concrete cylinders subject to low velocity hard impact using a drop hammer apparatus and concluded that the strength of concrete increases with the rate at which the concrete was stressed or strained until it reaches a constant maximum value. Green's work using the ballistic pendulum was continued by Hughes and Gregory (1968) who established a definite trend between the increase in the strength of impact loaded concrete and the compressive strength of a concrete cube.

The properties of the concrete and its constituents and their effect on the strength of the impacted concrete was also studied. Hughes and Gregory (1968) showed that the cement content, coarse aggregate content and the maximum aggregate size all affected the impact strength of concrete in similar ways to how they affected the static compressive strength. Hughes and Watson (1978) studied the properties of concrete which affect its impact strength and concluded that cubes which have a low cement/water ratio (c/w) have a low compressive strength but show a higher proportional strength increase when impacted than cubes with higher c/w ratios. The type of aggregate used in the manufacture of the concrete greatly affects its response at higher strain rates, which was illustrated by the work of Hughes and Gregory (1972) and Sparks and Menzies (1973). Apart from the strength differences resulting from the different surface textures of the aggregate, the impact strength increased as the maximum size of the aggregates decreased. Furthermore, both statically and at higher strain rates the stiffer aggregates produced stronger concrete and as the stiffness increased the rate sensitivity of the concrete was decreased.

The conditions under which the concrete is initially cured and then stored prior to testing also result in differences in its response to high strain rate loading. Neville (1995) illustrated that, under static conditions, if a concrete is wet cured it has a greater compressive strength than if air dried. Spooner (1971) showed that concrete which is wet cured exhibits a greater strength increase, over statically loaded wet concrete, when subject to higher strain rates than identical concrete when air dried. He concluded that the loading rate effect was greater in specimens which were saturated when tested, compared to those which were dry and that the loading rate effects decreased further as the drying time increased, which was similar to the results found by Ross *et al* (1995). The effect of age on the increases in the impact strength of concrete has not been studied by many researchers. Hughes and Gregory (1972) showed that there were limited increases in the impact strength of their concrete as it increased in age, if it had been continuously cured in water (until their final test was performed at 91 days). In the majority of tests, the effects of the curing conditions have a much greater influence on the strength increases and probably shadow the effects of any increases in the age of the concrete (Bischoff and Perry, 1991).

Both the strength and variation in the results have been shown to decrease as specimen size increases in the case of static loading (Neville, 1995), which complies with the weakest

link theory for Griffith type flaws. Both the aspect ratio and the restraint at the loading interface were found to be as important in impact loading as in static loading, and in some cases, reduction in the diameter of a specimen below a certain limit can result in considerable, and not necessarily representative, uni-axial strength increases (Bischoff and Perry, 1991). It is imperative that account be taken of the size of the specimen, when assessing strength increases as a result of high rate testing (Ahmad and Shah, 1985).

The propagation of stress waves through the concrete specimen away from the point of loading, in an attempt to dissipate the high stresses and strains generated as a result of the impact, also has an effect on the material strength (Bischoff and Perry, 1991). This stress pulse behaviour becomes significant at strain rates of approximately 5 sec^{-1}. Impacts generated using drop weight impact test machines are at the limit of the range at which stress wave propagation becomes important whereas tests with a split Hopkinson pressure bar, for example, must always account for the stress pulse propagation. Where possible, the specimen size for dynamic tests is chosen to avoid dispersion and allow the use of simple one-dimensional analysis for longitudinal wave propagation (Johnson, 1972). Very few of the drop weight impact tests take account of the wave propagation, excluding Hughes and Gregory (1972), Hughes and Watson (1978) and Perry and Bischoff (1990). However, all of these researchers considered that, if the stress wave propagation effects were neglected in the analysis, the failure strength of the concrete can be overestimated.

These and other researchers showed that there was a discernible increase in the uni-axial compressive strength of concrete as the strain rate increased. During impact and similar types of loading, at strain rates of 10 sec^{-1}, this results in the compressive strength of concrete being between 85 % and 100 % in excess of the equivalent static strength. Hughes and Watson (1978) suggested that concrete had a higher strength when impacted because the rise time of the stress pulse propagating in the concrete was less than the time required for a crack to form in the concrete and to cause failure. However, at what strain rate this strength increase definitively begins to occur is not agreed, with research undertaken by Hughes and Watson (1978) suggesting that the strain rates required for a strength increase are considerably lower than those defined by Evans (1942) as a result of his experimental work. Both Evans and Hughes and Watson concluded that concrete with a greater uni-axial compressive strength exhibits a smaller percentage increase in its strength than weaker concrete. Other researchers, including Atchely and Furr (1967)

showed experimentally that differences in the initial static compressive strength of the concrete did not result in different relative increases in the strength when subject to a higher strain rate. These findings are further evidence that the manufacture and the storage of the concrete are extremely important in the interpretation of the test results.

The CEB Report on Concrete Structures under Impact and Impulsive Loading (1988) and the CEB-FIP Model code (1990) assessed existing results and incorporate the static strength of concrete into the calculation of the relative increases in strength resulting from high rate loading. They both provide empirical formulae, based on the results of extensive experimental work by different researchers, which relate the strength of the concrete when tested to its static strength and to the stress or strain rate at which the test was performed. The values determined can then be used to estimate the concrete strength for a particular loading situation.

It is difficult to draw definitive conclusions regarding the increases in the strength of concrete by comparing the results of different researchers because, similar to the work reported on the static strengths of concrete (Neville, 1995), the strength of concrete varies greatly between batches as a function of their aggregates, overall mix design, size, shape and aspect ratio of a particular specimen and also their age and conditions of storage. This would suggest that comparisons are only possible between concretes in a particular test program. Furthermore, the loading conditions also greatly affect the magnitude and variation in the results, particularly in the case of high rate loading where often testing machines are pushed to their limits. This can result in the overestimation of some results and the underestimation of others. In a paper by Bischoff and Perry (1991) considerable work was undertaken to standardise test results from many researchers to facilitate comparisons between different researchers and their test programs. Figure 3.1 was assembled which summarised all of the standardised results and clearly shows the increases in the uni-axial compressive strength of concrete as the strain rate increases.

In conclusion, the static compressive strength of concrete and the rate at which the load is applied are the most important factors in the assessment of the expected increases in compressive strength. The mix proportions, shape and size of the specimen and the aggregate type affect the impact strength in a similar way to how they affect the static uni-axial strength and probably do not have a major importance in their own right.

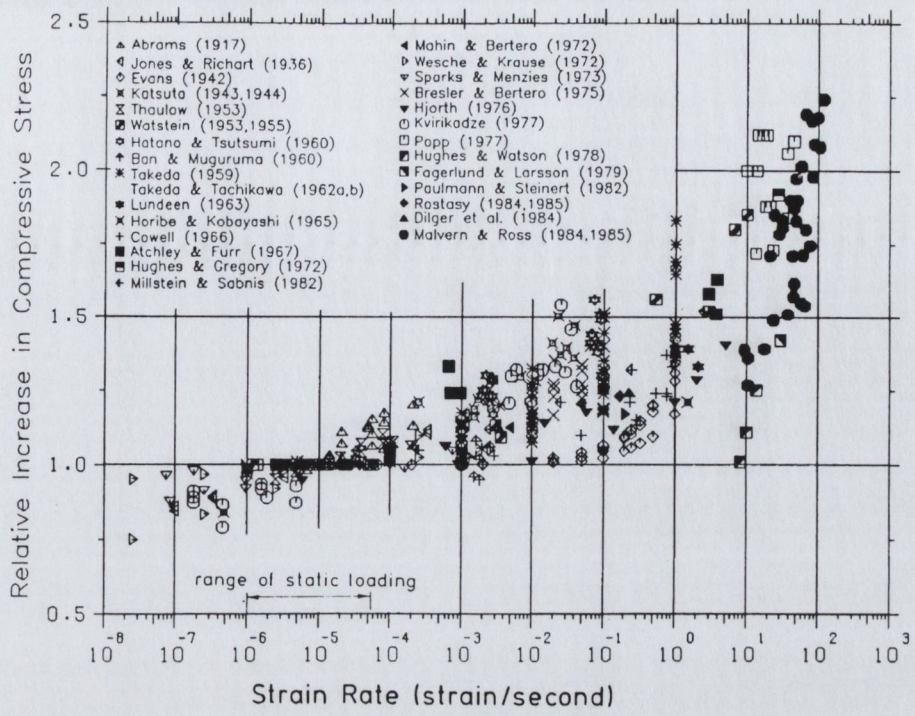


Figure 3.1 Strain-rate influence on compressive strength (Bischoff and Perry, 1991)

3.2.2. Contact force response of concrete subject to impact

The contact force response of concrete subject to impact is often not distinguished from its stress response which is a more familiar concept from the static loading of materials. Furthermore, the stress response allows the calculation of the strength or the strength increases in the concrete associated with impact loading. The contact force response can be defined as the force measured at the interface between the impactor and the impacted body, and is generally plotted against time for the duration of the impact event. It is not possible to measure the contact force, which is a dynamic phenomenon, in the case of concrete specimens loaded at high rates using hydraulic, pneumatic or mechanical machines, and its measurement against time is really only associated with impact tests which involve the collision of two bodies. All of the research examined in this literature survey concerns the response of materials to hard impact, where the impactor does not deform as a result of the collision and the loadcell measuring the contact force is usually incorporated into the impactor, close to its striking end.

Dinic studied the peak contact force response of impacted short span slabs (1985). He showed that the peak force was influenced only by the impact velocity and the target

thickness, whereas the overall contact force response was affected by the mass and the shape of the impactor and particularly whether the impactor was a solid or hollow object. Dinic and Perry (1990) showed that the contact force response could be broken down into two distinct phases, namely a very steep ascending and descending primary phase, predominantly associated with the contact velocity, and a secondary phase lasting the remainder of the duration of the impact event. The second phase includes the dynamic structural response and is controlled by the damage done initially to the impacted body. They also concluded that the peak contact force (and the associated kinetic energy of the impactor) had to reach a certain, critical level for damage to occur to the impacted body. They also studied fender layers placed on top of the concrete which absorbed the energy of the initial impact. Wet and dry sand, expanded clay and polystyrene aggregate concrete were all tested, and results showed that both the damage and contact forces were reduced because of this fender layer (Perry and Dinic, 1985). The resulting contact force plot was considerably less steep and was of longer duration than a similar impact on unprotected concrete. The impact response was a function of the thickness of the fender layer, with thicker layers absorbing more of the impact than thinner ones. They was found that polystyrene aggregate concrete, with a high proportion of polystyrene in the mix, was very effective at mitigating the severity of the impact (Bischoff *et al*, 1990a, 1990b).

The contact force response of conventionally and fibre reinforced beams was investigated by Bentur *et al* using a "tup loadcell" integrated into the falling impactor (1986). However, the focus of their work concerned the structural rather than the local response of the concrete beams (Banthia *et al*, 1989).

More recently in Japan, the effect of using sand and an absorption system comprising three different layers to reduce damage to rock shelters made of concrete was examined (Kishi, 1999). The contact force was calculated by measuring the acceleration in the impactor and multiplying it by its mass. Loadcells in the absorption layer were used to measure the transmitted stresses. The contact and transmitted forces were both proportional to the velocity of impact and decrease with an increasing thickness of either type of absorbing layer. Hertz's law was used to predict the maximum contact forces generated as a result of the impact. Sonoda *et al* (1999) studied how the presence of shock absorbers mitigates the effect of an impact, using results from loadcells at the location of impact and integrated into the shock absorber. They also showed that the contact force was proportional to the

velocity of impact for a simple elastic shock absorber. This system also absorbed the energy associated with the impact more effectively, and resulted in a lower maximum contact force, than a stiffer elastic-plastic shock absorber. Their experimental results showed that the contact force has a greater peak and is of longer duration, as the curve of the nose of the impactor decreases and a larger area comes in contact with the impacted body.

3.2.3. Change in material properties with increases in strain rate

The vast majority of early work in the field of impact concerned the strength increases associated with high strain rate loading, and it is only more recently that researchers have become directly interested in the deformational response of the impacted material.

The strain in the concrete at peak compressive stress, which is also known as the critical compressive strain, is important in the design of structures as it gives an indication of the deformability of the structure when the concrete reaches its maximum sustainable stress. Its measurement in the case of concrete is subjective, to some degree, as it depends on the test method, the location at which the strain in measured and the type of failure experienced. For static loads, the relationship between critical compressive strain and compressive strength has been studied by many authors, whom have proposed their own relationships, both linear and non-linear. These were summarised by De Nicolo *et al* (1994) whose non-linear empirical relationship combined many of the previous results. They showed that the value used for the critical strain greatly affects the accuracy of any subsequently predicted stress-strain curves.

It is equally important that the critical compressive strain should be known in an impact loading situation, but conclusions as to whether its value changes with increasing strain rate varies between different researchers and a consensus has not yet been reached.

Experimental work by Spooner (1971) showed that the failure strain of slowly strained specimens was twice that of those which were rapidly strained. Furthermore, the critical compressive strength also decreased with increasing strain rates, as creep and shrinkage which both affect the critical strain do not have time to occur, a fact which was particularly

evident in the case of the air dried specimens. Although Hughes and Watson (1978) did not report on the critical compressive strain, their experiments showed that the ultimate compressive strains decreased as the strain rate increased, which was consistent with the results of some earlier work, but inconsistent with results from Watstein presented in 1953. Other researchers, both before and since, have shown experimental increases in the critical compressive strain with increasing strain rates (Suaris and Shah, 1982). Atchley and Furr (1967) showed that there was small increase in the strain between a group of static and impact test results. More recently Tang *et al* (1992) showed that the increase in critical strain for their high strength concrete specimens varied in an almost linear manner with the increase in strain rate. Bischoff and Perry (1995) clearly showed that an increase in strain rate resulted in an increase in the critical compressive strain of concrete cylinders under static and impact loading. Furthermore, they also showed that the strain increase was greater for weaker concrete than for stronger concrete. This occurred because the stress-strain curves for the weaker concrete were flatter, allowing large increases in strain for minimal stress increases, than those for the stronger concrete tested.

The CEB Report (1988), which considered much of the existing literature, concluded that the critical strain (as defined here, and called ultimate strain, ε_u, in the report) increases with increasing strain rates (Figure 3.2). The report proposes the following empirical formula, based on the experimental results reported to that date, to predict the critical strain at a particular strain rate

$$\frac{\varepsilon_{u,imp}}{\varepsilon_{u,stat}} = \left(\frac{\dot{\varepsilon}}{\dot{\varepsilon}_0} \right)^{0.020} \tag{3.1}$$

where $\dot{\varepsilon}_0 = 30 \times 10^{-6}$ sec^{-1}. The report also suggests that the greater critical strain results from inertia effects and cracking in the concrete, which are less important at lower strain rates, and that the increases in the critical strain in compression are greater for lower strength concrete. However, the formula does not incorporate this into its prediction.

A comprehensive study on the effect of strain rate on the critical strain was undertaken by Bischoff and Perry (1991), the findings of which are summarised in Figure 3.3. The decreases in the critical strain were largely discounted because of the failure mechanisms experienced during these tests and the location at which the strains were measured. They concluded that the critical compressive strength increased with strain rate increases. However, they emphasised that the results were subject to variations in the composition

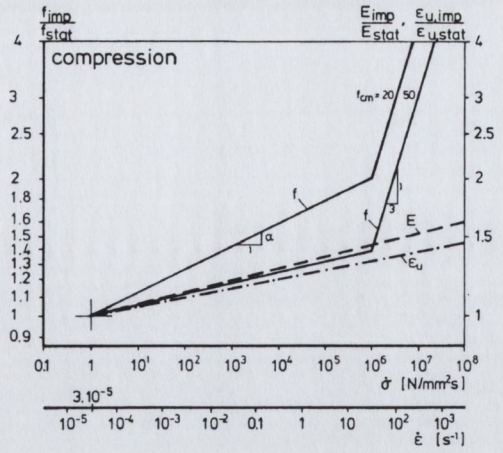


Figure 3.2 Influence of stress and strain rate on the compressive properties of concrete (CEB report, 1988)

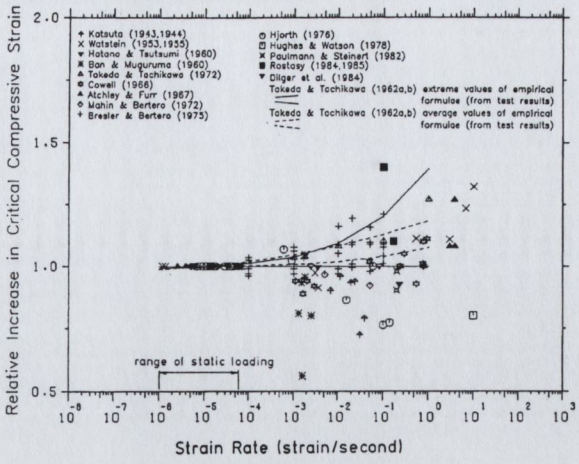


Figure 3.3 Strain-rate influence on critical compressive strain (Bischoff and Perry, 1991)

of the mix, the storage conditions, the compressive strength and in the accuracy of the measured stress-strain curve. Increases and decreases in the critical strain were evident for concrete tested hydraulically because of the way in which the concrete failed, depending on the particular type of equipment used. Yet, any impact test studied always showed evidence of increases in the critical compressive strain.

Changes in the dynamic modulii of elasticity over a comparative static value depend on the variation in the critical compressive strain and increase in the strength of concrete, which occur because of a considerable decrease in internal micro-cracking in the concrete at a particular stress level. Atchley and Furr (1967) reported a notable increase in the modulus of elasticity resulting from a strain rate increase, although they concluded that this modulus may not be a good indication of the dynamic strength of the particular concrete. Suaris and Shah (1982) examined results of impact tests prior to that date and concluded that, in all cases, the secant modulus of elasticity increased with increases in strain rate (Figure 3.4).

However, conclusions as to whether the initial tangent modulus of elasticity for concrete increases or decreases with an increase in strain rate vary between different researchers. Bischoff and Perry (1991) suggested that the tangent modulus does not vary with strain rate as there is no significant micro-cracking at this strain level which would cause it to change (Figure 3.5).

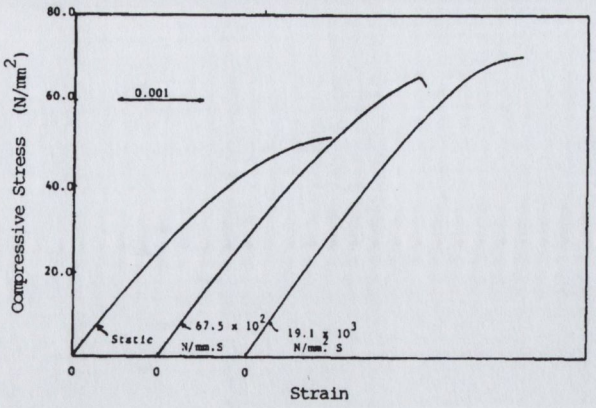


Figure 3.4 Compressive stress-strain curves for different strain rates (Suaris and Shah, 1982)

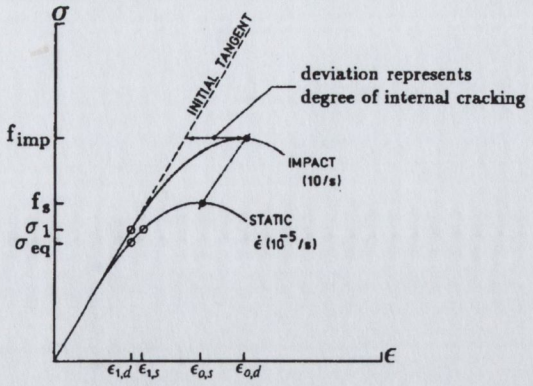


Figure 3.5 Idealised stress-strain response for static and impact loading (Bischoff and Perry, 1995)

Young's modulus of elasticity, which is defined as the secant value at one third of the failure stress, increases with strain rate as there is an enhanced stiffness due to a decrease in internal micro-cracking at a particular level of stress. The CEB-FIP Model Code (1990) gives equations for calculating the Young's Modulus of concrete with increases in strain rate for all standard grades of concrete.

The energy absorbed by concrete when loaded, either statically of dynamically, is defined as the area under the stress-strain curve up to the maximum or critical stress. It is well established that the energy absorption capacity of concrete increases with increasing strain rate (Bischoff and Perry, 1991). This is, again, consistent with the increase in the secant modulus and maximum stress when concrete is dynamically loaded, as discussed above. Atchley and Furr (1967) showed definite increases, of up to almost 50%, in the energy which their specimens absorbed when impacted. They concluded that this increase in the energy absorbed was as a result of the greater stress at a particular level of strain. The energy absorbed during a particular impact event can increase up to a certain critical level associated with the maximum strength or critical strain which, if exceeded, will result in concrete failure. The CEB Report (1988) concluded that the energy absorbed during a dynamic test was analogous to that during a static test, namely that it involved the entire area under the stress-strain curve. However, at that time, no complete stress-strain curve existed for concrete, due to the unstable fracturing of the concrete in the unloading curve (see section 3.2.5), however, the report did recognise that the energy absorbed did increase with increasing strain rate. Suaris and Shah (1982) acknowledged that the energy

absorption in the case of high strain rate loading was subjective between different researchers and varied with differences in the way in which the body was impacted.

Poisson's ratio has rarely been measured during impact testing, and the results which have been considered are conflicting, due to the difficulty of measurement. Bischoff and Perry (1995) concluded that Poisson's ratio was not affected by strain rate increases, until cracks began to occur in the concrete. The CEB Report (1988) concluded that Poisson's ratio is not a function of the strain-rate.

3.2.4. Failure patterns of concrete subject to impact

There are no major differences in the failure patterns between concrete specimens which are either statically or dynamically loaded. The predominant method of failure of both involves longitudinal cracks forming along the length of the specimen as a result of indirect tensile cracking in the direction of the maximum compressive load.

The presence of these longitudinal cracks at high strain rates has been reported by many researchers including Atchley and Furr (1967), Hughes and Gregory (1972) and Hughes and Watson (1978). Atchley and Furr examined the failure modes of concrete cylinders tested at three different, increasing strain-rates and observed that the typical cone or wedge, evident in the static tests, became smaller as the strain rate increased until, in the case of the impact tested concrete, the mode of failure was longitudinal splitting of the concrete from the centre of the top face. Hughes and Gregory examined the results of tests using Green's Ballistic Pendulum in which the tested cubes failed longitudinally from the centre of the top face as a consequence of failure of the aggregate-mortar bond, regardless of the strength of the concrete tested. Hughes and Watson (1978) tested concrete cubes and reported longitudinal splitting when the cubes were packed with rubber pads to reduce friction between the steel platten and the concrete. Where the rubber pad was not used the cubes failed with characteristic cones top and bottom because the centre of the specimen was in uni-axial compression and the ends were in tri-axial compression caused by platten restraint. They also explained the concentrations of cracking at the top or bottom of the packed cubes in terms of the magnitude of the stress waves propagating through the concrete, which were reduced or amplified by the presence of the rubber pads. The

fracture planes resulting from the high rate loading of the concrete were less jagged, straighter and shorter, and contained more aggregate failures than a failure plane of a similar static test. The authors explained this in terms of the differences in the duration of loading - when statically loaded, the cracks had time to spread and move around the aggregate particles to find the path of least resistance. When impacted, the stress increased so fast in the concrete that, before the cracks had time to find the path of least resistance, the stress had increased sufficiently to allow fracture of the higher strength aggregate particles. They used this to explain the strength increases resulting from high rate loading which they suggested occurred because the rise time of the stress wave travelling through the concrete was less than the time required for a crack to form at low stress. The critical rate of loading occurs when the time for the load to increase from being able to break the aggregate-mortar bond to the aggregate failure load, is equal to the time taken for the crack to propagate around the pieces of aggregate.

Similar logic was applied by Suaris and Shah (1984) in their development of a rate sensitive damage theory for concrete and brittle solids where they used a continuous damage theory explained at high rates by the reduction in the level of micro-cracking in the concrete at a particular level of strain. Bischoff and Perry (1995) compared the failure modes of static and impact tests on concrete cylinders. The statically tested cylinders failed by a characteristic bulking type failure and end cone formation. Their impacted cylinders failed in a similar manner, with failure concentrated in the centre of the specimen, and the failure of the aggregate-mortar bond rather than that of the angular aggregate. They concluded that the failure, which could be expected in the case of impact, was a function of the relative strengths of the mortar, the aggregate and the bond between them.

Janach (1976) studied the failure of rock, a material as brittle as concrete, at high rates using a Split Hopkinson Bar. He examined the role of bulking of the material as a mode of failure, and showed that the static and dynamic responses were quite similar and that end cones were only formed as a result of friction at the loading interface. He explained that bulking, or the lateral dilation of the material under a load, is a phenomenon which occurs whenever a material under compressive stress fails in a brittle manner as, close to failure, the material is subject to volumetric expansion. When a material is impacted, a stress wave propagates away from the impact location, and unlike a static case where the material has time to expand laterally due to a Poisson's ratio effect, the dynamic loading

does not allow instantaneous expansion. The material is in a state of uni-axial strain and the lateral stresses result in an effective confining stress on the central core of the specimen. In an elastic material, with an aspect ratio of at least 2, this lateral inertial confinement does not greatly effect the material behaviour, except if loaded at very high rates. However, brittle materials such as rock and concrete, are subject to volumetric expansion when loaded because of void formation, and are, therefore, sensitive to lateral inertial confinement at rates greater than 30 sec^{-1}, according to the CEB Report (1988). This lateral, inertial confinement partly may be the reason that impacted concrete exhibits increases in its strength and critical compressive strain (see section 3.2.3). However, Tang *et al* (1992) performed tests at rates of up to 100 sec^{-1} and suggested that even at this level the inertial confinement is insufficient to have an appreciable effect.

The CIRIA/UEG report on the Assessment of Impact Damage caused by Dropped Objects on Concrete Offshore Structures (Brown and Perry, 1989) predominantly studied the accidental impact of concrete slabs and domes. The report showed that the ratio of target thickness to the diameter of the missile was the most important factor in determining the type of failure which could be expected from an impact. The modes of failure included penetration, spalling, scabbing, and the formation of shear plugs. The report sets out a series of empirical equations to predict the magnitudes of each of the modes of damage as a result of different types of falling missiles.

The failure mechanisms for a brittle material, such as concrete, have been examined in an attempt to better understand why it fails locally in a particular way as a result of a load. Concrete is a highly non-linear material with inherent internal micro-cracks in its structure prior to any load being applied. It is widely accepted that fracture occurs within concrete due to the proliferation of flaws or micro-cracks, which are randomly distributed in the mortar aggregate matrix (Kotsovos and Pavlovic, 1995). These cracks cause high tensile stresses near their tips, which propagate, initially in a stable manner, if the energy reaches a critical level in the material. If the material is in a state of compressive stress, then the strain-energy concentrations near the crack tip are reduced by strain energy release resulting in material fracture. This results in the stress concentration being reduced below the critical level for cracking to occur. The cracking continues when further energy builds up in the material and exceeds the critical cracking level in a particular region. The crack propagation process is incremental and stable although non-linear, until the stage where

no more energy can be stored at the crack tips and any further energy goes straight into material fracture. The fracture process and cracking always occur in the direction of maximum compressive stress (Kotsovos and Newman, 1981)

With increases in strain rate, the development of internal micro-cracks is reduced and it is this which causes the differences in the failure mechanisms between low and high strain rate loading. The direct tensile strength is more affected by changes in strain rate than either the compressive or flexural strength (Suaris and Shah, 1982, 1984) which would suggest that, as concrete fails through tensile cracking, the material failure would be very sensitive to changes in strain rate. The cracks have only time to be created and travel a short distance prior to the passing of the stress wave. This suggests that the cracking in the concrete at high strain rates is related to the velocity of the propagating wave. This reduction in the crack length is consistent with a reduction in cracking at a particular stress level and in longitudinal deformation. The failure planes occur along the most direct path for crack propagation, as corroborated experimentally above, and spread longitudinally from the loaded face along the length of the specimen.

Vos and Reinhardt (1982) considered how the bond between concrete and steel is affected by increases in strain rate. They performed pull-out tests on both plain and deformed reinforcing bars. The plain bars rely on adhesion and friction between themselves and the concrete, whereas deformed bars also have support from the ribs on the steel. This means that the concrete has to be displaced and crack before the bond is overcome. They found that both plain reinforcing bars and strands of steel are not influenced by changes in strain-rate, but ribbed or deformed bars are very sensitive to changes in the rate of loading, as the concrete has to crack around each of the ribs or deformations individually.

3.2.5. Stress-strain response of concrete subjected to increasing strain rates

To ensure that the results from finite element or finite difference models are accurate it is necessary to have a good understanding of the constitutive relationships of the materials in question. The stress-strain behaviour of uni-axially and multi-axially statically loaded concrete is reasonably well understood at this time as a result of considerable research in the last thirty years (Popovics, 1973; Hobbs, Pommery and Newman, 1977; Darwin and

Pecknold, 1977; Kotsovos and Newman, 1978, 1979; Ahmad and Shah, 1982; Carreira and Chu, 1985; Almusallam and Alsayed 1995; Attard and Setunge, 1996). However, the constitutive relationships for dynamically loaded concrete are less well defined, but are very important. This is because of the limited number of uni-axial stress-strain results produced dynamically (see section 3.2.3) and the nearly total absence of high strain-rate multi-axial results. Some attempts to produce stress-strain relationships have involved modifications to the constitutive relationships for statically loaded concrete, usually by increasing them by a rate sensitive factor to account for the strain-rate effects.

Krajcinovic and Silva produced two papers in 1984 considering the collision of concrete blocks. Although the concrete was assumed to be both homogeneous and isotropic, the growth of micro-cracks resulted in its becoming highly non-linear. They suggested that a simple stress-strain relationship would relate the stress, strain and also the damage (which is also a function of the strain) and determined an empirical solution to the equation, based on their results, to predict the stress-strain curve. In their second paper, they showed that the unloading paths were not equal in slope to the loading paths because the damage caused was proportional to the stress applied, thereby creating a continuous damage theory.

In papers published in 1984 and 1985, Suaris and Shah presented another rate sensitive damage theory for quasi-static and dynamically loaded concrete, which accounted for the effects of micro-cracking (see section 3.2.4). Their theory also allowed continuous damage to occur as the stress increased, which meant that the strain history was incorporated into the model as the damage is a function of the strain and the strain rate. The model predicted that the tensile behaviour of the concrete was more sensitive to changes in strain rate than concrete loaded in compression. Furthermore, the model took account of the effects of pre-existing damage to the concrete on the stress-strain response, which has the effect of reducing the initial tangent modulus, and was capable of predicting the reduction in linearity of the curves with increasing strain rates (Figure 3.6).

Bischoff and Perry (1995) studied the stress-strain response of concrete loaded in compression, both impacted and statically. As bonded strain gauges were used to determine the response of the central zone of the cylinders, only the ascending portion of the response could be measured with certainty (Figure 3.7). Furthermore, the plots generated from the impact tests are subject to a large degree of fluctuation, possibly due to

the non-uniform states of stress in the specimen. The curves, statically and dynamically, are approximately bi-linear in shape and illustrate clearly the increases in strength of the concrete as the rate increases.

In 1998, Fujikake *et al* presented a complete stress strain curves for dynamically loaded concrete. They measured the strain response of the descending branch by casting a strain gauged rod into the centre of the 100×200 mm concrete cylinder. This method eliminated the post-peak stress-softening which causes failure of strain gauges attached to the surface of the cylinder. The ascending portions of the stress-strain curves were characteristic of impact loaded specimens, but the inbuilt rod showed that the descending portion of the curve became considerably steeper with increases in the strain rate (Figure 3.8).

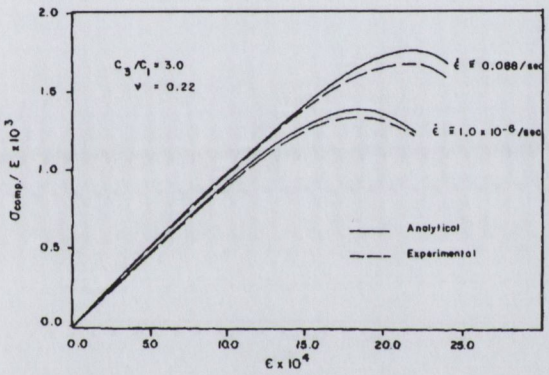


Figure 3.6 Analytical and Experimental stress-strain curves in uni-axial compression (Suaris and Shah, 1984)

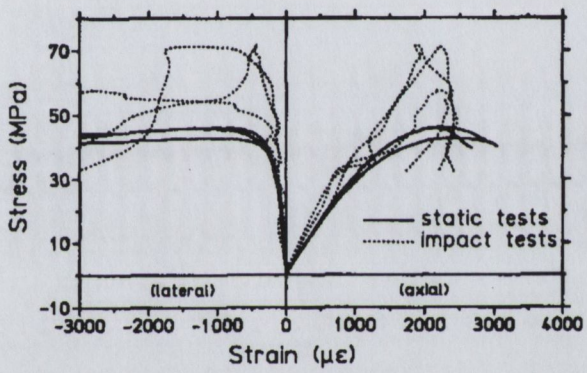


Figure 3.7 Typical static and impact stress-strain responses for 50 MPa concrete loaded in compression (Bischoff and Perry, 1995)

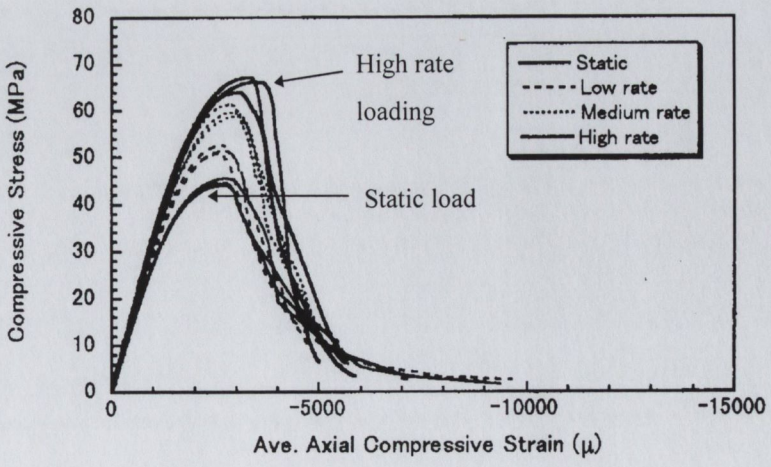


Figure 3.8 Complete stress-strain curves, at different strain-rates (Fujikake *et al*, 1998)

3.2.6. Conclusions

At strain rates which are higher than those of a typical static loading situation, some of the features of the response of concrete are well established, namely that the strength of the concrete increases and that the secant modulus of elasticity of the concrete increases with increases in strain rate.

Considerable inconsistencies exist in the strain or deformational response of concrete to high strain rate loading. This is because the response of the concrete is dependant on the properties of the concrete and the way in which the concrete is stored prior to testing significantly affects the results. Furthermore, the way in which the load was applied and the different locations at which the strain was measured complicate the results still further. The behaviour of the concrete depends on the local cracking caused by the loading, which eventually results in its failure. The reduced micro-cracking, which is a feature of high strain rate loading, reduces the deformation and changes the material behaviour, its energy absorption capacity and its stress-strain response.

It is still necessary to draw firm conclusions regarding other of the aspects of the response of concrete to high strain rate loading, which will allow more realistic information to be used in the numerical modelling of high rate behaviour using finite element analysis. Hence, although many features of the response of the concrete are well understood, more experimental work is needed to draw firm conclusions as to the other aspects of the behaviour.

3.3. CONCRETE CONFINEMENT

3.3.1. Experimental work on concrete confined by sleeves, spirals or hydraulically

In 1903 Considère published the results of his experiments on reinforced concrete including work on laterally confined concrete. He realised that the strength of laterally confined concrete was the sum of the material strength of the concrete under uni-axial loading and an additional contribution which was a function of the lateral confinement (Gardner and Jacobson, 1967). Considère showed that for equal weights of steel, circular hoops were twice as effective as rectangular links in increasing the strength. Hence, much of the subsequent research focused on this very effective form of reinforcement.

In the late 1920s, Richart *et al* examined the benefits of confining concrete both hydraulically and using steel spirals (1928, 1929) as part of extensive A.C.I. column investigation programme. In both of the groups of tests, the cylinders had a height to width ratio of 1:4 to minimise any column buckling effects, and two equal lateral stresses were applied which were different from the stress in the third, axial direction. The hydraulically confined tests, where the concrete was surrounded by a rubber membrane to prevent the hydraulic fluid penetrating into voids in the concrete and accelerating fracture, were split into two groups, one where the two lateral stresses were less than the third axial stress and one where the lateral stresses were greater than the axial stress. Both exhibited large deformations and high stresses, even when the expansion of the material was limited. They found, empirically, that

$$f_1 = f_c' + 4.1 f_2 \tag{3.2}$$

where f_1 is the axial stress, f_c' is the uni-axial strength of the concrete and f_2 is the confining lateral stress exerted on the concrete. The spirally confined concrete cylinders were formed by cold working the steel to form spirals, and the variables examined included the amount and type of spiral confinement. During testing, the longitudinal, radial and circumferential strains of the cylinder were measured. Up to two thirds of the maximum load, the volume of the concrete decreased with increasing load, but beyond that point, the volume increased and, at failure, an overall increase in the volume of the concrete had occurred, and the concrete under the spiral steel had been damaged. The

response of the spirally confined concrete could also be described by equation (3.2), as shown in Figure 3.9. The lateral stress was calculated by considering a section of the specimen bounded by two horizontal planes with a separation equal to the pitch of the spiral, s, and a vertical plane containing the longitudinal axis of the cylinder. The following equation was obtained by resolving the forces in the horizontal plane

$$f_2 = -\frac{2A_s}{sD} f_s \tag{3.3}$$

where f_s is the stress in the steel spiral which was assumed to have yielded, D is its diameter and A_s is its cross-sectional area. Hence, similar to the findings of Considère, the strength of a confined column could be determined by knowing the strength of the uni-axially loaded concrete and information about the confining material. The equation to predict the maximum stress was dependant on the slenderness of the column being small and bucking was prevented from occurring.

By the 1960s, researchers were confident that concrete columns could be reinforced more effectively using hoop reinforcement than using longitudinal bars. Gardner and Jacobson (1967) published work on the extreme case of axially loaded, hooped concrete - where the steel was confined by a tube of steel. This form of reinforcement had huge advantages in that the steel provides a uniform flexural stiffness and was prevented from buckling by the presence of the confined concrete core. As would then be expected, the concrete can resist higher stresses and strains than similar, unconfined concrete and, like the spirally confined concrete, has a much greater axial strength. The short columns were restrained and were

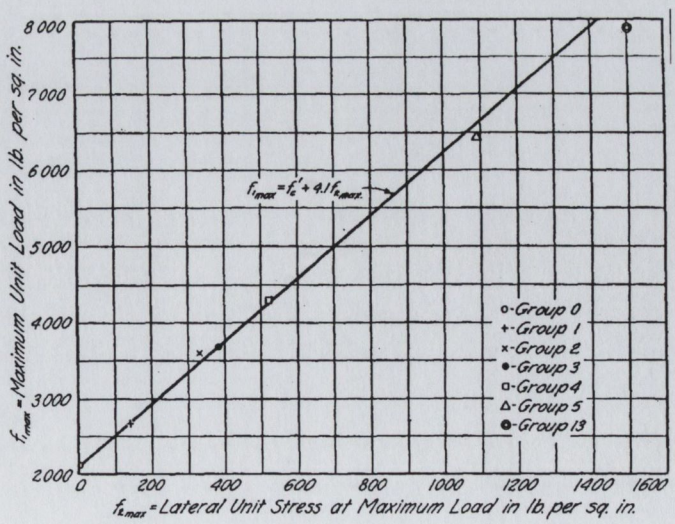


Figure 3.9 Maximum loads and lateral stresses for various columns (Richart *et al*, 1929)

loaded in three ways, namely by loading the confining steel only, by loading the concrete core only and by loading both the steel and concrete. Figure 3.10 summarises the results. The empty steel tube has a certain, not inconsiderable, strength (a) and, as can be seen in the figure, filling it with concrete and still only applying the load to the confining sleeve only increases the strength by a small amount (b), caused by the inability of the steel to buckle inwards due to the presence of the concrete core. If a cylinder of unconfined concrete was loaded, it would have a strength which is less than that of the empty tube. However, if the concrete core of a composite column is loaded, the confining sleeve prevents lateral dilation and cracking. The resulting strength (c) is considerably greater than the sum of the steel or the concrete on their own. Even if the steel sleeve is also loaded, the strength is only fractionally increased (d). This shows that the concrete core is very effective in taking and distributing the load within the composite. The authors concluded that because $\upsilon_c < \upsilon_s$, the steel initially does not provide any restraint to the concrete. However, as the concrete begins to dilate laterally, the tensile hoop stresses in the confining sleeve, σ_t, increase. These stresses can be described by

$$\sigma_t = \frac{r}{t}\sigma_r \tag{3.4}$$

where r is the average radius, t denotes the thickness and σ_r is the radial strain (Figure 3.11). When the steel in the short columns tested yielded, either longitudinally or axially, the cylinders failed by crushing, rather than by local buckling.

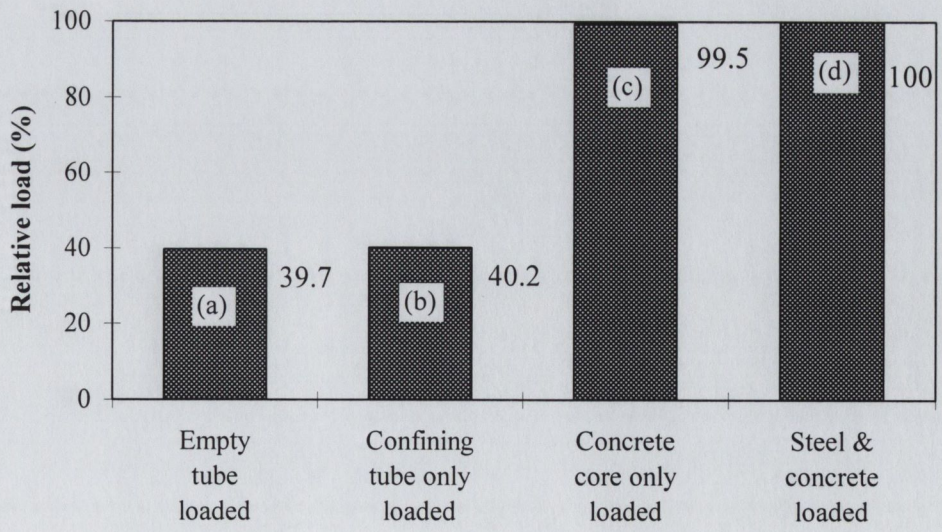


Figure 3.10 Relative loads taken depending on whether the steel or concrete was loaded (after Gardner and Jacobson, 1967)

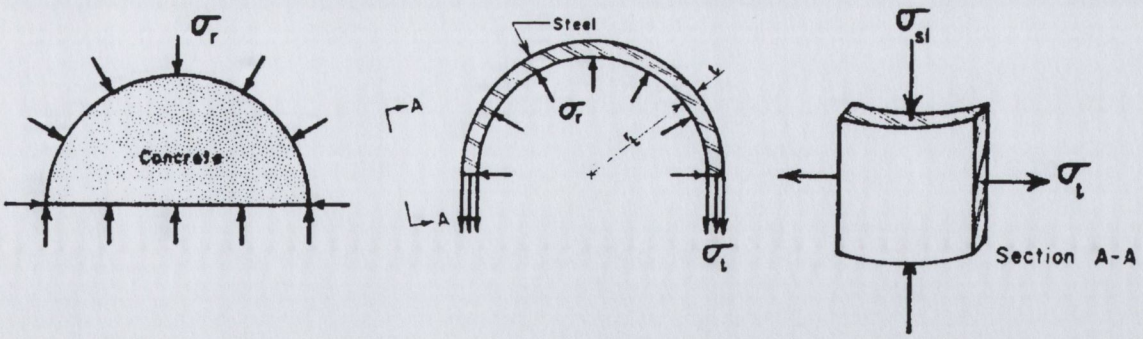


Figure 3.11 Free body diagrams of forces acting on concrete core and steel tube (Gardner and Jacobson, 1967)

Knowles and Park published papers in 1969 and 1970 on concrete filled tubular columns with a range of different slenderness ratios, predominantly considering the ultimate buckling stress. They loaded hollow steel tubes, concrete cylinders and concrete filled tubes and showed that the ultimate buckling load of a slender column could be predicted by summing the tangent modulus loads for the steel tube and concrete column. However, this method was not applicable to short columns as the strength enhancement from the confinement meant that the concrete strengths would have to have been between 1.5 and 1.7 times greater than the actual values to predict the ultimate capacity accurately. Using both circumferential and longitudinal strain gauges, they also showed that the concrete suddenly increases in volume at a certain value of longitudinal compressive strain (approximately 0.002). This creates an internal pressure inside the steel tube which causes the steel tube to exert a confining pressure on the concrete which increases the maximum compressive stress which the concrete can sustain. Until this limiting value of strain is reached, the tube cannot exert a confining pressure as the concrete has not dilated sufficiently laterally. They showed that these strength enhancements did not exist for concrete confined by square tubes as no hoop stress is generated in the sleeve. The authors derived an equation to predict the limiting value of the slenderness ratio above which increases in strength cannot be expected, thus

$$\left(\frac{KL}{r_s}\right)^2 = \pi^2\left(\frac{E_{ts}}{f_{su}}\right) \qquad \text{at } \varepsilon_s = \varepsilon_{vol} \tag{3.5}$$

where KL is the effective length of the column, r_s is the radius of gyration of the steel section, f_{su} is the buckling stress of the steel, E_{ts} is the tangent modulus of the steel tube, ε_s is the longitudinal compressive strain in the steel and ε_{vol} is the compressive strain at

which the concrete begins to increase in volume. A similar equation was derived for the slenderness of the confined concrete core.

Although previous researchers had concluded that square prisms did not experience as great strength enhancements as similar cylindrical columns, Somes (1970) proceeded to study the effects of confining columns with hoops of steel cut from a square tube. He found that the maximum load taken by the column is proportional to the cross-sectional area of the hoops and to the reciprocal of the hoop spacing, provided that this is not too large. Similarly, in 1971, Burdette and Hilsdorf published work on columns confined with rectangular ties showing that the strength and ductility of the column increased with increasing volumes of reinforcement. The circular links were more effective at restraining concrete than rectangular links because the circular ties are placed in direct tension whereas the rectangular ties act in a combination of bending and tension. Burdette and Hilsdorf showed that increasing the flexural rigidity of the rectangular links resulted in further increases to the strength and ductility of the column, as these reduced local failures at the corners of the concrete column.

Sundara Raja Iyengar *et al* considered the stress-strain relationship of concrete cylinders and prisms confined by steel spirals (1970). They defined a confinement factor as

$$C_i = p_b \frac{f_y}{f_c'} \tag{3.6}$$

where p_b is the volumetric ratio of the confinement (the ratio of the volume of the binder to the volume of the confined concrete), f_y is the yield stress of the confined steel and f_c' is the ultimate strength of the unconfined concrete. They showed that the confining steel had yielded by the time that the confined concrete reached its maximum strength. The increase in strength was plotted against the confinement factor for both cylindrical and prismatic specimens and, although the result was a straight line, it did not pass through the origin. This suggested that the confinement factor must reach a certain value before enhancing the concrete strength (Figure 3.12). Furthermore, they found that the pitch of the spiral should be no greater than the least lateral dimension of the column to provide substantial confinement to the concrete. They used linear regression to find empirical equations to describe the increase in the maximum stress and strain experienced by the specimen when axially loaded.

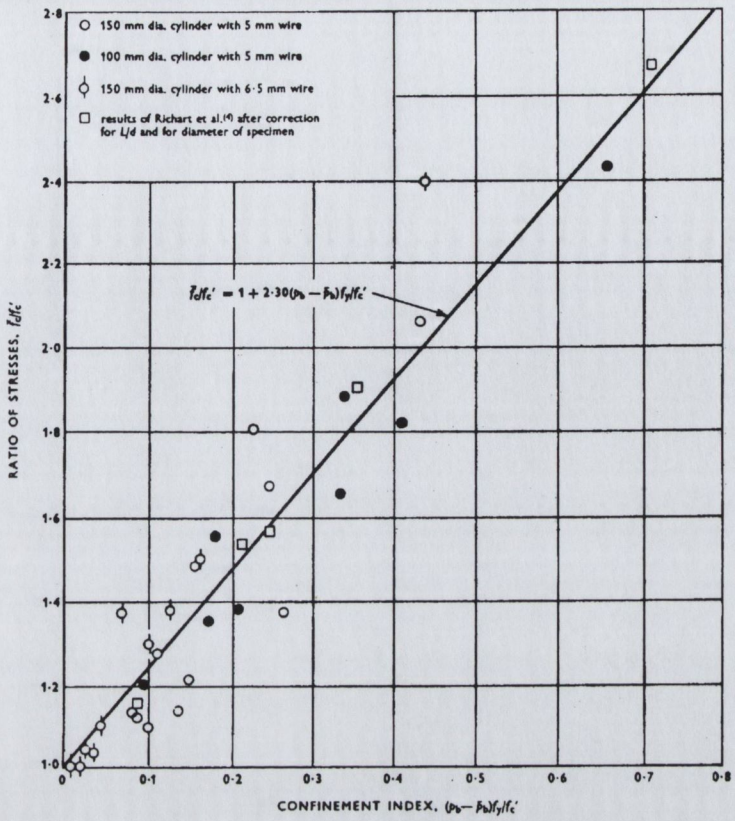


Figure 3.12 Influence of circular spiral on strength (Sundara Raja Iyengar *et al*, 1970)

The effects of cover on the stress-strain relationship of concrete confined in binders was studied by Gangadharam and Nagi Reddy (1980), who extended the work of Sundara Raja Iyengar *et al*, (1970). They proposed a modified, empirically based, confinement index, C_i', which took account of the breadth of the specimen, b, and the pitch of the spirals, s, the volumetric ratio of the binder to the concrete, p_b, and $\overline{p}_b$ which is the volume percentage of confinement with the pitch equal to the least lateral dimension of the specimen. The equation also incorporates the actual stress f_v which develops in the binder steel, thus

$$C_i' = (p_b - \overline{p}_b)\frac{f_v}{f_c'}\sqrt{\frac{b}{s}} \qquad (3.7).$$

They also modified a simple equation for the stress-strain curve of plain concrete which incorporated empirically calculated constants, by recalculating the coefficients for composite cylinders with confined cores and unconfined cover.

The behaviour of concrete subjected to passive confinement from steel tubes was considered by Kotsovos and Perry (1986). They axially loaded confined concrete cores of

cylinders with three different aspect ratios and thicknesses and found that an aspect ratio of 2 or greater reduced the frictional restraint at the loading interfaces. They compared the behaviour of the passively confined concrete to tests on concrete when actively confined and concluded that they behaved in a similar manner until the stress level where the volume of the concrete became a minimum. Beyond this 'minimum volume' the strength and deformation properties of the cylinders became significantly different. All of the cylinders failed when the steel yielded. However, the thicker confining sleeves behaved in a different manner to the thinner ones and sustained a considerably greater load due to their ability to allow consolidation of the concrete prior to the yielding of the steel.

Sheikh and Tokluku (1993) presented work on the earthquake resistance of concrete columns using both steel spirals and hoops. It was intended that these columns should be designed to ensure that the increase in compressive strength due to the confinement would offset the loss in strength due to the loss of the concrete cover due to spalling and that the columns should be able to sustain large deformations without significant losses in strength. They tested columns of different diameters, but with a constant L/D ratio. Increases in the volumetric ratio and decreases in the spacing of the confining spiral resulted in increases in the strength and ductility of the column. The hoops which were tested performed as well as the spirally confined concrete, with the added advantage that if one failed the whole column did not necessarily collapse.

The 1990s saw a considerable increase in the strength of concrete and 'high-strength concrete', with 28-day cylinder strengths in excess of 40 MPa, became much more common. However, this high-strength concrete is very brittle unless well confined. Razvi and Saatcioglu (1994) studied the strength and deformability of high-strength concrete columns subject to concentric loading. They found that the lateral confinement pressure required for high-strength concrete columns was significantly larger than that for normal strength concrete columns. This increased pressure could be provided by increasing the volumetric ratio of the confining steel or by using higher grades of steel. The authors also found that, similar to its effect on normal strength concrete, a reduction in the spacing of the steel links or an increase in the volumetric ratio of confinement results in an increase in strength and ductility of the confined column, as this results in a more uniform pressure distribution on the concrete. The use of high-strength concrete in a spirally loaded column situation was also considered by Pessiki and Pieroni in 1997. The lower strength concrete

was more ductile than the higher strength concrete. However, the high-strength concrete underwent larger overall displacements which might suggest that the columns required more spiral reinforcement than was provided. The cover concrete of the higher strength concrete columns cracked at a lower relative load to the peak load than the normal strength concrete and failed with an inclined failure plane rather than the bulging type failure exhibited by the lower strength concrete.

Schneider (1998) presented the results of an experimental and analytical study on the behaviour of short, concrete-filled steel tubes. He tested circular, square and rectangular columns, keeping the *L/D* ratio between 4 and 5 and varying the *D/t* ratio from 17 to 50. His results agreed with those of many previous researchers in that the circular steel tubes provided more post-yield axial ductility than similar square or rectangular sections. The strains measured in the steel tubes suggested that very little confinement is provided by the steel tube until the axial load reaches approximately 90 % of its ultimate strength and that local buckling of the steel tube walls occurred in the post-yield part of the curve. Furthermore, he showed that tubes with thinner walls carry a higher proportion of the load near yield than tubes with thick walls and, up to the yield strain, the ratio of the lateral and axial strains in the tube is approximately equal to Poisson's ratio.

In 1997, Shams and Saadeghvaziri produced a paper on the state of the art of concrete-filled steel tubular columns, therein summarising much of the previous work in the area. and showing that this form of structural member has an excellent earthquake resistance as its constituent elements act together. The confining steel puts the concrete into tri-axial stress whilst the concrete prevents the inward buckling of the steel, resulting in the column having excellent axial and flexural load carrying capacities, combined with a high shear resistance, ductility and energy absorption capacity. Initially the longitudinal strain in the concrete is small and the confinement contributes little, but as the longitudinal strain increases the concrete dilates and is subject to a radial pressure from the stiffer steel. The effectiveness of the confinement depends on the thickness (which affects the stress, as shown by equation (3.4) and Figure 3.13), slenderness ratio (which must be less than fifty to ensure that the elements act as a composite), eccentricity and the cross-sectional shape of the composite body. The mode of failure of the element depends on its slenderness - when long it fails by buckling along its length, whereas if short, it fails by concrete crushing. Concrete shrinkage, which usually occurs in reinforced concrete columns, is

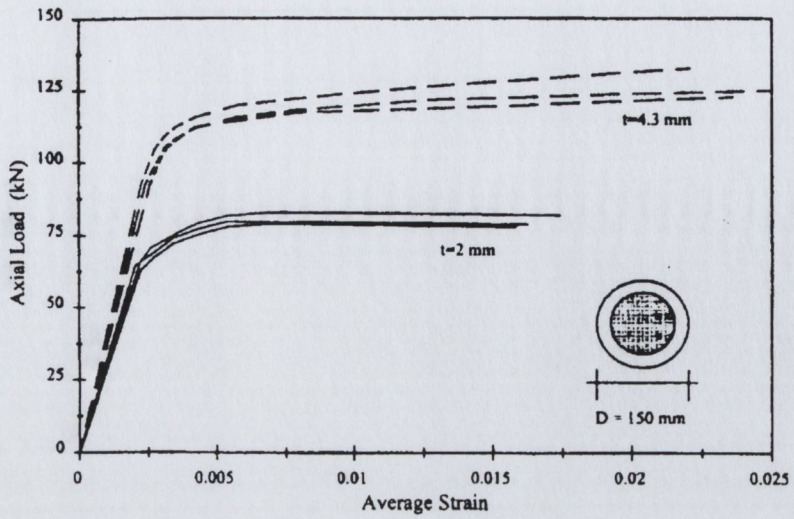


Figure 3.13 Relationship between applied load and overall strain for axially loaded circular CFT columns (Shams and Saadeghvaziri, 1997)

greatly reduced in the case of concrete filled tubes as the humid environment inside minimises the drying of the concrete and the bond between the concrete and the confining steel enhances the flexural stiffness of the column. Shams and Saadeghvaziri reported work which had been undertaken in Japan which showed that if the column is axially loaded, and slippage between the steel and the concrete is prevented, then the bond strength is not important, which was shown by axially loading a concrete filled steel tube with internal ribs. The authors also showed that concrete filled tubes subject to a cyclic load exhibited a ductile behaviour which was further enhanced by the addition of studs attached to the inside of the steel cylinder. Furthermore, steel jackets surrounding columns, with any gaps filled with grout, act in a very similar manner to true composite columns and could be used to retrofit concrete in seismic areas. The paper also examines many of the analytical studies on concrete filled columns and the numerous formulae to predict their ultimate strength and load-deformation relationship, and suggests that the load-moment relationship should be incorporated into the design of these columns.

The work on the bond between the steel and the concrete undertaken by Shams and Saadeghvaziri was examined further by Roeder *et al* in 1999 who investigated the effects of the diameter of the concrete core, the wall thickness of the steel tube and the shrinkage of the concrete core under concentric and eccentric loading, where slippage between the core and the sleeve was not prevented. The maximum average bond stress was related

directly to the applied force and the area along which slippage occurs. However, the bond stresses for the tubes where shrinkage was minimised were considerably larger than those under conditions where there was shrinkage of the concrete away from the steel cylinder. There was also a reduction in the bond stress capacity of tubes with greater diameters and in tubes with greater *d/t* ratios (Figure 3.14). The scatter in the results in this figure at low d/t ratios was caused by the variation in the diameter of the cylinders tested.

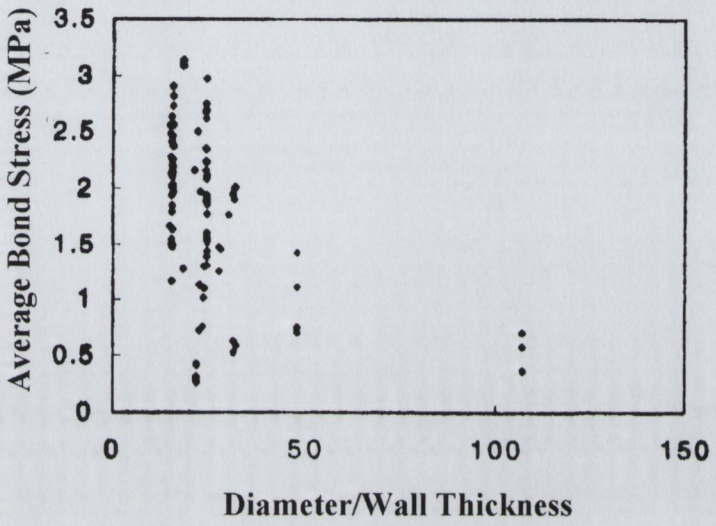


Figure 3.14 Bond stress for CFT as a function of the d/t ratio (Roeder *et al*, 1999)

3.3.2. Experimental work on confinement with confinement other than of steel

The use of materials other than steel to provide the confinement to concrete columns has been considered by researchers in an attempt to provide a system which is flexible and easy to use, both during construction and retrofitting, and economically viable. As early as 1978, Kurt considered using concrete filled plastic piping as a structural member. He found that the plastic pipe provided sufficient lateral support to the concrete core to result in a strength increase of up to three times more than the burst pressure of the pipe. He also found that at a slenderness ratio of approximately 20, which is considerably less than the value of 50 for a steel pipe found by Shams and Saadeghvaziri, the slenderness begins to effect the column behaviour. When short, however, the concrete in the columns failed in classical shear, which is different from the crushing failure exhibited by many of the steel confined pipes tested by other researchers.

More recently many researchers have considered using FRP (fibreglass reinforced plastic) as a way of confining concrete. Although its properties depend on the proportion of each of the materials used, the curing and the orientation of fibres, it is cheap, flexible, easy to use and its tensile strength in the direction of the fibres is excellent (Fardis and Khalili, 1982; Ahmad *et al*, 1991; Mirmiran and Shahawy, 1996, 1997; Toutanji, 1999; Saafi *et al*, 1999). Because of the low modulus of elasticity of the FRP the majority of the load is taken axially by the concrete and the FRP acts in tension to reduce the dilation, resulting in increases in strength and ductility of the column. Fardis and Khalili found that the following empirical equation described the critical strain, ε_u,

$$\varepsilon_u = 0.002 + 0.0005\frac{E_\theta t}{Rf_c'} \tag{3.8}$$

where E_θ is the Young's modulus of the FRP in the circumferential direction, R is the radius and t is the thickness of the circular section and f_c' is the uni-axial strength of the concrete. They assumed that the stress-strain curve was a hyperbola passing through σ_u, ε_u. In their 1997 paper, Mirmiran and Shahway described the stress-strain curves as being bi-linear with the first region similar to the response of plain concrete, a second transition zone where the pressure increases at the interface and a third zone where the confinement was activated and the pressure and dilation increased in a stable manner and proposed the following empirical relationship for FRP confined concrete

$$f_{cc}' = f_{co}' + 4.269 f_r^{0.587} \tag{3.9}$$

where f_r is the confining stress in the confining sleeve and is a function of the hoop stress, the thickness and the diameter. Toutanji compared different types of FRP and found that those sleeves made with carbon fibre could develop a higher lateral stress than those made with a glass fibre composite, as the composite sheets involved in the latter are much less stiff than those in the former. Also that year, Saafi *et al* showed that equations developed for FRP jackets are not applicable to FRP tubes as they tend to underestimate the axial strain and overestimate the axial compressive strength.

3.3.3. Theoretical work on confined concrete

The experimental work described above did not occur in isolation, but rather as a way of providing results to calibrate theoretical models and to allow researchers to understand better the mechanism of tri-axial confinement of concrete using spirals, tubes or hoops.

The majority of the theoretical work concerned attempts by different researchers both to create a unified stress-strain model for concrete with confinement and to predict the maximum strength obtainable by a confined column. However, a large proportion of the work is based on empirical analysis of experimental results as, although stress-strain relationships have been determined for actively confined concrete, similar relationships have not been derived for passively loaded concrete. This is because the lateral pressure is constant when confined actively, but varies with the axial load when confined passively.

Sargin *et al* studied the effect of lateral confinement on the strength and deformational characteristics of concrete (1971). They considered that a laterally confined section (where the overall section was described using the subscript *t*), which in their cases were rectangular prisms, consisted of two distinct parts - the cover (subscript *s*) and the core (subscript *c*). The stress in the concentrically loaded core, σ_c, was found by equating the forces on the cross section and rearranging the equation to determine the stress, thus

$$\sigma_c = \frac{A_t}{A_c}\left(\sigma_t - \frac{A_s \sigma_s}{A_t}\right) \qquad (3.10).$$

They proposed an expression for the longitudinal stress-strain curve of the confined concrete. The coefficients of the equation were determined empirically using regression analysis of experimental data. The stress is given in terms of strain, thus

$$\sigma = k_3 f_c' \frac{Ax + (D-1)x^2}{1 + (A-2)x + Dx^2} \qquad (3.11)$$

where $A = E_c \varepsilon_0 / k_3 f_c'$

$x = \varepsilon / \varepsilon_0$

f_c' = cylinder strength of concrete

E_c = initial modulus of elasticity

k_3 = ratio of maximum stress to cylinder strength

ε_0 = strain corresponding to maximum stress

D = a parameter mainly affecting the slope of the descending branch.

Sen *et al* also considered the relationship between stress and strain caused by tri-axial effects in circular stub columns when concentrically and axially loaded (1972). The stresses in the steel and concrete are calculated from experimentally observed strains throughout the elasto-plastic range using the following analytical formulae based on the 3-dimensional stress-strain relationships in polar co-ordinates

$$\sigma_{sL} = \frac{E_s}{\left(1-\upsilon_s^2\right)}\left(\varepsilon_{sL} + \upsilon_s \varepsilon_{sH}\right) \tag{3.12}$$

$$\sigma_{sH} = \frac{E_s}{\left(1-\upsilon_s^2\right)}\left(\varepsilon_{sH} + \upsilon_s \varepsilon_{sL}\right) \tag{3.13}$$

$$\sigma_{cL} = \frac{P - A_s \sigma_{sL}}{A_c} \tag{3.14}$$

$$\sigma_{cR} = -\sigma_{sH} \frac{2t}{d-2t} \tag{3.15}.$$

In these equations σ_{sH} and σ_{sL} are the hoop and longitudinal stresses in the steel, σ_{cL} and σ_{cR} are the longitudinal and radial stresses in the concrete, ε_{sH} and ε_{sL} are the measured hoop and longitudinal strains in the steel, E_s and υ_s are the modulus of elasticity and Poisson's ratio of the steel, A_s and A_c are the cross-sectional areas of the steel and concrete, t and d are the thickness and diameter of the tube and P is the applied load. Use of the Hencky-von Mises yield criterion allowed definition of when the steel yields. The equations were then modified for use in the post yield section of the graph. The strains were generated from statically loaded steel filled tubular cylinders, of slenderness $l/d < 5$, with gauges attached. These calculations showed that at failure the steel carries approximately three-quarters of the uni-axial yield stress in longitudinal compression and half that in hoop tension, while the tri-axially confined concrete core is twice as strong as when unconfined. The gain resulting from the confinement ranged from 36 % to 60 % above the sum of the failure strengths of the unconfined concrete and the steel tube.

Armstrong and Perry (1984, 1985) considered further the confinement of concrete using steel spirals. The stress in the spiral reinforcement is typically mobilised by its passive reaction to the deformation of the concrete, however, the confinement can be made 'active' and capable of resisting the load from the time it is applied, if the spiral is pre-tensioned, or if confinement is provided using pre-tensioned lateral bolts. They developed an analytical model to predict the strength and deformational behaviour of concrete with uniform active lateral confinement. Points on the stress path of a specimen were determined for increasing increments of axial stress and, for each state of stress, the deformational response was calculated using non-linear constitutive relationships (Kotsovos and Newman, 1978, 1979) and assuming compatibility of the steel strain and lateral concrete strain.

In 1973, Popovics proposed a stress-strain relationship for concrete based on a curve passing through a point which describes the maximum compressive strength of the concrete, f_0 in psi, and the corresponding strain, ε_0, thus

$$f = f_0 \frac{\varepsilon}{\varepsilon_0} \frac{n}{n-1+\left(\frac{\varepsilon}{\varepsilon_0}\right)^n} \tag{3.16}$$

where n is defined as a function of the compressive strength of the concrete

$$n_{concrete} = 0.4 \times 10^{-3} f_0 + 1.5 \tag{3.17}$$

The critical strain ε_0 can either be obtained experimentally, or as a function of the strength of the concrete

$$\varepsilon_0 = 2.7 \times 10^{-4} \sqrt[4]{f_0} \tag{3.18}.$$

Two companion papers by Mander, Priestly and Park (1988) examined, both experimentally and theoretically, the deformational response of uni-axially loaded concrete which is confined by circular or rectangular spirals or hoops. The formula which they used to model the stress-strain relationship was largely empirical and was based on that of Popovics. The curve passes through the maximum compressive stress f_{cc}' and the corresponding strain ε_{cc}, thus

$$f_c = \frac{f_{cc}' xr}{r-1+x^r} \tag{3.19}$$

where $x = \varepsilon_c / \varepsilon_{cc}$, where ε_c is the longitudinal compressive strain in the concrete. The maximum compressive strain is defined as

$$\varepsilon_{cc} = \varepsilon_{co}\left[1+5\left(\frac{f_{cc}'}{f_{co}'}-1\right)\right] \tag{3.20}$$

where f_{co}' and ε_{co} are the unconfined compressive strength and corresponding strain (which is usually assumed to be 0.002).

$$r = \frac{E_c}{E_c - E_{\sec}} \tag{3.21}$$

with

$$E_c = 5000\sqrt{f_{co}'} \text{ MPa} \tag{3.22}$$

and

$$E_{sec} = \frac{f'_{cc}}{\varepsilon_{cc}} \tag{3.23}.$$

The authors took account of the fact that the confinement provided by the spirals or hoops is not uniform over the length of the column and defined a confinement effectiveness coefficient, k_e which allows the effective lateral confining pressure f_l' to be defined as the product of the lateral pressure from the transverse reinforcement and k_e. Where the section is circular

$$f_l' = \frac{1}{2} k_e \rho_s f_{yh} \tag{3.24}$$

where ρ_s is the ratio of the volume of the transverse confining steel to the volume of the confined concrete core and f_{yh} is the yield strength of the transverse reinforcement. In the paper the confined compressive strength, which is a function of the unconfined compressive strength, f_{co}', required in equation (3.19) is defined empirically as

$$f'_{cc} = f'_{co}\left(-1.254 + 2.254\sqrt{1+\frac{7.94 f_l'}{f'_{co}}} - 2\frac{f_l'}{f'_{co}}\right) \tag{3.25}.$$

The resulting stress-strain curve is shown in Figure 3.15. The paper showed ways of extending this formula for use in cyclic loading situations and in the case of high strain rate loading. Account was taken of the changes in strength, stiffness and in the strain at peak stress associated with high strain-rate loading by incorporating empirical factors for the statically calculated values. The companion paper gives the results of a series of tests on both quasi-statically and dynamically loaded circular, square and rectangular columns.

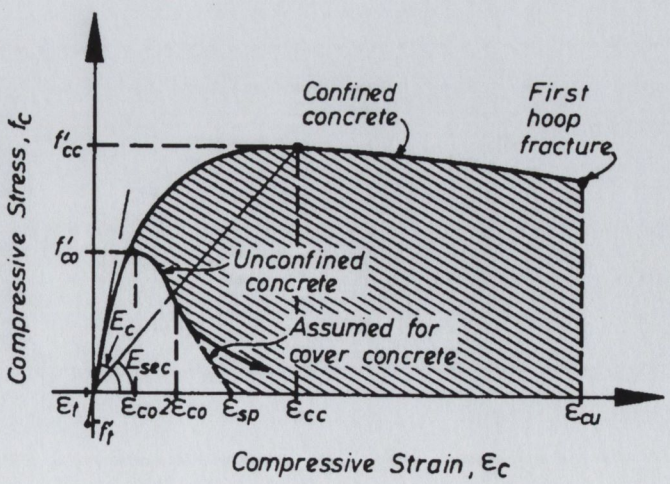


Figure 3.15 Stress-strain model proposed for monotonic loading of confined and unconfined concrete (Mander *et al*, 1988)

The confinement effectiveness coefficient, k_e, was used to predict the influence of the configuration of transverse reinforcement and the experimental results confirmed that the circular columns confined with spiral reinforcement are the most effective. The stress-strain relationship proposed by the authors was found to model the observed experimental behaviour quite accurately.

Ahmad and Shah (1982) proposed the following equation, similar to that of Sargin *et al* (1971), to predict the stress-strain curve of multi-axially loaded concrete. This equation was more sophisticated than that of Sargin *et al*, because it did not matter in which direction the maximum load was applied, provided that $\sigma_1 \geq \sigma_2 \geq \sigma_3$. The parameters, which described the relationship in a particular direction, could be determined from the experimental results and then used in the stress-strain relationship, thus

$$\frac{\sigma_1}{\sigma_p} = \frac{A_1 X_i + (D_i - 1)X_i^2}{1 + (A_i - 2)X_i + D_i X_i^2} \tag{3.26}$$

where $X_i = \varepsilon_i / \varepsilon_{ip}$

σ_i = principal compressive stress

σ_p = principal compressive strength

ε_i = strain in ith principal direction

ε_{ip} = peak strain in ith direction

$A_i = E_i / E_{ip}$

E_i = initial Young's modulus

$E_{ip} = \sigma_p / \varepsilon_{ip}$

D_i = parameter controlling descent curve.

This formed the basis for a series of later papers which model the stress-strain relationship of both normal and high strength concrete confined by spirals and hoops (Ahmad and Abdel-Fattah, 1991; El Dash and Ahmad, 1994, 1995; Ahmad and Mallare, 1994) with modifications of the factors above to take account of the particular types of confinement used. In these papers different equations are derived to predict the curve for spirally or hoop confined concrete, one using Boussinesq's equation to take account of the beneficial effect of the hoop confinement on the concrete and the other using empirical results gleaned from experiments. A third equation, which is also empirical, predicts the stress-strain relationship for rectangular confined, normal and high strength, concrete. All four

are compared to experimental results and appear to predict the deformational response closely.

The strength and ductility of confined concrete was also considered in the 1990s by Saattcioglu and Razvi and in two papers they attempted to produce a model which predicted both the ascending and descending branches of the stress-strain curve for concrete of different shapes with different confinement. They used the familiar expression to express the tri-axial strength of concrete, f_{cc}', in terms of the lateral confinement pressure, f_l, and the uni-axial strength, f_{co}'

$$f'_{cc} = f'_{co} + k_1 f_l \tag{3.27}$$

and used a value of k_1 generated from regression analysis of test data

$$k_1 = 6.7(f_l)^{-0.17} \tag{3.28}.$$

In 1992 the authors proposed using a modified value of the lateral confinement pressure, f_{le}, to account for differences in the section shapes and went on to develop work by Mander *et al* (1988) for the strain corresponding to the peak stress, ε_1

$$\varepsilon_1 = \varepsilon_{01}(1 + 5K) \tag{3.29}$$

with

$$K = \frac{k_1 f_{le}}{f'_{co}} \tag{3.30}$$

where ε_{01} is the strain corresponding to peak stress for unconfined concrete. They proposed the stress-strain relationship shown in Figure 3.16 to model the curve with the following used for the parabolic ascending branch

$$f_c = f'_{cc}\left[2\left(\frac{\varepsilon_c}{\varepsilon_1}\right) - \left(\frac{\varepsilon_c}{\varepsilon_1}\right)^2\right]^{\frac{1}{1+2K}} \tag{3.31}$$

and a linear descending branch passing through a point at 85 % of the peak strength, ε_{85} which is empirically defined. The model was modified in 1999 to take account of the differences between high and normal strength concretes, which the authors had previously studied (1994), and both give fairly accurate, and simple, predictions of experimental curves.

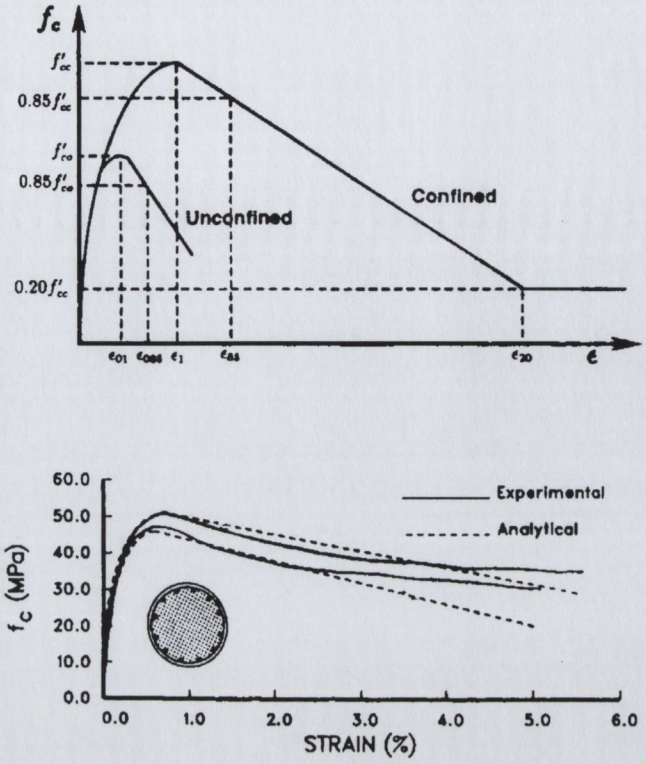


Figure 3.16 Proposed theoretical stress-strain relationship and comparison of experimental work with the model (Saatcioglu and Razvi, 1992)

In 1990 the CEB-FIP Model Code produced formulae to predict the differences in the constitutive law of concrete when confined, describing relationships between the tri-axial and unconfined compressive strength and strains based on empirical observation, and proposing a parabolic-rectangular diagram to model the stress-strain curve. De Nicolo, Pani and Pozzo (1997) used the confinement coefficient described in the model code as the basis for empirical work to find a unified prediction for the stress and strain increases associated with the axial loading of confined concrete.

3.4. DYNAMICALLY LOADED CONFINED CONCRETE

The study of concrete subject to both multi-axial loading and dynamic loads has been quite limited. This is both because of the difficulty of providing a system of confinement which is rugged enough to withstand high-strain rate loading, particularly when generated by impact, and because the complicated stress states existing within the concrete make it extremely difficult to model theoretically.

Early dynamic tri-axial tests undertaken by Takeda *et al* in 1974 and Yamaguchi *et al* in 1989 (reported by Bischoff and Perry, 1991) showed that both the maximum axial compressive stress and critical compressive strain were affected by the confining pressure and the axial strain rate. Furthermore, the failure criteria in compression increased considerably with increasing strain rate. Both Suaris and Shah (1982) and Bischoff and Perry concluded that there were no significant differences in the response of confined concrete between different strain rates when the deviatoric and hydrostatic stresses were normalised with the uni-axial compressive strength associated with each strain rate.

In 1991, van Mier *et al* performed a series of impact tests with both the target and striker specimens made of concrete, which focussed on generating an elasto-plastic contact model to estimate the contact force relationship. However, as both the target and striker were made of concrete, the specimens were cast into steel tubes to prevent premature splitting of the concrete when impacted and to simulate the concrete mass surrounding the impacted section, which would prevent lateral dilation in real concrete elements. The confining sleeve did not reach the contact interface which had one of three different surface geometries - spherical, conical and truncated conical. The presence of the confinement surrounding the concrete allowed it to be repeatedly impacted before the contact layers began to split off the top of the specimen. The authors attributed some of the stress increase to the tri-axial confinement of the concrete by the steel tube, which considerably enhanced the stiffness of the composite body. However, the benefits of confinement could have been increased if the sleeve had been in contact with the full length of the concrete specimens and reduced its dilation along the entire length. This would have reduced the plastic cracking phase of the contact force curve and it would have maintained its sinusoidal shape for longer, as the concrete tended to crack when repeatedly impacted.

Confinement was provided to ceramic specimens subjected to Split Hopkinson bar impact testing by shrink fitting a metal sleeve onto a 4.76 mm diameter cylinder (Chen and Ravichandran, 1996). Using this method, the cylinders were subject to active confinement with an effective pressure which was a function of the difference in the diameters of the confining and confined cylinder. They showed that the presence of confinement changed the constitutive behaviour of the specimen which exhibited a loading peak defined by the compressive strength, and a bi-linear unloading curve. Increasing the confining pressure resulted in considerable increases in the compressive strength and significant reductions in the crack density in the impacted specimen, which largely resulted from the active pressure minimising the lateral dilation.

Experimental work by Reider and Mindess (1998) studied the impact behaviour of bi-axially confined concrete. Cubes (100 mm sides) of high-strength concrete were bi-axially pre-stressed with screw type rams and were placed on a support anvil, all of which acted as loadcells to measure the stresses during the impact event. The contact force at the location of impact was measured using a loadcell incorporated into the falling hammer or 'tup'. They showed that the high strength concrete was stronger when it was actively confined prior to impact and that the strength increased as the lateral pre-loads increased. Similarly, the stresses measured by the 'tup' and support loadcells increased with increases in the confining pressures. The kinetic energy lost by the hammer W_{lm} was obtained from the impulse-momentum relationships

$$W_{lm} = \frac{1}{2} M_h \left[\left(\frac{1}{M_h} \int p(t)dt - \sqrt{2g_c h} \right)^2 - 2g_c h \right] \tag{3.32}$$

where M_h was the mass of the hammer, h the drop height, g_c was the corrected gravitational acceleration and if $p(t)$ was the load-time relationship of the hammer. The integral $\int p(t)dt$ represented the impulse during the impact, calculated by integrating under the tup-loadcell/time curve. Equation (3.32) is valid for any type of collision, but in the case of confined concrete, the kinetic energy lost by the hammer, and transferred to the cube was significantly increased when the concrete was preloaded, and increased with the pre-load. When the concrete was unconfined, the energy transfer split the specimen and accelerated the specimen halves, however, when confined, all the kinetic energy of the hammer has to be transferred to the specimen because the movement of the hammer is stopped by the specimen. This also results in a longer duration of impact. The authors

performed a Brazil tensile test on the undamaged concrete cubes and, although there was little visible damage, the tensile strength of an impacted cube was considerably reduced when compared to that of an un-impacted cube. However, these tests, although at a strain rate similar to those tested in the current research, are significantly different because the concrete was actively confined. The lateral pressures were constant throughout the duration of loading. It is probable that if the cubes were passively confined that the residual tensile strength would be reduced still further and that more cracks would be evident in the impacted surface.

High and very high-strength concrete are very brittle and need to be well confined laterally to improve their ductility and minimise spalling. Traditional reinforcement, which has to be closely spaced, is difficult to use because of problems with placing the concrete. As an alternative, Lahlou *et al* studied then response of concrete confined in a steel cylinder and rapidly cyclically loaded (1999). Three thicknesses of steel confining cylinder were also tested and although the evolution of damage and load-deflection curves were both characteristic of rapid cyclic loading, the presence of the confining steel greatly increased the ductility of the concrete cylinder. Furthermore, the confined columns showed a greater capacity for absorbing and dissipating energy under the dynamically applied load.

Madas and Elnashai (1992) derived a passive confinement model for analysing concrete subject to cyclic and transient dynamic loading. The intention of the work was to generate a model which incorporated the simplicity of the uni-axial models for concrete whilst accounting for the 3-dimensional effects on the strength and the deformational properties. It allowed the transverse confining stresses to be calculated, for increments in the applied axial strain, in either active or passive confinement situations. Initially, the axial strain, the Poisson's ratio and the confining pressure of the concrete corresponding to the yield strain of the confining steel were calculated. The variation of radial strain with the axial strain was assumed to be a cubic function, thus

$$\varepsilon_r = A\varepsilon_1^3 + B\varepsilon_1^2 + C\varepsilon_1 \tag{3.33}$$

with coefficients which could be determined from a knowledge of the initial Poisson's ratio, Young's modulus and strains. The confining pressure was calculated using

$$\sigma_r = \frac{\rho_s f_s}{2}\left(1 - \sqrt{\frac{S_{sp}}{1.25 d_{cc}}}\right) \tag{3.34}$$

if ρ_s is the volumetric ratio of the confining reinforcement to the concrete core, f_s is the stress in the confining steel, S_{sp} is the spacing of the stirrups and d_{cc} is the diameter of the concrete core. This equation assumed that the confining reinforcement becomes ineffective when the ratio of the spacing to the diameter of the cylinder is greater than 1.25. This lateral pressure was then used in an active confinement model for concrete to calculate the concrete stress. The process was repeated for each increment of axial strain and results in a passive confinement model for concrete which compared favourably with experimental results for confined concrete under monotonic and cyclic loading situations, when confined with circular steel spirals.

3.5. FINITE ELEMENT ANALYSIS OF CONFINED CONCRETE

Most of the theoretical work on confined concrete has been either an empirical analysis of existing experimental results or involved analytical models to predict the constitutive relationship of the composite. However, work in the area of finite elements has resulted in a highly detailed understanding of the complex states of stress and strain to which concrete is subject (Kotsovos and Newman, 1978; Gerstle *et al*, 1980) which can further facilitate the mathematical modelling of the response of concrete to axial loads when confined laterally.

Kotsovos and Pavlovic (1986, 1995) studied the three dimensional response of concrete when loaded and attempted to incorporate their findings into complex material and geometric models to predict the response of structural elements to many forms of loading and to gain an insight into the fundamental behaviour of concrete. The material response of the concrete is highly non-linear as a result of the fracture processes which are underway in the concrete when it is loaded. However, it is necessary to incorporate this non-linearity in order to model both the material and the structural behaviour. This process includes the extension and propagation of cracks in the direction of the maximum principal compressive stress which often exist prior to the application of the load due to the heterogeneous nature of the concrete and which can result in numerical instabilities during the period of load application. Kotsovos and Pavlovic produced a constitutive stress-strain model for concrete, based on existing experimental data, which allowed an accurate modelling of the structural behaviour for both uni-axially and multi-axially loaded concrete (with active confinement). The model generated could either be used as a finite element formulation or incorporated into existing finite element models. Furthermore, they successfully modelled the interaction of the reinforcing steel with the concrete element.

Limited finite element studies have been undertaken to model directly the response of concrete confined by a sleeve of another material. However, as part of his study on the behaviour of concrete filled tubes to axial loads, Schneider (1998) produced a finite element model, using the code ABAQUS, to compliment the results of his experimental work and to facilitate an understanding of the behaviour of cylinder sizes more likely to be used in construction. The concrete core was modelled using 20-node brick elements with

three translational degrees of freedom at each node. A 3-dimensional concrete element, incorporated in the code, was used to model the conditions of uni-axial strain at reasonably low confining pressures which the author determined experimentally to exist in the concrete until near the point of yield. The steel tube was modelled using 8-node shell elements with five degrees of freedom at each node. Inelastic material and geometric non-linear behaviour were used in the steel material model, with von Mises yield criteria defining the yield surface. An interface or gap element which transmitted friction if in compression, but could not hold the elements together if in tension, was used between the sleeve and the core. The results from the finite element model predicted both the elastic and in-elastic behaviour of the cylinder and provided a close approximation to the experimental results. However, the yield strength was not particularly well defined in the model and was, therefore, offset by 0.2 % in further models to predict the response of untested cylinders (Figure 3.17). The calibrated finite element model was used to predict the response of cylinders with varying wall thicknesses and diameters. The results illustrated that, for small diameter concrete filled tubes, the steel tube and the concrete core were both near their ultimate capacity when the tube reached its yield strength and caused failure. In the case of the large diameter tubes, the concrete stress eventually reached its compressive strength, although the steel sleeve did not achieve its full compressive strength due to the tri-axial stress state to which it was subject as it confined the concrete core. Furthermore, the confinement provided by the steel cylinder if of large diameter is considerably less than that provided by confinement at a small distance from

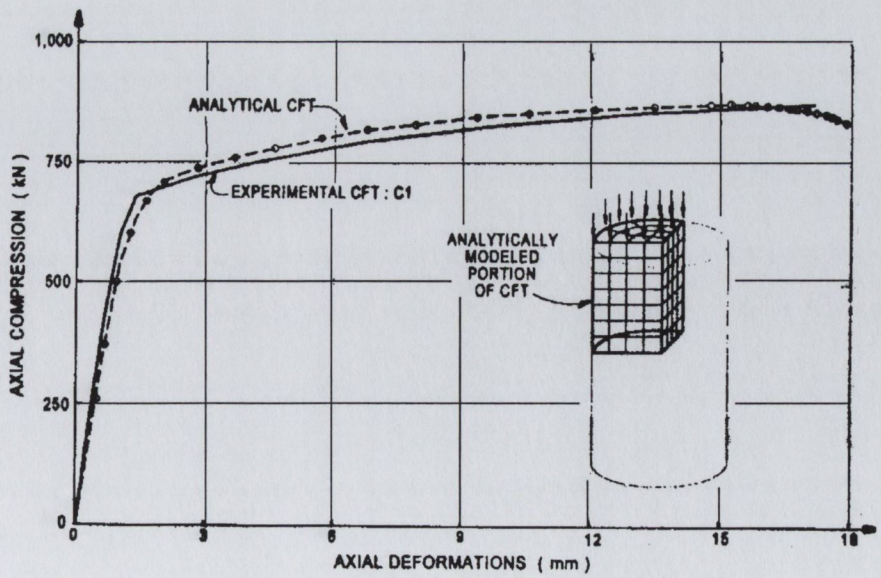


Figure 3.17 Comparison between numerical and experimental results (Schneider, 1998)

the location where it is loaded. The non-linear model was capable of modelling the local buckling of the wall of the tube and the strain hardening which occurred close to failure, due to the interaction of the steel and concrete elements.

Liu and Foster developed a finite element model to investigate the response of concentrically loaded columns with concrete strengths of up to 100 MPa (1998). A complex constitutive model derived by the authors incorporated the softening behaviour of concrete. They used a 2-dimensional, 4 or 8 node axi-symmetric, isoparametric elements to model the concrete. The modelling produced a good correlation with experimental results on columns with low confinement provided by steel spirals, and was used to model both small cylinders and full size confined columns. Although it was not capable of modelling the spalling of the cover concrete associated with the high loads applied to the column, it provided a good prediction for its load carrying capacity, which was confirmed by an analysis of experimental results.

A study of the non-linear response of concrete filled steel tubular columns under axial loading was undertaken by Shams and Saadeghvaziri (1999). They undertook the study because they realised that, although considerable experimental work had been undertaken to study to response of concrete filled tubes, the analytical studies were much more limited. They modelled the concrete using existing 3-dimensional solid elements which incorporated the non-linear stress-strain behaviour and the effects of a tri-axial state of stress on the concrete and the tendency of the concrete to fracture by incorporating an energy based constitutive model. The steel tube was modelled using isoparametric shell elements which allow local buckling to occur by incorporating a von Mises elastic-plastic model with kinematic hardening. A traditional contact element was used between adjacent nodes at the interface. When loaded initially, the steel took the majority of the load until it reached yield, whereupon the load was transferred back into the concrete core until this, in turn, reaches its maximum compressive strength. The load is then transferred back into the confining sleeve which undergoes hardening to withstand the increased load. The authors undertook a parametric study to determine the effects of changing the D/t ratio and the L/D ratio. They found that the compressive strength of the concrete and the critical strain were both affected by the D/t ratio, the cross-sectional shape (circular or square) of the column and the concrete strength. The increase in the thickness of a thick wall sleeve provided very little increase to the confinement because the stress distribution was not

uniform over the cross section of the confining steel and the dilation was already considerably reduced. For the same *D/t* ratio, the ratio of the confined strength to the unconfined strength was less for higher strength concrete than for lower strength concrete. This was because, as the strength of the concrete increased, the stiffness increased which meant that less lateral expansion can take place and that the confining pressure was reduced. The modelling also showed that the confinement was more effective in circular columns than in square ones because the stress distribution is more uniform. The finite element modelling was then used to calibrate an empirical model and to determine when buckling and failure of the steel tube would occur.

The finite element and finite difference analysis of bodies subject to impact is a second, highly complicated, area of theoretical analysis as it is necessary to model forces and changes in the material properties as time varying functions. In the finite element method the equations of motion are formulated through nodal forces for each element and do not depend on the shape of the neighbouring mesh, which means that complicated geometries are relatively easy to model. In the finite difference method, equations of motion are expressed directly in terms of the pressure gradients of the neighbouring meshes and the equations must, therefore, be formulated separately for irregular regions and boundaries (Zukas *et al*, 1982). The codes relating to impact dynamics subdivide into two categories - Lagrangian and Eulerian. Lagrangian codes follow the motion of fixed elements of mass and the computational grid is fixed in the material and distorts with it. They are useful for material models which vary with time and in situations where the distortions are not too great. In contrast, Eulerian codes are used where there are large deformations as the computational grid is fixed in space and the material passes through it, being either represented as discrete points or as a continuum. Both types of code are well described in a paper by Anderson (1987).

Zukas (1994) considered the importance of the use of accurate constitutive models which incorporate features observed experimentally during blast and impact situations. These facilitate accurate modelling of impacted bodies using wave propagation codes or hydrocodes, particularly when large deformation effects and failure are incorporated. Impact is a highly localised phenomenon, where the kinetic energy of the impactor is transferred to the target on collision. A compressive stress wave then propagates into the impactor and the target at a speed which related to the material properties, and can be

reflected or transmitted at the boundaries which it reaches. Zukas reported that, because of the localised nature of the impact, the geometries under consideration can be highly simplified and showed that, unlike a normal structural dynamics problem, catastrophic failure can occur before the distant boundaries can have any effect on the problem. The materials are typically modelled in two parts, one of which describes the properties of the material and the way it behaves during the loading, and a second which describes the failure criterion which can be instantaneous or time-dependant. These two features have to be well defined in order to model the response of a body to high strain rate loading.

Work in the area also involves mixing finite element codes to incorporate geometrical and constitutive non-linearites, for example Cescotto and Yhu (1994) studied the effects of incorporating solid and contact finite elements to better predict the stresses, strains and displacements. They compared the results of a number of finite element problems which modelled the collision of a rod with a solid wall using existing codes, and found that mixing the two types of codes gave the most accurate prediction for the behaviour of the rod. They also studied the low velocity impact of a die on a solid cylinder and showed that, at velocities of less than 10 m/s, the behaviour of the bodies was quite similar to a static solution, as barrelling of the specimen occurs at the centre, rather than the mushrooming effect at the end exhibited during higher velocity impact. The static simulation did not model the propagation of the stress wave in the material and a 3-dimensional model, which incorporated wave propagation effects, was required to model this accurately.

With the increases in the speed and capacity of computers over the last fifteen years the research into the numerical modelling of impact, shock and blast has grown considerably and is now the focus of many researcher's work on the response of bodies to high strain rate loading. Many papers have been written on the finite element modelling of concrete subject to impact, with increasingly complicated material models (for example, see Jiang and Rogers, 1989; Malvar *et al*, 1997, Gebbeken and Ruppert, 1999a) and on the development of hybrid codes which incorporate aspects of both the Lagrangian and Eulerian methods (see for example, Clegg *et al*, 1997; Sauer, 1999), which while computationally expensive are reducing the need for complicated and expensive testing to be undertaken. However, the work to calibrate the complicated geometries and models used in the finite element work against the results of extensive tests remains a necessity particularly at the highest of strain rates (Gebbeken and Ruppert, 1999b).

3.6. CONCLUSIONS

The research in the area of passively confined concrete to low velocity hard impact has not been unified, thus far. Considerable work has been undertaken on the response of concrete to hard impact and, similarly, other researchers have studied the effects of confining concrete and loading it axially.

The work in the area of impact has shown that high strain rate loading causes the material to act in a different manner to when it is statically loaded. Researchers have shown that high strain rate loading results in an increase in the compressive strength and in the critical strain of concrete. However, the main factor determining the concrete's response when impacted is its static strength. Research has also shown that increases in the strain rate influence the way in which the concrete fails, the secant modulus of elasticity and the energy absorbed during the collision. The material response is, by now, fairly well understood, but further research is still need to conclusively determine the effect that increasing rates has on the stress-strain response of the concrete which is of vital importance in the work to determine a realistic theoretical model of the concrete response.

The lateral confinement of concrete has also been studied in considerable detail and it has been shown that the effective lateral pressure generated by passive confining steel, which becomes effective when the concrete begins to dilate laterally under an axial load, increases the strength and ductility of the member considerably. This strength increase is particularly evident in the case of circular columns where the confinement goes into hoop tension evenly around the circumference, whereas, in the case of rectangular sections the confinement is partially in hoop tension and partially in bending. The confinement is effective when steel spirals or hoops are used and is even better when a sleeve, which stretches the entire length of the cylinder is employed as the confinement along the length is uniform. Other researchers have used other materials to replace the steel, and have found that materials which have a high tensile strength are almost as good as steel in resisting the lateral dilation of the concrete. Theoretical models to predict the response of the confined concrete to axial loading are quite limited due to the complicated stress state within the confined concrete, and because, when passively confined, the lateral pressure is not constant throughout the entire period of loading as it varies with the applied axial pressure. The majority of these models are either purely empirical or are semi-analytical

with empirically derived constants, but have had reasonable success in predicting the response of confined concrete to an axial load.

The combination of the high rate loading and confinement has been studied in a limited form within the last decade. However, it is complicated by the difficulty in applying a lateral load to the concrete in a sufficiently robust manner to withstand high strain rate loading caused by impact. The majority of the work in this area has involved applying an active pressure to the concrete. The presence of the confinement results in an increase in the strength of the concrete and a decrease in the cracking. However, the way in which the concrete resists this load is not considered, and the work on passively confined concrete is extremely limited.

Limited finite element studies have been undertaken on the passive confinement of concrete, and these tend to focus on the effects of the different parameters, such as the diameter and the thickness of the confinement and the strength of the concrete, rather than on the way in which the load is transferred to the base of the cylinder. Finite element studies with dynamic codes are highly complicated and focus on modelling complex geometries and using novel constitutive relationships to describe the materials involved. The studies have shown, however, that both statically and dynamically, the use of accurate models to describe the material response, particularly in the case of concrete, is the most important way of accurately predicting the response of either the material or the structure to an applied load.

It can be concluded that, although considerable work has been undertaken to date on the response of confined concrete to an applied axial load and on the response of materials to low velocity impact, considerable work must still be undertaken to generate a clear understanding of the response of passively confined concrete to impact. This is necessary, both experimentally and theoretically, in order that the response be quantified and that the load transfer mechanisms be properly understood.

4. DETAILS OF EXPERIMENTAL WORK AND TEST SPECIMENS

4.1. METHOD OF IMPACT LOADING

Any study of the response of concrete to impact loading is complicated by both the inhomogeneous composition of concrete and the stress wave propagation through both impactor and target following the impact event. It is, therefore, important in any experimental study that the equipment used to generate the impact is designed so as to result in a test which is easily and consistently repeatable and which minimises bias from variables other than in the impacted material. A simple way of designing equipment to provide an impact with the characteristics of a low velocity collision is to use the principle of a mass falling freely under the effects of gravity. An impact test rig was, therefore, constructed for the current research which allows a steel mass to fall under gravity onto the test specimen. It was modelled on a rig designed to perform low velocity impact tests on beams, slabs and cylinders in Imperial College London in the 1970's and 1980's (Brown and Perry, 1982).

Figure 4.1 shows the general arrangement of the impact test rig, in both elevation and plan. The test rig consists of a guide channel for the falling impactor which is attached to the side of a portal frame, as can be seen in Figure 4.2. The guide channel is constructed of two steel channels (200×75 mm), battened together using 50 mm steel plate; and it is attached to a sturdy portal frame in such a way as to allow adjustment to ensure perfect verticality.

The impactor consists of a solid steel cylinder, 150 mm in diameter, tapered to 100 mm at the lower end, into which a 'contact-force' loadcell is incorporated. The impactor has tapped holes, both at the top to allow a loop to be attached from which the impactor can hang, and at its base enabling a slightly rounded (radius of curvature 400 mm), hardened endstriker to be fitted, as in Figure 4.3, giving a total weight of 82.5 kg. It is fitted with two plastic rings (Figure 4.4) at its widest section to minimise friction between the steel cylinder and the steel guide channel as it is winched, by hand, up to the drop height for any particular test (a maximum of 3 metres). These rings did not bear when the impactor was falling as the guide channel was 50 mm oversized. In order to release the impactor, its winching cable was attached to a modified glider release connected to a Bowden cable.

Both confined and unconfined concrete cylinders were tested using this rig. A test assembly, consisting typically of the concrete cylinder, a flat-plate loadcell and a solid supporting aluminium billet was carefully prepared prior to each test. This assembly was in turn placed on a solid cube of concrete, with sides 500 mm, which was firmly bolted to the 1 metre thick reinforced structural floor of the laboratory, using a square restraining frame as can be seen in Figure 4.1 and Figure 4.2, and which was centred carefully beneath the impactor. The concrete block and floor, also, helped to dissipate the stress waves resulting from the impact.

The velocity of the free falling impactor was measured in a preliminary set of tests. This was achieved by using a magnetic triggering device which consisted of a thin magnet and two Hall Effect transistors, separated by 50 mm distance, and located close to the location of impact. The Hall Effect transistors are non-switching devices which react instantaneously to a magnetic field. This system was used to overcome switching delays which had been exhibited with an earlier system using light switching diodes. The earlier system failed because the light used was too diffuse and because the switching mechanism in the diode was not accurate enough to overcome the time delays. However, the Hall Effect transistors showed a distinct peak as a magnet attached to the impactor passed and the time difference between the peaks could be measured accurately. The basic equations of motion were used to determine the acceleration for each of the particular drop heights which, in turn, allowed the velocity of the impactor when it reached the top transistor to be calculated. Figure 4.5 shows a graph of the measured velocity at each drop height and a theoretical curve calculated with the acceleration due to gravity = 9.81 m/s^2. The average measured value for acceleration was found to be 9.79 m/s^2. This, very small, difference can probably be attributed to the following

- inaccuracies in the measurements taken with the hall effect transistors
- inaccuracies in the measurement of the distance between the two transistors
- resistance due to the movement of air around the impactor, although this was minimised as there was nothing preventing the free fall of the impactor, and the air was allowed to escape through the gaps in the side of the guide channel.

For the purpose of this research, the acceleration due to gravity was, therefore, taken as 9.8 m/s^2.

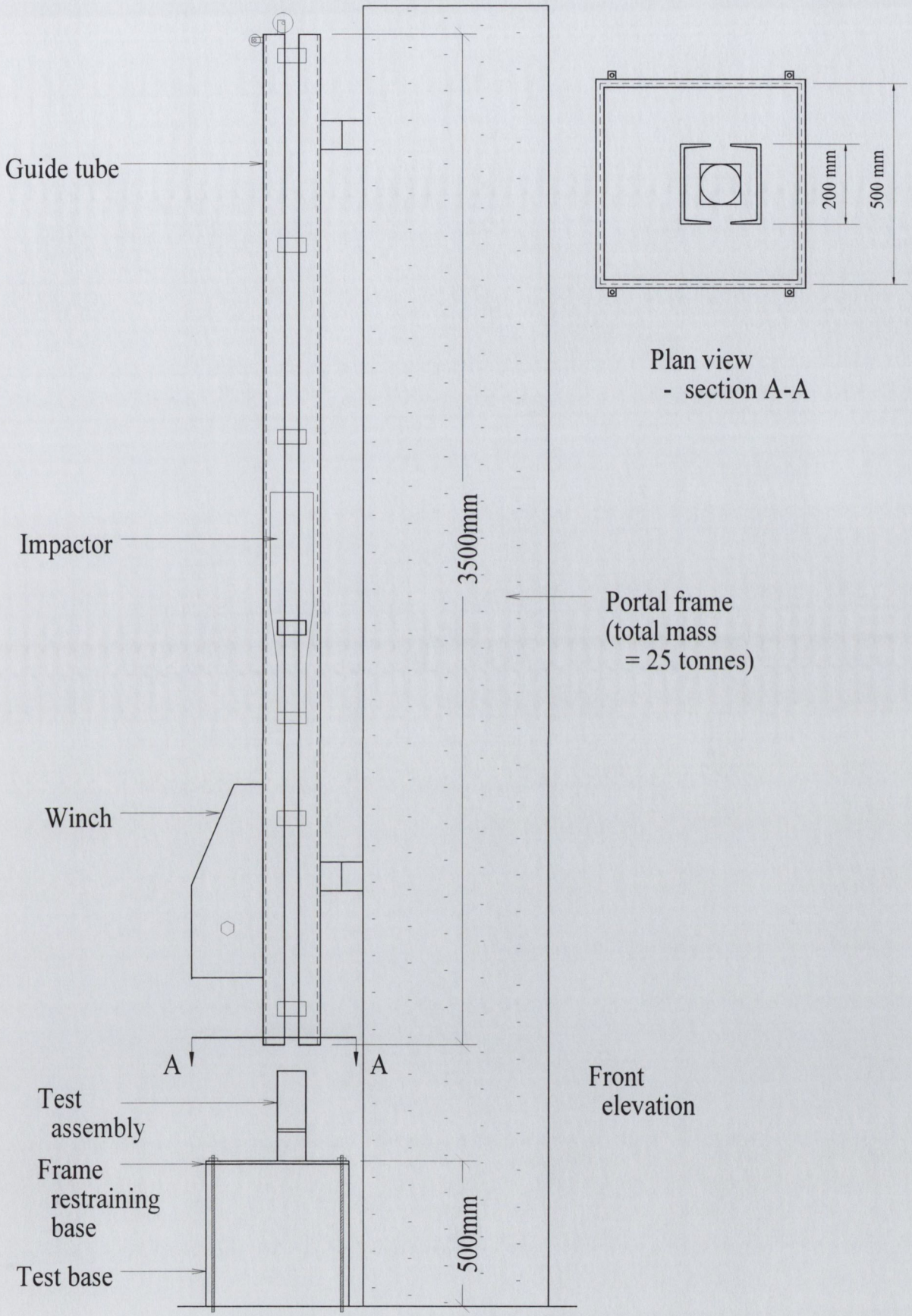


Figure 4.1 Schematic view of impact test rig (for further details of dimensions see text)

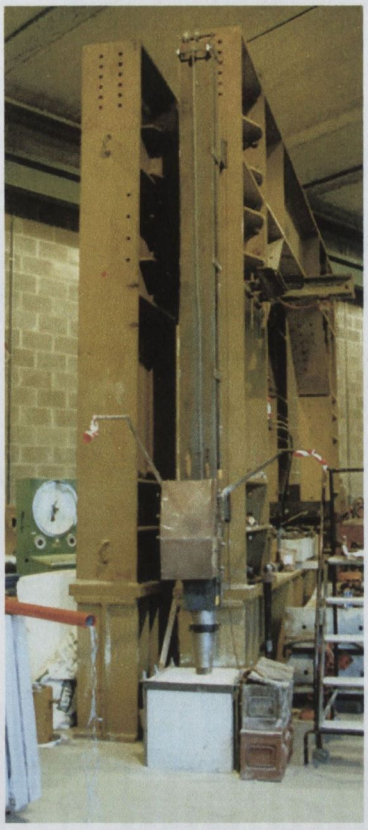


Figure 4.2 Photograph of impact test rig

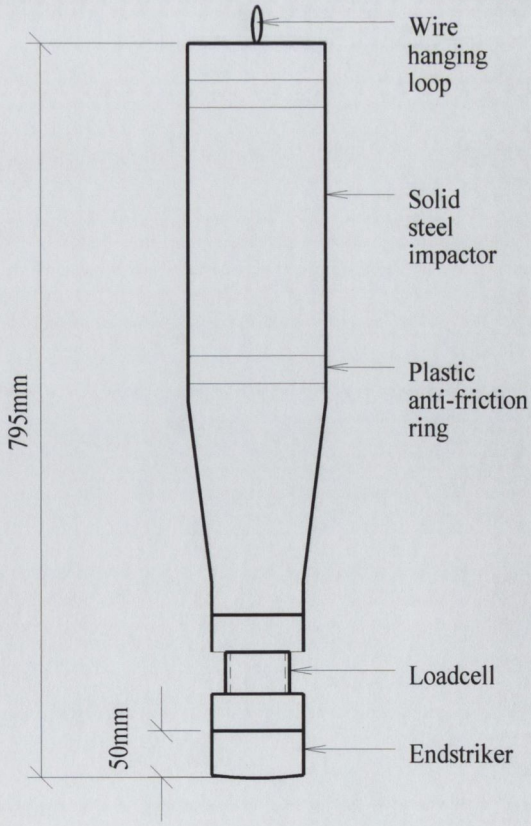


Figure 4.3 Schematic diagram of impactor

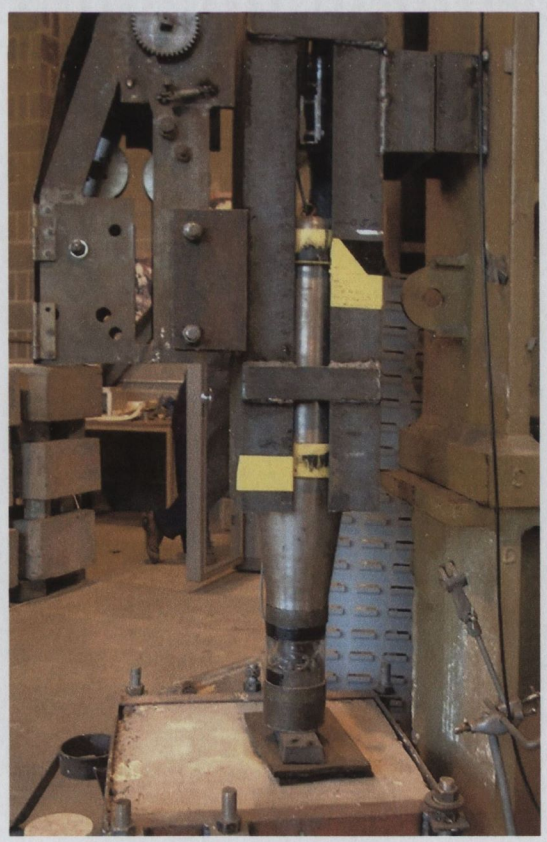


Figure 4.4 Photograph of impactor in guide tube, showing quick release mechanism

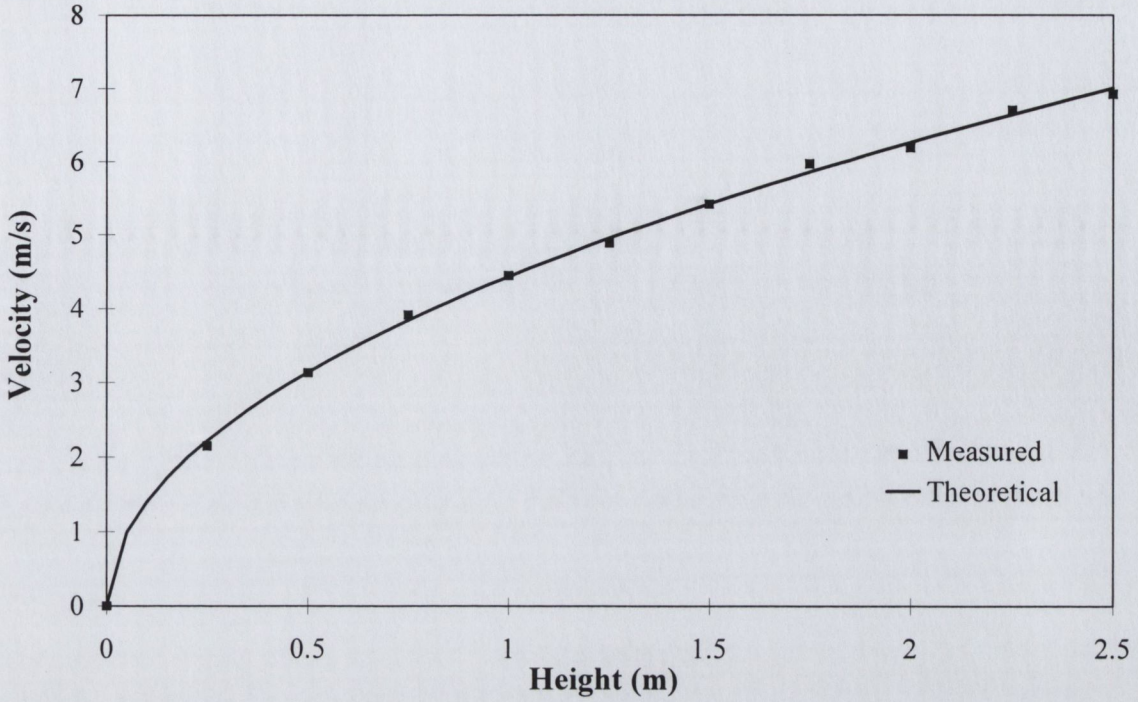


Figure 4.5 Experimental and theoretical determination of velocity

The impactor was dropped from three different heights during the current test series. These were 0.5 m, 1m and 2 m, and the corresponding contact velocities were 3.2 m/s, 4.4 m/s and 6.3 m/s. They resulted in different amounts of energy being transferred to the impacted cylinder as a result of the collision. These heights were chosen to ensure that the responses of the impacted cylinders should vary noticeably over the velocity range.

4.2. DETAILS OF TEST SPECIMENS

4.2.1. Geometry

All of the specimens tested were cylindrical, with a height of 200 mm. The majority were concrete cylinders, passively confined using hollow tubes, and one reference series of concrete cylinders was tested unconfined. There were two distinct series of tests. The main series of tests were on cylinders confined along their entire length, with diameters of between 110 mm and 115 mm and different types of sleeves. The second series examined cylinders whose sleeves were not supported at their base, of diameters again between 110 mm and 115 mm, cylinders of a greater diameter, both fully confined and unconfined, and the effects of static loads on unconfined and confined cylinders. The impact, or statically applied load, was always applied to the concrete core and not the confining cylinder using the slightly rounded, hardened endstriker.

According to BS 1881:Part 110:1983 the specimen diameter should be five times the maximum aggregate size to obtain an accurate representation of the concrete behaviour. The smallest diameter used for the unconfined cylinders was 100 mm, sufficient for the maximum aggregate size of 20 mm used throughout these tests.

Resulting from its composite nature, concrete is a highly heterogeneous material. Thus, failure can often be the result of stress concentrations associated with the method of testing. Carpinteri *et al* (1999) concluded that there are three main factors influencing its failure in compression, namely, contact due to the platen restraint, the shape and dimensions of the specimen and the aspect ratio. The latter is the ratio of the height to the characteristic cross-section dimension and, according to BS 1881 : Part 120 : 1983, should be between 1 and 2 to minimise the friction caused by the restraint at the loading plattens.

During impact loading, stress wave propagation is unavoidable and can result in stress variations along the length of a specimen. A more uniform stress condition can be achieved if the length of the specimen is reduced, allowing stress equilibrium, caused by internal wave reflection, to be obtained as quickly as possible. Lindholm (1964) proved experimentally that the aspect ratio for impacted specimens should ideally be less than one. It is, therefore, evident that the requirements for stress wave propagation and platen

restraint are contradictory. However, as the predominant method of failure of concrete under compression is indirect tensile cracking, which is governed by aspect ratio, it was decided that, for these tests, an aspect ratio of approximately two should be used to minimise end effects at the specimen interfaces and allow a good representation of the material properties, whilst ensuring that stress wave equilibrium was achieved reasonably quickly in the impacted cylinders.

4.2.2. Designation of test specimens

Each of the specimens tested was given a unique designation which describes the way in which it was confined and the way in which it was tested. Each had six different parameters, an example of which is given below.

a) The confinement was described in three ways

- C fully confined
- R reduced length of confinement
- U unconfined.

b) The external diameter of the sample, to the nearest millimetre, in parenthesis.

c) The confinement material

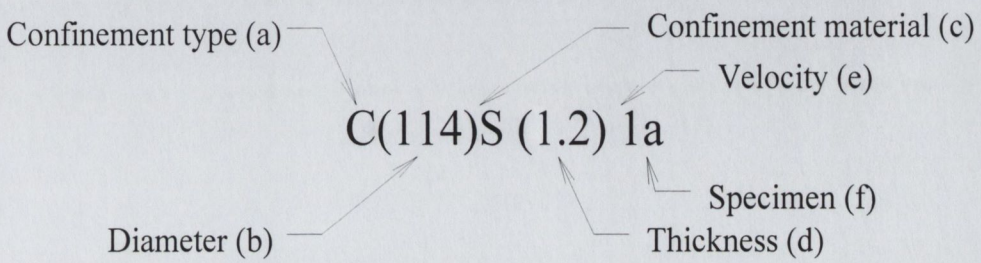
- S steel
- A aluminium
- P plastic.

d) The thickness of the confining material, in parenthesis.

e) The impact velocity

- 1 drop height 0.5 metres, contact velocity 3.2 m/s
- 2 drop height 1 metre, contact velocity 4.4 m/s
- 3 drop height 2 metres, contact velocity 6.3 m/s
- 4 used to describe cylinders tested statically, velocity 0 m/s

f) A letter (between a and g) to indicate the particular cylinder tested in the group.



4.2.3. Properties of confining cylinders

The confined concrete cylinders were selected and fabricated to investigate as wide a range of variables as was possible using simple, commercially available materials. The confinement consisted of thin walled tubes of steel, aluminium and PVC plastic pipe which were fabricated from long, cylindrical sections. All of the cylinders tested were 200 mm in length, which correspond to the size of the unconfined cylinders, cast in moulds 100 mm in diameter and 200 mm high.

The majority of the work on the static loading of confined concrete involved the use of steel as a confining material, either as spirals, hoops or sleeves. Therefore, it was decided that steel sections should form the basis of the experimental work on the response of confined concrete to low velocity hard impact. Four thickness of steel tube were used, namely 1.2 mm, 3 mm, 5 mm and 6.5 mm. For all but the thinnest section, the cylinders were commercially available structural hollow sections, conforming to EC3, with an external diameter of 114.3 mm. This resulted in an aspect ratio of approximately 2, as the cylinders were designed to act as short stub columns which did not undergo any local or overall buckling. These thicknesses were chosen with the intention of obtaining a wide range in the experimental results, where in some cases the concrete would undergo considerable dilation, and in others the dilation would be nearly negligible. Furthermore, it was hoped that the responses of the cylinders of these thicknesses would vary when tested at different contact velocities.

The cylinders, other than for the thinnest, were produced in the laboratory by cutting hollow tubes and machining them to the correct length with perfectly right angled edges. In the case of the thinnest steel section type, it was not possible to source cylindrical hollow sections of the required diameter and thickness. These sections were, therefore, fabricated by rolling and seam welding 1.2 mm thick steel sheet. From the outset, it was evident that these thin cylinders would behave slightly differently from the other cylinders because of the way in which they were fabricated. However, it was hoped that this thickness of sleeve would be near to the limit of the confinement required to prevent the fracture of the concrete when impacted. The 3 mm thickness of steel sleeve was chosen as the standard section, because it was fabricated from a single section of steel tubing and dilated in a consistent manner when the concrete was loaded.

Sleeves were also fabricated from sections of commercially available aluminium (of type 6082) and of UPVC plastic (6 Bar unplasticised PVC Wavin water main). These were chosen to be of similar thickness to the standard section of steel pipe (3 mm) but were, again subject to the limitations of what was available commercially. These materials were chosen because their properties were significantly different from the steel and, although their Young's modulii would suggest that they dilate considerably more under a load, they were still capable of generating a significant hoop stress in the sleeve and thereby reducing the dilation of the concrete core.

Larger diameter cylinders were also fabricated for comparison purposes to ascertain to what extent a sleeve at distance the centre of loading provided effective confinement to the core. To obtain a cylinder with a similar thickness to the standard cylinder (3 mm) a stainless steel sleeve was used. It had an external diameter of 168 mm, and was cut into 200 mm high sections like all of the other cylinders. Unconfined cylinders of the same internal diameter were also fabricated, by casting them in identical stainless steel tubes and then cutting the tube away with an angle-grinder, prior to curing the concrete.

A limited number of tests were performed on cylinders which did not have confinement along their entire lengths to study the effect of confinement when the sleeve was not being fully supported. The cylinders were also of 200 mm length. However, 5 mm was machined from the bottom of the confining sleeve after the concrete had be poured and cured. These tests were undertaken to examine how much of the load was transferred into and along the confining sleeve when loaded, and how this was affected by whether the confining sleeve could transmit the load directly into the support or whether it had to transfer the load back into the concrete core.

The properties of the confining cylinders used in the experimental work are listed in Table 4.1. The yield strength, Poisson's ratio and Young's modulus were determined in accordance with BS EN 10002-1:1990 for the metallic materials and BS 2782:Part 3:Method 320:1976, BS 2782:Part 3:Method 321:1993 and BS 2782:Part 11:Method 1110:1989 for the PVC plastic using, coupons cut from sections of each of the cylinders or sheet metal. Details of the experimental results of these tests are given in Appendix 2. The stress wave propagation speed of each material was determined using (2.17) and measured values for the density and Young's modulus.

	External Diameter (mm)	Thickness (mm)	Density (kg/m^3)	Co (m/s)	Poisson's ratio	Yield strength (N/mm^2)	Young's modulus (kN/mm^2)
C(114)S (1.2)	114.3	1.2	7820	5740	0.31	365	260
C(114)S (3)	114.3	3.0	7790	5765	0.36	365	260
C(114)S (5)	114.3	5.0	7850	5330	0.30	430	220
C(114)S (6.5)	114.3	6.5	7830	5360	0.33	365	225
C(115)A (3.25)	115.0	3.25	2810	4920	0.36	225	70
C(110)P (3.6)	110.3	3.6	1420	1390	0.36	-	3
R(114)S (3)	114.3	3.0	7790	5765	0.36	355	260
R(115)A (3.25)	115.0	3.25	2810	4920	0.36	255	70
R(110)P (3.6)	110.3	3.6	1420	1390	0.36	-	3
C(168)S (3)	168.0	3.0	7870	4910	0.28	265	190

Table 4.1 Properties of confining sleeves

4.2.4. Concrete properties and specimen production

The concrete mixes used in the tests were all of identical design. They were of grade C40 and details of the mix are given in Table 4.2. The water cement ratio of the concrete was chosen as 0.5 and the ratio of the 20mm:10mm aggregate was 2:1. The B.R.E. report *Design of normal concrete mixes* (Teychenne, 1988) was used as a guide to mix design.

The majority of the series of confined and unconfined cylinders were cast in separate batches, except when the number of cylinders cast was small (as in the case of the cylinders with reduced lengths of confinement), whereupon two series of cylinders were made together. A small laboratory concrete mixer, with a capacity of 0.2 m^3, was used to make the concrete. Each of the mixes was prepared in the following manner to ensure maximum uniformity in the resulting concrete.

1) The insides of the steel sections were cleaned with a wire brush, and the insides of all cylinders were wiped to remove any loose dust particles.
2) The confining cylinders were then attached to a specially made base using a dogging system for casting which provided a solid base for the confining sleeve to contain the concrete during pouring (Figure 4.6).

Mix per cubic metre			
Water		kg/m^3	180.00
Cement		kg/m^3	428.57
Fine Aggregate	(naturally occurring washed sand)	kg/m^3	830.22
20mm Coarse Aggregate	(pit run uncrushed gravel)	kg/m^3	624.14
10mm Coarse Aggregate	(pit run uncrushed gravel)	kg/m^3	312.07

Table 4.2 Test mix details

3) A thin bead of silicone sealant was placed at the join between the confining cylinder and the base to prevent the fines from leaking out during vibration of the concrete.
4) The coarse and fine aggregate and the cement were mixed well for 3 minutes
5) The water was added and the concrete was mixed for a further 3 minutes.
6) The confined specimens were cast into hollow cylindrical sections of steel, aluminium or PVC plastic pipe, each 200 mm high. The unconfined cylinders were cast in standard steel moulds in accordance with the requirements of BS 1881:Part 110:1983. For each mix, four 100 mm cubes were cast (in accordance with the requirements of BS 1881:Part 108:1983).
7) The cylinders were filled in four layers, with compaction on a vibrating table for 60 seconds for each layer. The cubes were filled in two layers, again with vibration between each addition.
8) The concrete was cured under wet hessian and polythene for 24 hours after mixing.

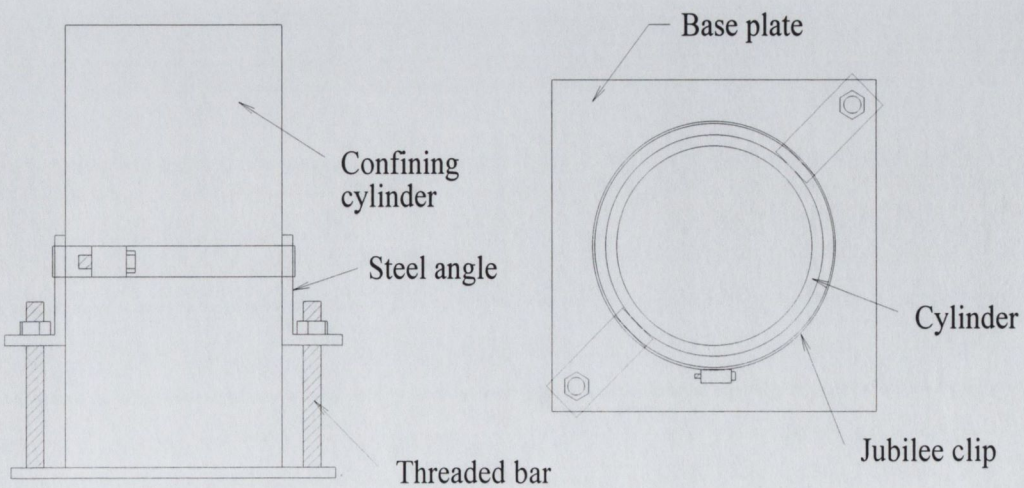


Figure 4.6 Dogging system for casting confined cylinders (schematic)

9) The unconfined cylinders and the cubes were then de-moulded and put in a curing tank at 20° ± 1° c for the following six days. The confining sleeves of the steel and aluminium cylinders were painted with a waterproof lacquer, prior to being placed in the tank, to prevent corrosion caused by the alkaline water.

10) The cylinders and cubes were removed from the curing tank at 7 days and two of the cubes were tested. The remaining cubes and the cylinders were stored in the laboratory at approximately 20° c for the remainder of the time before testing. This duration varied between 1 and 3 months and depended on the problems encountered with the testing equipment. However, the changes of the properties of the cylinders would have been very minor over this period as the curing had ceased and the cylinders had dried out fully before any were tested.

4.2.5. Static test results

For each batch of concrete, two of the four cubes were tested to failure at 7 days in a 300 tonne Losenhausen static testing machine. The other cubes were tested at 28 days to determine the density, longitudinal pulse velocity, and compressive strength of the concrete.

The density measurements were made in accordance with BS 1881:Part 114: 1983, by determining the air dried mass of each of the concrete cubes and then its volume by digital vernier calliper measurement, to within 0.01 mm. The longitudinal wave velocity, c_0, was determined using an ultrasonic pulse velocity test. Ultrasonic pulse velocities, c_L, were measured in accordance with BS 1881:Part 203:1986 for each of the cubes. A Pundit ultrasonic testing machine, with transducers operating at 50 kHz, was used to generate longitudinal ultrasonic vibrations in the concrete. After careful calibration of the equipment with a reference bar, the transducers were placed at opposite sides of the concrete cubes. A very thin layer of thick petroleum jelly was used at the contact points to ensure a good ultrasonic coupling. The time of transmission was divided by the path length, which was measured using a digital vernier callipers to an accuracy of ±0.01 mm, to give the pulse velocity. Equation (2.34) allowed the determination of the Young's modulus of elasticity of the material, which was used in equation (2.17) to determine the speed of elastic wave propagation, c_0, through the concrete. The cubes were then tested

	No. cyls.	Mass (kg)	Density (kg/m^3)	c_L measured (m/s)	Young's modulus (kN/mm^2)	c_0 calculated (m/s)	Strength (N/mm^2)
U(100)	10	2.27	2270	4535	41.0	4240	45.0
C(114)S (1.2)	10	2.30	2300	4620	43.0	4320	51.0
C(114)S (3)	16	2.30	2300	4600	42.5	4300	48.5
C(114)S (5)	10	2.29	2285	4795	46.0	4485	47.0
C(114)S (6.5)	10	2.25	2250	4650	42.5	4350	52.0
C(115)A (3.25)	10	2.29	2295	4525	41.0	4230	50.0
C(110)P (3.6)	10	2.25	2250	4660	42.5	4360	50.5
R(114)S (3)	6	2.28	2280	4505	40.5	4210	48.0
R(115)A (3.25)	5	2.28	2280	4425	39.0	4135	45.5
R(110)P (3.6)	5	2.28	2280	4425	39.0	4135	45.5
U(162)	3	2.31	2310	4475	40.5	4185	40.0
C(168)S (3)	3	2.28	2280	4505	40.5	4210	48.0

Table 4.3 Static test results at 28 days (average of results from two cubes)

for compressive strength according to BS 1881:Part 116:1983 in a Losenhausen Static machine, at a rate of 0.2-0.4 $N/mm^2 \cdot s$. The results of these static tests can be found in Table 4.3. A total of four of the cubes, selected at random, were strain gauged both laterally and axially (using a method described in the following section) at mid-height prior to being statically loaded. The results were used to determine Poisson's ratio for the concrete, which was found to be 0.21.

4.2.6. Cylinder instrumentation

The deformational response of the impacted cylinders was determined using strain gauges attached to the sample surface both laterally and axially. Four gauges were attached to each of the unconfined concrete cylinders, longitudinally and laterally, diametrically opposite each other at mid-height. These were Pl-90-11 electrical resistance strain gauges, manufactured by Tokyo Sokki Kenkyujo Co. Ltd. (TML). They had a nominal resistance of 120 ± 0.3 Ω and a gauge length of 90 mm, which was, in accordance with BS 1881: Part 206: 1986, greater than four times the maximum aggregate size used in the concrete. They were applied, according to the manufacturer's specifications, to the slightly roughened surface of the concrete cylinders, at least 24 hours prior to testing.

The response of the sleeved cylinders was determined using up to 25 strain gauges attached to the outer skin circumference of the confining sleeve. The gauges were fabricated by the Measurements Group and were C-930519-M, which had a resistance of 350 ± 0.3 Ω. These gauges were attached to the slightly roughened, but well cleaned sleeves, as advised by the manufacturers. Each of the gauges used was paired to another identical "dummy" gauge, mounted on a solid block, which formed part of a half Wheatstone bridge network. The cylinders had slightly different gauge configurations,

- One cylinder from each series was gauged on three equally spaced axes (at angles of 120° to one another), at three heights (at 10 mm from the top, at the mid-height and at 10 mm from the base of the cylinder), with lateral and axial gauges (Figure 4.7).
- A second cylinder was also gauged on three equally spaced axes. Two of the axes were gauged as previously described, and the third axis was gauged with lateral and axial gauges at five heights, at 10 mm and 50 mm from the top, at the mid-height and at 10 mm and 50 mm from the base of the cylinder.
- The rest of the cylinders in each of the series were gauged, laterally and axially at three heights on one axis, at 10 mm from the top of the confinement, at the mid-height and at 10 mm from the base of the cylinder.
- The cylinders with a reduced length of confinement were also gauged on one axis, at 10 mm from the top, at the mid-height and at 5 mm from the bottom of the confining sleeve (10 mm from the base of the cylinder), with axial and lateral gauges.

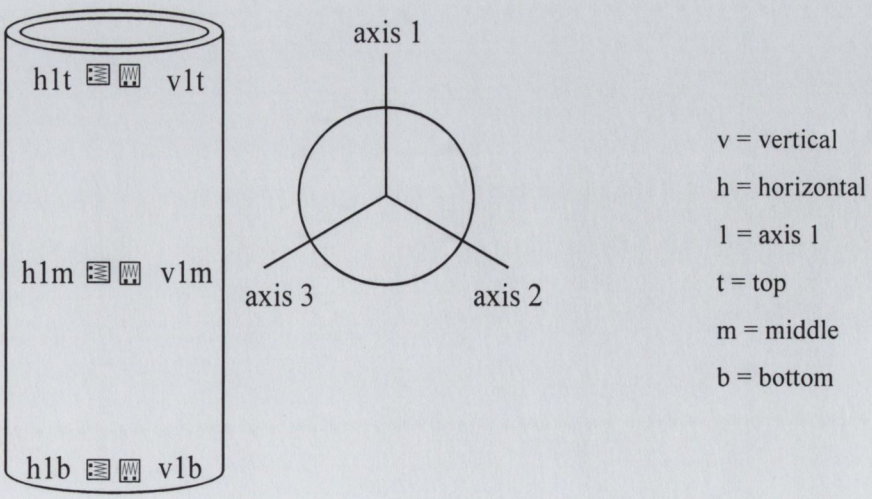


Figure 4.7 Gauge location on sleeved cylinder

4.3. MEASUREMENT OF CONTACT FORCE

Much of the work reported in the general area of impact loading has involved attempts to quantify the apparent increases in the strength of the impacted materials, when compared to their static strengths. This can either be determined qualitatively, by visual inspection and other post-event assessment techniques, or quantitatively, by measuring transient effects, such as the contact force at the time of impact. In the present study, a 'contact-force' loadcell is incorporated in the impactor between the tapered lower end and the endstriker (Figure 4.4 and Figure 4.8). This loadcell allows the forces at the time and location of impact to be found. It was necessary to design and fabricate a loadcell which would be sufficiently tough to withstand many severe impacts, yet sensitive enough to measure the contact force accurately.

The loadcell consisted of a hollow cylinder of hardened EN24 tool steel, with an internal diameter of 50 mm and a 4.5 mm wall thickness, as shown in Figure 4.9. It was 65 mm high, with 10 mm chamfered flanges at either end to allow its incorporation into the impactor, using stainless steel fixing bolts, nuts and washers, shown in Figure 4.10. Two contact force loadcells of identical dimensions were fabricated. The first was hardened, after machining, to 34.5 on the Rockwell C scale. The second, which was heat treated after the first loadcell failed, was hardened to 40 Rockwell C which, although it was slightly more brittle, gave it greater strength. The loadcells were strain gauged laterally and axially on their external faces using electric resistance strain gauges manufactured by Tokyo Sokki Kenkyujo Co. Ltd. (TML) of type QFCB-6·350. The eight gauges, each with a 350 Ω resistance, were bonded to the steel cylinder following the manufacturer's instructions and were wired to form a full bridge network. The resulting loadcell, in its housing, was calibrated statically in a Losenhausen testing machine (Figure 4.11). Each of the calibration tests were repeated four times, and a regression analysis with a 99 % coefficient of correlation showed that there was less than 0.05 % difference between the four calibration tests for each loadcell.

The initial loadcell failed after approximately 70 impact tests and, although the strain gauges were not broken, and its static behaviour remained constant, the dynamic properties of the loadcell changed considerably, possibly as a result of a hairline fracture to the steel hollow cylinder. The second was heat treated, gauged in an identical manner to

the first, and calibrated. There was approximately 0.25 % difference in the calibration factors. Both loadcells were re-calibrated during the testing period and, except when the loadcell broke, the calibration factors remained constant throughout.

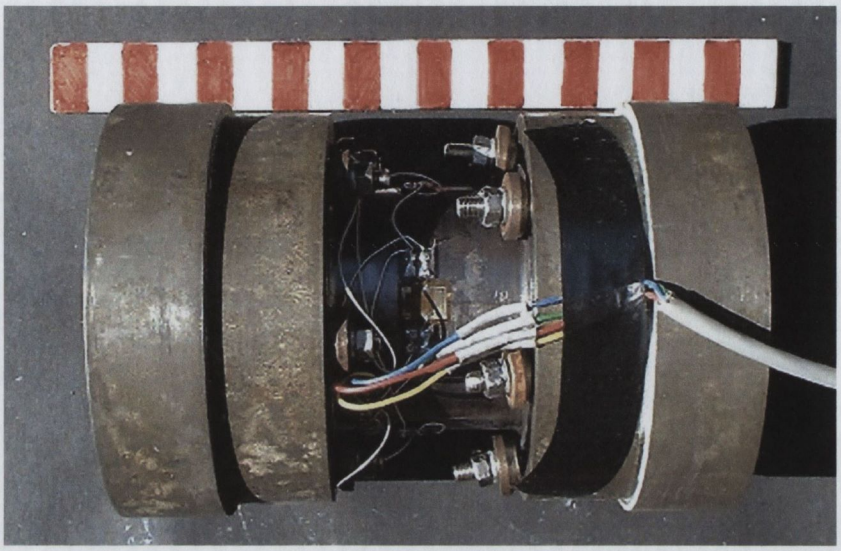


Figure 4.8 Photograph of impactor loadcell

The bar in the photograph is marked in units of 10 mm

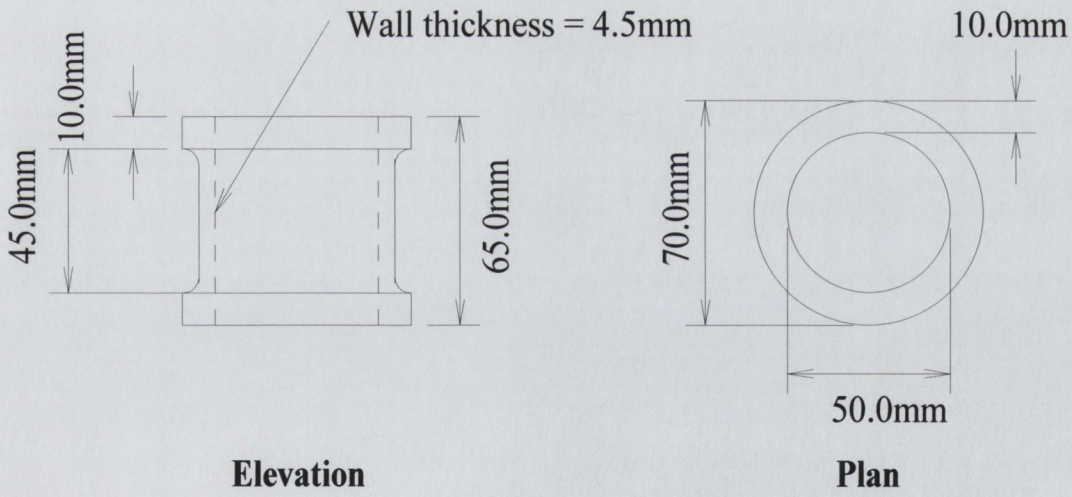


Figure 4.9 Hollow cylinder for impactor loadcell

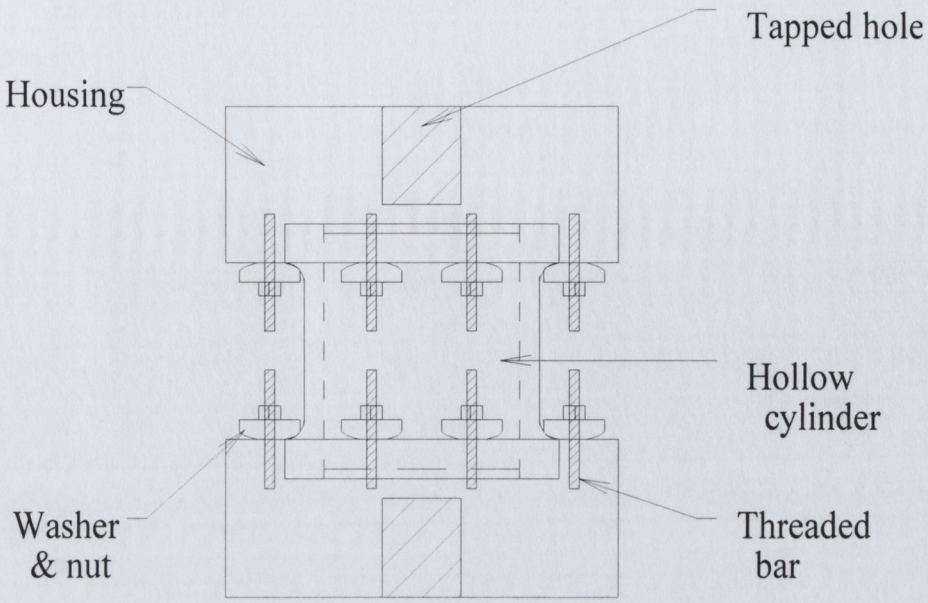


Figure 4.10 Housing for loadcell to facilitate attachment to impactor

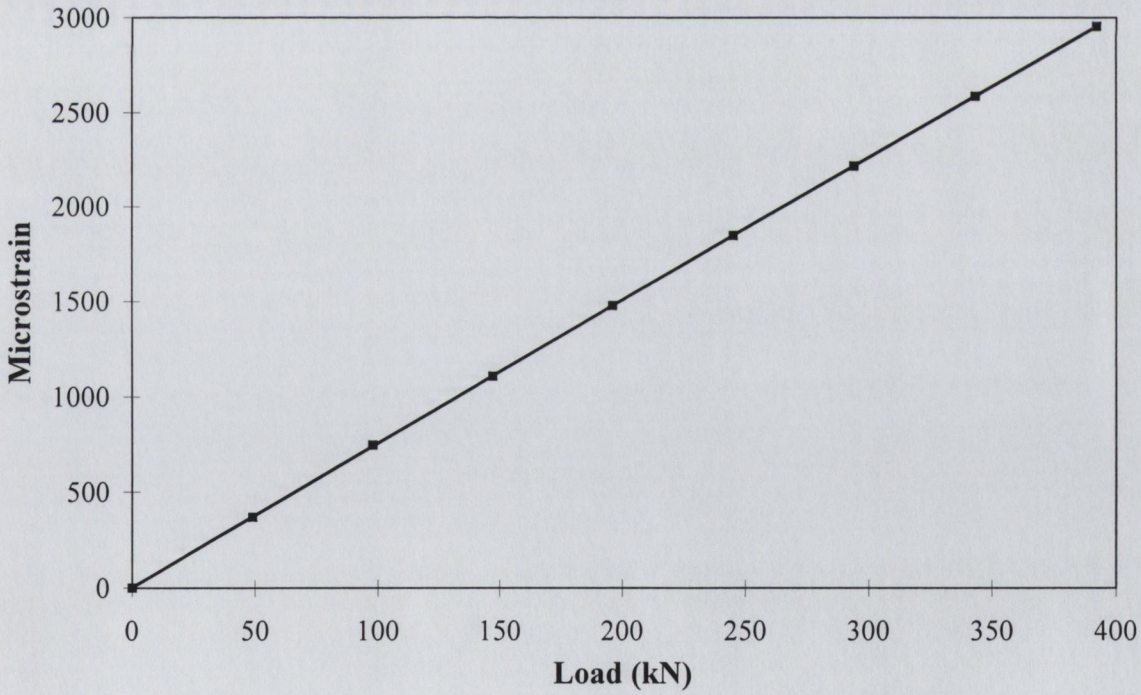


Figure 4.11 Calibration chart for impactor loadcell

4.4. STRESS MEASUREMENT

Traditionally, stress has been measured by placing a loadcell in series with the specimen. At constant rates of strain, for example when statically loaded, the loadcell can be placed either on top of or below the specimen. However, as shown experimentally by Chung (1978) and theoretically by Bischoff and Perry (1991), a loadcell which is placed at the location of impact, in this case at the top of the specimen, can overestimate the stress due to inertia effects. This effect is unimportant at constant, low strain rates, but is thought to become significant at higher strain rates than, perhaps, 10^{-1} sec^{-1}, which occur during impact loading. These effects can be eliminated if the loadcell measuring stress is placed at the bottom, or unloaded end of the specimen.

At rates of strain above approximately 10 sec^{-1}, stress wave propagation in the material must also be accounted for when interpreting test results. In order to obtain an accurate picture of the stress-strain response of the specimen, account must be taken of the time differences between measurements at different points. Similarly, as explained in section 2.4.5, when a wave travelling through a body meets a discontinuity, both reflection and transmission are experienced due to the impedance mismatch, which makes it increasingly difficult to determine the stress in the material. A conventional loadcell, suitable for measuring static loads, typically has an aspect ratio of at least one. If this is placed beneath the specimen, the resulting stresses which it measured could easily be misinterpreted, as a result of difficulties in defining the impedance values at the interface and because of stress wave oscillations within the loadcell.

A stress wave propagates through a body at a finite speed and is reflected at a boundary. A large number of oscillations occur within a thin body when compared to the number in a long body of identical material. If a very thin loadcell is placed beneath the impacted specimen then there will be many reflections within that body due to a transmitted wave, before the wave reflected from the top of the specimen causes interference. Equilibrium is quickly reached in the loadcell and it can be used to measure the stress in the specimen accurately (Perry and Bischoff, 1990).

Three 'base-plate loadcells' were used during the impact testing, each of which consisted of two 5 mm thick aluminium plates, between which commercial manganin gauges were sandwiched. This resulted in a 10 mm thick loadcell, one twentieth of the length of the specimen in which the stress was being measured. The plates were made from a high strength aluminium alloy (type 6082T6) and were carefully ground to ensure that the two sides were parallel. One plate was square, to which the gauges were attached (as can be seen in Figure 4.12) and which, when in contact with the test cylinder, protected the gauges from debris during the impact. The other plate was circular, of the same diameter as the length of the sides of the square plate. The three loadcells had different diameters, one had a diameter of 100 mm for the unconfined cylinders, a second had a 115 mm diameter and was placed beneath the confined cylinders, and a third, of diameter 110 mm was used to test the cylinders with a reduced length of confinement.

Manganin is a copper-manganese-nickel alloy which has a low strain sensitivity compared to its sensitivity to hydro-static pressures and its resistance change as a function of applied pressure is linear to very high pressures. It is commonly used to measure high-pressure shock wave propagation. Thin gauges fabricated from manganin foil can, therefore, be used to provide direct and accurate measurements of the stress-time history. The gauges used were manufactured by Measurements Group, Inc., and were LM-SS-210FD-050 / SP60. They were of 50 Ω resistance, and were encapsulated in a glass-fibre-reinforced epoxy-phenolic, approximately 0.025 mm thick, with only their tab ends exposed for

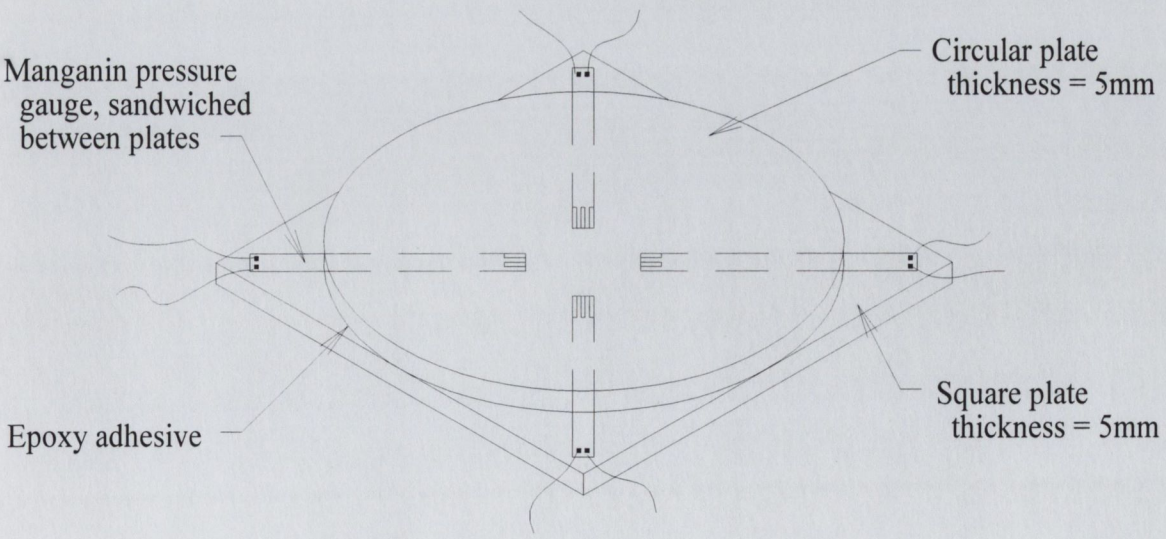


Figure 4.12 Base-plate loadcell (inverted)

soldering. The active grid measured 5.33 × 6.35 mm, the gauges had a tab length of 57.15 mm, and a nominal pressure sensitivity of 0.27 % per Mpa (0.0027 ohm/ohm/Mpa). The four gauges were wired in series, to form a single resistance and this was balanced by a resistor, situated away from the loadcell, to form a half Wheatstone bridge network.

The gauges were placed symmetrically on diagonals on the square plate. The loadcells were sensitive to variations in pressure distribution as the total active gauge area was small in comparison to the area of each of the plates (Table 4.4). In order to achieve consistent measurements, it was necessary to bed the loadcell well in 1mm of plaster prior to testing or calibration. The loadcell was also bedded onto a cylindrical aluminium billet, of the same diameter as the lower, circular plate, which provided solid restraint and minimised flexure in the loadcell. Hence, prior to testing, the trowelled face of the cylinder was bedded in plaster onto the square plate of the loadcell. This was, in turn, bedded by its lower surface onto the aluminium billet, and then onto the concrete test base (Figure 4.13 and Figure 4.14). The presence of the plaster had a second, equally important, function as it acted as a capping material for the slightly uneven trowelled surface of the cylinders. Stress concentrations can arise when cylindrical specimens, which always have one trowelled end, are tested and the three options for overcoming the ill-effects of an uneven end surface of the cylinder include capping, grinding and packing, the third of which is not recommended. The option of using dental plaster as a capping material was selected, as it increased the consistency of the measurements and was easier to achieve than grinding the specimens. If the cylinder is capped with a suitable material, such as high strength dental plaster, it does not adversely affect the strength of the cylinder and allows a uniform distribution of stress over the cross section to be achieved (Neville 1995). Furthermore, Atchley and Furr (1967) examined using different capping materials in a series of impact tests on concrete cylinders and concluded that the type of capping material used did not affect the results.

	Diameter (mm)	Area (mm^2)	Gauge area (%)
Small plate	100	7854	1.72
Plate for reduced confinement	110	9331	1.45
Large plate	115	10387	1.30

Table 4.4 Specifications of base-plate loadcells

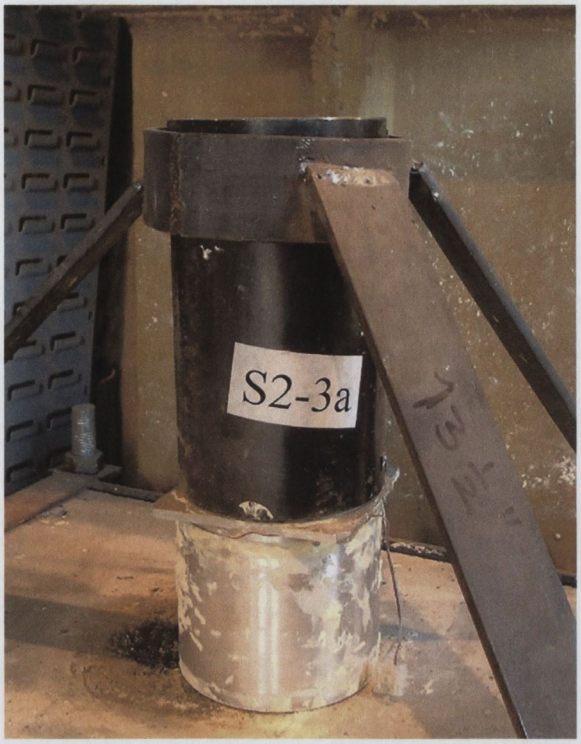


Figure 4.13 Photograph of the confined cylinder prior to being tested showing base-plate loadcell and aluminium billet

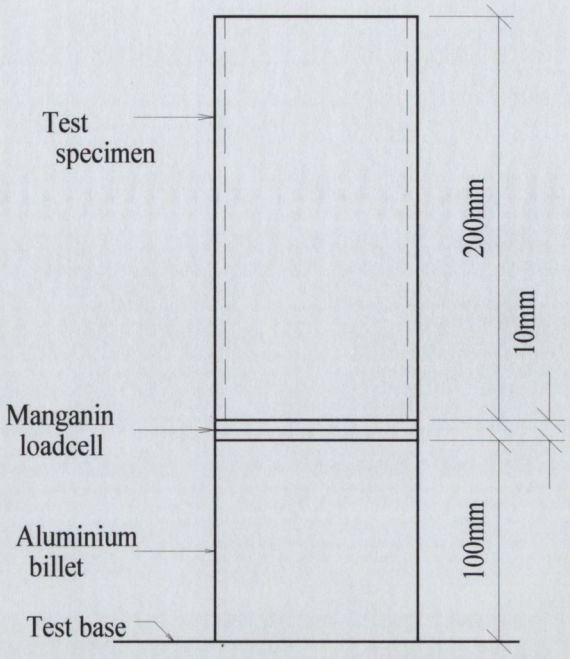


Figure 4.14 Base-plate loadcell and confined cylinder (schematic diagram)

The plaster chosen for bedding was a fast setting, hard dental plaster, Kaffir-D, which had a setting time of 5-7 minutes, with a water-plaster ratio of between 0.24 and 0.29. However, the plaster was allowed to cure for 20 minutes prior to testing, because Pundit testing showed that after 18 minutes, the speed of wave propagation through the cured plaster reached a plateau, and even a considerably longer curing period did not reduce the wave propagation speed further.

Considerable complications were experienced in the fabrication of the base plate loadcells, because of difficulties in finding a suitable method of bonding the two aluminium plates. Initially a standard cold cure epoxy (Araldite) was used to bond both the strain gauges to the square plate and to bond the two plates together. However, when this loadcell was loaded statically to produce a calibration curve it exhibited hysteresis and was, therefore, unsuitable for use as a loadcell. It is probable that, as the adhesive was very viscous, the epoxy-filled gap between the two plates was quite large and that this thickness of adhesive resulted in a plastic response.

Following advice from the strain gauge manufacturers, a special heat curable epoxy adhesive was then used, Measurements Group M-Bond 610 adhesive. This two part adhesive (resin and curing agent) was pre-mixed prior to application to the gauges and plates, and was then heat cured for two hours according to the manufacturer's instructions. Although this resulted in a thin loadcell which provided a linear calibration curve, its response to impact loading was less good. After two impact tests the brittle epoxy de-laminated, separating the plates and severing the strain gauges. This particular adhesive was used to make a second loadcell with Kapton film (0.001 mm shim), between the plates, but it failed in a similar manner to the first. The loadcell was then re-fabricated using an anaerobic adhesive (Loctite 326, with activator N). This tough structural adhesive was used to first bond the gauges to the square plate, and then was poured on to the circular plate. As it was extremely viscous, it was heated with a low flame on a gas torch to ensure that it covered the entire plate. The square plate was sprayed with activator prior to the plates being sandwiched together, and the gauges themselves acted as a consistent spacer between the two plates to prevent misalignment. This adhesive provided a highly reliable and repeatable method of bonding the two plates.

This method was then used to fabricate three base-plate loadcells which could be used to measure the stresses at the bases of cylinders with different diameters and a subsequent pair of large and small loadcells when the initial ones had failed. A photograph of the large base-plate loadcell is shown in Figure 4.15. In one case, the failure was as a result of flexure when the impactor rebounded and re-impacted the sample which had become misaligned after the initial impact and, in the other case, the second impact drove the steel confining cylinder down onto and through the loadcell, much like metal forming.

Each of the loadcells was calibrated statically in the laboratory using a Losenhausen static testing machine, with the loadcell bedded in dental plaster to both the loading platen and the solid aluminium billet (Figure 4.14). Rosenberg *et al* (1980, 1983) showed that if the aspect ratio of the epoxy layer is less than 0.5 %, as it is in the case of the loadcells manufactured for the current research, that the loadcell will experience uni-axial strain during static loading, and that it is possible to use a static calibration factor for impact loading. Each loadcell was calibrated four times and, although there was a 5 % variation in the calibration constants for different loadcells, a regression analysis with a 99 % coefficient of correlation showed that the results were consistent for each particular

loadcell. The calibration chart for the first large base-plate loadcell, which is typical of the other calibration curves, is shown in Figure 4.16. The loadcells were re-calibrated during and after testing and showed no variation in their calibration curves.

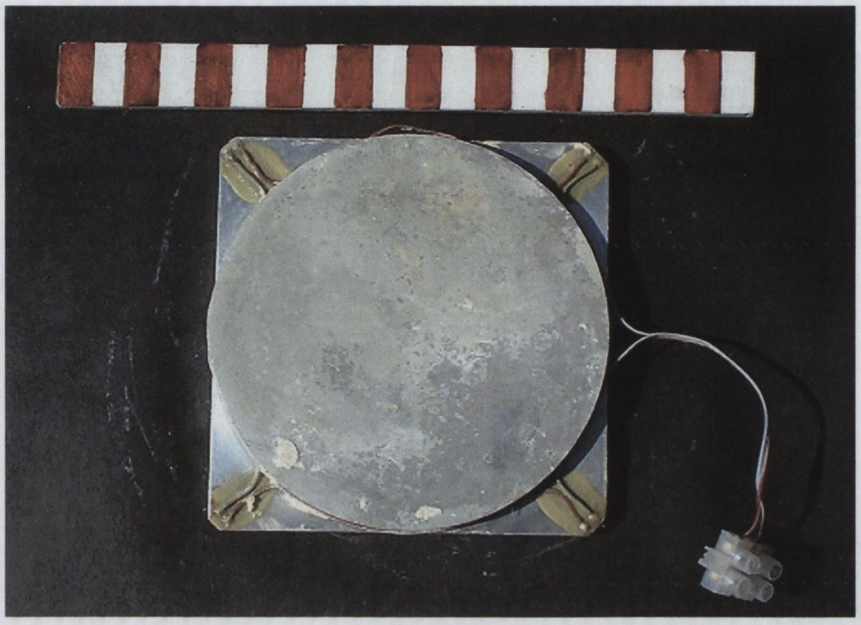


Figure 4.15 Photograph of large base-plate loadcell

The bar in the photograph is marked in units of 10 mm

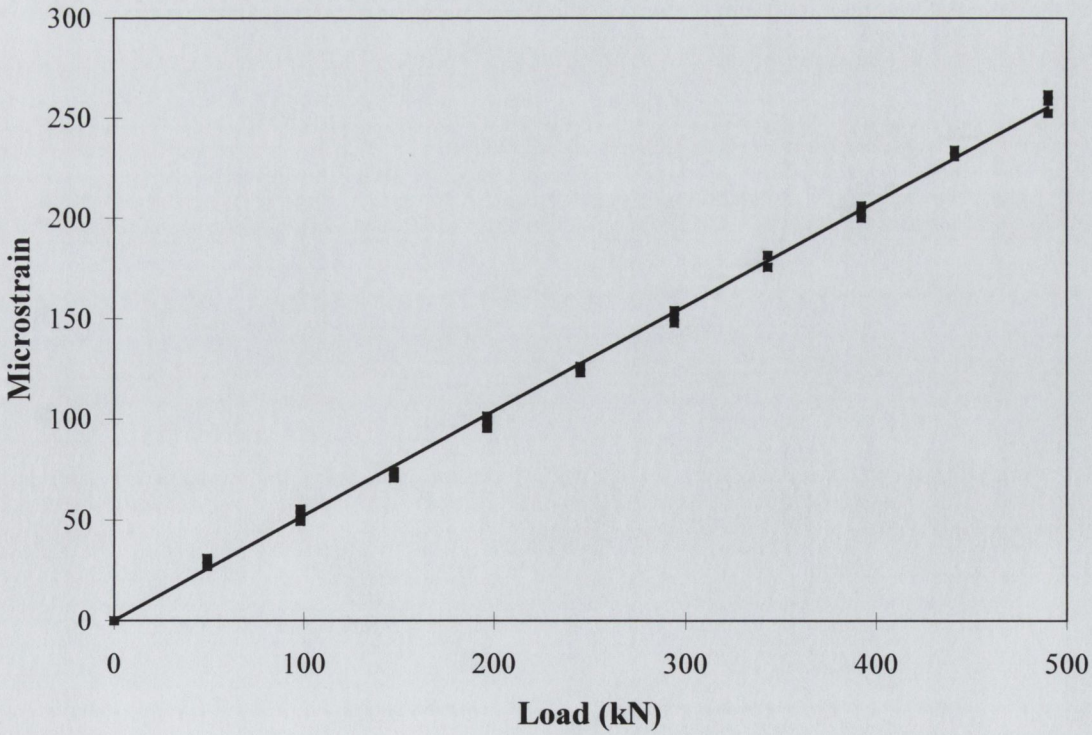


Figure 4.16 Calibration chart for first large base-plate loadcell (showing results from all four calibration tests and best fit line)

4.5. DATA ACQUISITION AND PROCESSING

The data acquisition system used was selected because of its ability to acquire accurate information from many channels at very high rates, within the short duration associated with impact loading. As can be seen from Figure 4.17, the system consisted of four parts, namely (1) the transducers, the strain gauges and the loadcells, which necessitated acquiring information from up to 27 channels simultaneously; (2) a signal conditioning system, which kept noise to a minimum while completing strain gauge Wheatstone bridges and amplifying and filtering all of the signals; (3) a data acquisition card, which multiplexed and converted the signal from analog to digital; and (4) a computer which used software to control the acquisition process, store the information during the test and then process the results.

A data acquisition system from National Instruments was chosen, which comprised a SCXI signal conditioning system, involving a chassis and conditioning modules, matched with a data acquisition card, designed for high accuracy analog input, fitted in a standard Pentium desktop computer.

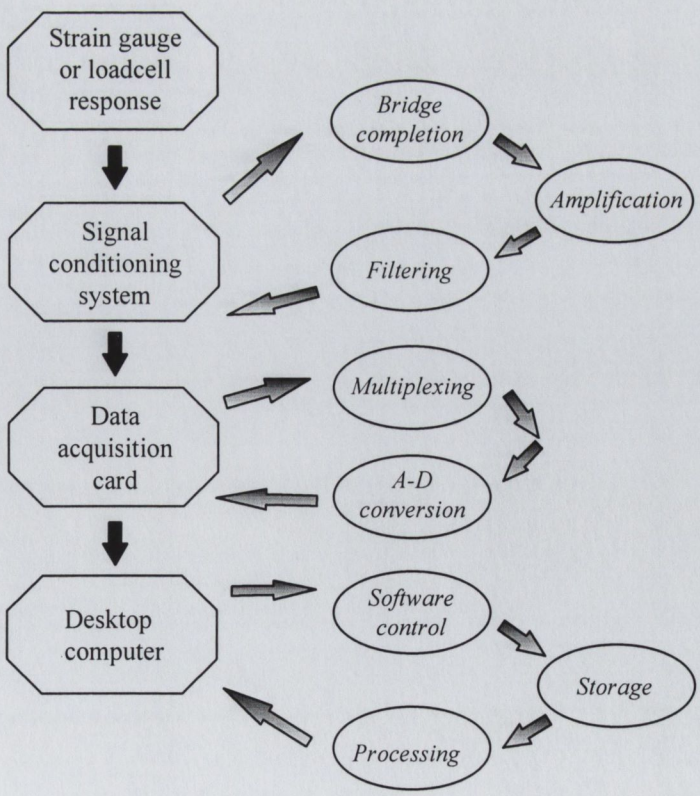


Figure 4.17 Data acquisition and processing

The SCXI 1001 chassis, operating on AC, with a maximum capacity of 32 channels, formed a rugged housing for signal conditioning modules, with shielded terminal blocks attached. The signals from the strain gauge transducers and the base-plate loadcell, paired to their "dummy" gauges, and the full-bridge contact force loadcell, were wired into screw terminals in SCXI 1321 terminal blocks. Each terminal block allowed offset nulling and shunt calibration of up to four strain gauges. The terminal blocks were plugged into SCXI 1121 signal conditioning modules, providing separate channel isolation amplifiers with excitation for each of the inputs. The strain gauge signals was amplified individually by 1000 and the loadcells signals by 500. All of the signals were excited with 3.33 volts using the in-built module voltage generation and were subject to a 10 kHz lowpass filter, to remove any extraneous noise. The filter, gain, completion network and excitation in the SCXI modules were controlled manually using jumpers. The signals from the modules were subject to a 0.15% error in the maximum reading.

The chassis was wired to a data acquisition card, of type PCI-MIO-16E-1, which multiplexed and then converted the signal from analog to digital, prior to writing it to the RAM of the computer. The maximum speed of the card was 1.25 Msamples per second (10^6 samples per second), however, a sampling rate of 30 ksamples/sec (10^3) was chosen. This was because the actual sampling rate is determined by how fast the card can combine or multiplex the signals, and is found by dividing the maximum rate by the number of channels. Sampling theory requires a minimum of two samples per cycle to properly define the maximum frequency of a digital signal and to prevent aliasing. This occurs if frequencies above the maximum limit are present in the original signal, and causes distortion, as these higher frequencies appear to be at a lower frequency, rather than at their true frequency. The Nyquist frequency is the maximum frequency which can be measured from a digital signal and can be determined from the rate at which data is sampled. If the time interval between samples is Δ, then the Nyquist frequency is $1/2\Delta$. A scanning rate of 30 ksamples/sec means that there is 33 microseconds between each sample point, and that the Nyquist frequency is 15 kHz. As the signals are previously subject to a 10 kHz lowpass filter, this ensures that for the system used the Nyquist frequency cannot be exceeded. The resolution of the card's analog to digital converter which controlled its precision was 12 bits. The voltage ranged between -3.33 and 3.33 which was divided into 4096 equal parts (2^{12}). This resulted in a quantisation error of 0.1% of the full scale on any one of the signals. The settling time, or the minimum time

which must be allowed for the data acquisition card to switch between signals whilst multiplexing, at a gain of 1000 and a sampling rate of 30 ksamples/sec, is 2 μs. As the scanning rate is 30 ksamples/sec on each of the channels, this did not have an effect on the present system.

The data acquisition card was fitted into a PCI slot of a Pentium 200 desktop computer, with 32 Mbytes of RAM. The entire data acquisition process was controlled by two software programs, NiDAQ 6.1 and LabVIEW 4.0, both supplied by National Instruments.

The NiDAQ software provided the device drivers for the hardware in the data acquisition system. This involved managing the DMA (Direct Memory Access) between the data acquisition card and the RAM of the computer and the configuration of the SCXI units, including the software controls for the gain and filter on each channel.

The application software, LabVIEW, was used to integrate the instrumentation hardware with the computer using a graphical programming system, allowing *virtual instruments* to be created to control data acquisition and analysis. The application consists of a graphical front panel user interface and a block diagram which specifies the functionality of the items in the front panel using a series of block diagrams with subroutines linked using wires. The program is compiled prior to execution which generates optimised code allowing maximum execution speeds. LabVIEW also incorporates sophisticated high speed data buffer management, which allows continuous or circular data acquisition. As information is read into the buffer through DMA operations from the card, the program pulls data out of the buffer for processing, which can include saving to disk or updating screen graphics. When the buffer is full, the DMA operation re-initialises to the beginning of the already cleared buffer, as shown in Figure 4.18. This means that continuous data acquisition and processing can be sustained indefinitely, assuming that the program can retrieve and process data faster than the buffer is being filled.

Two programs were written in LabVIEW to control the data acquisition and storage of the transducer responses from each of the impact tests. The first of these, "Impact Data Acquisition", a diagram of the front panel of which can be seen in Figure 4.19, was used to acquire data. It was necessary that this program could both control the acquisition at

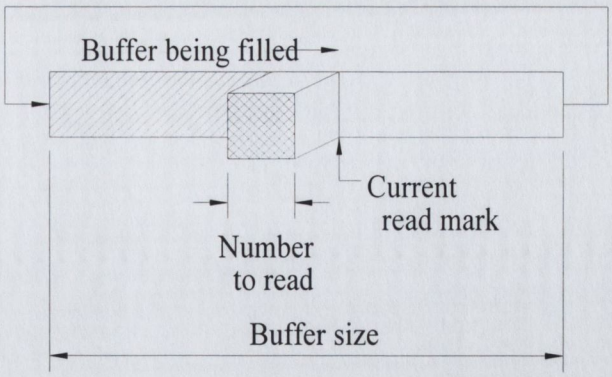


Figure 4.18 Circular buffer created for data acquisition by LabVIEW

very high rates and store the data. Information was inputted, prior to testing, on the file in which the test results would be stored, and on the channel and device information for the SCXI hardware. The speed of acquisition (or scan rate), the buffer size and the number of scans to be written to the file at any one time were also entered. It was necessary to set these rates to ensure that the buffer would not be overwritten during the acquisition period. The maximum number of scans to write was set to zero to ensure continuous acquisition until the stop button had been depressed. The only information written to the screen during the test period gave details of the total number of scans written to the file and the total backlog of scans in the buffer. Because of the high speed of acquisition, the program was not able to update the screen display without causing a buffer overwrite during the test, hence, the graph was only updated after the test. Figure 4.20 shows the block diagram programming for "Impact Data Acquisition". The while loop controled the information read to and taken from the buffer, as illustrated in Figure 4.18. The left hand side of the block diagram controls the initialisation of the program and the right concerns the writing of the information to file and the display of the graph.

The program ran for the entire duration of each impact test and, therefore, collected information for 5-7 seconds, and wrote it all to a binary file. As the information on the actual impact lasted for a maximum of 10 milliseconds, it was necessary to write a second program "Convert" to select the useful information, from somewhere in the 150×10^3 - 210×10^3 scans, and to write it to a decimal file. The front panel of "Convert" is shown in Figure 4.21. It reads in the rows and columns from the binary file and displays a graph of all the results.

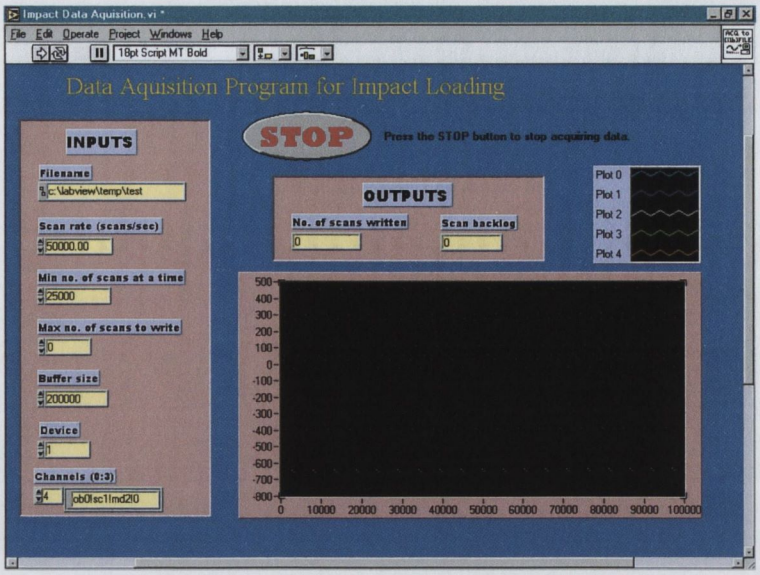


Figure 4.19 Front panel of "Impact Data Acquisition"

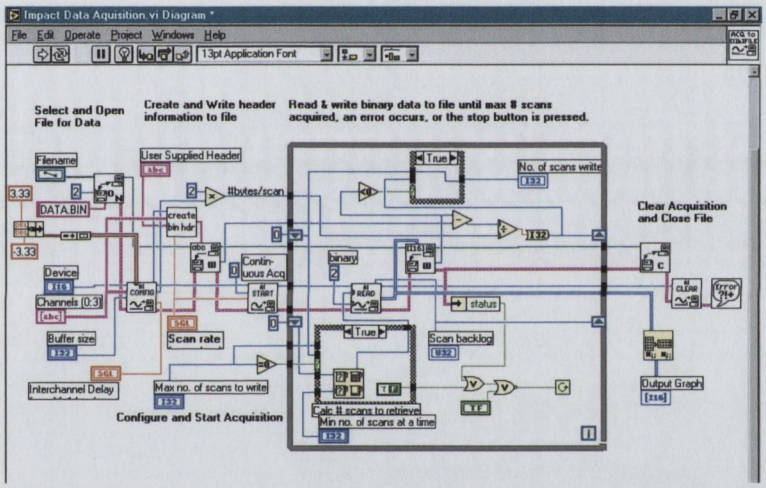


Figure 4.20 Block diagram of "Impact Data Acquisition"

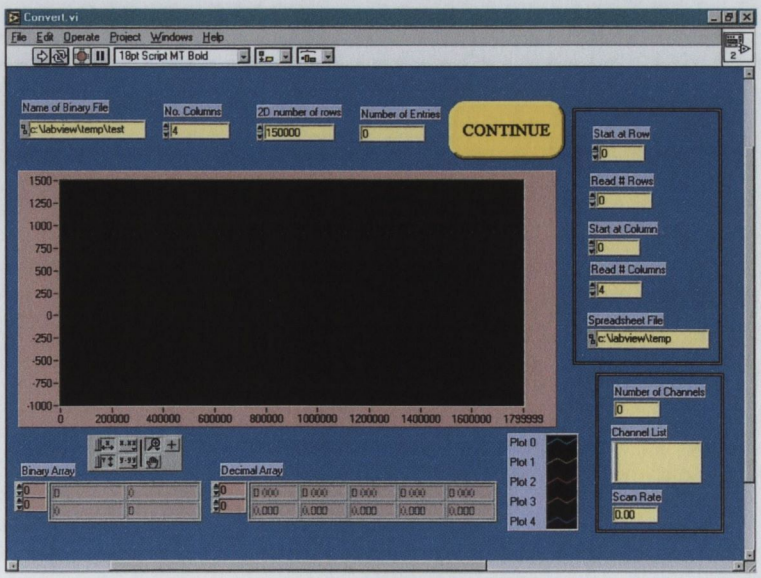


Figure 4.21 Front panel of "Convert"

The user can zoom in on the relevant part of the graph, the required rows and columns can be selected, and the program writes the selected information to a new file. The decimal file generated can be opened as a spreadsheet file, as tab-delimited text, for analysis. Although this method of acquiring data resulted in a lot of unnecessary information being collected it was a very effective way of data acquisition as, except in the rare case of the buffer being overwritten, the response of the bodies during the collision was not missed. Furthermore, information about the impactor rebound was also obtained which could be stored for subsequent analysis.

The final stage in the data processing involved converting the numbers recorded by the system into units of microstrain for further analysis. The system was, consequently, calibrated in the laboratory by loading a strain-gauged solid steel cylinder and using another calibrated system with units in microstrain. The results of the already calibrated system were equal to the calculated values for strain in the cylinder at a given load and were used to produce Figure 4.22, the clearly linear graph of SCXI units against microstrain.

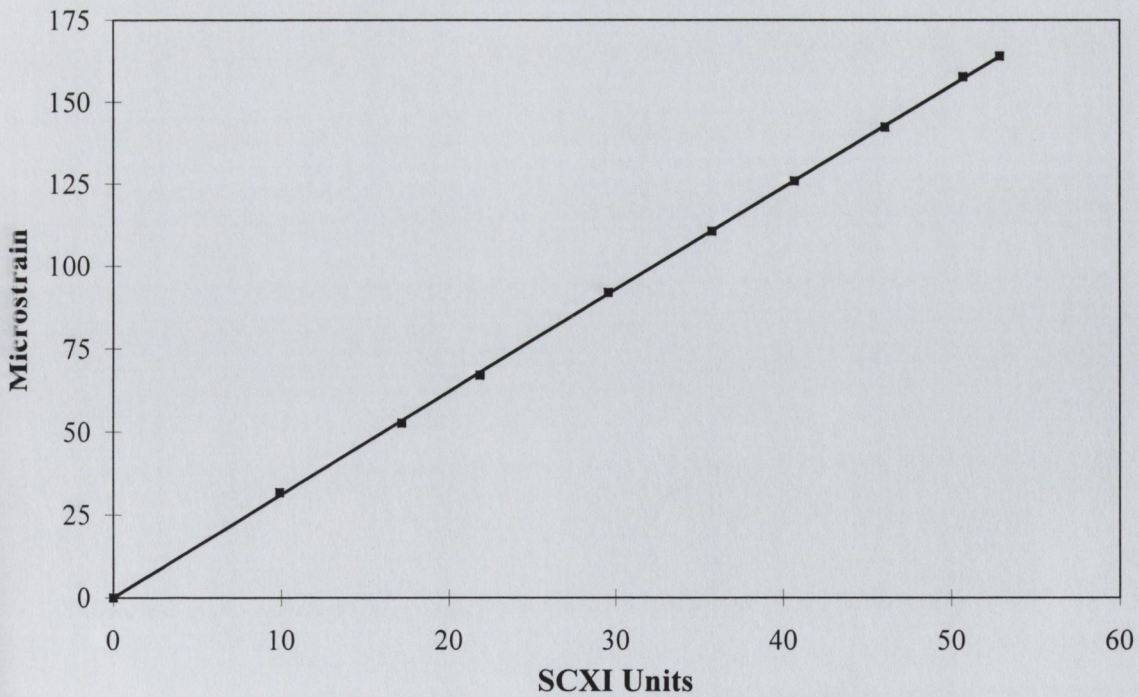


Figure 4.22 Calibration chart for SCXI units

4.6. TEST PROCEDURE

The impact of both confined and unconfined concrete cylinders was achieved by dropping a heavy steel mass at velocities of up to 6.3 m/s. Information from strain gauges and loadcells was acquired using a sophisticated data acquisition system and computer. The following, standard test procedure was used for all of the tests performed.

1) The cylinders were loaded axially, with care taken to prevent eccentric loading, by bedding it on to the solid concrete test base.
    - The circular side of the base plate loadcell was bedded on to a 100 mm long aluminium billet with a 1 mm layer of dental plaster with a water-plaster ratio of between 0.24 and 0.29.
    - The trowelled face of the cylinder was bedded to the square side of the loadcell with a similar layer of plaster.
    - Dental plaster was then placed on the base of the aluminium billet and the specimen was located directly beneath the impactor, with the impactor itself being used as a guide.
    - The plaster was allowed to set for at least 20 minutes.
    - A safety frame was placed around the cylinder and bolted to the concrete block (as shown in Figure 4.13).
2) The data acquisition system was allowed to warm up for 20 minutes prior to being used.
3) The NiDAQ configuration utility was run to set up the device drivers for the channels required during the acquisition.
4) The LabVIEW program 'Impact Data Acquisition' was then opened. Information about the file name, scan rate, buffer size and channel inputs required were entered.
5) The impactor was then winched by hand to the correct height, either 0.5 m, 1m or 2 m, depending on the test.
6) The safety pin in the quick release mechanism was removed and a large polystyrene block was placed around the impact area, to contain fragments of concrete during the test.
7) The LabVIEW program was started.

8) The impactor was released by pulling on the quick release mechanism handle, allowing it to fall on the specimen directly below. There was no braking system attached to the impactor, so a rebound occurred when a specimen was impacted, which, whilst it did not interfere with the initial impact, was also captured by the data acquisition system.
9) Immediately after the test the data acquisition program was stopped and the results were post-processed using the program 'Convert'.
10) The decimal results were then analysed on the hard-drive of the computer using an Excel spreadsheet.

5. EXPERIMENTAL RESULTS FROM IMPACT TESTS

5.1. INTRODUCTION

In excess of ninety impact tests were performed on cylinders of concrete with different types of confining sleeve. The experimental work on these cylinders was split into two groups. The larger group, which was undertaken first, included impact tests on six series of cylinders with different types of confinement, namely four thicknesses of steel, aluminium and UPVC plastic and an unconfined reference series. For simplicity, each of these test series was further broken down into three groups of cylinders, and tested at one of three different velocities by dropping the impactor from different heights, with a varying number of repeats in each group. The second, subsequent group of tests included statically loading confined and unconfined cylinders, on cylinders with a larger diameter than those tested in the main test series, on cylinders whose sleeves were not restrained at the base and impact tests where the impactor was repeatedly dropped on a particular cylinder.

Due to the density of information generated by the tests, particularly those in the main test group, the analysis performed on the results has been broken down into different sections, which are analysed separately in this chapter.

The contact force was measured using a loadcell integrated into the falling impactor and plots of its response against time are given in Figure 5.1 to Figure 5.7. A summary of the results, including the average value for each velocity group and its coefficient of variation are given in Table 5.1. A reduced factorial analysis of the contact force results is undertaken using analysis of variance techniques to assess the significance of various factors associated with the impact tests. This section also includes an analysis of the results with respect to the contact velocities at impact and the impulse caused as a result of the collisions.

Section 5.3 concerns the response of the thin base-plate loadcell which measured the force propagating to the base of the cylinders as a result of the impact. Plots of its responses are given between Figure 5.13 and Figure 5.19 and its results are summarised in Table 5.7.

The base-plate loadcell results were used to calculate the stress by dividing by the cross-sectional area of the cylinder. These results are also analysed in terms of their relationship with the initial contact velocity and the propagated impulse. In addition, the relationship between the response of the base-plate loadcell and the corresponding contact force measurement is also examined.

A qualitative analysis of the cylinders after the impact is included in section 5.4, with photographs of the cylinders after the impact between Figure 5.23 and Figure 5.43. The magnitude and length of the cracks in the top face of the cylinders were also quantified.

The strain gauge responses and stress-strain responses were determined using the base-plate loadcell and strain gauges attached to the circumference of each cylinder. Typical lateral and axial strain gauge responses are shown between Figure 5.44 and Figure 5.52. Stress strain responses for the cylinders are given in Figure 5.53 to Figure 5.59. In all of these plots the compressive stresses and strains are positive whilst tensile stresses and strains are negative. These responses were subject to considerable local fluctuations due to the inhomogeneous nature of the concrete close to where the strain was being measured.

The rebound of the impactor is quantified in section 5.6. This section only applies to the cylinders where not all of the energy of the impactor was dissipated in cracking the concrete and sufficient remained to allow the impactor to rebound after the initial impact. The analysis is undertaken in two ways - through an examination of the impulse and momentum associated with the impact and by an analysis of the time between which the impactor separated itself from the concrete and when it came in contact with the cylinder again, having bounced.

A further analysis of the energy involved in the impact is undertaken in the subsequent section which examines the energy absorption capacity of the concrete, determined by integrating under the curve of stress against mid-height axial strain, up to the point of maximum stress. This gives an indication of the energy dissipated by the concrete in the formation of cracks, in either the top surface, or along its entire length.

The damage caused to the concrete by the impact is studied in the results of a simple test undertaken on a representative selection of cylinders from each impact group. The

confining sleeve was cut away from the concrete cylinder which was then statically loaded to determine its residual strength, as cracking, both visible and invisible, had weakened the concrete as a result of the impact.

The chapter concludes with an analysis of the results from the supplementary group of tests - both loaded statically and by impact. This group of tests were designed to compliment and examine variables which had not been included in the main group of experiments. The section begins with the results of a series of static tests on confined and unconfined cylinders and compares the results of these tests to impact test results on similar cylinders. The results of impact tests on cylinders with larger diameters than those tested in the main series are also presented. These are both on unconfined and confined cylinders and are compared to one another and to the responses of cylinders with smaller diameters. The effect of removing some of the confining sleeve close to the base, and only allowing the core concrete to bear on the base-plate loadcell is also studied in a group of impact tests with sleeves of steel, aluminium and plastic. The responses of the cylinders are quite similar to those of the main group of results. The chapter concludes with the results of a series of impact tests where a particular cylinder was repeatedly impacted to see how its response changed as greater damage developed within the cylinder.

5.2. CONTACT FORCE RESPONSE

The contact force between the impactor and the impacted specimen was measured during the impact event, using a loadcell integrated into the falling impactor which is described in section 4.3. Graphs were plotted showing the contact force response over time, for each of the test series, as shown in Figure 5.1 to Figure 5.7. In the figures, the results from the three different velocities of impact, namely 3.2 m/s, 4.4 m/s and 6.3 m/s, are shown on the same graph. Separate graphs for each specimen are included in Appendix 3. Table 5.1 provides a summary of the contact force response, including the maximum force recorded, the area under the contact force-time graph (the impulse), and two pertinent times, namely the time at which the maximum contact force is reached, t_{max}, and the time to the end of the initial impact event, t_0. This table also includes the means and the coefficients of variation corresponding to each series, grouped by velocity.

It is evident that, occasionally in some of the results included in the table, the contact force response was far in excess of other values in the group, and also of what might have been expected. As previously mentioned in section 4.3, the initial impactor loadcell, used for measuring contact force at the location of impact, exhibited a very erratic response after approximately seventy tests had been completed (a number of preliminary tests had been completed prior to the main test series which added to the total). This was probably as a result of a hairline fracture in the steel cylinder and, therefore, a second replacement loadcell was used for the remaining tests. A regression analysis was performed on each of the test series to assess whether these high values of contact force were indeed outliers, (as might have been suggested by the damage to the loadcell), or were statistically significant. According to Montgomery and Runger (1999) a statistical outlier occurs if

$$\left| \frac{e_{ij}}{\sqrt{MSE}} \right| > 2 \tag{5.1}$$

where e_{ij} is the residual and MSE is the mean squared error of the sample. This allowed four outliers in the contact force results to be identified, namely, C(114)S (3)3a, C(114)S (5)3a, C(114)S (6.5)3a and C(114)S (6.5)3b, all of which were tests at the highest velocity undertaken in the period when the first impactor loadcell broke. Furthermore, as can be seen from the contact force graphs in the appendix, the results are

	Velocity (m/s)	Force (kN)	Impulse (Ns)	T_{max} (ms)	T_o (ms)
U(100) 1a	3.2	188	330.2	1.267	3.200
U(100) 1b	3.2	200	307.1	1.233	3.466
U(100) 1c	3.2	215	213.5	0.233	3.900
U(100) 1d	3.2	165	202.7	0.299	5.399
Average		192	263.4	0.758	3.991
COV %		11	25	75	25
U(100) 2a	4.4	329	128.9	0.400	1.733
U(100) 2b	4.4	304	143.1	0.167	1.933
Average		317	136.0	0.283	1.833
COV %		6	7	58	8
U(100) 3a	6.3	376	146.3	0.300	1.800
U(100) 3b	6.3	315	120.5	0.200	1.367
Average		346	133.4	0.250	1.583
COV %		12	14	28	19
C(114)S (1.2) 1a	3.2	411	401.2	0.667	1.933
C(114)S (1.2) 1b	3.2	385	413.3	0.867	1.900
C(114)S (1.2) 1c	3.2	388	402.2	0.867	1.867
C(114)S (1.2) 1d	3.2	362	392.8	0.567	1.733
Average		387	402.4	0.742	1.858
COV %		5	2	20	5
C(114)S (1.2) 2a	4.4	535	552.5	0.833	1.867
C(114)S (1.2) 2b	4.4	640	581.1	1.100	1.900
Average		588	566.8	0.967	1.883
COV %		13	4	20	1
C(114)S (1.2) 3a	6.3	767	989.8	0.500	1.817
C(114)S (1.2) 3b	6.3	715	764.3	0.600	1.773
C(114)S (1.2) 3d	6.3	908	972.2	0.533	1.566
Average		797	908.8	0.544	1.719
COV %		13	14	9	8
C(114)S (3) 1a	3.2	377	412.4	0.733	1.933
C(114)S (3) 1b	3.2	411	417.4	0.867	1.967
C(114)S (3) 1c	3.2	414	398.6	0.967	2.067
C(114)S (3) 1d	3.2	402	410.0	0.533	1.833
C(114)S (3) 1e	3.2	404	413.5	0.633	1.933
C(114)S (3) 1f	3.2	405	405.5	0.633	2.000
C(114)S (3) 1g	3.2	407	405.9	0.600	1.800
Average		403	409.0	0.709	1.933
COV %		3	2	22	5

Table 5.1 Contact force results from impact tests

	Velocity (m/s)	Force (kN)	Impulse (Ns)	T_{max} (ms)	T_o (ms)
C(114)S (3) 2a	4.4	647	578.8	0.567	1.967
C(114)S (3) 2b	4.4	593	581.5	0.667	2.133
C(114)S (3) 2c	4.4	561	554.2	0.800	1.900
C(114)S (3) 2d	4.4	570	585.7	0.833	1.867
Average		593	575.1	0.717	1.967
COV %		7	2	17	6
C(114)S (3) 3a	6.3	1686	1105.6	0.900	2.067
C(114)S (3) 3b	6.3	1131	1355.3	0.933	2.000
C(114)S (3) 3c	6.3	975	991.0	0.533	1.900
C(114)S (3) 3d	6.3	1079	1041.4	0.567	1.667
Average		1218	1123.3	0.733	1.908
COV %		26	14	29	9
Revised average		1062	1129.0	0.678	1.856
Revised COV %		7	17	33	9
C(114)S (5) 1a	3.2	425	399.8	0.633	1.767
C(114)S (5) 1b	3.2	417	416.0	0.600	1.767
C(114)S (5) 1c	3.2	401	408.7	0.600	1.900
C(114)S (5) 1d	3.2	429	402.9	0.867	1.900
Average		418	406.9	0.675	1.833
COV %		3	2	19	4
C(114)S (5) 2a	4.4	565	562.9	0.700	1.900
C(114)S (5) 2b	4.4	573	585.9	0.667	1.967
Average		569	574.4	0.683	1.933
COV %		1	3	3	2
C(114)S (5) 3a	6.3	1605	1147.3	0.833	1.900
C(114)S (5) 3b	6.3	996	-	-	-
C(114)S (5) 3c	6.3	1062	1065.2	0.900	1.667
C(114)S (5) 3d	6.3	937	863.1	0.533	1.800
Average		1150	1025.2	0.756	1.789
COV %		27	14	26	7
Revised average		1000	964.0	0.717	1.733
Revised COV %		9	15	36	5
C(114)S (6.5) 1a	3.2	441	408.9	0.833	1.967
C(114)S (6.5) 1b	3.2	386	426.8	1.100	2.167
C(114)S (6.5) 1c	3.2	430	404.4	0.867	1.867
C(114)S (6.5) 1d	3.2	439	402.9	0.567	1.733
Average		424	410.8	0.842	1.933
COV %		6	3	26	9

Table 5.1 Contact force results from impact tests (continued)

	Velocity (m/s)	Force (kN)	Impulse (Ns)	T_{max} (ms)	T_o (ms)
C(114)S (6.5) 2a	4.4	586	559.4	0.833	1.867
C(114)S (6.5) 2b	4.4	636	713.2	1.100	1.900
Average		611	636.3	0.967	1.883
COV %		6	17	20	1
C(114)S (6.5) 3a	6.3	1511	1229.5	0.500	1.817
C(114)S (6.5) 3b	6.3	2210	-	-	-
C(114)S (6.5) 3c	6.3	1236	1272.7	0.600	1.773
C(114)S (6.5) 3d	6.3	969	814.3	0.533	1.567
Average		1482	1105.5	0.544	1.719
COV %		36	23	9	8
Revised average		1103	1106.0	0.544	1.719
Revised COV %		17	23	9	8
C(110)P (3.6) 1a	3.2	260	369.8	1.467	2.466
C(110)P (3.6) 1b	3.2	310	373.8	1.067	2.433
C(110)P (3.6) 1c	3.2	270	361.7	1.100	2.866
C(110)P (3.6) 1d	3.2	269	376.7	1.067	2.600
C(110)P (3.6) 1e	3.2	305	387.2	1.133	2.400
Average		283	373.8	1.167	2.553
COV %		8	3	15	7
C(110)P (3.6) 2a	4.4	366	-	0.767	-
C(110)P (3.6) 2b	4.4	298	181.6	0.267	1.933
C(110)P (3.6) 2c	4.4	418	301.9	0.333	2.500
Average		361	241.8	0.455	2.216
COV %		17	35	60	18
C(110)P (3.6) 3a	6.3	445	255.5	0.233	1.734
C(110)P (3.6) 3b	6.3	443	180.9	0.300	1.400
Average		444	218.2	0.267	1.567
COV %		0	24	18	15
C(115)A (3.25) 1a	3.2	369	430.1	0.667	1.967
C(115)A (3.25) 1b	3.2	443	408.6	0.900	2.033
C(115)A (3.25) 1c	3.2	398	411.7	0.800	2.166
C(115)A (3.25) 1d	3.2	367	402.9	0.600	1.867
Average		394	413.3	0.742	2.008
COV %		9	3	18	6
C(115)A (3.25) 2a	4.4	529	547.4	0.700	2.100
C(115)A (3.25) 2b	4.4	548	556.2	0.600	1.867
Average		539	551.8	0.650	1.983
COV %		2	1	11	8

Table 5.1 Contact force results from impact tests (continued)

	Velocity (m/s)	Force (kN)	Impulse (Ns)	Tmax (ms)	To (ms)
C(115)A (3.25) 3a	6.3	807	1282.5	0.567	1.833
C(115)A (3.25) 3c	6.3	852	943.9	0.600	1.867
C(115)A (3.25) 3d	6.3	874	824.7	0.567	1.900
Average		844	1017.0	0.578	1.867
COV %		4	23	3	2

Table 5.1 Contact force results from impact tests (continued)

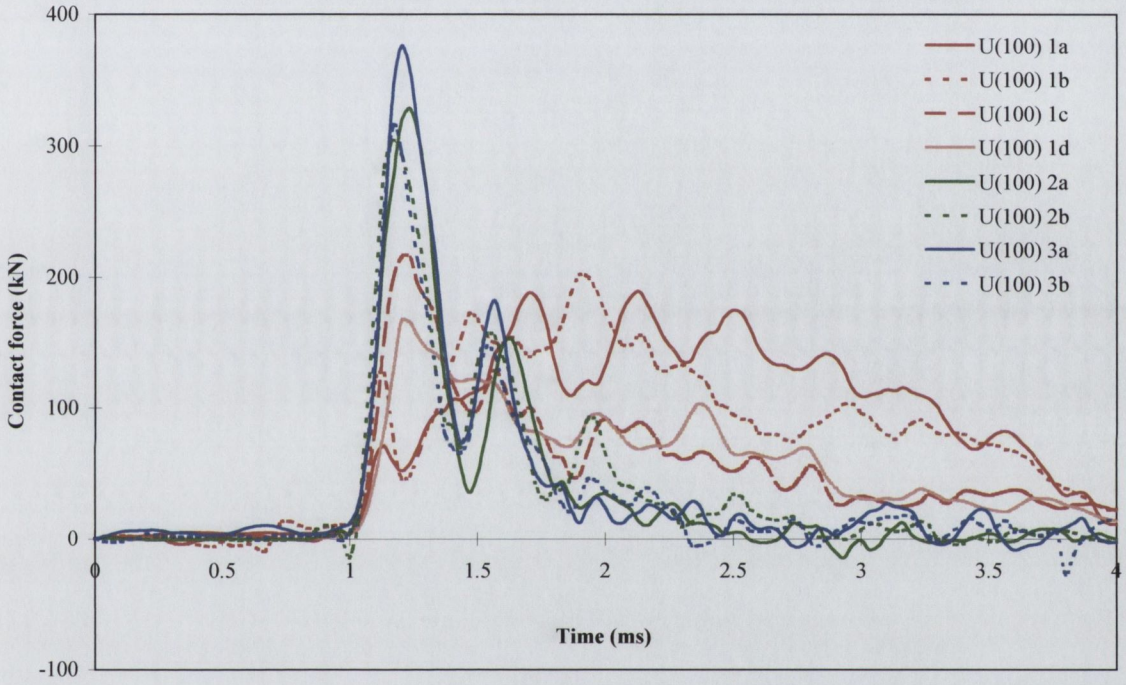


Figure 5.1 Contact force response of unconfined cylinders - U(100)

- repeats at velocities 1 = 3.2 m/s, 2 = 4.4 m/s, 3 = 6.3 m/s

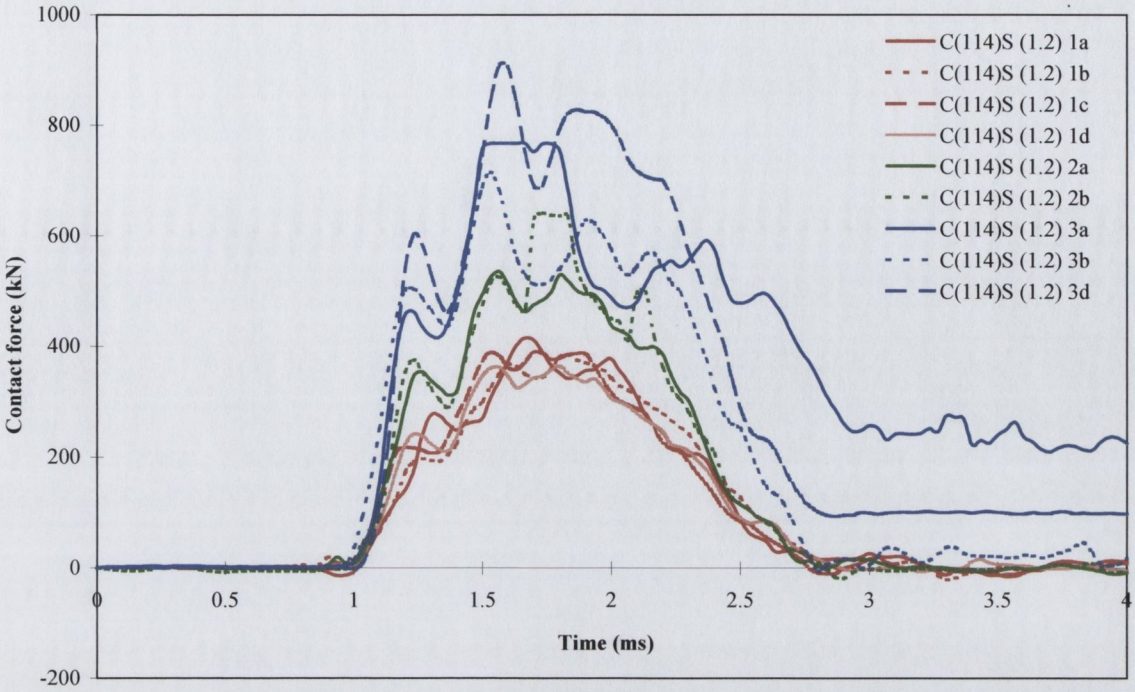


Figure 5.2 Contact force response of steel confined cylinders, thickness 1.2 mm - C(114)S (1.2) - repeats at velocities 1 = 3.2 m/s, 2 = 4.4 m/s, 3 = 6.3 m/s

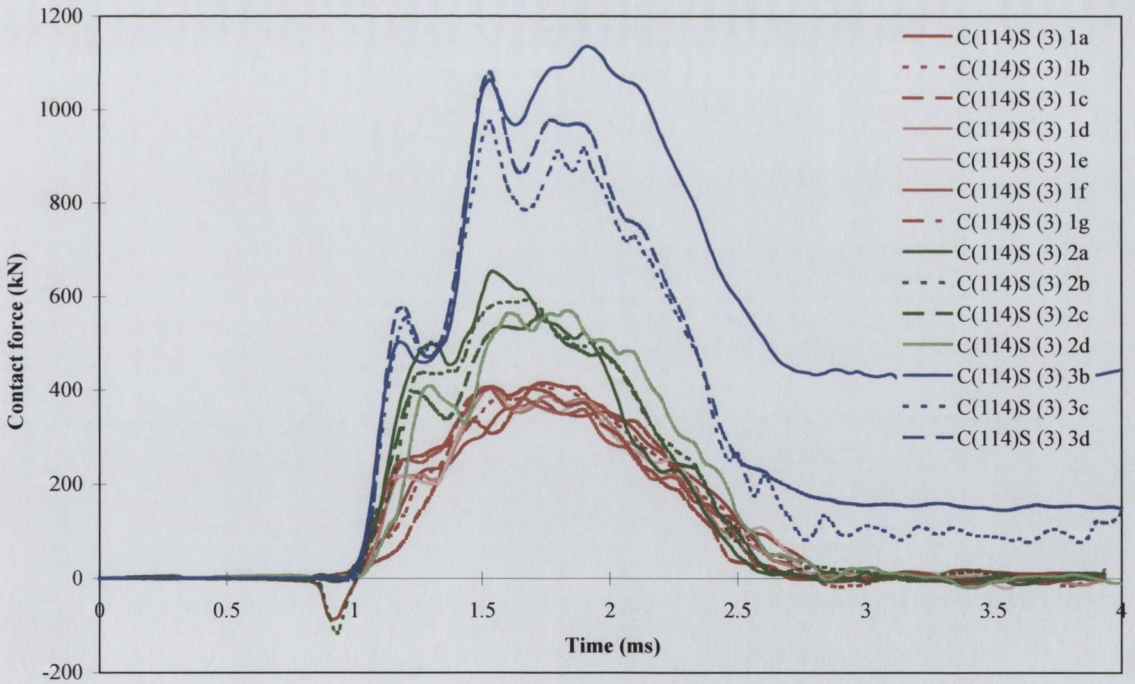


Figure 5.3 Contact force response of steel confined cylinders, thickness 3 mm - C(114)S (3) - repeats at velocities 1 = 3.2 m/s, 2 = 4.4 m/s, 3 = 6.3 m/s

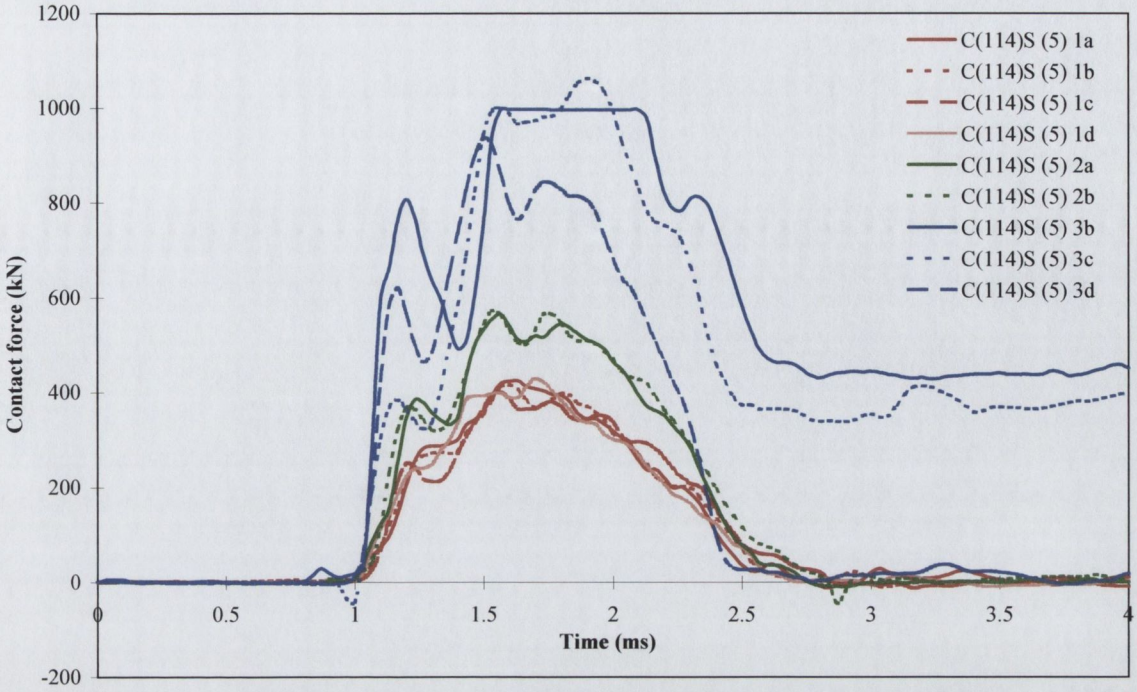


Figure 5.4 Contact force response of steel confined cylinders, thickness 5 mm - C(114)S (5) - repeats at velocities 1 = 3.2 m/s, 2 = 4.4 m/s, 3 = 6.3 m/s

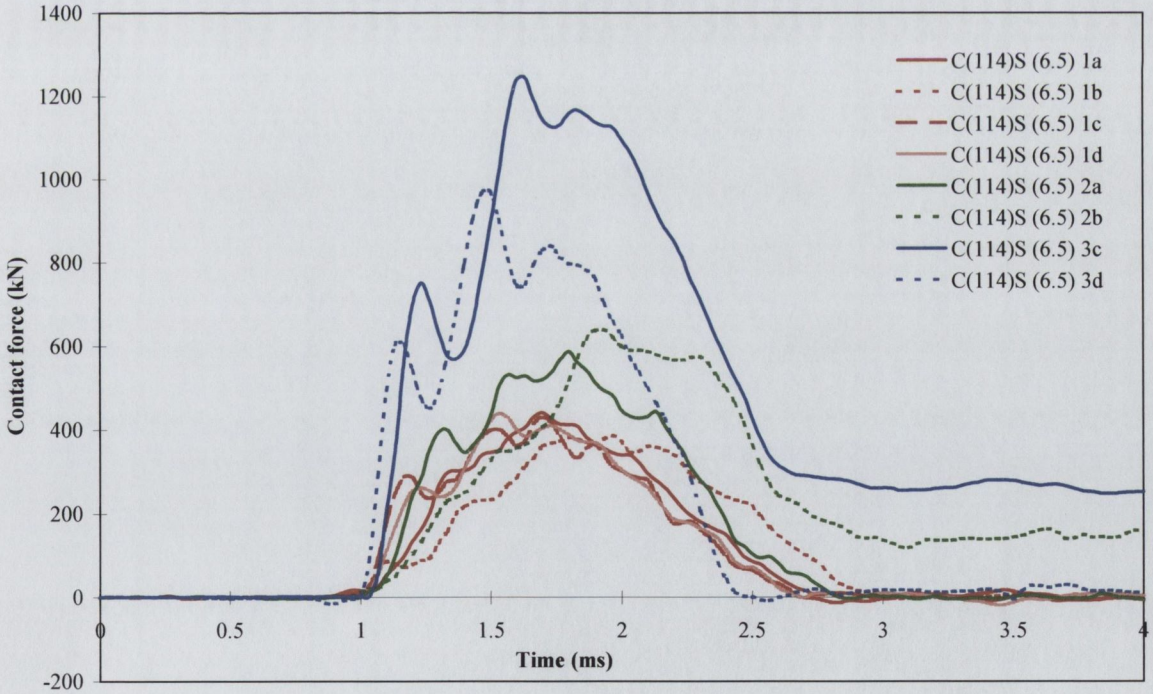


Figure 5.5 Contact force response of steel confined cylinders, thickness 6.5 mm - C(114)S (6.5) - repeats at velocities 1 = 3.2 m/s, 2 = 4.4 m/s, 3 = 6.3 m/s

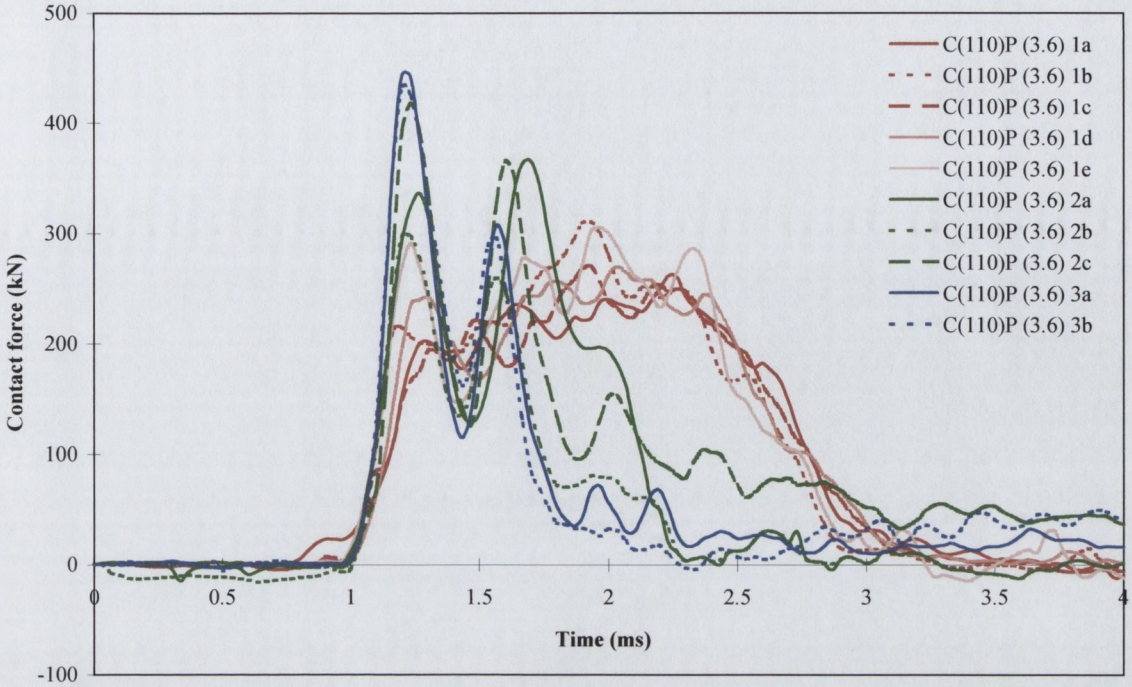


Figure 5.6 Contact force response of plastic confined cylinders, thickness 3.6 mm - C(110)P (3.6) - repeats at velocities 1 = 3.2 m/s, 2 = 4.4 m/s, 3 = 6.3 m/s

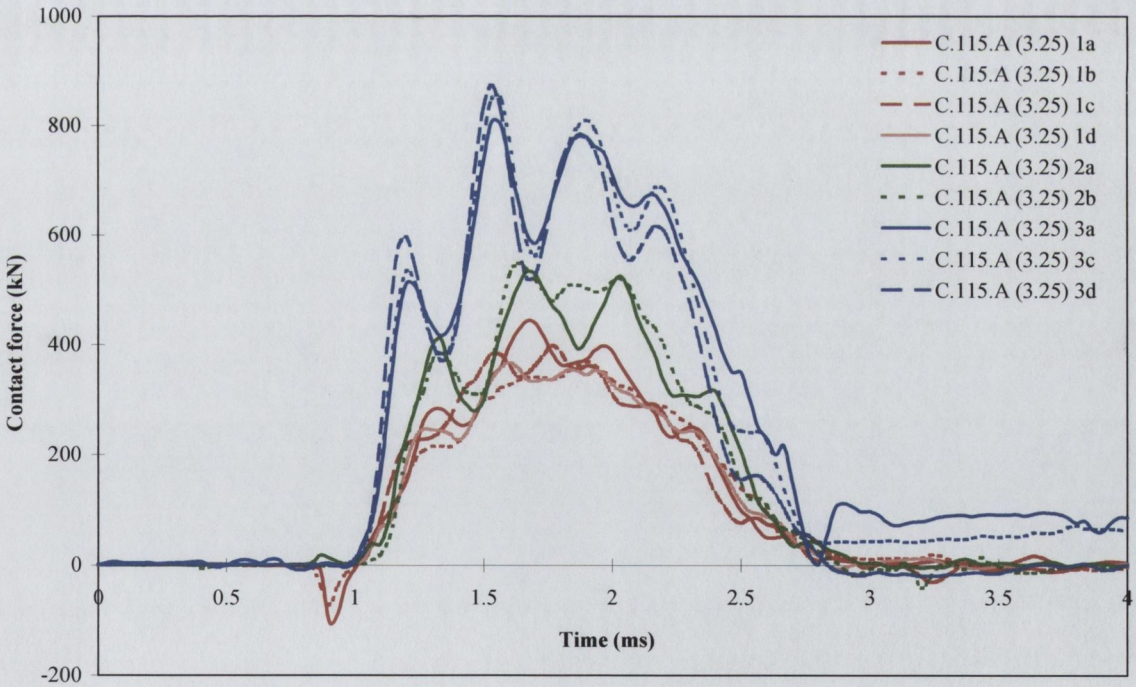


Figure 5.7 Contact force response of aluminium confined cylinders, thickness 3.25 mm - C(115)A (3.25) - repeats at velocities 1 = 3.2 m/s, 2 = 4.4 m/s, 3 = 6.3 m/s

atypical of those in the rest of their groups. The averages and coefficients of variation were re-calculated, with these values removed, for each of the test groups in question. The resulting values exhibited good consistency, with an average coefficient of variation of approximately 8 %. Values of the coefficient of variation which were above 10 % were associated predominantly with groups of tests in which there were a limited number of repeats, usually caused by a results shortage due to the failure of one of the loadcells.

5.2.1. Factorial analysis of maximum contact force results

The results from an experiment or series of experiments can be analysed in such a way as to eliminate the effects of extraneous variables which may conceal the effects of the variables being investigated and, therefore, improve the sensitivity of the experiment. This is performed statistically using a method known as *Factorial Analysis* using *Analysis of Variance* techniques. Although the experimental work on the impact response of sleeved concrete cylinders was not designed specifically to permit a full factorial analysis, the results do allow a modified factorial analysis to be used retrospectively. This method is described in detail in many statistical texts (for example, see Montgomery, 1997) and only a brief description will be given here.

Consider an experiment to investigate the effect of some factor A upon a certain quantity y. If the experiment is repeated n times at each of k levels of A, the results can be arranged as illustrated in Table 5.2. It is assumed that each result y_{ij} belongs to a distribution with a mean given by

$$u_{ij} = u + a_i \tag{5.2}$$

Level of A	Results of n repetitions	Means
1	y_{11} y_{12} ..... y_{1j} ..... y_{1n}	$\bar{y}_1$
2	y_{21} y_{22} ..... y_{2j} ..... y_{2n}	$\bar{y}_2$
	.....	
I	y_{i1} y_{i2} ..... y_{ij} ..... y_{in}	$\bar{y}_i$
k	y_{k1} y_{k2} ..... y_{kj} ..... y_{kn}	$\bar{y}_k$

Table 5.2 Arrangement of results for analysis of variance

where u is the expected value of the overall mean $(\bar{y})$, and a_i is the expected value of $\bar{y}_i - \bar{y}$. This assumption states that the mean of the quantity y_{ij} is the sum of the general mean, u, and the effect a_i of the ith level of the variable A. Furthermore, a second assumption is made that the variables y_{ij} are independently and normally distributed with the same variance, σ^2, such that

$$y_{ij} \sim N(u_{ij}, \sigma^2) \tag{5.3}.$$

The analysis proceeds by assuming that the level of factor A has no effect upon the outcome of the experiment, which is termed the null hypothesis, and is usually written thus

$$H_0 : a_i = 0 \quad (i = i,k) \tag{5.4}.$$

If, following the experiment, the null hypothesis is accepted then it is concluded that the quantity y is not affected by the level of A. However, if the null hypothesis is rejected, then the alternative hypothesis, given by

$$H_1 : a_i \neq 0 \quad (i = i,k) \tag{5.5}$$

is accepted, and it is concluded that the effect of factor A is indeed significant.

The components of the total variation of the experimental results (y_{ij}) are used to test the hypothesis. The total sum of squares, ($SS(T)$), is expressed as the sum of the treatment (or the level of the factor) sum of squares, ($SS(Tr)$), and the error sum of squares ($SS(E)$)

$$SS(T) = SS(Tr) + SS(E) \tag{5.6}$$

where

$$SS(T) = \sum_{i=1}^{k}\sum_{j=1}^{n} y_{ij}^2 - \frac{\bar{y}^2}{kn} \qquad \text{(kn-1 degrees of freedom)}$$

$$SS(Tr) = \frac{1}{n}\sum_{i=1}^{k} y_i^2 - \frac{\bar{y}^2}{kn} \qquad \text{(k-1 degrees of freedom)} \tag{5.7}$$

$$SS(E) = SS(T) - SS(Tr) \qquad \text{(k(n-1) degrees of freedom).}$$

If the null hypothesis is true, it may be shown that the mean square (or the sum of squares on the right hand side of (5.7) divided by its number of degrees of freedom) provides an unbiased estimate of the variance, σ^2. Therefore, if the effect of A is not significant, then the variation of the sample means will be the same as the variation caused by extraneous variables. If MS_1 and MS_2 are independent estimators of the variance of the same

population, and n_1 and n_2 are the number of degrees of freedom for each estimate, then the ratio MS_1/MS_2 possesses an F distribution with n_1, n_2 degrees of freedom. Thus, under the null hypothesis

$$\frac{MS(Tr)}{MS(E)} \sim F_{(k-1),k(n-1)} \tag{5.8}$$

where MS (Tr) = treatment mean square = SS(Tr)/(k-1)

MS (E) = error mean square = SS (E)/k(n-1).

The problem of testing the null hypothesis is reduced to deciding whether or not this ratio, often called the test statistic, belongs to the population described by the distribution. Usually a range of values of F, which contain a large percentage of the total population are selected, and the values of F corresponding to the remainder of the population are known as the critical region. When the test statistic falls in this region the test is described as being significant and the null hypothesis is rejected. If the critical region is chosen to contain 5 % of the population, its lower bound is written as $F_{0.05}$ and when a test statistic exceeds this value, the test is described as being significant, at a 5 % level.

Typically, experiments are undertaken with a number of replicates of each of the treatment levels, which results in balanced factorial design. However, it is not unusual to encounter situations where the number of results at a particular level may be unequal, which is termed unbalanced design. Unbalanced design results in calculations which are much more complicated than those for balanced design, predominantly because of the difficulty in calculating values for the sums of squares. One technique, considerably more complex, but with the same basic principals as the method described above, called the weighted sum of means method, was developed in the 1930s and is described in detail in Kuehl (2000). It is based on the sums of squares of the cell means, which are weighted in inverse proportion to their variances and provides an accurate method of testing for hypotheses about different factors.

This technique was used to perform a factorial analysis on the contact force results from the impact tests. The results were grouped in two ways, firstly by the thickness of the steel confining sleeve, which varied from 1.2 mm to 6.5 mm, and secondly by the Young's modulus of similar thicknesses of the confining sleeve, which varied from 0 kN/mm^2,

where there was no confinement, to 210 kN/mm^2, which represented the steel confining sleeve. Both were analysed at the three different impact velocities.

The contact force results from the first analysis, of varying thicknesses of the steel sleeve, are shown in Table 5.3, set out for factorial analysis according to Table 5.2, but with an unequal number of replicates in the different cells. An analysis of variance was performed, and the results are shown in Table 5.4. Since $F_{0.05,6,28} = 2.45$ and the F_0 value for interaction is 4.7 it is possible to conclude that there is a significant interaction between the velocity of impact and the thickness of the confining sleeve. Furthermore, $F_{0.05,2,28}$ and $F_{0.05,3,28}$ have the values 3.34 and 2.95 respectively, so the main effects of velocity and sleeve thickness are also of statistical significance to the maximum contact force.

A similar analysis was performed on the contact force results from concrete cylinders confined with sleeves of different Young's Modulii, with the values set out in Table 5.5. The results of an analysis of variance with different numbers of replicates are shown in Table 5.6. Again, a comparison of the test statistics, F_0, with the relevant F-test values show that the interaction between the velocity of impact and the type of confining material, and the main factor effects of the velocity and confining material type are all statistically significant.

At the time of analysis it became evident that a full factorial analysis could have been performed if the batches of concrete had been poured in a different way. As it was, each of the cylinder types was made with a different batch of concrete. Although the batches were all of identical design, the concrete, as would be expected, did not have identical material properties in each of the batches. Ideally, each batch of concrete should have been poured into cylinders with different properties, which could then have been tested randomly throughout the then factorially designed experiment to remove the extraneous variable of concrete variability. The effect of this variable can be seen in the results from the series C.114.S (5), which, at all but the lowest velocity, has an average maximum contact force response lower than the values with a thinner steel sleeve. This was probably because the concrete used in this series was less strong than in the other steel sleeved batches, as shown by the results of cube tests on the concrete at 28 days (Table 4.3). In an attempt to examine the effect of this variable, the analysis of variance on the different thicknesses of the confining sleeve was repeated, with

Thickness / Velocity	t = 1.2 mm	t = 3 mm	t = 5 mm	t = 6.5 mm	Velocity Means	Mean average
v = 3.2 m/s	411	377	425	441		
	385	411	417	386		
	388	414	401	430		
	362.0	402.0	429.0	439.0		
		404.0				
		405.0				
		407.0				
Means	386.5	402.9	418.0	424.0	407.1	407.8
v = 4.4 m/s	535.0	647.0	565.0	586.0		
	640.0	593.0	573.0	636.0		
		561.0				
		570.0				
Means	587.5	592.8	569.0	611.0	590.6	590.1
v = 6.3 m/s	767.0	1131.0	996.0	1236.0		
	715.0	975.0	1062.0	969.0		
	908.0	1079.0	937.0			
Means	796.7	1061.7	998.3	1102.5	979.5	989.8
Thickness Means	567.9	598.3	645.0	640.4		
Mean average	590.2	685.8	661.8	712.5		

Table 5.3 Contact force (kN) of different thicknesses of the steel sleeve

Source of variation	Sum of Squares	Degrees of Freedom	Mean Squares	F		
Velocity	2273321.0	2.0	1136660.5	346.6	$F_{0.05,2,28}$	3.34
Thickness	68109.6	3.0	22703.2	6.9	$F_{0.05,3,28}$	2.95
Interaction	91899.6	6.0	15316.6	4.7	$F_{0.05,6,28}$	2.45
Error	91833.6	28.0	3279.8			
Total	2537463.4	39.0				

Table 5.4 Analysis of variance for contact force of different thicknesses of steel sleeved cylinders with unequal replication of treatments

each of the contact force results being multiplied by the density (ρ) and the speed of stress wave propagation (c_0) for the particular type of concrete in each batch. However, this did not result in any significant change in the F_0 test statistic and the significance of the main factors and their interaction remained essentially unchanged.

E / Velocity	Unconfined E=0 kN/mm^2	Plastic E=3 kN/mm^2	Aluminium E=70 kN/mm^2	Steel E=210 kN/mm^2	Velocity Means	Mean average
v = 3.2 m/s	188	260	369	377		
	200	310	443	411		
	215	270	398	414		
	165	269	367	402.0		
		305		404.0		
				405.0		
				407.0		
Means	192.0	282.8	394.3	402.9	329.0	317.9
v = 4.4 m/s	329	366	529	647.0		
	304	298	548	593.0		
		418		561.0		
				570.0		
Means	316.5	360.7	538.5	592.8	469.4	452.1
v = 6.3 m/s	376	445	807	1131.0		
	315	443	852	975.0		
			874	1079.0		
Means	345.5	444.0	844.3	1061.7	729.7	673.9
E Means	261.5	338.4	576.3	598.3		
Mean average	284.7	362.5	592.4	685.8		

Table 5.5 Contact force (kN) of confined concrete with sleeves of different Young's modulus

Source of variation	Sum of Squares	Degrees of Freedom	Mean Squares	F		
Velocity	1096616.9	2.0	548308.4	428.4	F0.05,2,29	3.33
Young's modulus	994345.4	3.0	331448.5	259.0	F0.05,3,29	2.93
Interaction	316602.2	6.0	52767.0	41.2	F0.05,6,29	2.43
Error	37116.7	29.0	1279.9			
Total	2230257.5	40.0				

Table 5.6 Analysis of variance for contact force of confined concrete with sleeves of different Young's modulus

5.2.2. Analysis of contact force results

The variation of contact force over the duration of the impact is shown for each of the test series in Figure 5.1 to Figure 5.7, which summarise all of the individual results from the tests. The plots have two distinct shapes, depending on what occurred during the load transfer from the impactor to the target cylinder. The plot is broadly sinusoidal where the collision is nearly 'elastic', which occurs when the impactor collides with a well confined cylinder and the impactor does not have sufficient energy to rupture the confining sleeve through the lateral dilation of the confined concrete. All of the steel and aluminium confined cylinders exhibited this type of response as the sleeves prevented anything more than minor cracking occurring in the top face, regardless of the velocity of impact. The response of cylinder C(114)S (1.2)3a is unusual because of the flatness of the peak. An examination of the cylinder after the test showed that the weld, which held the confining sleeve together, had ruptured close to the top (the only case in which this happened), which would probably explain the unusual contact force response. However, when the cylinder, and occasionally its confining sleeve, ruptures during the impact test the shape of the curve is quite different, in that it has a very sharp initial peak which decays quite quickly as the concrete fractures. The unconfined concrete clearly shows evidence of this type of behaviour, as it fractures completely at any of the impact velocities. The slope of the initial part of each of the contact force graphs depends on the strain rate at which the test was conducted, as determined in section 5.5.

The plastic confined cylinders combine these two types of responses, depending on the contact velocity at which they are impacted. At a velocity of 3.2 m/s their response is of the former type, namely broadly sinusoidal, because the dilation was insufficient to cause the confining sleeve to rupture. However, at the two higher velocities the dilation of the concrete causes the splitting of the confining sleeve and the concrete fractures. The resulting response is of the latter form and exhibits a sharp initial peak in the response before decaying rapidly. However, the plastic confined cylinders at these velocities have a secondary sharp peak which is not as high as the first, but is considerably greater than the secondary peak in the unconfined responses. This occurs because, unlike the unconfined concrete which fractures instantaneously on impact, the fracture of the plastic confined concrete is progressive. The contact force reduces after the first peak before the loadcell realises that the concrete has some residual strength, which causes the contact force to

increase again and results in a second peak. This falls off as the rest of the concrete fails when subjected to this force.

As can be seen from the contact force/time graphs and Table 5.1, the presence of confinement leads to a considerable increase in the contact forces measured during impact, in some cases over double that measured for an unconfined case at the same velocity. This is illustrated schematically in Figure 5.8, which is a schematic graph of the contact forces against the product of the Young's modulus (in GPa) and the thickness of the confining sleeve, on a logarithmic scale. The increase in contact force is related to the stiffness of the confining materials, however, as would be expected, the increase is not linearly proportional. The presence of the plastic confining cylinders results in an increase in the contact force, and although the aluminium and steel sleeves have a much greater Young's modulus than the plastic, the difference in the contact force experienced by these cylinders is not as great as might have been expected. At the lowest velocity, the steel and aluminium confined sleeves have contact forces approximately twice that of the unconfined cylinders at the same velocity, but this increase is even more evident as the velocity increases and the confinement is able to reduce the dilation of the concrete. The relationship between the contact forces generated for the aluminium confined cylinders and the 1.2 mm thick steel cylinders varies as the velocity increases. At the lowest velocity, both are equally good at providing confinement to the concrete but, by the highest velocity, the aluminium experiences a higher contact force than the steel confined cylinder. It is evident that, for this amount of energy transfer, the thickness of the sleeve is very important in reducing the dilation, as even though it steel sleeve has a much higher Young's modulus its small thickness results in a considerably lower maximum contact force. As can be seen from Figure 5.8, the combination of the Young's modulus and the thickness in the 3 mm thick steel sleeve is very effective at resisting the dilation of the concrete. There is an increase in the contact force as the thickness of the steel increases, however, the benefit of the increase is not substantial, approximately 10 % at the lower two velocities, for a fivefold increase in the cross-sectional area of the confining material. Clearly, if lateral confinement is provided, beyond the minimum necessary to inhibit the dilation of the concrete, there is an increase in the maximum contact force, if the resulting hoop stresses are less than the yield strength of the sleeve. However, if the material response is elastic, further increasing the thickness or Young's modulus of the confining material does not reduce the dilation by any significant degree.

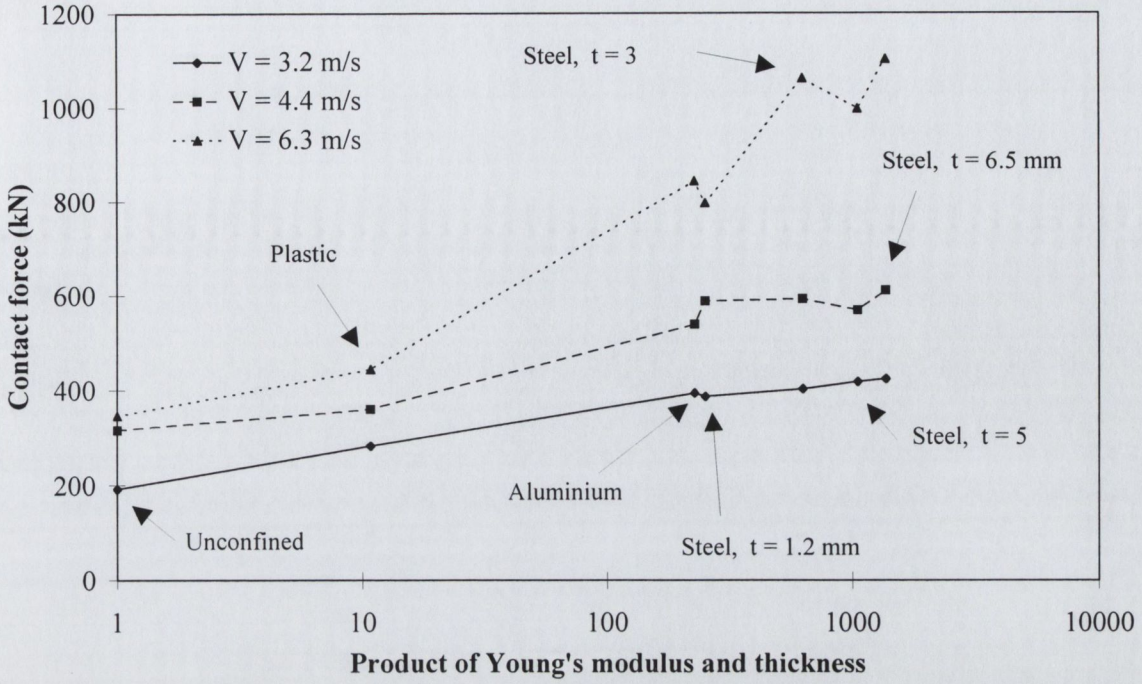


Figure 5.8 Graph showing average contact force with varying confinement (the lines joining the points are solely for illustrative purposes and do not show definitive trends in the variation of contact force with the properties of the sleeve)

In the case of the unconfined impact, the energy lost by the impact hammer is transferred to the concrete and is used to create fracture surfaces and to accelerate the fractured parts away from the location of impact. This results in kinetic energy absorption and little or no rebound of the impactor. If the concrete is confined, the kinetic energy is transferred to the concrete and into strain energy in the confining sleeve but is not entirely dissipated. This results in a significant rebound of the impactor, and a corresponding increase in the magnitude of the initial impact pulse.

Table 5.1 also includes values for the time to the maximum contact force and the time to the end of the impact event. The total duration of the impact is fairly consistent between groups at the same velocity for the confined tests (which is illustrated by its coefficients of variation being less than 10 %) and, in the majority of cases, the duration of impact decreases as the strain rate increases. Where the concrete fractured, the impact durations are longer and less consistent. The time taken to reach the maximum contact force is considerably more variable throughout all of the test series. Although the ascending slopes of the contact force/time graphs are similar at each impact velocity, different levels of irreversible cracking and deformation then occur in the concrete which result in a flattening

of the curve near its peak and variability in the time taken to reach the maximum contact force.

In section 2.4.4 the co-axial collision of two bars and the resulting stresses generated are described mathematically. According to equation (2.46), the stresses at the interface and, hence, the contact forces, are proportional to the difference in the initial velocities of the two colliding objects. In the current analysis, the impacted object is stationary and the stresses should be proportional to the velocity of the impactor. A graph was plotted of the peak contact forces of the cylinders confined by all thicknesses of steel against the contact velocity (Figure 5.9). A linear regression line, through the origin, was fitted to the contact force values and 95 % confidence limits were calculated, as illustrated in the graph.

The regression line confirms that there is indeed a relationship between the maximum contact force and the velocity of impact, particularly at the lower velocities. However, at the highest velocity, there is a considerable spread of results, and a large number of the measured contact force results do not fit within the confidence limits. As the outliers have already been identified and excluded from further analysis, all of these results are important in the interpretation of the experimental results. A second graph (Figure 5.10) was then plotted with a regression line through the origin and confidence limits, calculated

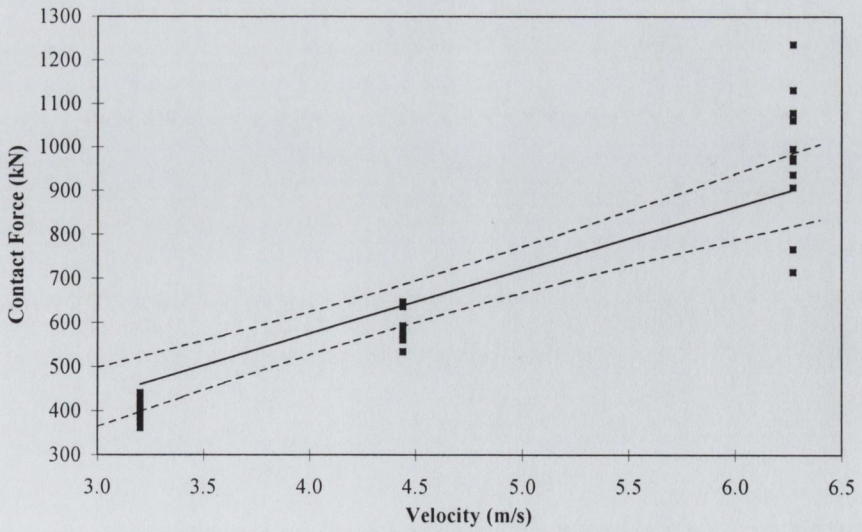


Figure 5.9 Contact force - velocity graph for steel confined concrete, with fitted regression line and 95 % confidence limits on all results

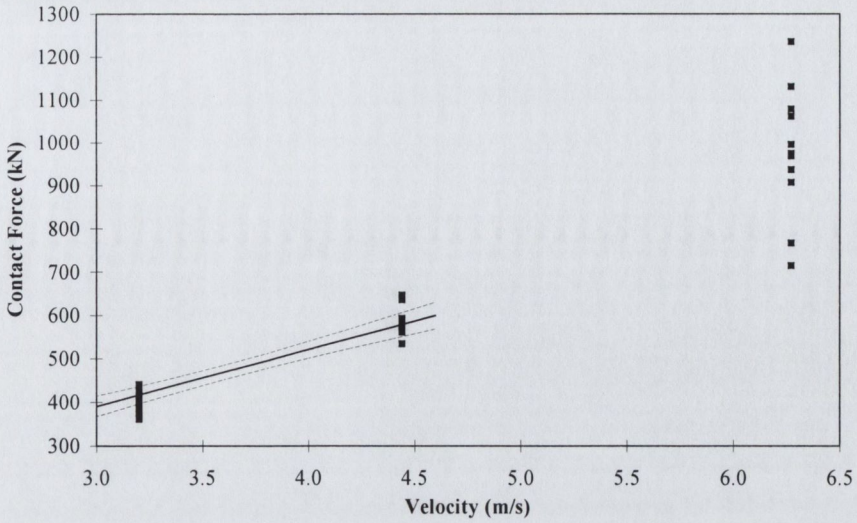


Figure 5.10 Contact force - velocity graph for steel confined concrete, with fitted regression line and 95 % confidence limits on results from lower two velocities

for the lower two contact velocities which provides a much closer fit to the results. The non-linearity of the relationship at high velocities might suggest one of two things, either that at the highest velocity the linearity of the contact force/velocity relationship is lost or that that the material properties of the impacted concrete change as a result of the much higher energy collision. It is more probable that the latter is occurring as the contact force equation was derived for materials behaving elastically, and it is probable that, at the highest velocity, the concrete is beginning to behave inelastically. At the lower velocities the response of the concrete confined by different thicknesses of steel is very similar, because all are sufficient to reduce the dilation of the concrete and to result in a nearly elastic response. However, at the highest velocity the thickness of the confinement is much more important in the contact force response as it takes the greater thicknesses of confinement to overcome the concrete's tendency to dilate under a load.

A similar figure of the maximum contact forces of the unconfined, plastic, aluminium and steel (thickness 3 mm) confined concrete is shown in Figure 5.11. Regression lines, through the origin, are fitted to each of the groups of data. The results of the unconfined and plastic confined cylinders at the lower velocities would suggest that the maximum contact force is related to the contact velocity, however, at the highest velocity the concrete fractures on impact and the results are lower than would be expected as the materials are not acting elastically and the maximum contact cannot be developed, as the concrete dilates and fractures. The aluminium shows the greatest degree of consistency

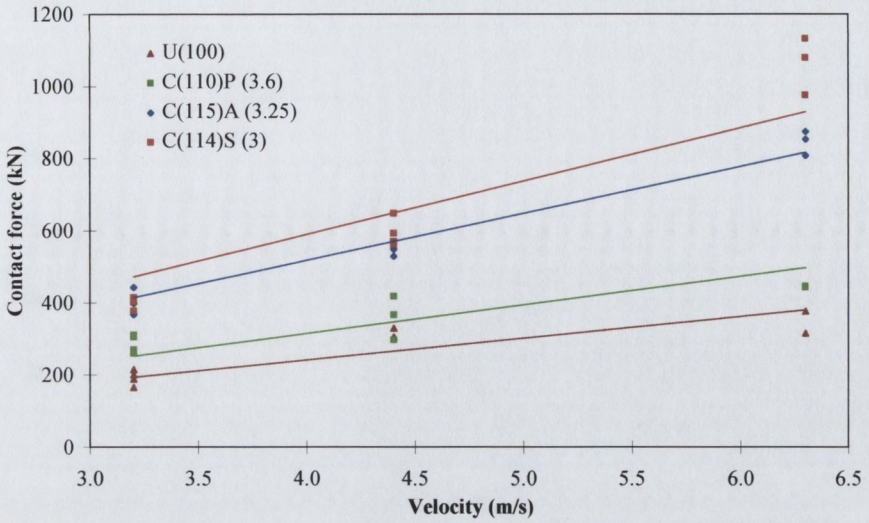


Figure 5.11 Contact force - velocity graph for unconfined, plastic, aluminium and steel confined concrete, with fitted regression lines

over the velocity range as the composite cylinder acts elastically over the entire range. The steel confined cylinder responds linearly at lower velocities, but shows an increase in the contact force at the highest velocity as the rigidity of the confinement is fully mobilised.

The impulse transferred from the moving impactor to the stationary specimen during the impact was calculated by integrating under the contact force/time graph and the values calculated are presented in Table 5.1, with their means and coefficients of variation. The impulse results have a slightly higher coefficient of variation than the maximum contact force results, due to the aforementioned variable flattening of the curve near its peak due to local crushing. However, there is evidence of a nearly linear relationship between the maximum contact force and the impulse, as can be seen in Figure 5.12 for the contact force results. The fitted linear regression line through the origin has a slope just greater than unity. The majority of the points on the graph relating to the responses of the steel and aluminium confined cylinders are within the 95 % confidence limits, as these act in an elastic manner and the sleeves dissipate the energy through elastic deformation. However, the unconfined concrete and the plastic confined concrete are predominantly outside the confidence limits. This is to be expected as the energy was absorbed by the dilation of the concrete and the sleeve in such a way that concrete cracked during the impact, resulting in reduced consistency in the calculated impulses.

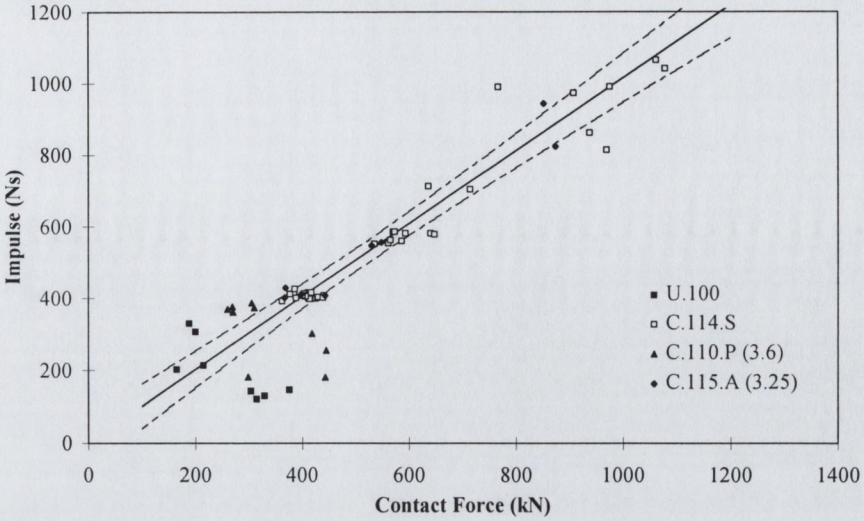


Figure 5.12 Graph of maximum contact force against impulse

5.3. BASE-PLATE FORCE AND STRESS RESPONSE

The manganin base-plate loadcell was used to measure the forces transmitted to the base of the impacted specimen, as described in section 4.4. These forces were then used to calculate stresses at the interface between the specimen and the loadcell. Graphs were plotted of the base-plate force against time for each of the impact tests, which can be found in Appendix 3. Summary graphs have also been plotted which combine the plate force responses for each of the types of specimen impacted, in Figure 5.13 to Figure 5.19. Table 5.7 is a summary of the results from each of the base plate response graphs, including the maximum force, the maximum stress at the interface, the integral under the base-plate force/time curve, the time to the maximum plate force and the time taken for the force to return to zero after the impact. This table also gives the average values and the coefficients of variation for each velocity group and for each type of confinement. The manganin base-plate loadcell was only developed during the testing period and, therefore, test results which include base-plate loadcell responses are not as numerous as those for the contact force loadcell. This resulted in there being fewer repeats in some of the test series and hence, larger degrees of variation within the results.

The identification of outliers was more difficult within these results because of the reduced number of repeats in each group. However, using a method identical to that used in the analysis of the contact force (described in section 5.2), the base-plate force results were analysed to identify any obvious outliers. Two outliers were identified, namely C(114)S (1.2)2b and C(114)S (3)3b which both had values far in excess of what would have been anticipated. Reasons for the presence of these outlying values are difficult to explain, but could be as a result of variations in the core concrete which resulted in an unusual pattern of wave propagation. Revised values of the average and the coefficient of variation were calculated for the group which included C(114)S (3)3b, as this was the only one which came from a group of greater than two, and for which it was possible to recalculate values. Even after removing the outliers, some variation still existed in the maximum base-plate force results, perhaps also as a result of the way in which the stress wave propagated through the concrete to the base of the cylinder. The largest variations were associated with groups with only two repeats, and would probably have been reduced if more tests had been performed.

	Velocity (m/s)	Force (kN)	Stress (N/mm^2)	Impulse (Ns)	T_{max} (ms)	T_o (ms)
U(100) 1c	3.2	156	19.9	43.2	0.367	0.567
Average		156	19.9	43.2	0.367	0.567
COV %		0		0	0	0
U(100) 2a	4.4	151	19.2	56.7	0.433	0.600
U(100) 2b	4.4	151	19.2	24.2	0.233	0.333
Average		151	19.2	40.4	0.333	0.467
COV %		0		57	42	40
U(100) 3a	6.3	156	19.9	24.6	0.300	0.433
U(100) 3b	6.3	146	18.6	33.2	0.200	0.367
Average		151	19.2	28.9	0.250	0.400
COV %		5		21	28	12
C(114)S (1.2) 1c	3.2	292	28.5	300.7	1.033	1.733
C(114)S (1.2) 1d	3.2	281	27.4	321.7	0.733	1.833
Average		287	27.9	311.2	0.883	1.783
COV %		3		5	24	4
C(114)S (1.2) 2a	4.4	409	39.9	410.4	1.267	1.900
C(114)S (1.2) 2b	4.4	552	53.8	300.6	0.467	0.767
Average		481	46.8	355.5	0.867	1.333
COV %		21		22	65	60
C(114)S (1.2) 3a	6.3	670	65.3	478.7	0.633	1.700
C(114)S (1.2) 3b	6.3	650	63.3	634.6	0.300	1.767
C(114)S (1.2) 3c	6.3	624	60.8	638.6	0.600	1.633
C(114)S (1.2) 3d	6.3	650	63.3	654.3	0.667	1.700
Average		649	63.2	601.6	0.550	1.700
COV %		3		14	31	3
C(114)S (3) 1d	3.2	259	25.2	240.8	0.633	1.533
C(114)S (3) 1e	3.2	311	30.3	269.3	0.800	1.567
C(114)S (3) 1f	3.2	338	32.9	339.9	0.733	1.700
C(114)S (3) 1g	3.2	266	25.9	266.2	0.933	1.667
Average		294	28.6	279.1	0.775	1.617
COV %		13		15	16	5
C(114)S (3) 2c	4.4	302	29.4	278.7	0.933	1.600
C(114)S (3) 2d	4.4	568	55.4	634.8	0.933	1.733
Average		435	42.4	456.8	0.933	1.667
COV %		43		55	0	6

Table 5.7 Base-plate forces and stresses

	Velocity (m/s)	Force (kN)	Stress (N/mm^2)	Impulse (Ns)	T_{max} (ms)	T_o (ms)
C(114)S (3) 3a	6.3	675	65.8	576.9	0.833	2.067
C(114)S (3) 3b	6.3	967	94.2	931.5	0.667	1.500
C(114)S (3) 3c	6.3	721	70.3	678.7	0.667	1.466
C(114)S (3) 3d	6.3	578	56.3	602.5	0.700	1.667
Average		735	71.7	697.4	0.717	1.675
COV %		23		23	11	16
Revised Average		658	64.1	619.4	0.733	1.733
Revised COV %		11		9	12	2
C(114)S (5) 1c	3.2	311	30.3	283.5	0.733	1.533
C(114)S (5) 1d	3.2	358	34.9	343.9	0.833	1.700
Average		335	32.6	313.7	0.783	1.617
COV %		10		14	9	7
C(114)S (5) 2a	4.4	660	64.3	661.5	0.800	1.733
C(114)S (5) 2b	4.4	552	53.8	582.7	0.833	1.733
Average		606	59.1	622.1	0.817	1.733
COV %		13		9	3	0
C(114)S (5) 3a	6.3	558	54.4	420.9	0.767	1.533
C(114)S (5) 3b	6.3	813	79.2	894.9	0.667	2.167
C(114)S (5) 3d	6.3	726	70.8	712	0.700	1.833
Average		699	68.1	675.9	0.711	1.844
COV %		19		35	7	17
C(114)S (6.5) 1c	3.2	409	39.9	408.4	0.667	1.733
C(114)S (6.5) 1d	3.2	425	41.4	407.4	0.700	1.700
Average		417	40.6	407.9	0.684	1.716
COV %		3		0	3	1
C(114)S (6.5) 2a	4.4	435	42.4	451.6	0.567	1.667
C(114)S (6.5) 2b	4.4	532	51.8	526.2	1.267	2.233
Average		484	47.1	488.9	0.917	1.950
COV %		14		11	54	21
C(114)S (6.5) 3a	6.3	532	51.8	518.5	0.433	2.366
C(114)S (6.5) 3b	6.3	951	92.7	782.9	0.667	1.367
C(114)S (6.5) 3c	6.3	900	87.7	733.9	0.667	1.367
C(114)S (6.5) 3d	6.3	748	72.9	603.4	0.667	1.400
Average		783	76.3	659.7	0.608	1.625
COV %		24		18	19	30

Table 5.7 Base-plate forces and stresses (continued)

	Velocity (m/s)	Force (kN)	Stress (N/mm^2)	Impulse (Ns)	T_{max} (ms)	T_o (ms)
C(110)P (3.6) 1b	3.2	198	20.8	69.9	0.467	0.633
C(110)P (3.6) 1c	3.2	246	25.9	200.2	0.533	2.433
C(110)P (3.6) 1d	3.2	230	24.2	147.9	0.400	1.800
C(110)P (3.6) 1e	3.2	240	25.3	212.4	0.467	1.833
Average		229	24.0	157.6	0.467	1.675
COV %		9		41	12	45
C(110)P (3.6) 2a	4.4	276	29.0		0.266	
C(110)P (3.6) 2b	4.4	281	29.6	174.5	0.333	1.366
C(110)P (3.6) 2c	4.4	252	26.5	173.1	0.433	1.867
Average		270	28.4	173.8	0.344	1.617
COV %		6		1	24	22
C(110)P (3.6) 3a	6.3	414	43.6	168.4	0.233	0.767
C(110)P (3.6) 3b	6.3	353	37.1	126.1	0.400	1.033
Average		384	40.4	147.3	0.317	0.900
COV %		11		20	37	21
C(115)A (3.25) 1c	3.2	312	30.0	313.7	0.667	1.633
C(115)A (3.25) 1d	3.2	368	35.4	401.2	0.767	1.767
Average		340	32.7	357.5	0.717	1.700
COV %		12		17	10	6
C(115)A (3.25) 2a	4.4	460	44.3	448.9	0.567	1.733
C(115)A (3.25) 2b	4.4	450	43.3	475.7	0.800	1.667
Average		455	43.8	462.3	0.684	1.700
COV %		2		4	24	3
C(115)A (3.25) 3a	6.3	629	60.6	701.5	0.600	1.433
C(115)A (3.25) 3b	6.3	639	61.5	632.9	0.650	1.616
C(115)A (3.25) 3c	6.3	598	57.6	677.3	0.733	1.767
C(115)A (3.25) 3d	6.3	612	58.9	682.6	0.667	1.800
Average		619.5	59.6	673.6	0.662	1.654
COV %		3		4	8	10

Table 5.7 Base-plate forces and stresses (continued)

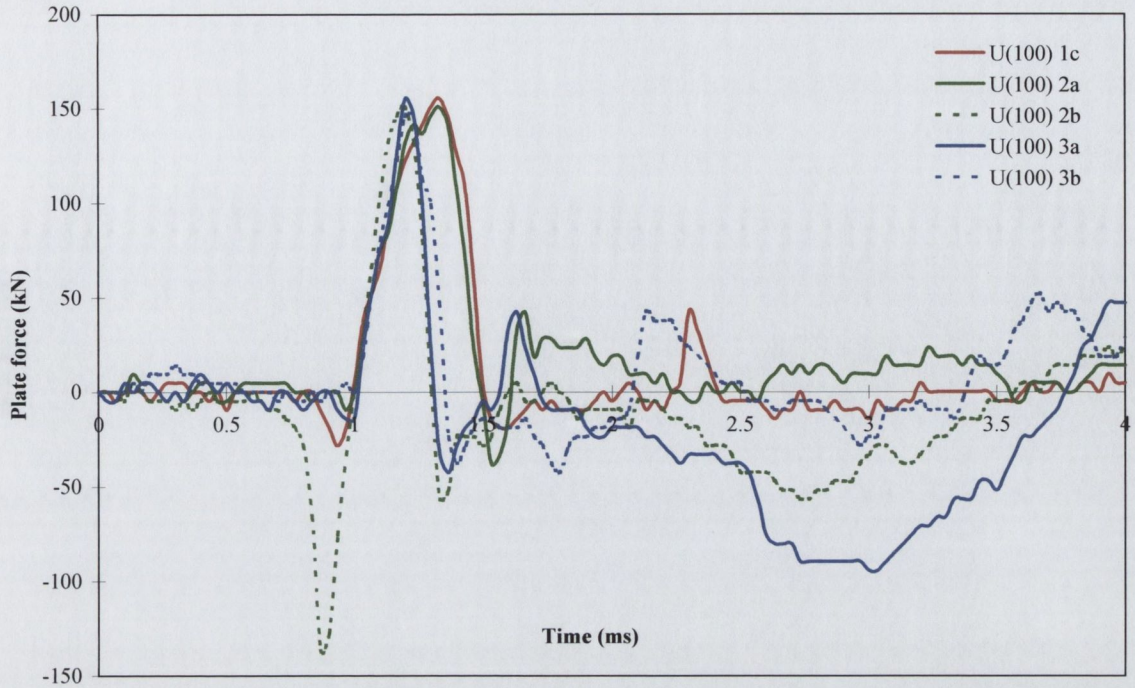


Figure 5.13 Plate force reponse of unconfined cylinders - U(100) - repeats at velocities 1 = 3.2 m/s, 2 = 4.4 m/s, 3 = 6.3 m/s

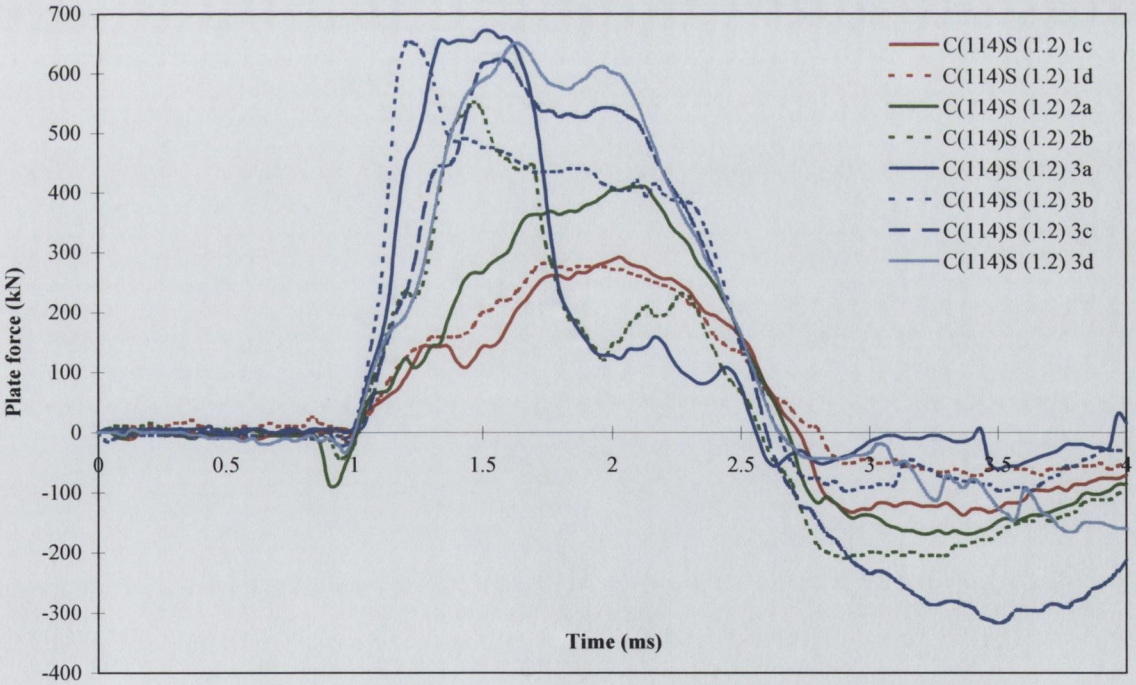


Figure 5.14 Plate force response of steel confined cylinders, thickness 1.2 mm - C(114)S (1.2) - repeats at velocities 1 = 3.2 m/s, 2 = 4.4 m/s, 3 = 6.3 m/s

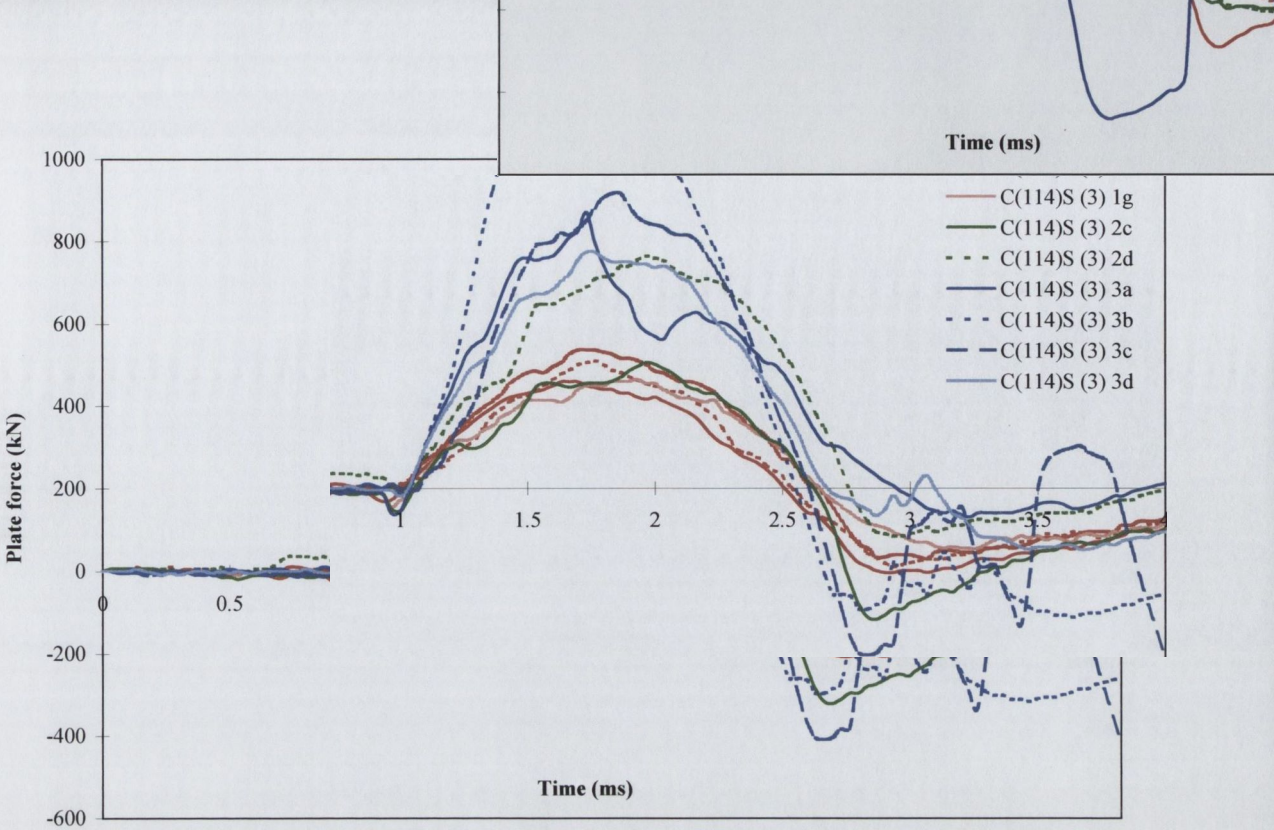


Figure 5.15 Plate force response of steel confined cylinders, thickness 3 mm - C(114)S (3) - repeats at velocities 1 = 3.2 m/s, 2 = 4.4 m/s, 3 = 6.3 m/s

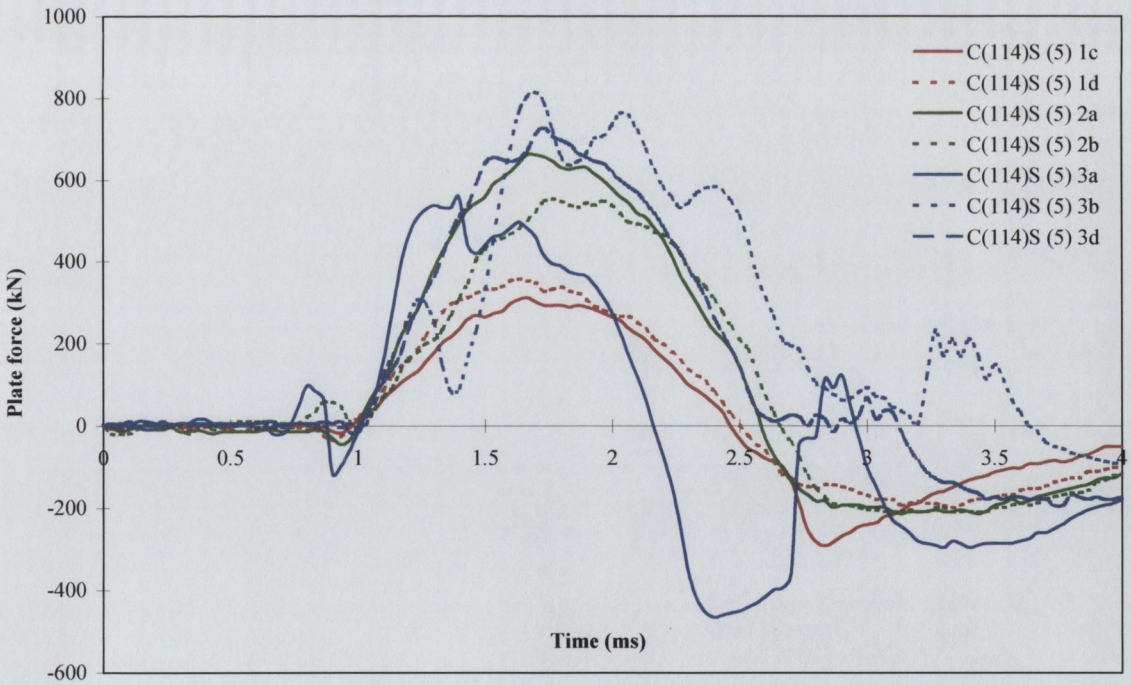


Figure 5.16 Plate force response of steel confined cylinders, thickness 5 mm - C(114)S (5) - repeats at velocities 1 = 3.2 m/s, 2 = 4.4 m/s, 3 = 6.3 m/s

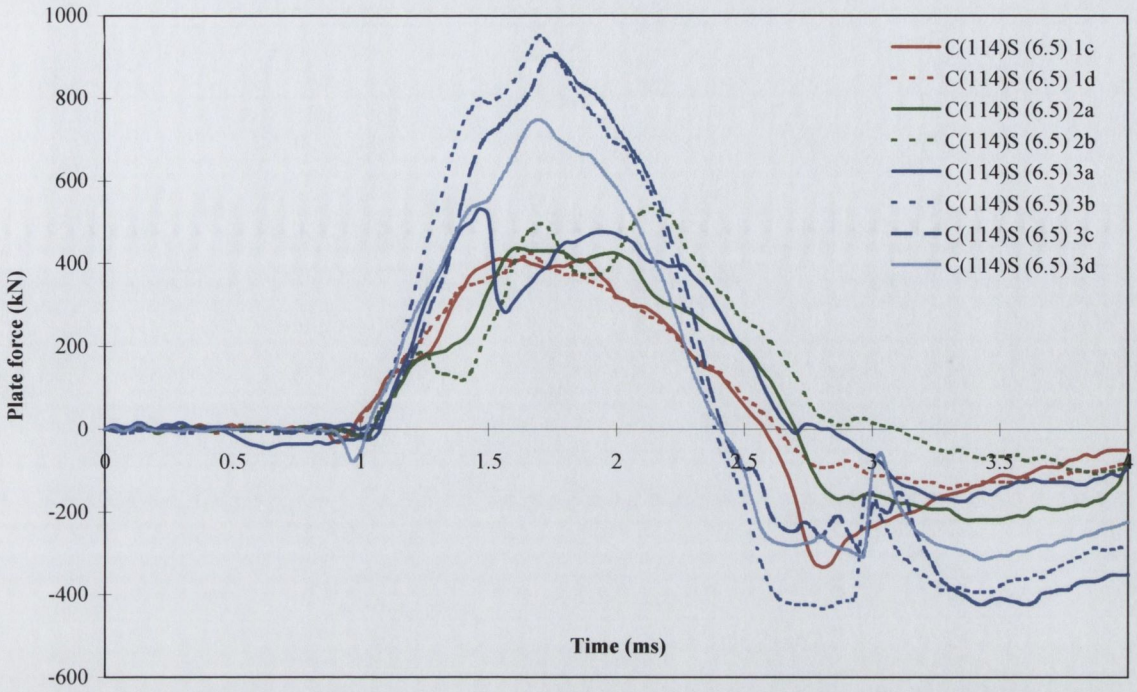


Figure 5.17 Plate force response of steel confined cylinders, thickness 6.5 mm - C(114)S (6.5) - repeats at velocities 1 = 3.2 m/s, 2 = 4.4 m/s, 3 = 6.3 m/s

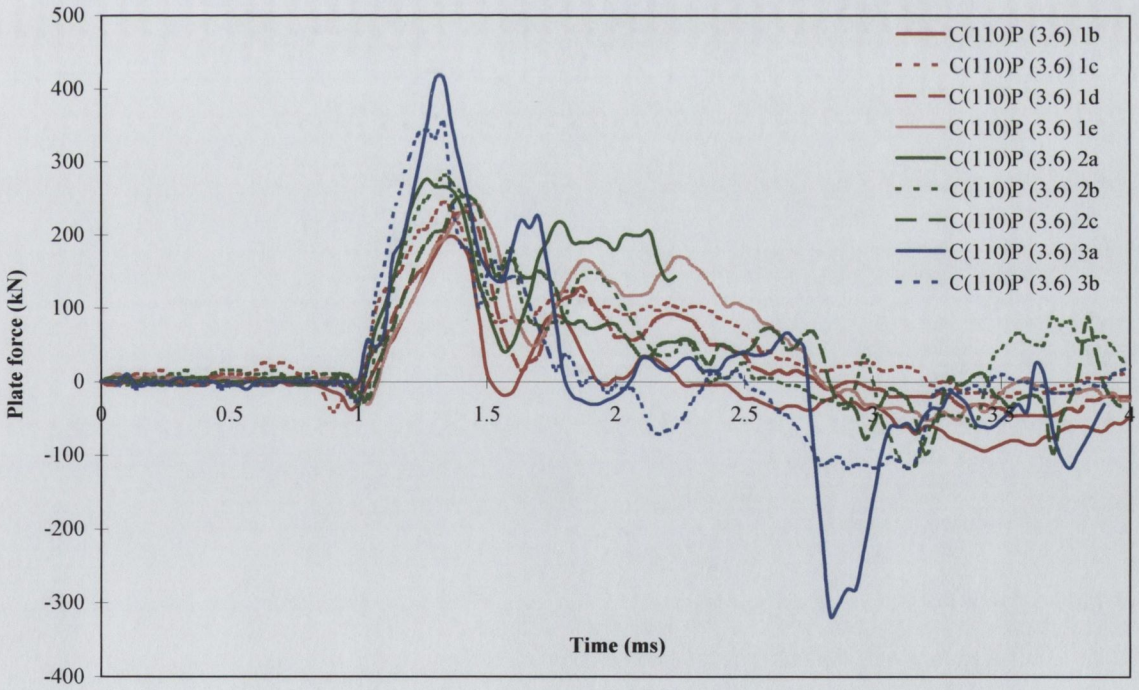


Figure 5.18 Plate force response of plastic confined cylinders, thickness 3.6 mm - C(110)P (3.6) - repeats at velocities 1 = 3.2 m/s, 2 = 4.4 m/s, 3 = 6.3 m/s

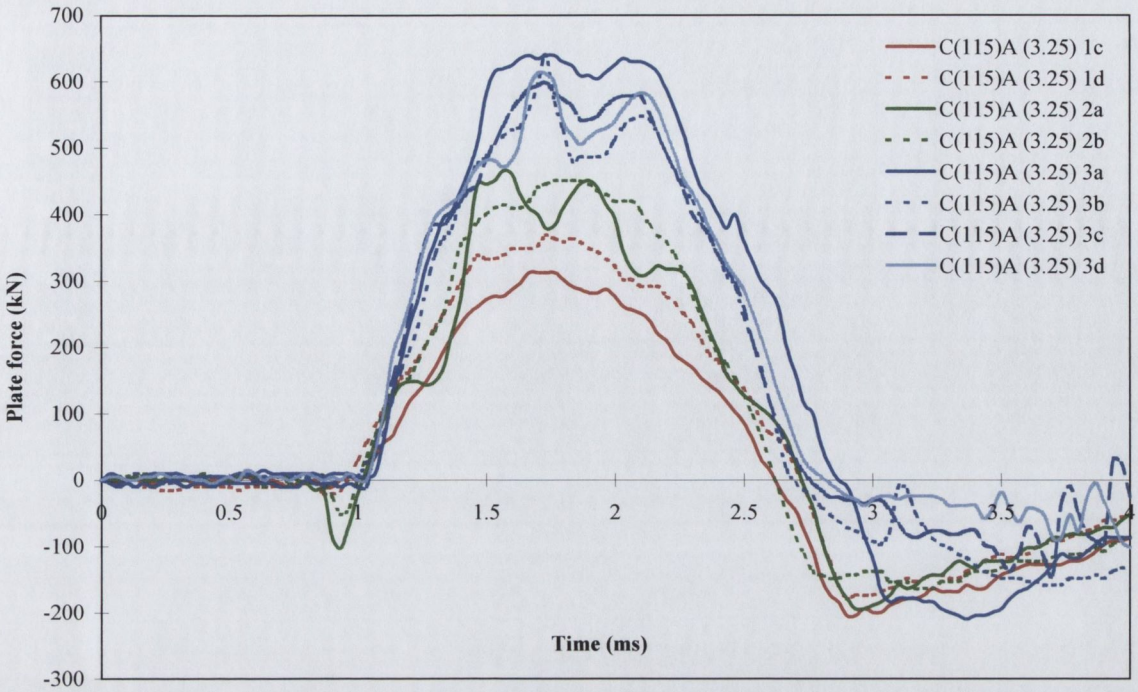


Figure 5.19 Plate force response of aluminium confined cylinders, thickness 3.25 mm - C(115)A (3.25) - repeats at velocities 1 = 3.2 m/s, 2 = 4.4 m/s, 3 = 6.3 m/s

The possibility of undertaking a factorial analysis on the base-plate force or stress results was considered. However, as it was only possible to perform a reduced factorial analysis on the much more numerous and consistent contact force results, it was decided that such an undertaking would probably not yield results which were statistically significantly different from the analysis undertaken for the contact force results.

The base-plate loadcell force values were used to determine the stress at the base of the cylinder resulting from the impact. As explained in section 4.4, it is preferable to use a loadcell at the unloaded end of the specimen to determine the stresses, rather than one at the location of impact, as this minimises any detrimental inertia effects. The stresses were calculated by dividing the base-plate force values by the cross-sectional area of the cylinder at its base. For the confined cylinders, the confining sleeve was bearing on the loadcell and, therefore, the cross-sectional area included the area of the confining sleeve. A proportion of the stress transmitted to the base passes into the confining cylinder and propagates along its length, as is evident by the presence of increasing longitudinal strains in the confining cylinder (section 5.5). The stresses are included in the table with averages, as their coefficients of variation are identical to those calculated for the base-plate forces.

The force measured by the base-plate loadcell is quite different to that measured by the contact force loadcell. Whereas the contact force loadcell determines the forces at the location of impact and is concerned only with the material properties and geometries at the interface, the base-plate loadcell measures the maximum force which the impacted cylinder was actually capable of propagating to its base, regardless of the energy initially transferred to it as a result of the impact. Figure 5.13 to Figure 5.19 show the base-plate force plots against time. In a similar way to the contact force analysis, these can be broken into two distinct groups, namely those in which the specimen fractured and those in which the confinement was sufficient to prevent overall failure of the concrete. The concrete fractured in both the unconfined case and the plastic confined case (particularly at higher velocities), resulting in a sharp peak, yet a small area under the base-plate force/time curve. The tests where the confinement was sufficient to prevent failure of the concrete are more sinusoidal in nature, because the material properties do not change significantly between the loading and unloading parts of the curve. These tests have a larger area under the compression part of the curve.

The base-plate forces of the unconfined concrete cylinders were very consistent with each other, over the range velocities, having a maximum coefficient of variation of 5%. If, as happened during the unconfined impact tests, the concrete fractures as a result of the impact, the material in the cylinder is not capable of transmitting all of the incident energy but transfers the maximum that it can prior to its fracture, at a value associated with the concrete properties, and not the velocity. This is consistent with the findings of Atchley and Furr (1967). In the case of the concrete in the unconfined cylinders, this maximum value was approximately 150 kN (Figure 5.13). It is quite probable that a limit could be found for a lower velocity of impact where the concrete does not fracture and allows nearly all of the contact force to be transferred to the base-plate loadcell. However, it was not possible or necessary to undertake tests to prove this. Similar logic can be applied directly to the confined cylinders in the interpretation of their base-plate force results. When impacted, the stress wave travelled through the concrete and, due to the presence of the confining sleeve, the concrete remained largely uncracked. The composite cylinder was capable of transferring the majority of the force measured at the top of the cylinder to the base-plate loadcell. As in the case of the contact force loadcell, the plastic sleeved cylinders responded in different ways depending on the velocity at which they were impacted. At the lowest velocity the plastic confined sleeves had not reached their load

capacity and it acted as a composite body but, by the highest velocity, the energy imparted to the cylinder was greater than it could resist and caused fracture of the cylinder and a levelling off of the maximum base-plate force measured.

Figure 5.20 compares the response of the contact force and base-plate loadcells for a confined and an unconfined cylinder impacted at 3.2 m/s. In both cases, the base-plate loadcell has a less steep initial gradient than the corresponding curve measured by the contact force loadcell because of the time delay associated with the transmission of the force along the length of the impacted cylinder. The force-time curves for the base-plate loadcell also exhibit a large negative phase when the concrete was confined. This occurred because the loadcell went into tension as the weight of the cylinder was removed when the impactor rebounded and was no longer in contact with the specimen. The impactor did not rebound when the concrete was unconfined, as the cylinder disintegrated and this negative phase does not occur for these types of cylinder. As can be seen in this figure and in others between Figure 5.13 and Figure 5.19, the base-plate force plots are slightly less uniform in shape than the contact force plots. This probably occurred because of variations in the wave transmission path through the inhomogeneous concrete and into the loadcell.

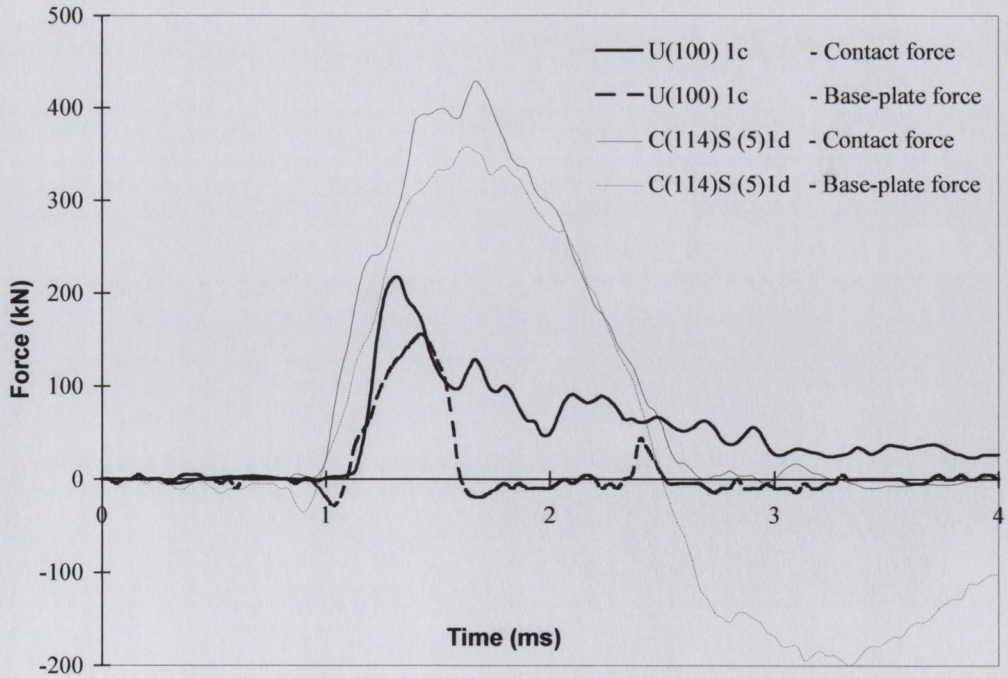


Figure 5.20 A comparison of the contact force and base-plate loadcell for unconfined (U(100)) and steel confined concrete (C(114)S (5))

Some of the base-plate force curves exhibit a slight either positive or negative "blip" prior to the start of the main loading curve, which happened sporadically throughout the test series, but can be clearly seen for both of the tests in Figure 5.20. It was difficult to explain because of its intermittent nature and because it often occurred before the stress wave should, theoretically, have reached the loadcell. It was thought initially that this might have occurred because the manganin gauges have a very fast response time and are very sensitive to pressure variations. However, the problem became increasingly apparent during an auxiliary set of tests and was, therefore, examined more thoroughly. The same phenomenon was reported by Bourne and Rosenberg (1996, 1997) whilst studying the response of ceramics to shock loading using manganin gauges. They found that when the gauges are mounted close to a metal surface that they can exhibit this "blip" when loaded at high rates. The gauge is supplied by a constant current through a Wheatstone bridge circuit. Although the gauge is assumed to be purely resistive so that the changes of resistance can be recorded, the gauge actually has a finite inductance. They suggest that the "blip" is as a result of a capacitive linkage between the gauge, the power supply and recording equipment, and showed that it has no effect on the overall results from the gauge. However, the problem was exacerbated when the base-plate loadcell was wired into the slot in the SCXI unit beside the impactor loadcell. Due to the calibration factors involved, the impactor loadcell exhibits a response far greater than the base-plate loadcell and was causing the base-plate loadcell's signal to peak sharply when the impactor loadcell began to respond to the impact (Figure 5.21). Wiring the base-plate loadcell into a separate terminal block, with an empty slot left beside each of the loadcells reduced the magnitude and the frequency of occurrence of the "blip".

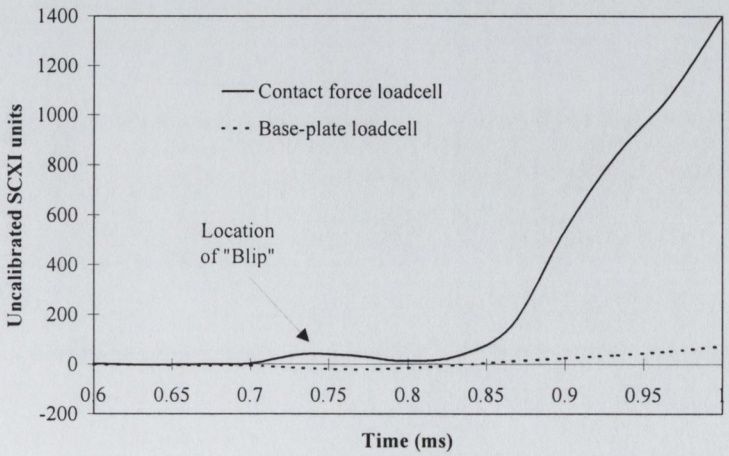


Figure 5.21 Loadcell responses, prior to calibration, of C(114)S (5)1d showing "blip"

Due to the variations in both the measured contact force and the base-plate force it is difficult to draw a definite conclusion as to how much of the force experienced at the top of the concrete cylinder propagated to its base. Table 5.8 shows the ratio of the contact force to the base-plate force. In the case of the confined concrete, at least 70 % of the force is transmitted to the base and into the loadcell. Some of the decrease in force can be explained by the transmission and reflection of stresses at the interface (using equation (2.51)). However, the rest of the reduction in the force probably occurs as a result of a slight deterioration in the material properties as the concrete fractures when impacted. No particularly evident pattern emerges as the velocity increases, however, it probably depends on the proximity of the cracks in the concrete to the path of the wave. The decrease in the transmitted stress is most evident in the case of the unconfined concrete, where the percentage of force transferred to the base-plate loadcell drops by approximately 30 % over the velocity range, as the concrete fractures and is unable to transmit any more load to the base.

The results were also analysed by considering their relationship with the velocity of impact. Because of the transfer of force through the cylinder, particularly when confined, it is not surprising that the force or stress transferred to the plate loadcell is proportional to the velocity of the initial impact, as illustrated in Figure 5.22, a graph of the average stress at the base of the cylinder against the velocity of impact. Regression lines were fitted to the data which, in all cases except the unconfined concrete for reasons previously explained, go through the origin and show the linear relationship between the velocity of the impactor and the stress at the base of the cylinder. The graph would suggest that the confinement offered by the steel of thickness 5 mm and 6.5 is very similar and that these sleeves are

Velocity (m/s)	3.2	4.4	6.3
U.100	0.73	0.48	0.44
C.114.S (1.2)	0.76	0.81	0.83
C.114.S (3)	0.73	0.77	0.71
C.114.S (5)	0.81	1.07	0.80
C.114.S (6.5)	0.96	0.79	0.75
C.110.P (3.6)	0.8	0.77	0.86
C.115.A (3.25)	0.89	0.85	0.73

Table 5.8 Ratio of contact force to base-plate force (average values)

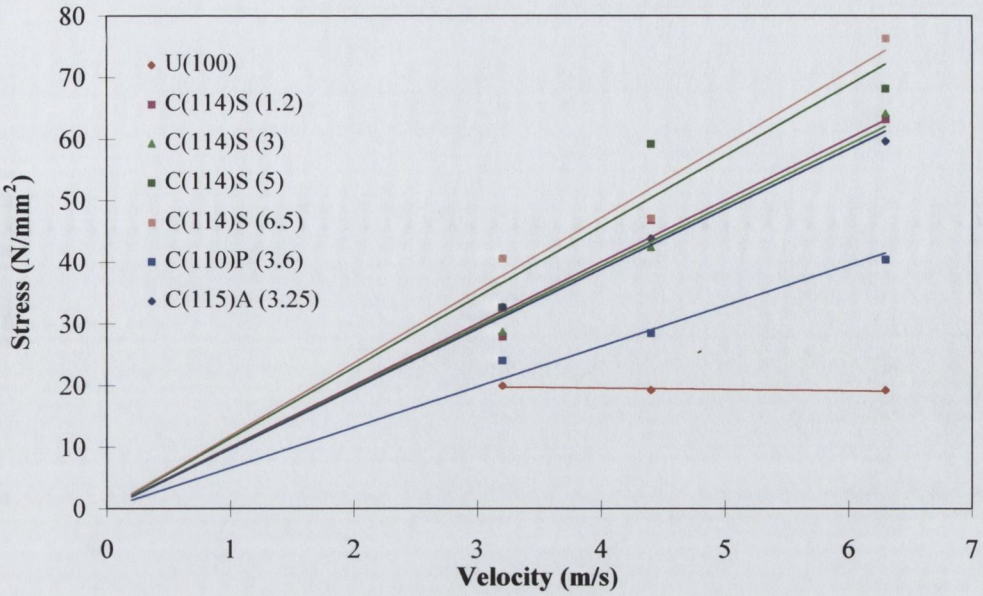


Figure 5.22 Relationship between average stress at the base of the cylinder and the velocity of impact, with fitted regression lines

best at resisting the dilation of the concrete under the load and allowing more of the force to be transmitted in an elastic manner to the base-plate loadcell. The results from the cylinders confined by steel of 1.2 mm, 3mm and the aluminium confined cylinders all provide similar levels of confinement along the length of the cylinder. The confinement provided by the plastic results in a much more effective response than if the cylinder is unconfined, but is much less effective than the other confining sleeves.

The time taken for the base-plate force to reach its maximum value and the time taken for it to return to zero after the impact are both given in Table 5.7, with the integral under the base-plate force/time plot within the compression part of the loading. As would be expected, the impulse determined from under the base-plate force plot is related to the maximum base-plate force in a similar manner to the relationship between the maximum contact force and the area under that curve. All of these values have considerably higher coefficients of variation than those for the maximum base-plate force or those for similar values measured by the contact force loadcell. Due to the nature of the propagating stress wave, all are dependant on the path taken by the wave between the top and base of the cylinder and the degree to which the wave encountered either aggregate or mortar, as both have different densities and stress wave propagation speeds, and this would affect the overall path and speed of stress wave propagation.

5.4. QUALITATIVE TEST RESULTS

All of the cylinders impacted were examined qualitatively to assess their response to the impact loads. However, unlike the measurements taken using the data acquisition system, the qualitative responses were more difficult to evaluate. The information captured by the data acquisition system was recorded sufficiently fast as to allow both the initial and subsequent impacts, caused by the rebound of the impactor, to be clearly and separately identified. The post-event examination of each cylinder was the outcome of the impact itself and any re-impact after rebound. Not surprisingly, the response of the unconfined and confined cylinders were entirely different, ranging from complete disintegration of the unconfined cylinders to minor cracking in the cylinders confined by the thickest steel sleeves. Photographs of a typical cylinder from each group are included in Figure 5.23 to Figure 5.43.

The unconfined concrete cylinders all failed dramatically in a consistent and uniform manner, regardless of the contact velocity. They split axially into three or four almost equal sections from the centre of the top face; Figure 5.23 shows an unconfined cylinder impacted at the lowest velocity (3.2 m/s). A proportion of each of the unconfined cylinders, especially at the higher velocities, was reduced to rubble by the impact, leaving some pieces of up to 100 mm in length. The axial splitting was associated with the slight curvature in the nosecone of the impactor, which reduced the effects of any surface irregularities in the concrete but did, initially, concentrate the loading in the centre of the cylinder. The concrete fractured this way because the compressive stress wave, which travels through the concrete after the impact, was reflected from the base of the cylinder as a tensile wave, the magnitude of which was greater than the tensile strength of the concrete. The rubble consisted of aggregate particles, pieces of mortar, aggregate particles which still had mortar attached to them and small pieces of concrete. Uncrushed aggregate was used in the fabrication of the concrete and on examination of the cracked faces of the particles, it was clearly evident that failure of the aggregate, the aggregate-cement bond and the cement paste itself had occurred. Meanwhile, the cylinders confined by a sleeve of either steel or aluminium remained sensibly whole after the impact but the majority exhibited radial and circumferential cracking in their top faces.



Figure 5.23 Unconfined - v 3.2 m/s

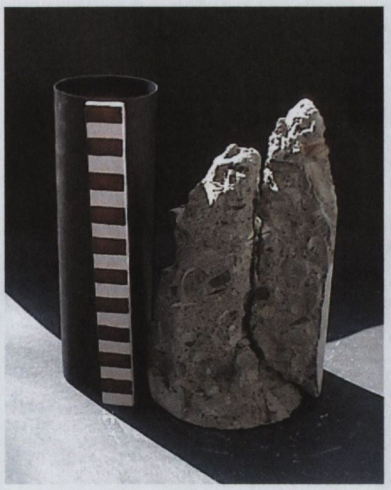


Figure 5.24 Unconfined v = 4.4 m/s



Figure 5.25 Unconfined v= 6.3 m/s



Figure 5.26 Cracking in C(114)S (1.2)1d

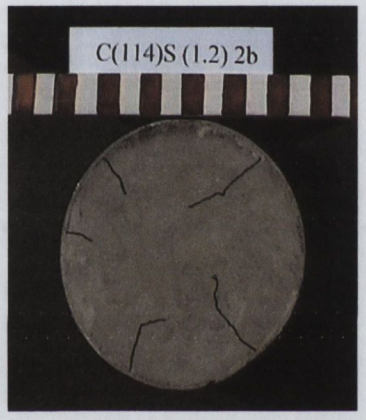


Figure 5.27 Cracking in C(114)S (1.2)2b



Figure 5.28 Cracking in C(114)S (1.2)3c



Figure 5.29 Top face of C(114)S (3)1b



Figure 5.30 Cracking in C(114)S (3)2a



Figure 5.31 Cracking in C(114)S (3)3d

The bar in the photographs is marked in units of 10 mm



Figure 5.32 Cracking in C(114)S (5)1d



Figure 5.33 Cracking in C(114)S (5)2a



Figure 5.34 Cracking in C(114)S (5)3a



Figure 5.35 Top face of C(114)S (6.5)1d



Figure 5.36 Top face of C(114)S (6.5)2b



Figure 5.37 Cracking in C(114)S (6.5)3a



Figure 5.38 Cracking in C(115)A (3.25)1c



Figure 5.39 Cracking in C(115)A (3.25)2a

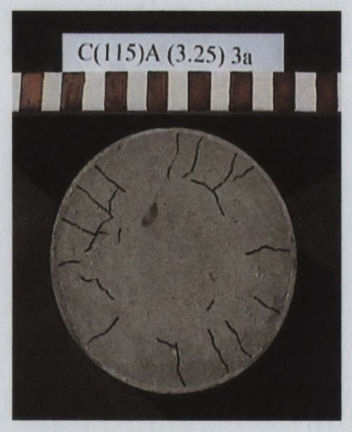


Figure 5.40 Cracking in C(115)A (3.25)3a

The bar in the photographs is marked in units of 10 mm



Figure 5.41 Cracking in C(110)P (3.6)1a



Figure 5.42 Disintegration of C(110)P (3.6)2b

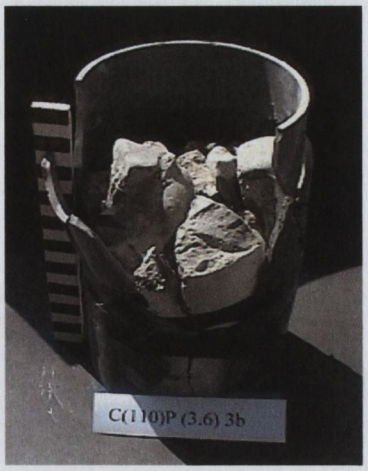


Figure 5.43 Disintegration of C(110)P (3.6)3b

The bar in the photographs is marked in units of 10 mm

These cracks were examined carefully under a spotlight using a magnifying glass, a crack-width microscope (accurate to 0.02 mm) and a micrometer (accurate to 0.1 mm), prior to being carefully marked with ink for photographic purposes. The total area of cracking in the top face of each cylinder was quite small in comparison to the total cross-sectional area of the cylinder. The cracked area was estimated by summing the products of the width and the length of the cracks. As would be expected, the crack widths varied along each of their lengths and the width was, therefore, determined by taking an average measurement at approximately half the length of the crack. The results of these findings, which are intended to be indicative of the damage done to the cylinder, are summarised in Table 5.9.

At a velocity of 3.2 m/s, little or no top face cracking was evident in the cylinders confined by the three thickest sleeves of steel. However, the cylinders confined by the 1.2 mm

	Velocity = 3.2 m/s	Velocity = 4.4 m/s	Velocity = 6.3 m/s
C(114)S (1.2)	6.03	9.09	23.93
C(114)S (3)	0	1.58	6.63
C(114)S (5)	0.44	2.59	2.01
C(114)S (6.5)	0	0	1.44
C(115)A (3.25)	3.93	4.88	27.39
C(110)P (3.6)	24.61	Disintegration	Disintegration

Table 5.9 Crack areas in typical confined cylinders (mm^2)

thick sleeve exhibited some top face cracking, as shown in Figure 5.26. As the velocity increased, radial cracking in the top faces of the concrete became increasingly common, with cracks ranging in width between 0.02 mm and 0.3 mm, and extending up to 30 mm from the inside face of the confining sleeve. The cracking was considerably more extensive in the cylinders confined by the thinner sections of steel sleeve, and became less extensive as the sleeve became thicker. However, as has previously been mentioned in the factorial analysis of the contact force results, the concrete in the 5 mm thick steel cylinders was weaker than that in the other cylinders and underwent more cracking than would be expected. Even at the highest velocity, these cracks in any of the steel confined cylinders were not extensive, either radially or circumferentially and rarely extended more than 20 mm from the concrete circumference (see for example Figure 5.31 and Figure 5.37).

The concrete cylinders confined by sleeves of aluminium were more susceptible to crack propagation, as shown in Figure 5.38 to Figure 5.40. This might have been expected because aluminium has a Young's modulus which is a third of the value for steel and allows more dilation to occur than a similar thickness of steel but, in most cases, less dilation than the thinnest steel sleeve. At the lowest velocity, the cylinders confined by plastic showed considerable top face cracking and permanent deformation of the sleeve, which remained visible after the test (Figure 5.41). However, although these cylinders had 10 times more cracks than the concrete confined by steel 1.2 mm thick, which underwent the next most severe degree of cracking, they remained whole after the impact. When the sleeve was cut away from the concrete considerable cracking was evident along the length of the cylinder. At a contact velocity of 4.4 m/s, the plastic sleeve split at the top and resulted in a considerable amount of cracking in the upper quarter of the concrete cylinder (Figure 5.42). At the highest velocity (6.3 m/s), the confining sleeve split along its entire length and was unable to provide confinement throughout the duration of the impact, leading to disintegration and fragmentation of the concrete (Figure 5.43).

These results are particularly interesting as they corroborate the earlier findings of the contact force analysis in that when the cylinders are well confined they are able to withstand impact of up to 4.4 m/s, whilst still remaining elastic and not cracking. However, at velocities greater than this, the energy involved in the impact is too great for the cylinders which are not totally rigidly confined, which is anything other than the 6.5 mm thick steel sleeve, and causes cracking and a deviation from 'elastic' behaviour.

5.5. STRESS-STRAIN RESPONSE

Each of the confined and unconfined cylinders was instrumented to allow both the stress at the base of the cylinder and the deformational response along the length of the cylinder to be assessed. The stress was measured using a thin, base-plate loadcell placed under the specimen, the responses of which, with respect to time, are described in section 5.3. As explained in section 4.2.6, each of the cylinders had between 4 and 25 strain gauges attached to its skin circumference to allow its deformational response to be determined. Compressive strains are shown as being positive throughout (and were predominantly from the axial gauges), whilst tensile strains are negative (which were usually associated with the lateral gauges). A large degree of variability was experienced between different test specimens for many of the strain results, which is to be expected when specimens are subject to impact. This is because the cracking which occurs in the concrete, even if minor, is less controlled than in the case of static loading, and can vary considerably between different specimens.

5.5.1. Strain gauge response

The strain measured by the gauges attached to the impacted cylinder varied from test to test. Because of the density of information obtained during each test, and then during the repeats in a particular group, it was not possible to present summary graphs of the strain gauge response with time for all of the specimens. Typical plots of strain against time, for each of the cylinder types, at a velocity of 3.2 m/s, are shown in Figure 5.44 to Figure 5.52,. The effects of changing the velocity are also shown for the cylinders C(114)S (3) in these figures. The strain/time response for each cylinder is given in Appendix 3.

Figure 5.44 shows a typical plot of the strain responses of an unconfined cylinder during the impact event. As was frequently the case, three of the four gauges attached to the unconfined cylinder broke as the concrete split apart during the test, as can be seen on the graph. There appears to be a difference in the strains at which the gauges failed, however, this occurred because of the way the gauges were calibrated and is dependant on the relative values of the initial strain and the off-scale limit. Due to the speed at which the data recorders were scanning information from the gauges, it was possible to pick up

accurately the strain information in the pre-fracture part of the graph. The response from the pairs of diametrically opposite lateral and axial gauges were similar to one another, particularly in the initial part of the loading, before substantial cracks had formed in the concrete. Therefore, the results from the pairs of diametrically opposite gauges were averaged. The graphs of the unconfined concrete strains against time were used to

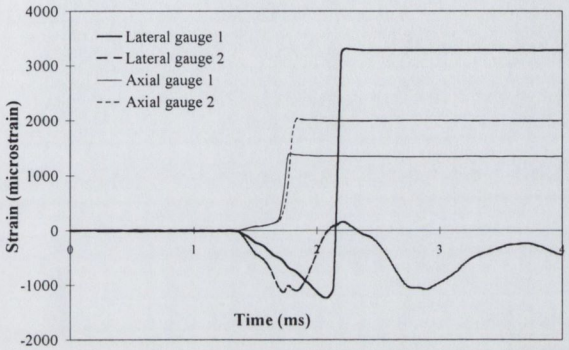


Figure 5.44 Strain gauge response of U(100)1d at 3.2 m/s

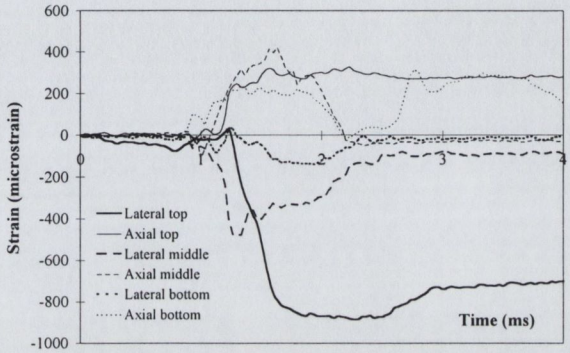


Figure 5.45 Strain gauge response of C(114)S (1.2)1d at 3.2 m/s

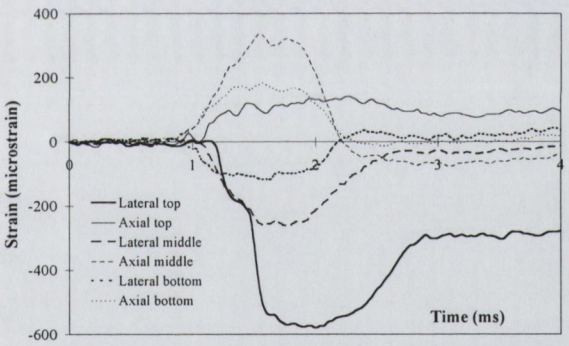


Figure 5.46 Strain gauge response of C(114)S (3)1d at 3.2 m/s

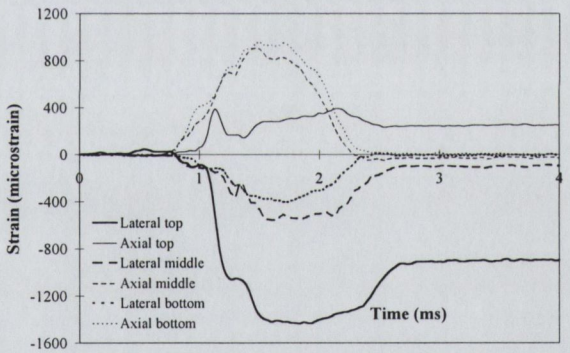


Figure 5.47 Strain gauge response of C(114)S (3)2d at 4.4 m/s

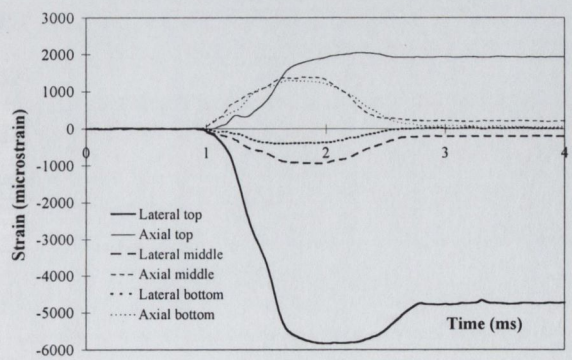


Figure 5.48 Strain gauge response of C(114)S (3)3c at 6.3 m/s

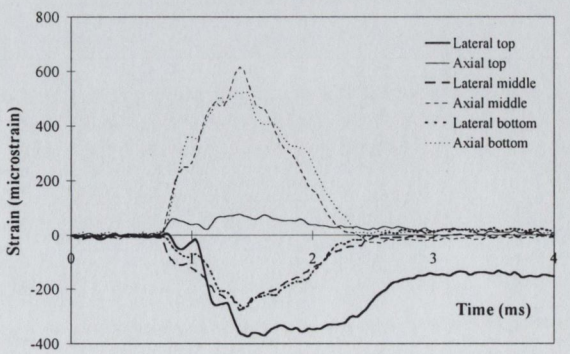


Figure 5.49 Strain gauge response of C(114)S (5)1d at 3.2 m/s

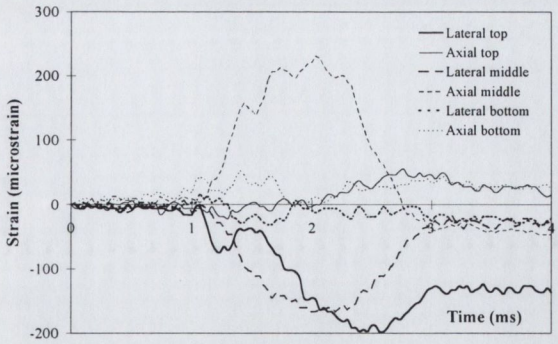


Figure 5.50 Strain gauge response of C(114)S (6.5)1b at 3.2 m/s

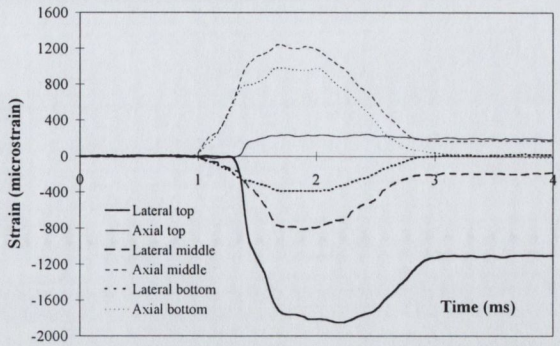


Figure 5.51 Strain gauge response of C(115)A (3.25)1c at 3.2 m/s

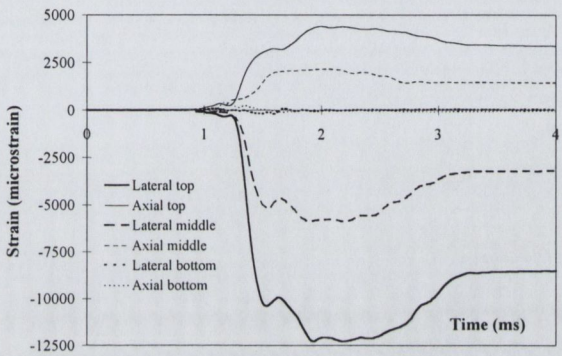


Figure 5.52 Strain gauge response of C(110)P (3.6)1e at 3.2 m/s

determine the loading rate induced by impact. As the strain rates were much higher than for static loading this can cause variability in the responses and corresponding variability in the strain rates because of the way in which the concrete fractures. Strain rates were determined, quite simply, from the strain gauge responses of the unconfined cylinders by dividing the axial strain at maximum compressive stress (which is known as the critical compressive strain, ε_0) by the time taken to reach this strain level. The strain rate at the lowest velocity (3.2 m/s) was found to be 2.5 sec^{-1}. At a velocity of 4.4 m/s the average strain rate was 5 sec^{-1}, and at a velocity of 6.3 m/s the average value was 9 sec^{-1}. The similarity of the results, over the entire group of unconfined cylinders, gives confidence that these strain rates are accurate, despite local fluctuations.

Figure 5.45 to Figure 5.52 show typical strain gauge responses from confined cylinders with 6 no. strain gauges attached, on the generator of the cylinder, at three different heights (as shown in Figure 4.7). Work was undertaken initially to strain gauge each of the confined cylinders more fully, by attaching up to 25 gauges to the outer circumference. However, when data was acquired from these cylinders, the signal, despite filtering, was

very noisy and inconsistent as can be seen from the results of those cylinders in Appendix 3. It was thought, initially, that this might be occurring as a result of a small degree of eccentricity in the loading. However, an identical sleeved cylinder was loaded concentrically and statically and exhibited similar results. Therefore, it was concluded that the steel or aluminium confining sleeve was affected by electrical interference caused by the number of gauges around the outside of the sleeve. The strain gauge responses from these cylinders, being very erratic and inconsistent, were largely neglected in the analysis. Much effort was made to ensure that each of the cylinders impacted at a particular velocity were loaded in an identical manner to ensure that the strains were comparable from test to test and that each cylinder was loaded concentrically. Therefore, the generator, to which the strain gauges were attached, was lined up prior to each test with a mark inscribed into the concrete support base.

The strain gauge responses are of a similar form to the curves for the contact force and base-plate loadcells described in sections 5.2 and 5.3. This is to be expected as the strains vary as the load is applied to and taken off the cylinder. As can be seen from the responses of any of the confined cylinders, the largest strains were experienced by the lateral gauge nearest to the location of impact, which was also where the smallest axial strains are experienced. The responses from the middle and bottom gauges were similar in magnitude to one another, with the axial gauges experiencing more strain than the lateral gauges at the same level. These phenomena will be discussed in conjunction with the stress-strain responses in the following section.

The results from these strain gauges clearly show that, as would be expected, the maximum strains in any of the gauges, lateral or axial, increase considerably as the velocity of impact increases. This can be seen in Figure 5.46 to Figure 5.48, which show the variation in the strain in the 3 mm thick steel confining cylinder with velocity. For example, the maximum strain in the middle lateral and axial gauges were

- -270 and 330 microstrain at a velocity of 3.2 m/s (C(114)S (3)1d)
- -550 and 900 microstrain at a velocity of 4.4 m/s (C(114)S (3)2d)
- -940 and 1390 microstrain at a velocity of 6.3 m/s (C(114)S (3)3c).

This trend can be seen throughout all of the results for the confining cylinders and is not surprising as the load transferred to the base of the cylinder increased as the velocity increased (see section 5.3), which caused more strain to be induced in the sleeve. At some

locations along the length of the confining cylinder the strains experienced, particularly at the highest velocity, exceeded the yield strength of the sleeve and result in its acting inelastically (as shown in Figure 5.48). Secondly, the presence of an increasingly thick confining sleeve resulted in a reduction in the maximum strains recorded. Again, this can be illustrated with an example of the middle lateral and axial gauges from the different thicknesses of steel confinement, at a contact velocity of 3.2 m/s. The middle lateral and axial strains measured were

- -470 and 420 microstrain for a thickness of 1.2 mm (C(114)S (1.2) 1d)
- -270 and 330 microstrain for a thickness of 3 mm (C(114)S (3)1d)
- -260 and 610 microstrain for a thickness of 5 mm (C(114)S (5)1d)
  (although the axial strain is atypical when compared to others in the series)
- -170 and 230 microstrain for a thickness of 6.5 mm (C(114)S (6.5)1b).

It is most noticeable in these figures that the uppermost lateral gauge does not return to zero after the impactor has bounced clear of the confined cylinder. Instead, a proportion of the strain remains, much like a residual strain. This occurs at the lowest velocity, as shown here, and occurs in a similar way in the other results. This could be expected in the case of the plastic confined cylinders which experience high strains because of their low Young's modulus, and which do not act elastically. However, in the majority of cases, the steel and aluminium do not even reach their yield strains, as shown in appendix 2, (except at the highest velocity), yet this residual strain exists in the top lateral gauge of the confining sleeve after the removal of the load. The ratio of the residual strain to the maximum strain varies from test to test, but is typically between 50% and 75%. The residual strains probably remain because the cylinder has undergone some lateral dilation and limited cracking has occurred in the top of the concrete core. These cracks do not close perfectly when the load is removed and their presence cause the persistent lateral dilation of the sleeve.

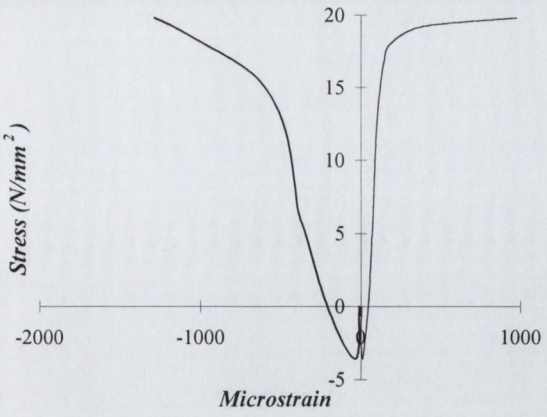
5.5.2. Plots of stress against strain for impacted cylinders

The results from the strain gauges attached to either the concrete of the unconfined cylinders or the outer skin circumference of the confining cylinder were coupled with the stress response of the base-plate loadcell between the points of zero stress (or as near as it

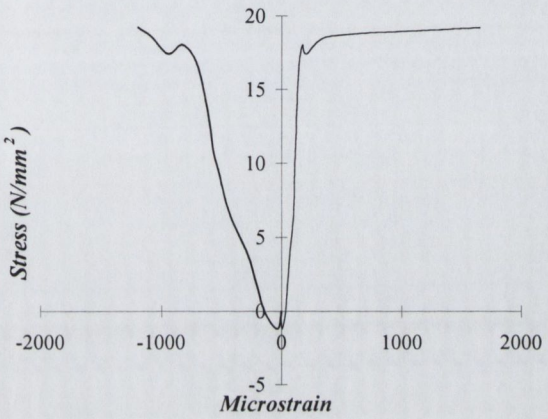
was possible to attain to zero stress) and maximum stress, to obtain plots of stress against strain. As is well established (Bischoff and Perry, 1995), due to the inhomogeneous nature of concrete, the stress-strain plots are not always very regular and are not always easily repeatable. However, Figure 5.53 to Figure 5.59 give typical stress-strain plots for each of the confinement types at each of the three velocities of impact. Again, due to the density of information it was not possible to present more than one set of results on each graph and similar plots for all of the other cylinders tested can be found in appendix 3.

Stress wave propagation is inevitable during impact loading and causes a time lag between measurement responses taken at the different locations. Hence, when comparing responses from strain gauges and loadcells at different locations, it is often necessary to offset the data points with respect to one another to ensure that the correct results are compared with one another. However, the time taken for a stress wave to travel half the length of the specimen through the concrete (the distance between gauges), as determined from the longitudinal wave velocities recorded in Table 4.1 and Table 4.3, was considerably less than the time between scans (0.023 milliseconds compared to 0.033 milliseconds scan time). It was, therefore, unnecessary to offset the stress-strain responses as doing this would have made the resulting graph less credible. Furthermore, it was impossible to determine from the experimental results whether the measured wave travelled through the concrete or through the confining sleeve. It was probable that a proportion of the load was transferred into the sleeve quite quickly and that the stress waves travel in the different media at different speeds, as the steel, aluminium and plastic have different stress wave propagation speeds to the concrete. Therefore, for the stress-strain diagrams in this research it was not necessary to offset the data points with respect to one another.

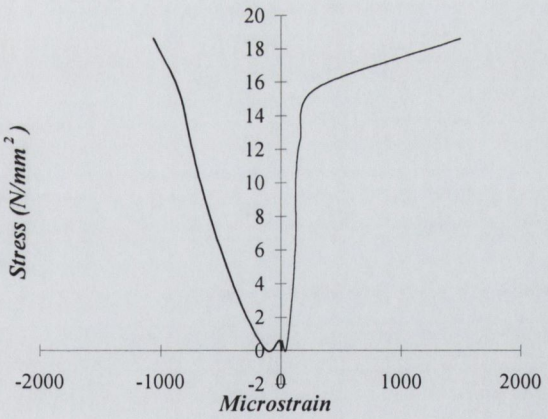
Three of the stress-strain graphs for unconfined concrete cylinders are shown in Figure 5.53. The strains were determined by using average values from the two diametrically opposite strain gauges. The strain gauges bonded to the concrete surface, measuring the deformational response, could only be relied upon to measure the ascending portion of the stress-strain plot accurately as, beyond the peak stress, the inner core of the specimen carries a larger portion of the applied load and the outer section, to which the strain gauges were attached, has a reduced load carrying capacity (Kotsovos, 1983). The axial gauges exhibit a bilinear response, with a flat, but still increasing plateau starting at approximately



U(100)1c, velocity 3.2 m/s



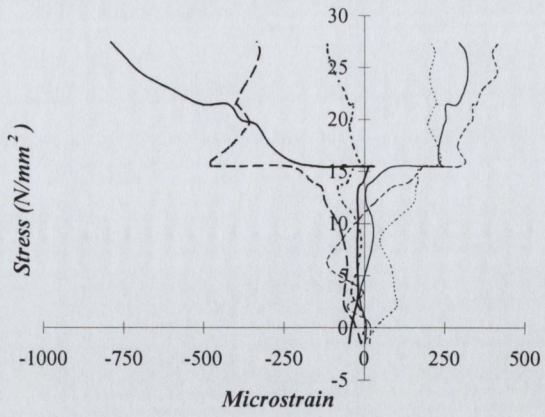
U(100)2a , velocity 4.4 m/s



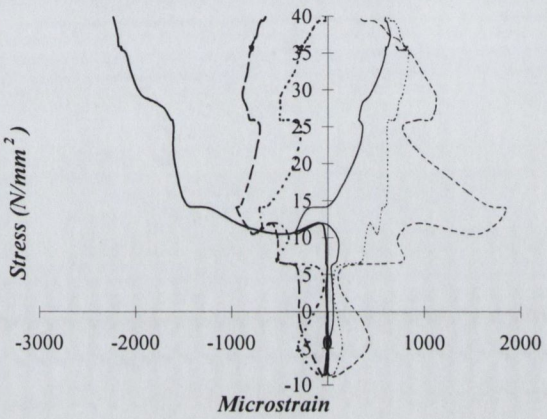
U(100)3b, velocity 6.3 m/s

Lateral top —— Axial top ——

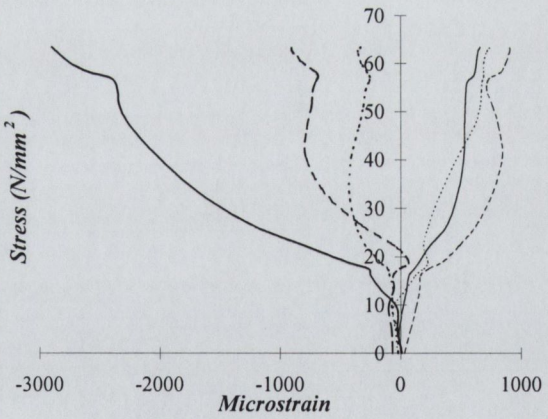
Figure 5.53 Stress-strain plots - unconfined



Co(114)S(1.2)1d, velocity 3.2 m/s



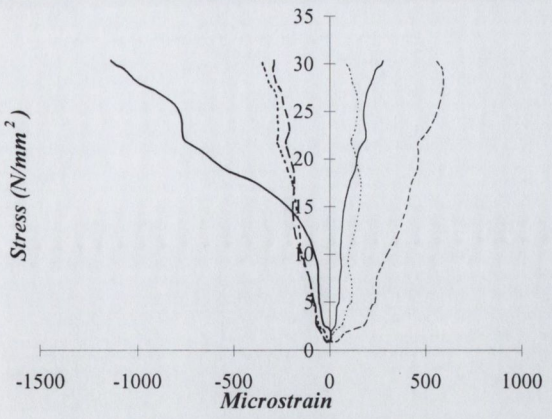
Co(114)S(1.2)2a, velocity 4.4 m/s



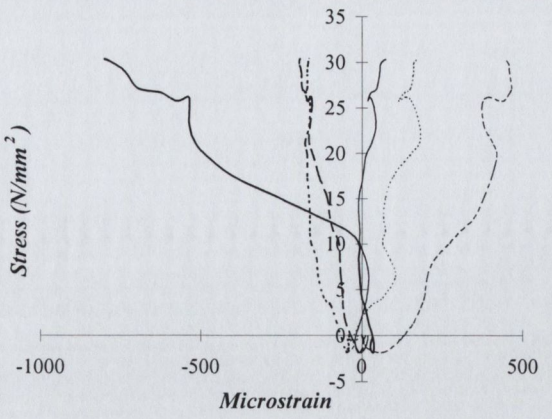
Co(114)S(1.2)3d, velocity 6.3 m/s

Lateral top —— Axial top ——
Lateral middle — — Axial middle - - - -
Lateral bottom - - - Axial bottom ·····

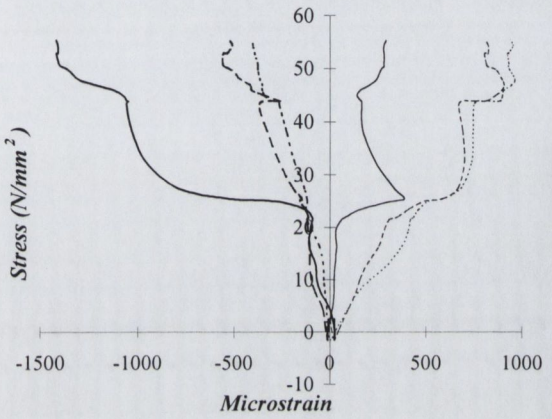
Figure 5.54 Stress-strain plots - steel confined, thickness 1.2 mm



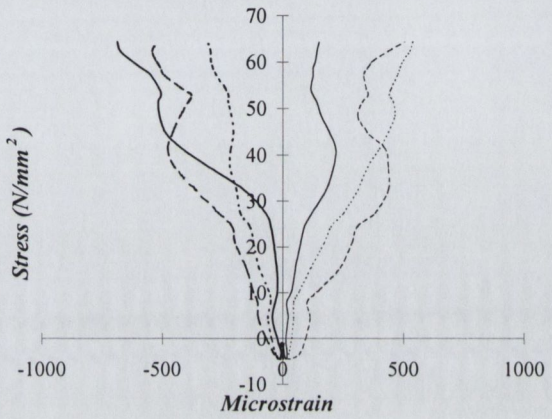
Co(114)S(3)1e, velocity 3.2 m/s



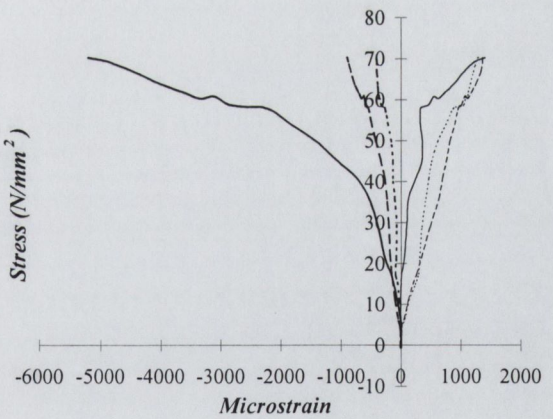
Co(114)S(5)1c, velocity 3.2 m/s



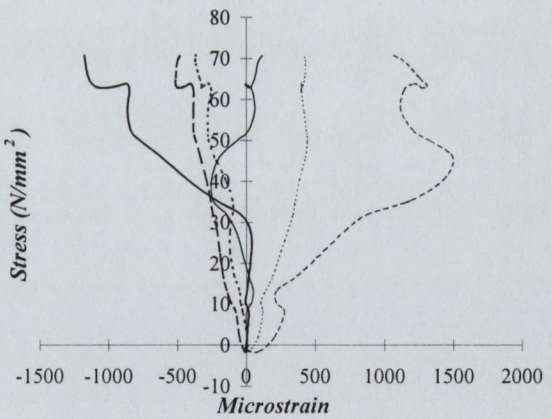
Co(114)S(3)2d, velocity 4.4 m/s



Co(114)S(5)2a, velocity 4.4 m/s



Co(114)S(3)3c, velocity 6.3 m/s



Co(114)S(5)3d, velocity 6.3 m/s

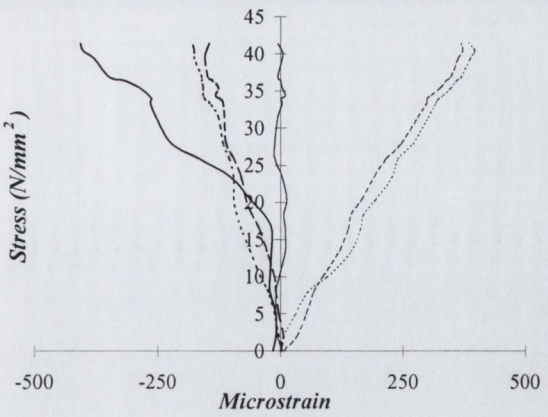
Lateral top —— Axial top ——

Lateral middle — — Axial middle - - - -

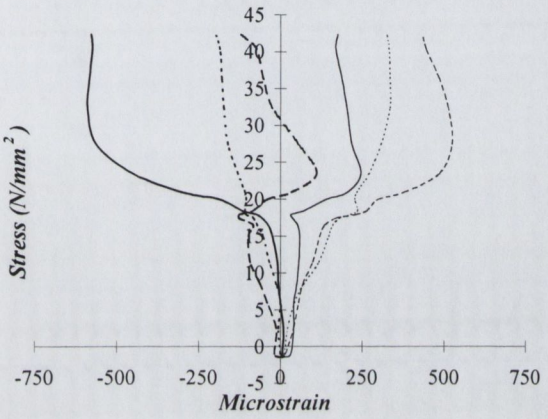
Lateral bottom - - - Axial bottom .....

Figure 5.55 Stress-strain plots - steel confined, thickness 3mm

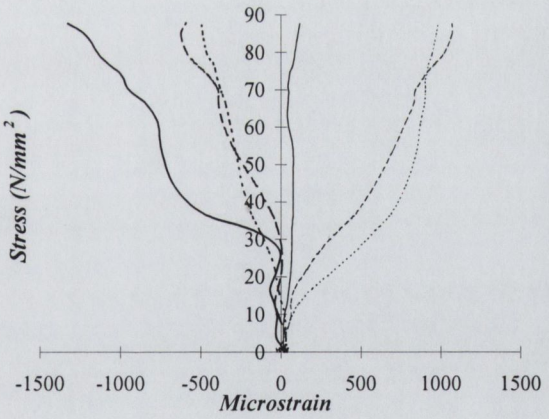
Figure 5.56 Stress-strain plots - steel confined, thickness 5mm



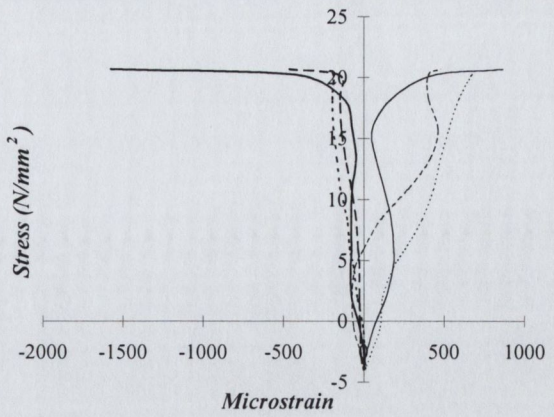
Co(114)S(6.5)1d, velocity 3.2 m/s



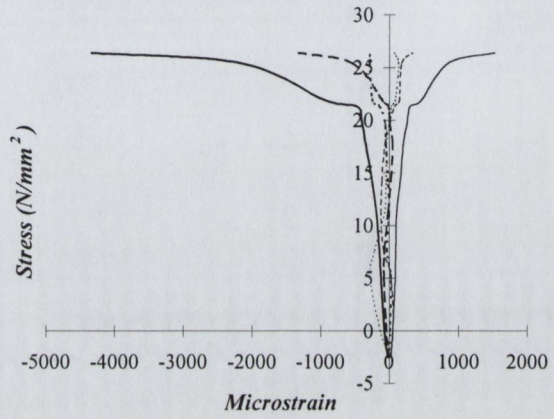
Co(114)S(6.5)2a, velocity 4.4 m/s



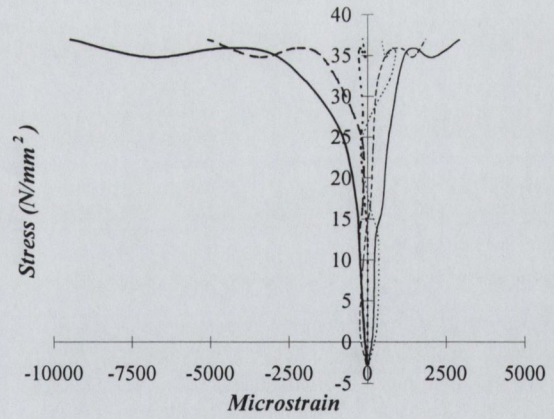
Co(114)S(6.5)3c, velocity 6.3 m/s



Co(110)P(3.6)1b, velocity 3.2 m/s



Co(110)P(3.6)2c, velocity 4.4 m/s



Co(110)P(3.6)3b, velocity 6.3 m/s

Lateral top —— Axial top ——

Lateral middle — — Axial middle - - - -

Lateral bottom - - - Axial bottom .....

Figure 5.57 Stress-strain plots - steel confined, thickness 6.5 mm

Figure 5.58 Stress-strain plots - plastic confined, thickness 3.6 mm

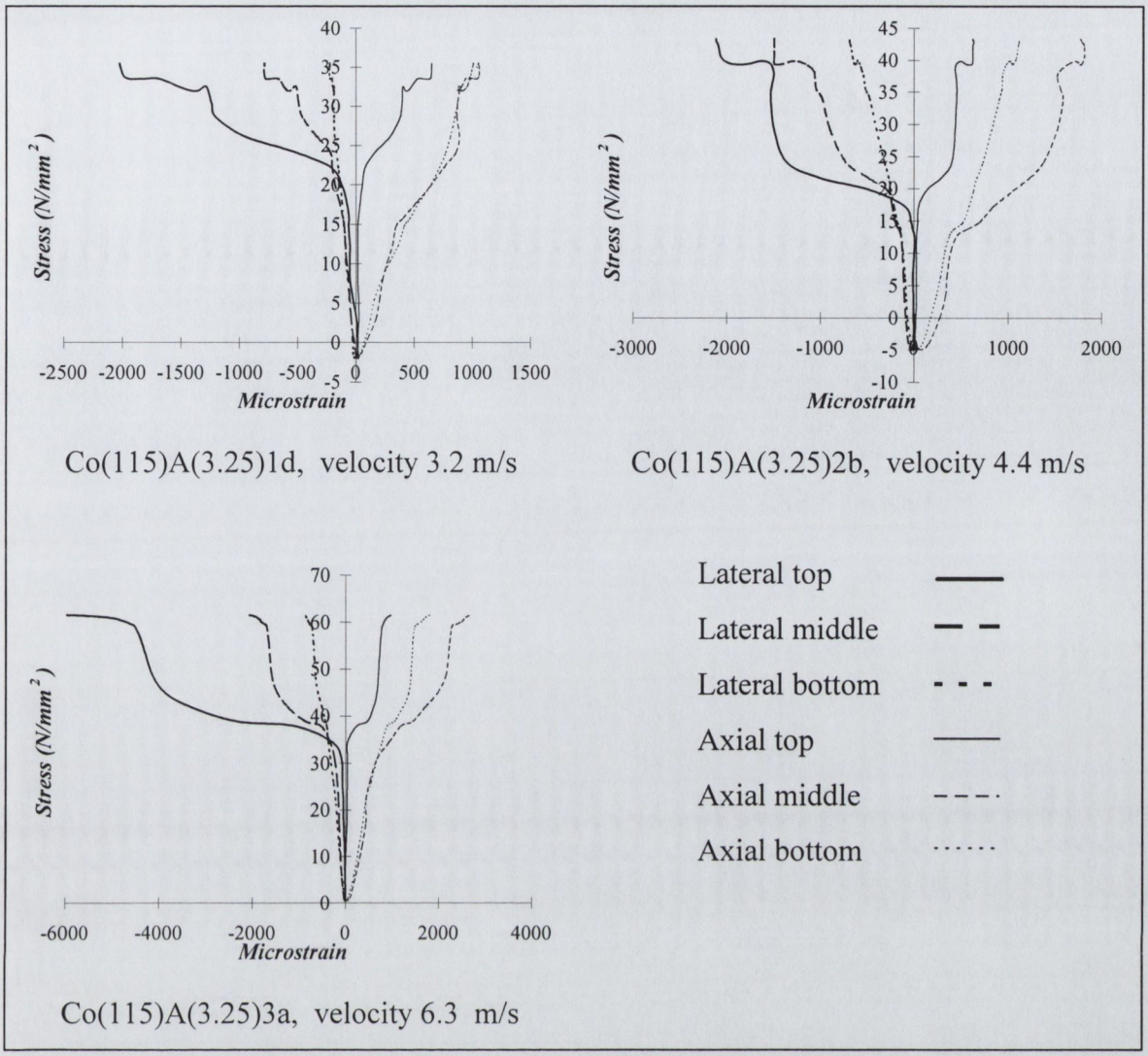


Figure 5.59 Stress-strain plots - aluminium confined, thickness 3.25 mm

200 microstrain. This 'yield' plateau continued until the concrete could not sustain any more axial load. The lateral gauges exhibited a more linear response up to their maximum value, which is typically less than the axial compressive strain on the concrete at maximum stress. The absolute values of both the axial and lateral strains at failure vary greatly between different concrete cylinders, probably because of the different proximities of the gauges to cracks in the concrete. The majority of the strain gauges attached to the concrete were broken as the cracks developed during the loading period.

The gradient of the plots generated from the lateral gauges were consistently less than the corresponding gradient of the axial gauges, which is the opposite of what might have been expected if Poisson's ratio had been considered. As the loading is axial, the axial strain would typically be considerably larger than the lateral strain for a particular level of stress.

The reverse possibly occurred because the loading is initially not over the entire surface of the unconfined cylinder, due to the slightly curved nose cone (as the surface becomes indented, the loading stretches over the entire area). Because of the high rate loading, the stress wave travels down the centre of the concrete cylinder, as it does not have time to equilibrate over its width. This central load would compress the centre of the cylinder and, due to a Poisson's ratio effect, would induce a lateral tensile strain. When this induced strain reaches the circumference of the concrete cylinder it induces a smaller axial strain at the surface due to a secondary 'Poisson's ratio' effect.

A stress-strain plot up to the point of maximum compressive stress was generated for each of the confined cylinders for which the base stress had been measured. A typical example of a stress-strain plot for each type of confinement, at each of the three impact velocities, can be found in Figure 5.54 to Figure 5.59. Due to the nature of impact loading, the stress-strain responses tended to vary considerably during the loading period and between cylinders which made some of the results difficult to compare. This is particularly evident in the case of the cylinders confined by a 1.2 mm thick steel sleeve, possibly because they were fabricated from rolled and welded sheet steel and although the strain gauges were placed diametrically opposite the weld some surface irregularity could have resulted in the output being considerably more erratic than those from other confinement types. The results from the steel and aluminium confined cylinders were unlike those from the cylinders confined by plastic and these will, therefore, be discussed separately at the end.

It is interesting to consider the different ways in which the six gauges attached to the skin of each sleeve respond to the impact. If one first considers the lateral and axial gauges separately it is evident that, in the vast majority of the tests, the lateral gauge closest to the top of the cylinder experiences the maximum strain, followed by the gauge at mid-height and the gauge closest to the base of the cylinder experiences the least strain. The pattern in the case of the axial gauges is quite different as, in most cases, the mid-height gauge records the highest strain, followed by the gauge nearest the cylinder base and the gauge closest to the top of the cylinder only experiences very small strains in comparison to both of these. The pattern for the lateral gauges can be explained by considering the restraint offered at the loading interface and at the support and the load transfer into the sleeve. When materials are tested statically, they are usually placed between two stiff platens which, during the loading, restrain the lateral expansion of the material in contact with the

platen and reduce the lateral strains due to friction at the interface. However, in the case of the current set of experiments, only the impactor is in contact with the concrete cylinder on its upper face, and this does not fully restrain the dilation of the concrete. In effect, this means that the concrete close to the top of the cylinder is relatively free to expand as a result of the loading. At the base of the cylinder, full restraint is provided by the base-plate loadcell which restricts the dilation of the concrete and the confining sleeve and, thereby, reduces the strains measured. The presence or lack of restraint makes has little effect on the strains at low stress values, but as the stress increases over time, its presence becomes increasingly important (see for example C(115)A (3.25)3a in Figure 5.59). Interpretation of the results from the axial gauges is considerably more complicated. The strains in the gauge closest to the top of the cylinder are very small throughout the period of loading. This occurs because the majority of the load at this level is being taken by the concrete core, as it has not had sufficient length along the friction interface between the sleeve and the core (10 mm), for the load to be transferred into the sleeve. Therefore, this strain is the result of a Poisson's ratio effect from the lateral strain at that level, which is large due to the dilation at this level. The gauge at mid-height and the gauge closest to the base of the cylinder often experience similar levels of strain. By the mid-height, a considerable proportion of the load has been transferred from the concrete into the stiffer confining material, which transmits the load to its base. The gauge closest to the base usually experiences slightly less strain because of the presence of the loadcell, which reduces axial dilation. This assessment of axial and lateral strains at the mid-height and closest to the base of the cylinder is corroborated by an assessment of the gradient of the ascending parts of these graphs. The gradient of the lower two axial gauges is typically considerably greater than that of the corresponding lateral gauge, which would suggest that the load is being transferred axially at these levels and is inducing the strains in the lateral gauges, through a Poisson's ratio effect. The opposite can be said of the gauges closest to the top which suggests that the loading is predominantly lateral at the top and induces the small axial strains. It can be concluded that, until the load is transferred from the concrete into the sleeve, the lateral strains will be high as a result of the lateral pressure from the concrete. If the gauges were located in the concrete it is probable that the lateral pressure would be less than the axial, throughout the length of the cylinder, as the concrete which is axially loaded at the top.

For many cases it is difficult to make an assessment of the shape of the stress-strain curve because of the variability in each individual curve. Nonetheless, it is possible to draw some conclusions by considering the stress-strain response of the top lateral gauge. In most cases, after a small initial strain, the stress increases considerably without causing any further increase in strain in the gauge. This probably occurs because the load is being taken by the concrete which does not dilate very much because of its low Poisson's ratio. At approximately one third of the maximum stress (see for example Figure 5.59), the gauges again begin to undergo an increase in strain, as the concrete has dilated sufficiently to affect the more rigid confining sleeve. However, the resulting considerable increase in strain is associated with a very small increase in stress, probably because the strains in the core concrete are quite high and the confining sleeve begins to take the load from the concrete, and reduces further cracking. At the end of this portion of the graph, there is a second region where the stress increases considerably with very little increase in the strain in the confining sleeve, probably because the sleeve is within its elastic limits and is easily able to withstand a considerable increase in stress. This is often followed by a second horizontal or nearly horizontal portion and the confining sleeve begins to yield near to the maximum stress.

This is similar to the load transfer mechanism described by Kotsovos and Perry (1986) for statically loaded sleeved concrete cylinders. If the confining sleeve is quite thin then the behaviour is characterised by the decreasing stiffness of the tube throughout the loading period, as in the case of the cylinders confined with a 1.2 mm thick sleeve of steel (Figure 5.54). However, for thicker confining tubes the loading is broken into stages (Figure 5.57). The first stage involves a reduction in the stiffness of the sleeve, as the confined concrete begins to fracture, and this is followed by an increase in load and stiffness as the concrete consolidates within the tube. The final stage occurs when the sleeve begins to yield, which only happens at high velocities of impact.

As would be expected, the response of the cylinders confined by a sleeve of plastic was very different to those confined by a sleeve of steel or aluminium and was much closer to the response of the unconfined cylinders. The plots of stress against strain are bilinear in appearance, both axially and laterally. The initial loading part of the curve shows a large increase in the stress for a minimal increase in the strain which, similar to the cases of the steel and the aluminium, probably occurred as the concrete takes the load initially. When

this had reached its limit, the load was taken by both the plastic sleeve and the concrete core. The plastic, which has a low modulus of elasticity, underwent large strains as a result of minimal increases in stress. At the lowest velocity, this strain increase was lower than the failure strain of the plastic and the sleeve did not break. However, at the two higher velocities, the strains increased beyond the failure strain, resulting in both fracture of the confining sleeve and of the confined concrete. The strains were highest nearest the top of the cylinder, which is where the cracking started prior to progressing down the length of the confining sleeve. For the plastic confinement, the axial strain at the top of the sleeve was larger than either of the other two axial gauges. This is probably because little of the load was transferred to the lower part of the sleeve, before the sleeve began to rupture at the top, and the majority of the load was, therefore, taken by the concrete core.

The interpretation of these strain results and the stress-strain plots is complicated by the transfer of load from the loaded concrete core into the confining sleeve through the interface between them. It probably takes a certain distance, from the point of load application for the load to be transferred into the sleeve, which then transmits the load to the base and causes the variation in the axial and lateral strains along the length of the sleeve. In a later chapter, the variation of the strains along the sleeve is examined using finite elements and a comparison will be made between the predicted and actual results, which will further aid the interpretation of the strain gauge results.

5.6. IMPACTOR REBOUND

As explained in section 4.5, the SCXI system used for data acquisition during the impact tests recorded information about both the initial collision and subsequent impacts which occurred as a result of the impactor bouncing. Therefore, it was possible to study what happened to each of the types of differently confined cylinder after the first impact and to determine the length of time prior to the second impact event. Furthermore, it was possible to compare these results with those obtained from a study of the momentum and kinetic energy transferred to the cylinder during the initial impact.

The impulse, or change of momentum, experienced by the impactor was determined by finding the area under the contact force/time plot (as described in equation (2.6)) using Simpson's Rule for integration and it was assumed that the self-weight of the impactor was negligible with respect to the contact loads. These impulse values, included in Table 5.1, are also shown in Table 5.10, together with values of the kinetic energy and the velocities before and after the initial impact. The velocity after the impact was calculated using equation (2.7) which illustrates the relationship between the impulse and the difference in the velocities. Average values and coefficients of variation for these velocities of rebound calculated from the impulse values (v_i) are also given in this table. The results generated by integrating under the curve, measured during the highest velocity impacts, are not particularly consistent with each other - as is illustrated by their large coefficients of variation. However, an examination of the contact force/time plots between Figure 5.1 and Figure 5.7, shows that the plot does not return to zero after the initial impact when the impactor bounces clear of the confined concrete cylinder. For these, high velocity impulse calculations, the area under the curve was calculated between the start of the impact and a point on the x-axis at which time the contact force should have returned to zero. This point was determined by extrapolating the unloading part of curve with the same gradient until it intersects with the x-axis. These high velocity impulse results are, therefore, only approximate and were largely neglected in the subsequent analysis.

In cases where the concrete cylinder disintegrated entirely, which happened when the unconfined cylinders were impacted at any of the three velocities and when the plastic confined cylinders were impacted at the two higher velocities, the impactor did not

rebound after the impact. This is because all of the energy in the moving impactor was transferred to the concrete and dissipated in the cylinder, creating fracture surfaces in the concrete and accelerating the pieces away from the location of impact. Hence, no residual energy remained in the impactor causing it to rebound and re-impact. The rebound velocities are subject to a degree of variation due to differences in the impulses. The variations are associated with the flattening of the curve at its peak because of the onset of cracking of the concrete (see section 5.2).

The kinetic energy transferred from the falling impactor to the confined cylinder was considered to be the energy associated with causing cracking or fracture in the concrete

	Initial velocity (m/s)	Initial momentum (Ns)	Initial K.E. (Nm)	Impulse (Ns)	v_i (m/s)	K.E. lost by impactor (Nm)	Intra-impact time (s)	v_t (m/s)
U(100)	3.2	264	422	263 (25)	-	-	-	-
	4.4	363	799	136 (7)	-	-	-	-
	6.3	520	1637	133 (14)	-	-	-	-
C(114)S (1.2)	3.2	264	422	402 (2)	1.71 (5)	291 (4)	0.382 (8)	1.87
	4.4	363	799	557 (4)	2.43 (10)	569 (9)	0.536 (0)	2.63
	6.3	520	1637	909 (14)	4.74 (32)	-	0.551 (33)	2.70
C(114)S (3)	3.2	264	422	409 (2)	1.78 (4)	286 (4)	0.426 (13)	2.09
	4.4	363	799	575 (3)	2.49 (6)	571 (6)	0.567 (6)	2.8
	6.3	520	1637	1129 (17)	-	-	0.746 (3)	4
C(114)S (5)	3.2	264	422	407 (2)	1.75 (5)	290 (5)	0.424 (9)	2.08
	4.4	363	799	574 (3)	2.52 (8)	550 (7)	0.553 (0)	2.71
	6.3	520	1637	964 (15)	5.41 (32)	-	0.749 (4)	3.67
C(114)S (6.5)	3.2	264	422	410 (3)	1.80 (7)	283 (6)	0.394 (7)	1.93
	4.4	363	799	636 (17)	3.27 (40)	-	0.528 (8)	2.59
	6.3	520	1637	1106 (33)	-	-	0.771 (2)	3.78
C(115)A (3.25)	3.2	264	422	413 (3)	1.83 (7)	278 (6)	0.388 (7)	1.90
	4.4	363	799	552 (1)	2.25 (3)	605 (2)	0.540 (3)	2.65
	6.3	520	1637	1017 (23)	6.05 (48)	-	0.706 (3)	3.46
C(110)P (3.6)	3.2	264	422	374 (3)	1.37 (9)	335 (5)	0.312 (6)	1.53
	4.4	363	799	242 (35)	-	-	-	-
	6.3	520	1637	218 (24)	-	-	-	-

Table 5.10 Average impulse and velocites pre- and post- impact (the coefficients of variation for each of the groups are shown in brackets beside the average values)

during the test. In a similar manner to that used by Reider and Mindess (1998), the kinetic energy lost by the impactor was determined from the impulse-momentum relationships in equation (3.32). The energy loss is also equal to the difference between the kinetic energy of the impactor before and after the impact. The average values and coefficients of variation for the energy lost by the impactor are also given in Table 5.10. The kinetic energy transfer tends to become smaller as the confinement becomes more effective and less cracking takes place in the concrete cylinder.

The rebound velocity was also calculated by measuring the time between the end of the first impact and the beginning of the second (t_{diff}). The time was determined by ascertaining when the impactor separated itself from the concrete cylinder and when the contact force/time plot began to record the bounce. The velocity at which the impactor rebounded (denoted as v_t, signifying that it was determined using time values) was calculated using the following equation derived from simple mechanics of moving bodies

$$v_t = \frac{at_{diff}}{2} \qquad (5.9).$$

The average values of the time between the end of the first and the beginning of the second impact and the calculated rebound velocity are given in Table 5.10. The coefficients of variation for the groups are the same for both and are given in brackets.

Although momentum is conserved during the impact, some energy is always lost in anything but a perfectly elastic impact. The coefficient of restitution (e) is an empirical parameter which describes the relationship between the velocities prior to and after the impact, and has a value of one if perfectly elastic and of zero if the impact is perfectly inelastic. Coefficients of restitution were calculated using the rebound velocities determined from the conservation of momentum equation and from the time duration between the first and second impacts, graphs of which are shown in Figure 5.60 and Figure 5.61. A line showing the average of the coefficients (excluding the values for the plastic confined concrete) is superimposed. The coefficients of restitution did not vary considerably between the lower two velocities. However, Figure 5.60 makes it clear that the values calculated for the impulse and, hence, the rebound velocity at the highest contact velocity are much greater than would have been expected. It can be seen that, using the time duration between the two impacts, the coefficient of restitution (and the

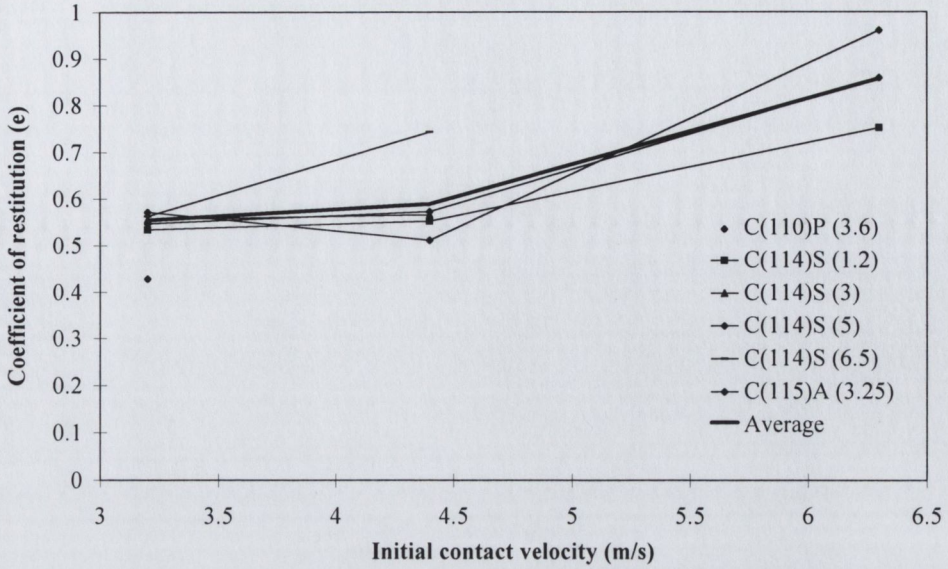


Figure 5.60 Coefficients of restitution calculated using the rebound velocity v_i, with a line showing the average trend of coefficients at different velocities

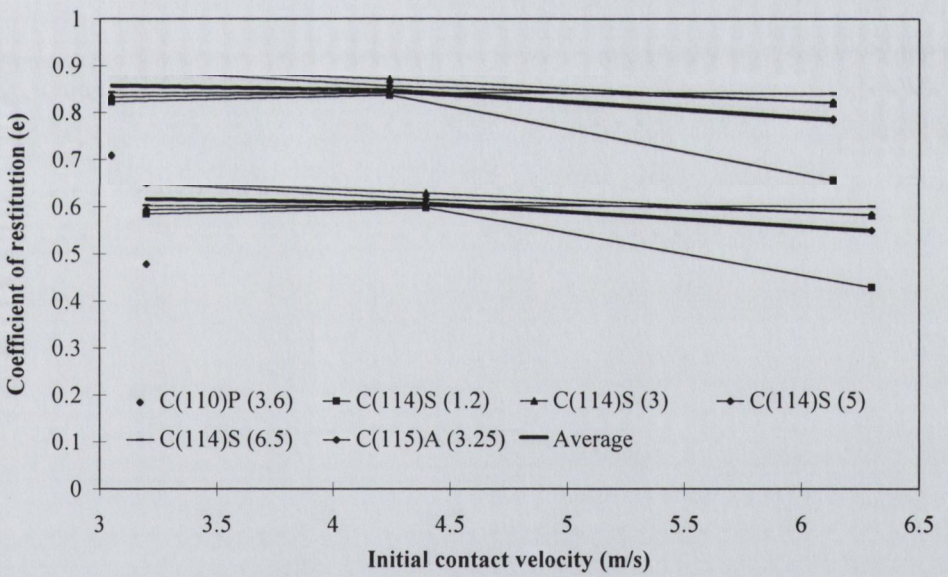


Figure 5.61 Coefficients of restitution calculated using the rebound velocity v_t, with a line showing the average trend of coefficients at different velocities

rebound velocity) decreases as the contact velocity increases. This would be expected because, as the contact velocity increases, a greater amount of damage is done to the impacted cylinder and more energy is thereby dissipated through cracking.

Both an examination of these graphs and of the values in Table 5.10 show that there is a difference between the velocities calculated using the two different methods, which has a

maximum value of 15 %. As previously discussed, both of the values are calculated from experimental results and are subject to a degree of variation, however, the results of each corroborate the other quite well, particularly at the lower velocities.

The rebound velocity values calculated using momentum considerations are only subject to a fraction of a percentage error in the calculation of the area under the curve using Simpson's rule. However, the calculations are slightly inaccurate in two other minor ways. Firstly, the area under the curve is only calculated between the time that the impactor contacts the concrete and when the curve first re-crosses the x-axis, and does not take any account of any part of the curve, including oscillations, beyond this point. Secondly, no account is taken of any movement of the impacted cylinder relative to the test base, which it was not possible to measure, nor of the relative velocities of the cylinder and impactor after the impact, which often occurred and could cause the velocity of rebound to be different from the value calculated. The velocity calculated using the time difference between the two impacts itself is also subject to some variability associated with the subjectively chosen "end" of one impact and the "beginning" of the next; - however, this variability is considered to be quite minor and is well within the accuracy of the results presented in Table 5.10. These factors do create some small variations, which could probably account for the difference between the results.

Figure 5.62 shows the variation in the rebound velocity, v_t, for each of the different types of confinement, at the three contact velocities. This chart is consistent with other observations made, thus far, about the effectiveness of different types of confinement. The plastic sleeve provides confinement at the lowest velocity at a level only slightly less than the 1.2 mm thick steel sleeve or the aluminium sleeve. However, at higher velocities the dilation caused by the impact is too great and causes the sleeve and the concrete to fracture and the impactor does not rebound. At the lower two velocities, the confinement provided by the metallic sleeves is very similar, and results in similar rebound velocities. The Young's modulus, provided it is sufficient to elastically resist the dilation, and the thickness of the confining sleeve had little effect on the rebound velocity. However, as the velocity increased, the properties of the confining sleeve had a significant effect on the rebound velocity. This is shown clearly in the case of the 1.2 mm thick steel sleeve, which, although it acts in a similar manner to the other steel and aluminium sleeves at lower velocities, is unable to withstand the higher velocity impact, and cracks under the

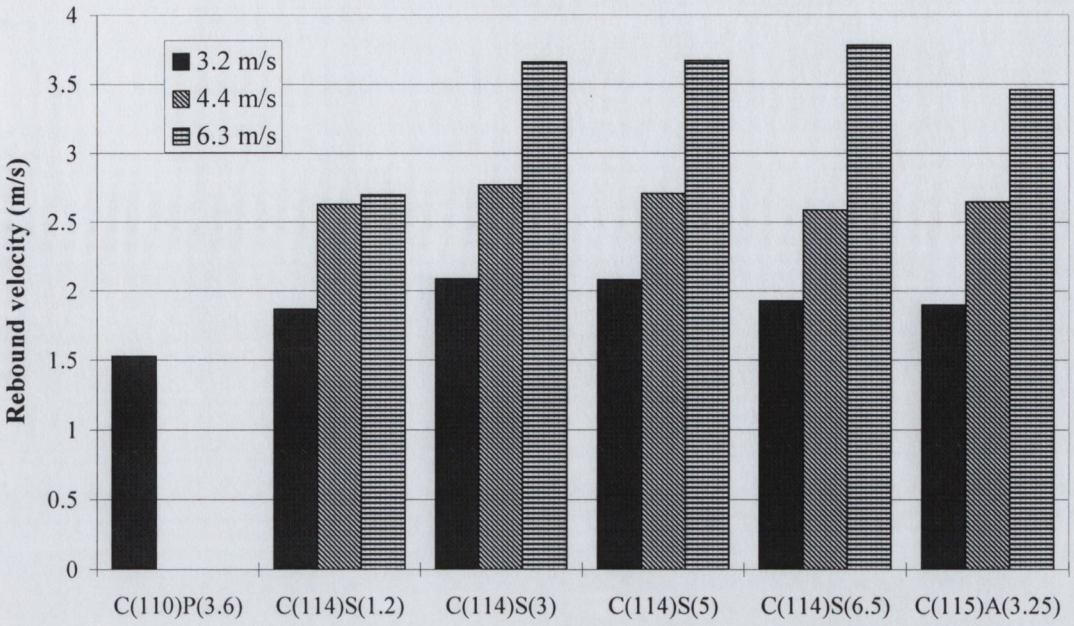


Figure 5.62 Rebound velocities for each type of confinement

load. The other, thicker steel sleeves all have similar rebound velocities as they are sufficiently thick to ensure that the collision is almost elastic and that little energy is dissipated in cracking. These results also confirm that it is a combination of the Young's modulus and the thickness which allows the sleeve to help to resist the impact because the aluminium sleeve, although it has a comparatively low Young's modulus, is of sufficient thickness to withstand the impact at the highest velocity and to make the impactor rebound with a velocity only slightly lower than a steel sleeve of similar thickness.

5.7. ENERGY ABSORPTION DURING IMPACT

The energy absorption by a loaded body is defined as the area under the stress-strain curve up to maximum stress value or the critical compressive strain (Timoshenko and Goodier, 1970). Values were calculated for the absorbed strain energy per unit volume for each impacted cylinder by numerically integrating under the stress-strain curve using the trapezoidal method. In static testing, the axial compressive strain in a cylinder is typically measured using a strain gauge on the mid-height circumference. In this research, the longitudinal strain was measured at three heights along the length of the cylinder and it was, therefore, decided that for consistency with other published results the energy absorption capacity should be determined using the mid-height axial gauge. The energy absorption is a function of the axial stress and of the critical compressive strain, both of which varied within a particular test series as explained in section 5.3 and section 5.5. Hence, the energy absorption results were not easily repeatable from test to test, and some test groups had coefficients of variation of up to 30 %. Nonetheless, some general trends in the results were evident and a graph of the average energy absorption capacity per unit volume is shown in Figure 5.63.

As would be expected, the absorption increases as the contact velocity, or strain rate, increases, in all cases except the unconfined, which has similar values at the higher two velocities. This is because, as explained by Atchley and Furr (1967), the unconfined concrete and similar materials are only capable of dissipating a certain amount of energy and when this level is exceeded, the concrete fails.

The concrete cylinders confined by steel all dissipated similar amounts of energy at a particular velocity. There is a trend towards a decrease in the energy dissipated as the thickness of the confinement increased. The energy dissipation at a given level is dependant on the maximum stress, the strain at this level of stress and the shape of the stress-strain curve until this point is reached. This is clearly illustrated by the following example where, at the highest velocity, the energy dissipated by the cylinder with a 1.2 mm thick steel sleeve dissipates less energy than the cylinder with, for example, a 6.5 mm thick sleeve, because although the former experiences more strain, the latter is capable of transmitting more stress to the base. In most cases, the aluminium confined

cylinders absorbed considerably more energy than similar steel confined cylinders because, although the stress levels experienced in both were quite similar, the aluminium confinement strained more because of its lower Young's modulus. However, its yield strain at lower velocities and failure strains at the highest velocity were sufficiently high to ensure that the sleeve did not fail when loaded, which would have caused a levelling off in the maximum strain.

The concrete confined by cylinders of plastic generally absorbed less energy than an unconfined cylinder at the lower velocities. This is because of the inter-relationship of the stress and strain. Although the plastic confined cylinders transmitted more stress as the sleeve remained in one piece and the confinement was maintained, they strained less under the load. However, at the highest velocity the confinement was split along its length and the concrete fractured. The plastic sleeve strained considerably as this occurred and the energy dissipation shown the figure is probably, like that for the unconfined concrete, the maximum that the plastic confined concrete can absorb.

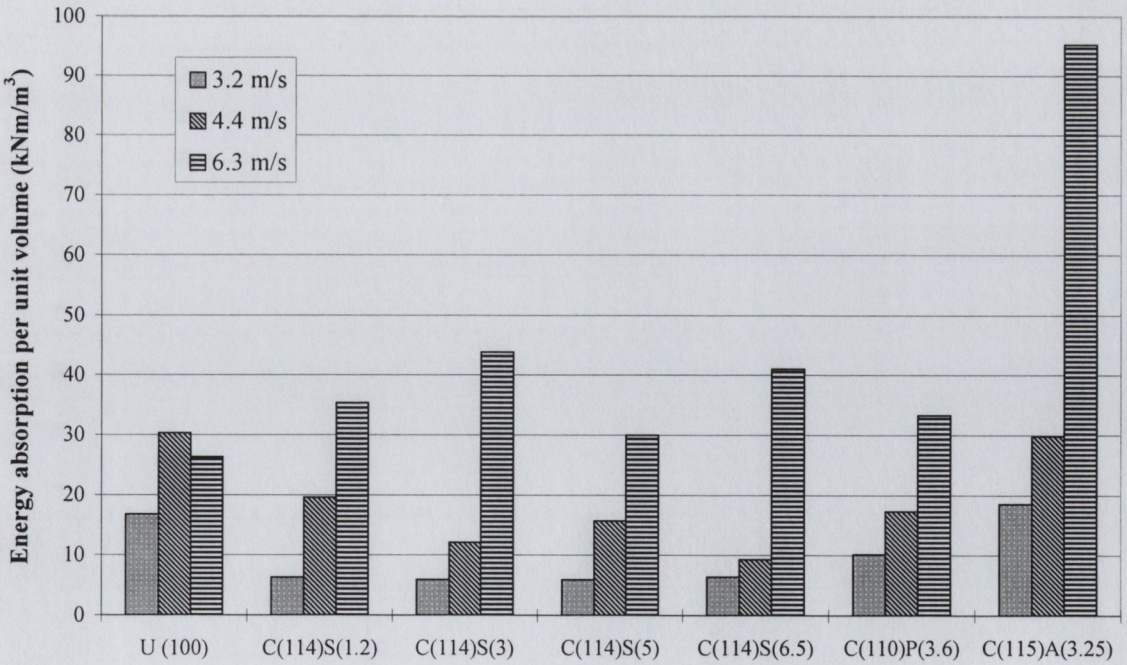


Figure 5.63 Absorbed energy per unit volume for impacted cylinders

5.8. CONCRETE STRENGTH AFTER CONFINEMENT REMOVAL

A visual inspection of concrete after it has been impacted normally gives a good indication of the damage which it has undergone. However, when confined, the cracks were predominantly only in the top face of the concrete (except in the case of the plastic confinement) and it was, therefore, difficult to make an assessment of the internal damage to which the concrete had been subject, beyond the determination of the energy dissipated during the impact.

In an attempt to quantify the damage to the concrete, the confinement was carefully removed from the concrete core of one representative cylinder from each impacted group. This was achieved by carefully cutting along the length of the confinement using an angle-grinder. The concrete cylinders were then tested statically according to BS 1881 : Part 120: 1983, and the residual strengths (f_r) were normalised by dividing by the original concrete strength (f_c). The plastic confined concrete impacted at the lowest velocity was the only one which could be tested statically as the others had collapsed when impacted. Of all of the cylinders tested statically, it underwent the greatest damage, with a residual strength only 33 % of the original strength of the concrete. The results of the other cylinders are shown in Figure 5.64. The residual strengths of even the well confined concrete are between 55 % and 85 % of their pre-impact strengths as, in all cases, the impact of the concrete results in cracking to the concrete and a loss of strength. The maximum damage in this group was done to the cylinders with the thinnest confining sleeves. The aluminium confined concrete performs well at the lower velocities but, as has been seen throughout the analysis, cannot withstand the energy of the highest velocity impact, and behaves in a similar manner to the 1.2 mm thick steel sleeve cylinder.

It is evident that, in the majority of cases, the residual strength of the concrete impacted at 4.4 m/s is greater than that at 3.2 m/s. This possibly occurred because at the lower velocity cracks were formed causing weakening of the concrete, whereas at the higher velocity these cracks did form but were then forced closed due to the longitudinal force and the presence of the confinement. This could have caused consolidation of the concrete, much like the temporary increase in contact force exhibited when concrete is re-impacted a second or third time before the onset of concrete failure (see van Mier *et al*, 1991).

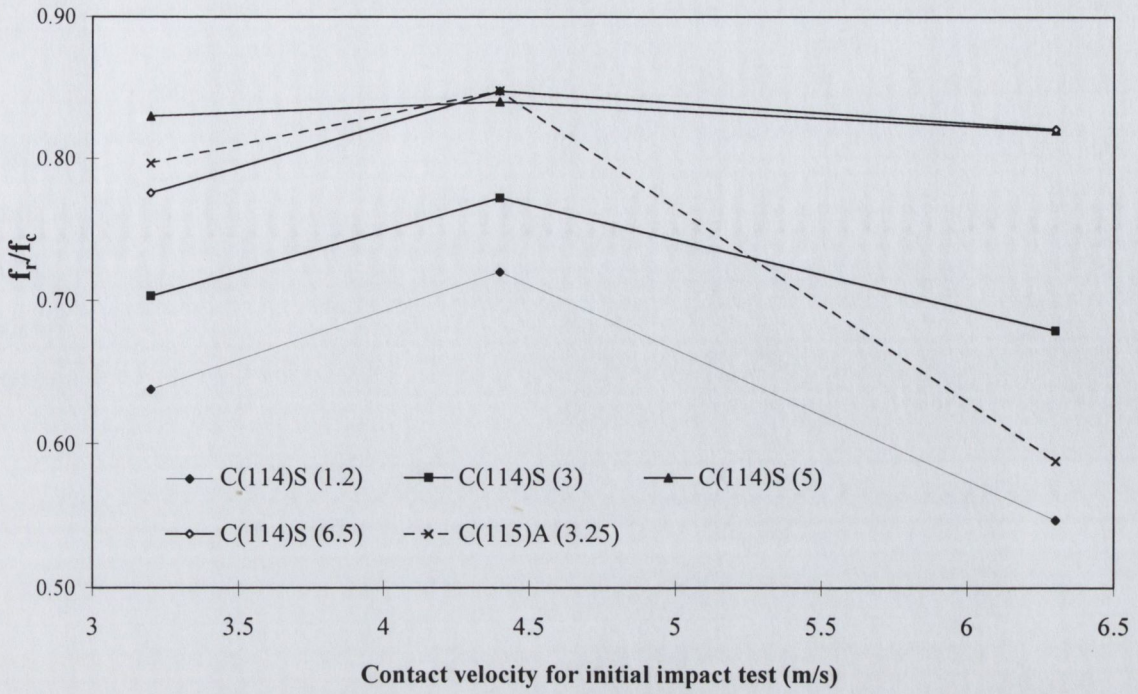


Figure 5.64 Relative strength of concrete cylinders with confinement removed, when statically reloaded after impact testing

It is possible that impacting the cylinders at this velocity might be approximately the optimum to provide consolidation to the concrete, to minimise the volume and to increase the compressive strength after the initial impact test.

At the highest velocity, except in the case of the concrete confined by sleeves of steel 5 mm or 6.5 mm thick, which were particularly good a withstanding the impact, the cracks induced were great enough to cause considerable degradation in the residual concrete strength.

It is possible that the three velocities of impact examined during the current research give the outline of an optimum consolidation curve for the concrete. At the lowest velocities, the impact results in damage which weakens the concrete strength. Although at mid-range velocity the concrete is less strong than if not impacted, the level of consolidation and damage is sufficient to cause a less severe loss in the strength. However, at the highest velocity, the cracking and fracture in the concrete results in considerable weakening and a low residual strength.

5.9. RESULTS OF SUPPLEMENTARY TESTS

The results of the main series of experimental tests on the response of confined concrete to hard impact are presented in sections 5.2 to 5.8 of this chapter. Whilst these tests were being undertaken, and subsequently analysed, other issues were raised which merited limited experimental exploration. With this in mind, a second, more limited, group of experiments were undertaken which examined the following variables

- the response of the confined and unconfined concrete to static loading
- the effect of increasing the diameter of the cylinder, both for the confined and unconfined cases
- the effect of reducing the length of confinement at the base of the cylinder so that solely the core concrete bears on the base-plate loadcell
- the effect of re-impacting a particular cylinder a number of times at the same velocity.

This section examines all of these different variables and compares their results with each other and with those generated in the main series of experimental work. It is an inevitable conclusion of this part of the experimental work that each of these variables could have been examined in considerable detail individually. However, they were not the main focus of the experimental study.

5.9.1. Static test results

Although the focus of the experimental work was on the response of sleeved cylinders to hard impact, it was necessary to examine how these cylinders responded to a statically applied load. A total of six cylinders were loaded statically, two of which were unconfined, two were confined by a steel sleeve, 3mm thick, one was confined by aluminium and the final cylinder was confined by plastic. The confined cylinders came from the concrete batches U(100), R(114)S (3), R(115)A (3.25) and R(110)P (3.6) described in Table 4.3, without the 5 mm section removed from close to the base.

The static loading was undertaken using a 300 Tonne Losenhausen Static test machine, at a rate of 0.2-0.4 $N/mm^2 \cdot s$. The static loading was designed to ensure that the method of load

application was similar to when the cylinders were impact loaded. This was achieved by removing the nose cone from the top of the impactor and placing it on top of the concrete, between the cylinder and the loading platten. This ensured that the load was only applied to the concrete core and that the cylinders would be similarly loaded by a slightly curved contact surface. The base-plate loadcell, which measured the stress, was placed beneath the cylinder and a standard mix of dental plaster was used to bed the cylinder to the plate and the plate to the loading platten and the aluminium billet. The confined cylinders were gauged in the normal manner with six gauges along one axes and the unconfined cylinders with one lateral and one axial gauge on the mid-height circumference.

The stress-strain relationships of each of the statically loaded cylinders are shown in Figure 5.65 to Figure 5.70. The steel confined cylinder C (114) S (3)4a was not loaded to the point of yield of the steel, but all of the other cylinders were either loaded until there was significant deformation of the cylinders or, in the case of the unconfined cylinders, until the concrete had failed. The unconfined cylinders failed by splitting longitudinally into three or four sections from the centre of the top face, which was similar to the mode of failure seen in the impact loading, and was probably caused by the slightly rounded nose-cone. The confined cylinders all experienced yield of the confining sleeve and, eventually, significant cracking in the confined concrete. With continuing loading, the confining sleeves of the aluminium and steel buckled near to the base in a ring or "elephant's foot" manner. However, the plastic sleeved cylinders failed in classical shear, in a similar manner to the composite cylinders tested by Kurt (1978). Photographs of the failure modes of one of each of the confined cylinders are shown in Figure 5.71 to Figure 5.73, with very obvious plastic deformation of the sleeves in all of the cases. The stress and strain in the plots increase until significant yielding occurs in the confining sleeve. However, they all reach a point where the stress increases for no further increase in strain. It is to be expected from the results of other researchers who have undertaken similar static loading tests (Kotsovos and Perry, 1986) that the strain and stress would have continued to increase gradually until the cylinder eventually failed due to the rupture of the steel. However, an examination of the cylinders after the test showed that the gauges measuring the strain had de-bonded from the confining sleeve and were not showing the increases in strain which occurred as the stress continued to increase.

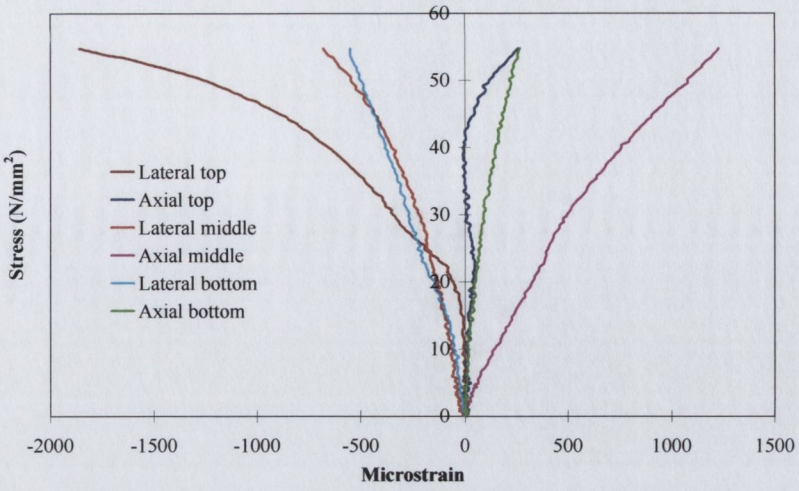


Figure 5.65 Static stress-strain response of C (114) S (3)4a

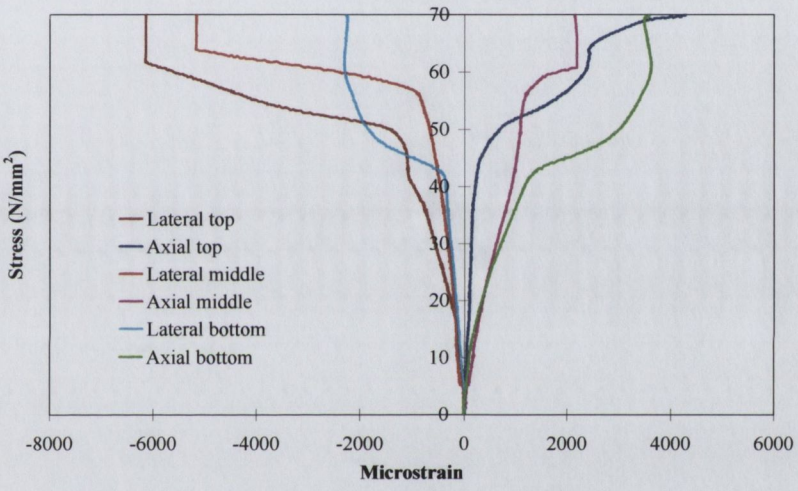


Figure 5.66 Static stress-strain response of C (114) S (3)4b

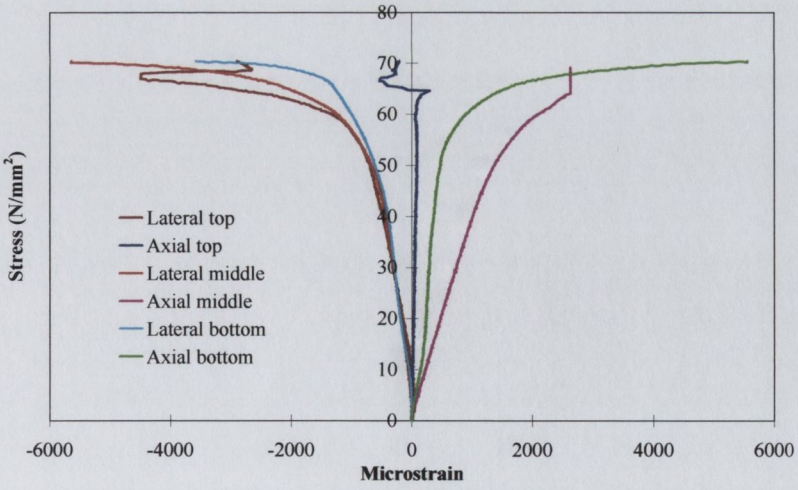


Figure 5.67 Static stress-strain response of C (115) A (3.25)4a

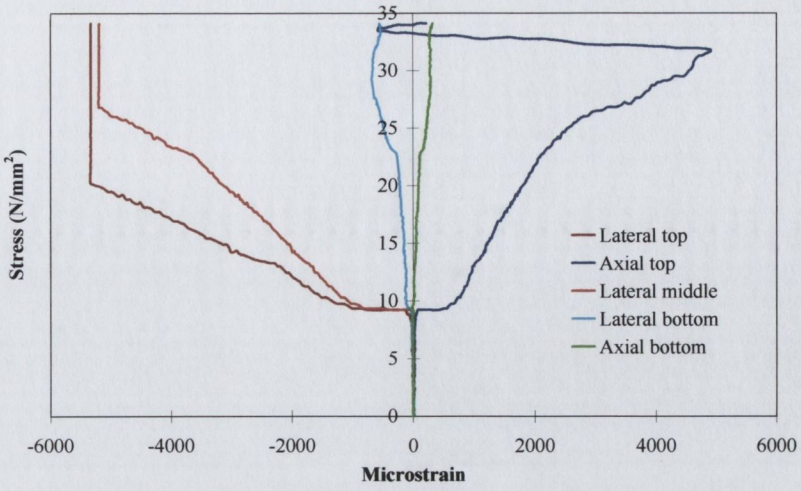


Figure 5.68 Static stress-strain response of C (110) P (3.6)4a

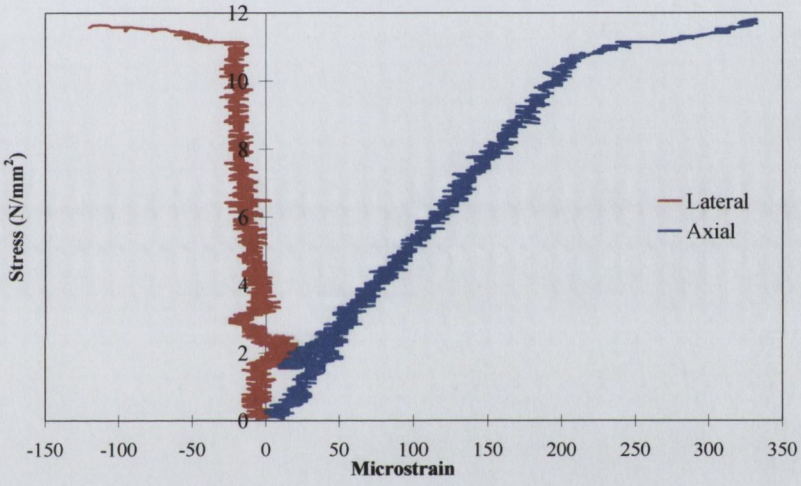


Figure 5.69 Static stress-strain response of U (100)4a

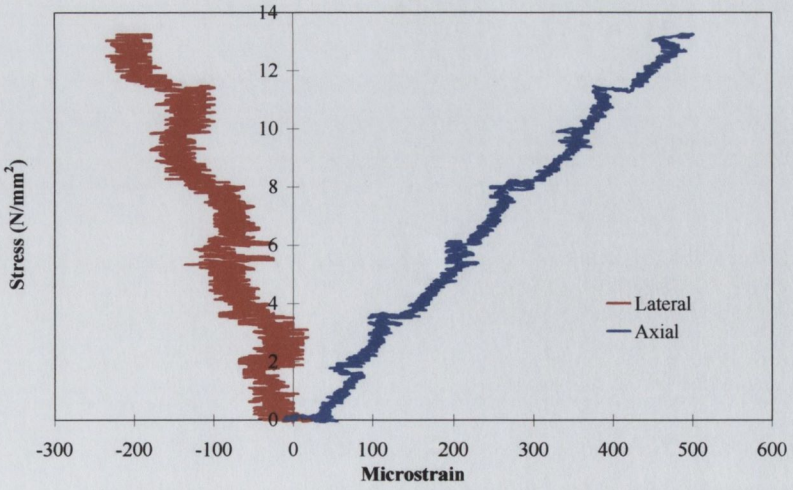


Figure 5.70 Static stress-strain response of U (100)4b

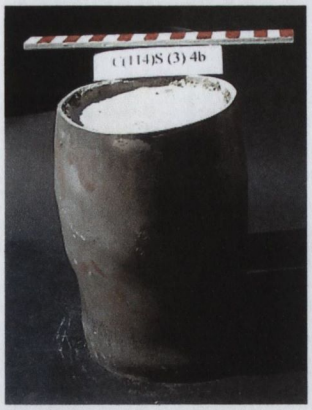


Figure 5.71 Failure mode of C (114) S (3)4b

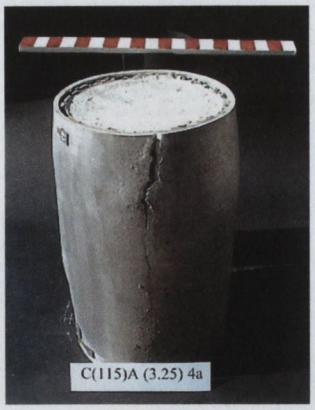


Figure 5.72 Failure mode of C (115) A (3.25)4a

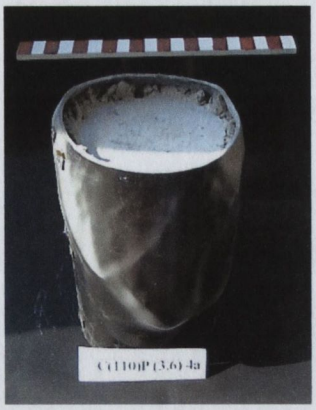


Figure 5.73 Failure mode of C (110) P (3.6)4a

The bar in the photographs is marked in units of 10 mm

The stress-strain results of the static loading tests show considerably greater levels of consistency with one another than the impact test results, however, it was not possible to obtain complete repeatability within the test series. The lateral strains in the steel were greatest close to the top of the cylinders, where the loading restraint was at a minimum. The strains at the middle and the bottom were similar both axially and laterally, as both underwent similar straining as, by the mid-height, the majority of the load has been transferred from the core into the sleeve. The impacted cylinders showed a similar pattern of strain when loaded and, in the majority of cases, exhibited high lateral and low axial strains close to the top of the cylinder and similar strain levels along the rest of the length.

The lateral strains in the aluminium sleeve were consistent along the entire length, and for the majority of the loading duration the axial strains were greatest at mid-height. However, the buckling close to the base of the sleeve can clearly be seen as the strain results close to the base increase considerably with very little increase in stress, close to the maximum stress applied to the cylinder. Their impact response is quite similar to both their static response and to the response of the steel sleeved cylinders. However, the impact occurs over such a short duration that buckling at the base of the sleeve does not occur.

The static response of the plastic sleeved cylinder is the closest of all of the static responses to its impact response. The strains initially in the sleeve were very low, until at approximately one quarter of the maximum load had been applied to the cylinder. Initially, the comparatively low Young's modulus of the plastic sleeve meant that the majority of the

load was taken by the concrete core. Beyond this point the lateral dilation of the cracking concrete meant that the strains increased rapidly in the confining sleeve began to take the load and yield continuously. Very little strain was experienced close to the base of the cylinder which is restrained by the base-plate loadcell, but the rest of the cylinder underwent considerable straining and plastic deformation along its length, as can also be seen in the photograph taken after the test.

The unconfined cylinders which were statically loaded exhibited a degree of variation in their stress-strain results. The maximum stresses reached in both cases were similar, but were lower than would have been anticipated from the strength of the concrete used in the cylinders. This, doubtlessly, occurred because the curved nose-cone applied a splitting force to the centre of the cylinder which fractured the concrete earlier than it would have with even loading. Furthermore, there was a significant difference in the maximum strains measured during the tests, which is probably a function of variations in the concrete, and like the stresses are lower than would have been expected, because of the curved nosecone. Unlike the impact test results, the axial strains are larger than the lateral ones, which is to be expected as the loading is axial. The lateral strains were probably induced by a Poisson's ratio effect caused by the axial strains. The impact test results exhibited greater lateral strains than axial strains, which was probably a stress wave propagation effect caused by the loading. The strains did not have time to equilibrate over the width of the cylinder when impacted, unlike in the static loading situation where, by the mid-height, the axial load was distributed evenly across the cross-section of the cylinder.

5.9.2. Large diameter cylinder tests

A total of six large diameter cylinders, with a core diameter of 162 mm, were manufactured and tested. They were made by casting concrete into a confining sleeve of external diameter 168 mm and 3 mm wall and, prior to curing, the sleeves were cut from those cylinders which were to be tested in an unconfined state. The confined cylinders were gauged in an identical manner to those of smaller radii, with six gauges along the length of the cylinder and the unconfined cylinders were gauged with four gauges, two laterally and two axially on the mid-height circumference. The cylinders were all impacted at the lowest velocity, 3.2 m/s, and the contact force response was measured for each

	Force (kN)	Impulse (Ns)
U (162) 1a	350	367.9
U (162) 1b	344	339.9
U (162) 1c	320	337.3
Average	338	348
COV %	5	5
C (168) S (3) 1a	474	433.9
C (168) S (3) 1b	450	379.6
C (168) S (3) 1c	460	393.9
Average	461	402
COV %	3	7

Table 5.11 Contact force response of large diameter cylinders impacted at 3.2 m/s

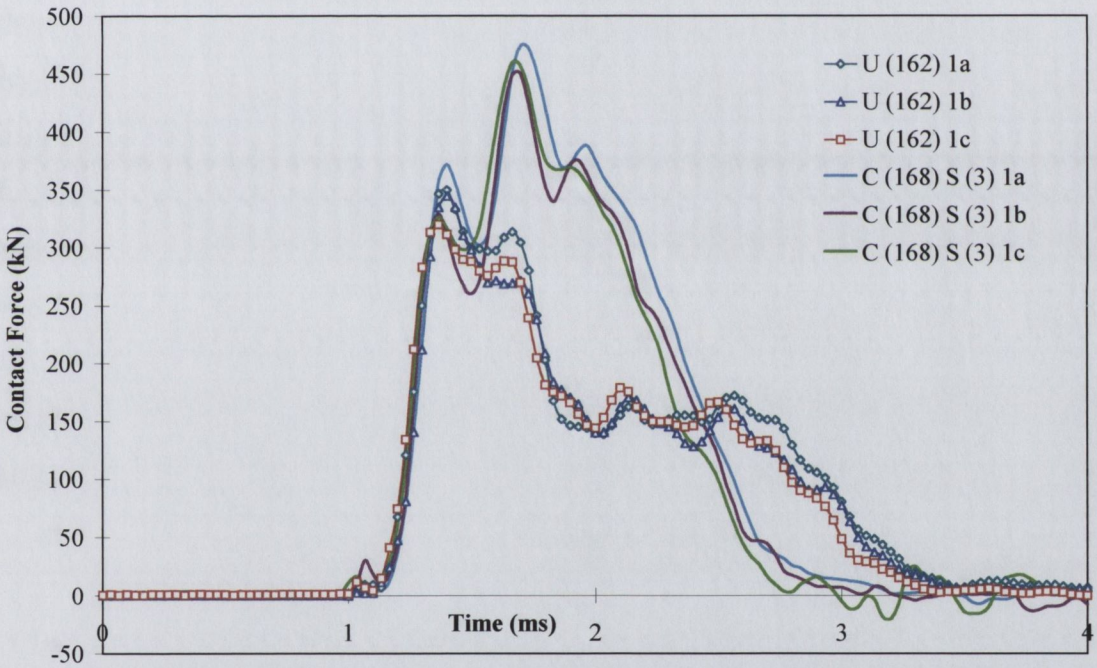


Figure 5.74 Contact force response of large diameter cylinders

cylinder. The base-plate response was not measured, as the accuracy of the response of a base-plate loadcell with a diameter of approximately 170 mm and four gauges, providing a total gauge area of 135 mm^2, would be questionable. The contact force responses are presented numerically in Table 5.11 and graphically in Figure 5.74, which combine the results of the confined and unconfined impact tests. Individual results for each of the tests are given in Appendix 4.

It is clear from the numerical results that the responses are very consistent with each other for both cases examined, with a maximum coefficient of variation of 5 % in the results of either the confined or unconfined case. Furthermore, an examination of these results shows that there are considerable similarities between the responses of all of the cylinders, of this diameter, during the initial period of the loading (Figure 5.74). The contact force response of the large diameter cylinders can also be compared to those examined in the rest of the experimental work, as shown in Figure 5.75, which clearly illustrates that the form of the curves is very similar, regardless of the diameter, but that the contact force increases with an increase in the cross-sectional area of the impacted body. In all cases, the cylinder appears to determine the limits of the concrete core quite quickly. If unconfined, the cylinder realises that it has reached the maximum force which it can sustain, and the contact force decreases as the concrete begins to fracture under the load. However, if the cylinder is confined the contact force can increase further as the concrete does not disintegrate and, during this period of the loading, the cylinder relies on the elastic properties of the sleeve to further develop the contact force. The increase in the duration of this loading period for the large diameter cylinders would corroborate the suggestion that the initial loading period, like the maximum contact force, is related to the area of the cylinder and it is the ratio of the area of the impactor to the area of the target which determines its response, as would be expected from equation (2.48). The high contact force exhibited by the smaller diameter confined cylinders occurred because the lateral dilation of the concrete is reduced by the rigid confining sleeve close to the location

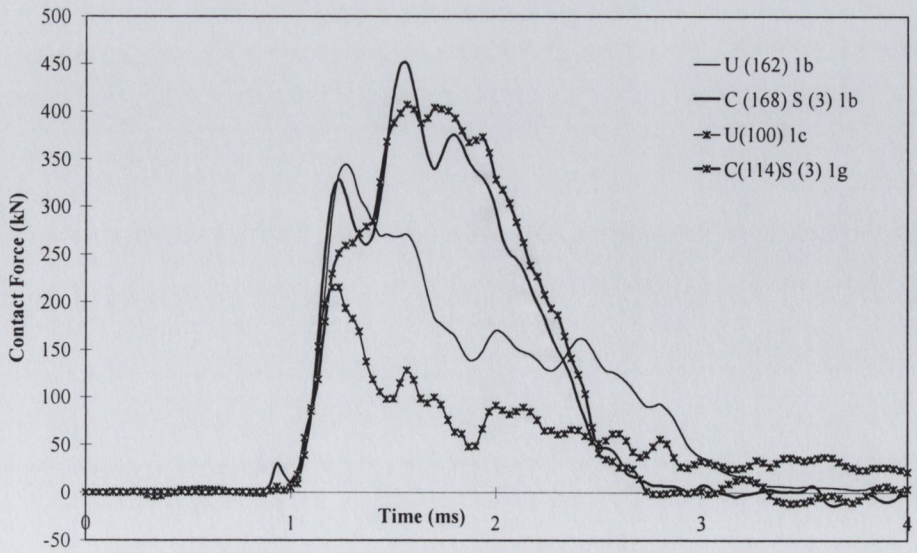


Figure 5.75 Contact force response of large and small diameter cylinders

of impact. The distance from the location of impact is considerably greater for the large diameter confined sleeves and, therefore, some dilation occurs which reduces the maximum contact force obtainable despite its considerably larger diameter. These findings are consistent with the results of Schneider (1998).

The following two hypotheses are the direct result of the findings from the larger diameter cylinders. If the diameters of two concrete core cylinders were the same, but the thickness of the confining sleeve was considerably greater in one case than the other, then it is probable that the primary loading phases would be very similar. The maximum contact force would be greater for the cylinder with the thicker sleeve, although not by a considerable amount because the dilation probably would not be reduced much further. If a second situation was postulated, regarding two identical concrete cores, and one of their sleeves was made of a material with a high Young's modulus, such as steel, and the other confining sleeve was made of concrete, of the same thickness. The primary phase of the loading would be similar for both cylinders. However, whilst the cylinder confined with steel would then show a considerable increase in contact force as the dilation was prevented, the cylinder confined by concrete would probably reach a maximum contact force at a level similar to that if the cylinder was made as one, of a slightly greater diameter. However, the maximum overall diameter of the concrete core and concrete sleeve would probably reach a limiting contact force, somewhere between the values measured for the small diameter unconfined cylinder and the small diameter confined cylinder, where the confinement offered by the concrete surrounding the impacted area did not have any further influence on the contact forces experienced during the impact.

The impulse values, obtained by integrating under the contact force curves are only subject to a small degree of variation for both the unconfined and confined situations. However, whereas typically in the response of the smaller diameter cylinders the impulse is greater than the maximum force, the same cannot be said for the confined concrete cylinders examined here which exhibit smaller impulses than might have been anticipated. The contact force response of the large diameter cylinder is much less flat near its peak than the smaller diameter cylinder, exhibiting a response much closer in form to the brittle fracture which occurs when the concrete is unconfined. This probably occurs because the confinement provided was less stiff and the cracks which form in the top surface of the cylinder were more numerous and larger than in the smaller diameter cylinder, and, hence,



Figure 5.76 Cracks in U (162) 1a



Figure 5.77 Cracks in C (168) S (3) 1b

The bar in the photographs is marked in units of 10 mm

near the top of the curve, the peaks and troughs are greater in magnitude, as this cracking occurs, and causes a reduction in the calculated impulse.

These findings are consistent with the results of a qualitative study of the large diameter cylinders after impact, shown in Figure 5.76 and Figure 5.77. It is evident that, although the unconfined cylinder has not split into pieces like the smaller diameter, unconfined cylinders, there is considerable cracking along the length of the cylinder and it is the interlock of the unfractured aggregate that keeps the cylinder from disintegrating entirely. The central circle where the impactor came into contact with the cylinder is also obvious in the figure. The confined cylinder exhibited much more top face cracking than a smaller diameter cylinder, as the confinement is quite removed from the centre of loading and allows more cracking to occur. However, the composite cylinder remains whole and the confining sleeve is unfractured.

The stress at the base of the cylinders was not measured for these large diameter cylinders and it is, therefore, not possible to plot the stress-strain response. However, the strain responses along the length of the cylinders were recorded and are compared to those of a smaller diameter cylinder in Figure 5.78 and Figure 5.79. The form of the curves at a particular gauge location are similar for both cylinders, however, the magnitudes of the strains are often different. The lateral strain in the top gauge in the large cylinder is approximately half that in the smaller diameter cylinder because, as the loading is not over the entire cross-section, it takes a certain distance along the length of the cylinders for

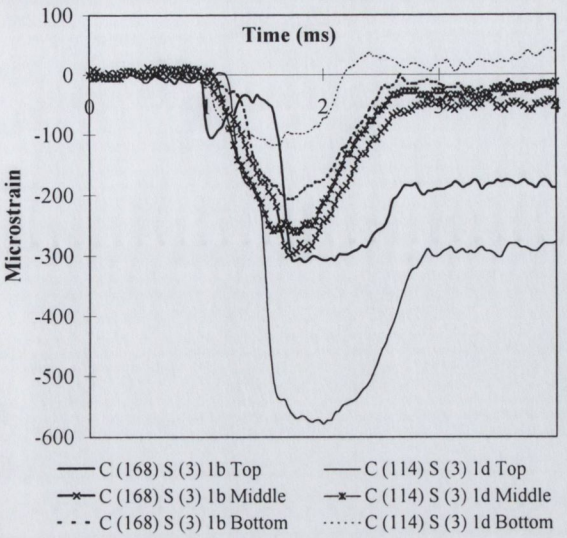


Figure 5.78 Lateral strain response of large and small diameter cylinders

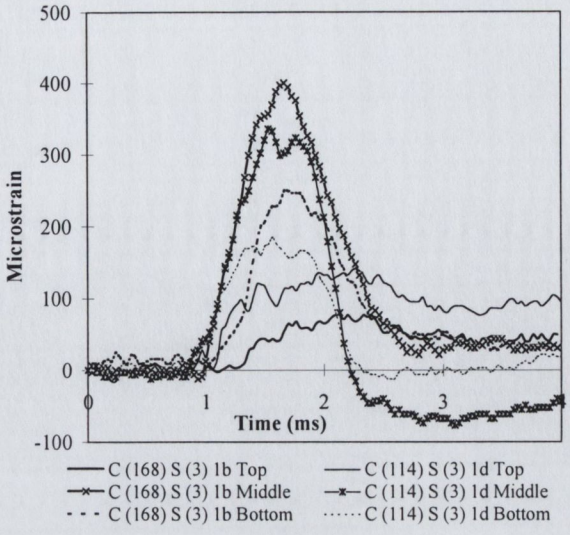


Figure 5.79 Axial strain response of large and small diameter cylinders

the stress waves, propagating away from the point of impact, to have an effect on the sleeve. By the mid-height, the lateral strains in both cylinders are very similar, whereas by the time that it reaches the base, the lateral strains are greater in the larger diameter cylinder, which is providing less rigid confinement and dilating more. The axial strains at the top of the cylinder are much smaller than the lateral strains and, as would be expected, are smaller in the larger diameter cylinder than in the smaller, as the strains have a greater distance to travel before they can have an effect on the sleeve. The axial strains are greater at the centre and reduce towards the base as the restraint from the block on which the cylinder was sitting has an effect. The concrete block is less rigid than the base-plate loadcell and, hence, allows a greater dilation of the sleeve close to the base.

5.9.3. Tests with reduced confinement at the base

The main test series involved testing cylinders confined by a sleeve of steel, aluminium or plastic which stretched along the entire length of the concrete core, and meant that, when the cylinder was tested, both the sleeve and the core were bearing on the base-plate loadcell. Hence, a considerable amount of the stress was transferred from the concrete core into the sleeve and then along the length of the sleeve and into the loadcell at the base. The purpose of this supplementary set of tests was to examine the differences in the response of the base-plate loadcell and the strain gauges when only the concrete cylinder

was in contact with the loadcell. The reduction in the confinement at the base of the cylinder was achieved by cutting 5 mm from the confining sleeve, using an angle-grinder, after the cylinders had been cast and cured. Preliminary tests showed that the response was unaffected by the length of confinement cut away, provided that the sleeve was not bearing on the loadcell. The base-plate loadcell was designed, with a reduced diameter of 110 mm, specially for these tests where only the concrete core was in contact with the square aluminium plate. Otherwise, the tests were identical to those in the main test series, with strain gauges at 10 mm, 100 mm and 190 mm from the impacted surface of the cylinder. All of the tests were performed with a contact velocity of 3.2 m/s.

The resulting shapes of the contact force and base-plate loadcell were very similar to those in the main test series, and a summary of the maximum points on the responses is presented in Table 5.12, with averages and coefficients of variation for each of the groups. The actual results of these impact tests are given in Appendix 4. The stress at the base was

	Contact force (kN)	Base-plate force (kN)	Stress at the base (N/mm^2)
R (114) S (3) 1a	390	375	42
R (114) S (3) 1b	386	316	34
R (114) S (3) 1c	384	412	45
R (114) S (3) 1d	388	358	39
Average	387	365	41
COV %	1	11	
R (110) P (3.6) 1a	291	187	22
R (110) P (3.6) 1b	310	273	33
R (110) P (3.6) 1c	304	222	27
R (110) P (3.6) 1d	274	250	30
Average	295	233	28
COV %	5	16	
R (115) A (3.25) 1a	390	380	41
R (115) A (3.25) 1b	392	342	37
R (115) A (3.25) 1c	394	316	34
R (115) A (3.25) 1d	348	193 (outlier)	21
Average	381	346	33
COV %	6	26	

Table 5.12 Response of cylinders with reduced confinement, impacted at 3.2 m/s

calculated by dividing the force measured by the base-plate loadcell by the area of the concrete core of the cylinder tested. The consistency of results is good for the contact force loadcell, but a greater degree of variation exists in the results from the base-plate loadcell. The results from the contact force loadcell from each of these tests is very similar to those for the equivalent tests with confinement along the entire length, shown in Table 5.1. This would have been expected as the contact force depends on the materials and geometry near the interface, and variations result from differences in the concrete properties.

The results of the base-plate loadcell can differ from those generated during the main test series. The magnitude of the force and the proportion of the load transmitted to the base for the plastic and aluminium confined cylinders is very similar when the confinement is reduced, to the results from the main test series. This probably occurs because the Young's modulii of these two materials are much closer to that of the concrete than that of the steel. Hence, the sleeves made of this material do not 'attract' load in the same way as a steel sleeve would. A smaller proportion of the load is transferred into the sleeve and it is less critical whether the sleeve is supported at the base as the concrete core retains most of the load. However, the results of the steel confined concrete with a reduced sleeve length are very different to those with a sleeve along the entire length, and all cases exhibit a much greater force at the base when reduced confinement is used. The reduced length of confinement results in almost 95 % of the force being transmitted to the base, compared to 73 % for similar tests with a full length of confinement. However, the increase in force at the base is possibly as a result of a slightly different load transfer mechanism. When the confinement is present along the entire length, the high Young's modulus results in a considerable proportion of the load being transferred from the loaded concrete core into the confining sleeve, and this is then transmitted along the length of the sleeve into the loadcell at the base. The presence of the longitudinal strain in the sleeve reduces its capacity to prevent the lateral dilation of the concrete core along its length and, hence, results in the reduction of force along the length of the cylinder caused by the cracking of the concrete. In contrast, the sleeve which is not supported by the loadcell provides the optimum conditions by which to resist the dilation of the concrete. It is free to dilate longitudinally to better resist the lateral dilation, particularly close to the base of the cylinder and does this so well as to transmit the majority of the load, almost elastically, along the length of the concrete, and minimises associated cracking.

As might be anticipated, the stresses experienced by the cylinders with reduced confinement at the base are greater than the equivalent stresses in the fully confined cylinders. The reasons for this are twofold. Firstly, in the case of the plastic and aluminium confined cylinders, the forces at the base are very similar, but the area by which this force is divided is smaller because only the concrete is bearing on the base-plate loadcell and is taken into account in the calculation of the stress. Secondly, as previously explained, the steel confined cylinders experience higher forces at the base because of the way in which the load is transmitted to the base and have a reduced area, resulting in much greater stresses.

The strains along the length of the cylinder when the sleeve is not supported at its base are different, at some locations, to the case where it is supported. This is particularly evident in the gauge near to the base of the cylinder as can be seen in Figure 5.80 to Figure 5.83 which compare the responses of lateral and axial gauges attached to steel and aluminium sleeves. The magnitudes of the strains differ between the tests considered, but the low level of horizontal strain near the base of the shorter steel sleeve is very evident in Figure 5.80. This reduction in the lateral dilation close the base is less in the aluminium confined cylinder, which still allows some dilation near to the base. Longitudinally, the reverse is evident, with very small strains being experienced near to both the top and the base of the shorter aluminium sleeve, which suggest that, whereas it undergoes axial straining at mid-height, the sleeve is slow to attract load and to transmit it along its length. The longitudinal strains close to the top of the shorter steel sleeve are slightly a-typical of the rest of the group, which are more like to those at the top of the full sleeve. The strains at the base of the shorter sleeve are typical of those in the rest of the series, being greater than those in the full length sleeve, as no restraint is provided which would reduce the strain.

These tests with reduced confinement were important because they developed the understanding of how the confined concrete cylinders withstand axial loading. When the cylinders are fully confined the amount of load which is transferred into the sleeve and down to the base, depends on the material of which the sleeve is made. However, the plastic and aluminium confining sleeves take less load than a similar steel sleeve, and the majority of the load being taken by the concrete core. It makes very little difference whether or not the sleeve is supported at the base because its main function is to minimise lateral dilation and fracture of the concrete. The steel confining sleeves also transfer the

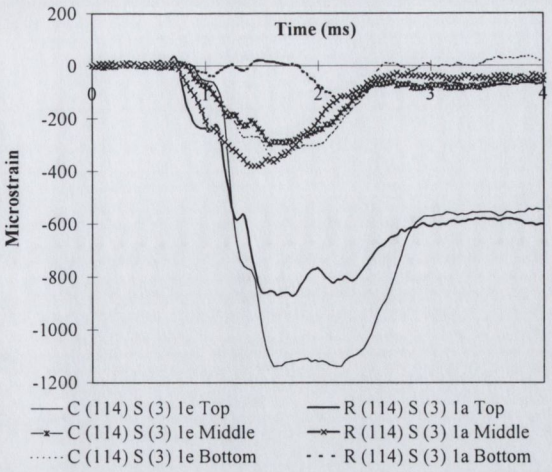


Figure 5.80 Lateral steel strain comparisons

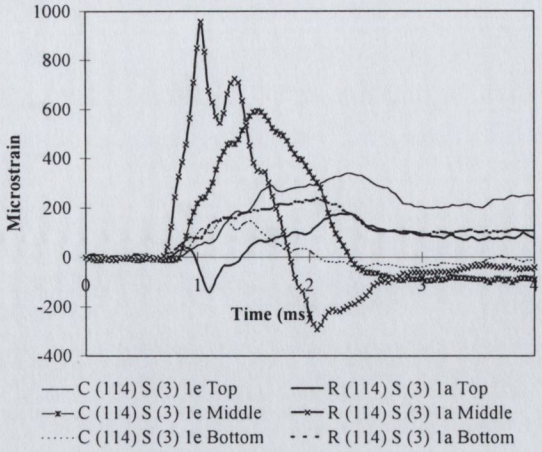


Figure 5.81 Axial steel strain comparisons

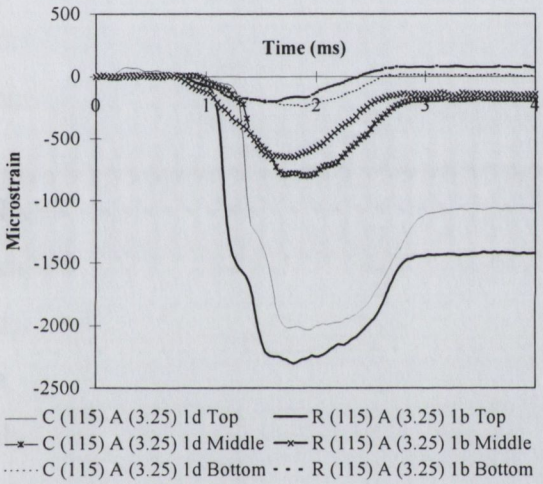


Figure 5.82 Lateral aluminium strain comparisons

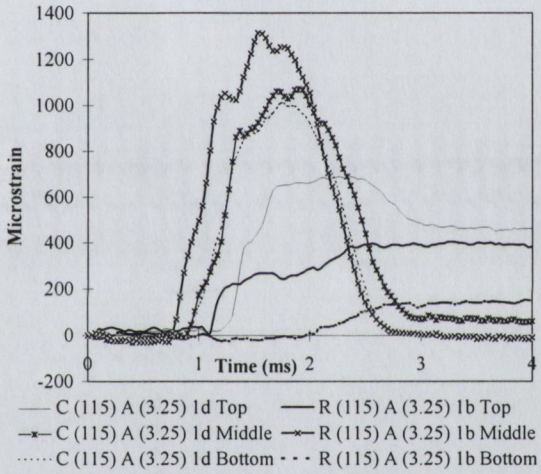


Figure 5.83 Axial aluminium strain comparisons

load along the concrete core when not fully supported. However, it is sufficiently elastic to minimise the dilation of the concrete and to transfer the majority of the load to the base. Therefore, the load transferred differs little regardless of whether the cylinder is fully confined along its entire length, as the main function of the sleeve is to prevent lateral dilation and cracking, which it achieves successfully in both cases.

5.9.4. Repeated impact tests

Limited tests were undertaken to assess the effect of repeatedly impacting the confined concrete cylinders which had not visibly failed as a result of the initial impact. As discussed and analysed in section 5.6, if the confinement was sufficiently thick and stiff, not all of the energy was dissipated during the collision and the impactor rebounded. Nonetheless, even after the two main collisions associated with this first impact test, the cylinders remained largely uncracked and unaffected by the impact. It was, therefore, decided to re-impact the cylinders at the same velocity a further three times and to assess their behaviour, particularly with respect to the responses of the contact force and base-plate loadcells. Four cylinders were chosen for these re-tests, namely, C(114)S (3)1d, C(114)S (1.2)1d, C(115)A (3.25)1c and the large diameter cylinder C(168)S (3)1a. The responses of their loadcells are compared in Figure 5.84 to Figure 5.90. The individual results of each of the tests are given in Appendix 4.

These experimental results show that the contact force and the base force vary between subsequent tests. From an analysis of the test results thus far, it might be considered that this variation occurs as a result of differences in the concrete in a particular cylinder, or as a result of very minor variations in the exact centre of impact. However, the results of these tests show trends which are consistent with each other, and with the results of other researchers (van Mier *et al*, 1991). In the majority of the repeats, the maximum contact force increases when the cylinder is impacted for a second and third time, and then

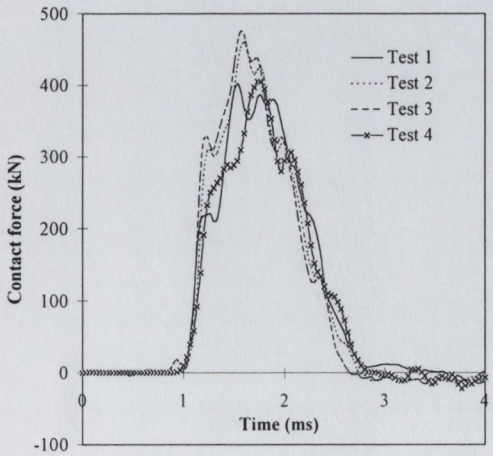


Figure 5.84 Contact force variation for repeated testing of C(114)S (3)1d

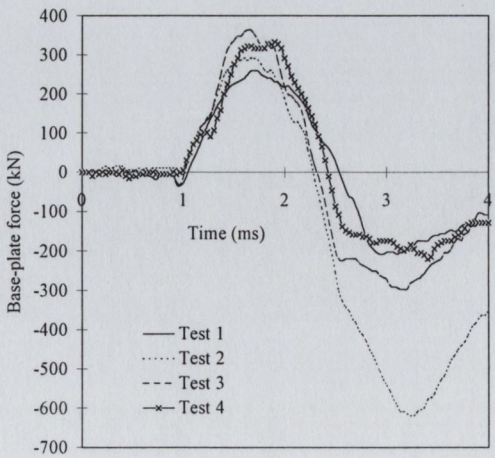


Figure 5.85 Base-plate force variation for repeated testing of C(114)S (3)1d

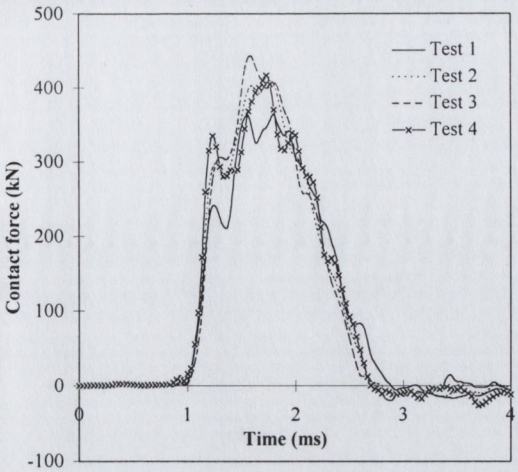


Figure 5.86 Contact force variation for repeated testing of C(114)S (1.2)1d

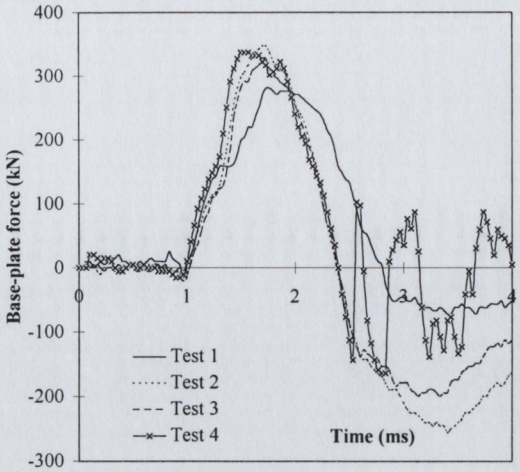


Figure 5.87 Base-plate force variation for repeated testing of C(114)S (1.2)1d

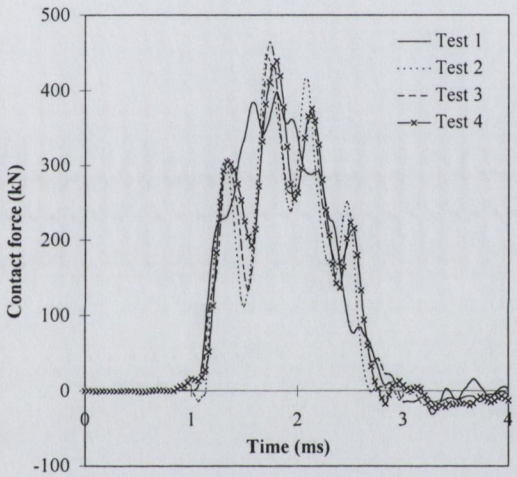


Figure 5.88 Contact force variation for repeated testing of C(115)A (3.25)1c

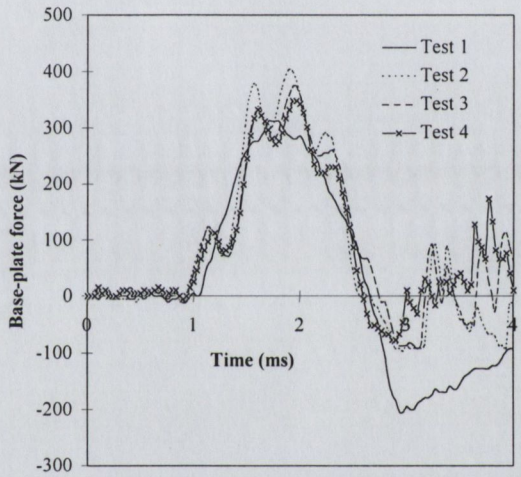


Figure 5.89 Base-plate force variation for repeated testing of C(115)A (3.25)1c

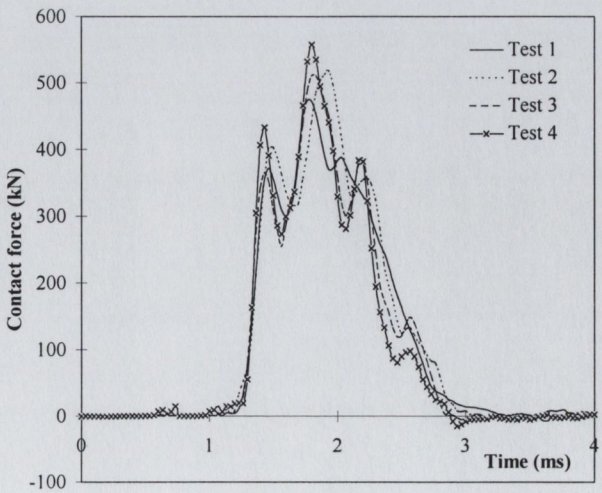


Figure 5.90 Contact force variation for repeated testing of C(168)S (3)1a

decreases when impacted subsequently. It is probable that the maximum contact force continues to decrease with subsequent impacts until the eventual disintegration of the specimen. Evidence of this is shown in the repeat tests of C(114)S (3)1d, C(114)S (1.2)1d and C(115)A (3.25)1c. The large diameter cylinder is slightly different in that it shows an initial increase, and then a small decrease in the third impact test, which might not be significant, prior to an increase on the final repeat. These patterns of contact force responses can be explained by variations in the density of the impacted concrete, which increases initially in response to the impact loading to which it is subject. It reaches a limit, beyond which it begins to significantly fracture, and the density decreases.

An examination of the plots in the area where the contact force returns to zero after the impact shows that the duration of the first impact loading is greatest, and that as the maximum load increases the duration of the loading becomes shorter as the system.

The base-plate loadcell acts in a similar way to the contact force loadcell. The maximum force increases when the cylinder is impacted for a second time, but can decrease when impacted again, as shown in Figure 5.87 and Figure 5.89. The force experienced resulting from the final test can either be an increase or a decrease on the third test. The loadcell always goes into tension after the impact as the impactor looses contact with the top of the concrete core. In some cases, a considerable amount of oscillation is experienced by the loadcell during this part of the loading cycle. However, the steel confined cylinder shows that the tension phase also increases when the test is repeated. It is difficult to make an assessment of exactly why this occurs, other than that the magnitude of the unloading tension wave is a function of the compressive loading wave and that this tends to increase as the tests are repeated.

The top faces of the cylinders which were repeatedly impacted were examined visually after the fourth test. The number of cracks in the top face increased from the inspection after the initial impact test, but the cylinders remained otherwise intact and capable of bearing a load.

5.10. CONCLUSIONS FROM THE EXPERIMENTAL RESULTS

The experimental work was divided into two sections - a large group of impact tests which examined how varying the confinement affected the impact response and a second, supplementary group, which complimented the first series and examined features brought to light during the major test series.

For ease of analysis, the interpretation of the impact test results was broken down into distinct sections, however, certain trends do run through all of the experimental results which should be considered together. Two particular features were examined throughout this analysis - namely the effect that the confinement was having on the response of the concrete and the way in which the load was transferred into the sleeve.

The following are the main conclusions of the experimental analysis

- The unconfined cylinders split longitudinally from the centre of the top face and the energy was dissipated in the creation of fracture planes and the acceleration of the pieces away from the point of impact. These cylinders exhibited an increase in the contact force as the velocity increased, but fairly constant load transfer to the base at a level associated with the properties of the concrete, over the range of velocities tested.
- The contact force and base-plate force were greatly enhanced when the concrete cylinder was surrounded by a confining sleeve, capable of generating a hoop stress and, thereby, reducing the dilation of the concrete.
- A reduced factorial analysis was used to show that the velocity of impact, the thickness of the confining sleeve and the Young's modulus of the confining material were all statistically significant factors in the response of confined concrete to impact.
- The plastic confined cylinders were better at resisting the impact than the unconfined cylinders. Whilst the strains in the sleeve did not exceed the relatively low failure strain of the plastic, it was able to contain the concrete, prevent failure of the specimen and the response of the composite was, in many ways, elastic. When the critical strain was exceeded at higher velocities, this resulted in the complete disintegration of both concrete and confining sleeve.

- When the sleeve was sufficiently stiff to reduce the dilation of the concrete the composite cylinder behaved in an elastic manner, in the majority of cases this was when the confinement was provided by a metallic sleeve. The sleeves did not allow much visible cracking to occur in the concrete core and caused the impactor to rebound with a significant velocity. The concrete confined by the stiffer sleeves also had a high residual strength when statically reloaded and was able to resist repeated impacts.
- The responses of the metallic sleeved cylinders were similar at low velocities, exhibiting increases in the contact force and the base-plate force over similar unconfined values. However, at a velocity of 6.3 m/s, the contact forces were up to 150 % greater than the measured unconfined values, and the combination of thickness and Young's modulus of the sleeve significantly affected the results. The 1.2 mm thick steel sleeved cylinder and the aluminium sleeved cylinder responded in a similar manner but neither was as good as the thicker sleeves at steel at resisting the impact. At this velocity, the 5 mm and the 6.5 mm steel sleeves were clearly the most effective at reducing the dilation
- The supplementary tests showed that the proximity of the confining sleeve to the point of load application was also important in the contact force response. If the distance from the centre of loading to the confining sleeve was large, dilation occurred which reduced the maximum forces measured by the loadcell.
- The results also illustrated that the unconfined strength of the concrete has a effect on the response of the composite. The results of the C(114)S (5) cylinders, whose concrete had a low cube strength, were consistently less good at resisting impact than otherwise might have been expected.
- In all cases, particularly in the analysis of the unconfined cylinders and the base-plate results, an increasing number of test repeats would have useful in the removal of outliers and in increasing the confidence in some of the results.

The way in which the load was transferred from the loaded concrete core into the sleeve and to the base of the cylinder was also examined, both under impact and static loads. The strain results and stress-strain results lead to the following conclusions.

- The thickness and Young's modulus of the confining sleeve affected the strains in the sleeves, with increases in either reducing the measured strains. However, the yield and tensile strength of the confining sleeve were also important in the

response because, if the maximum stress was exceeded, the sleeve ruptured and the benefits of the confinement were significantly reduced.

- The load was initially taken by the concrete core resulting in considerable lateral dilation close to the top of the cylinder. Little or none of the load was taken by the sleeve at this level, as it takes a certain distance along the friction interface between the core and the sleeve for the load transfer to occur.
- By the mid height, a significant proportion of the load had been transferred into the confining sleeve which then propagated axially down to the loadcell at the base. This meant that the axial strains were considerably larger than the lateral strains in the lower half of the cylinder, which are predominantly induced by a Poisson's ratio effect. This is the opposite of the relationship in the uppermost strain gauges.
- The load transfer along the sleeve had little effect on the overall response, as shown by tests with reduced confinement at the base. These tests showed that the main function of the sleeve was the reduction of the dilation of the core concrete and that when the load cannot be transferred to the base through the sleeve it will find an alternative path.
- An understanding of the load transfer mechanism into and along the sleeve is extremely complicated and it is hoped that the understanding will be facilitated by the use of finite elements in a later chapter.

It is possible to use the results obtained during the experimental work to generate an outline for a design curve for the response of sleeved concrete cylinders to low velocity hard impact. Any such curve has limitations because the cross-sectional area of the impactor and the target have to be similar to be applicable to this experimental work, however, it is probable that, with modest adaptation, it could be used for cylinders of other cross-sectional areas. Figure 5.91 gives an indication of such a design curve for the steel sleeved concrete. Clearly, there is a upper bound velocity beyond which unconfined concrete (which has a sleeve of thickness 0 mm) can not be impacted without significant fracturing. However, this value was not determined experimentally during the current series of tests.

Such a design curve might be bi-linear as, up to a certain velocity and thickness of confinement, the sleeved concrete would be able to withstand the impact without significant dilation or cracking. The initial slope of the curve would be quite steep as the

presence of a sleeve has a significant confining effect, even at low velocities. However, as has been shown in the current research, there is a limit whereupon the thickness of the sleeve is of importance to the response. If the velocity of the impactor is greater than the maximum allowable for a given thickness of sleeve, the design curve would show that the confined cylinder would be unable to withstand the impact without considerable cracking. An example of this occurred with the 1.2 mm thick steel sleeved concrete which was able to withstand the impact at the lower two velocities but, at the highest velocity, dilated resulting in considerable cracking to the concrete.

Similar relationships for aluminium or plastic sleeved concrete would fall inside the curve shown in the figure for steel. However, by no means does the author wish to contend that this graph in its current form should be used in design. It is merely indicative of the physical behaviour of steel confined concrete when subject to impact. More experimental work, along similar lines, would have to be undertaken before the shape of the curve be accurately determined - this might then allow the use of such a curve in design.

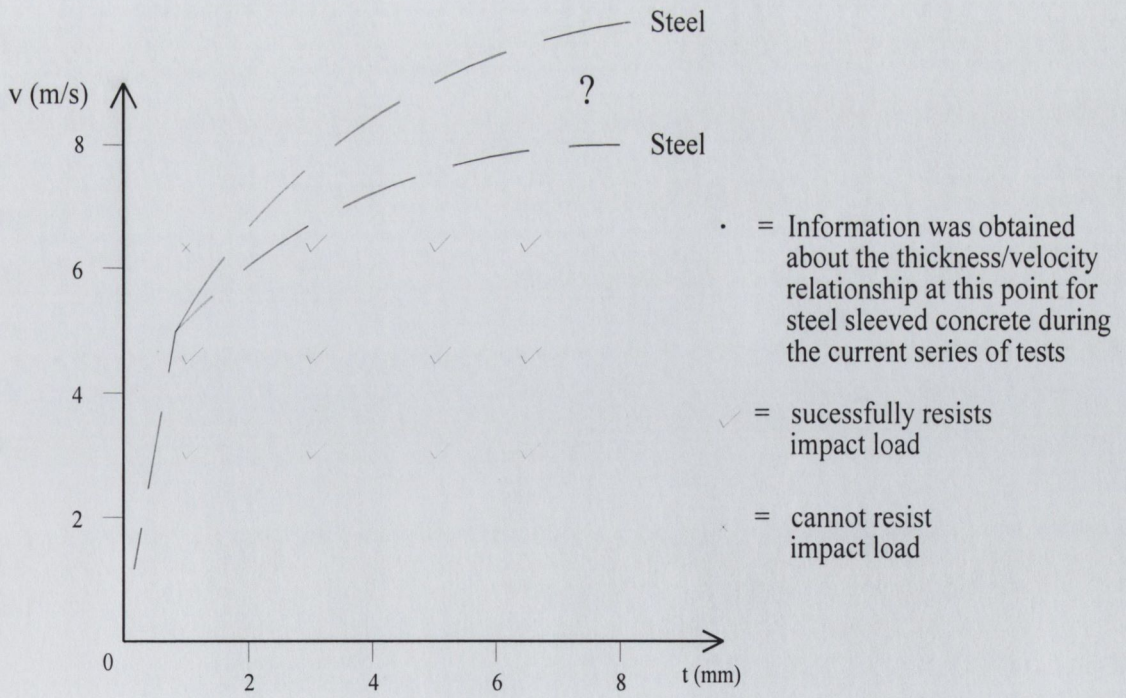


Figure 5.91 Approximate design curve for steel sleeved concrete of different thicknesss

6. ANALYTICAL STUDY

6.1. INTRODUCTION

The results of the experimental work can be examined analytically through the use of existing equations and others derived by the author which model the responses of the confined cylinders to impact. These formulae can be classified in two ways, namely, those which are derived analytically though a knowledge and understanding of the parameters of the subject and those which are obtained empirically by researchers by an analysis of their experimental results. The former can sometimes be useful and, although they are often simplified, can provide a closed-form solution to the particular problem. However, the empirical formulae, determined through the analysis of experimental results to obtain coefficients for equations which allow the problem to be described, are limiting because they only provide an accurate solution to a particular problem and in some cases only fit the results from which they were generated.

This chapter describes three analytical studies which allow certain aspects of the response of the confined concrete cylinders to be modelled. The study involves (a) the determination of a relationship to predict the maximum contact force generated by an impact, (b) the use of Hertzian contact theory to model the contact force response of the concrete cylinders and (c) the generation of stress-strain curves based on existing empirical equations to model the deformational response of the unconfined and confined concrete to both static and impact loading. The theoretical results produced are compared to the experimental work to which they correspond.

6.2. CONTACT FORCE PREDICTION

6.2.1. Theory

The high contact force associated with dynamic loading, and particularly impact, is generated by the transmission of stress waves away from the point of impact as the body attempts to dissipate the high stresses resulting from the collision. Much of the work in the field of impact has involved an attempt to quantify the contact forces associated with the collision, and the current work has measured the contact force using a loadcell incorporated into the impactor close to the point of impact.

When the impact occurs (in the z direction in Figure 6.1) the impactor hits the confined concrete, but not the confining cylinder, resulting in a sharp increase in the local longitudinal stress in the concrete. As the concrete is loaded axially, an effective compressive pressure is generated at the boundary between the concrete core and the confining sleeve due to lateral dilation. At the boundary of the concrete core, this effective pressure, p_0, is equal to the radial stress, σ_{rc}, and the circumferential stress, $\sigma_{\theta c}$ in the concrete and to the radial stress on the inside of the confining sleeve, σ_{rp}. Furthermore, the dilation of the core and the sleeve are assumed to be equal at the interface, as the radial and circumferential strains in the core are equal to the circumferential strains in the

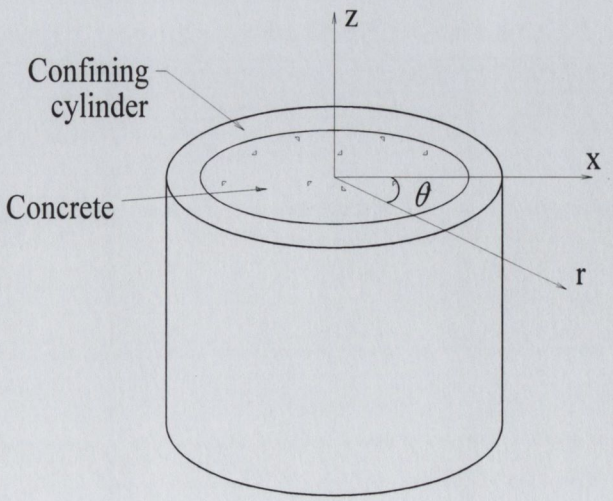


Figure 6.1 Concrete filled tube with axes illustrated

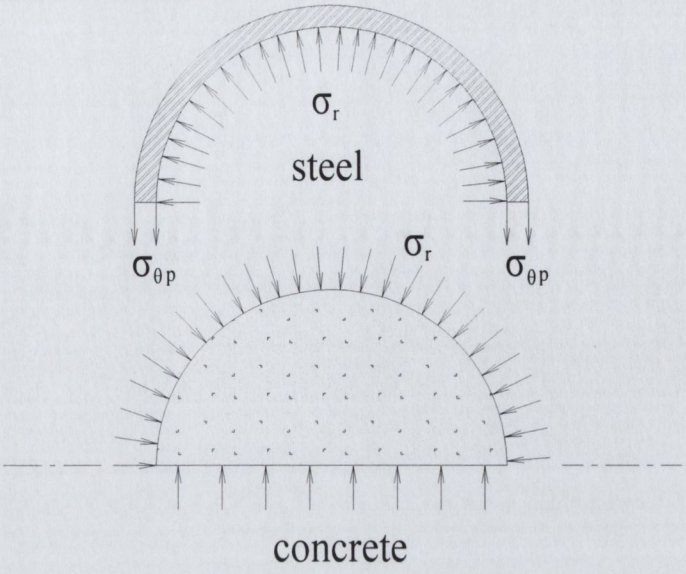


Figure 6.2 Free body diagram of stresses in half a concrete filled tube

confining sleeve. The radial stress in the sleeve creates a hoop or circumferential stress, σ_θ, in the confining sleeve, as shown in Figure 6.2, of magnitude

$$\sigma_{\theta p} = \frac{r}{t}\sigma_{rp} \tag{6.1}$$

where r is the radius and t is the thickness of the sleeve (Timoshenko and Goodier, 1970). The concrete is, therefore, in tri-axial compression as the wave passes and the confining cylinder is in hoop tension, created by an internal pressure. It is assumed that the concrete is sufficiently well confined to behave as a linearly elastic, isotropic material, and that longitudinal friction in the cylinder is not important. Although the experimental results have shown that friction is important, it takes a certain distance along the sleeve before it has an effect on the sleeve and thus, the friction at the interface is negligible. The following expression can then be written for the static radial strain in the concrete at the interface

$$\varepsilon_{rc} = \frac{1}{E_c}\left(\sigma_{rc} - \upsilon_c(\sigma_{\theta c} + \sigma_z)\right) \tag{6.2}$$

where, σ_z is the applied longitudinal stress, σ_{rc} and $\sigma_{\theta c}$ are the radial and circumferential stresses in the concrete. The material properties of the concrete, Poisson's ratio and Young's modulus are denoted by υ_c and E_c.

When the concrete is confined, even if only by a small thickness of confining material, the radial strain in the concrete is significantly reduced when compared to the case when

there is no confinement present. The experimental work showed that there were lateral strains close to the top of the confined cylinder, however, these were measured below the surface where the material has had some distance to dilate, rather than actually at the top of the cylinder. If the confining sleeve is sufficiently strong to remain elastic during the period of loading then, as an upper bound it can be assumed that the radial strain tends to zero, on the basis that there is no lateral dilation of the concrete at the interface, due to the presence of the confining material. Hence,

$$\varepsilon_{rc} = 0 = \frac{1}{E_c}\left(\sigma_{rc} - \upsilon_c(\sigma_{\theta c} + \sigma_z)\right) \tag{6.3}.$$

As the radial and circumferential stresses are equal, this equation can be re-written to give a value for the confining pressure, p_0, thus

$$p_0 = \sigma_{rc} = \frac{\upsilon_c \sigma_z}{1 - \upsilon_c} \tag{6.4}.$$

The presence of a lateral load on concrete, provided either hydro-statically or using spirals, hoops or tubes, has been found to increase the longitudinal strength of the concrete. Richart *et al* (1928) were the first to show that the strength of concrete, when confined by an active hydrostatic fluid pressure, could be described using the following relationship

$$\sigma_c = \sigma_z + k\sigma_r \tag{6.5}$$

where σ_c is the strength of the confined concrete, and k is an empirical factor. Other experimental work has successfully used this formula to describe the increase in the concrete strength when confined passively by closely spaced circular spirals or tubes of steel which cause an equivalent lateral pressure (Richart *et al*, 1929; Gardner and Jacobson, 1967). The factor k has been empirically determined to be 4·1. This value is now widely accepted as a good empirical solution and was used in the A.C.I. Building Code for the design of composite columns (Saatcioglu and Razvi, 1992)

The increase in strength of a cylinder of concrete when confined by a pressure which is sufficiently great to prevent the lateral dilation of the concrete can be described by substituting equation (6.4), which describes the pressure, into equation (6.5), which describes the strength increase and, hence,

$$\sigma_c = \sigma_z\left(1 + k\frac{\upsilon_c}{1 - \upsilon_c}\right) \tag{6.6}.$$

Research has also shown that there is a significant increase in the uni-axial compressive strength of concrete and other materials, compared to their equivalent static strengths, when they are subjected to high strain rate loading. Furthermore, the current experimental work has shown that there is a further increase in this contact force when the concrete is confined. Johnson (1972) derived an expression, using momentum considerations and the formula for one dimensional stress in a bar due to a compressive pulse, to describe the maximum stress, at the location of impact, generated by the collision of two bars. In this equation the cross-sectional areas of the impactor and target can be either the same or different (equations (2.46) and (2.48)).

The derivation of these equations involve equating the forces at the contact interface, which are the products of the stress and the area of the surface, as shown in equation (2.47). If a third, confining, material is present at the contact interface then the equation for the forces at the interface can be modified to incorporate this. Hence,

$$A_i\sigma_i = A_c\sigma_c + A_p\sigma_p \tag{6.7}$$

where the subscripts i refer to the impactor, c to the core concrete and p to the confining sleeve. If the stresses are replaced by their components from the one dimensional stress wave propagation, given in equation (2.43), then equation (6.7) becomes

$$A_i\rho_i c_i(v_1 - u_0) = A_c\rho_c c_c(u_0 - v_2) + A_p\rho_p c_p(u_0 - v_2) \tag{6.8}$$

where v_1 and v_2 are the initial velocities of the impactor and the target, prior to impact, and u_0 is the common velocity of the interface after the impact, whilst the impactor and the confined cylinder are in contact. If the increase in the longitudinal strength of the core is incorporated into this equation, then

$$A_i\rho_i c_i(v_1 - u_0) = A_c\rho_c c_c(u_0 - v_2)\times\left(1 + k\frac{\upsilon_c}{1-\upsilon_c}\right) + A_p\rho_p c_p(u_0 - v_2) \tag{6.9}.$$

The common velocity after the impact is, therefore,

$$u_0 = \frac{A_i\rho_i c_i v_1 + A_c\rho_c c_c\left(1 + k\frac{\upsilon_c}{1-\upsilon_c}\right)v_2 + A_p\rho_p c_p v_2}{A_i\rho_i c_i + A_c\rho_c c_c\left(1 + k\frac{\upsilon_c}{1-\upsilon_c}\right) + A_p\rho_p c_p} \tag{6.10}.$$

The maximum contact force, P_c, of a concrete cylinder passively confined by an unloaded sleeve, can, therefore be found by substituting equation (6.10) into equation (6.8), thus

$$P_c = \frac{A_i \rho_i c_i \left[\left(A_c \rho_c c_c (1 + k \frac{\upsilon_c}{1 - \upsilon_c}) + A_p \rho_p c_p \right) \times (v_1 - v_2) \right]}{A_i \rho_i c_i + A_c \rho_c c_c (1 + k \frac{\upsilon_c}{1 - \upsilon_c}) + A_p \rho_p c_p} \qquad (6.11)$$

6.2.2. Comparison of predicted contact force with experimental results

Equation (6.11) was used to predict the maximum contact force for confined concrete for the specimens which were tested as part of the current research, as described in Prichard and Perry (1999). Table 6.1 compares the average measured contact force found in Table 5.1 with the calculated contact force value for each of the groups of results and shows the percentage difference between the two values.

The results of the predictions for the steel and aluminium confined concrete cylinders impacted at the lower two velocities fall, predominantly, well within 10 % of the measured contact force value and are typically over-predictions because of the assumption that there was absolutely no lateral dilation at the interface. The variance in the over-prediction can probably be attributed to the variation in the concrete properties of the specimen. The largest discrepancy between the measured and predicted values, at the lower two velocities, is in the case of the concrete confined by steel of 5 mm thickness, but it should be noted that, as discussed in Chapter 5, the experimental results from these cylinders do not conform to what would be expected from an analysis of the other velocities of impact or other thicknesses of confinement at the same velocity, because of the low cube strength of the concrete.

The predicted values for identical cylinders impacted at the highest velocity are much less close to the experimental results. This was particularly the case for the thicker types of sleeve, and in some cases the theoretical predictions were 20 % less than the measured value. This probably occurred because, as has already been discussed in chapter 5, the contact force values are dependant on both the impactor and the target acting elastically. This occurs with the thinner sleeves. However, the cylinders with a greater thicknesses of

confinement and a high Young's modulus exhibit higher contact forces at high velocities because the properties of the confined concrete are changed by the collision. The concrete is so well restrained by these thicknesses of steel sleeve that, at the higher velocities, the concrete is compacted, perhaps increasing the density of the material, altering the material properties and resulting in this increase.

The theoretical prediction for cylinders confined with sleeves of plastic produced results which were much less accurate, but this happened at all three velocities and the reason for its occurrence is different to that in the steel confined case. The over-predictions in the maximum contact force are between 25 % and 57 %. This, however, is not surprising as the underlying assumption for the above relationship was that there was no lateral dilation of the concrete or the confining cylinder. Not only was the plastic cylinder found to dilate during the impact event, but the deformations which occurred were unrecoverable and, in some cases, led to the splitting of the sleeve, considerable cracking and failure of the concrete. Hence, in the case of the plastic confinement, the assumption of zero dilation is invalid and the over-prediction is very large.

The simple equation for the collision of two bars, (2.46), was used to predict the contact force for unconfined concrete. At the lowest velocity, the results which it produced were in close agreement with the experimental results as, although the concrete fractured longitudinally, it was not as catastrophic as the instantaneous shattering of the whole cylinder at higher velocities. The assumption that it was acting elastically, at these higher velocities, was clearly invalid and the equation was increasingly unable to accurately predict the maximum contact force.

The contact forces of the large diameter cylinders, both confined and unconfined, were over-predicted by the two equations. The dilation of the concrete is much greater in the larger cylinders because of the considerable distance from the centre of the impact to the confining sleeve which inhibits the dilation. Like the plastic sleeved cylinders, the assumption that the sleeve is capable of sufficiently reducing the radial dilation is probably not strictly valid and means that the contact force cannot be predicted accurately. Furthermore, the over-prediction is also high in the case of the unconfined cylinder which would suggest that the equation, originally derived for the collision of two bars of similar

Velocity (m/s)		3.2	4.4	6.3
Unconfined	Average measured (kN)	192	317	346
	Calculated (kN)	195	271	383
	Difference (%)	*1.5*	*-14.6*	*10.7*
Steel t = 1.2 mm	Average measured (kN)	387	588	797
	Calculated (kN)	414	575	814
	Difference (%)	*7.0*	*-2.2*	*2.1*
Steel t = 3 mm	Average measured (kN)	403	593	1062
	Calculated (kN)	427	593	839
	Difference (%)	*5.9*	*-0.1*	*-21.0*
Steel t = 5 mm	Average measured (kN)	418	569	1000
	Calculated (kN)	447	621	878
	Difference (%)	*6.8*	*9.1*	*-12.2*
Steel t = 6.5 mm	Average measured (kN)	424	611	1103
	Calculated (kN)	447	621	879
	Difference (%)	*5.4*	*1.6*	*-20.3*
Aluminium	Average measured (kN)	394	539	844
	Calculated (kN)	393	546	773
	Difference (%)	*-0.2*	*1.3*	*-8.4*
Plastic	Average measured (kN)	283	361	444
	Calculated (kN)	355	494	698
	Difference (%)	*25.5*	*36.7*	*57.3*
Large unconfined	Average measured (kN)	338		
	Calculated (kN)	389		
	Difference (%)	*15.1*		
Large confined	Average measured (kN)	461		
	Calculated (kN)	606		
	Difference (%)	*31.4*		

Table 6.1 Measured and calculated contact forces

cross-section, might not be able to successfully predict the contact force when there is such a large difference in areas between the impactor and target.

The theoretical predictions for the maximum contact forces, in the majority of cases, are within 10 % of those measured. A summary of the results for the lower two velocities is shown in Figure 6.3, which compares the measured results (shown as bars) with the results calculated using the theoretical equation (shown as lines). Where the confinement provided was stiff, for the steel and aluminium, the over-prediction was small, but would

suggest that there was a some lateral dilation of the concrete. However, where the assumption that the lateral dilation was zero is least accurate, is in the case of the plastic sleeved cylinder or the large diameter cylinder. The plastic was more flexible and the thickness provided was not sufficient to prevent the dilation of the confined concrete.

Regardless of the dilation along the length of the cylinder, the radial and circumferential strains at the top of the cylinder must be nearly negligible at the top of the sleeve. The contact force, both experimentally and theoretically, is a phenomenon associated with what happens at the instant of the collision at the interface between the target and the impactor. The two objects experience nothing more than the velocity, density and speed of stress wave propagation of the object by which they have been hit (nothing is known, for example, about the mass or length). The contact force at the interface is solely a function of the material and physical characteristics at that location, including whether any dilation has occurred or not, and it is this which dictates the contact force response.

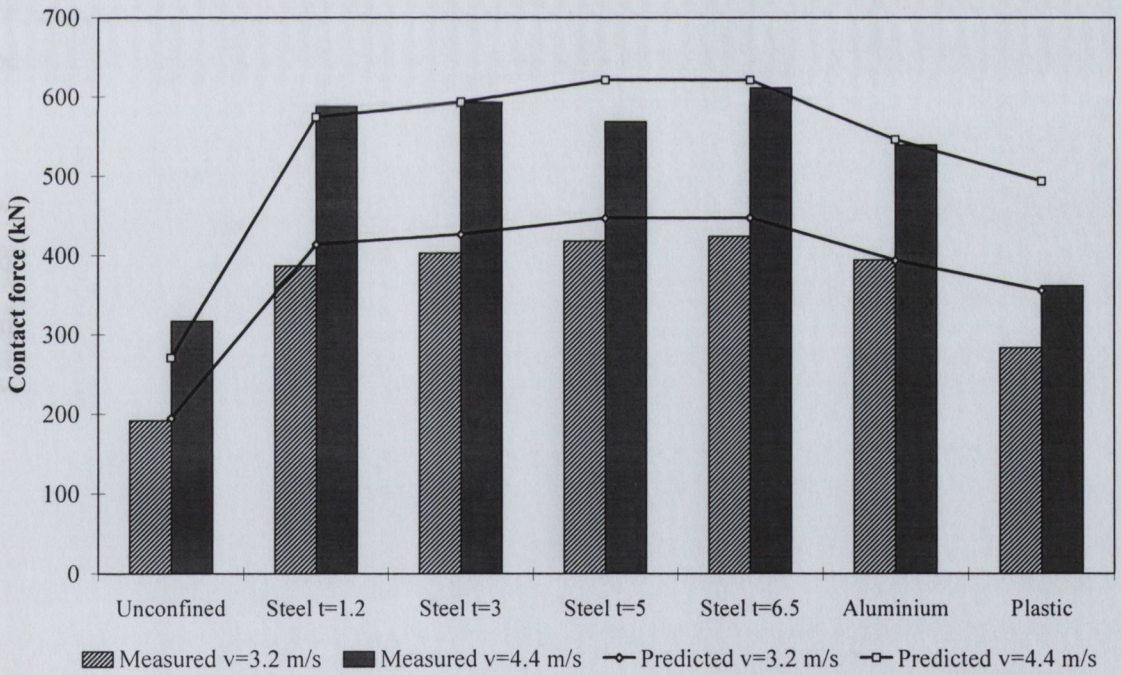


Figure 6.3 Comparison of measured and predicted contact force results

6.3. HERTZ'S CONTACT LAW

6.3.1. Theory

A force-deformation relationship for the static elastic compression of two isotropic bodies was derived by Hertz. It is valid for any bodies whose surfaces, in the region of contact, can be assumed to be smooth paraboloids. However, this law can also be used to describe the elastic impact of two masses if the vibrations produced by the impact can be neglected. This force-deformation phenomenon is extremely important as a considerable amount of the initial kinetic energy can be absorbed by the deformation of the bodies (Goldsmith, 1960; Timoshenko and Goodier, 1970).

If the two surfaces are assumed to be paraboloids in the region of contact, the law will take account of the majority of surface types, except for discontinuous surfaces such as the apex of a cone or a wedge. The equations of the surfaces, which are initially in contact at point 0, as illustrated in Figure 6.4, are

$$z_1 = A_1 x_1^2 + B_1 y_1^2 + C_1 x_1 y_1 \qquad z_2 = A_2 x_1^2 + B_2 y_1^2 + C_2 x_1 y_1 \qquad (6.12),$$

where the z-axes are normal to the tangent plane at the contact point and are positive towards the interior of the bodies. The x_1-y_1 axes can be rotated to remove the x_1y_1 terms in the equations above and, hence, the distance, $\bar{d}$ separating the two bodies along the z-axis is given by

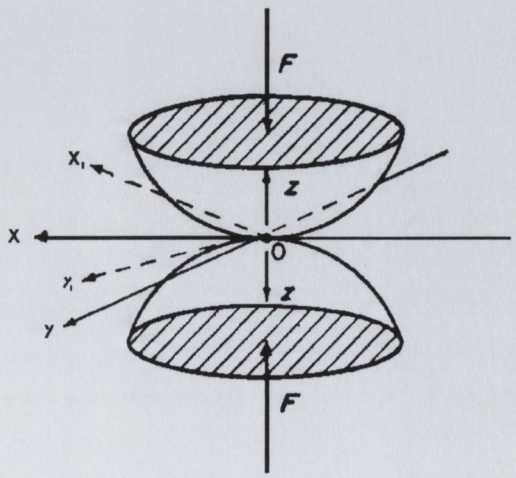


Figure 6.4 Contact between two paraboloids in Cartesian geometry (Goldsmith, 1960)

$$\bar{d} = z_1 + z_2 = Ax^2 + Bx^2 \tag{6.13}$$

where A and B are related to the principal radii of curvature of the two bodies, which are R_1 and R_1' for body 1, and R_2 and R_2' for body 2. Goldsmith showed that the following can be determined,

$$A + B = \frac{1}{2}\left(\frac{1}{R_1} + \frac{1}{R_1'} + \frac{1}{R_2} + \frac{1}{R_2'}\right)$$

$$A - B = \frac{1}{2}\left[\left(\frac{1}{R_1} - \frac{1}{R_1'}\right)^2 + \left(\frac{1}{R_2} - \frac{1}{R_2'}\right)^2 + \left(\frac{1}{R_1} - \frac{1}{R_1'}\right)\left(\frac{1}{R_2} - \frac{1}{R_2'}\right)\cos 2\beta\right] \tag{6.14}.$$

$$\text{and} \quad \cos 2\beta = \cos\theta = \frac{B - A}{B + A}$$

A further assumption is made that the contact is never between two perfectly flat bodies and, therefore, causes indentation to occur in one of the surfaces. Thus, when a normal force is applied to the bodies, some local deformation will occur at the point of contact. The contact surfaces of the bodies can be described by

$$w_1 + w_2 = \alpha - Ax^2 - By^2 \tag{6.15}$$

where w_1 and w_2 describe the displacements of the two bodies in the z-direction. The approach, α, is the sum of the displacements along the z-axis and represents the maximum relative compression of the bodies. It is assumed that the two bodies are deformed in such a way as to produce coincidence of the corresponding nodes within the area of contact, which is only strictly valid when both materials have the same elastic constants. The deflections caused by a pressure, p, on the area $dxdy$ can be described by

$$w\big|_{z=0} = \frac{1 - \upsilon^2}{\pi E} \iint \frac{p\, dxdy}{s} \tag{6.16}$$

or

$$w = \delta \iint \frac{p\, dxdy}{s} \qquad \text{where} \qquad \delta = \frac{1 - \upsilon^2}{\pi E} \tag{6.17}$$

and s is the distance between the element in its original position and the origin after application of pressure, p. This can be substituted into equation (6.15) to give

$$[\delta_1 + \delta_2] \iint \frac{p\, dxdy}{s} = \alpha - Ax^2 - Bx^2 \tag{6.18}.$$

To solve the equation for p, the pressure distribution over the contact area, Hertz determined that the intensity of pressures over the surface could be represented by the

ordinates of a semi-ellipsoid constructed over the surface of contact with the maximum pressure p_{max} at its centre and a and b its semi-axes. The maximum pressure is, therefore, determined from

$$F = \iint p\, dxdy = \frac{2}{3}\pi abp_{\max} \tag{6.19}$$

and, hence

$$p_{\max} = \frac{3}{2}\frac{F}{\pi ab} \tag{6.20}.$$

The magnitudes of the semi-axes are required to find the maximum pressure which are determined in Goldsmith, thus

$$a = q_a \sqrt[3]{\frac{3F(\delta_1 + \delta_2)}{4(A+B)}} \quad \text{and} \quad b = q_b \sqrt[3]{\frac{3F(\delta_1 + \delta_2)}{4(A+B)}} \tag{6.21}.$$

The Hertz force-deformation law determines the relationship between the applied force, the resulting deformation and a factor relating the geometric and material properties of the surface, thus

$$F = k_2 \alpha^{3/2} \tag{6.22}$$

where

$$k_2 = \frac{4}{3}\frac{q_k}{(\delta_1 + \delta_2)\sqrt{A+B}} \tag{6.23}.$$

The coefficients q_a, q_b and q_k are all functions of the angle θ or of the ratio A/B, and when θ is 90° then $q_a = q_b = 1.4645$ and $q_k = 0.3180$ and, in this case, the area of contact is a circle (Goldsmith, 1960). Similar values can be found in Timoshenko and Goodier (1970) but these differ by a factor of π, which is incorporated in the equations (6.21) rather than in the coefficients.

The Hertz law of contact can also be used to describe the collision of two bodies, when incorporated into Newton's Second Law of motion, which takes account of the masses of the bodies and the acceleration, thus

$$F(t) = -\frac{m_1 \times m_2}{m_1 + m_2} \times \frac{d^2\alpha}{dt^2} \tag{6.24}$$

where $F(t)$ is the contact force and the masses of the bodies are m_1 and m_2. If the Hertz contact law is substituted into equation (6.24) then

$$\frac{m_1 m_2}{m_1 + m_2} \ddot{\alpha} = -k_2 \alpha^{3/2} \tag{6.25}$$

$$\text{or} \quad \ddot{\alpha} = -k_1 k_2 \alpha^{3/2} \quad \text{where} \quad k_1 = \frac{m_1 + m_2}{m_1 \times m_2} \tag{6.26}.$$

Equation (6.25) can be solved by integration with the initial conditions

$$\frac{d\alpha}{dt} = v_0 \; at \; \alpha = 0 \quad and \quad \frac{d\alpha}{dt} = 0 \; at \; \alpha = \alpha_{\max}$$

where v_0 is the velocity of the impactor just prior to the impact. The maximum deformation occurs when there is zero relative velocity between the two bodies, or when $\dot{\alpha} = 0$, and is equal to

$$\alpha_{\max} = \left[\frac{5 v_0^2}{4 k_1 k_2} \right]^{\frac{2}{5}} \tag{6.27}$$

Similarly, the maximum load, P_{max}, and the contact time, t_{max}, at which P_{max} occurs can be found to be

$$P_{\max} = \left(\frac{5 \times v^2 \times k_2^{2/3}}{4 \times k_1} \right)^{\frac{3}{5}} \tag{6.28}$$

and

$$t_{\max} = 1.47 \times \left[\frac{5}{4 \times v^{1/2} \times k_1 \times k_2} \right]^{\frac{2}{5}} \tag{6.29}.$$

The idealised elastic impact, modelled by a sine wave because the integration of equation (6.24) involves elliptic integrals, is shown in Figure 6.5, with P_{max}, t_{max} and $t_0 = 2t_{max}$ as

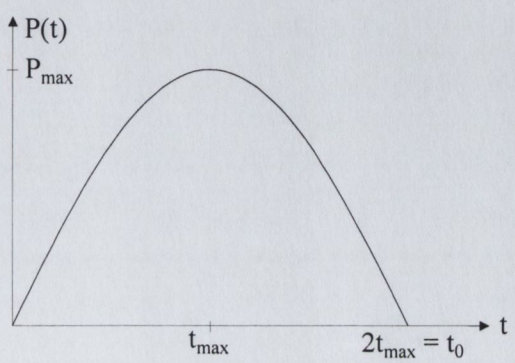


Figure 6.5 Elastic impact modelled as a sine wave

indicated. The value of the contact parameter, K_2 in the equations above, is the same for the approach (K_a) as for restitution (K_r) as the collision is assumed to be elastic. The force/time relationship can be described by

$$P(t) = P_{max} \sin\left(\frac{\pi t}{2t_{max}}\right) \qquad (6.30).$$

6.3.2. Model 1 - A sine curve

The current research examines what happens when a cylinder of concrete, confined by a thin walled cylinder of a different material, is subjected to low velocity hard impact along its major axis. The experimental work has shown that, when the concrete is impacted in this way, it results in an increase in the maximum contact force measured when compared to an unconfined cylinder. In this section, an attempt is being made to model both the maximum contact force and the shape of the contact force/time curve using Hertzian contact theory. Six different series of confined and one series of unconfined concrete cylinders were tested. It was evident, on examination of the contact force/time graph for the well confined tests, that the response was nearly sinusoidal and was almost symmetrical about its maximum point and that the collisions were, therefore, showing evidence of being elastic. This was backed up by the considerable rebound of the impactor after the impact, as discussed in section 5.6.

The Hertzian Contact Law is an idealised model of impact, but has been used by many researchers to model the response of the impact zone. It is appropriate to use it for well confined impact where it can be assumed that there is only minimal cracking in the top face of the impacted concrete, that the collision is almost elastic and that the contact force curves are nearly sinusoidal.

It was assumed that the target comprised the confined cylinder and the solid concrete block on which it was placed, and the effective mass, k_1, was calculated using their combined mass and the mass of the impactor, as in equation (6.26). However, the results for k_1 were dominated by the mass of the block rather than the particular type of cylinder tested. Equation (6.23) was then used to calculate a value for k_2. This incorporated the assumption

that the impactor, which has a curved base with a radius of curvature of 400 mm (R_1), impacts a plane surface and, hence,

$$A = B = \frac{1}{2R_1} \tag{6.31}.$$

The value calculated for k_2, using equation (6.23), was 3.17×10^{10} N/m$^{3/2}$ (or 1002.9 N/mm$^{3/2}$), which was used in the determination of the maximum contact force, using equation (6.28) with a value of k_1 which incorporated the mass of the cylinder and the block. For a velocity of 3.2 m/s the force was found to be 896.4 kN, which was considerably larger than any of the measured values. This way of calculating k_2 had several problems, including

- there was no way of differentiating between the prediction for any of the particular types of confined cylinder. A value of k_2 determined in this manner would be the same for all types of cylinder,
- there was no obvious way to change any of the variables incorporated in the equations above to better predict the maximum force, or the contact duration,

Hence, another way of calculating the value of k_2 was considered.

Other researchers have determined values for k_2 experimentally, typically using penetration results generated by static tests, and then incorporating these values in the calculation of the contact force versus time curve (Hughes and Speirs, 1982; van Mier *et al*, 1991). Similar static penetration values were not generated during the current research. However, values for the maximum contact force, F_{max}, the time at which this maximum force was reached, t_{max}, and the total duration of impact, t_0, were measured for each of the impact tests (and are given in Table 5.1), and from these it was possible to determine values for k_2 using equations (6.28) and (6.29) as had been done by other researchers. The individual values of force and time for each group of results, at all three contact velocities, were substituted into these equations, and into a third equation for the overall impact duration, which was double that of the time to the maximum force. These three equations were combined and the solution was then iterated to find a single optimum (least squares) value of K for each of the types of confined and unconfined cylinders, which took account of all of the individual forces and times in each group. The values determined for each of the groups of results for K are given in Table 6.2.

The values of K were then used to determine values for F_{max} and t_{max}, using equations (6.28) and (6.29) which were in turn used in equation (6.30) to estimate the contact force-time curve for each type of cylinder at each of the three contact velocities. The sine curves which were generated are shown in Figure 6.6 to Figure 6.14, denoted as "Model 1". They are compared directly to the experimental results from the tests at the particular velocity. These sine curves and form a reasonable approximation for the measured plots whilst not taking any account of the degradation in the material properties as the concrete cracks. However, because a combined value of K for each confinement series was used in the calculation, the graphs exhibit a considerable overestimation in some areas, predominately in the calculation of the duration of impact (Prichard and Perry, 2000).

	Model 1	Model 2		
	K (kN/mm$^{3/2}$)	K_{force} (kN/mm$^{3/2}$)	$K_{t\,max}$ (kN/mm$^{3/2}$)	$K_{t\,0}$ (kN/mm$^{3/2}$)
Steel 1.2 mm	126.3	109.2	228.6	127.9
Steel 3 mm	154.6	165.6	255.8	113.9
Steel 5 mm	171.9	159.6	252.4	130.4
Steel 6.3 mm	132.4	187.9	180.8	123.6
Aluminium	114.6	115.6	282.2	110.5
PVC Plastic	65.4	34.3	191.2	68.9
Unconfined	21.2	17.1	529.5	39.7

Table 6.2 Calculated optimum values of the contact parameter for Model 1 and Model 2

6.3.3. Model 2 - A quasi-sine curve

The assumptions which were made in the case of model 1 resulted in a curve which was simple but did not always accurately represent the contact force-time response during the impact event. In practical cases of impact, even when confined, the material response is not perfectly elastic, as some of the energy is absorbed by the concrete through micro-cracking. This can result in slightly different values for the contact parameters for approach (K_a) and restitution (K_r). Thus a second model was produced which improved on the simple elastic model shown.

As before, the values for the maximum contact force, namely the time at which this maximum force was reached and the total duration of impact for each test, were used. The maximum contact force values were used in equation (6.28) to find an optimum value for the contact parameter, K_{force} for each of the types of confinement, that is, the four types of steel and the aluminium, plastic and the unconfined cylinders. The times at which the maximum force was reached and the total duration of impact were both used with equation (6.29), or double equation (6.29), to find two other values for the contact parameter, K_{tmax} and K_{t0} respectively. These separate least squares, optimum values can also be found in Table 6.1. These values for, 'K' are associated with the physical properties of the colliding bodies and should, theoretically, be similar, regardless of whether it is calculated using the maximum force or the maximum time. The differences were probably associated with the assumptions in the modelling and because the concrete underwent some micro-cracking during the collision.

Each of K_{force} and K_{tmax} presented in Table 6.1 was then used in equations (6.28) and (6.29) to calculate values for F_{max} and t_{max}. Equation (6.29) was also used with K_{t0} to find a value for t_0. These values (F_{max}, t_{max} and t_0) were used in equation (6.30) to find the contact force-time curve. Different values of K were used for the approach and restitution because the concrete properties changed during the impact. Account was taken of this by changing from the value for K_{tmax} to K_{t0} in the calculation of t_{max}, when the maximum force was reached, resulting in an overall curve formed by two different sine curves with the same amplitude, determined by K_{force}. The curves generated by this equation are also shown in Figure 6.6 to Figure 6.14 as the dashed line, "Model 2".

6.3.4. Comparison between models

Figure 6.6, Figure 6.7 and Figure 6.8 are of the contact force responses of one of the thicknesses of steel (3 mm) at the three different velocities of impact. Model 2 provided a curve which was considerably closer to the curves acquired during the impact than model 1, for all three velocities of impact. This was predominantly because the curves are not true sine curves and are, therefore, capable of modelling the degradation in properties which occur as a result of concrete fracture during impact loading. Similarly, Figure 6.9 to Figure 6.12, which show the models for steel (with thickness 1.2 mm, 5mm and

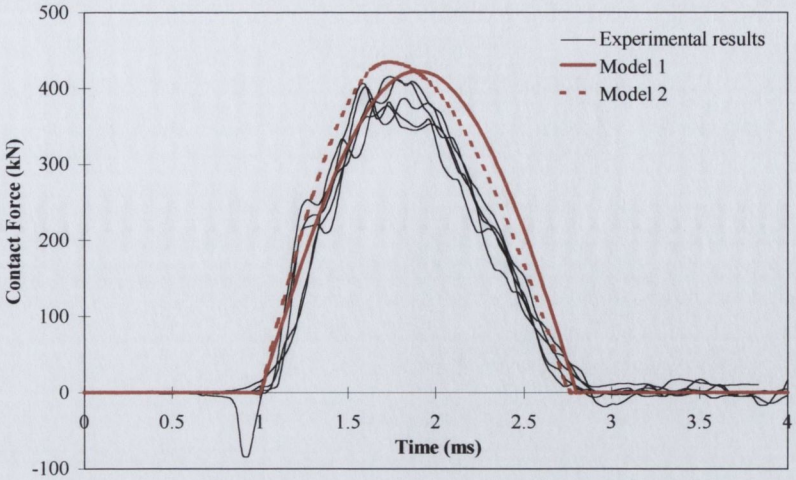


Figure 6.6 Steel sleeved cylinder, thickness 3mm, velocity 3.2 m/s

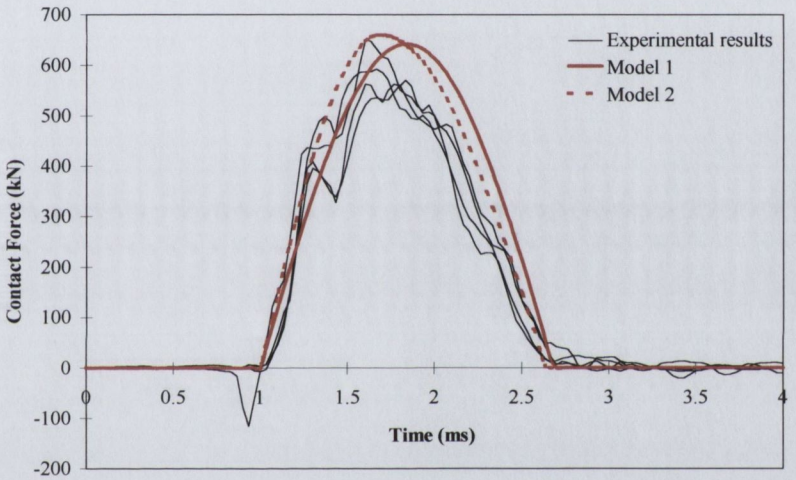


Figure 6.7 Steel sleeved cylinder, thickness 3mm, velocity 4.4 m/s

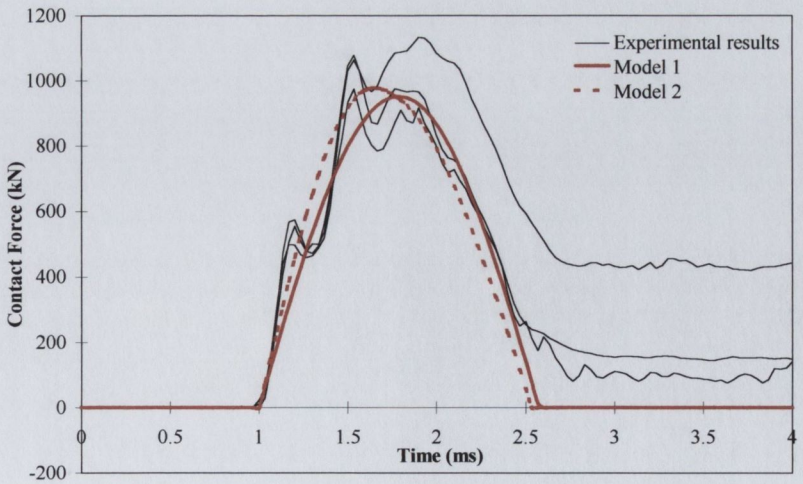


Figure 6.8 Steel sleeved cylinder, thickness 3mm, velocity 6.3 m/s

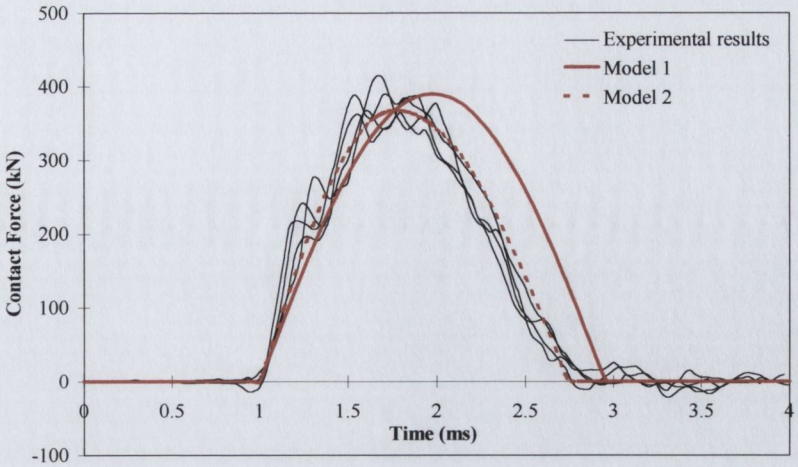


Figure 6.9 Steel sleeved cylinder, thickness 1.2 mm, velocity 3.2 m/s

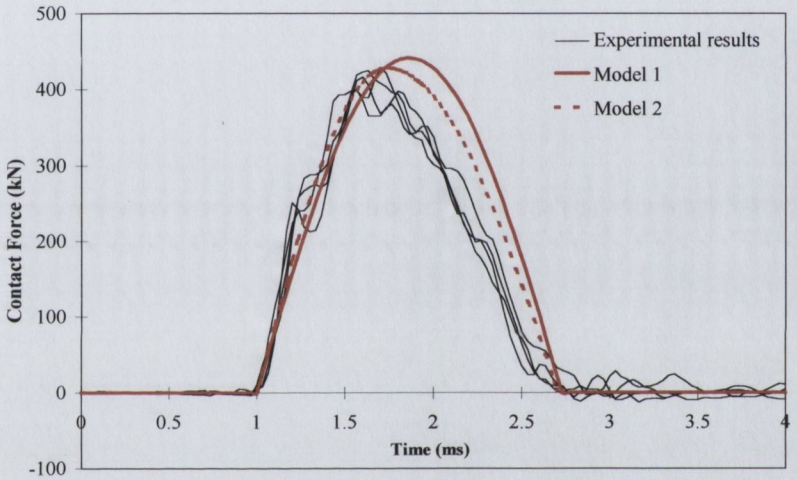


Figure 6.10 Steel sleeved cylinder, thickness 5 mm, velocity 3.2 m/s

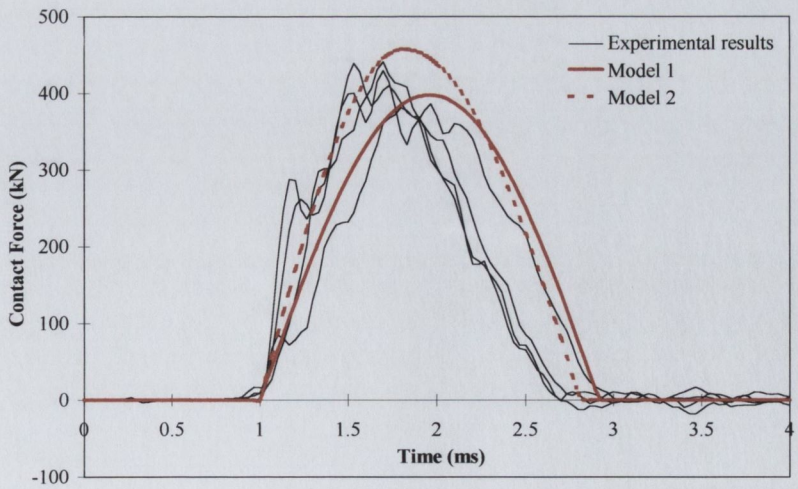


Figure 6.11 Steel sleeved cylinder, thickness 6.5 mm, velocity 3.2 m/s

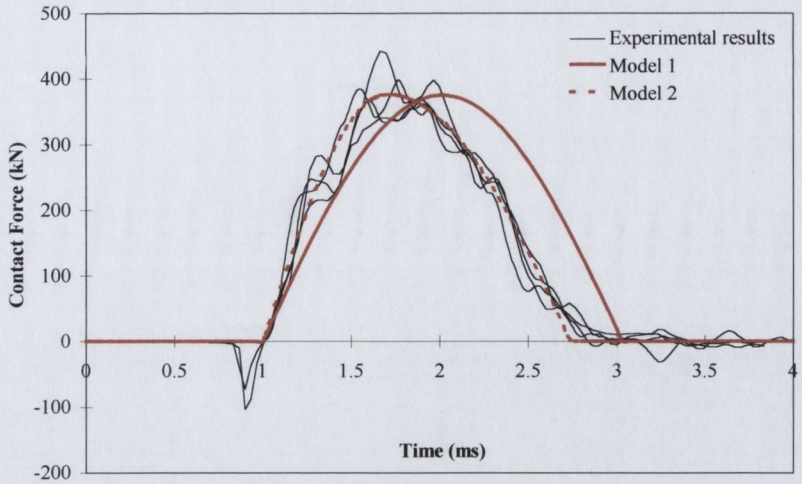


Figure 6.12 Aluminium sleeved cylinder, thickness 3.25 mm, velocity 3.2 m/s

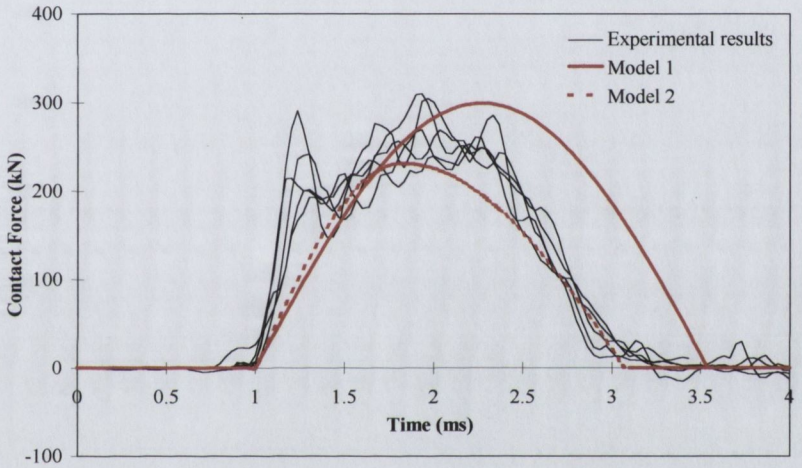


Figure 6.13 Plastic sleeved cylinder, thickness 3.6 mm, velocity 3.2 m/s

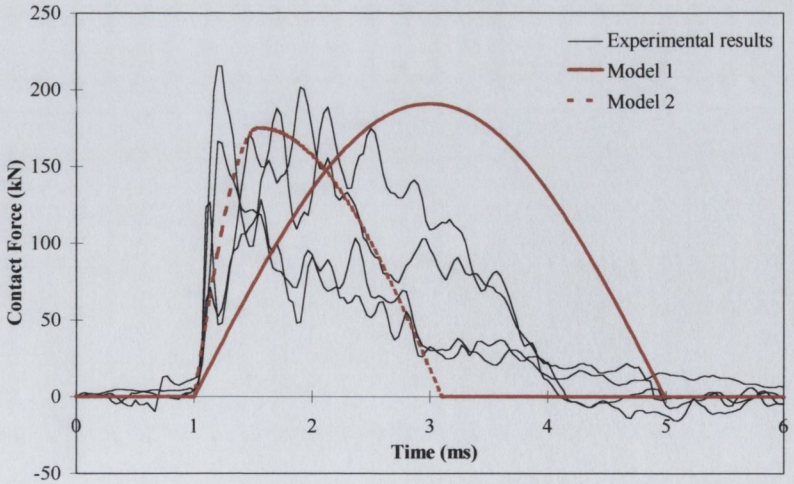


Figure 6.14 Unconfined cylinder, velocity 3.2 m/s

6.5 mm) and aluminium, and are evidence that model 2 is more effective for different types and thicknesses of sleeve provided the confinement is sufficiently thick and stiff to make the composite act in an quasi-elastic manner, and prevent anything more than minimal cracking in the top of the concrete. However, as seen in Figure 6.13 and Figure 6.14, the plastic sleeved cylinder and the unconfined concrete are examples of where the concrete fractures. As a result, the response is definitely not elastic and neither model is able to estimate the response. In the case of the plastic confined concrete, model 1 overestimates both the time and the maximum contact force, and model 2, whereas it approximately models both the time taken to reach the maximum force and the time for the total impact event, it underestimates the maximum contact force. Similarly, the modelling of the unconfined concrete is inaccurate when a single parameter is used to generate the curves (model 1). When three different parameters are used, the curve is better at estimating the maximum force and the time taken to reach the maximum, but cannot model the shape of the curve. This is particularly evident in the difference between the model and the measured steep fall of the force resulting from the brittle fracture of the concrete or the time taken for the force to return to zero after the impact.

The assumption that the curve should be described using different parameters for approach and restitution is, therefore, quite plausible in the case of well confined impact of cylinders. However, when the concrete is confined by a sleeve of plastic or is unconfined, these results cannot predict the response as the assumption of elasticity is totally invalid as the concrete disintegrated.

In many cases, the modelling of the collision between the falling impactor and the concrete cylinder can be greatly simplified if account is taken not only of the solid concrete block, but also of its being bolted to the 0.9 metre deep strong floor of the laboratory. The mass of the whole "target", i.e. the floor, the reaction block and the confined cylinder is, therefore, practically infinite and much greater than the mass of the impactor (82.5 kg). Hence, the movement of the target can then be assumed to be limited to local deformation in the top of the concrete cylinder. As the mass of the impacted body is then assumed to be infinite, the ratio k_1 reaches a limit at the mass of the striker, m_s. Equations (6.28) and (6.29) can be rewritten as

$$P_{\infty} = \left(1.25 \times m_s \times v^2 \times K^{2/3}\right)^{\frac{3}{5}} \tag{6.32}$$

$$t_{\infty} = 1.47 \times \left[1.25 \times \frac{m_s}{v^{1/2} \times K} \right]^{\frac{2}{5}} \tag{6.33}$$

where the subscript ∞ is used to indicate that the mass of the target is assumed to be infinite, a limiting case of the problem. The following equation can then be used to generate a reasonable approximation for the contact force history

$$F(t) = F_{\infty} \sin\left(\frac{\pi t}{2t_{\infty}} \right) \tag{6.34}.$$

Previous researchers, (Hughes & Speirs, 1982) used these equations to generate generalised curves for the variations of both the maximum contact force, P_{∞}, and the peak time, t_{∞}, with the contact parameter K and the initial velocity, v_0, for a given striker mass. Similar generalised curves for the current research can be found in Figure 6.15 and Figure 6.16 below, where the mass of the striker is taken as 82.5 kg, the mass of the falling impactor. It would, alternatively, be possible to input the values of the maximum contact force or the time which it took to reach that maximum value onto the graphs and to determine graphically an optimum value for the contact parameter. If a value is determined for K using these two graphs (resulting in a value of 139 $N/mm^{3/2}$ in the case of the 3 mm thick steel sleeved concrete) and then substituted into equations (6.32) and (6.33), equation (6.34) can be used to model the contact force response of the body. However, the contact force curve is considerably over-predicted by this curve, when compared to the equivalent curve from model 1, both in terms of the maximum force and the duration of the impact. This would suggest that, in the current situation, the mass should not be assumed to be infinite. The assumption that the mass of the target is greater than that of the cylinder alone is more accurate, as if the mass was assumed to be that of the cylinder it would result in considerable under-predictions.

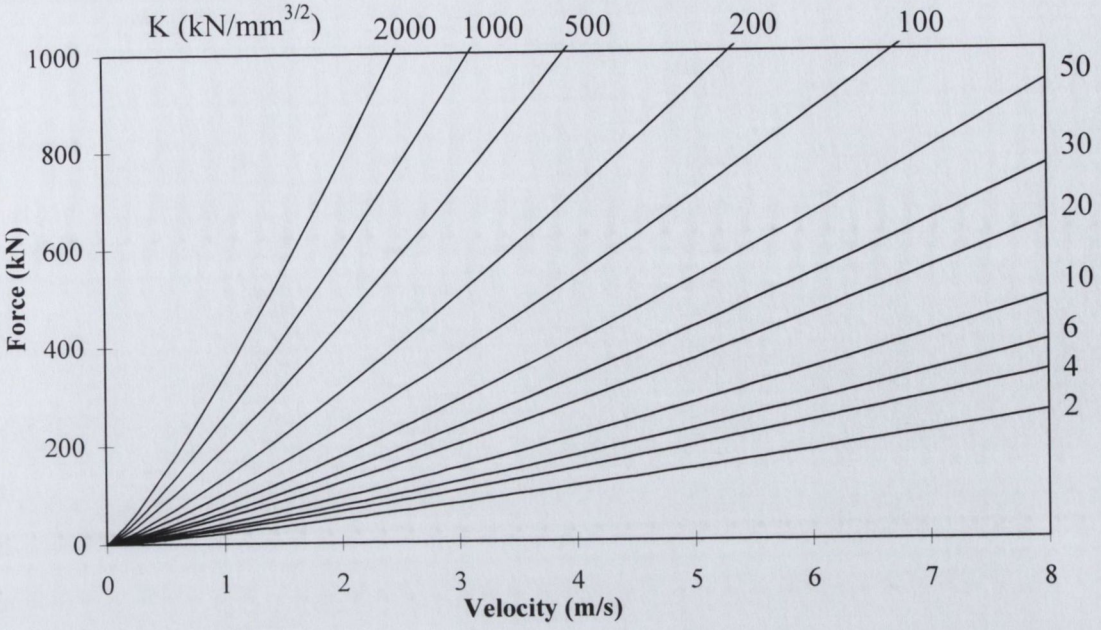


Figure 6.15 Variation of P_∞ with velocity and K

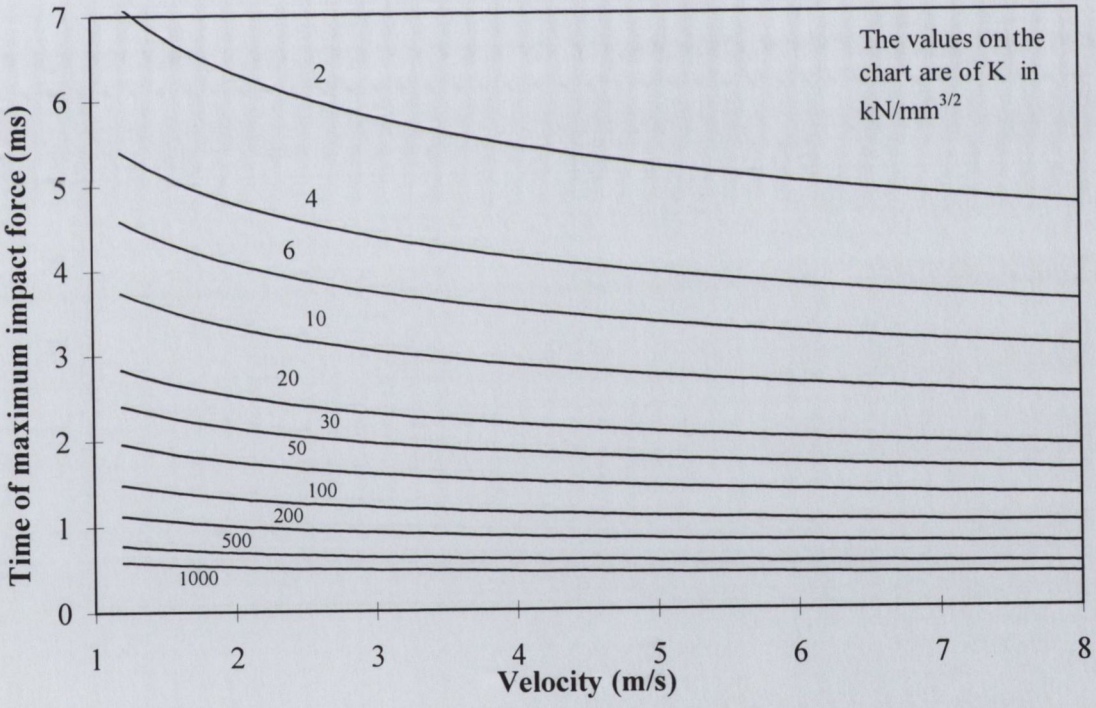


Figure 6.16 Variation of t_∞ with velocity and K

6.4. STRESS-STRAIN CURVES

6.4.1. Theory

The deformational response, characterised by the stress-strain relationship, is important in the understanding of how a body acts under a given load. However, the stress-strain response is usually a function of the rate of loading and, particularly in the case of concrete, of the level of confinement to which the material is subjected when loaded. The stress-strain response of concrete is also non-linear which complicates its response and, therefore, the majority of researchers have generated empirical relationships which describe the stress-strain response for their particular loading regime. Some of the equations which exist have been generated from extensive test results, from several different researchers, whereas others are more limited and can only model the response of the particular test set up. As would be expected, the former are much more valuable as they have the potential to be used even more extensively to predict the results of further research. This section examines some of the existing stress-strain formulae which were generated for static loading situations, described in section 3.3.3, and uses some of the more appropriate models to predict the ascending portion of the stress-strain curve for the results from the current test series, as discussed in sections 5.5 and 5.9.1.

Four distinctly different types of tests were undertaken, all of whose stress-strain curves have the potential to be modelled using existing formulae. Static tests were performed on unconfined and confined concrete cylinders and some empirical formulae exist to approximately predict their responses. In the unconfined case, the curves couple the strain at the mid-height of the cylinder with the stress at its base and, when confined, the stress is coupled with the mid-height strain on the outside of the confining sleeve. The majority of the results were generated by impact testing both confined and unconfined cylinders. However, equations which can accurately predict the response of concrete to impact, even if unconfined, are very limited, predominantly because the curves are different for each loading rate, making it difficult to generate a generic formula. Typically, static formulae have been used to predict the higher rate impact test results with modifications to the variables inputted, with varying levels of success (Bischoff, 1988).

Before theoretical curves were generated, certain obvious limitations existed which hinder the comparison between the predicted and experimental results. Firstly, the theoretical results generated are closed form estimations of the stress-strain curves, in that they predict the deformation of the entire body rather than the strains at a particular location. Secondly, all of the stress-strain models assume that the stress is applied evenly over the entire loading surface. In all of the tests performed during this research series, the load was applied using the slightly curved nosecone which was designed to reduce the effects of any irregularities in the loading surface. Due to the slight radius, the load was initially slightly more concentrated towards the centre of the loading area, rather than being evenly distributed across the entire surface. Furthermore, the diameter of the nosecone was 100 mm, and the diameter of the concrete core in the case of the confined cylinders was, in some cases, nearly 112 mm, which meant that not all of the top surface was loaded. Thirdly, the empirical formulae produced for confined concrete were predominantly determined for either spiral or spaced hoop reinforcement, rather than the full confining sleeves provided during the current set of tests. The empirical constants can result in a considerable overestimation in the confining forces when the equations are modified to predict the response of sleeved cylinders. Models do exist which predict the deformational response of concrete when subject to active, tri-axial stresses but these do not model the response of the confinement. The deformational response of the sleeve can be estimated from these results but is complicated due to variations in the restraint at the base and the friction interface between the core and the sleeve which transfers the load axially into the sleeve. Finally, the models for the confined concrete typically assume that the maximum stress is reached when the steel, or other confining material yields. Although this does occur when the confined cylinders are statically loaded, it does not occur when they are impacted, as the stresses and strains involved are usually insufficient to cause yield.

The stress-strain curves of unconfined concrete were modelled using an equation generated by Popovics (1973), described in section 3.3.3. This non-linear formula estimates the ascending branch of the stress-strain curve for concrete whilst incorporating the changes in the ratio of the strain at a particular stress to the critical strain, which can take account of the material properties of the concrete (equation (3.16)). This equation incorporates the uni-axial concrete strength and the corresponding critical strain into the curve generation and uses empirical parameters to account for the non-linearity of the relationship. It allows either solely the concrete strength or the concrete strength and critical strain to be inputted

into the model. The relationship (which is based on psi units) takes account of a wide range of concrete strengths and is valid for specimens with an aspect ratio not less than two. Furthermore, it forms the basis of some of the stress-strain relationships used by other researchers for confined concrete modelling.

A number of stress-strain models for confined concrete were considered in the literature survey and were examined for their potential to provide models for the stress-strain curves generated in the current series of tests. Four of these, by Sundara Raja Iyengar *et al* (1970), Sargin *et al* (1971), Gangadharam and Nagi Reddy (1980) and by de Nicolo *et al* (1997) were not suitable because they were empirically designed for either spiral or hoop based confinement and relied heavily on the spacing between the confinement being inputted into the model. However, two models were examined in further detail, namely those by Mander *et al* (1988) and by Saatcioglu and Razvi (1992) which describe the deformational response of the composite column tested. The theory behind these models can be found in section 3.3.3. Another model, which finds the stress-strain curve of the tri-axially confined concrete, derived by Ahmad and Shah (1982), was not suitable for use as it could not realistically be compared or accurately developed to model the results measured experimentally in the sleeve. This was because of the differences in the way that the load was applied and in the restraint provided at the base of the confining sleeve.

A stress-strain model was developed by Mander *et al* in which the concrete is subject to uni-axial compressive loading and is confined by transverse reinforcement. It is based on the concrete model of Popovics and, hence, the curve passes through the point of maximum compressive stress and the corresponding strain. The model requires that values for the unconfined concrete strength and corresponding critical strain be known and that the lateral pressure, created by the confining material, be determined using equation (3.24). It is possible to use this formula to predict the strength of the sleeved concrete cylinders because the lateral pressure is calculated using the ratio of the volume of the transverse reinforcement to the ratio of the confined concrete. This can incorporate the spacing between the reinforcement hoops, in such a case, but does not necessarily have to. The model proceeds to calculate the maximum compressive stress (equation (3.25)) and the corresponding critical strain (equation (3.20)). It then determines the tangent modulus of elasticity of the unconfined concrete as a function of the unconfined compressive strength and the secant modulus of the confined cylinder using equations

(3.22) and (3.23). The stress strain curve is a function of these variables, and is described in equation (3.19). The paper illustrates how the stress-strain model can be used for high rate loading of concrete, where account is taken of the increases in strength and stiffness of the material when dynamically loaded, by suitably modifying the input parameters.

The model proposed by Saatcioglu and Razvi is partly based on the work of Mander *et al*, however, a different formula is proposed to describe the parabolic ascending branch of the curve, given in equation (3.31). In the case of confined cylinders, the model assumes that the tri-axial strength is a function of the unconfined strength of the concrete, the lateral pressure (which was calculated from the free body diagram of the cross-section of the cylinder) and a factor which varies with the lateral pressure (as shown in equations (3.27) and (3.28)). The maximum strain of the confined cylinder can then be calculated as a function of all of these variables above using equations (3.29) and (3.30). However, when the lateral pressure was calculated, it resulted in an extremely large value, which then overestimated the confined strength of the concrete (106 N/mm^2 as opposed to 58 N/mm^2). However, in 1978, Kurt published a paper which took account of the stress compatibility at the interface between the confined and confining material and used this, and the formulae for the stresses in a thin pipe, to derive an equation for the lateral pressure as a function of the applied axial pressure (equation (2.64)). The model by Saatcioglu and Razvi was modified by the author to incorporate the formula for the lateral pressure, determined by Kurt, into the stress-strain model.

6.4.2. Comparison of models with experimental stress-strain curves

The static unconfined tests, described in section 5.9.1, are compared to the model by Popovics. The results of the two static unconfined tests were not identical, but were similar and the differences were probably as a result of variations in the properties of the concrete in the two cylinders. However, although the strains at a particular level differed between the tests, the strengths of the cylinders were quite similar, and their average was found to be 12.5 N/mm^2. This value was used in equations (3.17) and (3.18) to determine values for $n_{concrete}$ and ε_0 and was then used to generate a curve to describe the stress-strain relationship. This curve is shown in Figure 6.17, as "Popovics - attempt 1", and it can clearly be seen that it overestimates the critical strain experienced by the concrete cylinder.

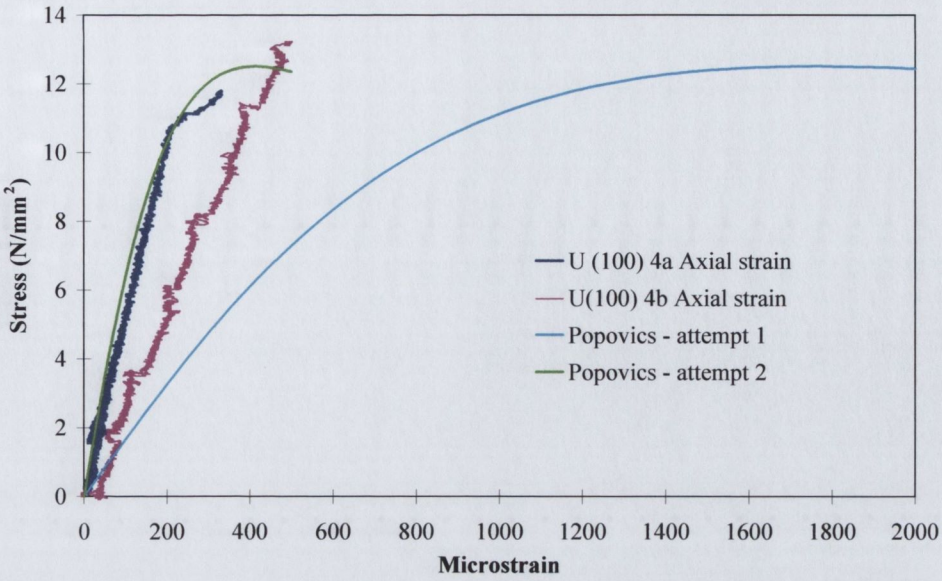


Figure 6.17 Unconfined static test results compared to model proposed by Popovics

However, as discussed in section 5.9.1, the strains measured during the static tests are lower than would typically have been expected, and the prediction by the model is very close to the accepted value of critical strain. These low strains are probably due to the curved nose cone which tended to initially apply the load to the centre of the cylinder, rather than evenly spreading it across the top. This caused a splitting action which resulted in the cylinder fracturing at a lower stress and strain than if the cylinder had been evenly loaded. The model by Popovics also allowed the critical strain value to be inputted to correspond to an experimental value, rather than be calculated as a function of the maximum stress. An average value was calculated for the critical strain from the two measured results which was inputted into the Popovics model, the results of which are shown as the curve "Popovics - attempt 2" in Figure 6.17. As expected, this curve is much closer to the experimental results, as the ordinates through which it passes, those of maximum stress and critical strain, are both separately defined. The steep parabolic shape of the curve generated models the reasonably linear experimental curves reasonably well.

The same model was used to predict the stress-strain relationship of the unconfined cylinders which were impacted, as Popovics suggested that the model was valid for any situation where there was a constant rate of straining, which would probably be appropriate for the impact situation examined here. Typical stress-strain curves shown in chapter 5 for each of the three velocities of impact are compiled in Figure 6.18. As has previously been explained, the maximum stresses for the three different velocities are very

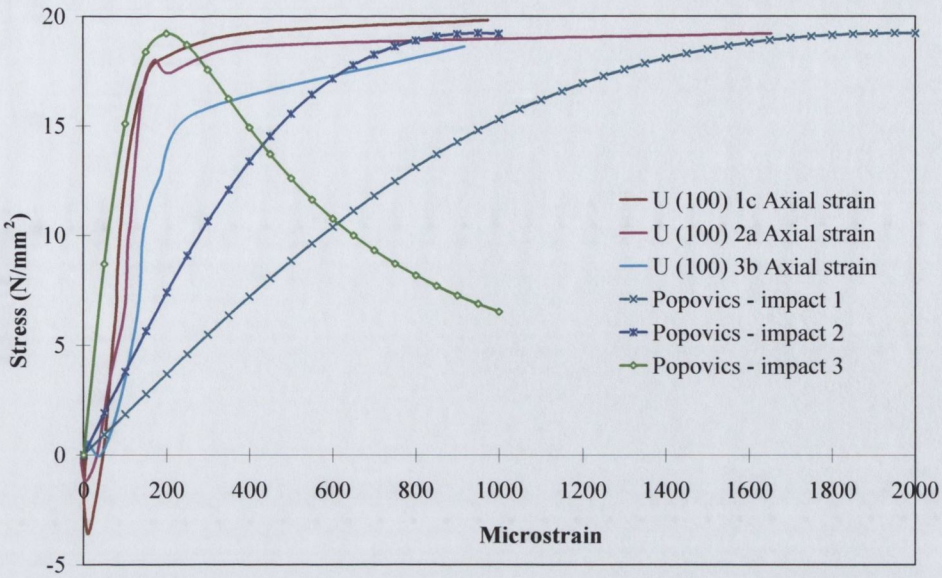


Figure 6.18 Unconfined impact test results compared to model proposed by Popovics

similar because the unconfined concrete can only achieve a certain level of stress prior to failure. The stress-strain curves are bi-linear axially, with a steep initial section and a comparatively long, nearly horizontal, section where the strain increases at a fairly constant level of stress until failure occurs. Unlike the static case where the stresses have time to equilibrate during the period of loading when an impact occurs the stress is concentrated in the centre of the cylinder because of the curved nosecone. The stress wave propagates along the length causing lateral dilation, which induces the initial axial strains. However, when the stress propagates out to the edge of the cylinder, the strains increase rapidly as the circumference is subjected to the axial load. This bi-linear curve is, not surprisingly, difficult to model analytically. An initial attempt was made using Popovics model, and is shown as "Popovics - impact 1" on the graph, where the average strength of the three impacted concrete cylinders was inputted and the critical strain and the curve were calculated using the model. This curve greatly overestimates the maximum strain and underestimates the slope of the stress-strain curve. A second attempt "Popovics - impact 2" was then tried, where the average maximum strain was inputted into the model. The maximum point on the curve is, therefore, fully defined yet it still fails to model the curve accurately because of the bi-linear effect associated with the significant increase in stress axially when the load equilibrates over the cross-section. The initial loading portion was then considered separately in "Popovics -impact 3", where the average strain at the end of the initial loading period was entered into the model. Although this predicted the initial loading curve, it was unable to predict the second, horizontal, part of the curve.

It can be concluded that a typical model which predicts the stress-strain curve of unconfined concrete when loaded, in this case generated by Popovics, only had limited applicability to this experimental work. The reasons for this included the effect of the shape of the nosecone, through which the load was applied and, in the case of the impact loading, non-uniform stress distribution along the specimen length, which resulted in a bi-linear stress-strain curve.

Two different models were used in an attempt to accurately predict the stress-strain curve for the confined concrete cylinders when either loaded statically or by impact. The two models were chosen to predict the results of one of the confined concrete cases, namely the 3 mm thick steel sleeves, as this type of cylinder had been loaded at both strain rates.

The first model examined was that by Mander *et al*, and the initial inputs included the ratio of the volume of the confinement to the volume of the confined concrete, the static strength of an unconfined concrete cylinder and the corresponding critical strain. Using these inputs the lateral pressure, the confined concrete strength, the corresponding critical strain and the tangent modulus of elasticity (E_c) of the unconfined concrete were calculated, which allowed the secant modulus of elasticity of the confined concrete (E_{sec}) to be determined. As would be anticipated from Figure 3.15, the value of E_c always had to be greater than E_{sec} to allow the stress-strain relationship to be generated. The results of the model are shown in Figure 6.19, as "Mander - attempt 1". However, this model does not accurately predict the stress-strain relationship measured experimentally, as the slope of the curve is lower, and is largely affected by the initial tangent modulus of elasticity of the unconfined cylinder. This, as it is calculated in the model as a function of the unconfined concrete strength (determined using the curved nosecone), is quite low.

The model was, therefore, modified in two ways in an attempt to better represent the experimental stress-strain curves. Firstly, the measured confined critical strain value was inputted into the model directly, rather than being generated as a function of the unconfined and confined strengths. Like the unconfined cylinders, the strains measured are much lower than those predicted because the load is not applied evenly across the top surface of the cylinder and, as in the unconfined case, a more accurate model can be produced if the critical strain is entered from the experimental results. Secondly, as this greatly increases the value of the secant modulus of elasticity of the confined concrete, the

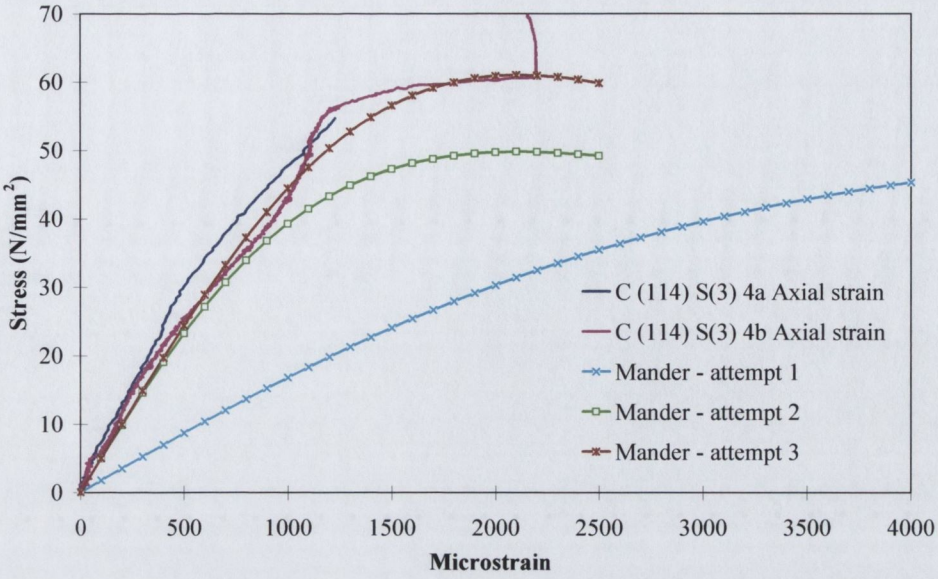


Figure 6.19 Confined static test results compared to two different proposed models

tangent modulus of elasticity of the unconfined concrete was also inputted directly from the experimental results of the unconfined static tests. A value of 50×10^3 N/mm^2 was calculated from unconfined stress-strain plots and was used in the model. The resulting curve is shown on the graph as "Mander - attempt 2". It is clear that this models the stress-strain curve, particularly initially, where it is affected by the tangent modulus, much more accurately than the first attempt. However, as discussed in section 5.9.1, in a situation where the confinement is sufficiently thick, the stiffness of the composite can increase considerably prior to the yielding of the steel tube (Kotsovos and Perry, 1986), which results in the curve not being uniform throughout. Furthermore, it is clear from this model that the calculated increased strength of the cylinder due to the presence of the confining sleeve is nearly 20 % less than that measured experimentally. The value calculated is a function of the calculated lateral pressure and the strength of the unconfined cylinder. However, the calculation also depends on empirical values which were determined for cylinders with non-continuous confinement and this would probably result in the low calculated value of the strength of the composite cylinder.

A third attempt was made to predict the stress-strain curve, by inputting a more accurate value for the strength of the confined cylinder, determined from the experimental results. This is also shown in Figure 6.19 as "Mander - attempt 3". This model, which is very simplified due to the loading constraints involved, estimates the slope of the curve

accurately, particularly at low stresses. Although it reaches the point of critical stress and strain, is unable to model the change in the slope of the curve near the maximum stress.

The model generated by Saatcioglu and Razvi in 1992 was also used to predict the stress-strain curve of the confined concrete to a static load. The lateral pressure, f_l, was calculated from the forces applied to the cross section of the cylinder using the following equation

$$f_l = \frac{2A_s f_y t}{d \times s} \tag{6.35}$$

where A_s is the cross sectional area of the steel, f_y is the yield strength of the steel, t is the thickness, d is the diameter and s is the spacing between particular links. The reinforcement used was a continuous sleeve and there was no spacing. However, as the formula determines the pressure over a distributed length, the length of the cylinder was used instead. When this was inputted into the formulae to derive the curve, it determined that the strength of the confined cylinder was 106 N/mm^2 and that the corresponding critical strain was 16,000 micro-strain. The curve produced is shown in Figure 6.20 as "Saatcioglu and Razvi - attempt 1", but the maximum strain shown is 4000 microstrain, and the curve continues nearly horizontally until it reaches the maximum strain. As this greatly overestimated the maximum stress and strain, the model was modified to incorporate the maximum measured stress and a more realistic value for the lateral force

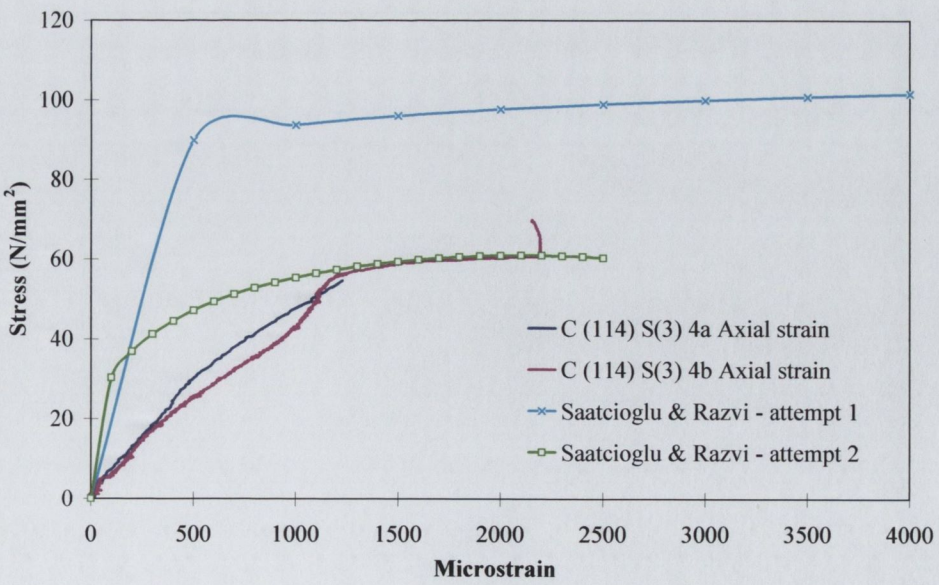


Figure 6.20 Confined static results compared to the model by Saatcioglu and Razvi

was calculated using an equation derived by Kurt in equation (2.64). These formulae were then combined in the prediction of the stress-strain curve and are shown on the graph as "Saatcioglu and Razvi - attempt 2".

Although the curve produced is much more realistic in estimating the response of the confined cylinder, it still overestimates the initial slope probably because of the estimate in the spacing of the reinforcement, before producing the closest estimate of the horizontal part of the curve as the steel begins to yield. This ability to model the horizontal part of the curve occurs because the curve shape used by Saatcioglu and Razvi was selected to take this form using a power term which has a greater effect as the lateral confinement becomes more important when the concrete dilates under the applied load.

The stress-strain curves produced for the static loading of the confined cylinders did not initially produce results which accurately predicted the deformational response of the specimens. However, with certain modifications, estimates were made, particularly those based on the model created by Mander *et al*, which predicted some of the aspects of the stress strain curves. With the limitations which had already been considered for the static analysis, three stress-strain curves, described in section 5.5, one for each velocity of impact, for the cylinders confined with 3 mm thick sleeves of steel, were compared to models generated.

The stress-strain response of the lowest velocity impact (3.2 m/s) was considered initially and was compared to the results from three different models, as can be seen in Figure 6.21. The first curve was produced ("Mander - impact 1") by using the model by Mander and only entering the values for volumetric ratio, the unconfined compressive strength and the critical strain from an impacted, unconfined cylinder. As in the static case, this curve greatly overestimates the maximum stress and the critical strain in the cylinder. This would probably be expected as the value calculated for the maximum stress is based on the assumption that this value is reached when the steel yields. In the case of an impact, at this velocity and with this thickness of sleeve, the stress transferred to the cylinder by the falling impactor is much lower than the strength of the composite cylinder and does not cause yielding of the sleeve. Mander's model was modified in a similar manner to the statically loaded case, by inputting the maximum stress experienced by the impacted sample, the critical strain and the tangent modulus of the impacted unconfined concrete,

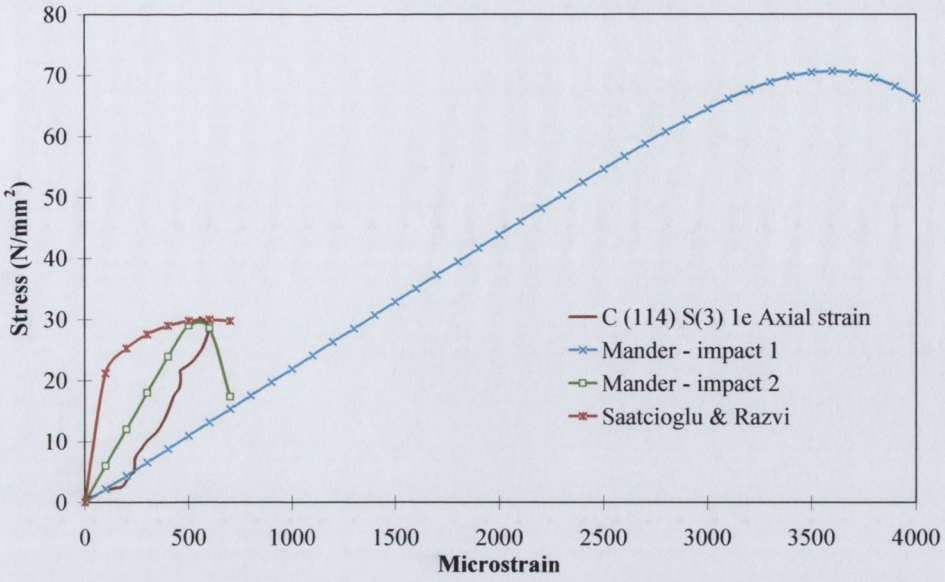


Figure 6.21 Stress-strain curve for a steel confined cylinder subject to impact at 3.2 m/s, compared to the results of three different models

resulting in the curve "Mander - impact 2". The resulting curve, as expected, is much closer to the experimental result but, although the slopes of the curves are quite similar, it is not capable of modelling the initial transfer of strain to the sleeve just after the impact. The model produced by Saatcioglu and Razvi, with the lateral pressure predicted using the equation by Kurt, was also used to predict the stress-strain curve and is shown on the graph. Values for the maximum stress and corresponding critical strain were used in the equation, but in a similar manner to the static case, this model overestimates the slope of the curve, and does not produce a good estimate of the experimental stress-strain curve.

The closest model for the stress-strain response of the confined cylinders was that generated by the modified version of the Mander model (impact 2) and although this provided a fairly loose estimate of the curve, it was decided that it could be used to attempt to model the stress-strain curves of similar impacts at higher velocities. The maximum stress experienced in the sample and the corresponding critical strain from each of the three velocities of impact were used to generate curves, the results of which can be seen in Figure 6.22. The model at the lowest velocity "Mander - velocity 1" corresponds to the curve "Mander - impact 2" in Figure 6.21. The experimental curves, particularly at the lower two velocities are subject to a considerable amount more variation as the stress and strain increase which makes them particularly difficult to model. However, the model for

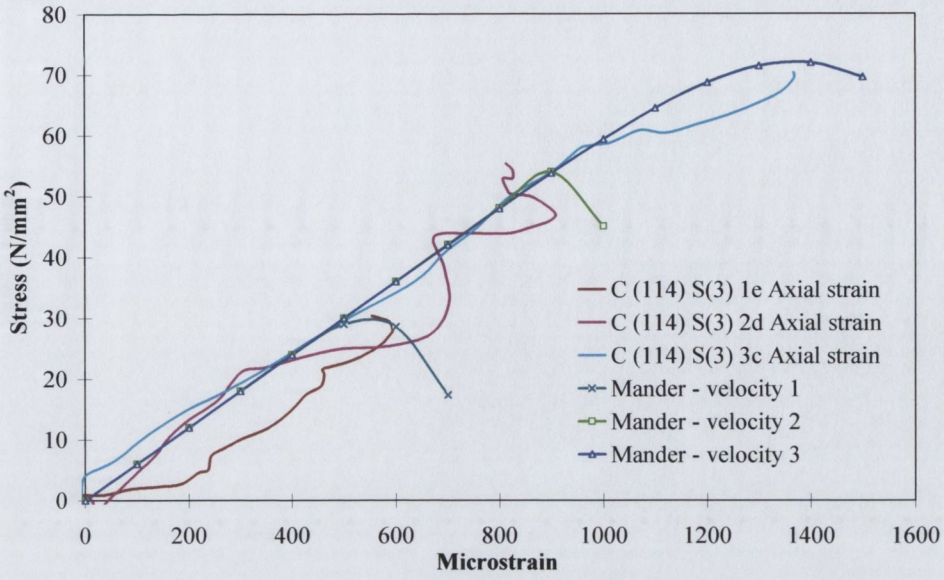


Figure 6.22 Stress-strain curve for steel confined cylinders subject to impact at three different velocities, compared to the results of the model by Mander *et al*

the highest velocity impact provides a fairly good estimate of the stress-strain curve measured experimentally.

The stress-strain curves which were generated experimentally for either impact or static loading of confined or unconfined cylinders showed that there were obvious trends and similarities between curves within the same group of results. Well established models produced by three other researchers were used to model the experimental stress-strain curves. However, for a combination of reasons these did not always accurately predict the results of the current study. This included the following :

- The models themselves were empirical and the coefficients used were designed for specific testing situations.
- Although the confined concrete models have been used to predict the results of tests from other researchers, the confinement was steel spirals or hoops, not the continuous sleeved confinement used during these tests. This meant that, in some cases, the confining pressures were significantly overestimated.
- When the confined cylinders were impacted, the maximum stress transferred to the target by the impactor was not sufficient to cause the steel to yield. This meant that the predicted ultimate strength of the confined cylinder was not reached.

- The loading in the models was intended to be evenly distributed across the top face of the concrete cylinders, either when confined or unconfined. The loading was over the entire surface when unconfined but, when confined, did not cover the entire surface of the concrete. Furthermore, the loading was not evenly distributed across the top because of the slight curvature of the nosecone of the impactor which, particularly in the unconfined case, caused the cylinders to have an increased tendency to split apart from the centre of the top face and reduced the critical strains in the cylinder.
- The inputs to the models were modified slightly to take account of the increase in the strength and the stiffness of the concrete resulting from the increase in strain rate. However, the models were not capable of predicting the stress wave propagation in the cylinder resulting from the impact which did cause them, in some cases, to act very differently from a similar, statically loaded cylinder.

Nonetheless, the models were modified to take account of some of the differences between the way in which the original models were designed and how the actual experimental work was carried out during the current test series. In the majority of the loading situations, at least one curve was found which made a reasonable estimation of the stress-strain curves measured experimentally for the limited cases considered.

6.5. CONCLUSIONS

This chapter describes three different types of analytical work to model the response of passively confined concrete to impact. A relationship has been postulated which predicts the maximum contact force for passively confined concrete. The derivation of the equation involves two fundamental assumptions, namely that the materials in the composite cylinder act elastically and that the lateral dilation of the concrete was negligible at the top of the cylinder due to the presence of the confining sleeve. The theoretical predictions for the maximum contact forces in the majority of cases were within 10 % of those measured. The equation did not accurately predict the maximum contact forces when either of the two fundamental assumptions was invalid. This was due to the material properties of the sleeve, the distance between the centre of impact and the confining sleeve, or, in some cases, where the impact was so severe as to cause the properties of the impacted materials to be changed.

This chapter has shown that Hertz's Contact Law, which was originally derived for the static contact of two parabolic surfaces, can be applied to an impact situation, even when permanent deformations are produced. An initial attempt to apply the contact law produced a sinusoidal model which gave a reasonable indication of the shape of the contact force curve. However, the preliminary model generally overestimated the maximum force, the time to reach the maximum force and the duration of impact. A second model was produced in which the curves were not perfectly symmetric. This was because the parameters for approach and restitution are slightly different as the impact of the steel impactor onto the concrete target results in cracking and fracture of the concrete. The second model gave a good estimation of the curve when the experimental response of the concrete was nearly elastic. It used a quasi-sine curve with different coefficients of approach and restitution to incorporate the minor levels of cracking which take place in the well confined cylinders when impacted. It can be concluded that Hertz's Contact Law can provide an accurate model for the contact force response of confined concrete cylinders subjected to impact, if the confinement provided is sufficient to prevent concrete fracture and ensure that the response is nearly elastic. Where this is not the case, the law overestimates considerably the contact force response, both in terms of the maximum contact force and the duration of the impact.

This chapter also makes an attempt to model the stress-strain relationship of cylinders of concrete loaded statically and by impact when confined and unconfined. Three well established, empirical models, created by other researchers to estimate the deformational response of confined and unconfined concrete were used. The models had been used to predict the results of these and other researchers and the empirically determined constants were accurate enough to provide a good model for the different results. However, in the confined case, the models were formulated for spirally or hoop confined concrete, rather than the sleeved concrete used here, which resulted in the lateral confining pressure being significantly overestimated. Furthermore, the way in which the load was applied, through a slightly curved nosecone, and the differences between the static and impact loads made it even more difficult to obtain an accurate prediction for the stress-strain relationship. These issues were addressed and the models were used, with some modifications, to provide reasonable estimates for the deformational response of the confined and unconfined concrete cylinders subject to two different forms of loading. These results show, however, that more work is required in the future to generate a better estimate of the stress-strain curve for confined concrete when impacted.

It can be concluded that this chapter provides three different models to predict some of the features examined during the experimental work. All of the solutions are closed form and are, therefore, subject to considerable limitations, often associated with the assumption of elasticity and the way in which the load is applied. Nonetheless, the models generated form genuine and fairly accurate predictions for the response of sleeved cylinders subject to hard impact.

7. FINITE ELEMENT ANALYSIS OF CONFINED CONCRETE

7.1. INTRODUCTION

Experimental work, where sleeved concrete cylinders were subject to hard impact, clearly showed that there was a good degree of repeatability between the behaviour within a particular group or series. However, as shown in Chapter 5, the results from tests on different types of confinement showed that, although there were trends between the different series, these were not always linearly related as the contact velocity increased. This was due to different combinations of the thickness, Young's modulus and yield strength of the confining material which resulted in its acting differently as the imparted energy increased.

The results generated by the contact force and the base-plate loadcell were both examined extensively in Chapter 5 and the important features of each particular loadcell and the inter-relationships between the two were examined closely with respect to both the type of confinement and the contact velocity. It was clear that whilst the sleeve can provide sufficient confinement to prevent fracture of the concrete, and to ensure that it acted like an elastic material, the maximum contact force was related to the velocity of impact. The amount of energy that was transferred to the concrete which was sufficient to overcome the strength of the sleeve varied between each of the types of confinement. The force transferred to the base plate loadcell was found to be between 20 % and 30 % lower than the corresponding contact force in the case of the confined concrete and was fairly consistent across the range of velocities. This was quite different to the unconfined case where the proportion of load transferred reduced with increases in velocity, as the concrete could only absorb and transfer a certain amount of stress prior to fracture. The reduction in the load transferred in the case of the unconfined concrete is consistent with results from other researchers and with what might have been anticipated. However, the consistent level of load transfer in the confined cylinders, which underwent different levels of straining, is more difficult to explain.

When concrete is impacted, stress waves propagate away from the point of impact along the length of the concrete core in an attempt to dissipate the high strains, some of which

are transferred from the loaded concrete to the confining sleeve. The variation in the strains along the outside of the sleeve was measured experimentally and was found to vary continuously along the length. The strains were subject to a considerable degree of fluctuation because of the nature of the concrete when impacted, and varied with different types and thicknesses of confinement. In section 5.5, the strain and stress-strain response of the cylinders was considered. Whereas the results of different cylinders were consistent with one another, it was difficult to draw firm conclusions as to the mechanism of transfer of the load from the core into the sleeve. Furthermore, the relationship (Poisson's ratio or otherwise) between the responses of the lateral and axial gauges attached to the outer skin of the confining sleeve, at different locations along its length, was also very complicated.

Chapter 6 involved an analytical study of the response of sleeved concrete to impact. The assumptions made were justified by the comparisons between the experimental results and the analytically determined values. However, the results of these analyses were limited because they provided a closed form solution to the problem and could not be reliably extended to find the responses of other, untested cylinders.

It was decided to undertake a limited numerical study of the response of the sleeved cylinders to various forms of loading using the finite element method. It was intended that this model, unlike the analytical work, would provide a solution which could predict the responses of the cylinders at different locations and could be more easily and accurately extended to determine the responses of untested specimens.

As discussed in chapter 3, much research has been undertaken within the last twenty years to predict the response of concrete and other materials to both static and dynamic loads using the finite element method (FEM). However, the studies which have been reported are usually highly complicated and seek to model complex geometries, highly non-linear, often novel, materials or unusual loading cases (Zukas, 1982). It was the intention of this study to keep both the geometry, material models and the loading cases as simple as possible and to study both the transfer of loads from the top to the bottom of the concrete cylinder and the variation in the strains in the confining sleeve in an attempt to better understand the mechanisms of transfer and the relative magnitudes of the stresses and strains.

The study comprised two parts using different commercially available finite element packages for each. Each was subject to modelling limitations associated with the computers and the software available. Simple static analyses, both 2- and 3- dimensional, were undertaken using the finite element package ANSYS which allowed the strain transfer mechanism to be studied in detail for a range of different loading conditions. A simple dynamic analysis was performed using DYNA-3D, on a UNIX workstation, which modelled moving bodies colliding with a stationary cylinder and allowed the stresses and strains to be examined for a variety of confinement types and thicknesses.

This chapter is, therefore, broken into two distinct sections, one for each of the finite element packages used, corresponding to the different static and dynamic analyses undertaken. Both sections include simple introductions to the finite element package, the rationale for its use and theory behind the workings of the software. This chapter does not attempt to go into any great depth regarding the theory behind finite elements as it is covered in great detail in many of the standard finite element texts (Zienkiewicz and Taylor, 1989; Ottosen and Petersson, 1992; Cook, 1995). Each of the sections outlines the model or models created for the particular finite element analysis and the simplifying assumptions made, prior to presenting the results from the analysis. The results from the two separate analyses are then compared and analysed.

7.2. STATIC ANALYSIS USING ANSYS

7.2.1. Theoretical background

ANSYS is a three dimensional finite element program for the solution of a variety of common engineering problems, including structural, mechanical, fluid, thermal and magnetic applications. The focus of the current work is on its structural capabilities which can range from a simple, linear, static analysis to a complex, non-linear, transient dynamic analysis. ANSYS has an extensive range of element types (over 100) for use in different types of analysis and material properties can conform to simple inbuilt models or can be inputted, by the user, prior to the analysis.

The version of ANSYS used in the analysis was version 5.5.1 (Research/FS package) developed by the ANSYS Corporation in 1999. It was installed on a Gateway Pentium 333 computer with 64 Mbytes of RAM and a 4 GB hard drive, running Windows NT. The use and theory behind this version of ANSYS is described in its online manual (ANSYS Online Manuals, Release 5.5, 1999). An add-on package "LS-DYNA Explicit Dynamics Capability" is available from ANSYS and creates an interface to the LS-DYNA finite element analysis program, capable of providing solutions to large deformation dynamics, complex contact problems, transient dynamic analysis and the analysis of non-linearities. However, this package was not available within the University and the analysis was performed using the standard ANSYS package.

The purpose of finite element analysis is to re-create numerically the behaviour of an actual engineering system through the creation of an accurate numerical *model* of a physical prototype. The model which is created includes all the nodes, elements, material properties, real constants, boundary conditions and other features which are used to represent the physical system. An analysis using ANSYS has three distinct steps, namely,

- building the model, using the ANSYS integrated pre-processor
- load application followed by problem solution, using the solver
- results review, with an integrated general or time varying post-processor

ANSYS does not assume a system of units for the analysis and it is the responsibility of the user to ensure that units are consistent for all input data.

The ANSYS pre-processor goes through a number of logical stages in the formation of a model, starting with the definition of the elements to be used in the analysis. The ANSYS element library contains more than 100 different element types including beam, contact, fluid, mass, plane, shell, solid and visco-elastic or visco-plastic. It allows the determination of the degrees-of-freedom of each type and whether the element lies in 2- or 3-dimensional space. The use of element *real constants* allow further details to be defined which can include the cross-sectional properties of a beam element, the second moments of area, initial strain and the mass per unit length. The material properties can be (a) linear or non-linear, (b) isotropic, orthotropic or anisotropic (c) constant temperature or temperature-dependent. Furthermore, ANSYS has the facility to create material libraries where archival material properties can be stored for repeated use in different analyses.

The next stage involves the creation of the model geometry which can be undertaken in one of three ways, namely by (a) solid modelling, (b) through direct generation or (c) by importing a model created in a computer-aided design (CAD) system. With direct generation, the location of each node and the connectivity of each element is "manually" defined by the user. Despite the options of copying patterns of existing nodes and elements and symmetry reflection, this method of generation can both be time consuming and potentially subject to a considerable number of errors. In contrast, solid modelling involves the definition of the geometric shape of the model which is automatically meshed by ANSYS. However, certain mesh controls allow the user to define the element shape, the location of a mid-side node and the element size to be used in meshing which can greatly affect the accuracy and economy of the analysis. This can be undertaken manually by setting defined parameters or through the use of the ANSYS *MeshTool*. This also allows refinement of the initial mesh and adaptive meshing. The resulting geometry and mesh can be analysed using either global co-ordinate systems (including Cartesian, cylindrical and spherical) or user-defined local co-ordinate systems. When the solid model is meshed, contact interfaces can be defined between elements which are in contact or may move relative to each-other during the analysis.

Contact problems are highly non-linear and require significant computer resources to solve. Furthermore, contact analysis poses two further problems in that, firstly, the regions of contact are not always evident until the solution has been determined and, secondly, most contact problems need to account for friction. Although there are several friction laws and

models to choose from, all are non-linear. In ANSYS, contact problems can be either rigid-to-flexible (where one body has a much greater stiffness than the other) or flexible-to-flexible (where both of the bodies are deformable). Three contact models exist within ANSYS - node-to-node, node-to-surface, and surface-to-surface, all of which use different contact elements in the analysis. The contact can be created manually by positioning contact elements (which cannot penetrate the target surface) and target elements (which can penetrate the contact surface) at potential contact boundaries. The most common, surface-to-surface contact, can be generated using ANSYS's *Contact Wizard* which generates the elements required for the contact along lines or planes, determines their relative stiffness and allows a friction value to be specified by the user. The regions of contact are determined for surface-to-surface elements using Gaussian integration points to establish when one surface comes in contact with, or penetrates, the other, as shown in Figure 7.1. The contact algorithms used can vary between different analyses but for surface-to-surface contact elements, ANSYS uses either the augmented Lagrangian algorithm (which is an iterative series of penalty updates) or the penalty method, both of which are described in Zhong (1993). The contact stiffness is user defined and determines the amount of penetration which can occur between the two surfaces. It can often be difficult to determine because of the balance between minimising the penetration at the surface and solution convergence. The contact between nodes or surfaces also requires a friction model, which is typically the basic Coulomb friction model allowing two contacting surfaces to carry shear stresses up to a certain magnitude across their interface before they start sliding relative to each other. Contact problems which involve friction produce non-symmetric stiffness matrices. ANSYS reduces the computation time by using a symmetrization algorithm to solve the frictional contact problem.

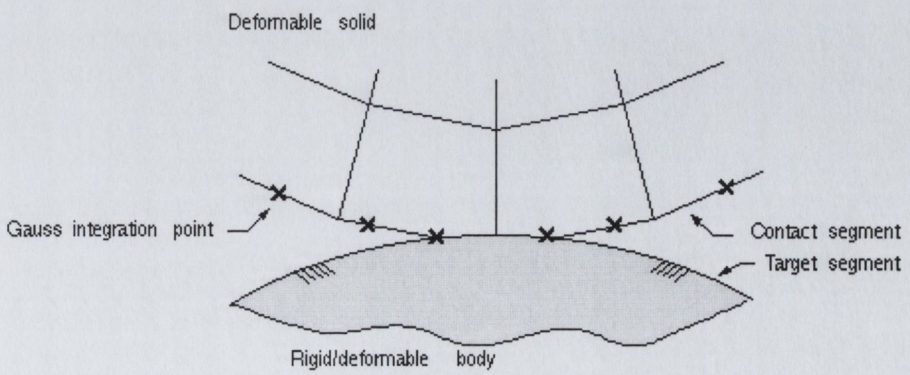


Figure 7.1 Detection of contact point location at Gauss point using ANSYS

The loads are applied to the model and the problem is solved using the Solution-processor in ANSYS. The type of analysis to be performed depends on the loading conditions and the required type of response. It can be one of the following - static (or steady-state), transient, harmonic, modal, spectrum and buckling. This processor also incorporates the definition of loads on the structure. These include

- boundary conditions (constraints, supports, etc.) and other externally and internally applied loads such as DOF constraints which are fixed to a known value and include symmetry and anti-symmetry boundary conditions and the ability to specify displacements;
- forces or moments which are applied to a particular node in the model;
- surface loads including pressure, which is applied as a distributed load over a surface;
- body loads such as temperature;
- inertia loads associated with the inertia or mass matrix of the body, incorporating gravitational acceleration, angular velocity, and angular acceleration.

Most of these can either be applied to the solid model geometry (onto keypoints, lines and areas), which the program then automatically transfers as loads onto particular nodes or elements, or the load can be applied directly to the model (on the nodes and elements).

The loads can be applied in one of two ways - (a) instantaneously at the start of the analysis (*stepped*) or (b) gradually over the duration of the analysis (*ramped*), by using different time and load related commands. A *load-step* is simply a configuration of loads for which it is possible to obtain a solution at a particular time and its use allows different loads to be applied separately. Sub-steps are incremental steps taken within a load step and are used for accuracy and convergence purposes in non-linear analyses. ANSYS uses the concept of time in both static (or steady-state) analyses and in transient analyses. In a transient analysis, time represents actual time in seconds, minutes or hours. In a static or steady-state analysis, time simply acts as a counter to identify particular load steps and sub-steps.

The program proceeds to solve the problem through the use of simultaneous equations which are generated as part of the finite element method. The finite element method generally requires that the problem should be described in the form

$$[K]\{a\} = \{F\} \tag{7.1}$$

where [K] is the global stiffness matrix, {a} is the vector of nodal degrees of freedom and {F} is the vector of loads or forces at the nodes. This can then be re-formulated to allow calculation of the nodal degrees of freedom. ANSYS can take these nodal degree-of-freedom values (which form the primary solution), and calculate derived values (which form the element solution) at the elements' integration points. ANSYS has several methods of solving the simultaneous equations, which are described in its online manual, but the frontal solver is the default option. This solver does not assemble the complete global matrix, but performs the assembly and solution steps simultaneously as the solver processes each element. The solver reads in the degrees-of-freedom for the first element when the individual element matrices are calculated, and eliminates any degrees of freedom which can be expressed in terms of the other, previously defined, degrees-of-freedom. ANSYS then calculates the nodal DOF solution by back substitution, and uses the individual element matrices to calculate the element solution.

Data is then written to an output file which includes load summary information, mass and moments of inertia of the model, solution information, the total CPU time and elapsed time. Once the solution has been calculated, ANSYS has two post-processors to review the results, a general and a time varying. The primary unknowns (nodal degrees of freedom) calculated in a structural analysis are displacements. Other quantities, such as strains, stresses and reaction forces, are then derived from the nodal displacements.

The general postprocessor is capable of reviewing results at one time step over the entire model or selected portion of the model. However, the particular time step chosen can be changed during the processing for analysis of different loading conditions. It is possible to generate contour displays which show how a result such as stress, temperature or strain varies over the model; deformed shapes for the whole or part of the model; and reaction force displays. These can also be in the form of tabular listings for reviewing and interpreting the results of the analysis and can all be generated for both the nodal and element solutions. This post-processor can also be used to estimate the magnitudes of the errors and to combine different load cases. The plots from the post-processor can be generated on screen with or without using the *PowerGraphics* display capability of ANSYS. Using *PowerGraphics* means that graphics displays are plotted at a much faster rate. However, the averaging calculations for *PowerGraphics* include results for only the model surface, whereas, those for the *full model method* of display include results for the

entire model (interior and exterior surfaces), which can cause differences in the listed and plotted results when *PowerGraphics* is used. The time history postprocessor is used to review results at specific points in the model over a range of time steps. It allows graphs to be generated of particular data values against time (or frequency) and tabular listings to be created and stored.

The static (steady-state) analysis performed using ANSYS determines the effects of *steady* loading conditions on a structure or body, while ignoring inertia and damping effects, such as those caused by time-varying loads, and allows the calculation of the displacements, stresses, strains and forces. The analysis can be either linear or non-linear, which means the effects of large deformations, plasticity, creep, stress stiffening, contact and friction can all be determined if desired.

7.2.2. Model creation - 2D

A simple axi-symmetrical, 2-dimensional model was created in ANSYS to model both a confined and an unconfined cylinder. A typical, annotated, *logfile* created by ANSYS during the model generation, and modified by the user to create subsequent models, can be found in Appendix 5. Geometrically the model consisted of two rectangles, a larger one representing the concrete core from the centre to its edge and a thinner rectangle representing a slice through the confining sleeve, adjacent to the core rectangle. The left hand longitudinal edge of the larger rectangle acted as a line of symmetry for the problem, about which the body would, theoretically, be rotated to form a full cylinder (as seen in Figure 7.2) was given initial axi-symmetrical boundary conditions. Both rectangles consisted of solid "PLANE 42" elements which are suitable for structural solid applications as a plane element (plane stress or plane strain) or as an axi-symmetric element. The four noded element has two degrees of freedom at each node (x and y translations) and it is possible to apply a pressure as a surface load onto the element. The bodies were meshed in very similar ways for each of the models created. The length of the rectangle (200 mm) was divided into 40 sections of equal lengths. The top of the large rectangle, representing half of the concrete core, was divided into 10 equal lengths, whose length varied slightly as the radius of the cylinder changed depending on which confinement type was being modelled. The sleeve was similarly divided into 40 sections along its length and into no

less than two sections along its shorter edge. The number of divisions was increased as the thickness of confinement increased, from a minimum of 2 for the thinnest confining sleeve up to a maximum of 6 divisions for the thickest confinement. A plot of the elements for a typical analysis can be seen in Figure 7.3.

The materials defined for the two-dimensional models were both isotropic elastic materials. This type of material was chosen because it was very simple, which was one of the aims of the FEA. As the yield strains and failure strains for each of the materials in the sleeves had been measured during the experimental work using coupon tests, it was easy to establish whether these strains had been exceeded in the finite element analysis. Account could then be taken of this in the examination of the results. Hence, this method provided a simple way of modelling each type of material. Elastic material properties (Young's modulus, density and Poisson's ratio) of concrete, steel, aluminium and plastic were entered for each as appropriate.

When the model had been meshed, contact between the core and the sleeve was established using the *Contact wizard*. The surfaces were both equally densely meshed and, therefore, the choice of target and contact surface was not critical. The line at the edge of

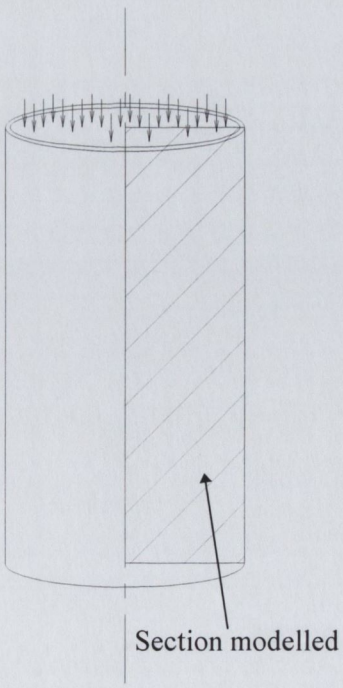


Figure 7.2 3-D cylinder showing from where the section was taken

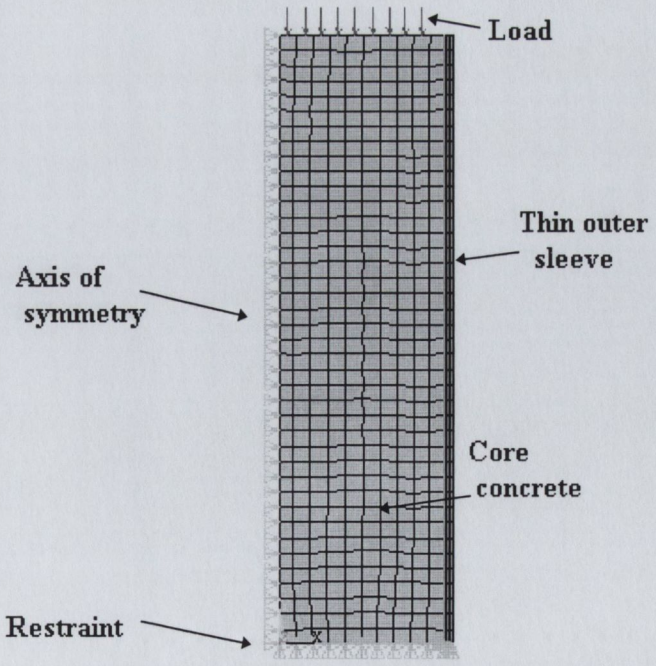


Figure 7.3 2-D model geometry showing elements, boundary conditions and load

the concrete was chosen as the target and the inner line of the sleeve was chosen as the contact (although a model was run with these two reversed and it was found that it made no difference to the results generated). The *Contact wizard* selected the target (TARGE169) and contact (CONTA172) elements. The elements chosen are used to represent 2-D 'target' and 'contact' surfaces which can either be rigid or flexible to represent contact and sliding. The contact surfaces are paired using a shared real constant set. Coulomb friction and shear stresses are allowed at the interface. The elements have two degrees of freedom at each node (x and y translations) and are located on the surfaces of 2-D elements. They have the same geometric characteristics and stress states as the solid element face on which they are situated. Contact occurs when the contact element surface penetrates one of the elements on the specified target surface. The only material property required is the interface coefficient of friction for the Coulomb friction model.

Initial boundary conditions were defined along the base of the rectangles. All of the nodes along the base had all of their degrees of freedom restrained. This was an acknowledged simplification of the problem as, in the experimental work, the axial restraint was coupled with complicated lateral friction and restraint provided by the loadcell and plaster placed beneath the cylinder. However, this fully restrained boundary condition provided a simple means of restraining the cylinders and, as shall be seen, slightly over-exaggerated the friction levels causing lateral restraint at the base. Symmetrical boundary conditions were applied along the left side of the core concrete cylinder.

A simple, static pressure load was applied to the top surface of the core concrete for 50 mm from the centre of the cylinder to represent the 100 mm diameter impactor. In the experimental work, the bottom of the nose-cone of the impactor is slightly curved which, until significant indentation of the concrete occurs, causes the pressure to be slightly unevenly applied along the loading interface. Therefore, two loading conditions were considered, one where the pressure was constant along the radius and a second where the pressure varied linearly across the surface to a maximum at the axis of symmetry. The pressures were calculated by determining the maximum impact stress transferred to the confined cylinder by the falling impactor (using equation (2.10)) and the linearly varying pressures were calculated to apply an identical overall load to the concrete.

The program iterated over one time step, with 10 sub-steps, to find a solution to the problem. When the solution had been found, the stresses and strains in three directions (radial, axial and circumferential) were plotted. Lists were created of the strains along the outer edge of the sleeve, the strains along the interface between the sleeve and the core and the stresses along the base of the composite.

The fundamental assumptions made during the static 2-D analysis performed with ANSYS were

- the composite cylinder was axi-symmetric and it was, therefore, suitable to model using only 2-dimensions and perfect axi-symmetry,
- the concrete and the sleeve material both remain linearly elastic, which could be confirmed or otherwise by considering the strains generated during the analysis,
- the boundary between the concrete and the sleeve was perfect with a particular, pre-defined coefficient of friction,
- the composite cylinder was fully restrained at its base,
- the loading was applied statically to the top of the cylinder, as a pressure.

The two dimensional model was solved within minutes by ANSYS and, therefore, provided a suitable platform to examine input parameters for other models. With this in mind, the following were examined

- unconfined and confined models,
- constant and varying pressure over the top surface of the core rectangle,
- changing the restraint at the base from fully restrained to only axially restrained,
- changing the coefficient of friction for the contact plane from 0, for frictionless contact, to 0.25, 0.5, 0.75 and 1.0,
- changing the material properties of the confining material and the dimensions of the sleeve to represent each of the types of confined cylinder,
- changing the constant pressure across the top face to represent the different equivalent pressures associated with different contact velocities to see whether this would make the strains exceed their measured elastic limits.

Table 7.1 provides a summary of the models created in 2-dimensions in ANSYS to model the different features described above.

Model No.	Confinement	Pressure	Restraint	Friction	Velocity
1	Steel, 3mm	Constant	Full	0.25	3.2 m/s
2	Steel, 3mm	Constant	Only axial	0.25	3.2 m/s
3	Steel, 3mm	Varying	Full	0.25	3.2 m/s
4	Steel, 3mm	Constant	Full	0	3.2 m/s
5	Steel, 3mm	Constant	Full	0.5	3.2 m/s
6	Steel, 3mm	Constant	Full	0.75	3.2 m/s
7	Steel, 3mm	Constant	Full	1	3.2 m/s
8	Steel, 3mm	Constant	Full	0.25	4.4 m/s
9	Steel, 3mm	Constant	Full	0.25	6.3 m/s
10	Unconfined	Constant	Full	N/A	3.2 m/s
11	Steel, 1.2mm	Constant	Full	0.25	3.2 m/s
12	Steel, 5mm	Constant	Full	0.25	3.2 m/s
13	Steel, 6.5mm	Constant	Full	0.25	3.2 m/s
14	Aluminium	Constant	Full	0.25	3.2 m/s
15	Plastic	Constant	Full	0.25	3.2 m/s
16	Steel, large dia.	Constant	Full	0.25	3.2 m/s

Table 7.1 Different 2-D models created in ANSYS

7.2.3. Results from ANSYS in 2-dimensions

When each of the analyses had been performed using ANSYS, the results were examined both graphically and numerically. The graphical results showed the outputs, at the end of the single time step, of the deformed shapes and the stresses and strains in the radial, axial and circumferential directions, which could be examined on the screen and saved in *metafile* format for later analysis and printing. However, numerous models were examined and generated considerable results which it was found were easier to analyse if lists of the results at pertinent nodes only were generated. Hence, the strains along the outside length of the sleeve, the strains at the interface and the stresses along the base of the cylinder and sleeve were all listed and examined by converting them into Excel spreadsheets.

7.2.3.1. Preliminary analysis

Prior to considering the variables which were examined in the course of the analysis it is informative to examine the overall results from one particular load case. The load case chosen models the response of a concrete cylinder confined by a 3 mm steel sleeve to a pressure of 120 N/mm^2 (approximately equivalent to the maximum overall impact stress associated with impacting the cylinder at 3.2 m/s), and is denoted Model no. 1 in Table 7.1. The base of the cylinder and the sleeve were fully restrained and a coefficient of friction of 0.25 was chosen for the contact between the sleeve and the core (which was consistent with a value chosen by Schneider (1998) for his analysis).

Figure 7.4 and Figure 7.5 show the lateral and axial deformation of the cylinder. The lateral dilation shows that the sleeve and the core move by equal amounts, which would have been anticipated, and is a maximum close to the top of the cylinder. The figure showing the axial displacements show that these are greatest at the top beneath where the pressure is applied. As a result of Poisson's ratio, this axial compression causes radial dilation of the concrete and radial movement of the confining sleeve. The stresses and strains in the composite are shown in Figure 7.6 to Figure 7.11. The diagram of axial stress (Figure 7.8) shows that it is at a maximum 10-20 mm below where the pressure is applied and is reduced by the time that it reaches the base of the cylinder. The model is elastic and cannot incorporate any compression or bearing failure under these large stresses.

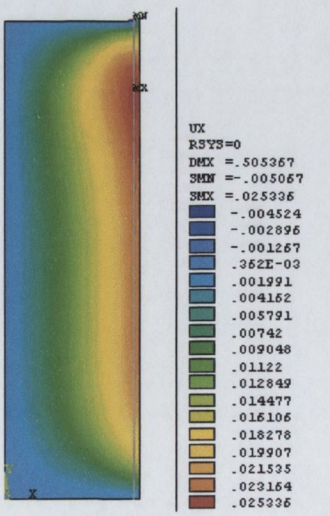


Figure 7.4 Model no.1, lateral displacement

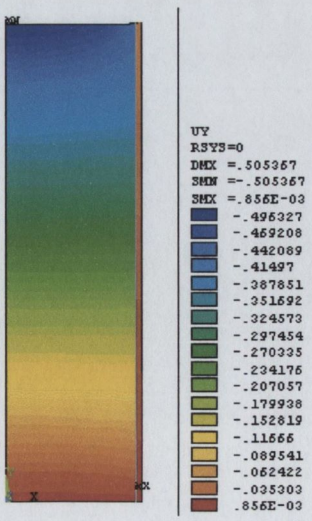


Figure 7.5 Model no. 1, axial displacement

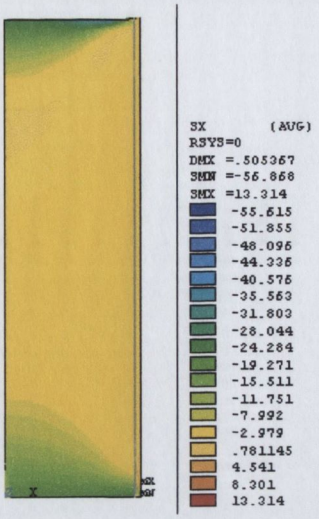


Figure 7.6 Model no. 1, radial stress

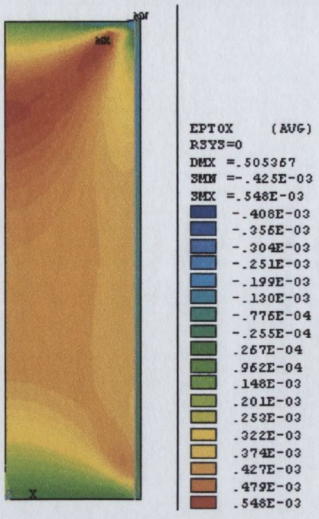


Figure 7.7 Model no. 1, radial strain

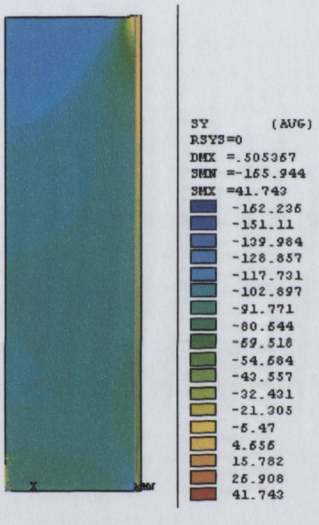


Figure 7.8 Model no. 1, axial stress

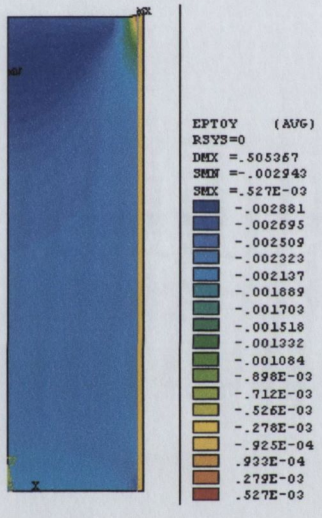


Figure 7.9 Model no. 1, axial strain

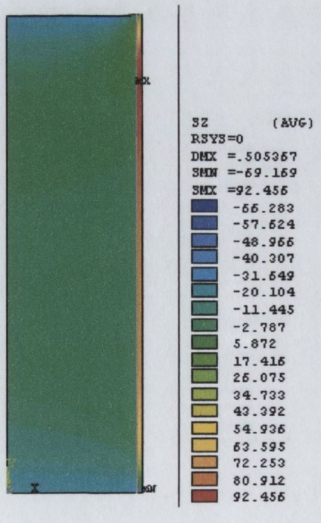


Figure 7.10 Model no. 1, circumferential stress

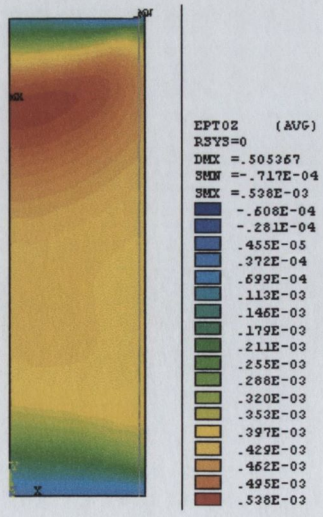


Figure 7.11 Model no. 1, circumferential strain

The axial stresses, similar to those which would have been measured by the base-plate loadcell at the base of the specimen were plotted in Figure 7.12. The stresses along the base of the core cylinder (from nodes no. 1 to no. 11) were very consistent as the load has had the entire length of the cylinder to equilibrate across the full width. However, there is a stress discontinuity at the interface between the core and the sleeve. The stresses in the sleeve (from no. 11, as the nodes are coincident at the interface, to no. 14) show a considerable variation over the width. The inner edge of the sleeve is in axial tension. However, the rest of the sleeve experienced compression, which increased linearly to a maximum at the edge. This would suggest that the sleeve is bending outwards to incorporate the dilation of the confined concrete. The inside of the sleeve is trying to lift off the base, whereas the outside is being forced down, in compression, onto the base as the sleeve bends. The smaller stresses in the radial and circumferential directions show that the base was being restrained from lateral dilation, which is similar to what would have occurred in the plaster during testing. The actual loadcell is only capable of measuring the overall force or stress to which it is subject and cannot take account of the stresses in different locations. However, although the magnitude of the stresses here are greater than those measured by the cell, the relative values between the stresses at the top and the bottom are similar to those in the experimental work.

The strains in the core and sleeve were also plotted and listed in all three directions. The strains are highest in all directions a little below the top of the cylinder, rather than actually at the top. This occurs because the top section is close to the line of load application and,

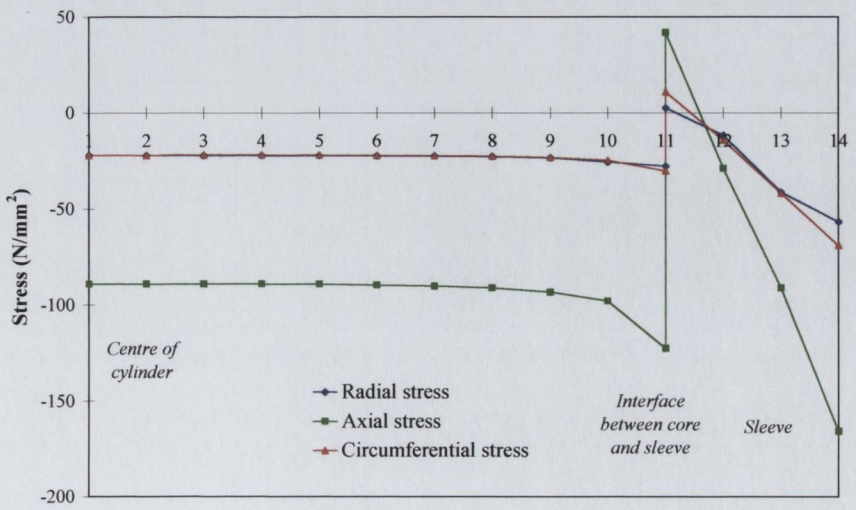


Figure 7.12 Model no. 1, variation of stress across the cylinder base

therefore, moves as a solid section. The effects of the load are really felt at a distance below, where the material is free to move in response to the load. The response is a "shear band" effect, at a characteristic 45° angle to the line of load application. A similar feature can be seen in the compression testing of metals (Rao, 1989).

As can be seen from a plot of the circumferential stresses (Figure 7.10), the values are not equal across the interface between the core and the sleeve which is expected because of the differences in the Young's modulii of the two materials. The stresses in the sleeve are caused by a combination of the radial and circumferential strains applied to the sleeve resulting from the dilation of the core and as a result of frictional transfer of load from the core across the contact interface.

However, the tensile strains circumferentially were identical at the interface between the core and the sleeve, which is what would have been expected due to strain compatibility at this interface and formed an excellent check on the validity of the model. This can be seen in the contour plot of the circumferential strains (Figure 7.11) and also in the graph of the strain variations along the length of the sleeve at the interface (Figure 7.13). This graph also shows that the circumferential strain increases at the top of the cylinder near to the point of load application, up to a maximum 2.5 cm below the top of the cylinder. The experimental results would suggest that, at this level, the lateral strains should be quite high because the concrete core is taking the majority of the load and is causing lateral dilation. The strains are measured experimentally 10 mm from the top of the cylinder, and are highest laterally at this level, as shown in Figure 5.46. The high strains in the model are at a greater depth along the length of the cylinder than might have been expected from the experimental results. However, it should be remembered that the lateral strain gauge on the cylinder is 10 mm below the top surface and, in the absence of further gauges, it is impossible to ascertain whether the strain increases further at greater depths below the surface.

The strain is fairly constant along the mid-section of the cylinder, at a slightly lower strain than the maximum, and remains constant until close to the base where it decreases to zero as the lateral restraint prevents circumferential dilation. This finding gives further confidence in the choice of experimental strain gauge location, showing that the central strain gauge is representative of the response of the majority of the cylinder. The axial

compressive strains in the core are considerably greater than those in the sleeve and reduce slightly along the length as the corresponding compressive strains in the sleeve increase (Figure 7.13). This shows that the loads are being transferred through the contact interface from the core to the sleeve. The majority of the transfer occurs within 60 mm from the top.

The radial strains in the core are tensile and are similar to the circumferential strains in the mid-section, whereas the radial strains in the sleeve are compressive, as it prevents the dilation caused by an outward pressure from the core. The variation of the strains along the outside length are shown in Figure 7.14. The circumferential strains on the outside of the sleeve exhibit the same pattern as the strains on the inside (Figure 7.13) but are fractionally smaller. The axial strains increase slightly more slowly on the outside of the sleeve as the load has to be transferred from the core across the friction interface and then across the

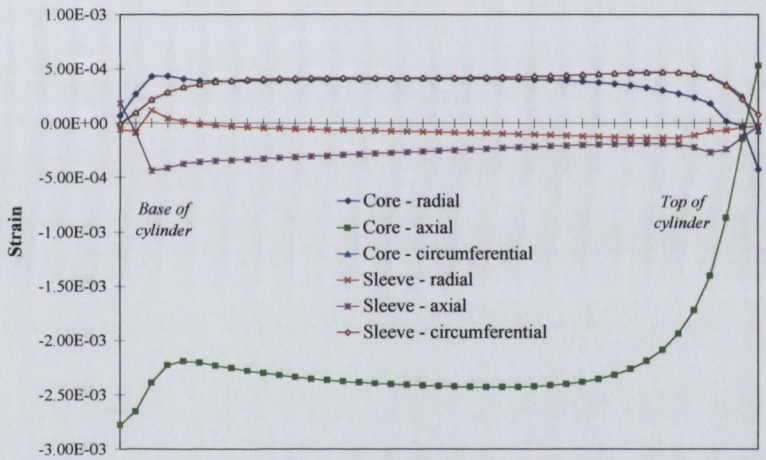


Figure 7.13 Model no. 1, strains at the interface between the sleeve and the core

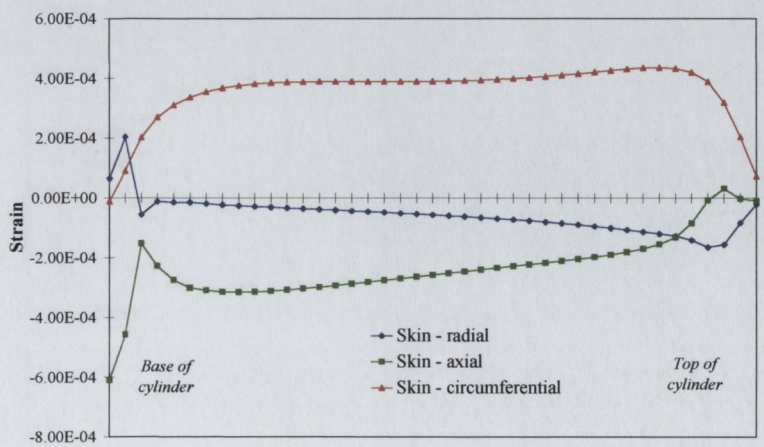


Figure 7.14 Model no. 1, strains along the outside of the sleeve

thickness of the sleeve, but are equal within 40 mm from the top. The axial strains continue to increase along the length of the cylinder, and exhibit some fluctuation near the base due to the presence of end effects. These are both consistent with experimental results (Figure 5.46) which show a small axial strain near the top, the greatest axial strain at the centre and a slightly reduced strain near the base. Furthermore, at the top of the cylinder there are considerably larger circumferential strains than axial strains, which would be expected from the experimental results (Figure 5.55), and the shape of the curve would suggest that the axial strains near to the top of the cylinder are as a result of a Poisson's ratio effect from the large circumferential strains, before the friction at the interface begins to transfer axial load into the sleeve. Although the measured strains are not always identical to the strains determined by this model, they are not very different and are always well within the same order of magnitude. The difference can largely be explained by considering the simple elastic model used. As can be seen from these figures, the maximum tensile strain in the steel is approximately 4.00×10^{-4} which, even accounting for the difference between the experimental and theoretical results, is less than the yield strain for the steel used (Appendix 2). These strains would suggest that the initial assumption that the materials in the sleeve, for this material and thickness and under this particular loading condition, can be modelled elastically. If the concrete had been unconfined, the strains which were determined for the core would have exceeded what it was capable of sustaining. However, because it was confined the concrete was prevented from dilating and, hence can sustain a greater load without failing. The results, however, facilitate a clearer understanding of the load transfer mechanism from the core to the sleeve.

7.2.3.2. End restraint

Two different conditions of end restraint were examined using the 2-dimensional finite element model. In the experimental work the composite cylinder was bedded onto the flat plate loadcell using dental plaster. It was, therefore, prevented from being longitudinally displaced at its base and was subject to some friction and 'platten restraint'. Initially, the base of the core cylinder and the confining cylinder were assumed to be fully restrained (axially and radially), by constraining their displacements to be zero (Model no. 1), modelling a case of full or sticking friction. In Model no. 2, the radial restraint was removed and the cylinders were solely prevented from being displaced in the axial

direction, which modelled sliding friction. The stress results along the base of the cylinder and the external skin strains in the sleeve are shown in Figure 7.15 and Figure 7.16.

The axial stress in the core concrete is very similar in all of the models regardless of the type of restraint provided, however, the stresses in the confining sleeve are much more uniform over its width, when only axially restrained. This occurs because the sleeve is not forced into bending as it is free to move outwards. Furthermore, the radial and circumferential stresses are minimal because there is no restraint for the material to overcome. The axial strains along the length of the cylinder are similar for both types of restraint until the end effects become important at approximately 40 mm above the base of the cylinder. At this height, the axial strains continue to increase as there is no platten restraint preventing them from doing so. Near to the base, the circumferential strains in the fully restrained cylinder reduce considerably as the initial conditions dictate that there should be no movement at the base. The partially restrained cylinder, in contrast, exhibits a fairly constant strain level as it approaches the base of the cylinder. In reality, the experimental results would suggest that the restraint offered at the base falls somewhere between the two simple cases modelled here. There is, without doubt, full axial restraint provided by the presence of the loadcell, however, there is also some restraint provided by friction at the cylinder/loadcell/plaster interface which prevents unrestricted lateral dilation, although perhaps not as much as the fully restrained case. It was not possible to model partial restraint.

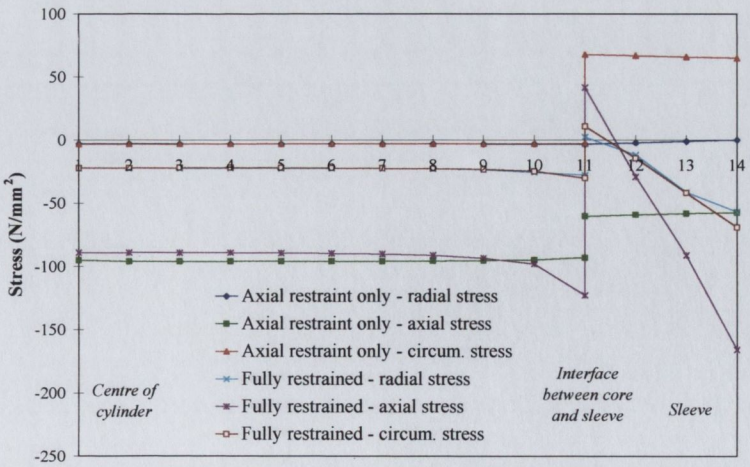


Figure 7.15 Effect of changing restraint at the base on the stresses at the base

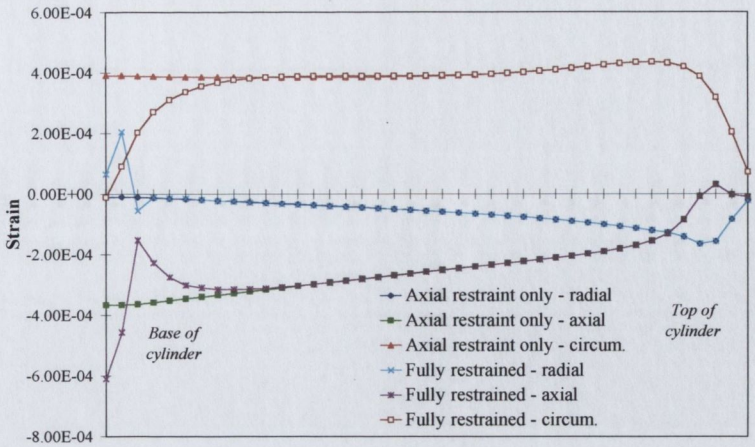


Figure 7.16 Effect of changing restraint at the base on the strains along the outside

7.2.3.3.Constant and linearly varying pressure loading

Two types of load were applied to the 50 mm from the centre of the confined cylinder to represent the forces exerted on a confined cylinder by an impact load, namely a constant pressure (Model no. 1) and a linearly varying pressure between ½ and 1½ times the constant pressure (Model no. 3). The result of the two models were both very similar but, although the total pressure was the same in the two cases, the strains and the stresses in the variable pressure case were consistently lower those with a constant pressure. In contrast to the model with the constant pressure, the model with the varying pressure experienced no circumferential strains until 20 mm below the top of the confining sleeve, as no load reached this part of the cylinder. As the experimental work showed that the circumferential strains were both present and larger than in the numerical modelling, it was decided to adopt the constant pressure model for the rest of the numerical studies.

7.2.3.4. The effect of varying friction

The importance of friction between the sleeve and the concrete core were examined by changing the coefficient of friction in 0.25 increments from 0 (frictionless contact) to 1 (perfect friction) and running separate simulations for each (Model no.1 and Models no. 4 to no. 7) . As the friction increased, the amount of load which was transferred from the concrete core to the confining sleeve increased, with the largest amount of load transfer

when the friction was greatest. This directly affected the amount of stress experienced at the base of the concrete and at the base of the confining sleeve. The cylinder with the highest coefficient of friction (Model no. 7) transferred the smallest load to the base of the concrete cylinder and the greatest load to the base of the confining sleeve (Figure 7.17). This is consistent with the results of the axial strain in the sleeve (Figure 7.18) where the sleeve which had a coefficient of friction of 1 exhibited the highest axial strain, almost six times higher than the cylinder with frictionless contact (Model no. 4). The cylinder in Model no. 4 experienced a constant level of strain over the centre portion of its length because, after an initial load transfer associated with dilation, there was no friction interface across which more load could be transferred. The strains close to the top of the cylinder were of very similar magnitude, regardless of the coefficient of friction, because the friction interface becomes important in the load transfer with a greater distances from

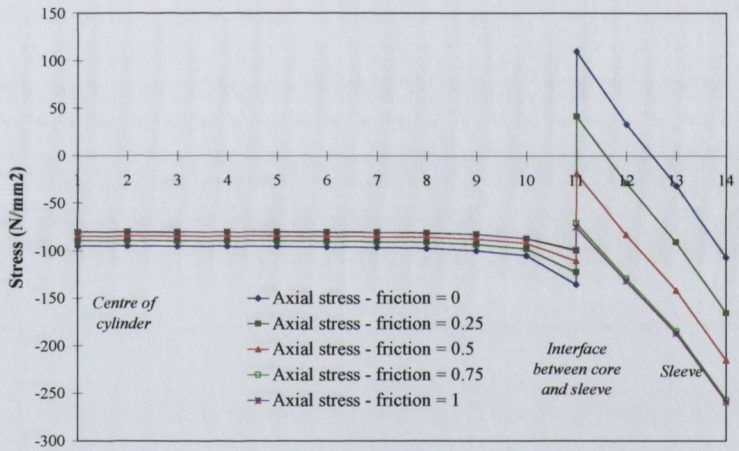


Figure 7.17 The effect of varying friction on the stresses at the base

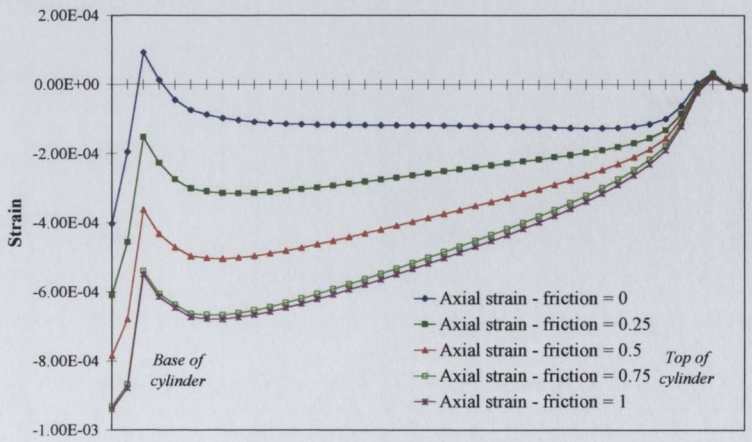


Figure 7.18 The effect of varying friction on the axial strains

the point of loading. The circumferential strains were the same regardless of the friction as the load was always the same and dilation of the sleeve was caused by Poisson's ratio. As the presence of some friction was of critical importance in the modelling, a coefficient of friction of 0.25, which was consistent with values used by other researchers (Schneider, 1998), was chosen for use in the rest of the analysis (Model no. 1) as there was no reason to assume that the friction at the interface in this situation was any greater.

7.2.3.5. Modelling of concrete with different types of confinement

A major part of the experimental work involved comparing the results of cylinders with different types of confinement. It was interesting to compare the results of these different confinement options using ANSYS. Models no. 1, no. 8 and no. 9 were prepared for the 3mm thick steel confined cylinder and were run with three different pressure loads, equivalent to the three different velocities of impact. As would be expected (Figure 7.19), the strains increase as the pressure applied to the top surface of the confined cylinder increases, with curves identical in shape and characteristic to those described above in section 7.2.3.1 (as all the materials in question were assumed to be elastic). Similar effects can be seen in the experimental results in Figure 5.46 to Figure 5.48. The same pressure increases were applied to the other types of confined cylinders. In the cases of the metallic sleeves, the maximum strains experienced were less than the yield strain of the material. However, the plastic sleeved cylinders began to yield as soon as they were loaded, and would have strained unrecoverably as a result of any of these pressure loads, regardless of the contact velocity.

It is, therefore, more interesting to make a direct comparison between the different types of confinement if all are subject to the same applied pressure. The pressure of 120 N/mm^2 (used in the initial model) was chosen for this purpose and was applied to each of the confined cylinder types in turn. The axial strains in the unconfined concrete were considerably higher than those in the confined cylinders as this cylinder was not surrounded by a sleeve into which it could shed load by friction. The unconfined concrete experienced similar circumferential strains to the other materials yet, these, when combined with the high axial and radial strains, would have been sufficient to cause cracking in the concrete (Figure 7.20).

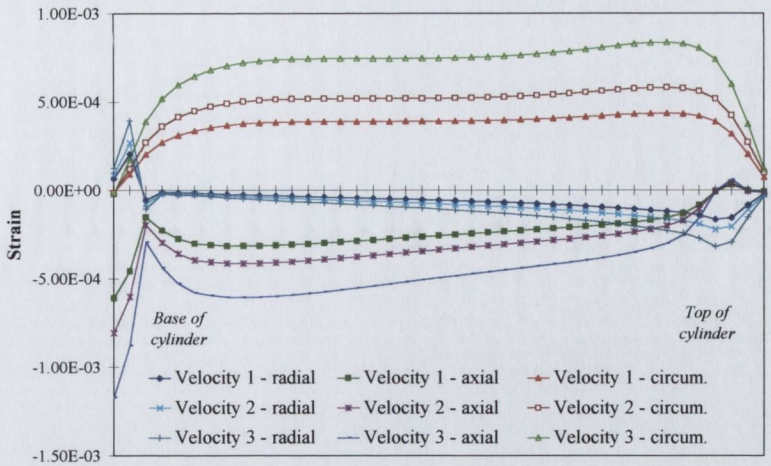


Figure 7.19 Variation of skin strains with pressure increases

As might have been anticipated, the strains in the steel confined concrete decrease as the thickness of the sleeve increases (Figure 7.21). Whereas this causes a significant reduction in the circumferential strains, the axial and radial strains are much less affected, which are similar to the experimental findings in Figure 5.45, Figure 5.46, Figure 5.49 and Figure 5.50. Figure 7.22, compares the results of cylinders confined plastic, aluminium and steel of similar thicknesses. The straining reduces as the Young's modulus of the confining sleeve increases, and the difference is greatest between the plastic and the aluminium sleeved cylinders. This is not as significant as might have been thought by the difference in Young's modulii, which might suggest, similar to the experimental work, that it is the presence of any sleeve that reduces the dilation by the greatest degree and the thickness and stiffness of the sleeve are less important, beyond a certain limit (Figure 5.51

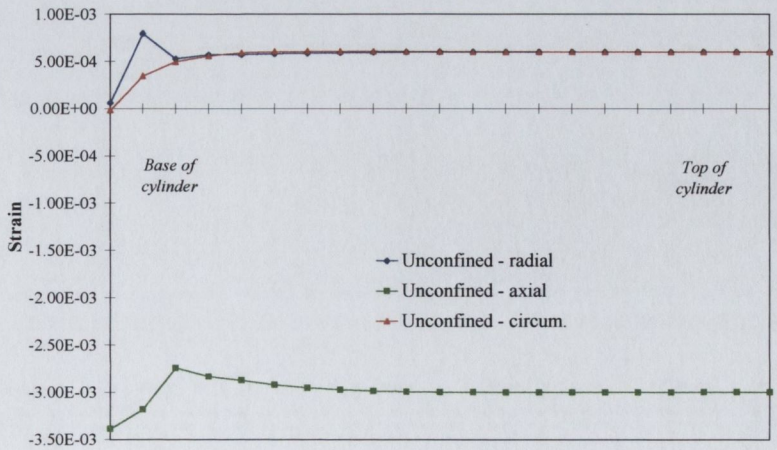


Figure 7.20 Strains along the outside of the unconfined concrete

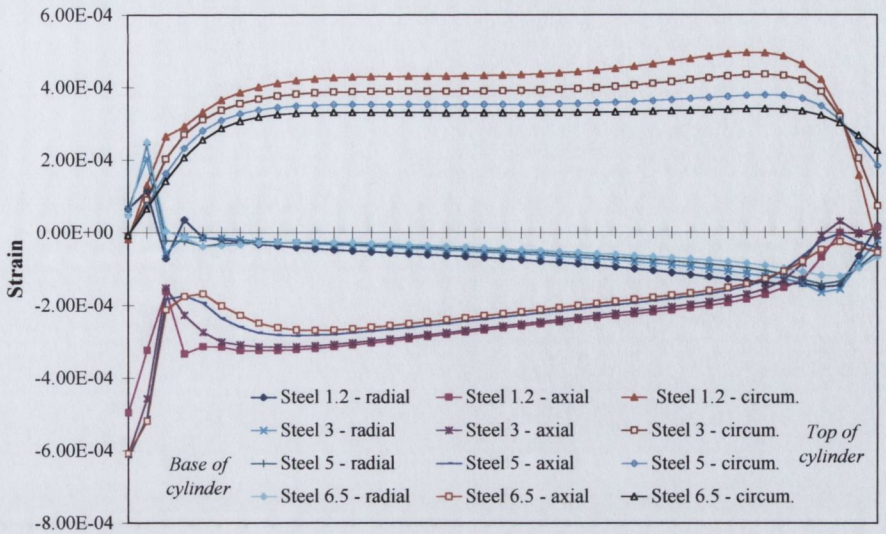


Figure 7.21 Strains along the outside of the sleeve of the steel confined concrete cylinders

to Figure 5.52). A comparison of Figure 7.21 and Figure 7.22 further corroborate experimental results in that the aluminium sleeve (Figure 5.51) is slightly less effective at providing confinement than the 3mm thick steel sleeve, but is probably almost as effective as the 1.2 mm steel sleeve (Figure 5.45).

These strain results are consistent with the assumptions made in Chapter 6 regarding the prediction of the maximum contact force. As can be seen in Figure 7.22, which is of the stains in the confining sleeves along the length of the cylinders, the radial and circumferential strains at the top of the cylinder are negligible in the case of the steel and aluminium confined cylinders. However, considerably more lateral dilation exists, particularly at the top, in the case of the plastic confined cylinders which would make the assumptions of zero radial strain at the top invalid and any contact force predictions overestimations.

A final simulation was run which modelled a cylinder with a considerably larger diameter, that of 168 mm diameter, similar to that tested and discussed in section 5.9.2. It was subjected to a pressure load of 120 N/mm^2 in the central 50 mm. The strains in the outside of the sleeve are shown in Figure 7.23. The circumferential strain in the sleeve increases gradually from the top of the cylinder, as in this case it takes a considerable distance for the load to be transferred from the centre of the cylinder to its edge and then into the sleeve. This is corroborated by the axial strains which are also shown. The results from a

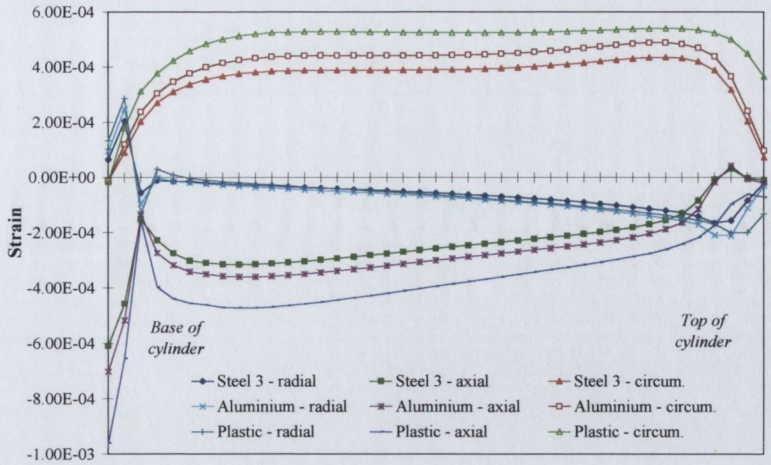


Figure 7.22 Strains along the outside of the sleeve with different materials

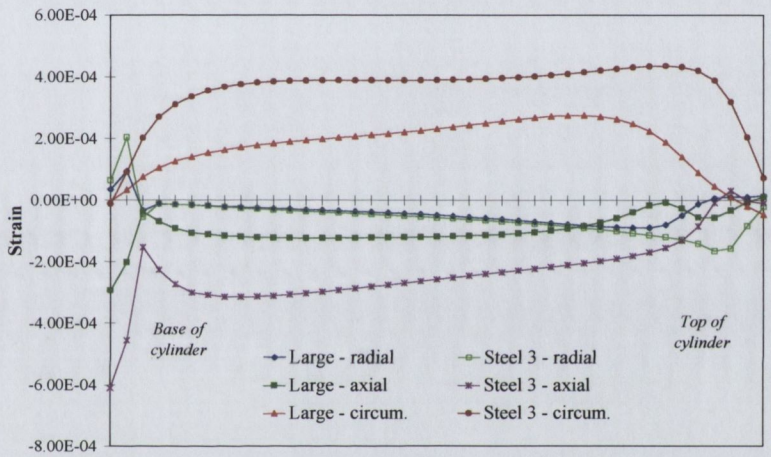


Figure 7.23 Variation of strains along the outside of the sleeve for large diameter cylinder

smaller diameter cylinder are also shown, and it can be seen that the load transfers across the interface into the sleeve a lot more quickly. The strains, both circumferentially and longitudinally are also much smaller in the larger diameter cylinder than those in a smaller diameter cylinder. However, they are similar to the experimentally measured strains in the larger cylinder shown in Figure 5.78 and Figure 5.79.

7.2.4. Model creation - 3D

Although the composite cylinder was easily modelled symmetrically in 2-dimensions, it was useful to confirm this by creating a 3-dimensional model with quarter symmetry planes along the edges. The model created was designed to be simple, symmetrical and to be subjected to a static load. Only one representative model was created in 3-dimensions,

representing the concrete cylinder confined by a steel sleeve of 3 mm thick, impacted at the lowest velocity (Model no. 1).

The model geometry was formed by creating three quarter circles of different diameters, as shown in Figure 7.24. The inside quarter circle had a radius of 50 mm which described the area over which the load was applied [1], an inner annulus which had an inner radius of 50 mm and an outer radius of 54.15 mm [2] representing the area between the edge of the loading and the inside of the confining sleeve, and an outer annulus which represented the confining sleeve which had an inner radius of 54.15 mm and an outer radius of 57.15 mm [3]. These 3 no. ¼ circles were then extruded for 200 mm in the axial direction to form a quarter cylinder. The inner two volumes were merged to form one volume at all locations except at the top, to which the load was applied.

In a manner very similar to the 2-dimensional analysis, the areas at the base of the cylinders were fully restrained in all directions and symmetry boundary conditions were applied along the extruded flat areas. A simple, static pressure load was applied to the top surface of the core concrete cylinder over the 50 mm inner circle to represent the 100 mm diameter impactor. The pressure was calculated in an identical manner to the 2-dimensional analysis and, in the particular case analysed, was 120 N/mm^2. A contact interface was created between the core concrete cylinder and the outer confining sleeve, which incorporated the outer circumference area of one cylinder and the corresponding inner area of the other. 3-dimensional contact elements (TARGE170 and CONTA174), similar to the 2-dimensional elements described above, were used in the surface creation. The coefficient of friction between the two surfaces was again assumed to be 0.25.

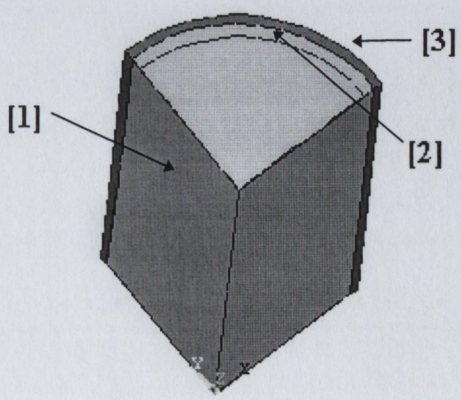


Figure 7.24 3-dimensional model showing ¼ circles

The tetrahedral elements used in the elastic modelling were of the SOLID92 formulation. These can model irregular meshes, such as the ¼ cylinder in question. The element is defined by ten nodes with three degrees of freedom at each node, namely translations in the nodal x, y and z directions, and is capable of modelling plasticity, creep, large deflection and large strains. The number of elements generated in the analysis had to be restricted because of the limitations of the particular version of ANSYS and the computational power of the computers used. The cylinder length was divided into 12 equal sections and each of the top surface radii into 6 sections. The sleeve had 8 elements along the quarter circumference and was one element thick. A total of 2368 elements were used in the modelling of the quarter cylinder.

The program iterated over ten time steps, with up to twenty sub-steps, to find a solution to the problem, and took four hours to converge. The standard post-processor was then used to find the stresses and strains graphically and to list the strain values in the nodes along the outer edge of the confining sleeve, the strains along the interface between the sleeve and the core and the stresses along the base.

The fundamental assumptions made during the 3-D analysis performed with ANSYS were

- the geometry and loading is axi-symmetric and can be modelled using quarter symmetry,
- the boundary between the concrete and the sleeve is perfect with a coefficient of friction of 0.25,
- the cylinder is fully restrained at its base,
- the loading is a static pressure applied to the top surface

7.2.5. Results from ANSYS in 3 dimensions

The three dimensional model described above generated a quarter symmetry solution to the loading of the concrete composite. This had the potential to create many plots of the stress and strain contours as the cylinder was loaded. However, this section will look briefly at a few of the solutions generated and at the results gathered from the nodes along the length of the cylinder.

Figure 7.25 shows the three dimensional model with the axial strains illustrated and is similar to the 2-dimensional result in Figure 7.9. This diagram particularly illustrates the axi-symmetry of this model as the strains are mirrored on either side along the length. The strains are highest slightly below the area of load application, because of shear bands, and reduce along the length in a similar manner to the 2-dimensional model. Figure 7.26 and Figure 7.27 show the radial and circumferential strains in the cylinders and these compliment each other almost perfectly as the model is described in global Cartesian co-ordinates. Figure 7.28 shows a close up of the strains, particularly focusing on the strains in the right hand side which show the circumferential strains on that plane. As would be expected from the 2-dimensional analysis (Figure 7.11), the circumferential strains are continuous across the boundary between the sleeve and the core concrete, as the composite dilates by equal amounts. The tensile strain in the sleeve is clearly at a maximum just below the top of the cylinder, and is fairly constant along its length. Figure 7.29 compares the strains in the outside of the confining sleeve on the two edges, generated by finding the strains at the nodes along the outside of the sleeve. It illustrates the nearly perfect axi-symmetry of the problem and, even at the location of greatest discrepancy, the results are within 3 % of each other. This probably occurred as a result of imperfect symmetry of the elements on the left and right sides of the model.

The difference between the 2- and 3-dimensional models is no greater than the 3 % difference in the two sides of the 3-dimensional model, as can be seen if this figure is compared to Figure 7.14. Similar figures can be generated for the stresses at the base and the strains at the interface which all corroborate the decision to predominantly model the cylinder in 2-dimensions as its geometry and loading are both axi-symmetric.

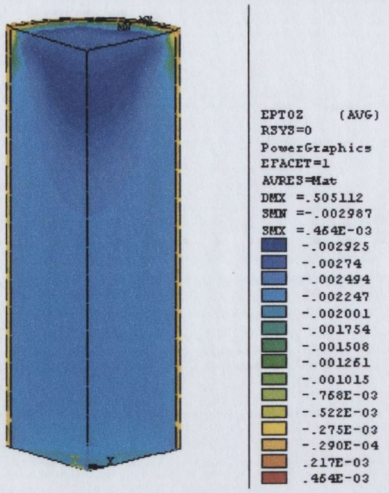


Figure 7.25 Axial strains in 3 dimensions

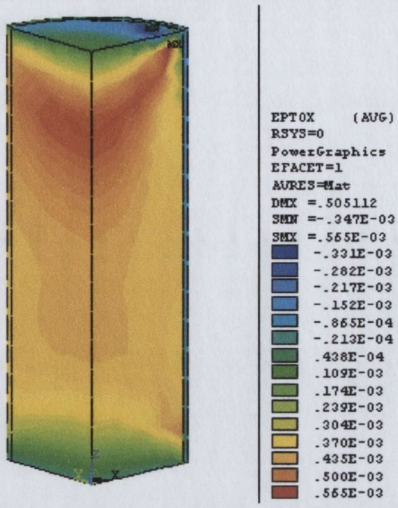


Figure 7.26 Strains in the cylinder - circumferential on left, radial on right

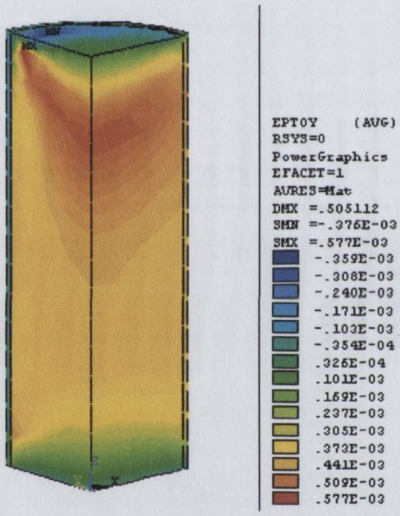


Figure 7.27 Strains in the cylinder - circumferential on right, radial on left

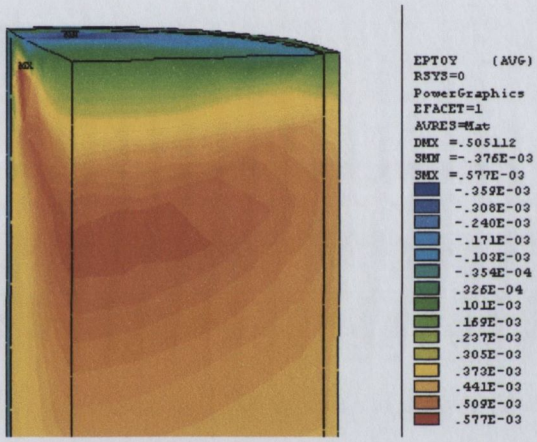


Figure 7.28 Detail of strains - circumferential on right, radial on left

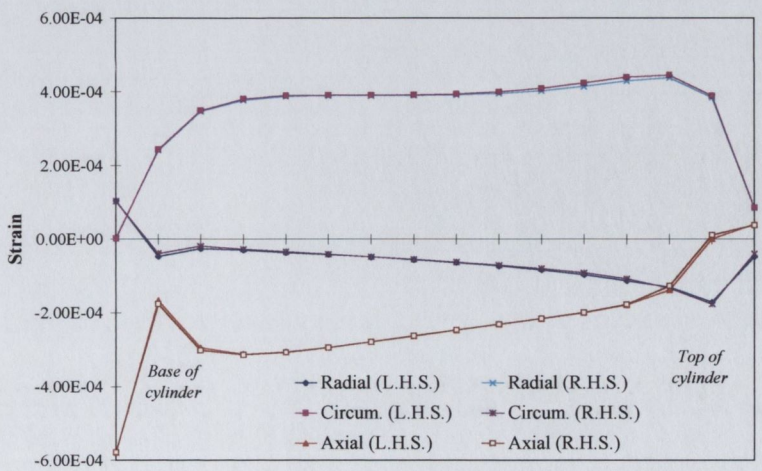


Figure 7.29 Comparison of strains along the outside of the sleeve in the 3-d cylinder

7.3. WORK USING DYNA3D

7.3.1. Theoretical background

DYNA3D is a non-linear, finite element code for the transient dynamic response of three-dimensional solids and structures, developed by the Lawrence Livermore National Laboratory (LLNL). DYNA3D is appropriate for problems where high rate dynamics are important, as it is designed to use small time steps to integrate the equations of motion. A similar code for static and low strain rate problems, NIKE3D, was also developed by LLNL. DYNA3D incorporates a material library to represent a wide range of material behaviour including elasticity, plasticity, composites, thermal and rate dependence and its element library includes solid, shell and beam elements. DYNA3D also has a range of contact interfaces available, and can model contact between different bodies and different parts of the same body. DYNA3D is the dynamic processing part of a series of software and was used in conjunction with the pre-processor INGRID and the post-processor TAURUS. The graphics were produced using the DIGLIB public domain graphics library, all of which were also produced by LLNL

All of the software was installed on a Sun Solaris workstation, running UNIX, with a 3 ½" floppy drive and a 4" tape drive. The copy of DYNA3D used in the analysis was version 3.0.1 and was produced in 1991. Similarly, INGRID was version 1991b and the version of TAURUS used was revision 2.0.91e, complied in 1992. It was recognised, throughout the analysis, that the versions of the software used were not the most up to date available and that newer versions would have had more friendly user-interfaces and a greater variety of material models and contact elements. However, as the intention of the analysis was to provide a simple model, both in form and in properties, of the impact produced in the laboratory, it was decided that the codes could be deciphered with "some" work and that the material and contact models would be adequate for the analysis undertaken. The three dimensional mesh generator and pre-processor INGRID was used to produce complete input files for DYNA3D, with the geometries being described using index space concepts (a 3-dimensional discrete co-ordinate system with integer values greater than or equal to 1 in all directions), with up to 30,000 elements. The basic use of INGRID is described, poorly, in its manual by Stillman and Hallquist (1985).

The INGRID file is divided into sections with an control section followed by a section for each of the physical parts in the analysis. The control commands are sub-divided and dictate how the analysis is to be undertaken. These include the type of analysis to be performed, for example a DYNA3D dynamic analysis, the length of time for which the analysis is to be run, and the time duration, in response terms, between each DYNA3D node and element calculation and data dump interval. The type or types of material used in the analysis, and its properties, are also entered. When this version of INGRID was created, it had up to 35 distinct material types, and this number has increased considerably in the time duration since, with up to 47 material types available in the version released in 1998. The material model types include elasticity, plasticity (both isotropic and anisotropic), finite elasticity, volumetric compaction, rate dependence, thermal effects and failure accompanied by eleven equations of state. This control part also includes input data on any sliding or contact interfaces and boundary conditions for the problem. A range of different sliding interfaces are available for use in DYNA3D including *sliding only*, *sliding with separation and friction*, *tied* and *single surface contact*. Careful use of boundary conditions allows the model to be created and then reduced, taking advantage of any axes of symmetry to minimise the number of nodes and calculations performed.

The part definitions are in individual sections which describe the problem further. Nodes are generated by creating an index space and then mapping them onto the object of interest to create its particular geometry. The material type and the velocity of the body, prior to impact, are also entered. Other controls allow nodes regions or surfaces in the index space to be deleted or moved. Each part then allows definition of the index progression over which either the master or slave part of the contact interface acts, and the boundary conditions which fix the displacements and rotations of particular nodes.

The file which is created is read and manipulated by INGRID, allowing the problem geometry to be viewed, rotated and scaled, either as a whole or in parts. The boundary conditions, including the displacements, symmetry planes, sliding interfaces and load cases can also be viewed. INGRID then writes the problem into a format which DYNA3D is capable of reading, by creating very specific input cards, or occasionally into a TAURUS database so that the location of nodes and elements can be viewed prior to the execution of the problem.

The use of DYNA3D is outlined sketchily in its accompanying users manual (Whirley and Hallquist (the originator of the code), 1991) which describes the control cards created by the pre-processor INGRID. The elements used by DYNA3D include truss, beam, shell, thick shell and continuum elements, all of which are capable of dealing with geometric non-linearities. The material properties, boundary conditions, interface contacts and pressure behaviour all are compatible with, and are defined by, the INGRID pre-processor. The code has no embedded unit formulation and it is, therefore, imperative that the system of units used should be consistent with each-other.

DYNA3D is based on a finite element method for the discretisation of the three spatial directions and a finite difference formulation for the discretisation of time. A central difference method is used to integrate the equations of motion with respect to time. A limit is placed on the time step interval by the program and, for 3-dimensional elements, is the time required for a stress wave to propagate across the shortest dimension of the smallest element in the mesh. The processor automatically calculates the maximum step size at each step of the calculation and adjusts the time step to minimise the number used in the solution, thereby minimising the total time taken for the analysis to be performed. DYNA3D uses a lumped mass formulation for efficiency which produces a diagonal mass matrix M. The solution is, therefore, a function of the applied external forces f^{ext} and the element internal forces f^{int}, thus

$$Ma_{n+1} = f^{ext} - f^{\text{int}} \tag{7.2}$$

where the a_{n+1} is the new acceleration at each stage. This formulation of the solution in this manner means that the solution process at each stage is trivial as no simultaneous system of solutions must be solved.

The elements, which are typically the 8-node solid brick continuum type, are integrated using one-point Gauss quadrature or a constant stress formulation. Spurious 'hourglass modes', which have zero energy, can arise as a result of using this integration type. Their periods are much shorter than that of the structure and often are oscillatory. They are stabilised using 'hourglass viscosity' or 'hourglass stiffness'. Through the use of this formulation, the elements can deal with large displacements and strains associated with contact impact problems. However, other element types, including lumped parameter elements such as springs and dampers, are also available for use in DYNA3D and involve different, specific finite element formulations. Rayleigh damping, when required, is used

in DYNA3D to provide global damping in linear and non-linear analysis. Further details of the theoretical background behind DYNA3D can be found in its theory manual (Hallquist, 1983, 1993).

Several initial conditions can be set in DYNA3D to ensure that the problem is completely defined. These are defined by the pre-processor INGRID and include the specification of the initial velocities of particular nodes or entire parts, and contact and symmetry planes, as described above. The interface contact of two bodies involves the mechanical interaction of two surfaces or of discrete nodes on the surfaces, where the master surface is prevented from being penetrated by nodes on the slave surface. Boundary conditions are of two types, namely nodal single point constraints, which restrict the rotational or translational movement of particular nodes, and nodal constraint equations, which specify that two or more nodes share a global degree-of-freedom. DYNA3D is also capable of defining non-reflecting or transmitting boundaries which allow the definition of semi-infinite domains to prevent spurious wave reflections during the period of analysis. Loads can be applied to nodes or over surfaces as load curves which can vary over time. Body forces can also be used to represent physical phenomena such as gravity, electromagnetic and centrifugal forces and are defined as functions of the base acceleration defined in the model. Furthermore, DYNA3D can be initialised by determining initial stresses and strains due to static loading through the analysis program NIKE3D which can incorporate both stress and deformation effects.

DYNA3D creates up to three binary plot databases, including a state database containing information about each node at each time interval, a time history database containing information about particular nodes at particular time intervals, and interface force database containing information on the normal and shear forces on the DYNA3D slide surfaces. The post-processing is undertaken using TAURUS, an interactive post-processor with a graphical display. TAURUS incorporates two separate parts - one which displays the deformed geometry and state data on a deformed mesh and a second which allows the analysis of results of particular nodes or elements as a function of time. It is both capable of processing large amounts of data created by the processor and of deriving relevant quantities which are spatial or time dependant functions of the primitive variables (consisting of displacements, history variables and element stresses or resultants). It is possible to examine the data generated by TAURUS on the screen or by creating a hard

copy postscript file (with extension .ps) which can be then be examined using the DIGLIB program on the Sun workstation. This file can then be transferred through UNIX to a floppy disk and brought to a PC whereupon a program called 'Ghostscript view' can be used to open the file and create a bitmap image.

Within the state data processing phase, TAURUS has the capability to display results for a given time, or *state*, of the model. If the result required falls between two particular time states TAURUS will linearly interpolate between the states, providing it lies within the program duration. If the time required lies beyond the program duration the processor will extrapolate to find the results (which may be erroneous). The program is capable of producing plots of the deformed shape of the mesh and of *contours* or *fringe* patterns derived from the primitive results, including displacements, stresses, pressures and strains. The time history post processing is an important part of analysis with TAURUS, and can display the variation of global, nodal, element and material data over the duration of the analysis. It is necessary to specify particular nodes or elements which must be 'gathered' prior to the creation of any plots. The plots which it is possible to generate are much more extensive for the element formulations than for the nodal formulations. The use of TAURUS is described in its manual (Spelce and Hallquist, 1991).

The creation, analysis and processing of a model for dynamic analysis with these programs is a highly complicated, three stage process, with certain obvious limitations and idiosyncrasies. These range from complications associated with the use of the code on the UNIX workstation, the way in which the command-line code is formulated and the sparse details provided on the use of the programs in each of their user manuals. Notwithstanding, a three dimensional model, albeit simplified, was created to study the response of a sleeved cylinder to impact by a body travelling with varying initial velocity.

7.3.2. Model creation - 3D

As an entirely separate code exists to analyse 2-dimensional bodies in the DYNA family of codes, all of the dynamic modelling was undertaken in three dimensions. A model was created which was made as simple as possible, whilst still striving for accuracy in the final solution. As DYNA3D performs an essentially unit-less analysis, the units inputted to the

model were in millimetres, milliseconds and kilograms or combinations of these. Therefore, the model was set to run for 1.6 units of time (milliseconds) in total and added information to the output file every 0.02 milliseconds. The experimental results showed that in the majority of cases the initial impact was over within approximately 1.5 milliseconds and the data acquisition system only scanned once every 0.033 milliseconds. It was hoped that that the computer model would, therefore, produce results with an accuracy similar to those of the experimental work.

Similar considerations were made in the material modelling using DYNA3D as had been made using ANSYS, in that a fundamental assumption was made that the materials, including the concrete, remained essentially elastic because of the presence of the confining material. Material properties including the density, Young's Modulus and Poisson's ratio were entered for the material type 1 (isotropic elastic) for each of steel, concrete, aluminium and plastic. Using the information about each of the materials generated by the coupon tests (Appendix 2) it was possible to determine whether this assumption of elasticity was valid, after the analysis had been performed. The model created was quarter-symmetric, with planes of symmetry going through the centre points of the impactor and cylinder. Also within the control part, two sliding interfaces were defined, one a *sliding interface with voids* for between the impactor and the top of the concrete core cylinder, and a second *sliding interface with voids*, incorporating friction, for between the core concrete and the confining sleeve.

The geometric modelling was undertaken in three parts, by splitting the geometry into sections for the impactor, core concrete and the sleeve. The impactor was defined first. It consisted of two quarter cylinders with different radii. The impactor in the experimental work was 795 mm long and consisted of a top section with a diameter of 150 mm and a bottom section with a diameter of 100 mm with tapering between the two. Although it was possible to create an identical model using INGRID, the amount of complication added to the model, on top of the number of elements created in the impacted object, resulted in an input file which DYNA3D was inexplicably incapable of processing. Furthermore, as the focus of the results was on the impacted object and not the impactor, the accuracy with which the impactor was modelled was not as important. The geometry of the impactor was simplified - resulting in two joined cylinders of distinctly different diameters (Figure 7.30). The material properties given to the impactor were those of steel and the mass and volume

of the impactor were carefully checked to ensure that they provided a similar input in terms of mass and kinetic energy to the impactor itself. The location of the step from the smaller diameter cylinder to the larger diameter cylinder was selected so as to ensure that the calculated mass of the impactor was within 0.002 kg of the actual mass. It was given an initial velocity in the positive z direction (downwards) which was identical to that measured for the experimental impactor just prior to when it impacted the concrete cylinder. The impactor was prevented from moving laterally or wobbling as it began to rebound, using boundary conditions. A *sliding interface with voids* was defined at the base of the impactor where it would come into contact with the concrete cylinder with the strong steel impactor as the master so that its nodes could not be penetrated by the nodes of the concrete.

The confined composite cylinder was designed to provide a more accurate mesh for the analysis than the impactor whose sole function was to generate a collision similar to that created experimentally. The focus of the investigation was on the strain results in the confined concrete cylinder. The 200 mm cylinder length was divided into 19 elements by 20 rows of nodes, and the quarter cross-section into ten sections. Whereas the element divisions along the length were all of identical size, those on the cross-section were divided into a 5×5 square of elements over 25 mm and the index points of the other nodes were moved out to different radii, all greater than 36 mm, to form the circular shape of the core concrete, as can be seen in Figure 7.31. This layout of elements was chosen to maintain quadrilateral elements, as DYNA3D is better at manipulating these than tetrahedral shaped elements. Furthermore, a series of preliminary analyses were undertaken which showed that 10 elements were necessary to provide consistent calculations of the strain on the outside circumference of the cylinder. The considerable length of these sleeve elements relative to their breadths was of little further importance to the analysis as the stresses and strains did not change significantly over the breadth (Cook, 1995). The outside sleeve was generated in a very similar manner to the core concrete cylinder but had all of its central elements removed. The resulting sleeve was formed, two elements thick, and with ten elements around the circumference, and also had 20 nodes along its length. A *sliding interface with voids* and friction was used in the interface between the core cylinder and the outer sleeve, which was defined with the sleeve acting as the master surface and the core cylinder acting as the slave surface. The core was also modelled using a linearly elastic material, with properties similar to concrete, and the

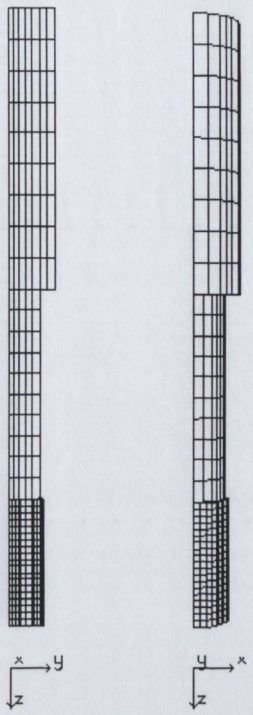


Figure 7.30 Elements along the length of impactor and target

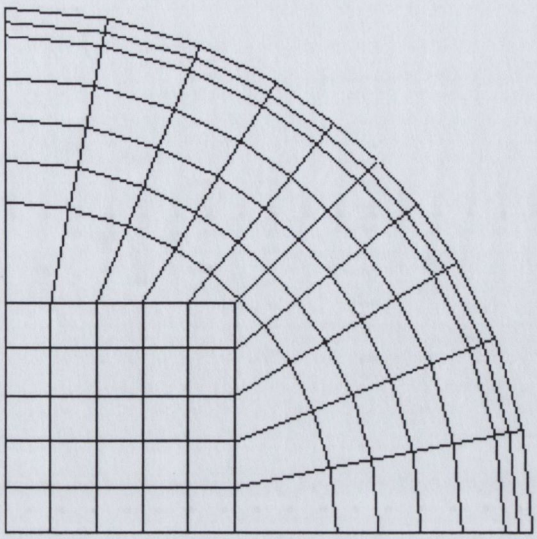


Figure 7.31 Elements in the cross-section of the composite cylinder

sleeve was defined to have elastic properties of steel, aluminium or plastic. The composite element was initially situated 0.2 mm below the base of the impactor, and the top of the inner cylinder was defined as the slave surface corresponding to the impactor's sliding interface. Boundary conditions identical to those provided in the ANSYS analysis, namely that of full restraint, were defined over the entire base surface of both the sleeve and the core. An annotated INGRID file, created for a typical analysis, is given in Appendix 5.

When the model had been created, INGRID was run allowing checks to be made on the geometry, mass and volume of the parts. Within the INGRID program, nodes which were within 0.1 mm of each other, which existed along the length of the cylinder which was created by moving a square grid into the required shape, were merged by the user, which was very important for the accuracy of the resulting model. On exiting from INGRID, an input file for DYNA3D was created, called "*ingrido*". This file was then modified manually by the author to incorporate static friction because the input file for INGRID only defined kinetic friction which meant that none of the load would have been transferred longitudinally into the confining sleeve. The DYNA3D program was then run. This started by removing any interpenetrating nodes on the contact surface between the core and the

sleeve and checking the initial kinetic energy. The program, which modelled the collision and the subsequent movement of the impactor took approximately 8 hours to converge and generated a file of the nodal displacements and the forces at the interfaces.

The fundamental assumptions made during the analysis performed with DYNA3D were

- the concrete and the sleeve material are both linearly elastic which could be confirmed or otherwise by considering the strains generated during the analysis,
- the model is axi-symmetric and can be modelled as a quarter cylinder,
- the boundary between the concrete and the sleeve is perfect and incorporates *sliding with voids* and a pre-defined coefficients of static and dynamic friction,
- the composite cylinder is fully restrained at its base.

7.3.3. Results from DYNA3D analysis

7.3.3.1. Preliminary analysis

The impact response of different cylinders was modelled using DYNA3D. Models were created for each of the types of confinement, including an unconfined and a large diameter cylinder, with the contact velocities of 3.2 m/s. The cylinders confined by a steel sleeve of 3 mm were also "impacted" at 4.4 m/s and 6.3 m/s, as listed in Table 7.2. This generated a considerable number of results for analysis, as plots of the variation of the stresses, strains and displacements with time could be generated for each node or element, or for particular groups of nodes or elements. Similarly, fringe and contour plots could be generated for each of the different stresses or strains at a particular point in time or state of the analysis. It was decided to analyse one of the sets of results in considerable detail, namely the confined cylinder with a 3 mm sleeve impacted at 6.3 m/s (Model no. D1) and then examine the differences between these results and those of other simulations.

Furthermore, due to the manipulation of units mentioned above, the results are shown as functions of the input units and the times along the x axes of the graphs are, therefore, in milliseconds, the displacements in millimetres, the forces in kN, the stresses need to be multiplied by 10^3 to be in units of N/mm^2 and the strains are in units of strain. It was not possible to modify the graphs which DYNA3D creates to change the values of the axes.

Model No.	Confinement	Velocity	Equivalent ANSYS model
D1	Steel, 3mm	6.3 m/s	9
D2	Steel, 3mm	4.4 m/s	8
D3	Steel, 3mm	3.2 m/s	1
D4	Unconfined	3.2 m/s	10
D5	Steel, 1.2mm	3.2 m/s	11
D6	Steel, 5mm	3.2 m/s	12
D7	Steel, 6.5mm	3.2 m/s	13
D8	Aluminium	3.2 m/s	14
D9	Plastic	3.2 m/s	15
D10	Steel, large diameter	3.2 m/s	16

Table 7.2 Different 3-D models created using DYNA3D

No more than four variables are plotted on any of the graphs during this analysis and each of the variables are labelled [A], [B], [C] and [D]. Diagrams on each of the charts show the location of the three points. The analysis focuses on elements at the top, middle and bottom of the cylinder at

- the centre of the concrete core,
- the outside of the concrete core,
- on the inside of the sleeve and
- on the outside of the confining sleeve.

The results compare the responses at each location and at each measurement height and also the responses along the length.

Figure 7.32 illustrates the displacement response of the central nodes of the impactor and the target in the z-direction. The impactor [A] collides with the target and continues to move into it causing it to deform [B], also in the positive z direction (axially). The impacted target then oscillates around its zero point while the impactor rebounds and moves away from the location of impact. As no gravity forces are applied to the model to cause deceleration of the impactor, it continues to move away for the entire duration of the analysis (even if taken over a considerably longer time period) and never impacts again.

Figure 7.33 shows the interface force at the base of the impactor and top of the confined cylinder. It shows the familiar steep sloped rise of the contact force up to a maximum of 534 kN. This value is somewhat lower than would have been expected from an

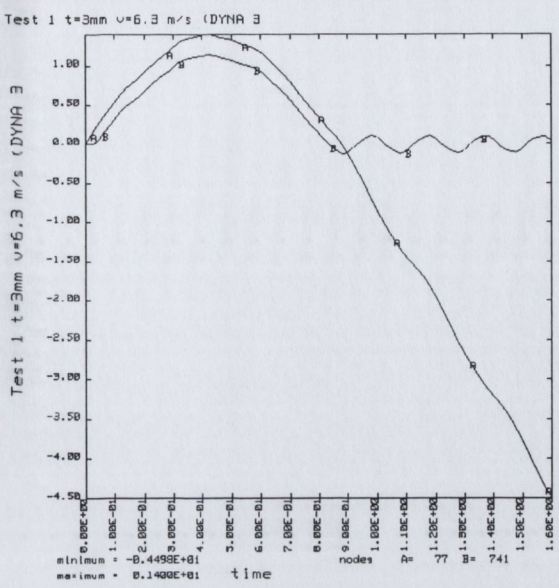


Figure 7.32 Axial displacement of impactor [A] and target [B]

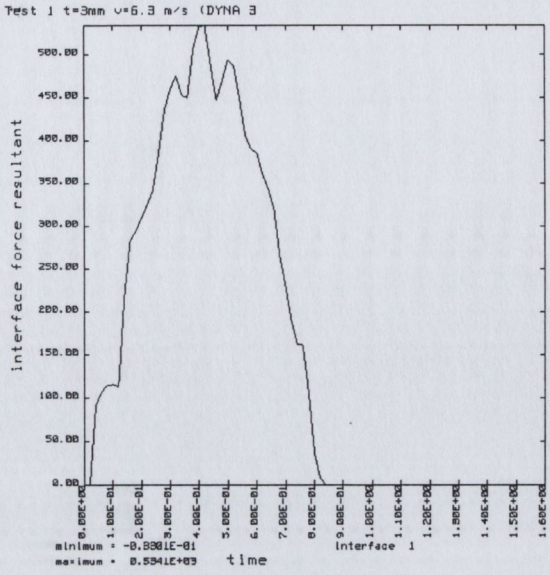


Figure 7.33 Force at the impactor - target interface

examination of the experimental results (1060 kN). However, this interface force is determined as part of the contact-impact algorithm and is the force in the interface springs between penalty nodes at the contact surface. Hence, it is a function of the velocity of impact. It is not related to the stress wave propagation forces which were measured experimentally. However, the slope of the graph is discontinuous, similar to the experimental graph, as the forces in both the experimental and numerical cases vary as the impactor realises that the concrete, which it has just impacted, is restricted from dilating laterally. The duration of the impact is shorter than that which would have been expected experimentally (Figure 5.3). However, the difference in the results is probably due to the fact that experimentally the concrete is subject to inelastic deformation and crushing which is not accounted for within the DYNA3D modelling (a similar phenomena occurred during the Hertz modelling in Chapter 6).

This graph is complimented by Figure 7.34 which compares the stress in the central top element of the concrete core [A] and the corresponding central element at its base [B]. The stresses determined by DYNA3D are much larger than those measured by the contact force or base plate loadcell. Again, the experimental stresses are generated by stress waves travelling in the composite cylinder after the impact. However, the theoretical stresses are calculated by assuming that the kinetic energy of the impactor is absorbed as strain energy during the collision, as described by equations (2.9) and (2.10).

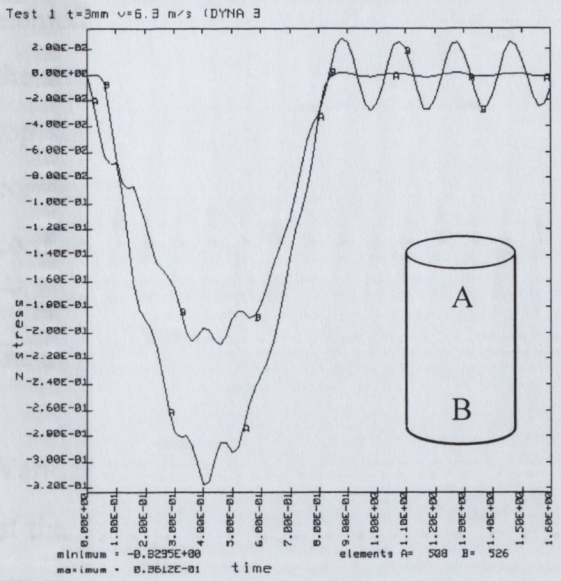


Figure 7.34 Axial stress in central elements at top and bottom of the concrete

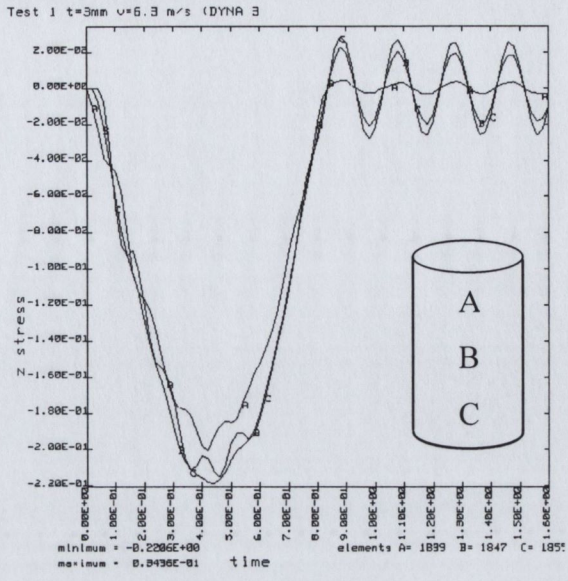


Figure 7.35 Axial stress along the outside edge of the concrete core

The compressive stress at the base of the concrete core is approximately 65 % of that at the top of the core, whose overall slope of response is considerably steeper and whose peak occurs just before that at the base. This reduction in the amount of stress transferred to the base would have been expected from the experimental work where the base-plate loadcell experienced less stress than the contact force loadcell at the location of impact.

Figure 7.35 is of the stresses in the axial direction along the outer elements of the concrete core, comparing elements from the top [A], half way along the length [B] and from the bottom [C]. The stress increases slightly along the length of the cylinder, and does not show the decrease in stresses evident in the stresses at the core centre (Figure 7.34). This occurs, quite simply, because the impact only occurs over a radius of 50 mm from the centre of the cylinder and is, therefore, not directly applied to the element at the edge of the top surface, and is much lower in magnitude than the stress in the centre. By half way along the length the stresses have equilibrated across the cross-section and do not increase further. They are practically identical to the stress at the base in the centre.

The tensile, circumferential strains along the outside length of the concrete core, shown in Figure 7.36, are what might have been anticipated from the results of the experimental work, from the gauges along the outside of the sleeve. The circumferential strain decreases from the top of the cylinder to base. A comparison of the strains in the topmost

element and the element one from the top shows that there is a considerable difference in the strains at this level, which again occurs because the load is not applied over the entire top surface of the cylinder and needs some distance to equilibrate within it. This also corroborates the assumption made of there being negligible dilation at the top of the confined cylinder, which was used in the prediction for the maximum contact force in Chapter 6. The strains are approximately one quarter of the magnitudes of the strains in the axial direction.

Various comparisons were made between the stresses and strains in the core and the sleeve at the three heights along the length of the cylinder. At the top of the cylinder, the axial stresses are much greater in the concrete core [A] than in the confining sleeve. Furthermore, the stresses in the element at the inside top of the sleeve are compressive [B] and the stresses at the outside of the sleeve are tensile [C], as is shown in Figure 7.37. This corresponds to the static analysis and occurs because the stress is only just being transferred through the sliding interface from the concrete into the sleeve at that level and does not have sufficient time to move out to the edge of the sleeve. This part is being pulled down into tension by the compressive stresses in the lower sections of the sleeve. Figure 7.38 shows the axial stresses at mid-height and by this stage much more stress has transferred into the sleeve and has equilibrated over the width of the sleeve [B] and [C].

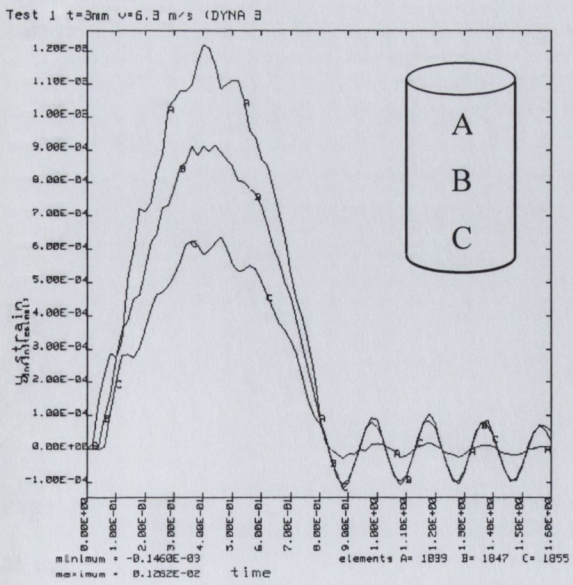


Figure 7.36 Circumferential strains along the outside edge of the concrete core

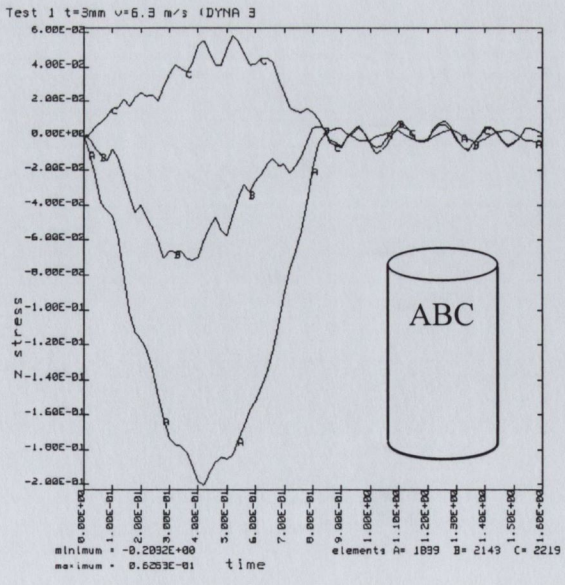


Figure 7.37 Axial stress at the top of the concrete, inside and outside of the sleeve

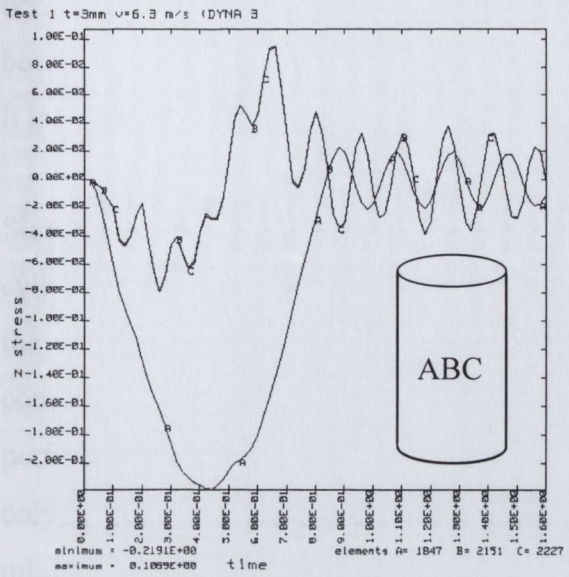


Figure 7.38 Axial stress at the mid-height of concrete, inside and outside of sleeve

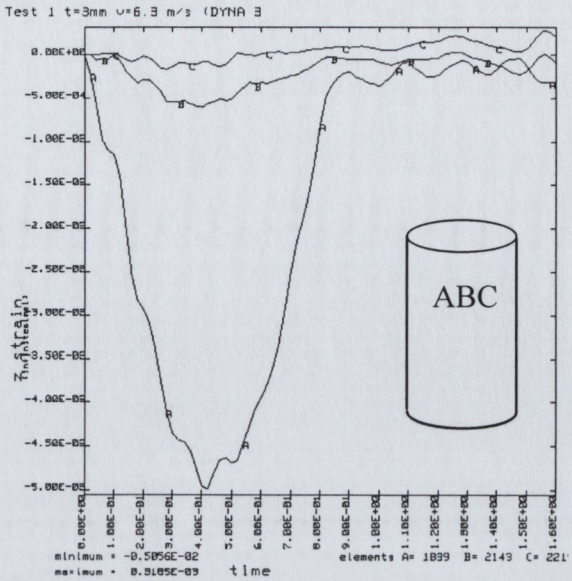


Figure 7.39 Axial strains at the top of the concrete, inside and outside of the sleeve

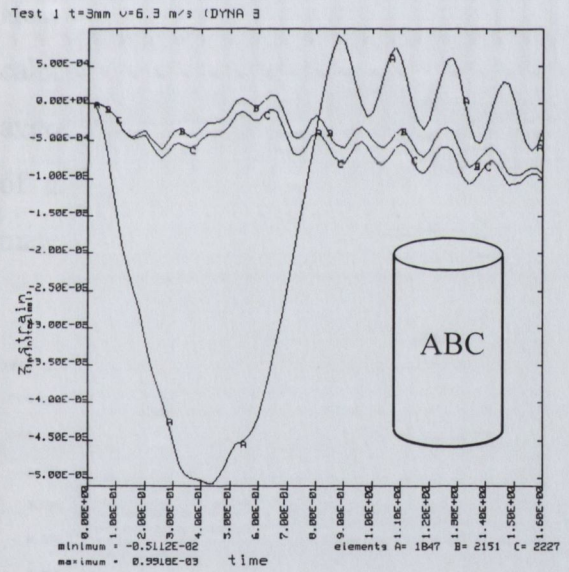


Figure 7.40 Axial strains at the mid-height of concrete, inside and outside of sleeve

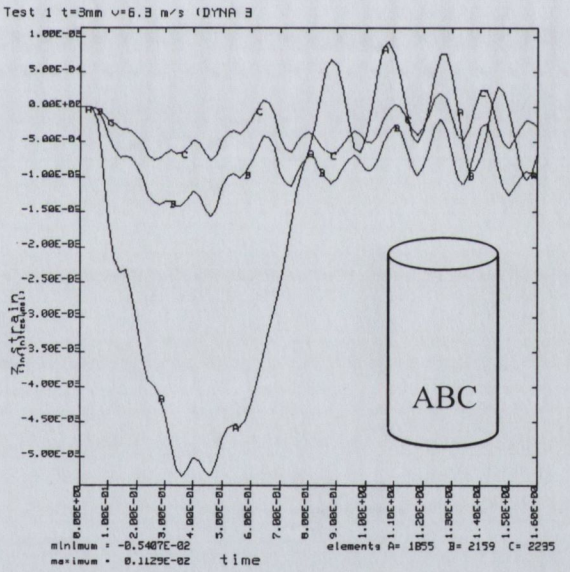


Figure 7.41 Axial strains near the base of concrete, inside and outside of sleeve

Figure 7.39, Figure 7.40 and Figure 7.41 compare the axial strains in the core and sleeve at the top, mid-height and base of the cylinder. The strains are considerably larger in the core [A] than in the sleeve, as would be expected from the stress analysis and the ANSYS analysis and are minimal at the outside top of the sleeve. By the mid-height, the strains in the sleeve are larger in magnitude than at the top, are much more similar to each other and the strain in the outside of the sleeve [C] is larger than that on the inside [B], possibly

because it is less constrained. The strains at the base, on the inside, have increased further because, at this stage, a considerable amount of the load has been transferred to the sleeve. It is larger on the inside than on the outside because of the restraint imposed at the base.

Similar observations can be made about the circumferential strains along the length of the cylinder by comparing Figure 7.42, Figure 7.43 and Figure 7.44. It would be expected that the circumferential dilation of the cylinder would be equal at the interface between the concrete core and the inside of the confining sleeve, as occurred in the static analysis performed using ANSYS. However, an examination of the three figures shows that this only occurs near the base of the cylinder, where the circumferential strains are at a minimum. The core cylinder and the confining sleeve are defined geometrically as being in contact with each other along their entire lengths and this difference in the strains might suggest that there are problems with the model. Different models with different levels of coarseness in the element shapes were tried and the results were the same in all cases. However, as hinted in the manual, the difference probably occurs because the values calculated at the interface are the overall strains in the elements at that location, which are averages over the element volume and associated nodes, due to grouping and vectorisation of the elements in the model formulation. Because of the different stiffness of the materials and gauss points, TAURUS is only able to find average values for the strains in

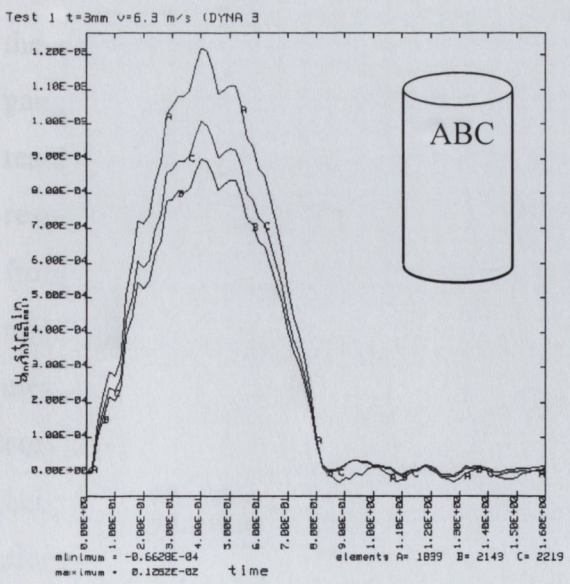


Figure 7.42 Circumferential strains at top - concrete, inside and outside of sleeve

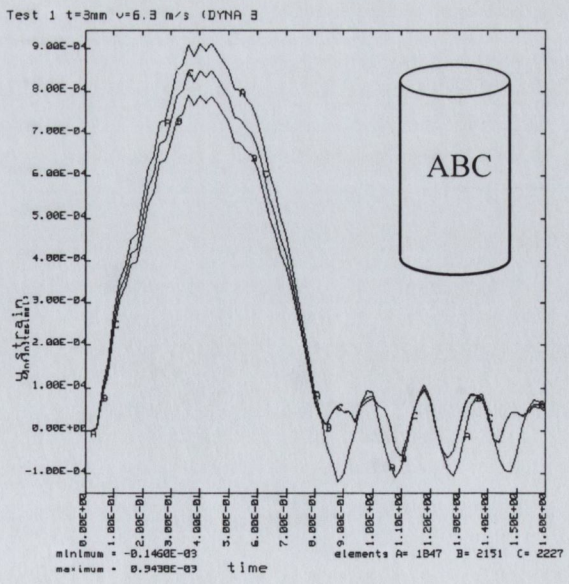


Figure 7.43 Circumferential strains at mid-height - core, inside and outside of sleeve

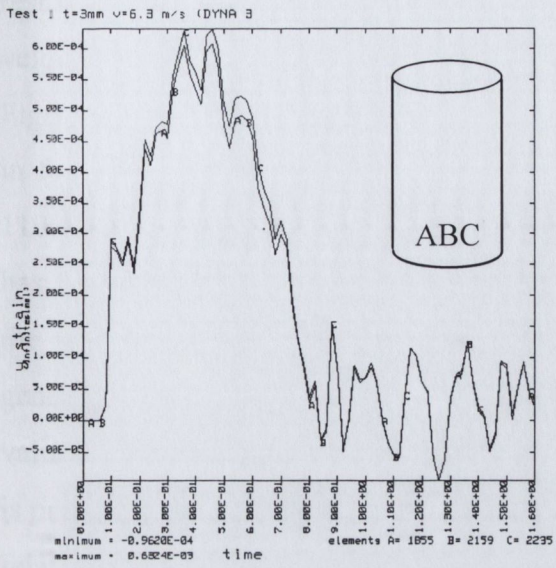


Figure 7.44 Circumferential strains at base of concrete, inside and outside of sleeve

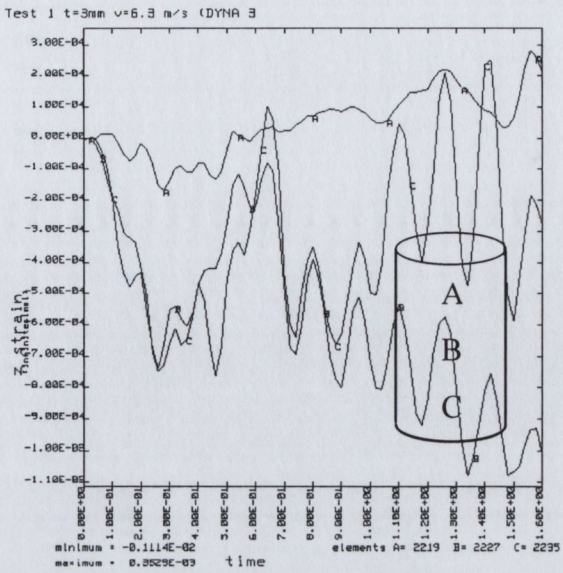


Figure 7.45 Axial strains along the outside of the confining sleeve

the elements at the boundary which causes in the difference shown until near the base of the cylinder where the stresses are very similar across the section. This is unlike the analysis performed using ANSYS which is capable of finding the strains at the particular nodes at the interface.

Figure 7.45 to Figure 7.47 examine the strain response of the elements along the outside of the confining sleeve and form the closest comparison between the outputs of the strain gauges attached to the skin of the confining sleeve during the experimental work and the results of the finite element modelling using DYNA3D. Figure 7.45 is of the axial strain response of the elements along the outside of the sleeve and compares the element one from the top [A] to that in the middle [B] to that one from the base [C]. The strain in the uppermost element is the smallest in magnitude and the axial strains in the lower two elements are considerably greater and are similar to each other. All of the strains are compressive. The strain at the top is small (175 microstrain) because in the model, at this height, only a small proportion of the stress has transferred through the boundary into the sleeve. The experimental results for these cylinders show that the highest strains are experienced close to the top of the cylinder (2100 microstrain). However, this is a phenomenon associated with the loading at the highest velocity where the lateral strains at the top of the cylinder are high enough to exceed the elastic limit (5800 microstrain) and

result in very high axial strains also. The results from other cylinders, impacted at lower velocities show that the axial strain in the top gauge is often the smallest (Figure 5.46 and Figure 5.47). The axial strains at the mid-height and at the base of the cylinder are similar in form and magnitude to those measured experimentally (800 microstrain in the model, 1100 microstrain experimentally). This is because, by the mid-height, much of the load has been transferred into the sleeve and the strains hardly increase in magnitude between the mid-height and the base. It should be noted that the DYNA3D results, like those generated in the ANSYS analysis, do not always result in exact predictions for the strain values measured experimentally, although the values are not significantly different. This is predominantly as a result of the simple elastic model used in the analysis. However, the relative magnitudes of the different strains are well modelled numerically both within a model and between different models.

The circumferential strains in the sleeve are shown in Figure 7.46. These can also be compared to the experimental results (Figure 5.48). As has been mentioned, the lateral strains measured close to the top of the cylinder are large, and at the highest velocity, exceed the elastic limit. This cannot happen in the DYNA3D model as all the materials are elastic. However, the lateral strains are greatest near the top of the cylinder, and decrease along its length because more of the load is being taken axially by the sleeve and due to

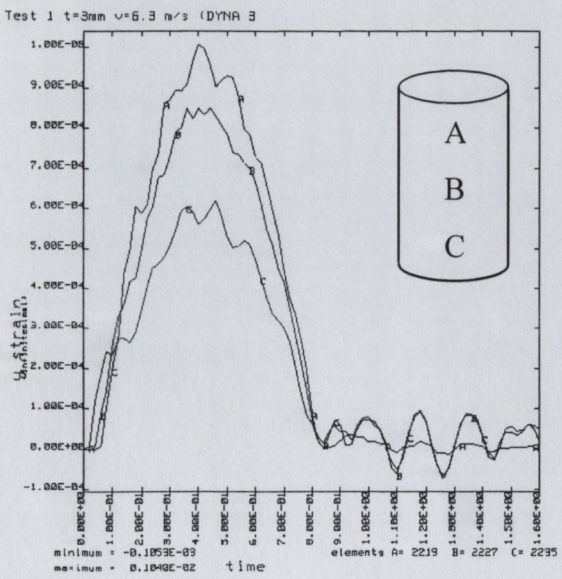


Figure 7.46 Circumferential strains along the outside of the confining sleeve

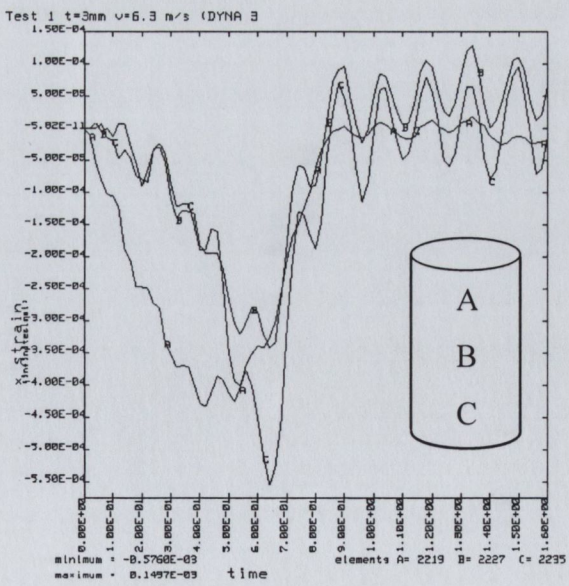


Figure 7.47 Radial strains along the outside of the confining sleeve

microstrain and 500 microstrain respectively). The circumferential and axial strains are of similar magnitudes at the mid-height and base of the cylinder, both experimentally and in the model. However, the strains at the top in the circumferential direction are much greater than those axially, which suggests that these axial strains exist because of a Poisson's ratio effect from the circumferential strains. Figure 7.47 shows the radial strains in the outside of the sleeve, which are the smallest in magnitude of all three directions and are compressive. This would be expected, as the confining cylinder wishes to move outwards due to the internal pressure caused by the dilation of the concrete. However, as a result of the hoop stiffness it is prevented from doing so and, hence, the dilation is small.

Two examples of fringe plots generated using DYNA3D for this particular model are shown in Figure 7.48 and Figure 7.49. They include a plot of the axial strains in the impacted cylinder and a plot of the y-strains. The strains on the left side of the latter plot describe the circumferential strains and are equal over the interface and those at the right side are the radial strains and are discontinuous.

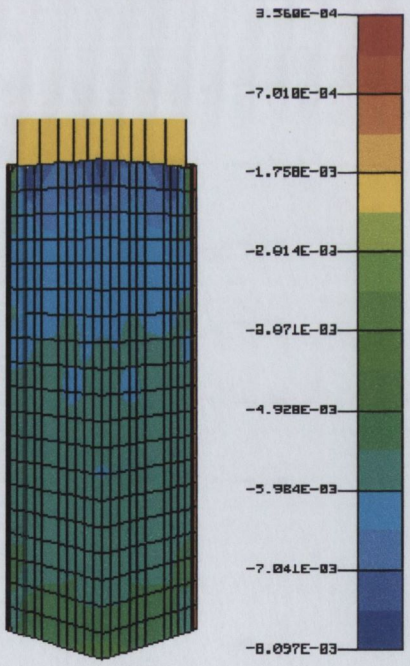


Figure 7.48 Axial strains in target at 0.42 ms

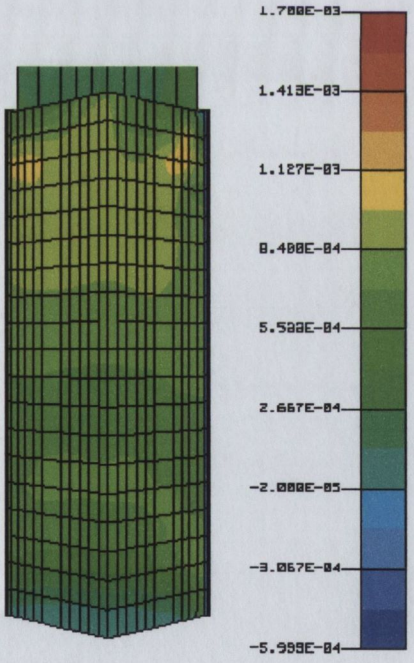


Figure 7.49 Strains in target - circumferential on the left, radial on the right at 0.4 ms

7.3.3.2. Variation in contact velocity

For the 3mm thick confining sleeve the model was re-run at three different velocities corresponding to the velocities at which the impactor collides with the target during the experiments, namely 6.3 m/s (as described in section 7.3.3.1 above), 4.4 m/s and 3.2 m/s (Models no. D1, D2 and D3). The plot generation in DYNA3D does not allow graphs from different analyses to be overlain on one another. As the form of the results were as would have been expected from the analysis above, a predominantly quantitative analysis of the relative strains, focusing on the forces, stresses and strains along the outside of the sleeve, will be undertaken in this section.

Table 7.3 shows the variation of the interface force and the stresses at the top and base of the central elements of the concrete core cylinder with the contact velocity. As discussed above, the interface force varies linearly with the velocity of impact, but does not predict the experimentally measured values. The impact stresses at the top and base of the cylinder are also directly a function of the contact velocity and in all three cases the proportion of the stress transferred to the base is approximately 65 %, a decrease which would probably have been expected from a comparison of the loadcells responses from the experimental results, as discussed in section 5.3.

The axial strain transferred into the sleeve through the sliding interface is at a maximum in the mid-height element on the outside of the sleeve. These maximum axial strain values are included in Table 7.3 with the stress and force results. They are compared to the experimental results from Figure 5.46 to Figure 5.48. The strain decreases as the velocity decreases because there is less stress generated at the top of the cylinder, resulting from the impact at lower velocities, to be transferred to the base of the cylinder through the contact interface into the confining sleeve. Even at the lowest velocity, however, the strain in the

Velocity	Model no.	Interface force	Stress - at top	Stress - at base	Max. axial strain at mid-height (model)	Max. axial strain at mid-height (meas.)
6.3 m/s	D1	534	324	215	770	1100
4.4 m/s	D2	375	225	142	710	850
3.2 m/s	D3	273	164	106	590	360

Table 7.3 Summary of model results generated by varying the contact velocity

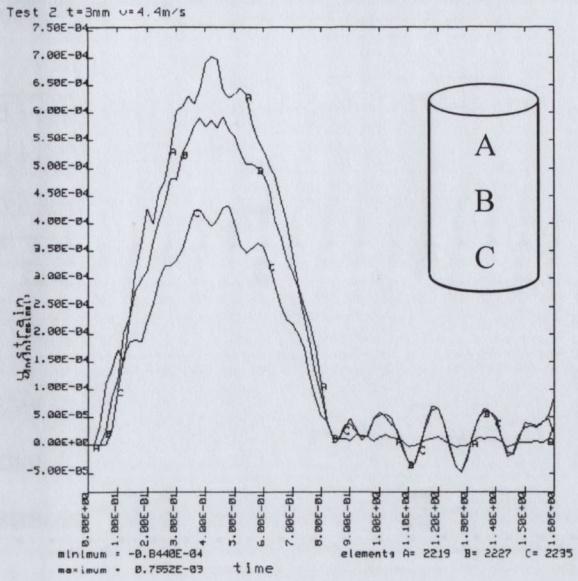


Figure 7.50 Circumferential strains - 3mm steel sleeve, at 4.4 m/s (Model no. D2)

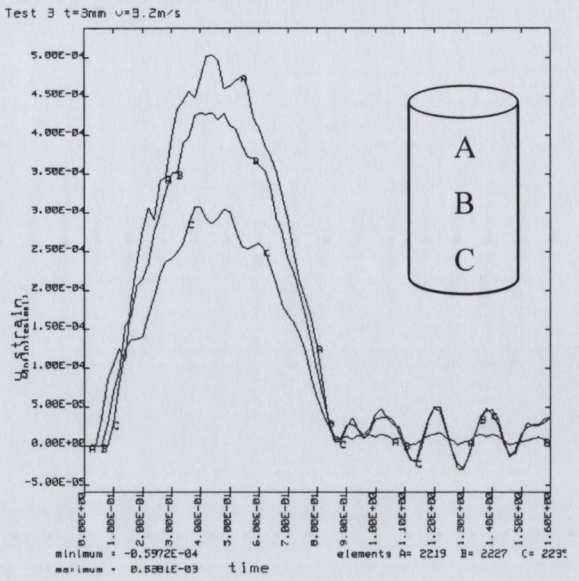


Figure 7.51 Circumferential strains - 3mm steel sleeve, at 3.2 m/s (Model no. D3)

sleeve at mid-height is quite high because, due to its stiffness, it takes a considerable proportion of the load. The circumferential strains also decrease as the velocity decreases, as can be seen from a comparison of Figure 7.46 (Model no. D1), Figure 7.50 (Model no. D2) and Figure 7.51 (Model no. D3). The lateral strains are always at a maximum near to the top of the cylinder, as the load is taken by the concrete core which is relatively free to dilate. The strain is slightly smaller at mid-height than at the top and decreases considerably by the time it has reaches the base, which is fully restrained. The proportions in which the strains decrease are very similar regardless of the velocity of impact which would suggest, as corroborated by the ANSYS analysis, that the friction influences the load transfer more than the increase in the force. These three figures of circumferential strain can be compared to similar experimental plots in Figure 5.46 to Figure 5.48. The magnitudes of the strains in the mid-height and bottom gauges in the experiments are very similar to those predicted using the finite element model, particularly at lower velocities. However, those at the top are much larger than the predicted values. A direct comparison is made between the actual and measured values in Table 7.4. The underestimation of the strains near to the top is probably because of the assumption that the materials are elastic and do not yield (or fracture in the case of concrete). The model cannot, because of its elasticity, take account of any small cracks which form in the concrete and cause further dilation of the sleeve near the top nor of any yielding of the steel sleeve at the highest velocity, resulting from the large amounts of dilation. Nonetheless,

Velocity	Top calculated	Top measured	Middle calculated	Middle measured	Bottom calculated	Bottom measured
6.3 m/s (D1)	1040	5800	860	900	600	500
4.4 m/s (D2)	750	1400	590	540	430	400
3.2 m/s (D3)	540	590	430	250	300	120

Table 7.4 Lateral strains - calculated and measured for three different impact velocities

this comparison of the experimental and theoretically modelled results provides evidence that the finite element work, even when kept simple, is a good way of estimating the strains in the sleeve caused by the impact.

7.3.3.3. Variation in the confining sleeve

The confining sleeve was then varied to model each of the different confinement types and thicknesses used in the experimental work, and the model was re-run at one velocity, namely 3.2 m/s. This generated a series of seven further models, one for each of the different thicknesses of steel, one for the large diameter cylinder and one for each of the aluminium and plastic sleeves. A final model, created without a confining sleeve, was used to model an unconfined cylinder when impacted. Each of the models generated a number of graphs, similar to those described above and the key points from each of these numerous graphs are summarised in Table 7.5. These include

- the maximum interface force,
- the ratio of the stresses in the central element at the top of the concrete core to the corresponding element at the base,
- the maximum axial strain in the mid-height element on the outside of the confining sleeve,
- the maximum horizontal or circumferential strain near the top of the outside of the confining sleeve.

In the case of the unconfined concrete model the strains correspond to those in the mid-height and top elements on the outside of the concrete cylinder.

The interface forces listed in Table 7.5 corroborate the analysis of the forces in section 7.2.3.1, in that DYNA3D calculates the interface forces as part of the penalty function in

the contact algorithm and, hence, only considers the materials of the impactor and target, their respective cross sectional areas and, most importantly, the contact velocity. The ratio of the stress in the central element at the top of the core concrete to the corresponding element at its base is predominantly depends on the confinement offered by the sleeve. Noticeably, it increases as the thickness of the steel sleeve increases.

However, the material the high transmission ratios in the case of the aluminium, plastic and unconfined cylinders would suggest that it also depends on the cross-sectional area of the cylinder. The cylinders with the smallest cross sectional areas, namely the plastic confined and the unconfined cylinders transmit the highest stresses. It is probable that the proportion of the stress transferred should increase as the confinement becomes more important in the behaviour of the composite cylinder, however, although the stress at the base does increase slightly, the consistent level of stress at the top of the cylinder tends to dominate these results.

The strains in the confining sleeve could have been predicted from the experimental results, as both axial and circumferential strains decrease as the thicker confinement prevents the dilation of the core concrete resulting from the impact. Experimental results corresponding to these model predictions are given in Figure 5.44 to Figure 5.52. The thinnest steel sleeve (1.2 mm) experiences axial strains at mid-height nearly twice those of the 3 mm steel sleeve and also experiences higher circumferential strains. The axial strains in the confining sleeve at mid-height decrease considerably as the thickness of the sleeve

	Max. interface force (kN)	$\frac{Stress@base}{Stress@top}$	Max. axial strain at mid-height	Max. lateral Strain at top
Steel 1.2 mm (D5)	265	0.63	1020	550
Steel 3 mm (D3)	273	0.64	590	540
Steel 5 mm (D6)	260	0.65	375	445
Steel 6.5 mm (D7)	258	0.68	340	410
Steel 3 mm dia. 168 mm (D10)	303	0.29	175	95
Aluminium (D8)	262	0.71	490	600
Plastic (D9)	261	0.73	620	860
Unconfined (D4)	257	0.72	3100	1040

Table 7.5 Summary of model results generated by varying confinement

increases as, although load is still being transferred to the sleeve, the increased thickness of the sleeve reduces dilation. A similar effect is experienced circumferentially by the elements close to the top of the cylinders. The thinnest sleeves experience higher strains than the thicker sleeves because the dilation is less restricted as the hoop stresses in the sleeves are smaller.

The high Young's modulus of the steel also reduces the dilation as can be seen when the steel, aluminium and plastic sleeves are compared. The aluminium undergoes axial straining of a similar level to the steel of a similar thickness at this velocity. However, the strains are very high circumferentially as its lower Young's modulus reduces the ability of the sleeve to resist strains in this direction. The plastic confinement is even less effective as, due to its low Young's modulus, it experiences high strains. It is less well able to resist these strains than shown in the results because the material begins to yield as soon as it is loaded, which is not modelled. As would be expected, the strains are at their highest in the unconfined concrete which does not have a confining sleeve into which load can be transferred. The cylinder undergoes straining which would lead to the fracture of the concrete during a test.

The strain response of the large diameter cylinder is different to the other cylinders. This occurs because the diameter of the cylinder is considerably larger than that of the impactor and it takes both time and a certain distance for the load to be transferred from the core into the sleeve, similar to the findings in ANSYS in Figure 7.23. Figure 7.52 compares the stress at the top [A] and base [B] elements in the centre of the core of the concrete and the elements at the top [C] and base [D] elements on the edge of the concrete core. The stresses of the concrete reduce along the length in a similar way to the smaller diameter cylinders. However, the stress at the top edge of the cylinder is very small as there has been insufficient distance along the sleeve for the stress to be transferred to its edge. The stresses at the edge and centre of the base of the cylinder are very similar as there has been sufficient time and distance for the stress to be transferred and equilibrate over the width. The circumferential strains in the sleeve for the same cylinder are shown in Figure 7.53. The model shows that little strain has reached the sleeve near its top and caused dilation. The difference between this and the model is possibly because some cracking is occurring in the top face of the experimental cylinder which is increasing the actual dilation near to the top of the confining steel sleeve which this simple elastic model is not capable of

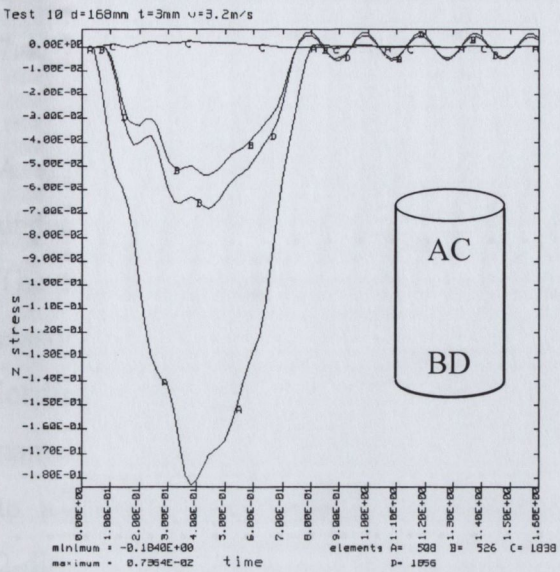


Figure 7.52 Axial stress in the concrete core, top and bottom, centre and edge

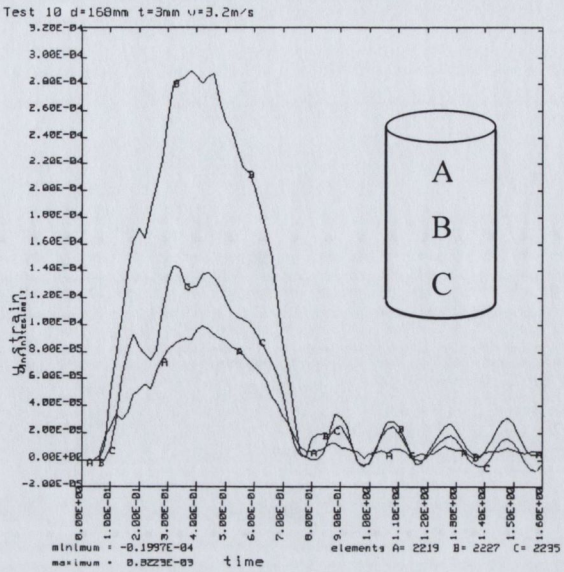


Figure 7.53 Circumferential strain in the sleeve of the large diameter cylinder

incorporating. The model strain is, therefore, greatest at the centre where is has had sufficient distance to dilate the sleeve and for the load to be taken by the sleeve but before it experiences the effects of restraint provided at the base. The experimental results (Figure 5.78 and Figure 5.79) show that the strain, at the location where it is measured experimentally, is very similar to the model strain at the mid-height (300 microstrain compared to 290 microstrain).

7.4. COMPARISONS BETWEEN THE DIFFERENT MODEL TYPES

A static analysis of the application of a pressure load to the top of a cylinder was undertaken using ANSYS and allowed the problem to be modelled in 2- and 3-dimensions. The fundamental assumption made was that the composite cylinder could be modelled elastically. The observation that the problem was axi-symmetric, both in geometry and in loading was exploited in the modelling. Models were run which had the same geometries, namely cylinders with 54.15 mm radii and 3 mm thick confinement and which were subject to a pressure load applied to the top of the cylinder over a 50 mm radius. The 2-dimensional model took a slice through the cylinder and analysed it assuming perfect axi-symmetry about the centre, whereas the three dimensional model looked at a quarter of the cylinder and assumed that this section was quarter symmetrical about its edges. The problems were both designed to be very simple, in that they assumed that all of the materials used in the modelling were isotropic and elastic, and that the cylinders were fully restrained at the base. As shown in section 7.2.5, the 3-dimensional model produced results which were within 3 % of each other across the two edges of the quarter cylinder and this difference was greater than the difference between the this and the two dimensional model.

DYNA3D was used to perform a complimentary piece of analysis by allowing a simplified impactor to collide with a cylinder which had the same properties as that used in the 2- and 3-dimensional analysis using ANSYS. However, the analysis iterated over time and provided a model which could take account of the dynamic effects. The analysis using DYNA3D generated time varying plots of the stresses and strains at different locations in the cylinder, whereas the ANSYS model produced more simple plots of the variation of the stresses and strains at particular locations for a single static load only. However, it was possible to compare the two models in terms of the relative magnitudes of strains at similar locations. The strains determined in both analyses were of similar magnitudes and values, as the pressure applied to the static model was calculated to be equivalent to an impact stress in the cylinder at a particular velocity. Furthermore, because the velocity of impact was quite low, shock waves, which would travel through the bodies after the impact if loaded at high velocities, did not complicate the dynamic problem. The strains along the outside of the sleeve varied in a similar manner in both models, namely the axial

strain was lowest near the top and base of the cylinder and was at a maximum towards the centre of the cylinder. This occurred because it takes a finite time and distance for the load to transfer from the loaded core into the sleeve through the friction interface. Whereas the strains increase along the length, they are reduced close to the base as a result of a the lateral and axial restraint at the base. As has been shown throughout this analysis, the relative values of the axial strains along the length of the cylinder was in agreement with the results generated by the experimental work. Furthermore, both models were able to model the transfer of load from the loaded core into the sleeve and, thereby, facilitate and understanding of the experimental results. Both models also found that the circumferential strains were at a maximum a short distance below the top of the sleeve as the maximum dilation of the core is slightly below the point of load application and similarly causes dilation of the sleeve. The circumferential strains decreased along the length of the cylinder as the loading in the sleeve became axial and dropped quite sharply at the base due, again, to the restraint. The experimental results showed that the strains close to the top of the cylinder were considerably greater than those along the length and that, when impacted at high velocities, some of the sleeves underwent unrecoverable deformation near to their top. However, the simple, elastic material models used in the analysis were not capable of incorporating this effect.

The strains at the interface found by ANSYS were identical in the circumferential direction, and are what would have been expected from an analysis of the problem. This also corroborates the assumptions made in the contact force analysis in chapter 6. However, although the strains were very close in the DYNA3D modelling, they were not identical. This probably occurred because the ANSYS program was capable of listing the precise strain at the node on the edge of the core cylinder and the inside of the confining sleeve, whereas DYNA3D was only capable of determining the strain in the adjacent elements and was the average of the eight nodes in the element. The strains were, therefore, not perfectly identical at the interface. The strains on the outside of concrete core, both circumferentially and radially, generated by the DYNA3D analysis were similar to those which what would have been expected from the ANSYS analysis both in actual and relative magnitudes, as the dynamic effects in the model did not influence the results greatly because the impact velocity was quite low in this case.

A comparison of the stress at the top and the base of the cylinders was performed in both cases. The stress which was transmitted to the base of the cylinder was reduced to between 63 % and 75 % of the stress at the top depending on the particular model. The shapes of the stress/time curves generated by DYNA3D were similar to those measured experimentally. There was also a 20 % to 30 % difference in the results of the contact force loadcell at the top of the concrete cylinder and the flat-plate loadcell measuring the stress and forces at its base in the experiments.

The 2-dimensional model in ANSYS was used to compare cylinders with different types of confinement and the ¼ symmetry model in DYNA3D was also re-run with different confinement properties. The shapes of the curves or plots generated by either of the two programs were very similar in all cases because of the assumption that all of the materials were assumed to be elastic. However, the magnitudes of the strains differed depending on the thickness of the confinement and its material properties. In both analyses, the strain, both axially and circumferentially, decreased as the thickness of the confinement increased. Furthermore as the material properties, particularly the Young's modulus, decreased the strains in both directions increased. The strains were at a maximum when there was no confining sleeve to reduce the dilation of the concrete. The aluminium sleeved concrete was found, particularly in the analysis using ANSYS, to respond in a very similar manner to the concrete cylinder confined with a 1.2 mm thick steel sleeve, which is consistent with the experimental results which suggest that the Young's modulus, the thickness of the sleeve and the combination of the two are important in determining its response to axial loading.

7.5. CONCLUSIONS

Three simple pieces of analysis were undertaken using two distinct pieces of software, both of which tackle the problem in different ways. The Windows based software, ANSYS, was used to model the loading of a confined cylinder statically in 2- and 3-dimensions. The Unix based software, DYNA3D, was used to model the impact of a simple impactor onto a confined cylindrical target. All of the modelling cases assumed that the material properties were elastic and that the geometry and the loading were symmetric about the centre of the cylinder.

The 2-dimensional work using ANSYS involved rectangles and elements which were defined as axi-symmetric. The model was quick to converge and was used to examine some of the parameters of the problem. The restraint at the base was changed to model fully restrained situation and axially restrained case and it was possible to conclude that the former overestimated the restraint while the latter underestimated it, but that the fully restrained model was more accurate for the simple modelling undertaken. The 2-dimensional model also allowed calculations to be performed to determine the effects of friction between the core concrete and the sleeve. As would have been expected, changing the coefficient of friction did not change the circumferential strains, but markedly increased the axial strain transferred into the sleeve along its length. Two ways of applying the static load were examined - a constant pressure and a pressure which varied linearly along the line to which it was applied. It was found that the former, constant pressure application generated a strain profile in the sleeve which was closer to that measured during the experimental work.

As was discussed in the previous section, the simple 2-dimensional model was compared to a 3-dimensional quarter symmetry model generated in ANSYS and analysed statically, and to a dynamic model created in 3-dimensions using DYNA3D. The results from the different models compared very favourably to one another because of the low contact velocity. The two static analyses generated results which were within 3 % of each other. The dynamic analysis exhibited a very similar strain profile to both the static analysis and to the results produced during the experimental work. Even if the magnitudes of the strains in the numerical and experimental work were not always identical, they were not

very dissimilar and were accurate regarding the relative values and the load transfer mechanism, which was the intention of the modelling. The models also showed that the strains calculated in the sleeve, particularly away from the location of loading where some inelastic deformation took place at high velocities, were such that due to the presence of the confinement, the materials, including the concrete, were nearly acting elastically. The 2-dimensional ANSYS analysis and the 3-dimensional DYNA3D analysis allowed the variation of the sleeve material properties and thickness to be modelled. It was found that, similar to the experimental results, the strains in the sleeve decreased as the confining material became thicker and stiffer but that, in all cases, the presence of a confining sleeve, regardless of its properties, caused the greatest reduction in the dilation of the concrete core under a load.

The finite element modelling which was undertaken was very simple. It was based on a number of assumptions, namely

- the problem is symmetric about the central line of the cylinder,
- in the majority of cases, the materials used act elastically (This even included the concrete when sufficiently confined),
- the composite cylinder is fully restrained at the base,
- there is a friction interface between the core concrete and the confining cylinder.

In the course of the modelling each of the above assumptions was examined and found to be justifiable. Furthermore, the results from the finite element modelling were consistent with each other and with the results of the experimental work.

8. EXECUTIVE SUMMARY AND CONCLUSIONS

8.1. EXECUTIVE SUMMARY

The aim of the current research was to gain a more thorough understanding of the response of sleeved concrete subject to low velocity hard impact. The response of concrete to impact has been studied in considerable detail over the last fifty years in an attempt to better understand how this brittle inhomogeneous material responds to strain rates which are higher than those of a typical statically applied load. The research has resulted in a considerable amount of experimental and theoretical knowledge and the responses are now fairly well understood. It has been shown that concrete has a greater strength and stiffness when loaded at higher strain rates. Simultaneously, the response of concrete when loaded tri-axially has also been studied. When concrete is confined in two out of three mutually perpendicular directions its compressive strength in the third direction is considerably enhanced. This research intended to build on, and uniquely combine, these two phenomena, and to examine how concrete responds when passively confined by a cylindrical sleeve and then impact loaded.

The specimens tested were cylindrical and the composite units were formed by pouring the concrete into a sleeve of another material. Various types of confining sleeve were examined in the experimental study. The main test series consisted of concrete cylinders with six different confining sleeves, four of which were made of different thicknesses of steel, ranging from 1.2 mm to 6.5 mm, and two other sleeve types, namely aluminium and plastic, of similar thicknesses to one of the steel sleeves. A seventh group of tests, which formed a reference series, was performed on an unconfined group of cylinders. All of these cylinders were 200 mm high and had an aspect ratio of approximately 2. In a supplementary set of tests, two further types of cylinder were tested, those with a greater diameter, but an identical length, and cylinders of the same dimensions as those in the main test series but whose sleeves did not extend for the entire length of the concrete core and were, therefore, not supported at the base. In all cases, only the core concrete was loaded and the sleeve provided a mechanism for confining the concrete.

The majority of the cylinders were tested by impact, using a hard impact test rig in the Civil Engineering Laboratories of Trinity College Dublin. The rig allowed an impactor to fall, under gravity, at velocities of up to 8 m/s, onto the concrete cylinder situated directly below. Three velocities of impact were used during the current test series, 3.2 m/s, 4.4 m/s and 6.3 m/s, equivalent to drop heights of 0.5 m, 1 m and 2 m, which allowed different amounts of energy to be imparted to the test cylinder. The impactor was a solid steel cylinder, weighing 82.5 kg, with a hardened steel endstriker, and incorporated a loadcell which measured the contact force close to the location of impact. The cylinder was placed on a thin base-plate loadcell which allowed the stress at the base of the cylinder to be measured during the impact event. The measured stress was coupled with the response of strain gauges along the length of the outer circumference of the sleeve, which allowed the determination of the deformational response of the concrete composite. A data acquisition system, scanning at 30 ksamples/sec, recorded the responses of the loadcells and strain gauges during the tests. Also, for comparison purposes, a limited number of static compression tests were performed in a Losenhausen testing machine.

The experiments were not undertaken in isolation but were compared to the results of two theoretical studies - an analytical study and a finite element study. The analytical work was broken into three sections, one which studied the contact force response, one which studied the variation in the contact force over time using Hertz's law and one which modelled the stress-strain relationship of the cylinders tested. The contact force analysis involved the derivation of a formula to predict the maximum contact force of an unconfined or a confined cylinder, using momentum considerations, one dimensional stress wave propagation theory and elastic deformation theory. Hertz's law was then used to provide an analysis of the variation in the contact force with respect to time, with empirical constants determined from the experimental results, including the maximum force, the time taken to reach this maximum force and the total duration of the initial impact event. Two models were generated, one of which used a true sine curve and the other a quasi-sine curve which took account of the degradation in the material properties as a result of the impact. The final section used well established, existing empirical formulae to model the stress-strain response of unconfined and confined cylinders subject to static and impact loads. The empirical models were limited because they were developed for static loads and where the confinement was provided by spirals or hoops. The models were subject to numerous approximations because of the way in which the load was applied

during the current series of tests and the way in which the confinement was provided to the concrete through the use of a sleeve along the length of the concrete core. However, account was taken of these factors and the original models were slightly modified in an attempt to predict, more accurately, the deformational response of the cylinders tested.

Two finite element analyses were performed, one statically using ANSYS and the other dynamically using DYNA3D. It was intended from the outset that the modelling should be quite simple and should facilitate an understanding of how the load is transferred from the loaded concrete core into and along the confining sleeve. The geometry of the problem was reasonably easy to model, when advantage was taken of symmetry, and the models were intentionally further simplified by assuming that the materials acted in a linearly elastic manner. The magnitudes of the stress and strain illustrated clearly, for the cases analysed whether this assumption was realistic or not. The model created using ANSYS was studied in 2- and 3- dimensions and was statically loaded by applying a pressure on the top surface of the cylinders. The dynamic model created using DYNA3D modelled the impact by forcing an impactor, travelling at a pre-defined velocity, to strike the composite cylinder. The program was able to determine the change in the stresses, strains and displacements with respect to time.

8.2. CONCLUSIONS

The experimental and theoretical work undertaken within the scope of this research leads to the following conclusions :

(1) Within the framework of the limited number of variables monitored, the experimental evidence showed that the main factors influencing the response of sleeved concrete cylinders to hard impact included the material properties of the confining sleeve, the thickness of the sleeve, the diameter of the impacted cylinder and the velocity of the impactor just prior to impact. However, the experimental work clearly showed that the significance of these factors depends on the energy imparted to the specimen by the collision. Whilst the presence of a confining sleeve is of primary importance at low velocities, the properties of the sleeve, predominantly its Young's Modulus and its thickness, become increasingly significant at higher velocities of impact, as they reduce the dilation of the confined concrete when loaded.

(2) For the range of velocities which were investigated during the current research, the confinement was extremely important in reducing the cracking and fracture of the concrete when subject to an impact, as was shown by a post-event qualitative analysis of the impacted cylinders. The unconfined cylinders failed catastrophically during the impact, splitting longitudinally into three or four equal sized sections from the centre of the top face, regardless of the contact velocity (within the current range). The presence of the confinement very significantly reduced the cracking and fracture of the concrete. Where the sleeve was sufficiently thick, stiff and elastic, which was the case for all of the thickness of steel sleeves and the aluminium sleeve, the impact resulted at most in a few small radial cracks in the impacted face, from the edge of the cylinder, even at the highest velocity. The plastic confining sleeve, which acted elastically at the lowest velocity, was unable to withstand the increase in energy at the higher velocities and dilated beyond its yield strength which resulted in splitting of the sleeve and the eventual fracture of the confined concrete.

(3) The confinement had a significant effect on the contact force measured by the impactor loadcell during the impact event. The contact force was shown experimentally and theoretically to be proportional to the material properties of the impactor and impacted body, to the cross-sectional area of the bodies at the location of impact and to the relative velocities of the two bodies. However, when the impacted body was confined close to the location of impact, the contact force was greatly increased, and the degree to which this affected the maximum force depended on the ability of the sleeve to reduce the lateral dilation. An analytical study showed that where Young's modulus of the material is low, the thickness is small or the confinement is at a considerable distance from the location of impact, the hoop stresses generated in the sleeve are unable to prevent considerable dilation of the concrete and sleeve and both materials from acting in-elastically. Experimentally, the steel and aluminium confining sleeves increased the contact force by approximately 100 % over the measured unconfined values, at the lower velocities, and by significantly greater amounts at the higher velocities. Whereas the plastic confining sleeve increased the contact force by almost 40 % at low velocities, it was unable to maintain this at higher velocities, where it fractured in a similar manner to the unconfined cylinders.

(4) The force transmitted to the base of the impacted cylinders was measured by a flat-plate loadcell, incorporating manganin strain-gauges. This force was typically 20 % lower than the value measured by the contact force loadcell and was proportional to the velocity of impact. The reduction in force was because some of the energy was used in fracturing the concrete, and because of the reflection and transmission of the wave at the loadcell boundary. However, where the concrete fractured on impact, which happened when the cylinders were unconfined, the maximum force measured by the flat-plate loadcell was fairly constant, and consistent with the properties of the impacted concrete.

(5) The deformational response of the impacted confined and unconfined cylinders was difficult to accurately and consistently quantify due to the inhomogeneous nature of the concrete. The resulting stress-strain curves were typically bi-linear which occurred because the cylinders were capable of sustaining a certain level

of stress with minimal expansion, yet, subsequent increases in stress, beyond this level, caused considerable dilation. The deformational responses of the confining sleeves also illustrated the way in which the load was transferred from the impacted surface to the base of the cylinder. The lateral dilation at the top of the cylinder was high, as there was little to prevent outward movement as the concrete core. The core initially takes all of the load and dilates laterally due to a Poisson's ratio effect which results in circumferential expansion of the sleeve. This circumferential dilation was reduced down the length of the cylinder as the concrete core takes less of the load and because the restraint provided by the loadcell at the base reduces the lateral movement. As the load moved away from the top of the cylinder, it was transferred, by friction and the bond force at the interface, into the stiffer confining sleeve. Hence, the axial strains at the top of the sleeve were very low as it took little axial load at this level. However, the strains increased considerably by the mid-height, by which stage, the sleeve was taking a sizeable proportion of the axial load.

(6) The stress-strain response was modelled using well established empirical formulae produced by different groups of researchers. The way in which the models were constructed and the way in which the loads were applied and the concrete was confined during the current research, resulted in modifications being made to the models, particularly to the maximum stress and the corresponding critical strain. However, the resulting solutions provided reasonable models of the shape for the stress-strain curves of both confined and unconfined concrete when loaded statically. The models were modified further to take account of the enhanced strength and stiffness of concrete when loaded at higher rates and made reasonable estimations of the deformational response of the impacted cylinders.

(7) The response of unconfined concrete when impacted was largely inelastic. However, the confining sleeve surrounding the concrete cylinders resulted in their responding as, predominantly, elastic bodies. This was illustrated by two separate phenomena. Firstly, the shape of the contact force response curve was largely sinusoidal, suggesting that the coefficients associated with the approach and restitution were similar and that there was very little degradation in the

material properties during the impact event. Secondly, the velocity of rebound could be determined by measuring the impulse under the contact force curve and by measuring the length of time between the first and second collision. The ratio of the velocities before and after the impact showed that, although there was a reduction in the velocities, the rebound was significant and consistent with a quasi-elastic response. These phenomena became less evident as the velocity of impact increased and caused increased dilation of the sleeve and cracking of the concrete. Nonetheless, the elasticity of the response allowed Hertz's law to be used to describe the variation of the contact force with time and, where they acted in an 'elastic' manner it was found to model the response reasonably accurately.

(8) The finite element modelling using ANSYS and DYNA3D corroborated the findings of the experimental and analytical work, particularly with respect to the relative values between locations on one cylinder and between identical locations on differently sleeved cylinders. The transfer of load from the concrete core into the confining sleeve through a friction interface between the two was found to be largely complete by approximately 1/3 down the length of the cylinder. This reduced the lateral dilation of the sleeve which was caused by a Poisson's ratio effect of the load in the concrete core, and increased the axial strains as the sleeve took an increasing amount of the load. The fundamental assumption that the materials act elastically was found to be reasonably accurate as the resulting strains were predominantly below the elastic limits of the materials and the strains predicted were of similar magnitudes to those measured. Furthermore, the comparison between the results of the static analysis performed using ANSYS and the dynamic analysis performed using DYNA3D both provide similar results for confined cylinders impacted at these quite low velocities.

As can be seen from the conclusions made in this section, the presence of a confining sleeve has a beneficial effect on the response of concrete to low velocity hard impact. The experimental results clearly showed evidence of increased loads and reduced dilation when the concrete was confined, which was corroborated by the results of both analytical and finite element analyses.

8.3. RECOMMENDATIONS FOR FURTHER WORK

Although an attempt has been made, within the scope of the present research, to cast more light on the problems related to low velocity hard impact on concrete, a great deal more research is required in this area before one can, as an engineer, fully understand concrete as a material during this type of discontinuous dynamic loading. It would, therefore, be desirable to examine the following areas in further detail :

(1) A modification to the low velocity impact test rig to increase the contact velocity of the falling impactor. This could be achieved in one of two ways, either by increasing the maximum drop height or by evacuating the guide tube, but, in both it cases, would allow a greater range of energies to be imparted to the impacted concrete. Some of these impact velocities are being examined currently through the use of the Split Hopkinson Bar technique, but are subject to considerable limitations in the size of the specimens because of the complex stress wave patterns established using this method of loading.

(2) Modifications to the sleeved concrete specimens to examine further their response to impact, in a similar manner to the comprehensive study undertaken statically, by changing the following :

- The thickness of the confining sleeve, which could include reducing it in the case of the metal sleeves to determine the minimum thickness which would be sufficient to minimise the dilation of the concrete core under a load, or increasing it in the case of the plastic confinement to establish what minimum thickness, for this material with a low Young's modulus, could resist the higher velocities of impact and provide cheap, flexible way of providing confinement to the concrete.
- The way in which the confinement is provided could be examined by testing concrete cylinders confined by steel hoops or spirals which do not provide continuous confinement along the length of the cylinder. Extensive work has been undertaken on the response of these types of cylinder to static loading but their response to impact loading is, as yet, unexamined.

- The use of an enhanced friction interface between the concrete core and the sleeve. The numerical study showed that the friction interface between the concrete core and the sleeve was responsible for transferring much of the load from the core into the sleeve. Friction could be increased by using sleeves with ribs or corrugations on the inside surface.
- The use of man made fibres wrapped around the concrete core, particularly those such as fibre reinforced polymers which have a high tensile strength but are too thin to successfully resist an axial load.
- Different properties of the confined concrete, including low strength concrete, potentially made from recycled aggregates such as Recycled Paper Waste (RPW Concrete). These have a low static compressive strength but in preliminary tests (Decard *et al*, 2001) have been shown to have a good energy absorption capacity when impacted, but disintegrate during the event. If these concretes were coupled with a confining sleeve it could provide an excellent, cheap energy absorption mechanism.
- Other ways of confining the concrete, such as the use of the wireball technique, which provides internal confinement to the concrete and also has the potential to act as an efficient energy absorption mechanism (Ryan *et al*, 2001).

(3) The way in which concrete itself provides confinement within a slab. This could be examined by fabricating a slab and then coring it. The hole in the slab could be filled by replacing the core of concrete which was removed or by substituting it for a similar cylinder, which can be gauged and grouted back into place. The slab could then be impacted where the core was originally taken in an attempt to determine to what extent this large structural member provides lateral confinement to a particular area when loaded.

(4) The mechanism of confinement could be changed from passive to active by either hydro-statically pre-loading a cylinder in two directions in a tri-axial cell before impacting it in the third direction, or by the use of orthogonal plattens providing active confinement to the sides of a cube before impacting in the third direction. A limited amount of work has been undertaken recently in this area, however, as the material response to this active loading has been shown

statically to be significantly different to when passively loaded, both cases should be examined further to provide an better understanding of the concrete's response. Similarly, active confinement could be provided using spirals of pre-tensioned wire wrapped around the concrete core. This would act in a similar way to steel spirals but would be easier to fabricate on site, and would probably still provide excellent lateral confinement to the concrete core.

(5) The simple outline of a potential design chart was presented at the end of the experimental work, which was loosely based on the findings of the experimental results. It shows which combinations of velocity and confinement thickness would successfully allow an impact on confined concrete to be withstood. With some more experimental work, along similar lines, this design chart could be made more accurate and could potentially be used in a design situation.

(6) The intention of the finite element work conducted during the present research was to produce a simple model to determine how the load was transferred from the concrete core into the confining sleeve, which it successfully achieved. This work should be extended to model the impact using more realistic material properties, both statically and dynamically. The finite element tool, if it modelled these tests more comprehensively, could be used to predict the results of different geometries of impacted confined concrete cylinders, with different types of confinement, at different velocities of impact. However, this would require advances in the finite element packages, especially in the ability to model cracks in the concrete, and the computational ability of the computers.

(7) The work on the stress-strain relationship of the unconfined and confined concrete was intended to assess how the current research fitted into a broader series of experimental work on the response of confined concrete when loaded. Although the work was restricted because of the way in which the load was applied, the results were not too dissimilar. The derivation of an analytical model, rather than a further empirical models, to predict the stress-strain relationship of passively confined concrete, at different loading rates is necessary in order to better understand and model this extremely important material, and to provide accurate inputs for further analysis using the finite element technique.

REFERENCES

1. Abbott, D. : 'The biographical dictionary of scientists - physicists', Blond Educational, London, 1984
2. Ahmad, S.H., Abdel-Fattah, H. : 'A rational model for the stress-strain relationship of circular hoop-confined concrete', *Mag Concrete Res*, 1991, 43 (154), 23
3. Ahmad, S.H., Khaloo, A.R., Irshaid, A. : 'Behaviour of concrete spirally confined by fibreglass filaments', *Mag Concrete Res*, 1991, 43 (156), 143
4. Ahmad, S.H., Mallare, M.P. : 'A comparative study of models for confinement of concrete by circular spirals', *Mag Concrete Res,* 1994, 46 (166), 49
5. Ahmad, S.H., Shah, S.P. : 'Behaviour of hoop confined concrete under high strain rates', *Am Concr Inst J*, 1985, 82 (5), 634
6. Ahmad, S.H., Shah, S.P. : 'Complete triaxial stress-strain curves for concrete', *A.S.C.E J Struct Div*, 1982, 108 (ST4), 728
7. Almusallam, T.H., Alsayed, S.H. : 'Stress-strain relationship of normal, high-strength and lightweight concrete', *Mag Concrete Res*, 1995, 47 (170), 39
8. Anderson Jr., C.E. : 'An overview of the theory of hydrocodes', *Int J Impact Engng*, 1987, 5, 33
9. ANSYS Corporation : 'ANSYS online manuals', Release 5.5, ANSYS Corporation, 1999
10. Armstrong, W.E, : 'Axially loaded concrete prisms with lateral confinement', PhD Thesis, Imperial College, University of London, 1983
11. Armstrong, W.E., Perry, S.H. : 'Spirally bound concrete columns', *Proc R Soc Lond*, 1985, A400, 127
12. Armstrong, W.E., Perry, S.H. : 'Stress-strain relationships for concrete with steel confinement', *International Conference on Concrete Under Multiaxial Conditions*, Toulouse, France, 1984, 1, 263
13. Atchley, B.L., Furr, H.L. : 'Strength and energy absorption capabilities of plain concrete under dynamic and static loadings', *Am Concr Inst J*, 1967, 64, 745
14. Attard, M.M., Setunge, S. : 'Stress-strain relationship of confined and unconfined concrete', *Am Concr Inst Mat J*, 1996, 93 (5), 432
15. Banthia, N., Mindess, S., Bentur, A., Pigeon, M. : 'Impact testing of concrete using a drop-weight impact machine', *Exp Mech*, 1989, 29 (1), 63
16. Bentur, A., Mindess, S., Banthia, N. : 'The behaviour of concrete under impact loading : Experimental procedures and methods of analysis', *Mater Struct / Mater Constr*, 1986, 19 (113), 371
17. Bischoff, P.H. : 'Compressive response of concrete to hard impact', PhD Thesis Imperial College, University of London, 1988
18. Bischoff, P.H., Perry, S.H., Eibl, J. : 'Contact force calculations with a simple spring-mass model for hard impact : a case study using polystyrene aggregate concrete', *Int J Impact Engng*, 1990, 9 (3), 317

19. Bischoff, P.H., Yamura, K., Perry, S.H. : 'Polystyrene aggregate concrete subjected to hard impact', *Proc Inst Civ Eng*, 1990, 89 (2), 225

20. Bischoff, P.H., Perry, S.H. : 'Compressive behaviour of concrete at high strain rates', *Mater Struct / Mater Constr*, 1991, 24, 425

21. Bischoff, P.H., Perry, S.H. : 'Impact behaviour of plain concrete loaded in uni-axial compression', *A.S.C.E. J Eng Mech Div*, 1995, 121 (6), 685

22. Bourne, N.K., Rosenberg, Z. : 'Fractoemission and its effect upon noise in gauges placed near ceramic interfaces', *Journal of the American Institute of Physics*, 1996, 1053

23. Bourne, N.K., Rosenberg, Z. : 'On the ringing observed in shock-loaded piezoresistive stress gauges', *Meas. Sci. Technol.*, 1997, 8, 570

24. British Standards Institution : 'BS 2782 : Part 11 : Method 1110 1989 Methods of testing plastics, Thermoplastics pipes, fittings and valves, Method 1110. Tensile properties of dumb bell specimens from PVC gutter profiles or pipes for non pressure applications', London, 1989

25. British Standards Institution : 'BS 1881 : Part 108: 1983, Testing concrete, Method for making test cubes from fresh concrete', London, 1983

26. British Standards Institution : 'BS 1881 : Part 110: 1983, Testing concrete, Method for making test cylinders from fresh concrete', London, 1983

27. British Standards Institution : 'BS 1881 : Part 114: 1983, Testing concrete, Methods for determining the density of hardened concrete', London, 1983

28. British Standards Institution : 'BS 1881 : Part 116: 1983, Testing concrete, Method for determining the compressive strength of concrete cubes', London, 1983

29. British Standards Institution : 'BS 1881 : Part 120: 1983, Testing concrete, Method for determination of the compressive strength of cores', London, 1983

30. British Standards Institution : 'BS 1881 : Part 203: 1986, Testing concrete, Recommendations for measurement of the velocity of ultrasonic pulses in concrete', London, 1983

31. British Standards Institution : 'BS 1881 : Part 206; 1986, Testing concrete, Recommendations for determination of strain in concrete', London, 1983

32. British Standards Institution : 'BS 2782 : Part 3 : Method 321 1994 Methods of testing plastics, Mechanical properties, Method 321. Determination of tensile properties, general principles', London, 1994

33. British Standards Institution : 'BS 2782 : Part 3 : Methods 320A to 320F 1976 Methods of testing plastics, Mechanical properties, Methods 320A to 320F. Tensile strength, elongation and elastic modulus', London, 1976

34. British Standards Institution : 'BS EN 10002-1: 1990 : Tensile testing of metallic materials, Part 1. Method of test at ambient temperature', London, 1990

35. British Standards Institution : 'Eurocode 3, Design of steel structures : Part 1.1 General Rules', London, 1992

36. British Standards Institution : 'Eurocode 4, Design of composite steel and concrete structures', London, 1994

37. Brown, I.C., Perry, S.H. : 'An experimental method to investigate impact on concrete slabs', *RILEM-CEB-IABSE-IASS Interassociation Symposium on Concrete Structures under Impact and Impulsive Loading*, (ed. Plauk, G.) Berlin, BAM, 1982, 202

38. Brown, I.C., Perry, S.H. : 'CIRIA/UEG - The assessment of impact damage caused by dropped objects on concrete offshore structures, Part 2', Concrete in the Oceans, Technical report 17, H.M.S.O., London, 1989

39. Burdette, E.G., Hilsdorf, H.K. : 'Behaviour of laterally reinforced concrete columns', *A.S.C.E J Struct Div*, 1971, 97 (ST2), 587

40. Carpinteri, A., Ferro, G., Monetto, I. : 'Scale effects in uniaxially compressed concrete specimens', *Mag Concrete Res*, 1999, 51 (3), 217

41. Carreria, D.J., Chu, K-H. : 'Stress-strain relationship for plain concretes in compression', *Am Concr Inst J*, 1985, 82 (6), 797

42. Cescotto, S., Zhu, Y.Y. : 'Mixed finite elements for contact-impact of solids undergoing large strains, *Shock and Impact on Structures*, (Eds. Brebbia, C.A., Sanchez-Galvez, V.) Computational Mechanics Publication, Southampton, 1994, 231

43. Chen, W., Ravichandran, G. : 'An experimental technique for imposing dynamic multiaxial-compression with mechanical confinement', *Exp Mech*, 1996, 36 (2), 155

44. Chung, H.W. : 'Shear strength of concrete joints under dynamic loads', *Concrete*, 1978, 27

45. Clegg, R.A., Sheridan, J., Hayhurst, C.J., Francis, N.J. : 'The application of SPH techniques in AUTODYN-2D to kinetic energy penetrator impacts on multi-layered soil and concrete targets', *Proceedings of the 8th International Symposium on the Interaction of the Effects of Munitions with Structures*, Virginia, U.S.A., 1997,

46. Comite Euro-International du Beton : 'C.E.B.-F.I.P. Model Code', Thomas Telford, London, 1990

47. Comite Euro-International du Beton : 'Concrete Structures Under Impact and Impulsive Loading', *C.E.B. Bulletin d'Information* No. 187, 1988

48. Cook, R.D. : 'Finite element modelling for stress analysis', Wiley, New York, 1995

49. Darwin, D., Pecknold, D.A. : 'Nonlinear biaxial stress-strain law of concrete', *A.S.C.E. J Eng Mech Div*, 1977, 103 (EM2), 229

50. De Nicolo, B., Pani, L., Pozzo, E. : 'Strain of concrete at peak compressive stress for a wide range of compressive strengths', *Mater Struct / Mater Constr*, 1994, 27, 206

51. De Nicolo, B., Pani, L., Pozzo, E. : 'The increase in peak strength and strain in confined concrete for a wide range of strengths and degrees of confinement', *Mater Struct / Mater Constr*, 1997, 30, 87

52. Decard, J.D., West, R.P., Prichard, S.J., : 'The impact response of recycled paper waste concrete', *International Symposium on Recovery and Recycling of Paper*, 2001, Dundee, U.K. (to be published)

53. Dinic, G. : 'Hard impact of reinforced concrete domes, circular slabs and fender materials', PhD Thesis, Imperial College, University of London, 1985

54. Dinic, G., Perry, S.H. : 'Shear plug formation in concrete slabs subjected to hard impact', *Engineering Fracture Mechanics*, 1990, 35 (1/2/3), 343

55. Dugas, R., : 'A history of mechanics', Dover Publications, New York, 1988

56. Eibl, J. : 'Behaviour of critical regions under hard missile impact', *RILEM-CEB-IABSE-IASS Interassociation Symposium on Concrete Structures under Impact and Impulsive Loading*, (ed. Plauk, G.) Berlin, BAM, Introductory report, 1982, 113

57. El-Dash, K.M., Ahmad, S.H. : 'A model for stress-strain relationship of spirally confined normal and high-strength concrete columns', *Mag Concrete Res*, 1995, 47 (171), 177

58. El-Dash, K.M., Ahmad, S.H. : 'A model for the stress-strain relationship of rectangular confined normal and high strength concrete columns', *Mater Struct / Mater Constr*, 1994, 27, 572

59. Evans, R.H. : 'Effect of rate of loading on the mechanical properties of some materials', *J Inst Civ Eng*, 1942, 18 (5), 296

60. Fardis, M.N., Khalili, H.H. : 'FRP-encased concrete as a structural material', *Mag Concrete Res*, 1982, 34 (121), 191

61. Fujikake, K., Mizuno, J., Suzuki, A., Ohno, T., Nonaka, T. : 'Dynamic strain softening of concrete in compression under rapid loading', *Proceedings of Structures Under Shock and Impact V (SUSI V)*, (eds. Jones, N., Talasidis D.G., Brebbia C.A. & Manolis, G.D.), Computational Mechanics Publications, Southampton, 1998, 481

62. Gangadharam, D., Nagi Reddy, K. : 'Effect of cover upon the stress-strain properties of concrete confined in steel binders', *Mag Concrete Res,* 1980, 32 (112), 147

63. Gardner, N.J., Jacobson, E.R. : 'Structural behaviour of concrete filled steel tubes', *Am Concr Inst J*, 1967, 404

64. Gebbeken, N., Ruppert, M. : 'A new concrete material model for high dynamic hydrocode simulations', *Archive of Applied Mechanics*, 1999 a

65. Gebbeken, N., Ruppert, M. : 'On the safety and reliability of high dynamic hydrocode simulations', *Int J Numer Methods Engng*, 1999 b, 46 (6), 389

66. Gerstle K.H., Aschl H., Bellotti R., Bertacchi P., Kotsovos M.D., Ko H.M., Linse D., Newman J.B., Rossi P., Schickert G., Taylor M.A., Traina L.A. : 'Behaviour of concrete under multiaxial stress states', *A.S.C.E. J Eng Mech Div,* 1980, 106 (EM6), 1383

67. Gillispie, C. : 'Dictionary of scientific biography', Charles Scribner's Sons, New York, 1973

68. Goldsmith, W. : 'Impact, The theory and physical behaviour of colliding solids', Arnold, London, 1964

69. Green, H. : 'Impact strength of concrete', *Proc Inst Civ Eng*, 1964, 28, 383

70. Hallquist, J.O. : 'LS-DYNA3D Theoretical manual', Livermore Software Technology Corporation, LSTC Report 1018, Rev 2, 1993

71. Hallquist, J.O. : 'Theoretical manual for DYNA3D', University of California, Lawrence Livermore National Laboratory, Report UCID-19401, 1983

72. Hobbs, D.W., Pomeroy, C.D., Newman, J.B. : 'Design stresses for concrete structures subject to multi-axial stresses', *Structl Engnr*, 1997, 4, 151

73. Hughes, B.P., Gregory, R. : 'Concrete subject to high rates of loading in compression', *Mag Concrete Res*, 1972, 24 (78), 25

74. Hughes, B.P., Gregory, R. : 'The impact strength of concrete using Green's ballistic pendulum', *Proc Inst Civ Eng*, 1968, 41, 731

75. Hughes, B.P., Watson, A.J. : 'Compressive strength of concrete and ultimate strain of concrete under impact loading', *Mag Concrete Res*, 1978, 30 (105), 189

76. Hughes, G., Speirs, D.M. : 'An investigation of the beam impact problem', Cement and Concrete Association, Technical report No. 546, Cement and Concrete Association, 1982

77. Janach, W. : 'The role of bulking in brittle failure of rocks under rapid compression', *Int J Rock Mechanics*, 1976, 13, 177

78. Jiang, L., Rogers, R.J. : 'Proportional material damping in finite element impact analysis', *Comput and Struct*, 1989, 31 (2), 235

79. Johnson, W. : 'Impact strength of materials', Edward Arnold, London, 1972

80. Kishi, N. : 'Absorbing performance of sand cushion and three-layered absorbing system', *3rd Asia Pacific conference on Shock and Impact Loads on Structures*, (eds. Lok. T.S., Lim, C.H.), Singapore, 1999, 195

81. Knowles, R.B., Park, R. : 'Axial load design for concrete filled steel tubes', *A.S.C.E J Struct Div*, 1970, 96 (ST10), 2125

82. Knowles, R.B., Park, R. : 'Strength of concrete filled steel tubular columns', *A.S.C.E J Struct Div*, 1969, 95 (ST12), 2565

83. Kolsky, H., : 'Stress waves in solids', Dover Publications, New York, 1963

84. Kotsovos, M.D. : 'Effect of testing techniques on the post-ultimate behaviour of concrete in compression', *Mater Struct / Mater Constr*, 1983, 16(91), 3

85. Kotsovos, M.D., Newman, J.B. : 'Generalised stress-strain relations for concrete', *A.S.C.E. J Eng Mech Div*, 1978, 104 (EM4), 845

86. Kotsovos, M.D., Newman, J.B. : 'A mathematical description of the deformational behaviour of concrete under complex loading', *Mag Concrete Res*, 1979, 31 (107) 77

87. Kotsovos, M.D., Newman, J.B. : 'Fracture mechanics and concrete behaviour', *Mag Concrete Res*, 1981, 33 (115), 103

88. Kotsovos, M.D., Pavlovic, M.N. : 'Structural concrete', Thomas Telford, London, 1995

89. Kotsovos, M.D., Pavlovic, M.N. : 'Non-linear finite element modelling of concrete structures : basic analysis, phenomenological insight, and design implications', *Eng Comput.*, 1986, 3 (3), 243

90. Kotsovos, M.D., Perry, S.H. : 'Behaviour of concrete subjected to passive confinement', *Mater Struct / Mater Constr,* 1986, 19 (112), 259

91. Krajcinovic, D., Silva, M.A.G. : 'Analysis of tests on impact strength of concrete armour blocks', *Int J Impact Engng*, 1984, 2 (4), 3331

92. Krajcinovic, D., Silva, M.A.G. : 'Damage of Colliding Concrete Cubes', *A.S.C.E J Struct Div*, 1984, 110 (8), 1822

93. Kuehl, R.O. : 'Design of Experiments : Statistical principles of research design and analysis', 2nd Edition, Duxbury, Pacific Grove, 2000

94. Kurt, C.E. : 'Concrete filled structural plastic columns', *A.S.C.E J Struct Div*, 1978, 104 (ST1), 55

95. Lahlou, K., Lachemi, M., Aitcin, P.-C. : 'Confined high-strength concrete under dynamic compressive loading', *A.S.C.E J Struct Div*, 1999, 125 (10), 1100

96. Lindholm, U.S. : 'Some experiments with the Split Hopkinson Pressure Bar', *J Mech Phys Solids*, 1964, 12, 317

97. Liu, J., Foster, S.J. : 'Finite element model for confined concrete', *A.S.C.E J Struct Div*, 1998, 124 (9), 1011

98. Lovejoy, S.C., Whirley, R.G., : 'DYNA3D example problem manual', Lawrence Livermore National Laboratory, Report UCRL-105259, 1990

99. Madas, P., Elnashai, A.S. : 'A new passive confinement model for the analysis of concrete structures subjected to cyclic and transient dynamic loading', *Earthquake Eng Struct Dyn*, 1992, 21, 409

100. Malvar, L., Crawford, J.E., Wesevich, J.W., Simons, D. : 'A plasticity concrete material model for DYNA 3D', *Int J Impact Engng*, 1997, 19 (9-10), 847

101. Mander, J.B., Priestley, M.J.N., Park, R., : 'Observed stress-strain behaviour of confined concrete, *A.S.C.E J Struct Div*, 1988, 114 (8), 1827

102. Mander, J.B., Priestley, M.J.N., Park, R. : 'Theoretical stress-strain model for confined concrete', *A.S.C.E J Struct Div*, 1988, 114 (8), 1804

103. Mirmiran, A., Shahawy, M. : 'A new concrete-filled hollow FRP composite column', *Composites*, 1996, 27B, 263

104. Mirmiran, A., Shahawy, M. : 'Behaviour of concrete columns confined by fibre composites', *A.S.C.E J Struct Div*, 1997, 123 (5), 583

105. Montgomery, D.C. : 'Design and analysis of experiments', Fourth Edition, Wiley, New York, 1997

106. Montgomery, D.C., Runger, G.C. : 'Applied statistics and probability for engineers', Wiley, Chichester, 1999

107. Narayanan, R. : 'Steel-concrete composite structures : Stability and strength', Elsevier Applied Science, London, 1988

108. Nash, W.A., : 'Schaum's outline of theory and problems of strength of materials', McGraw Hill, London, 1972

109. Neville, A.M. : 'Properties of concrete', 4th Edition, Longman, London, 1995

110. Ohanian, H.C. : 'Physics', 2nd Edition, Norton, London, 1989

111. Ottosen, N.S., Petersson, H. : 'Introduction to the finite element method', Prentice Hall, London, 1992

112. Perry, S.H., Bischoff, P.H. : 'Measurement of the compressive impact strength of concrete using a thin loadcell', *Mag Concrete Res*, 1990, 42 (151), 75

113. Perry, S.H., Brown, I.C., Dinic, G. : 'Factors influencing the response of concrete slabs to impact', *Proceedings of the international conference and Exposition on Structural Impact and Crashworthiness*, (ed. Morton, J.) London, Elsevier Applied Science Publishers, 1984, Vol. 2, 617

114. Perry, S.H., Dinic, G. : 'Fender layer protection of sub-surface concrete caissons', *Behaviour of Offshore Structures, BOSS* (ed. Battjes, J.A.), Delft, 1985, 889

115. Pessiki, S., Pieroni, A. : 'Axial load behaviour of large-scale spirally-reinforced high-strength concrete columns', *Am Concr Inst Struct J*, 1997, 94 (3), 304

116. Popovics, S. : 'A numerical approach to the complete stress-strain curve of concrete', *Cement Concrete Res*, 1973, 3, 583

117. Prichard, S.J., Perry, S.H. : 'A comparison between experimental and predicted contact forces of confined concrete under impact', *Proceedings of the 9th International Symposium on the Interaction of the Effects of Munitions with Structures*, Berlin, May 1999, 355

118. Prichard, S.J., Perry, S.H. : 'Contact force response of confined concrete cylinders subjected to hard impact', *Conference on Abnormal Loading on Structures - Experimental and Numerical Modelling,* (Eds. Virdi, K.S., Matthews, R.S., Clarke, J.L., Garas, F.K.), E & FN Spon, London, 2000, 201

119. Rao, S.S. : 'The finite element method in engineering', 2nd Edition, Pergamon Press, Oxford, 1989

120. Razvi, S., Saatcioglu, M. : 'Confinement model for high strength concrete', *A.S.C.E J Struct Div*, 1999, 125 (3), 281

121. Razvi, S.R., Saatcioglu, M. : 'Strength and deformability of confined high strength concrete columns', *Am Concr Inst Struct J*, 1994, 91 (6), 678

122. Richart, F.B., Brandtzaeg, A., Brown, R.L. : 'A study of the failure of concrete under combined compressive stress', Bulletin No 185, Engineering Research Station, University of Illinois, 1928

123. Richart, F.B., Brandtzaeg, A., Brown, R.L. : 'The failure of plain and spirally reinforced concrete in compression', Bulletin No 190, Engineering Research Station, University of Illinois, 1929

124. Rieder, K.A., Mindess, S. : 'New test method to evaluate the impact behaviour of bi-axially confined concrete', *Mater Struct / Mater Constr*, 1998, 31, 669

125. Roeder, C.W., Cameron, B., Brown, C.B. : 'Composite action in concrete filled tubes', *A.S.C.E J Struct Div*, 1999, 125 (5), 477

126. Rosenberg, Z., Partom, Y., Keren, B. : 'Calibration of commercial manganin stress gauges under static uni-axial strain conditions', *Journal of applied physics*, 1983, 54 (5), 2824

127. Rosenberg, Z., Yaziv, D., Partom, Y. : 'Calibration of foil-like manganin gauges in planar shock wave experiments', *Journal of applied physics*, 1980, 51 (7), 3702

128. Ross, C.A., Tedesco, J.W., Kuennen, S.T. : 'Effects of strain rate on concrete strength', *Am Concr Inst Mat J*, 1995, 92 (1), 37

129. Ryan, C.A., Broderick, B.M., West, R.P. : 'Performance of wireball reinforced concrete under seismic loading conditions', *CONSEC Conference*, Vancouver, 2001 (to be published)

130. Saafi, M., Toutanji, H.A., Li, Z. : 'Behaviour of concrete columns confined with fiber reinforced polymer tubes', *Am Concr Inst Mat J*, 1999, 96 (4), 500

131. Saatcioglu, M., Razvi, S.R. : 'Strength and ductility of confined concrete', *A.S.C.E J Struct Div*, 1992, 118 (6), 1590

132. Sargin, M., Ghosh, S.K., Handa, V.H. : 'Effects of lateral reinforcement upon the strength and deformation properties of concrete', *Mag Concrete Res*, 1971, 23 (75-76), 99

133. Sauer, M. : 'Simulation of dynamic material behaviour using a hybrid (mesh based/meshless) numerical method', *Proceedings of the 9th International Symposium on the Interaction of the Effects of Munitions with Structures*, Berlin, May 1999, 475

134. Schneider, S.P. : 'Axially loaded concrete-filled steel tubes', *A.S.C.E J Struct Div*, 1998, 124 (10), 1125

135. Sen, H.K., Chapman, J.C., Neogi, P.K. : 'Concrete filled tubular steel columns - triaxial effects in circular stub columns under concentric loading', *Construction Research Industry, Technical Note 39*, London, 1972

136. Shams, M., Saadeghvaziri, M.A. : 'Nonlinear response of concrete-filled steel tubular columns under axial loading', *Am Concr Inst Struct J*, 1999, 1009

137. Shams, M., Saadeghvaziri, M.A. : 'State of the art of concrete filled tubular columns', *Am Concr Inst Struct J*, 1997, 94 (5), 558

138. Sheikh, S.A., Toklucu, M.T. : 'Reinforced concrete columns confined by circular spirals and hoops', *Am Concr Inst Struct J*, 1993, 90 (5), 542

139. Somes, N.F. : 'Compression tests on hoop-reinforced concrete', *A.S.C.E J Struct Div*, 1970, 96 (ST7), 1495

140. Sonoda, Y., Hikosaka, H., Matsuba, Y. : 'Basic study on the effect of shock absorber by the one dimensional stress wave analysis', *3rd Asia Pacific conference on Shock and Impact Loads on Structures*, (eds. Lok, T.S., Lim, C.H.) Singapore, 1999, 445

141. Sparks, P.R., Menzies, J.B. : 'The effect of rate of loading upon the static and fatigue strengths of plain concrete in compression', *Mag Concrete Res*, 1973, 25 (83), 73

142. Spelce, T., Hallquist, J.O. : 'TAURUS : An interactive post-processor for the analysis codes NIKE3D, DYNA3D AND TOPAZ3D', Lawrence Livermore National Laboratory, Report UCRL-105401, 1991

143. Spooner, D.C. : 'Stress-strain-time relationships for concrete', *Mag Concrete Res*, 1971, 23 (75-76), 127

144. Stillman, D.W., Hallquist, J.O. : 'INGRID : A three-dimensional mesh generator for modelling nonlinear systems', Lawrence Livermore National Laboratory, Report UCID-20506, 1985

145. Suaris, W., Shah, S.P. : 'Constitutive model for dynamic loading of concrete', *A.S.C.E J Struct Div*, 1985, 111 (3), 563

146. Suaris, W., Shah, S.P. : 'Mechanical Properties of Materials Subjected to Impact', *RILEM-CEB-IABSE-IASS Interassociation Symposium on Concrete Structures under*

Impact and Impulsive Loading, (ed. Plauk, G.) Berlin, BAM,, *Introductory Report*, 1982, 33

147. Suaris, W., Shah, S.P. : 'Rate sensitive damage theory for brittle solids', *A.S.C.E. J Eng Mech Div*, 1984, 110 (6), 985

148. Sundra Raja Iyengar, K.T., Desayi, P., Nagi Reddy, K.N. : 'Stress-strain characteristics of concrete confined in steel binders', *Mag Concrete Res*, 1970, 22 (72), 173

149. Tang, T., Malvern, L.E., Jenkins, D.A. : 'Rate effects in uni-axial dynamic compression of concrete', *A.S.C.E. J Eng Mech Div*, 1992, 118 (1), 108

150. Teychenne, D.C. : 'Design of normal concrete mixes', Building Research Establishment, Department of the Environment, U.K., 1988

151. Timoshenko, S.P., Goodier, J.N. : 'Theory of elasticity', McGraw-Hill, Singapore, 1970

152. Toutanji, H.A. : 'Stress-strain characteristics of concrete columns externally confined with advanced fiber composite sheets', *Am Concr Inst Mat J*, 1999, 96 (3), 397

153. Van Mier, J.G.H., Pruijssers, A.F., Reinhardt, H.W., Morrier, T. : 'Load-time response of colliding concrete bodies', *A.S.C.E J Struct Div*, 1991, 117 (2), 354

154. Viest, I.M., Colaco, J.P., Furlong, R.W., Griffis L.G., Leon, R.T., Wyllie, L.A. : 'Composite construction - design for buildings', American Society of Civil Engineers, 1997

155. Virdi, K.S., Dowling, P.J. : 'Bond strength in concrete-filled steel tubes', *IABSE Symposium, Periodica* 3/1980, 1980, 125

156. Vos, E., Reinhardt, H.W. : 'Influence of loading rate on bond in reinforced steel', *RILEM-CEB-IABSE-IASS Interassociation Symposium on Concrete Structures under Impact and Impulsive Loading*, (ed. Plauk, G.) Berlin, BAM, 1982, 170

157. Warnock, F.V. : 'Strength of Materials', Pitman, London, 1958

158. Whirley, R.G., Hallquist, R.G. : 'DYNA3D A non-linear, explicit, three-dimensional finite element code for solid and structural mechanics - User manual', Lawrence Livermore National Laboratory, Report UCRL-MA-107254, 1991

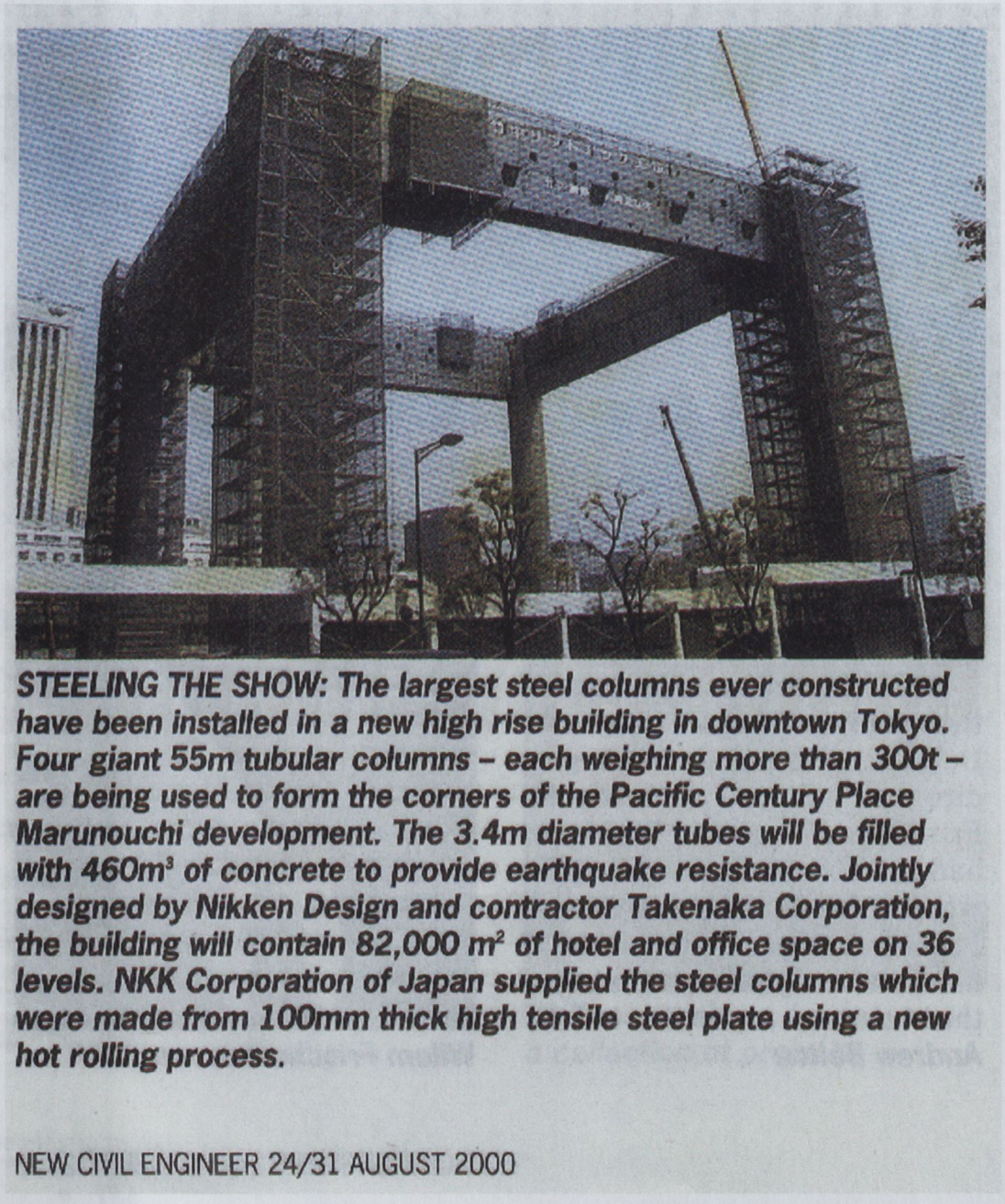
159. Zhong, Z-H. : 'Finite element procedures for contact impact problems', Oxford University Press, Oxford, 1993

160. Zienkiewicz, O.C., Taylor, R.L. : 'The finite element method', McGraw Hill, London, 1989

161. Zukas, J.A. : 'Numerical simulation of high rate behaviour', *Shock and Impact on Structures*, (eds. Brebbia, C.A., Sanchez-Galvez, V.), Computational Mechanics Publication, Southampton, 1994, 1

162. Zukas, J.A., Nicholas, T., Swift, H.F., Greszczuk, L.B., Curran, D.R. : 'Impact Dynamics', Wiley Interscience Publication, New York, 1982

APPENDIX 1. CONCRETE COMPOSITE COLUMNS - APPLICATION



STEELING THE SHOW: The largest steel columns ever constructed have been installed in a new high rise building in downtown Tokyo. Four giant 55m tubular columns – each weighing more than 300t – are being used to form the corners of the Pacific Century Place Marunouchi development. The 3.4m diameter tubes will be filled with 460m³ of concrete to provide earthquake resistance. Jointly designed by Nikken Design and contractor Takenaka Corporation, the building will contain 82,000 m² of hotel and office space on 36 levels. NKK Corporation of Japan supplied the steel columns which were made from 100mm thick high tensile steel plate using a new hot rolling process.

NEW CIVIL ENGINEER 24/31 AUGUST 2000

Figure A1.1 Real application for steel composite columns - on a large scale

From New Civil Engineer, 24/31 August 2000

APPENDIX 2. MATERIAL PROPERTIES OF THE CONFINING SLEEVES

Tensile tests were performed on samples of the material which formed each of the different types of sleeves used to confine the concrete during the experimental work. These tests were performed in accordance with the relevant British Standards. In the case of the metal sleeves, BS EN 10002-1 : 1990 was used, whereas the plastic sleeves were tested in accordance with BS 2782:Part 3:Method 320:1976, BS 2782:Part 3:Method 321:1993 and BS 2782:Part 11:Method 1110:1989.

Dog-bone shaped coupons were cut from each of the cylinders, or the sheet metal, adjacent to the sections from which the sleeves were fabricated, in accordance with the codes. The dimensions in the dog-bone coupons depended on the thickness of the pipe from which the piece was cut and were, therefore, different for each material. Three pieces were cut from each of the metal tubes, and five were cut from the plastic tube.

All of the coupons were tested to failure in a calibrated tensile testing machine, at a rate of 6 $N/mm^2 \cdot sec$. Each of the coupons were gauged laterally and axially in the mid-section to allow the elastic properties of the material to be determined. Similarly, the load which the machine applied was measured which was used to determine the stresses in the cross section of the coupon. The results of the tests, both the stress-strain results and the axial strain/lateral strain results, are shown for each of the types of specimen in Figure A2.1 to Figure A2.7 below. Only two results are shown from each because, of the three coupons tested, one of each of the groups failed outside the gauge length and the test was, therefore, deemed invalid.

The elastic material properties were then calculated in accordance with Warnock (1958).

- The Young's modulus was determined as being the slope of the linearly elastic section of the stress/strain graph, and the value determined was the average of the two results measured. The calculated value was rounded to the nearest 5 kN/mm^2, in all cases except the plastic.
- The materials tested did not have clearly defined elastic limits or yield strength. In the case of the plastic coupon, the material began to yield as soon as it was loaded. However, in the case of the metallic materials the 2 % offset value was

used in the determination of the yield strength. A line was drawn, parallel to the straight line portion of the loading curve, through the 2 % offset and the yield strength was determined at the point at which this curve crossed the stress-strain curve. This line and the yield points for each of the curves are clearly shown in the figures. The calculated yield strength was rounded to the nearest 5 N/mm^2.

- Poisson's ratio was determined by plotting the results of the lateral gauge against those for the axial gauge, for the linear portion of the graph. These plots are also shown in the figures below. Poisson's ratio was determined as the average of the two values measured, and is given to two places of decimals.

The density of the sleeves was determined using the water displacement technique. The coupons were weighed in air using an electronic balance. They were then weighed when fully immersed in water. The volume of the coupon was determined by subtracting its weight in water from its weight in air and dividing by the density of water (1000 kg/m^3). The density of the material was calculated by dividing the mass of the coupon in air by the value calculated for its volume, and the value was rounded to the nearest 10 kg/m^3.

The values calculated for each of the material properties are given in Table 4.1, with the dimensions of each of the sleeves. The length and the thickness of each of the cylinders were determined by careful measurement using a callipers and a micrometer.

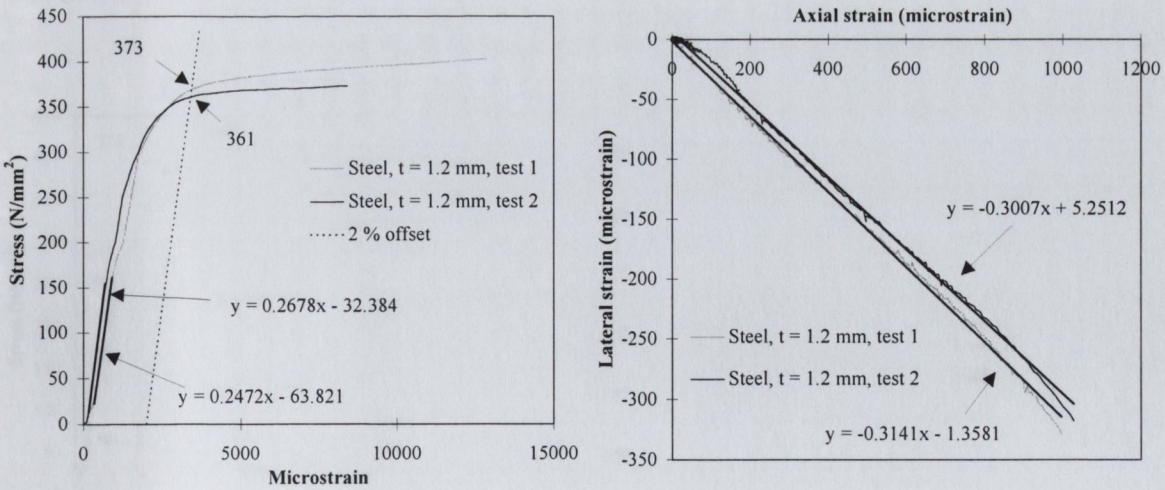


Figure A2.1 Young's modulus, yield strength and Poisson's ratio determination for 1.2 mm thick steel sheet

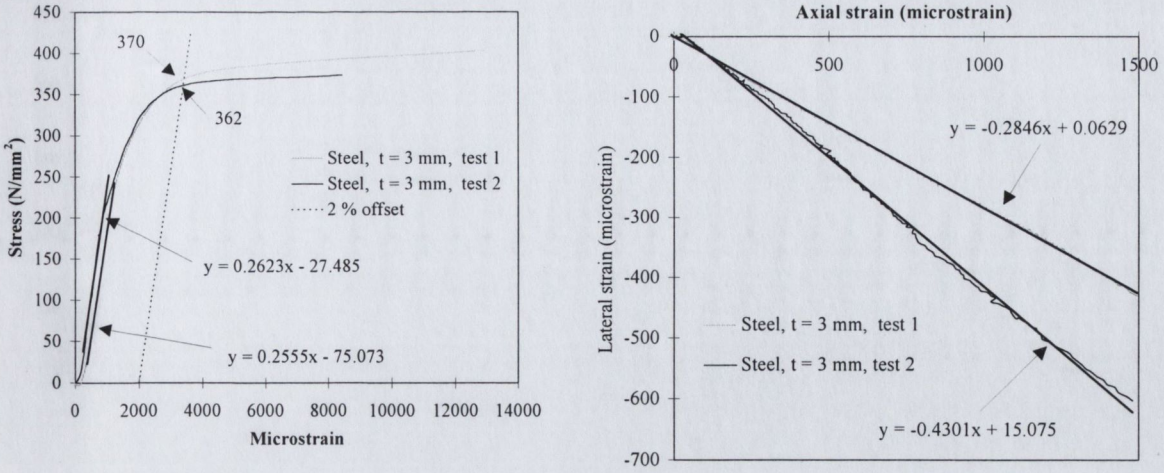


Figure A2.2 Young's modulus, yield strength and Poisson's ratio determination for 3 mm thick steel cylinder

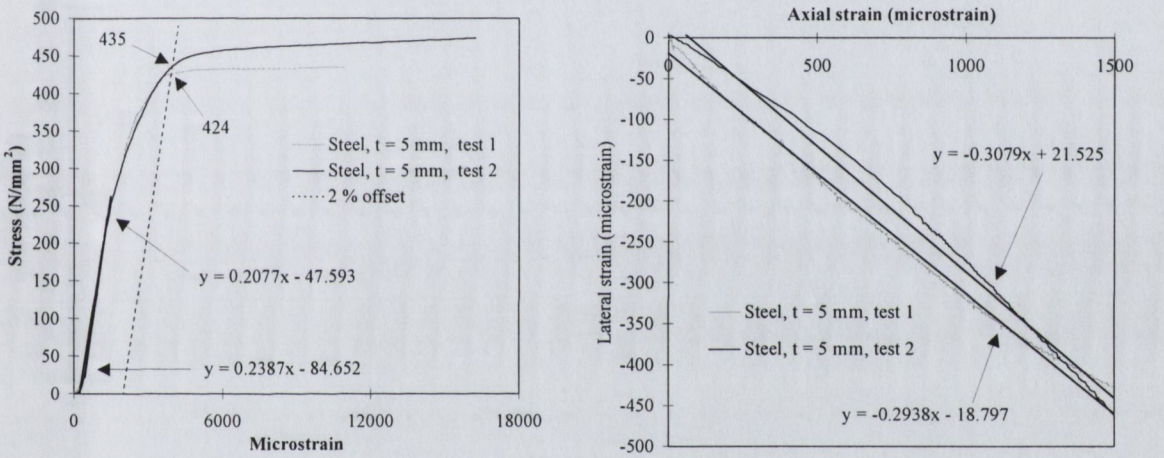


Figure A2.3 Young's modulus, yield strength and Poisson's ratio determination for 5 mm thick steel cylinder

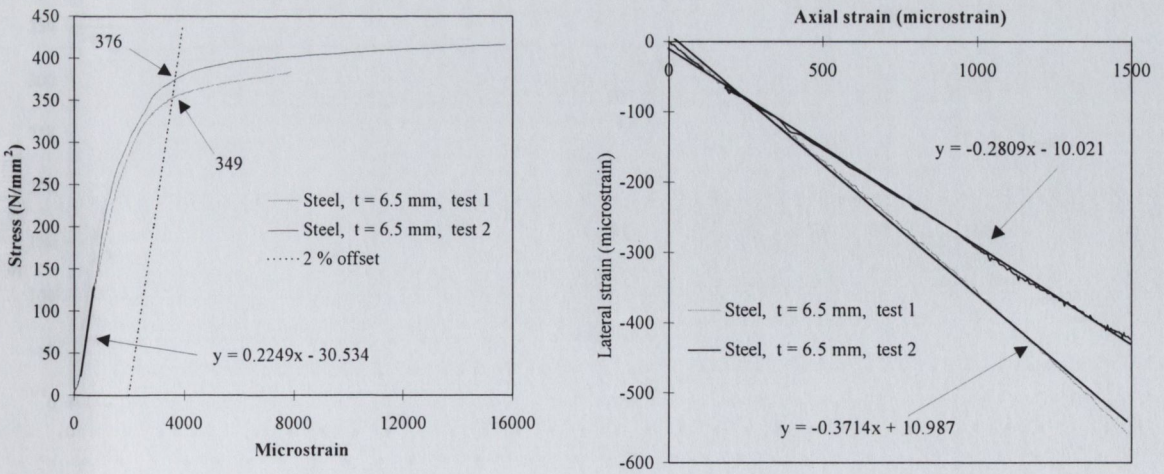


Figure A2.4 Young's modulus, yield strength and Poisson's ratio determination for 6.5 mm thick steel cylinder

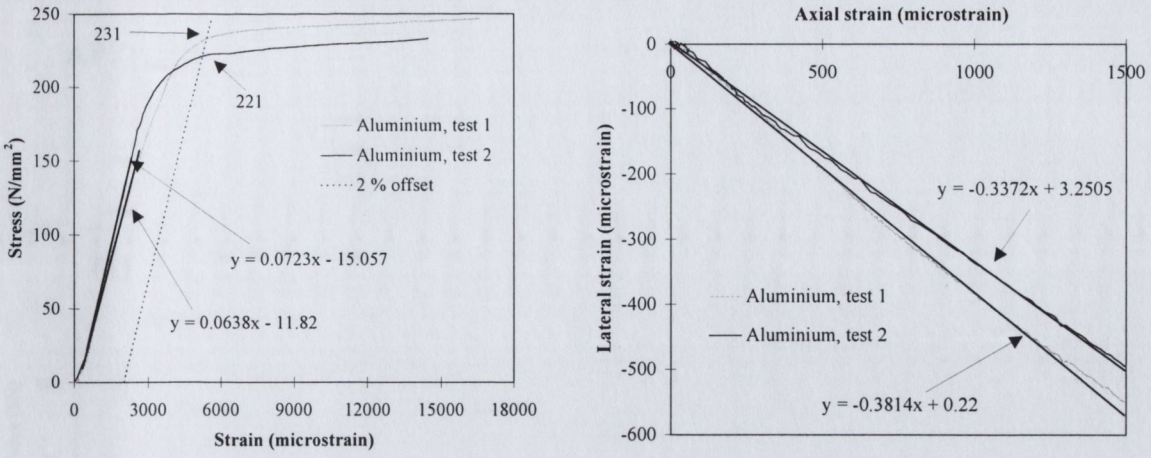


Figure A2. 5 Young's modulus, yield strength and Poisson's ratio determination for aluminium cylinder

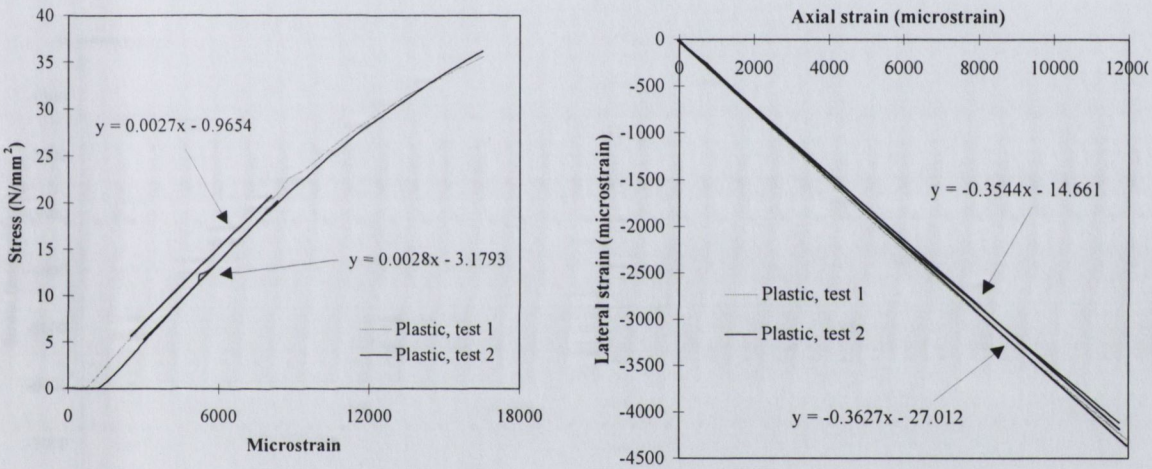


Figure A2. 6 Young's modulus, yield strength and Poisson's ratio determination for plastic cylinder

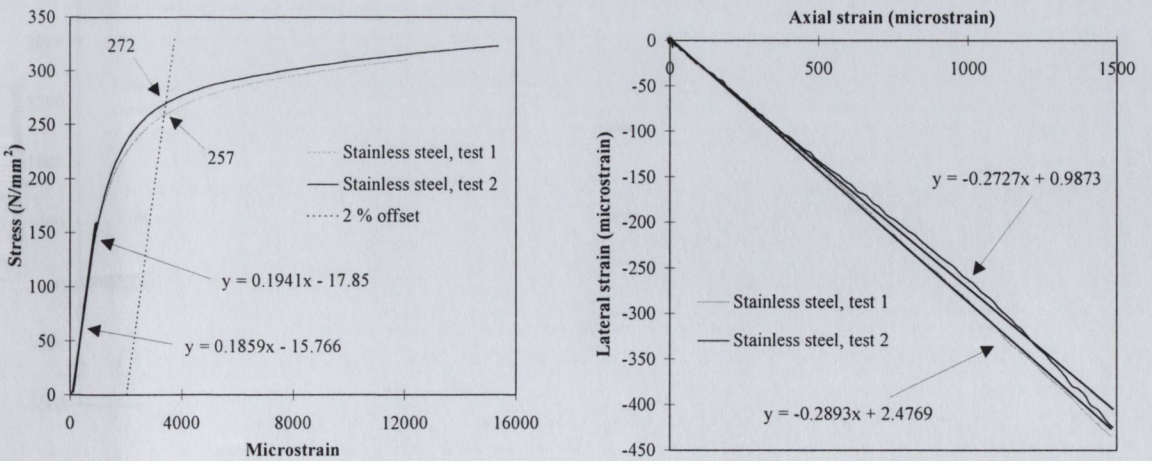


Figure A2.7 Young's modulus, yield strength and Poisson's ratio determination for 3 mm thick large diameter steel cylinder

APPENDIX 3.1. IMPACT RESPONSE OF UNCONFINED CONCRETE CYLINDERS

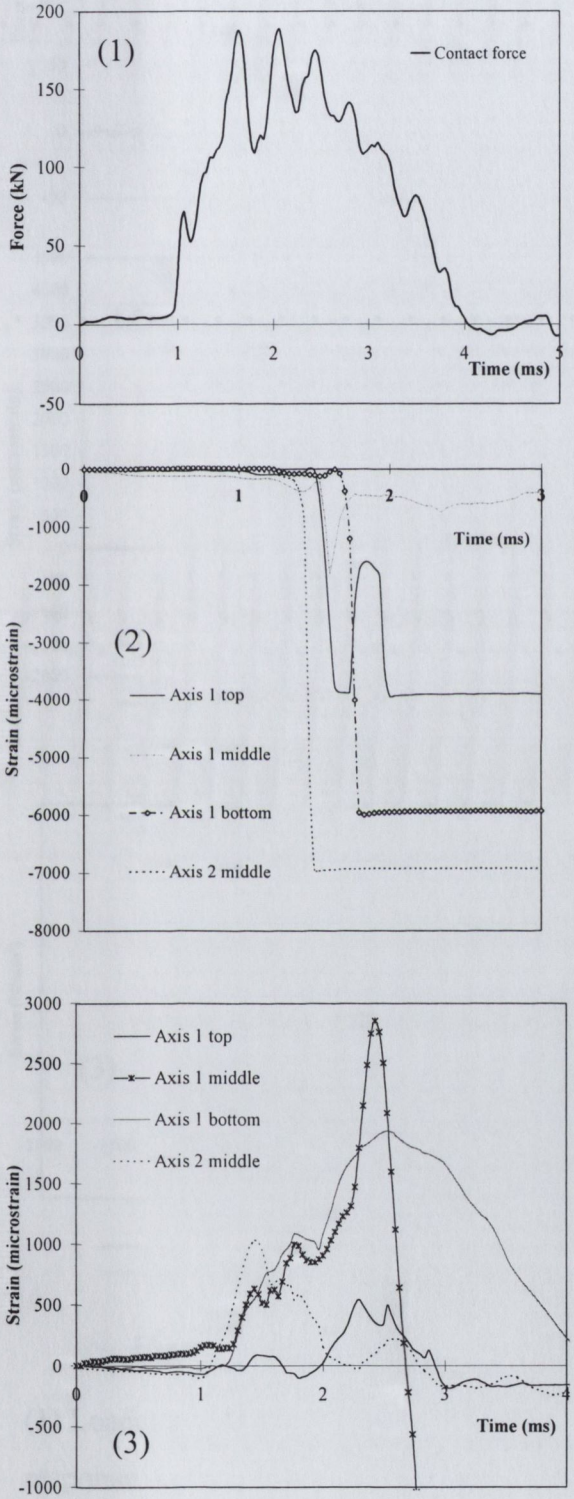


Figure A3.1 U(100)1a

(1) Loadcell response, (2) lateral strain gauge and (3) axial strain gauge response

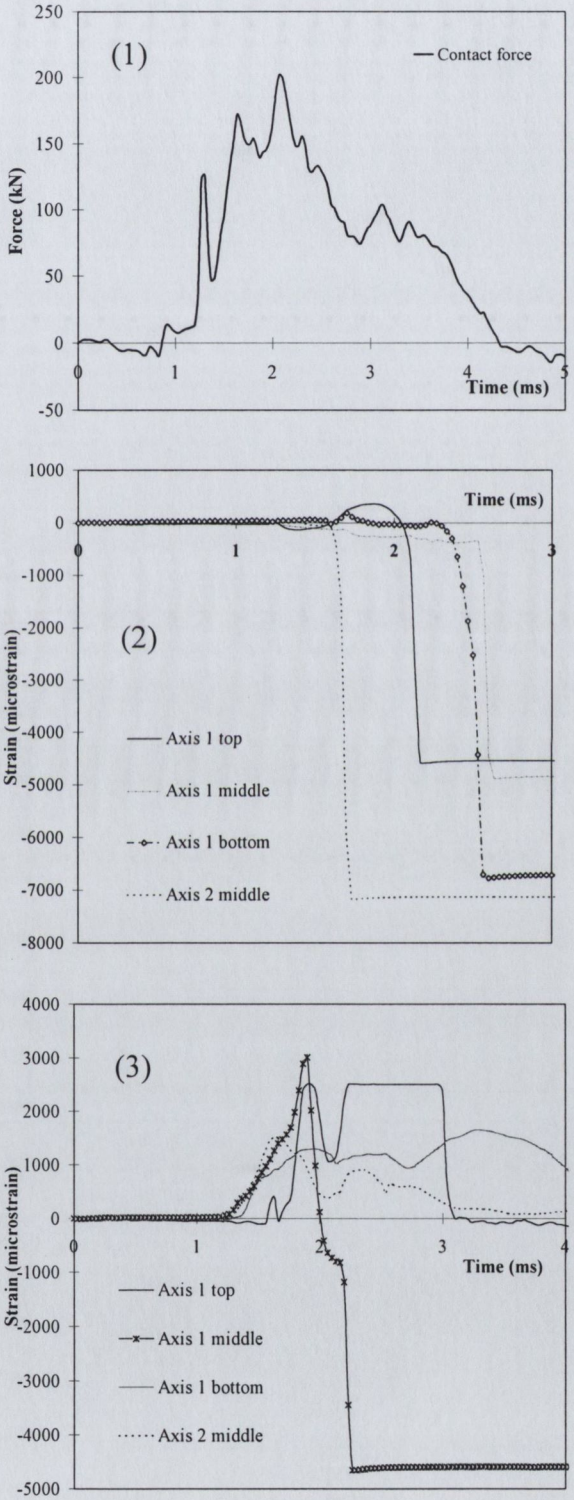
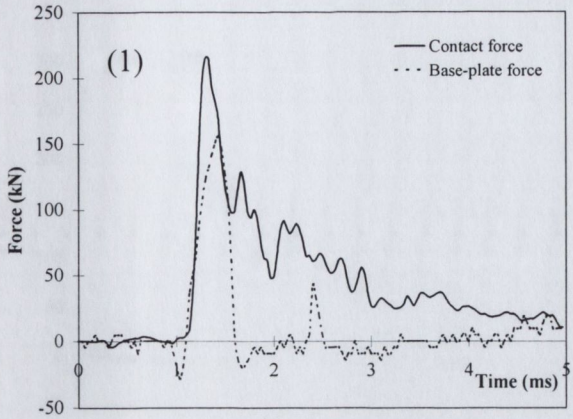
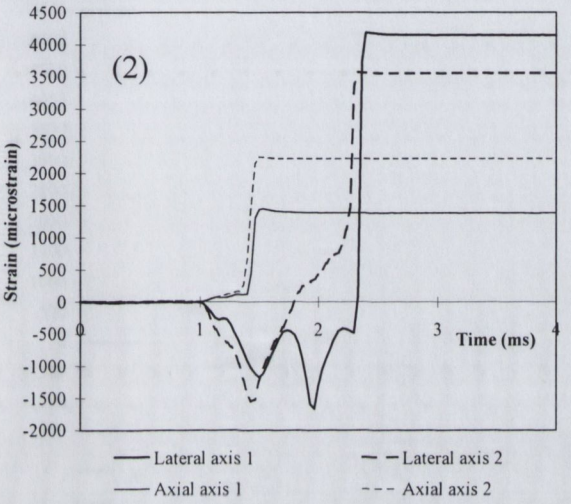


Figure A3.2 U(100)1b

(1) Loadcell response, (2) lateral strain gauge and (3) axial strain gauge response





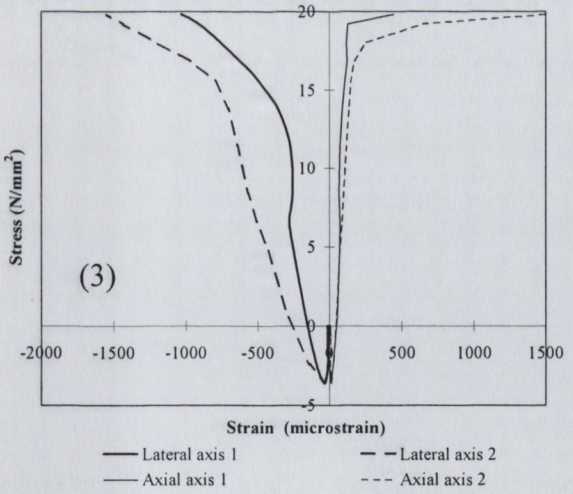
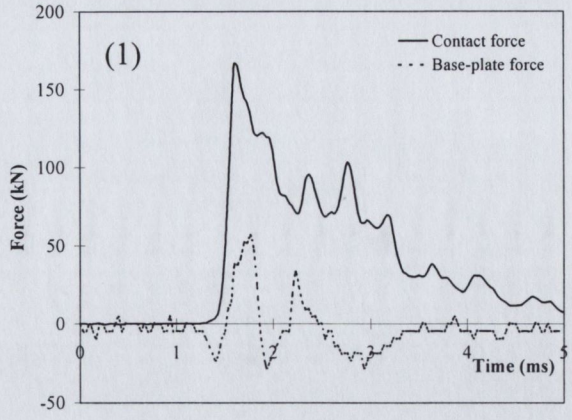
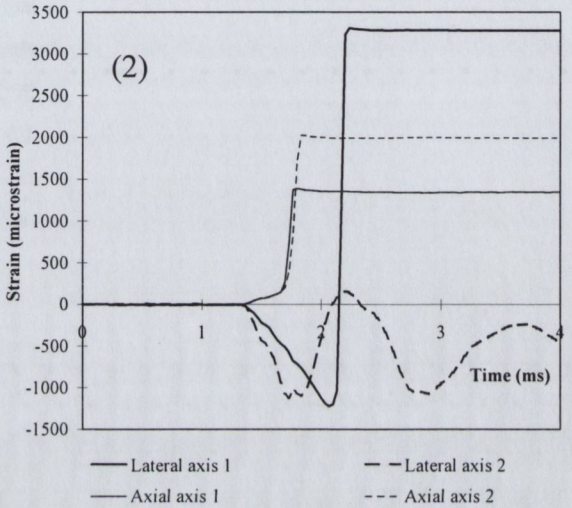


Figure A3.3 U(100)1c

(1) Loadcell response, (2) strain gauge response and (3) stress-strain response





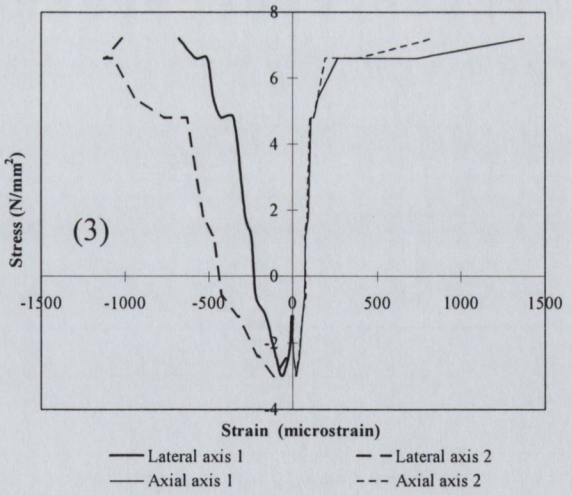
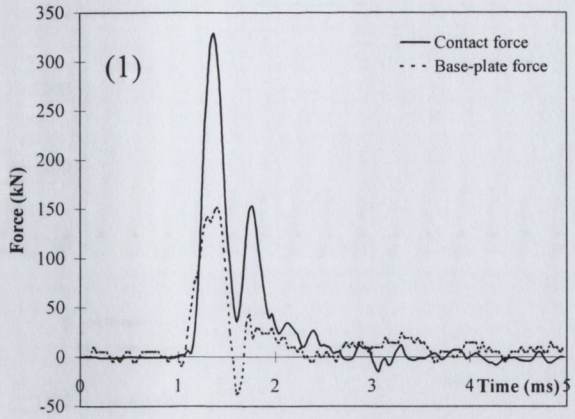
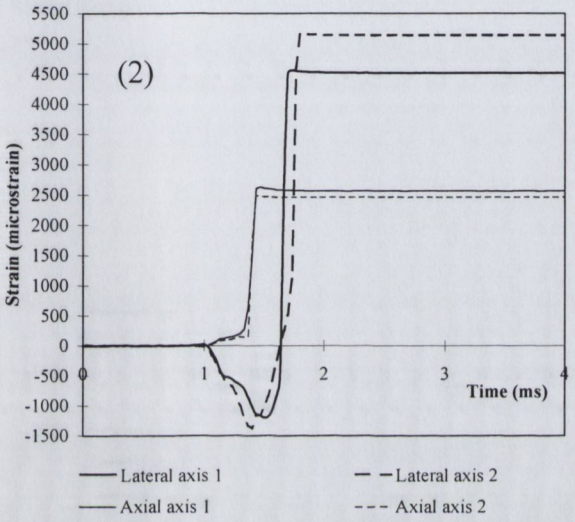


Figure A3.4 U(100)1d

(1) Loadcell response, (2) strain gauge response and (3) stress-strain response





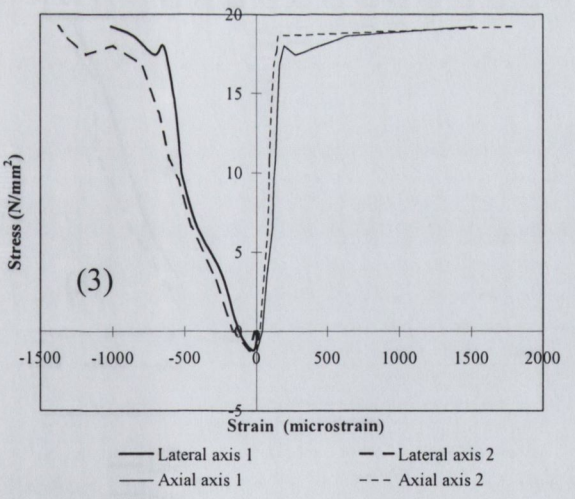
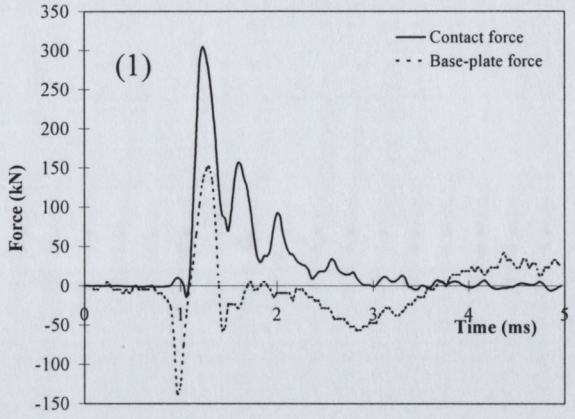
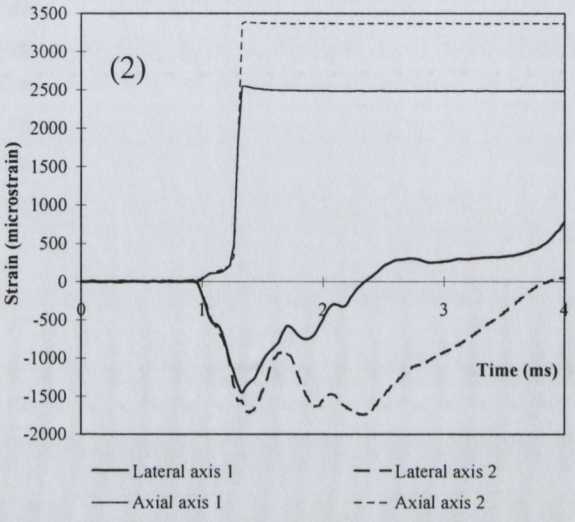


Figure A3.5 U(100)2a

(1) Loadcell response, (2) strain gauge response and (3) stress-strain response





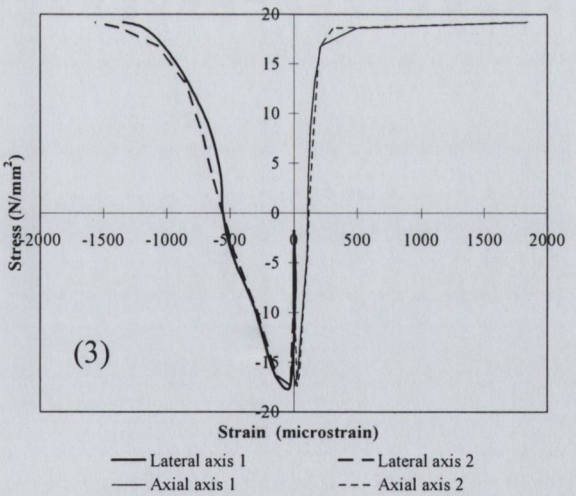


Figure A3.6 U(100)2b

(1) Loadcell response, (2) strain gauge response and (3) stress-strain response

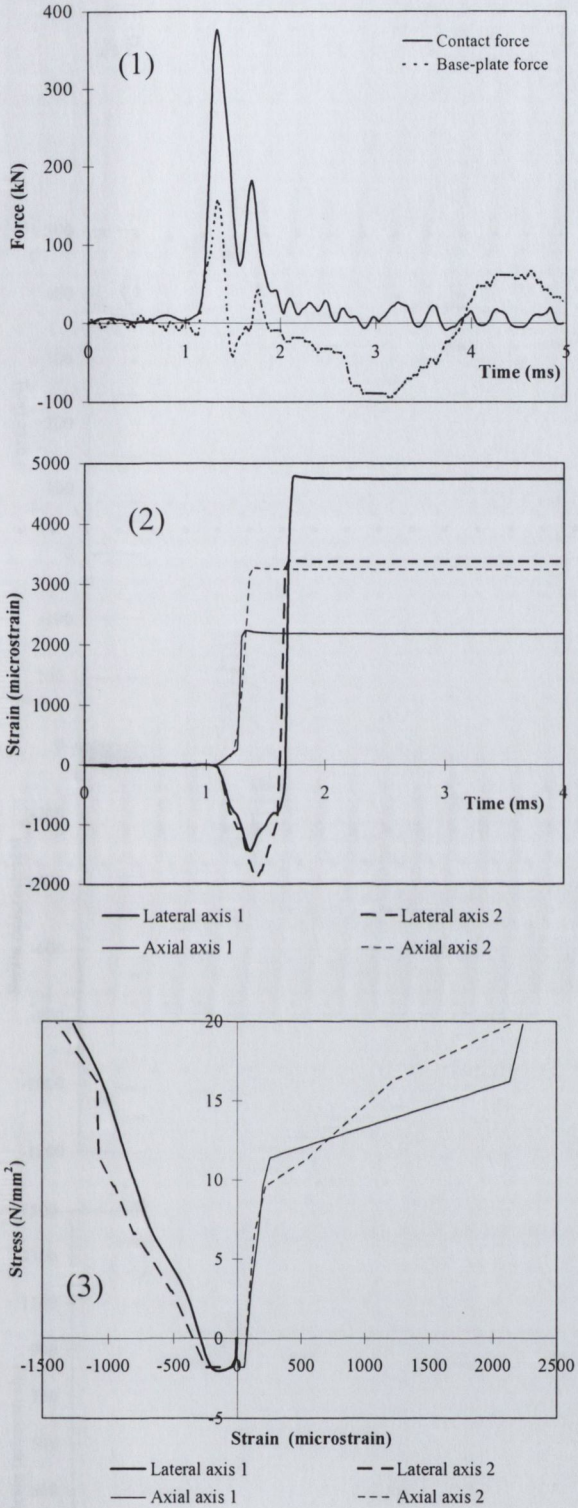


Figure A3.7 U(100)3a

(1) Loadcell response, (2) strain gauge response and (3) stress-strain response

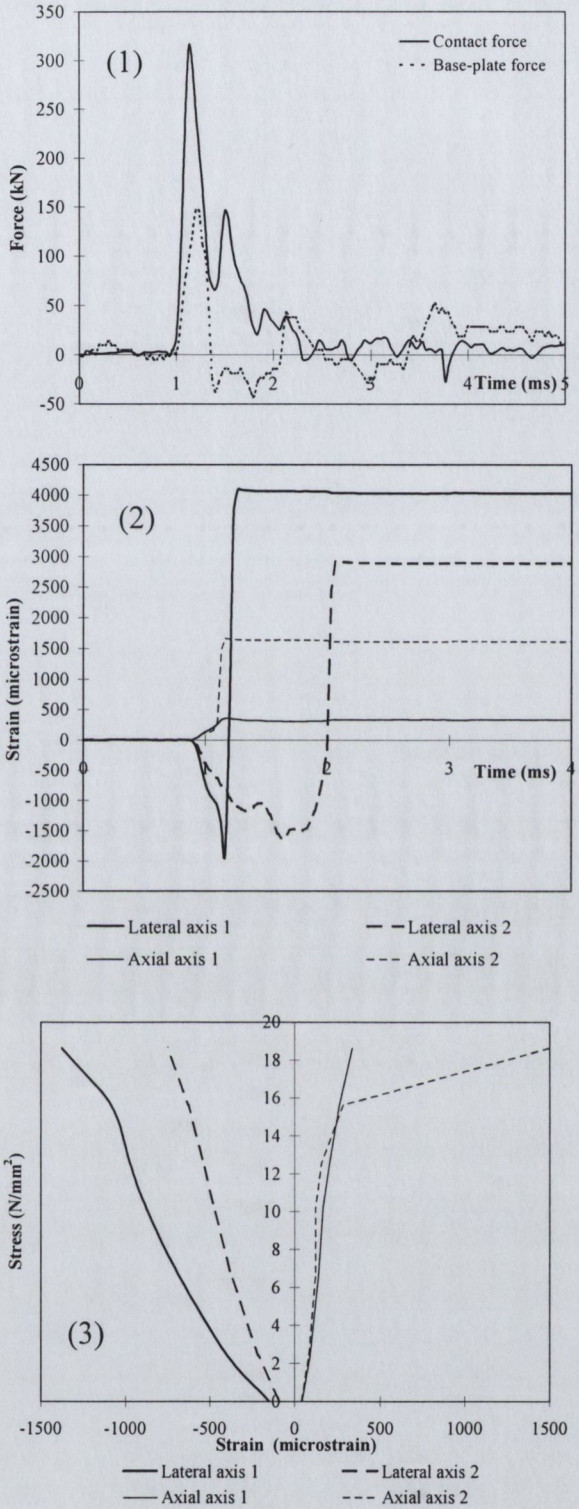


Figure A3.8 U(100)3b

(1) Loadcell response, (2) strain gauge response and (3) stress-strain response

APPENDIX 3.2. IMPACT RESPONSE OF SLEEVED CYLINDERS, 1.2 MM STEEL

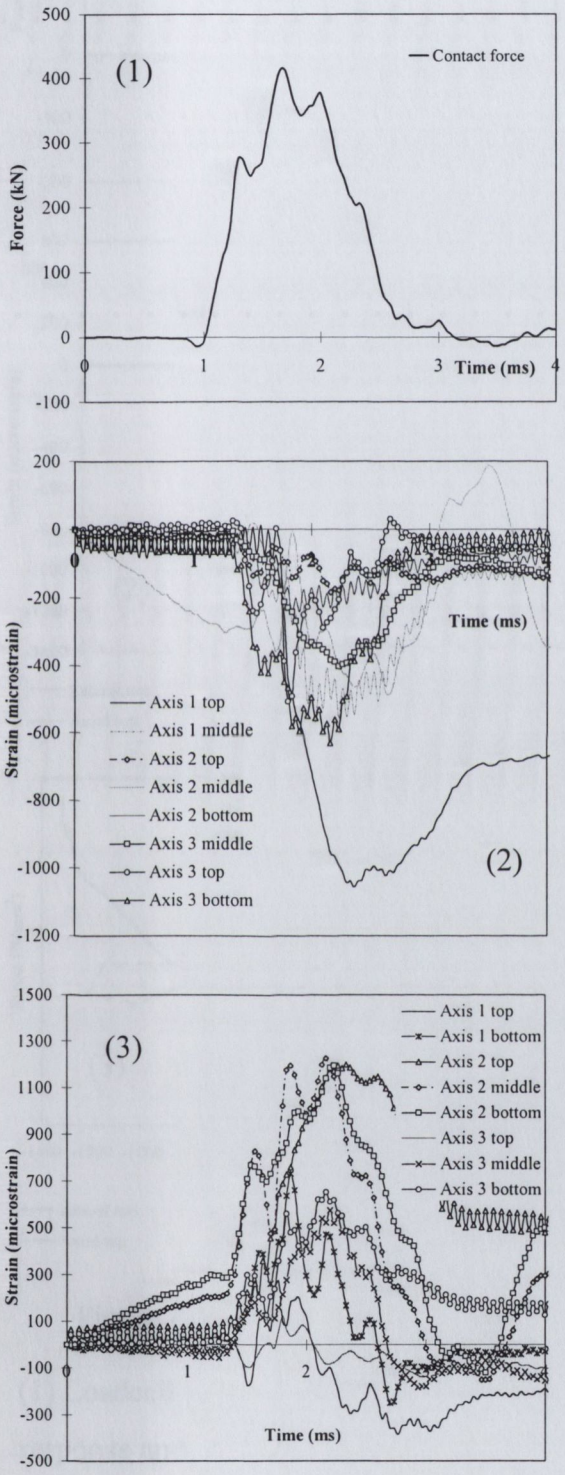


Figure A3.9 C(114)S (1.2)1a

(1) Loadcell response, (2) lateral strain gauge and (3) axial strain gauge response

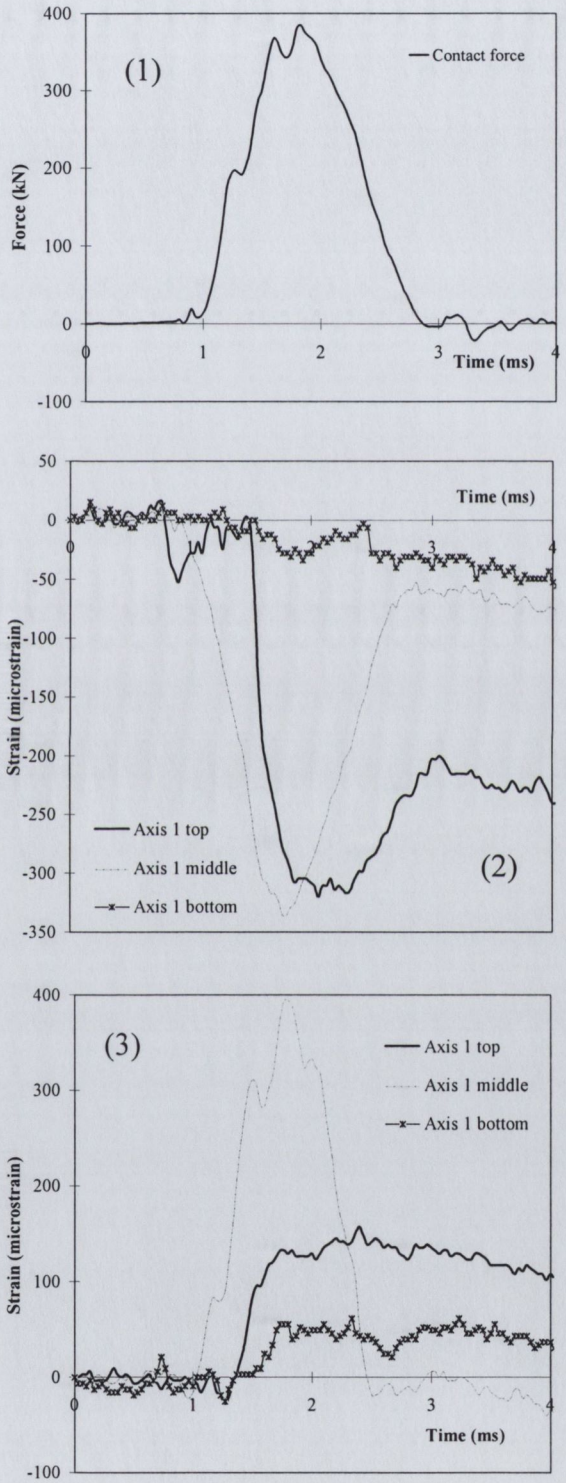


Figure A3.10 C(114)S (1.2)1b

(1) Loadcell response, (2) lateral strain gauge and (3) axial strain gauge response

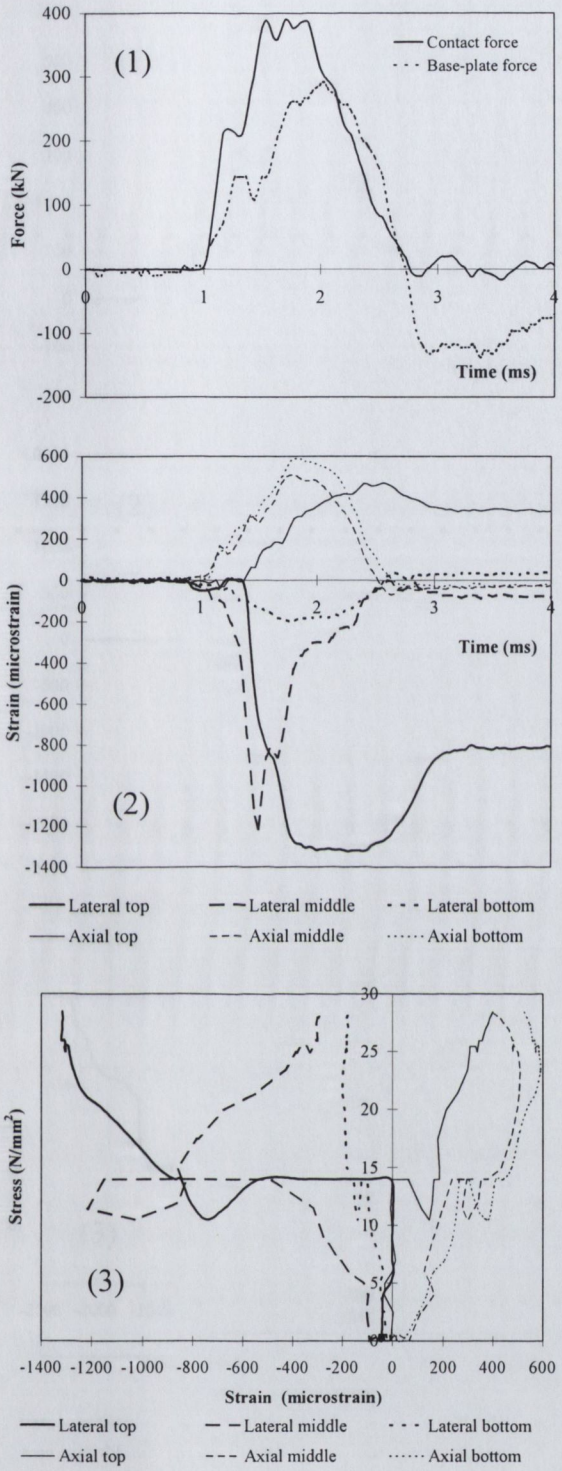


Figure A3.11 C(114)S (1.2)1c

(1) Loadcell response, (2) strain gauge response and (3) stress-strain response

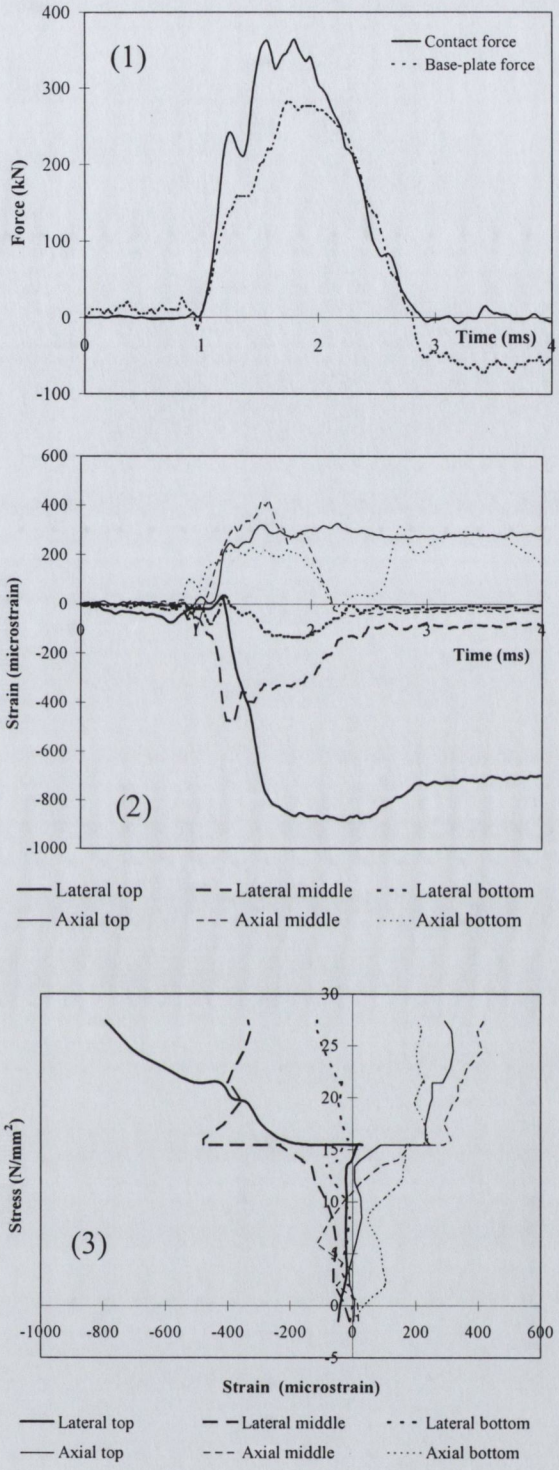


Figure A3.12 C(114)S (1.2)1d

(1) Loadcell response, (2) strain gauge response and (3) stress-strain response

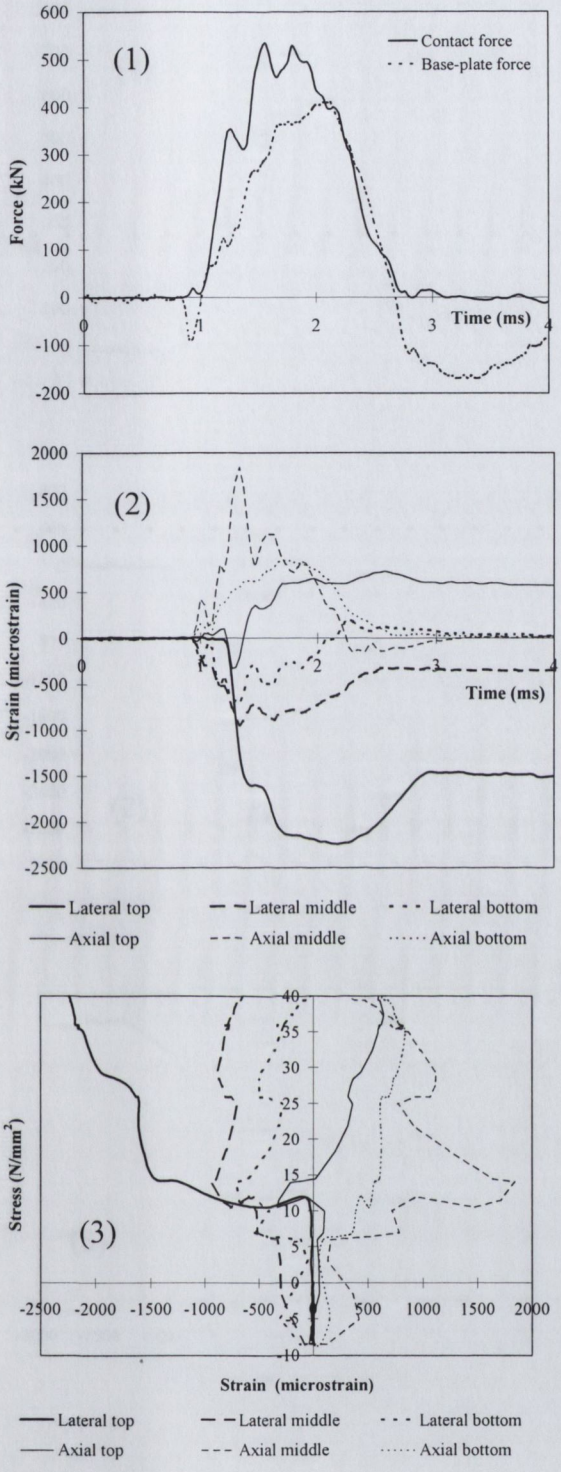


Figure A3.13 C(114)S (1.2)2a

(1) Loadcell response, (2) strain gauge response and (3) stress-strain response

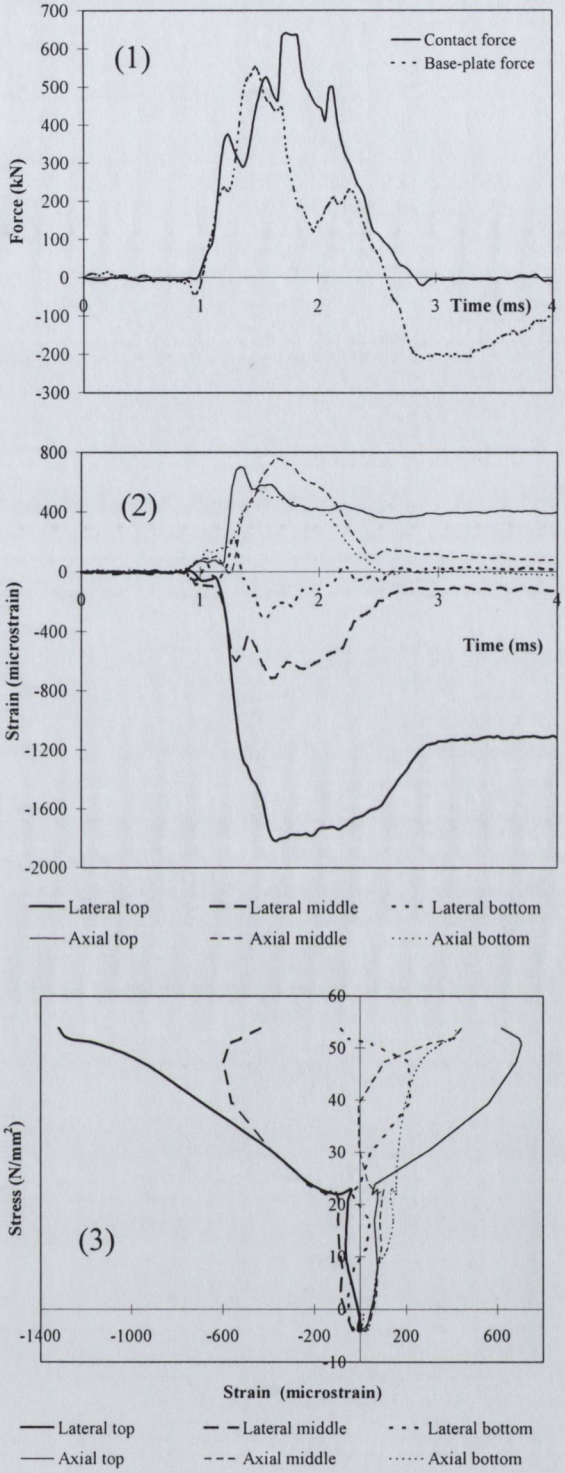


Figure A3.14 C(114)S (1.2)2b

(1) Loadcell response, (2) strain gauge response and (3) stress-strain response

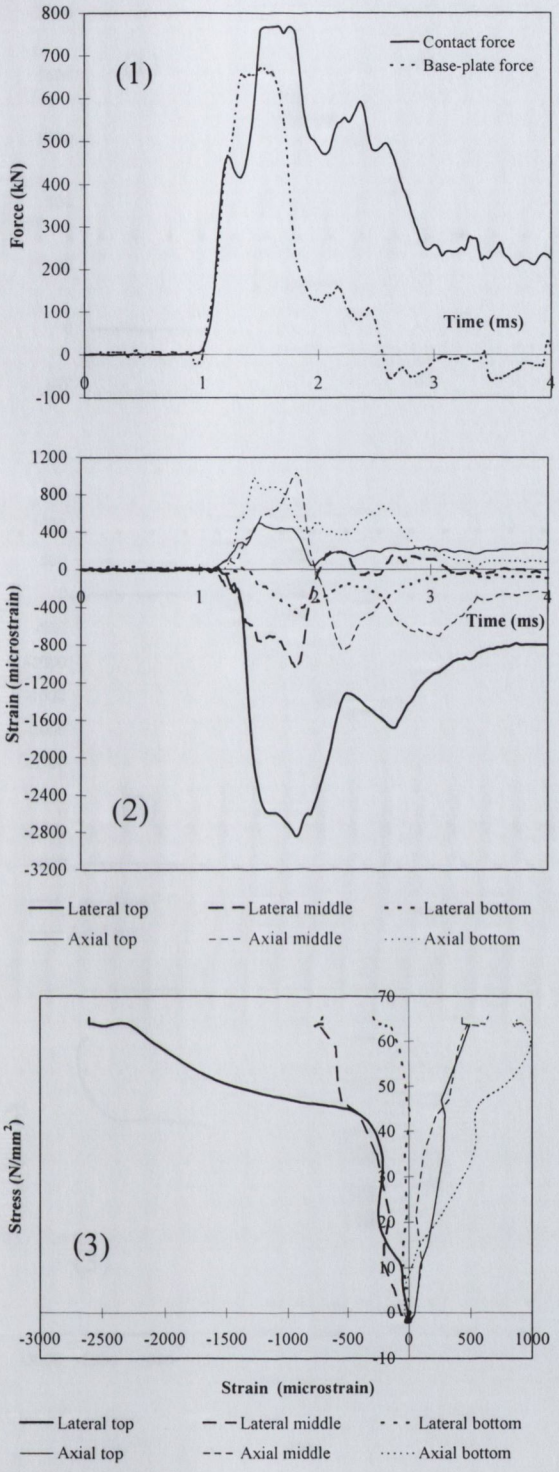


Figure A3.15 C(114)S (1.2)3a

(1) Loadcell response, (2) strain gauge response and (3) stress-strain response

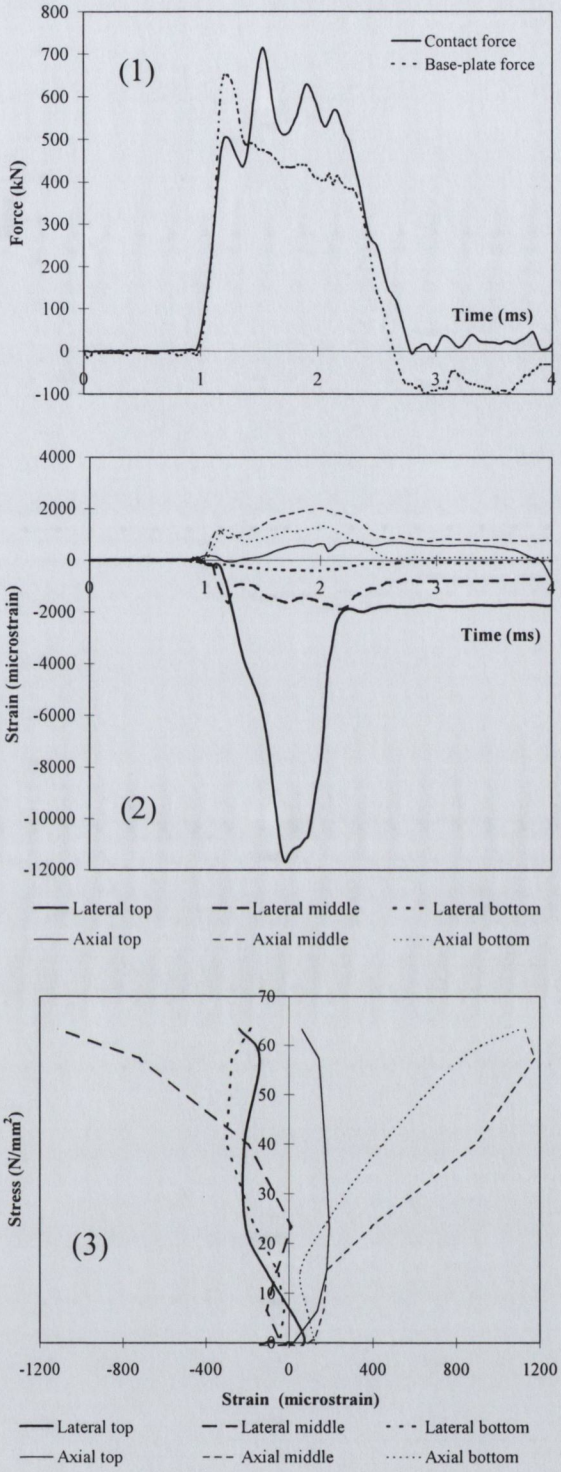


Figure A3.16 C(114)S (1.2)3b

(1) Loadcell response, (2) strain gauge response and (3) stress-strain response

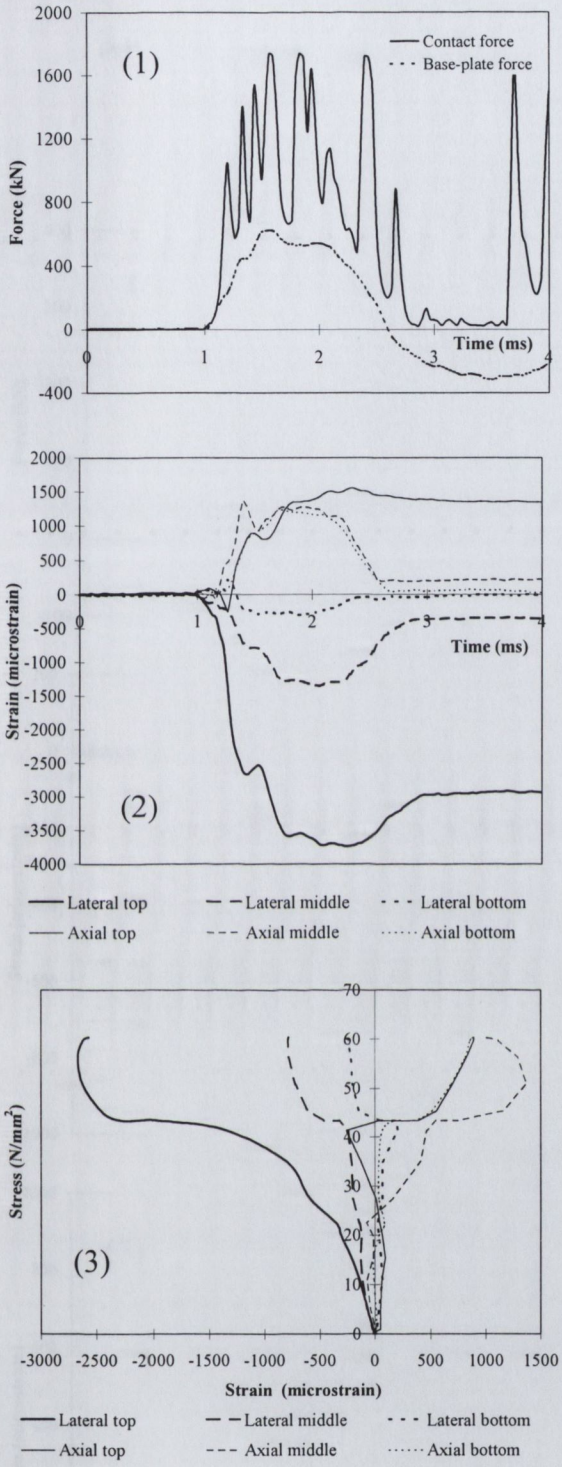


Figure A3.17 C(114)S (1.2)3c

(1) Loadcell response, (2) strain gauge response and (3) stress-strain response

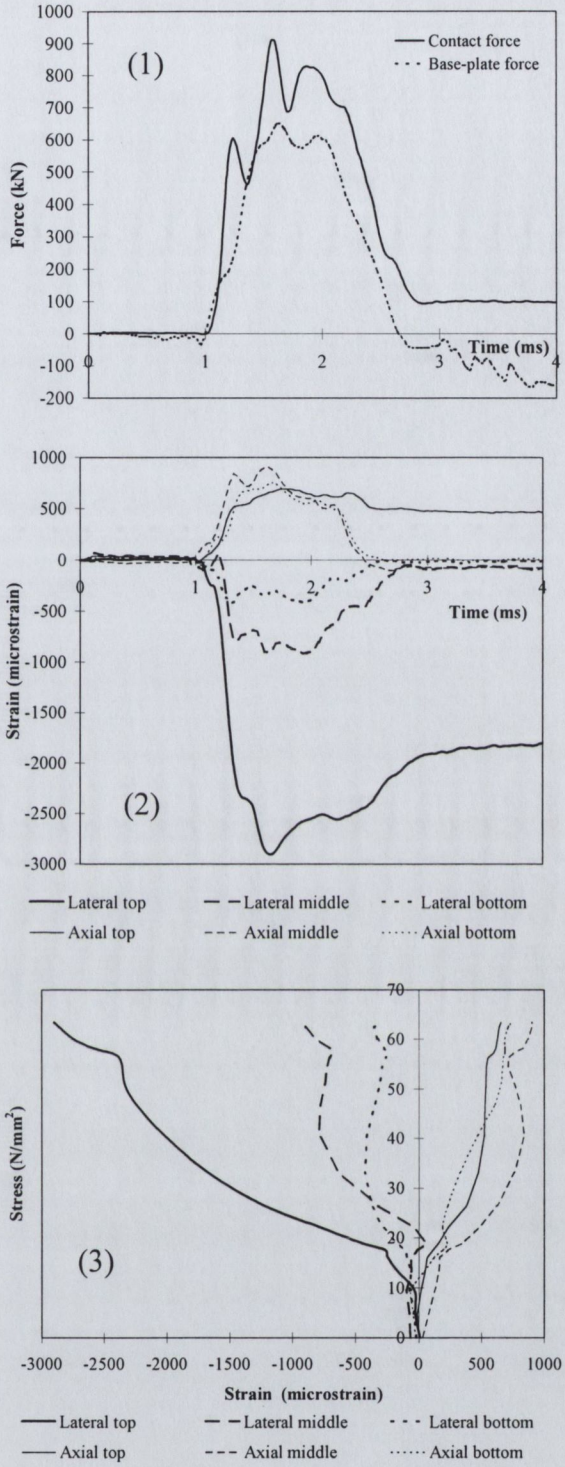


Figure A3.18 C(114)S (1.2)3d

(1) Loadcell response, (2) strain gauge response and (3) stress-strain response

APPENDIX 3.3. IMPACT RESPONSE OF SLEEVED CYLINDERS, 3 MM STEEL

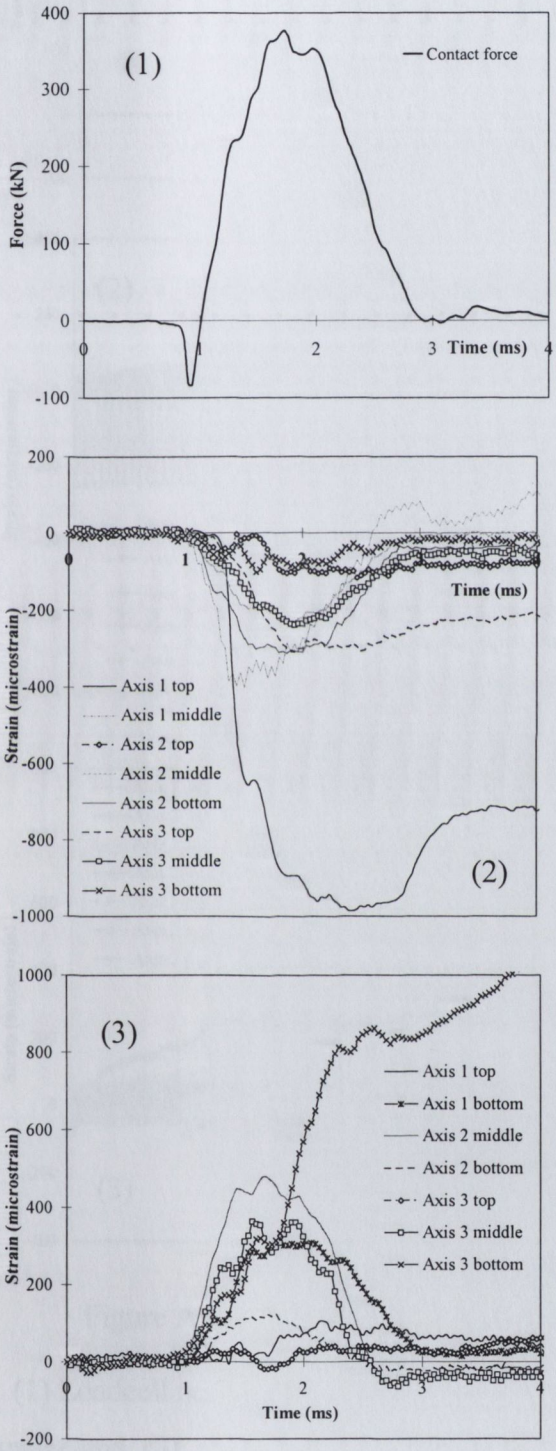


Figure A3.19 C(114)S (3)1a

(1) Loadcell response, (2) lateral strain gauge and (3) axial strain gauge response

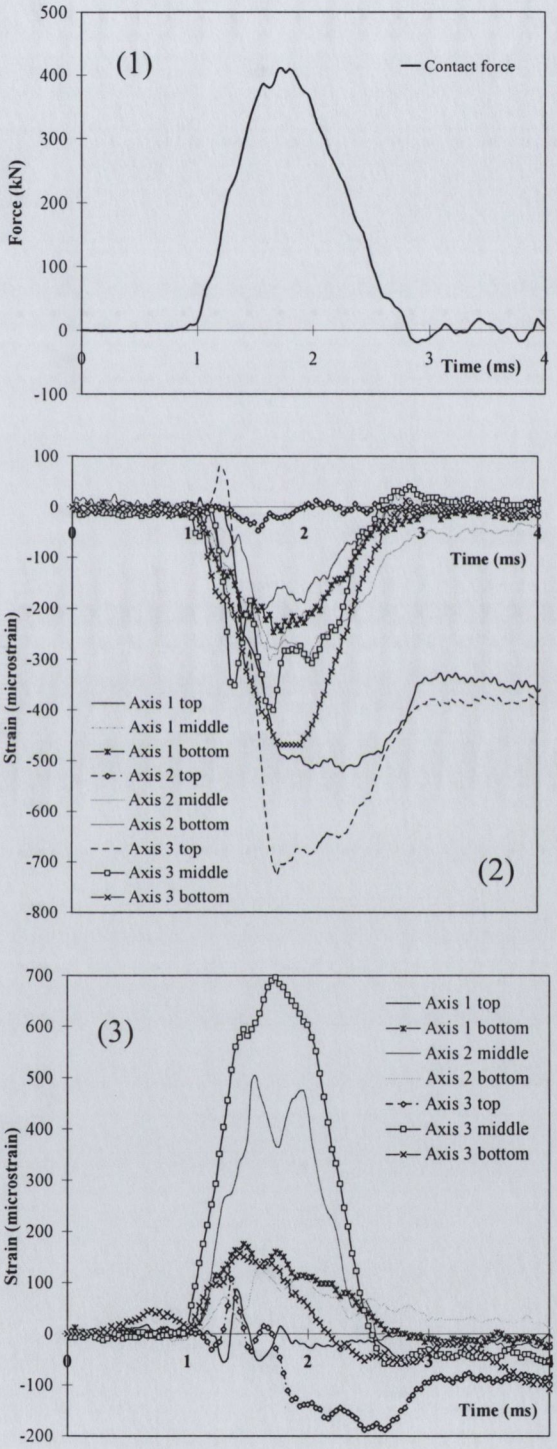


Figure A3.20 C(114)S (3)1b

(1) Loadcell response, (2) lateral strain gauge and (3) axial strain gauge response

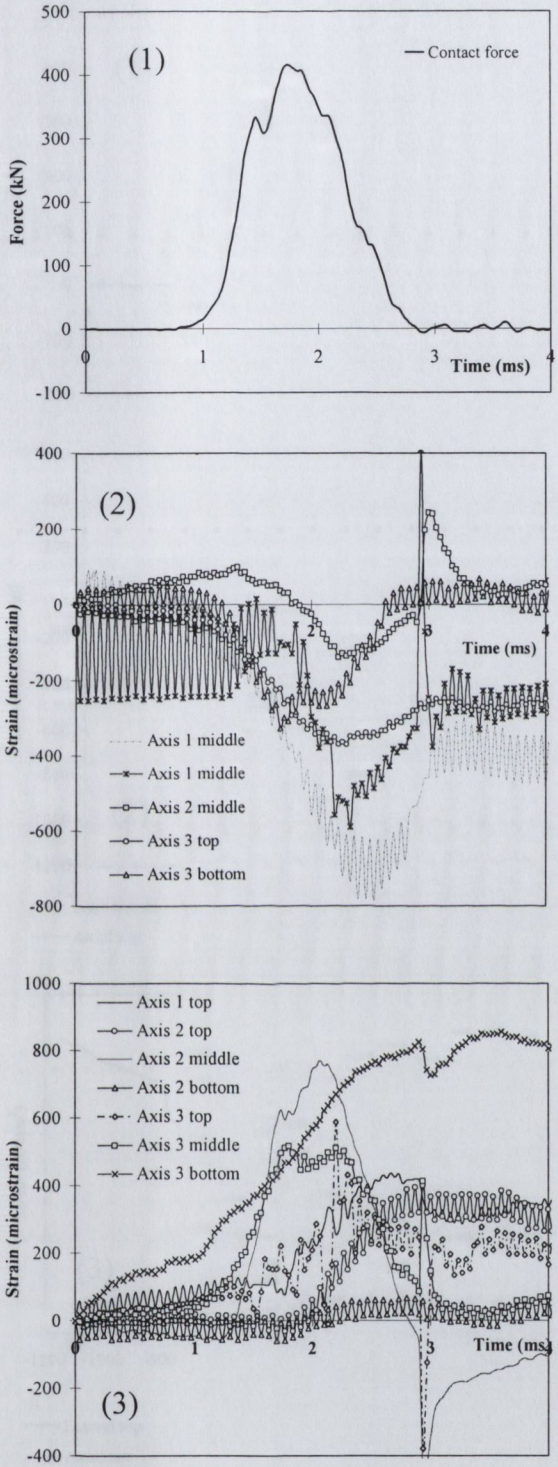


Figure A3.21 C(114)S (3)1c

(1) Loadcell response, (2) lateral strain gauge and (3) axial strain gauge response

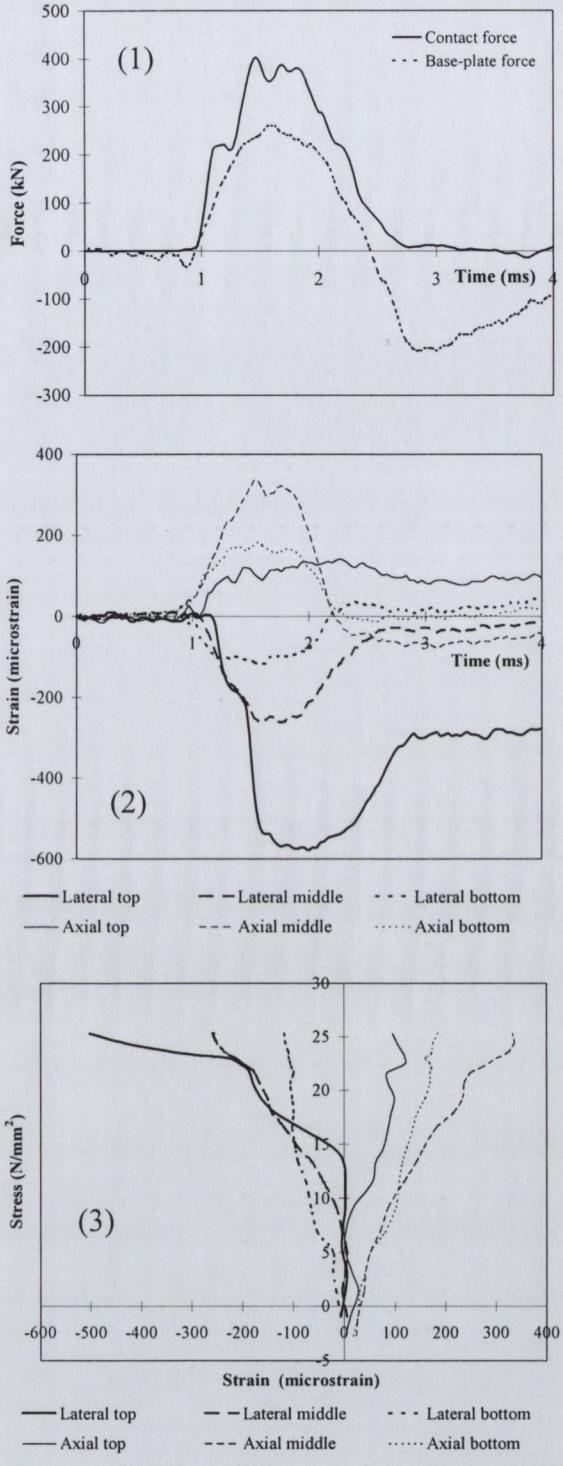


Figure A3.22 C(114)S (3)1d

(1) Loadcell response, (2) strain gauge response and (3) stress-strain response

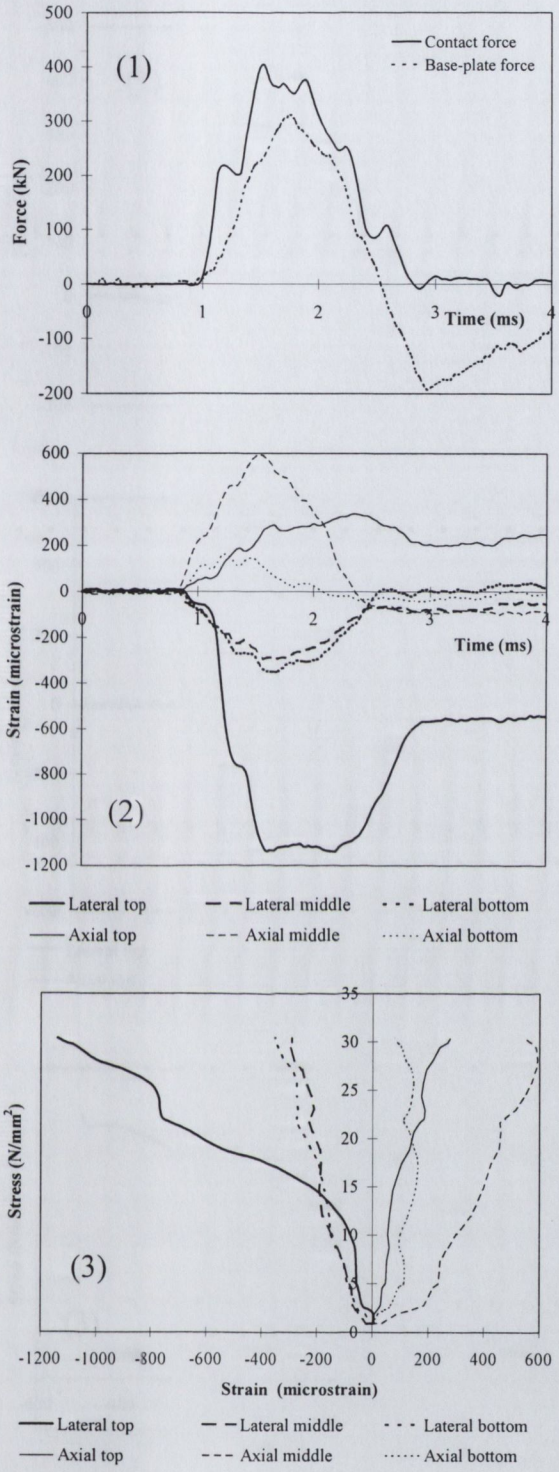


Figure A3.23 C(114)S (3)1e

(1) Loadcell response, (2) strain gauge response and (3) stress-strain response

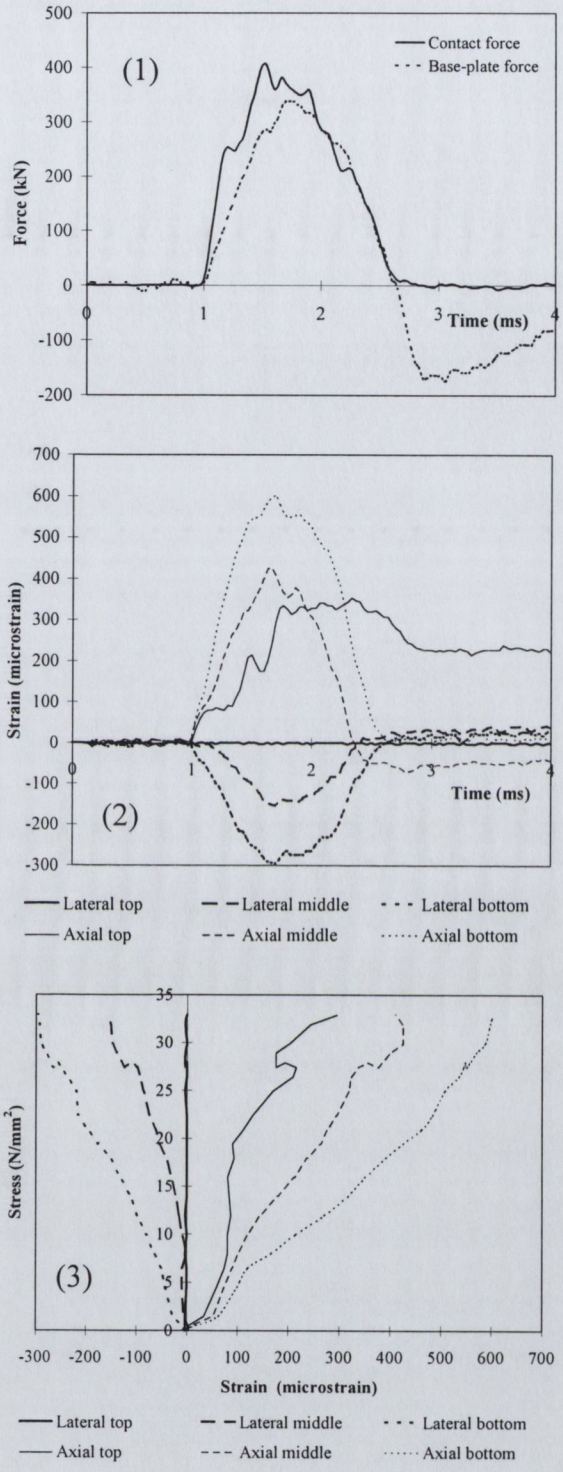


Figure A3.24 C(114)S (3)1f

(1) Loadcell response, (2) strain gauge response and (3) stress-strain response

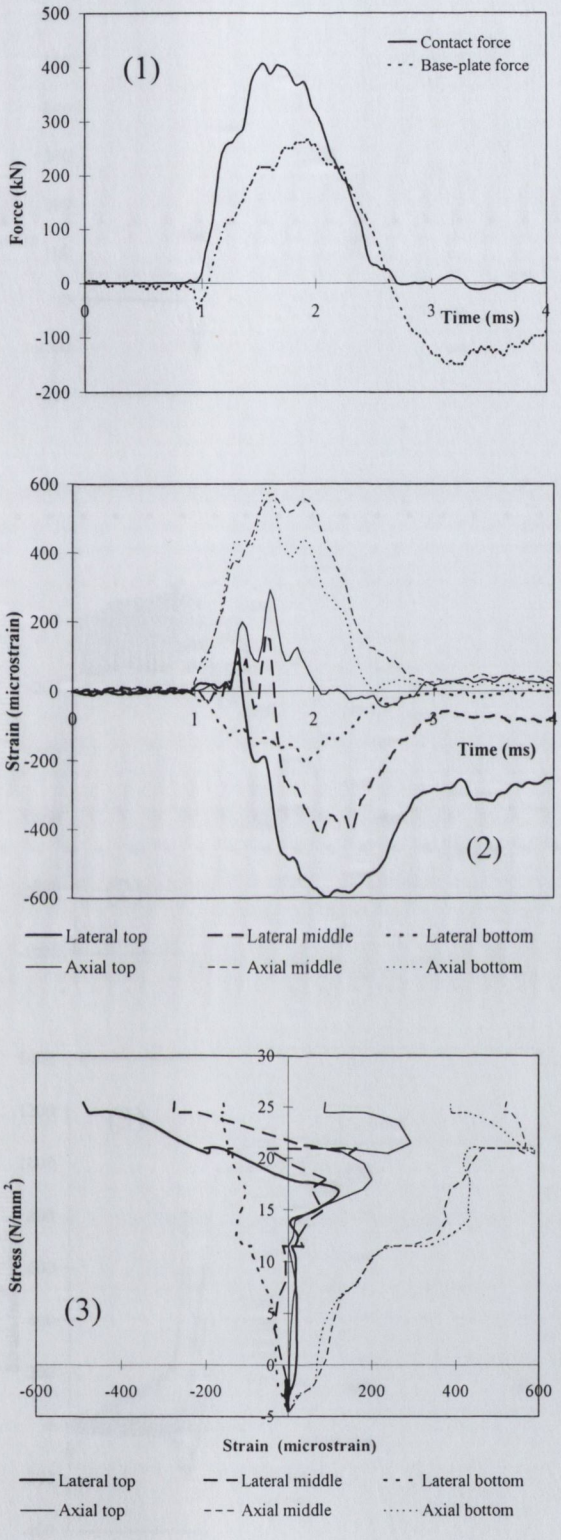


Figure A3.25 C(114)S (3)1g

(1) Loadcell response, (2) strain gauge response and (3) stress-strain response

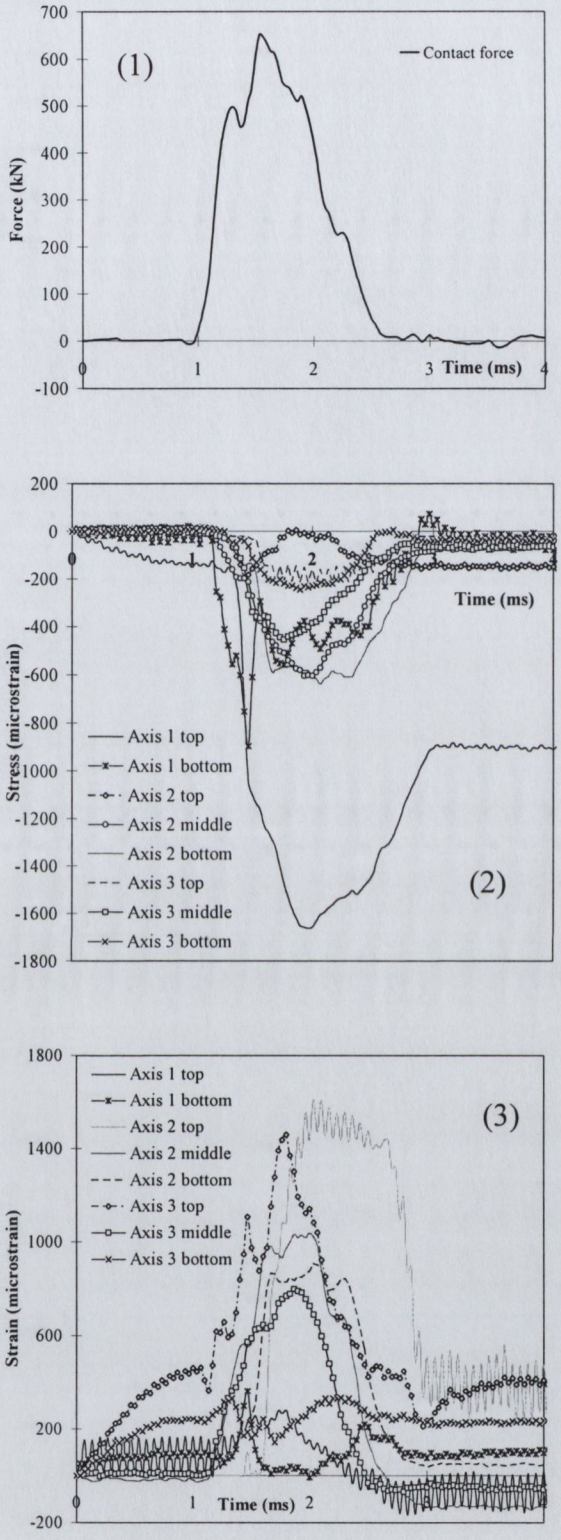


Figure A3.26 C(114)S (3)2a

(1) Loadcell response, (2) lateral strain gauge and (3) axial strain gauge response

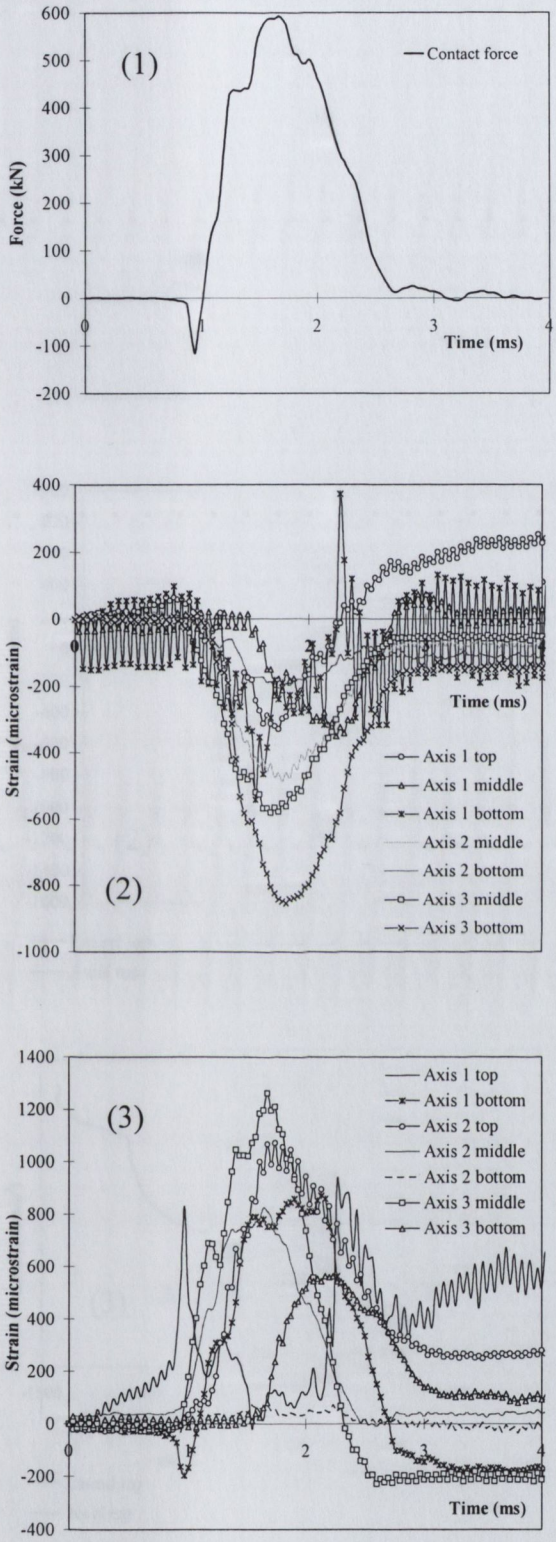


Figure A3.27 C(114)S (3)2b

(1) Loadcell response, (2) lateral strain gauge and (3) axial strain gauge response

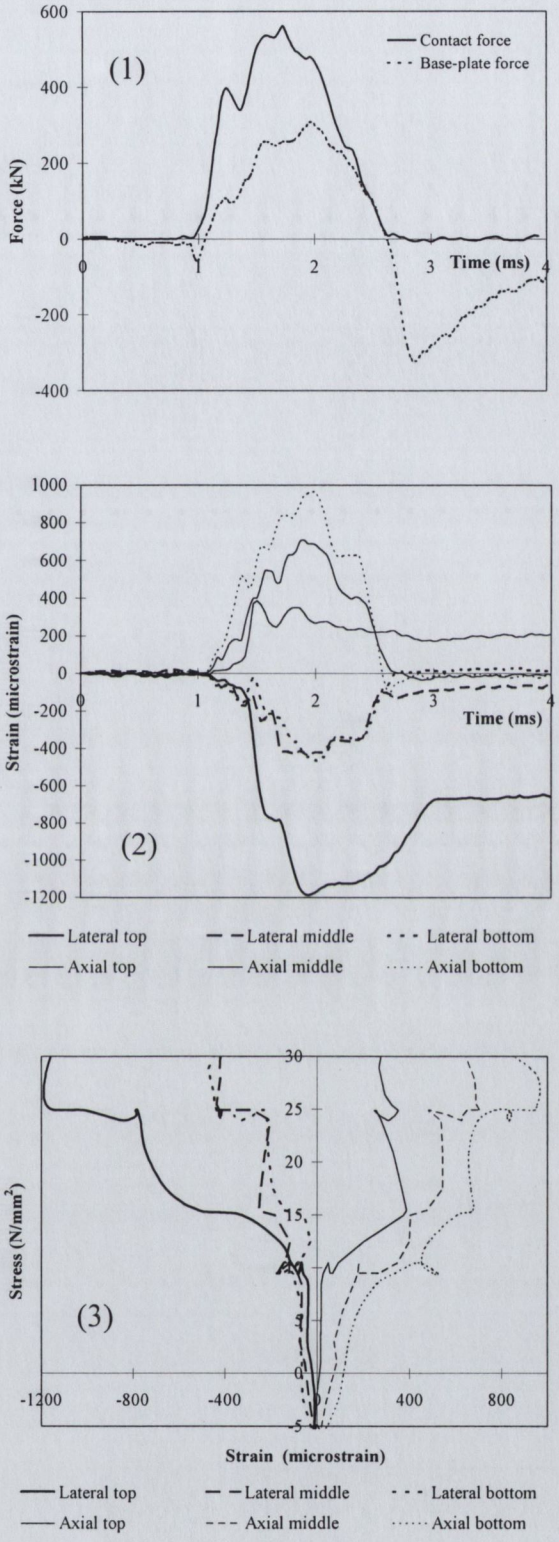


Figure A3.28 C(114)S (3)2c

(1) Loadcell response, (2) strain gauge response and (3) stress-strain response

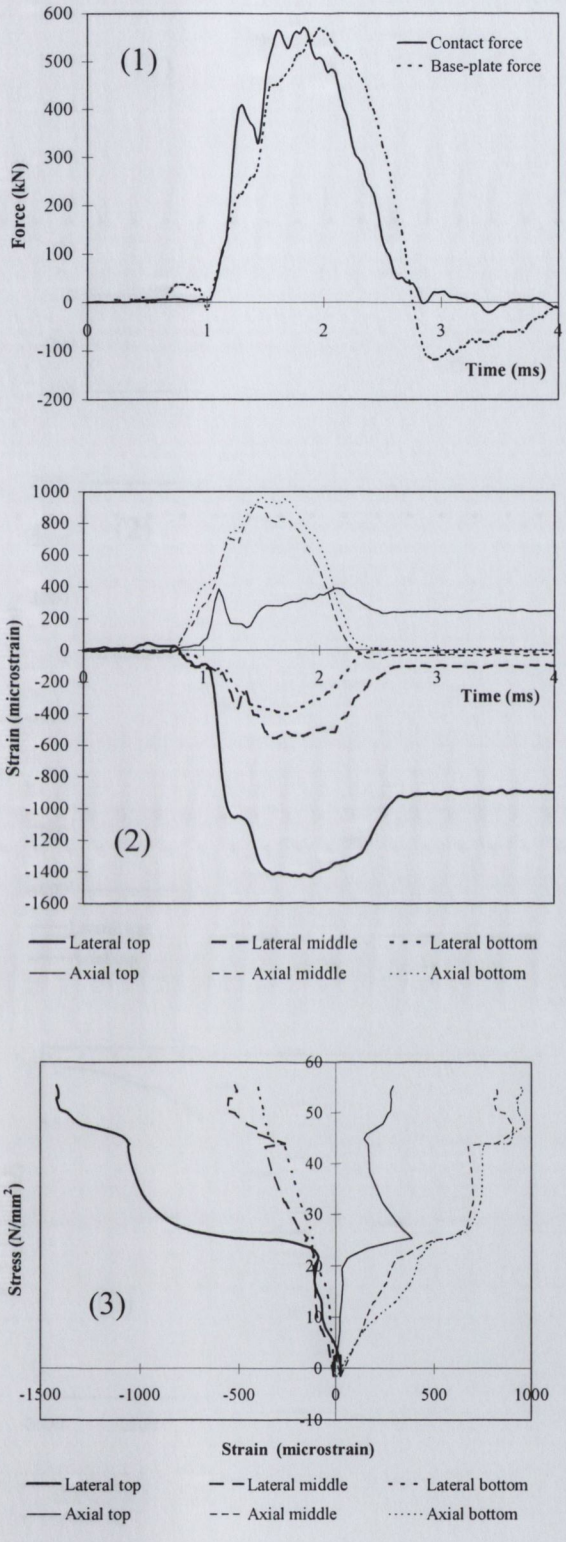


Figure A3.29 C(114)S (3)2d

(1) Loadcell response, (2) strain gauge response and (3) stress-strain response

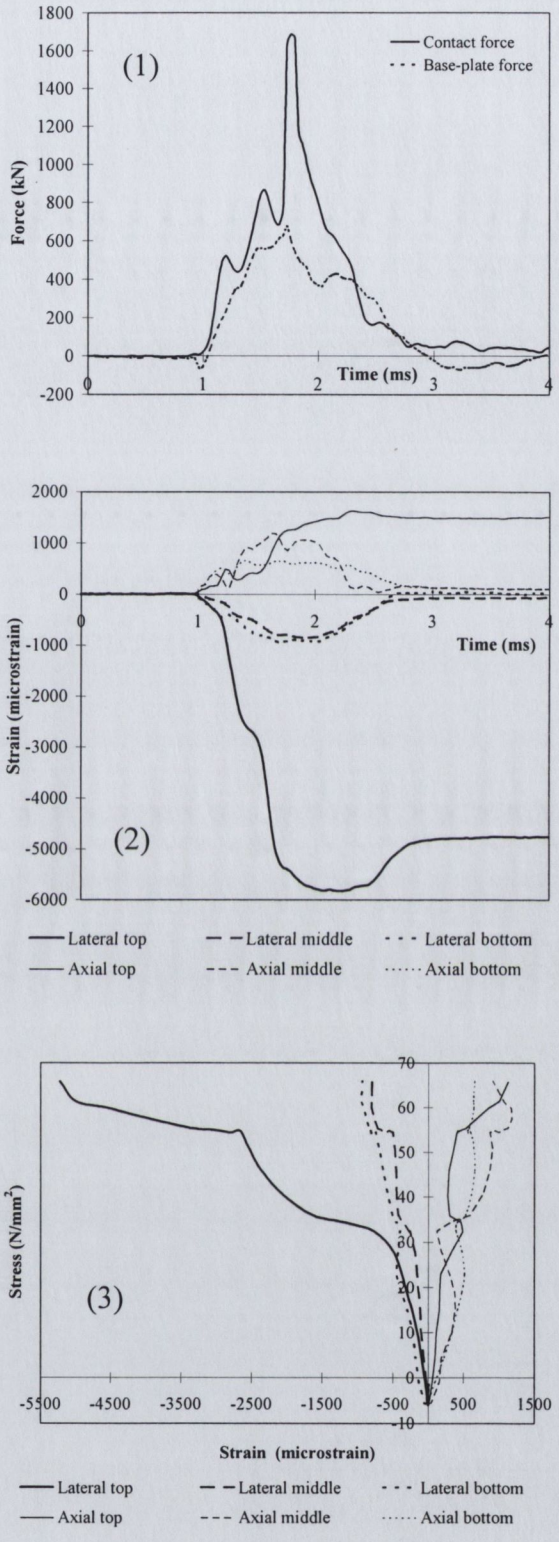


Figure A3.30 C(114)S (3)3a

(1) Loadcell response, (2) strain gauge response and (3) stress-strain response

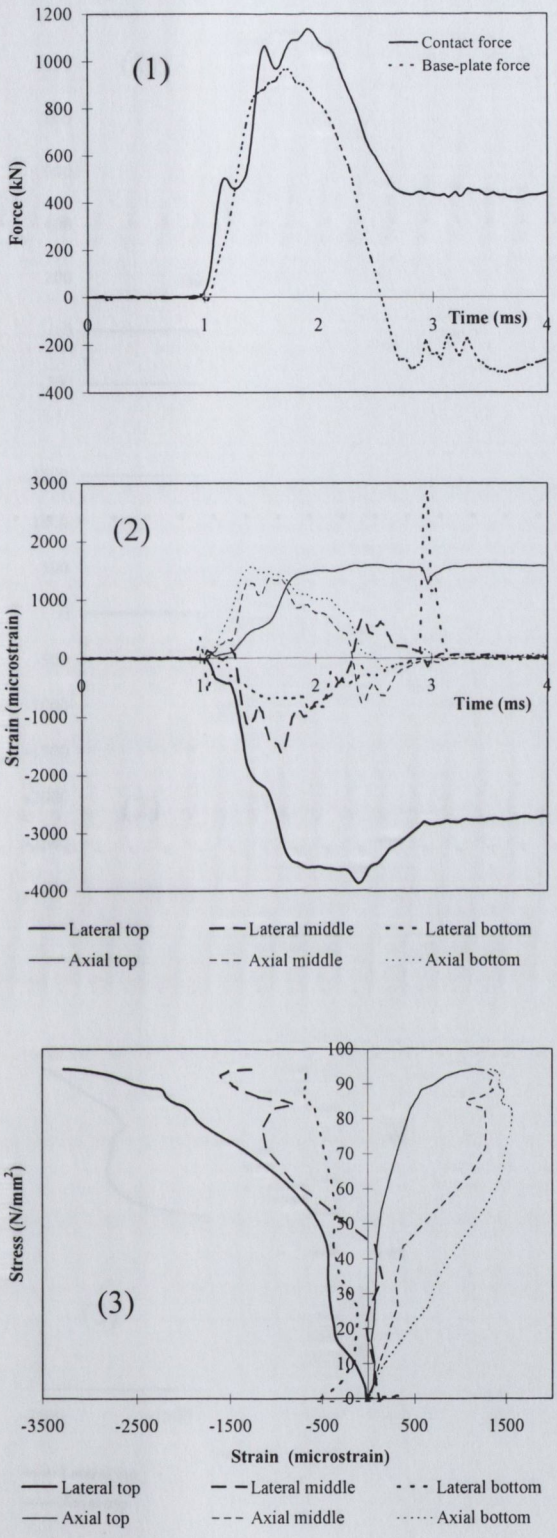


Figure A3.31 C(114)S (3)3b

(1) Loadcell response, (2) strain gauge response and (3) stress-strain response

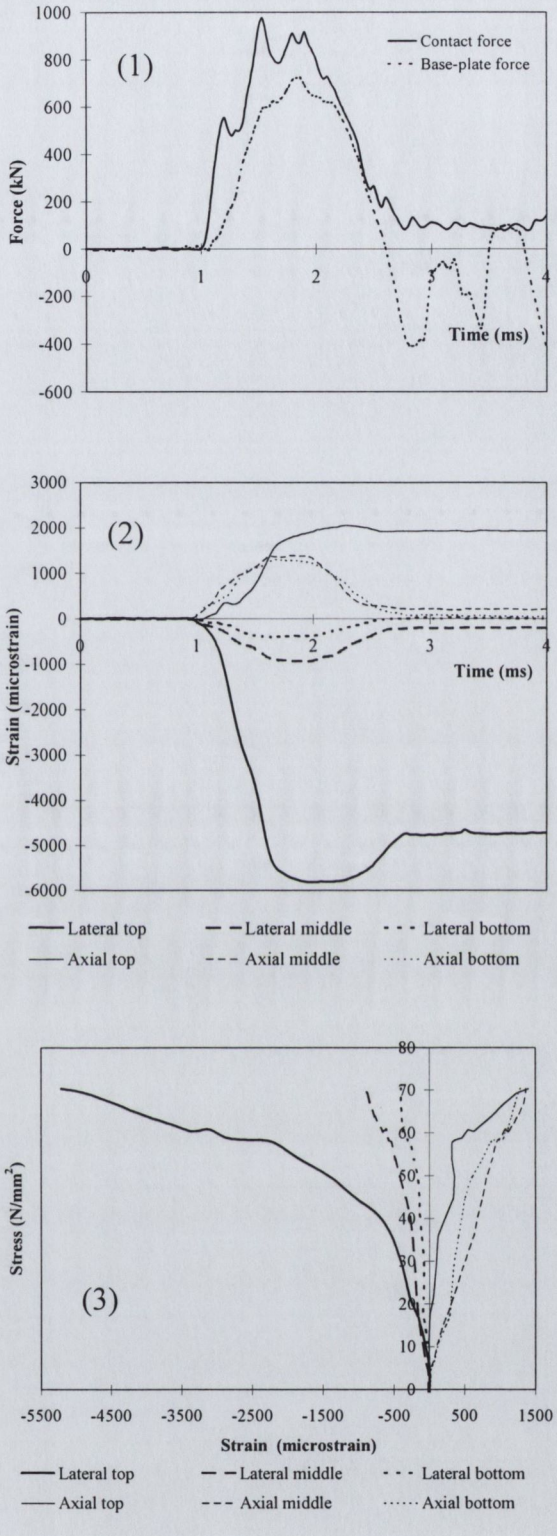


Figure A3.32 C(114)S (3)3c

(1) Loadcell response, (2) strain gauge response and (3) stress-strain response

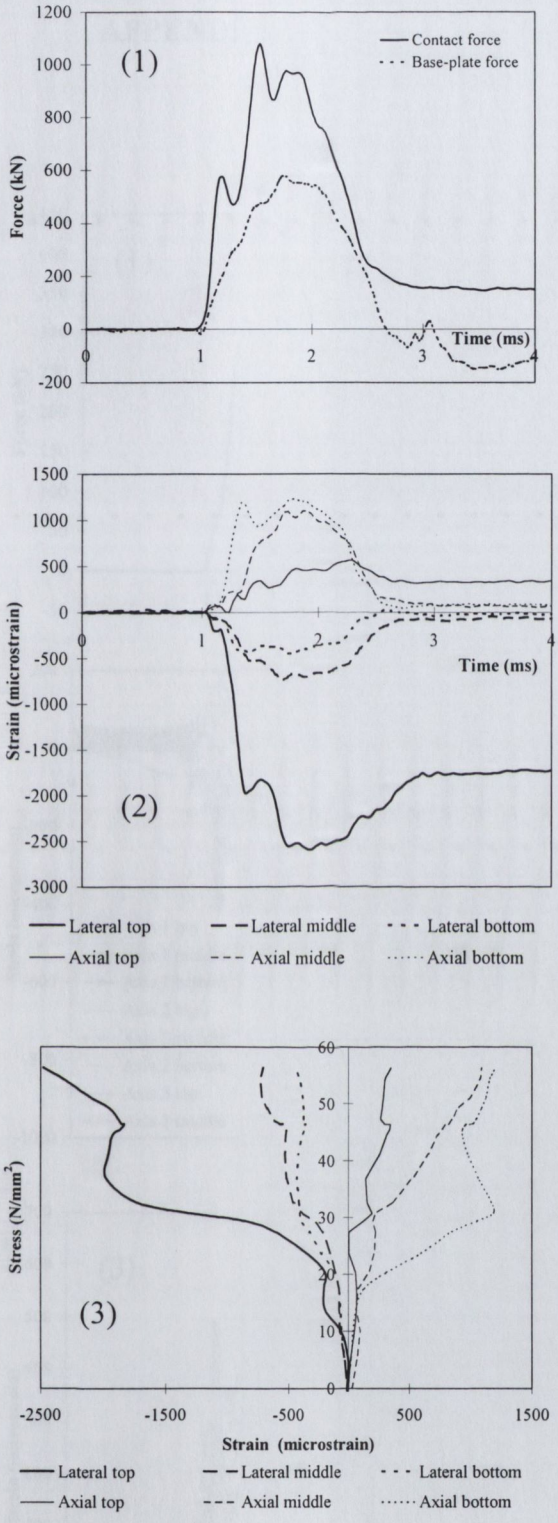


Figure A3.33 C(114)S (3)3d

(1) Loadcell response, (2) strain gauge response and (3) stress-strain response

APPENDIX 3.4. IMPACT RESPONSE OF SLEEVED CYLINDERS, 5 MM STEEL

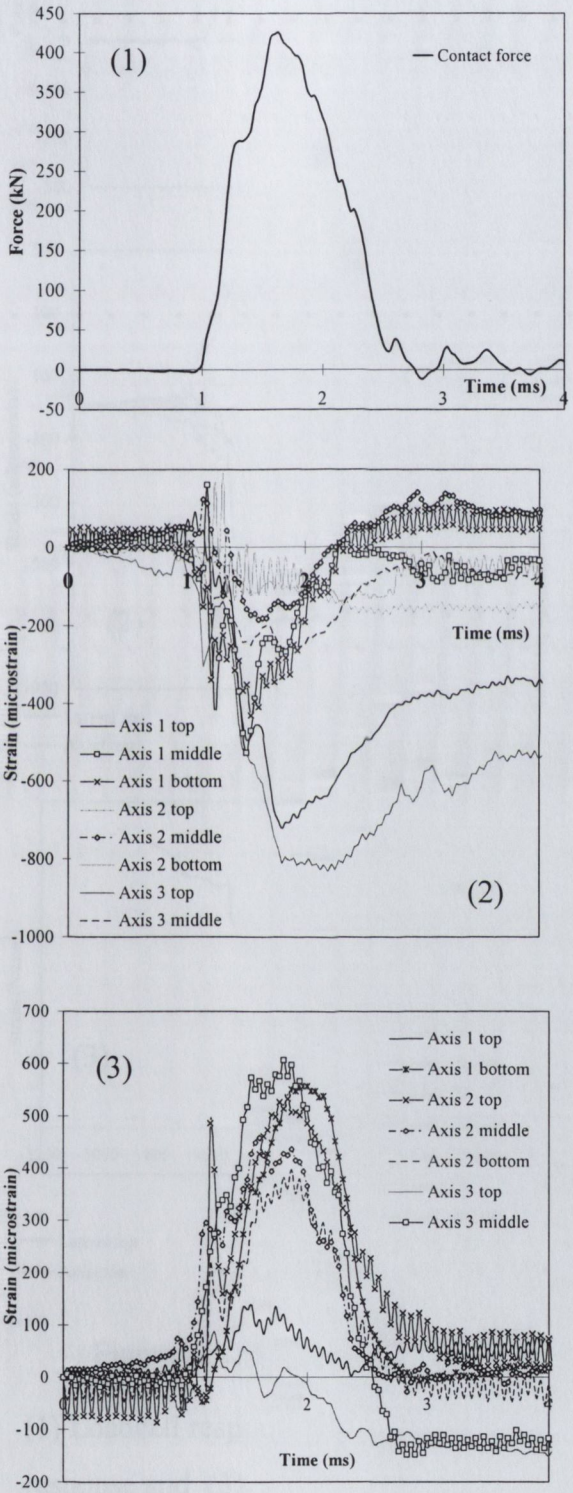


Figure A3.34 C(114)S (5)1a

(1) Loadcell response, (2) lateral strain gauge and (3) axial strain gauge response

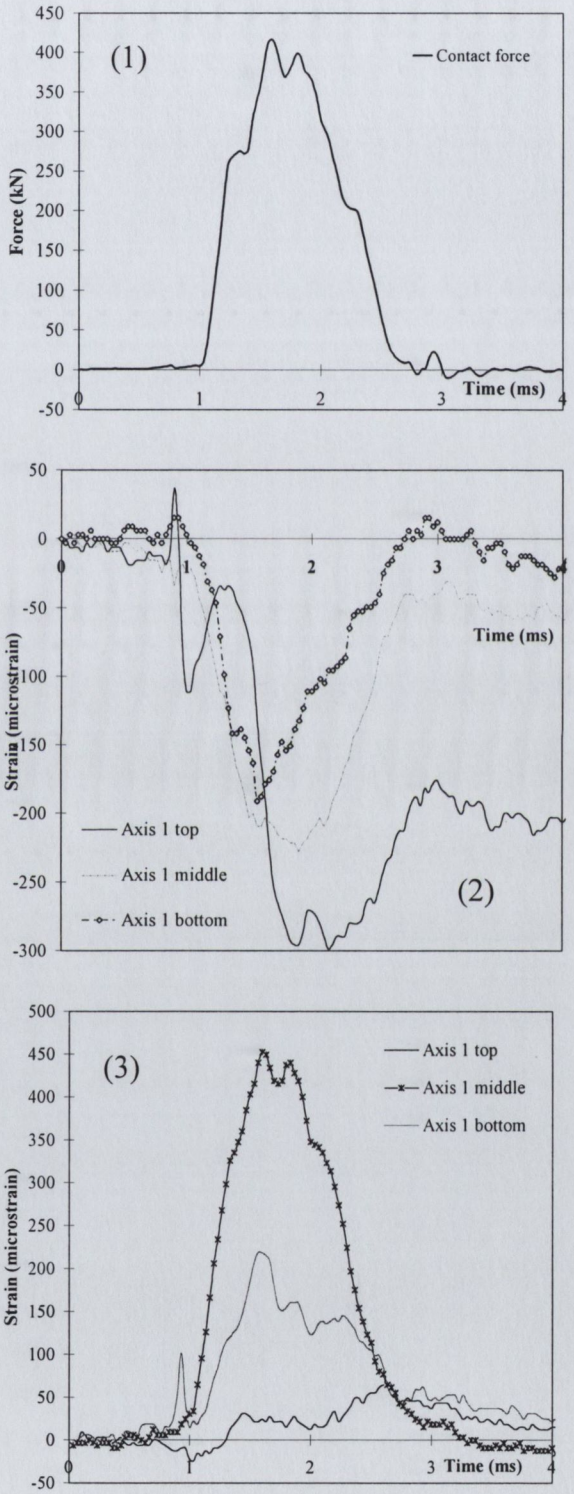


Figure A3.35 C(114)S (5)1b

(1) Loadcell response, (2) lateral strain gauge and (3) axial strain gauge response

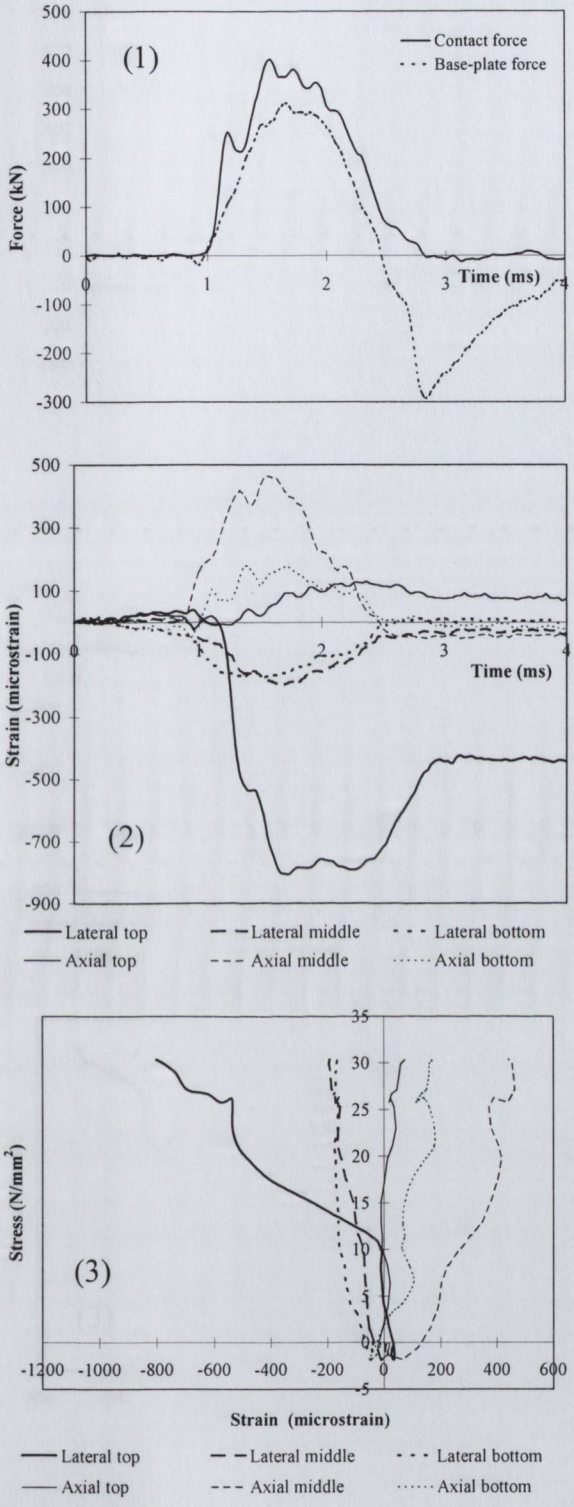


Figure A3.36 C(114)S (5)1c

(1) Loadcell response, (2) strain gauge response and (3) stress-strain response

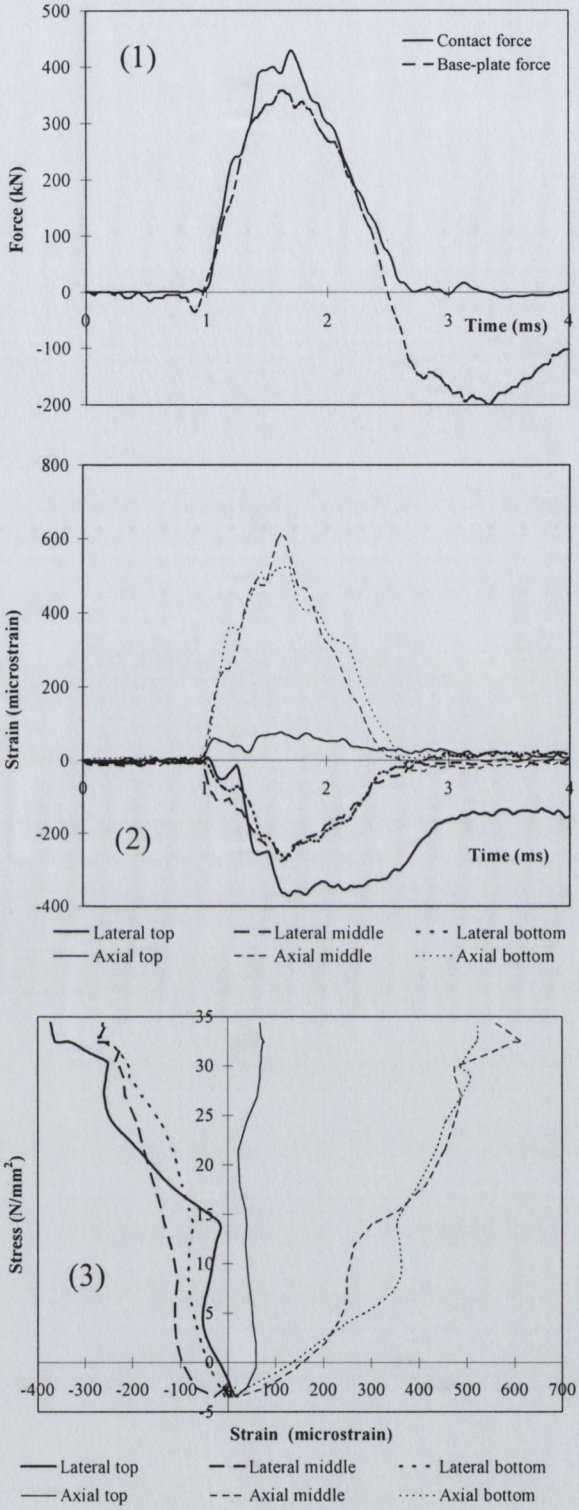
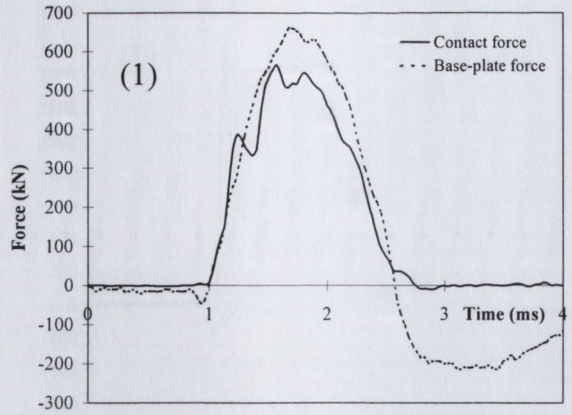
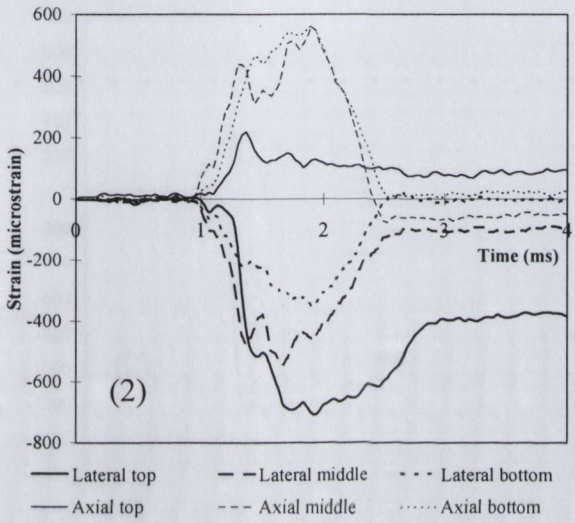


Figure A3.37 C(114)S (5)1d

(1) Loadcell response, (2) strain gauge response and (3) stress-strain response





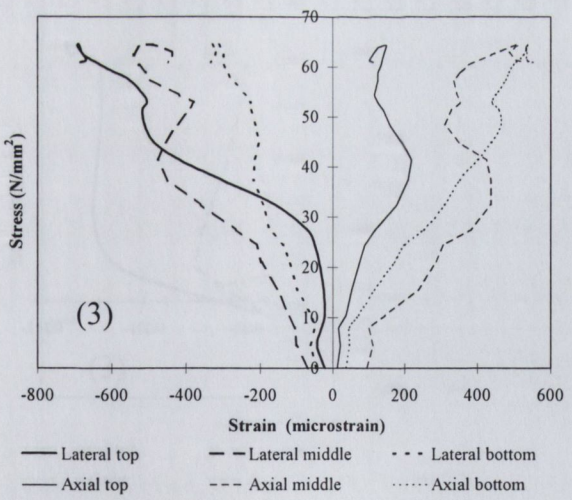
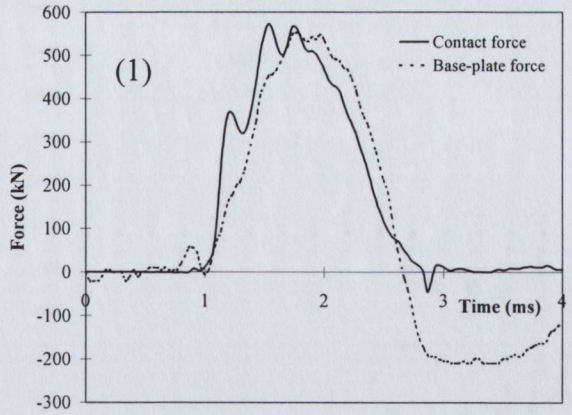
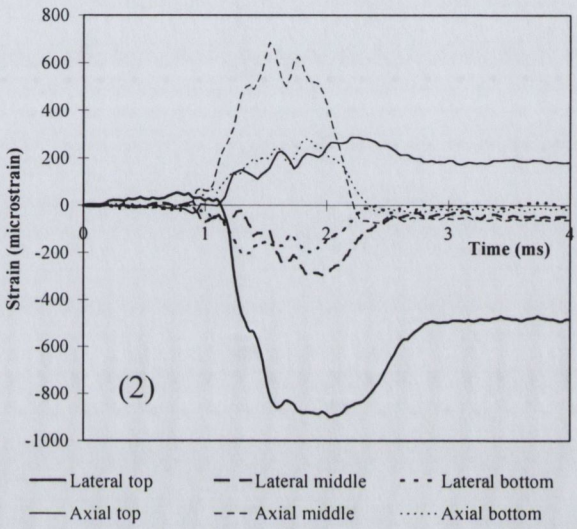


Figure A3.38 C(114)S (5)2a

(1) Loadcell response, (2) strain gauge response and (3) stress-strain response





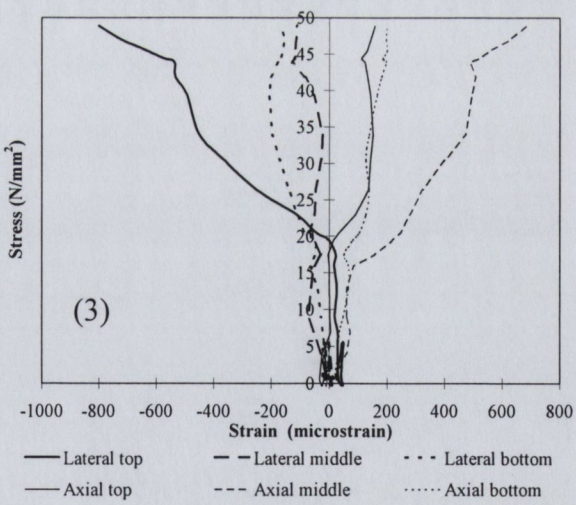


Figure A3.39 C(114)S (5)2b

(1) Loadcell response, (2) strain gauge response and (3) stress-strain response

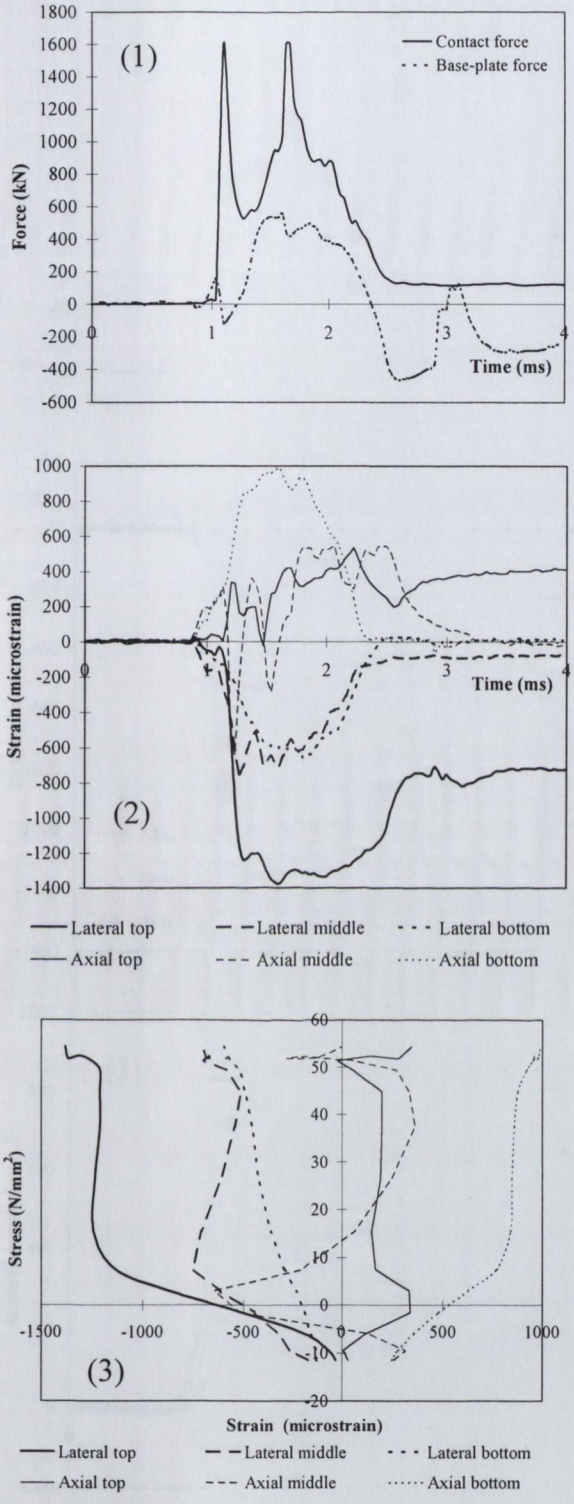


Figure A3.40 C(114)S (5)3a

(1) Loadcell response, (2) strain gauge response and (3) stress-strain response

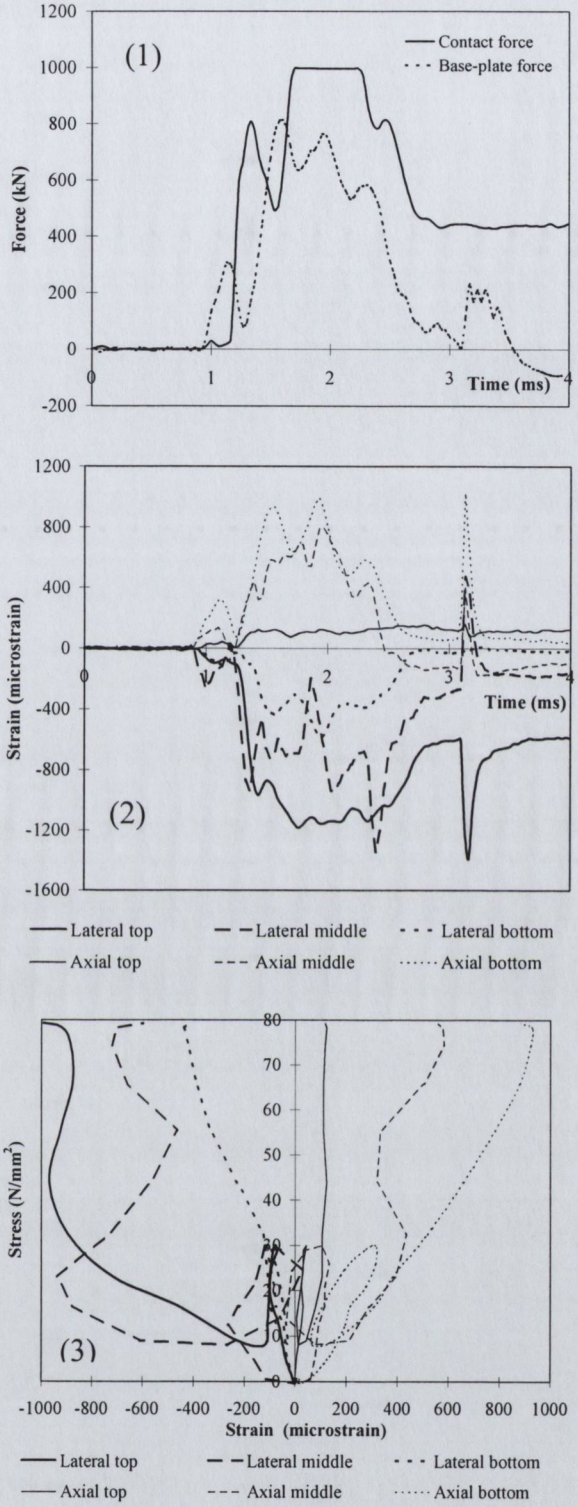


Figure A3.41 C(114)S (5)3b

(1) Loadcell response, (2) strain gauge response and (3) stress-strain response

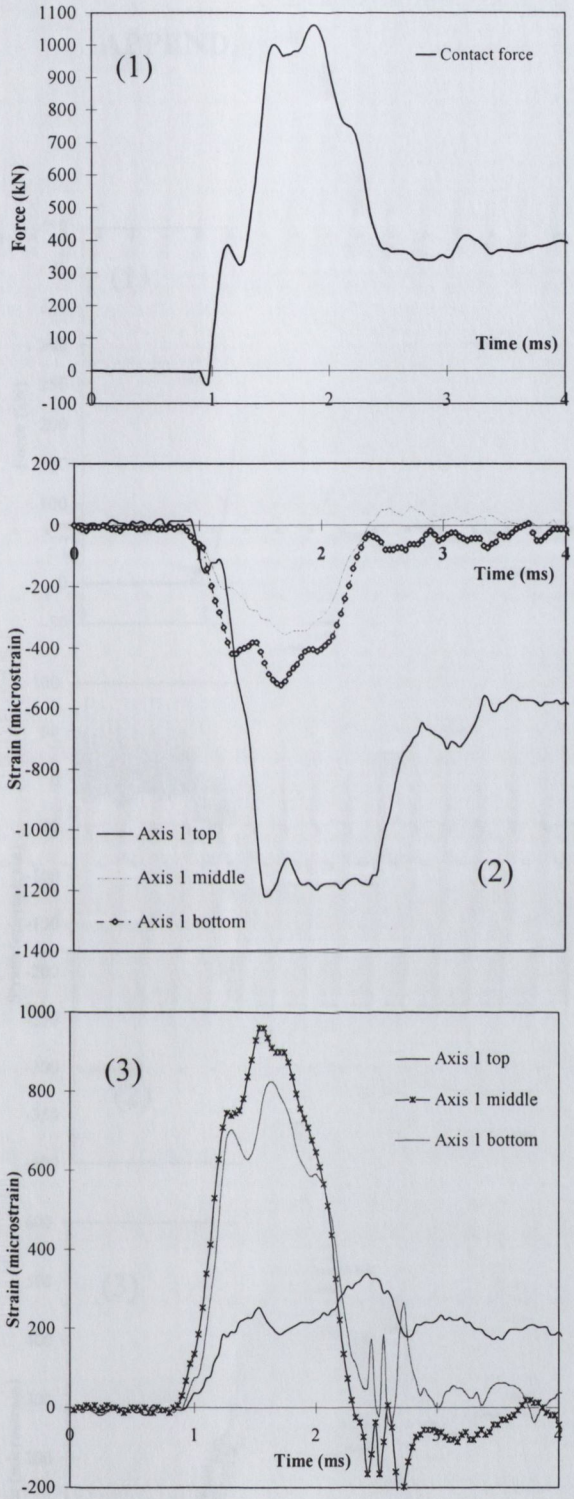


Figure A3.42 C(114)S (5)3c

(1) Loadcell response, (2) lateral strain gauge and (3) axial strain gauge response

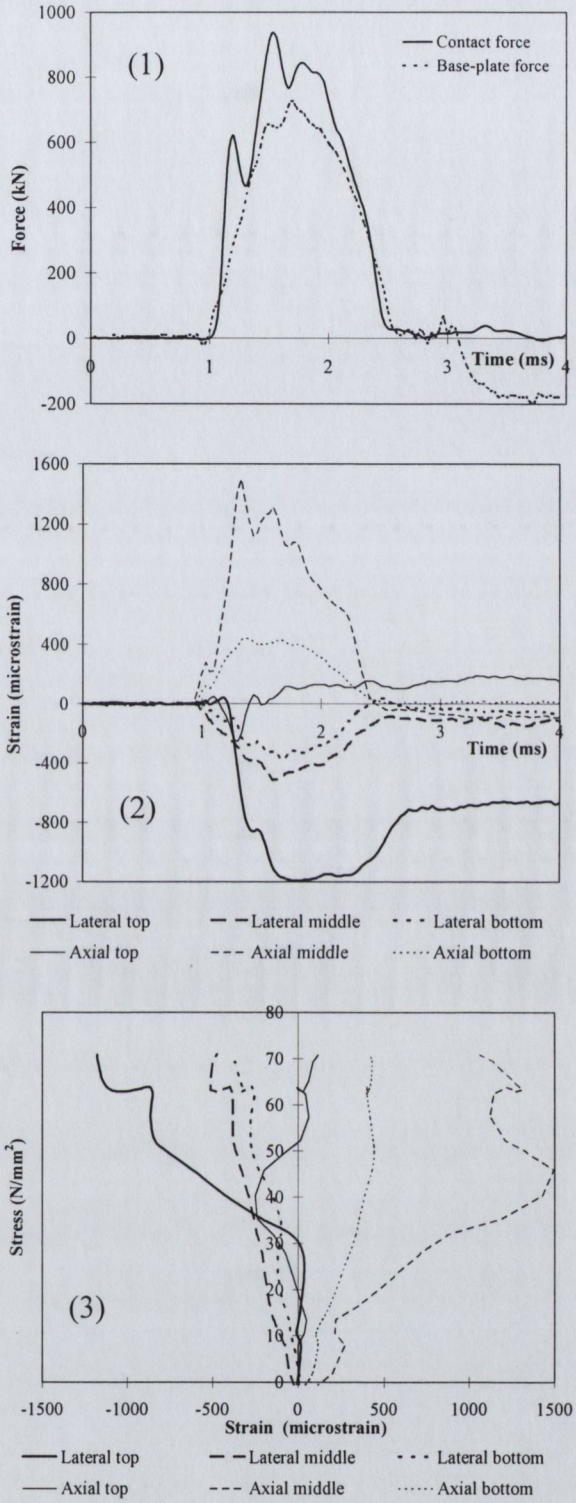


Figure A3.43 C(114)S (5)3d

(1) Loadcell response, (2) strain gauge response and (3) stress-strain response

APPENDIX 3.5. IMPACT RESPONSE OF SLEEVED CYLINDERS, 6.5 MM STEEL

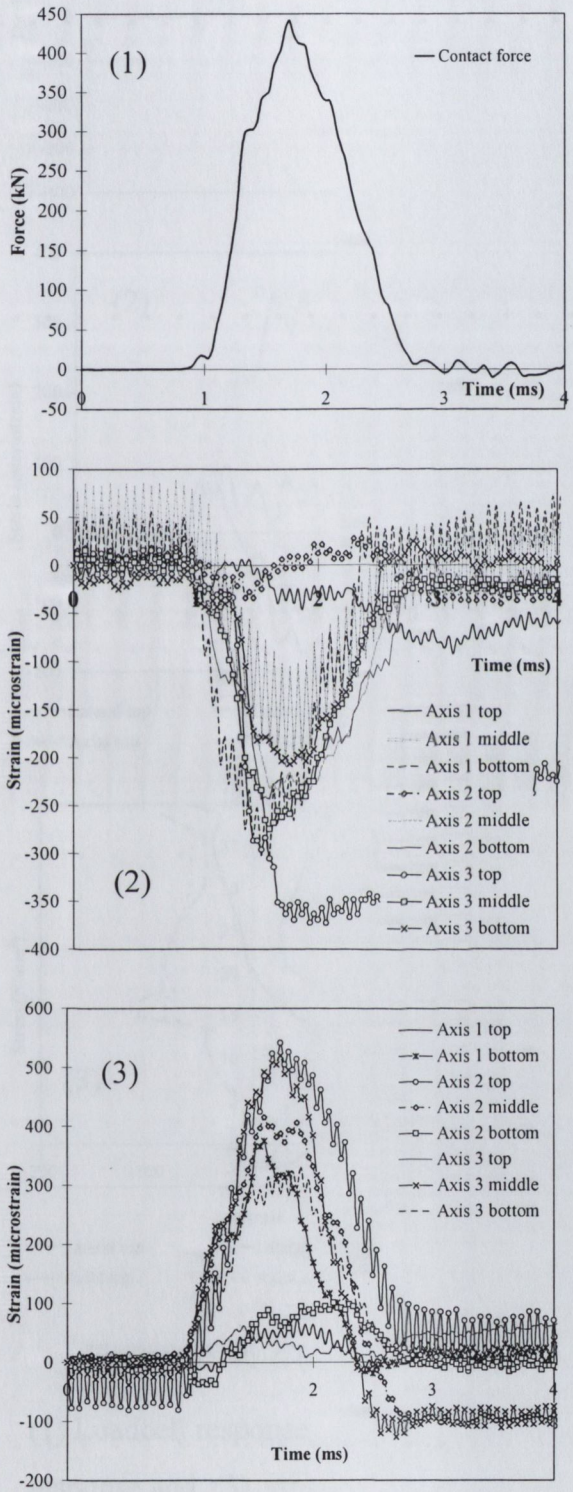


Figure A3.44 C(114)S (6.5)1a

(1) Loadcell response, (2) lateral strain gauge and (3) axial strain gauge response

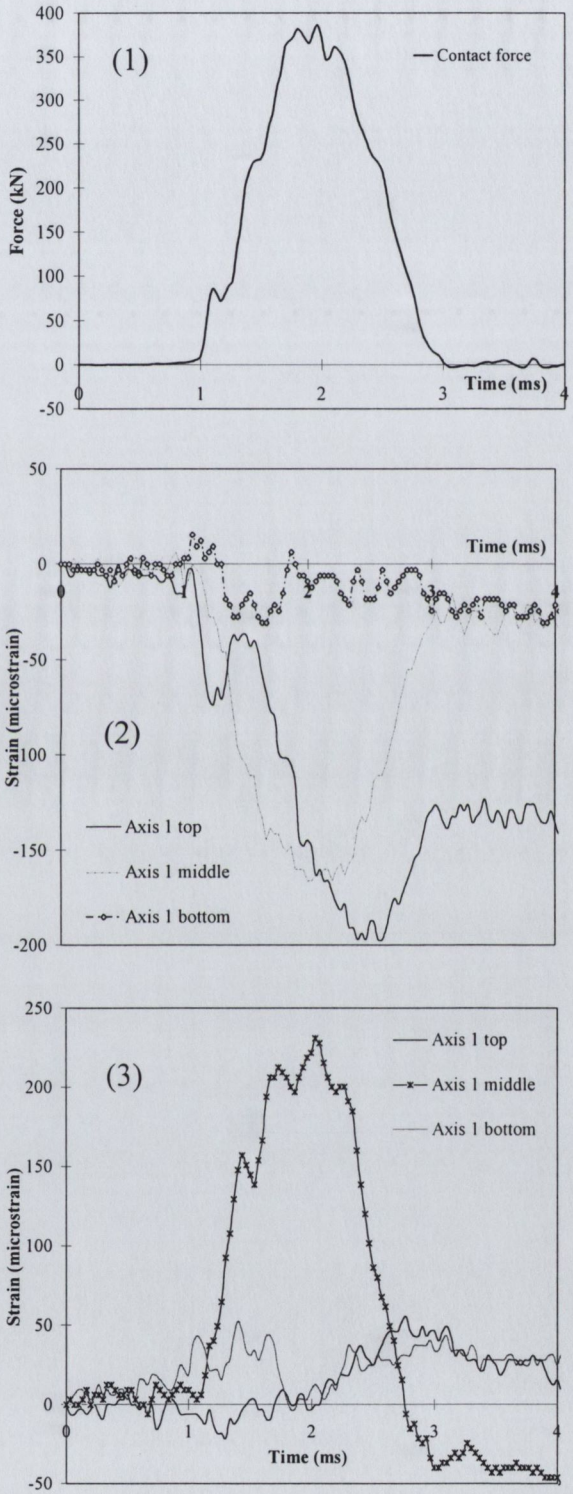
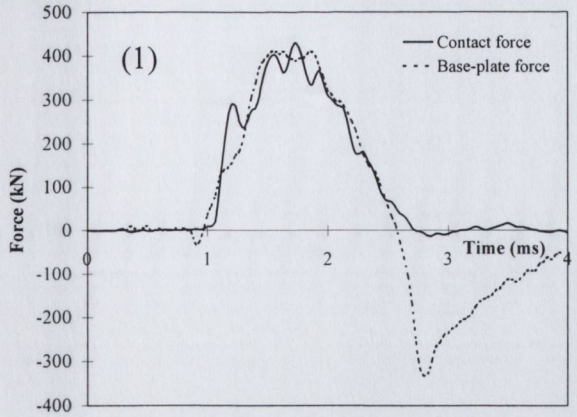
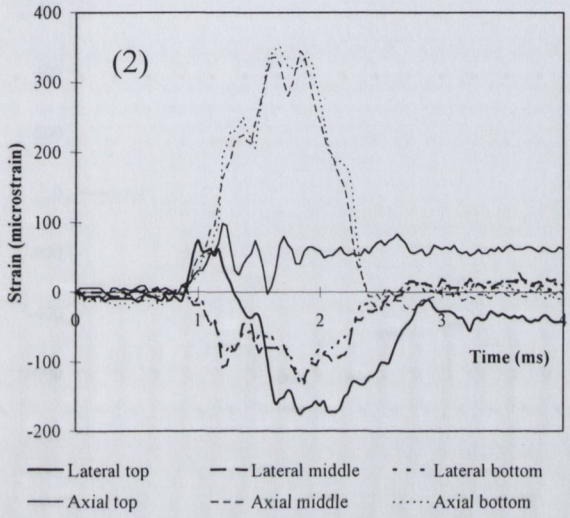


Figure A3.45 C(114)S (6.5)1b

(1) Loadcell response, (2) lateral strain gauge and (3) axial strain gauge response





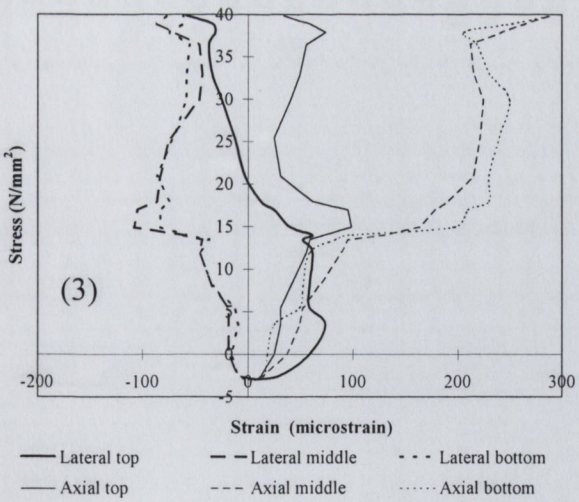
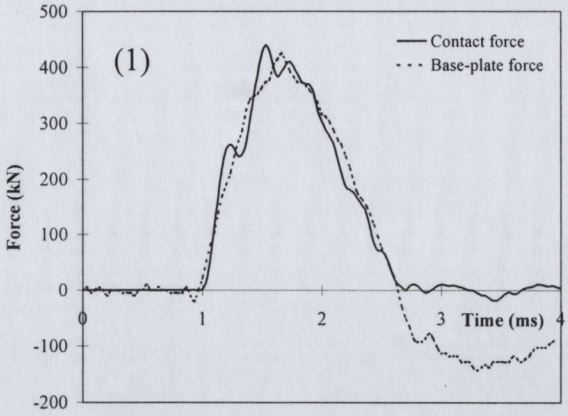
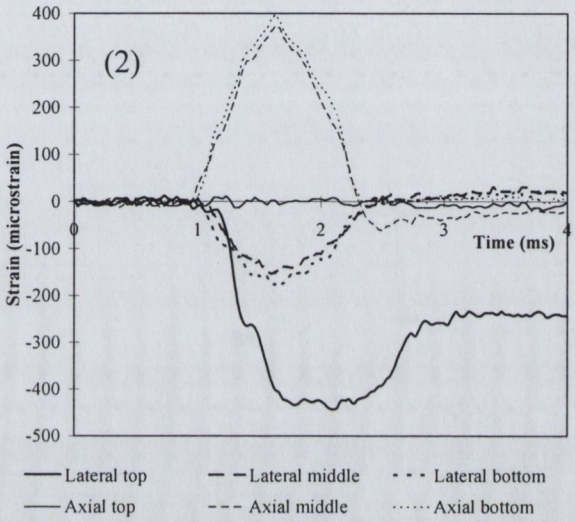


Figure A3.46 C(114)S (6.5)1c

(1) Loadcell response, (2) strain gauge response and (3) stress-strain response





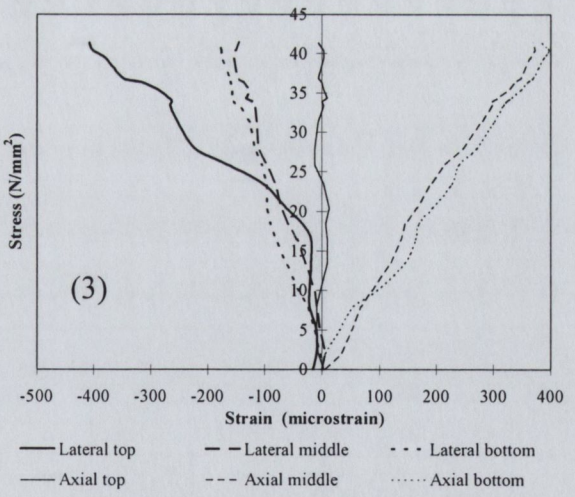


Figure A3.47 C(114)S (6.5)1d

(1) Loadcell response, (2) strain gauge response and (3) stress-strain response

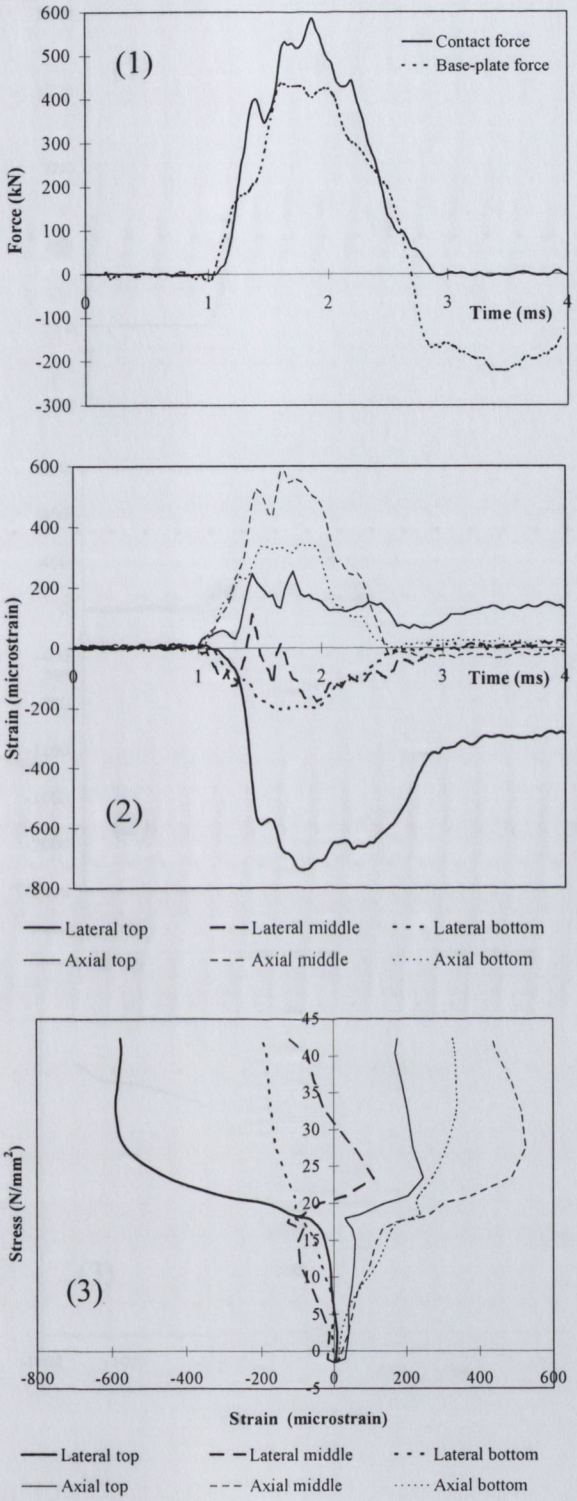


Figure A3.48 C(114)S (6.5)2a

(1) Loadcell response, (2) strain gauge response and (3) stress-strain response

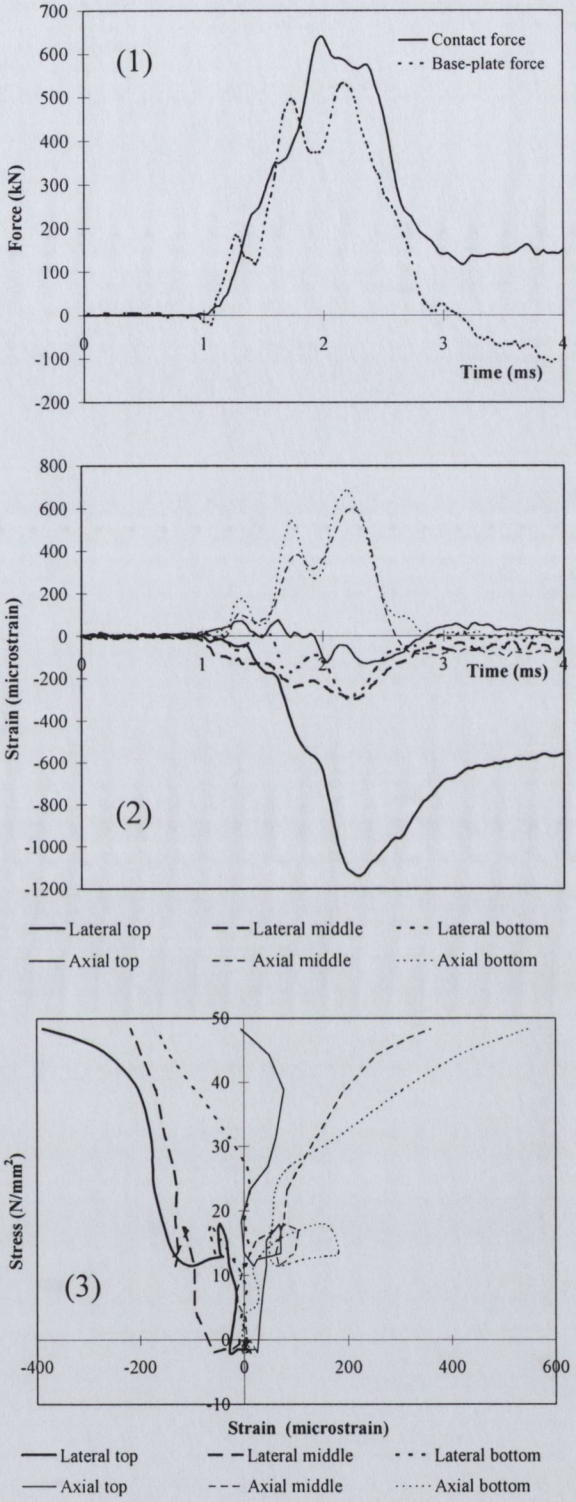


Figure A3.49 C(114)S (6.5)2b

(1) Loadcell response, (2) strain gauge response and (3) stress-strain response

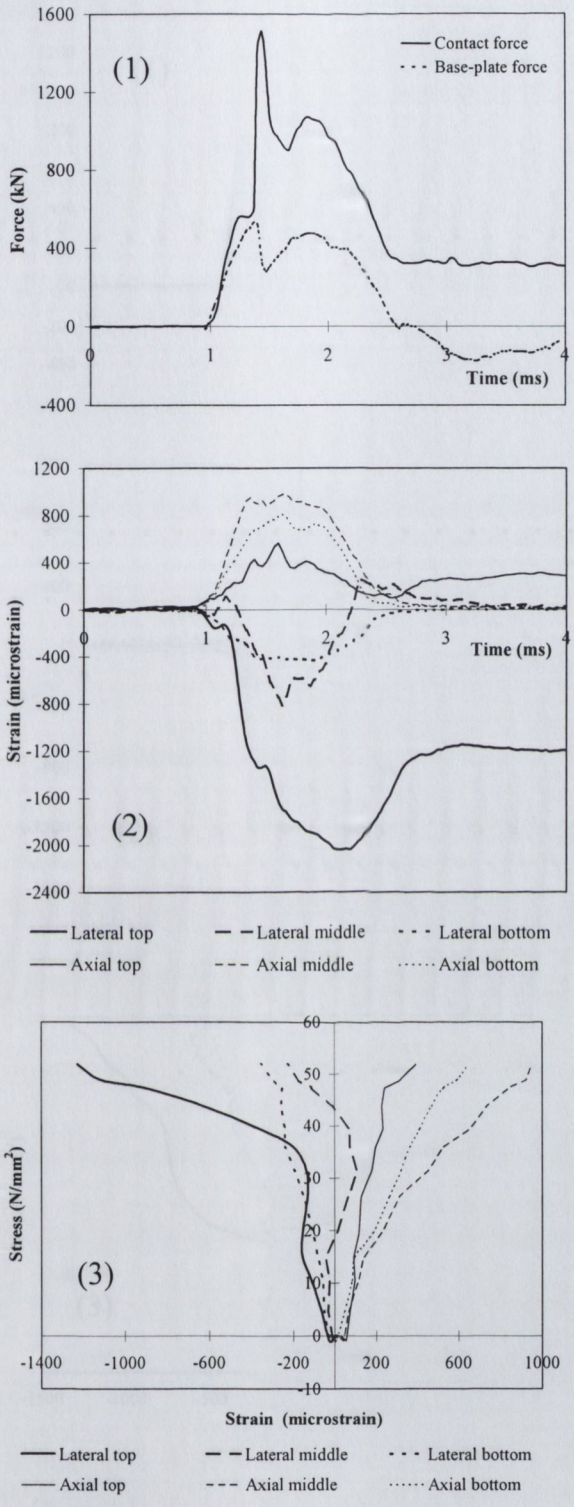


Figure A3.50 C(114)S (6.5)3a

(1) Loadcell response, (2) strain gauge response and (3) stress-strain response

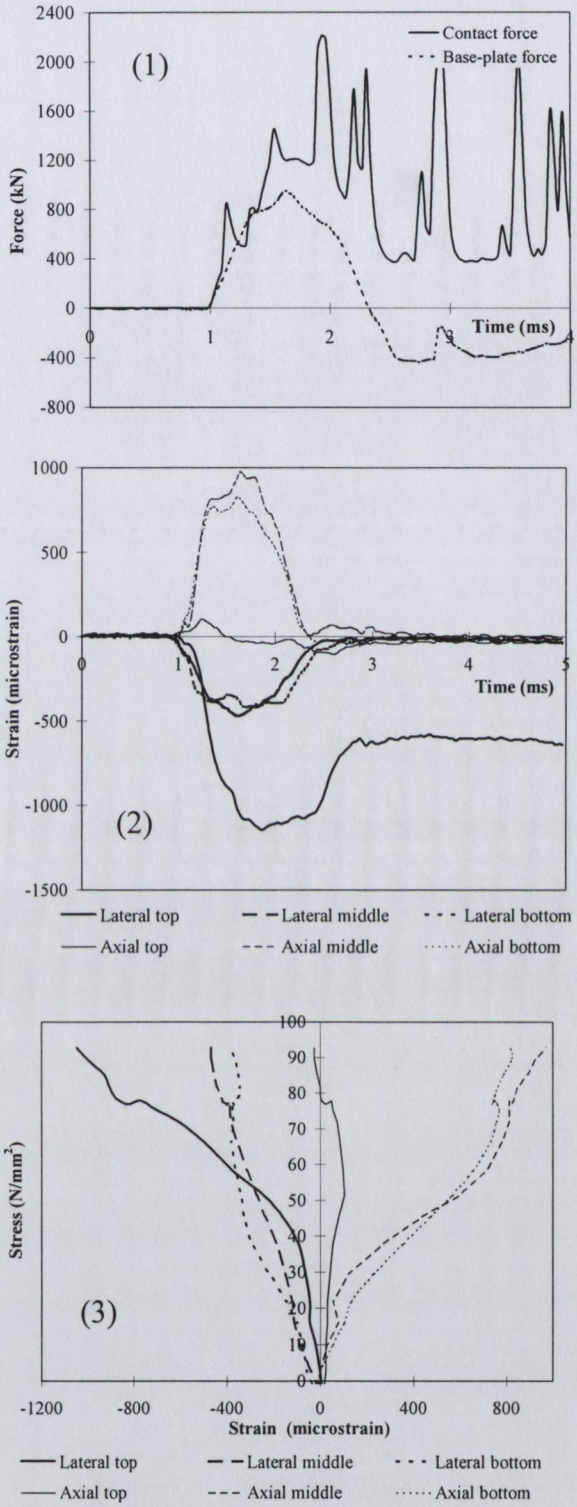


Figure A3.51 C(114)S (6.5)3b

(1) Loadcell response, (2) strain gauge response and (3) stress-strain response

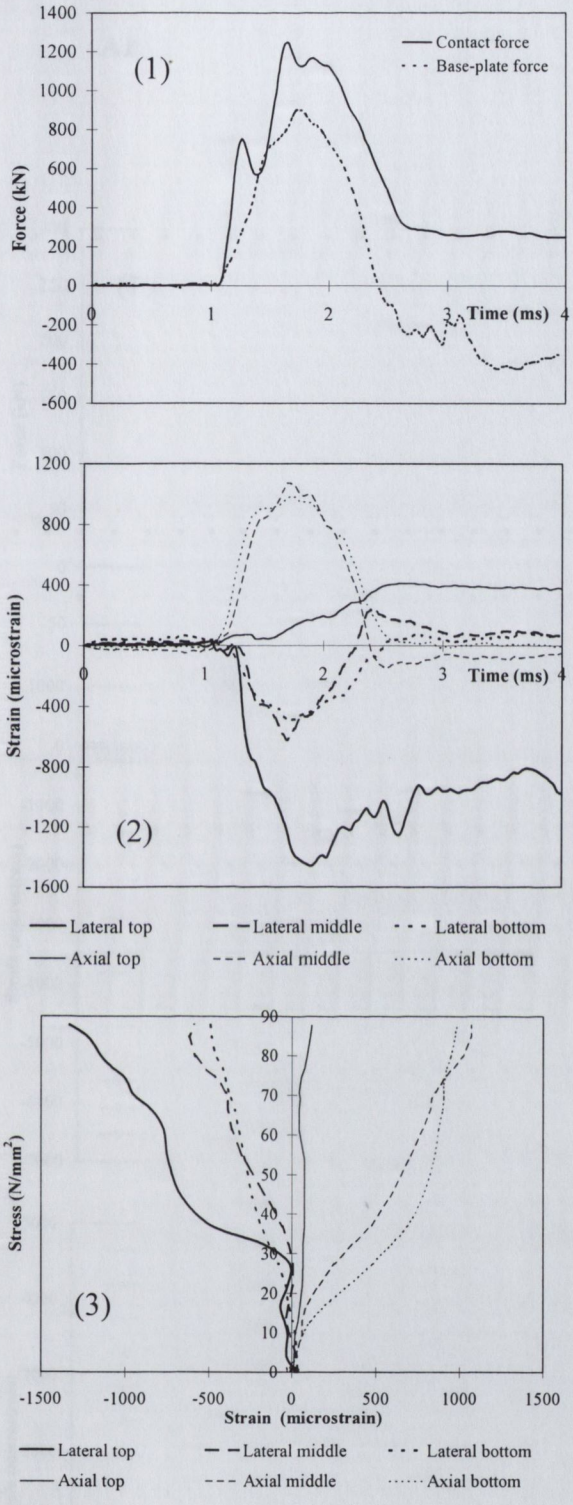


Figure A3.52 C(114)S (6.5)3c

(1) Loadcell response, (2) strain gauge response and (3) stress-strain response

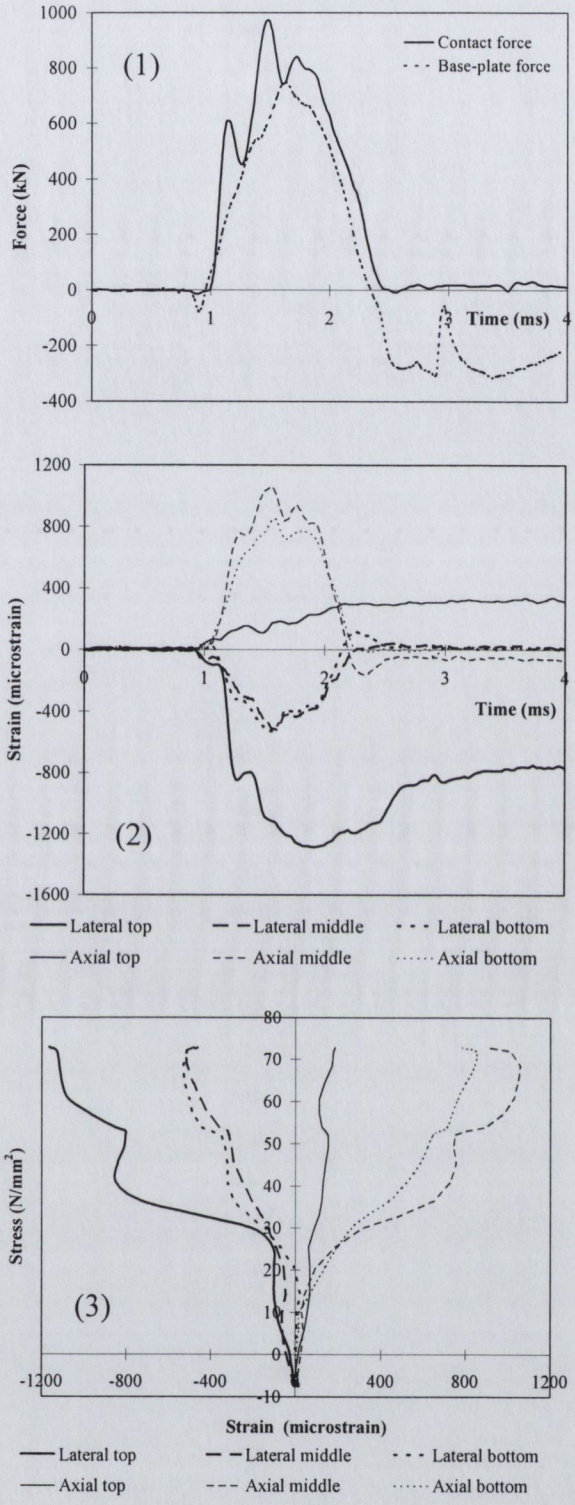
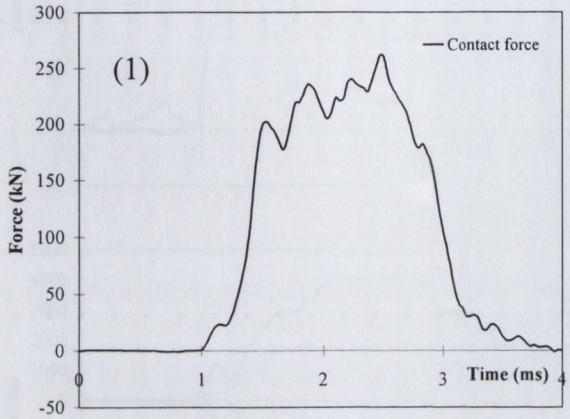
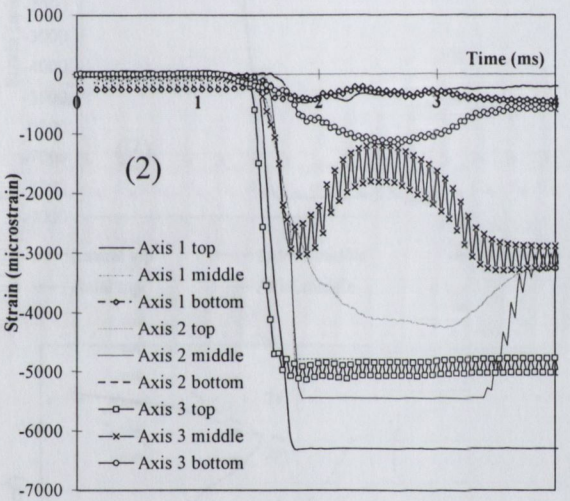


Figure A3.53 C(114)S (6.5)3d

(1) Loadcell response, (2) strain gauge response and (3) stress-strain response

APPENDIX 3.6. IMPACT RESPONSE OF SLEEVED CYLINDERS, 3.6 MM PLASTIC





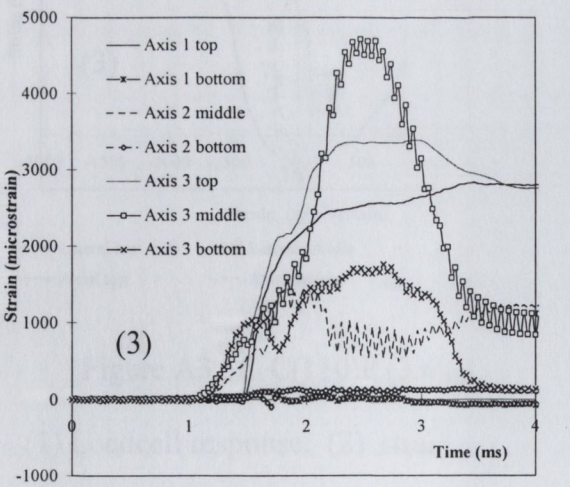
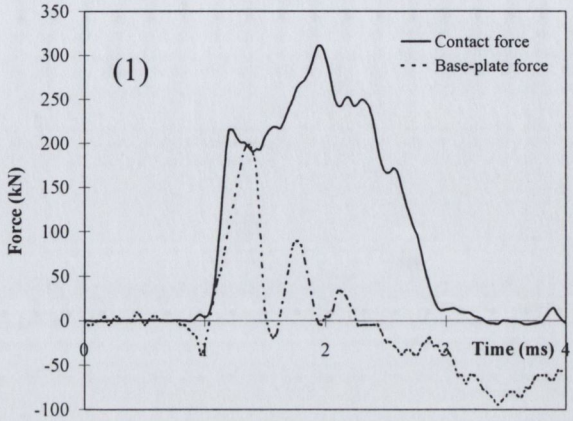
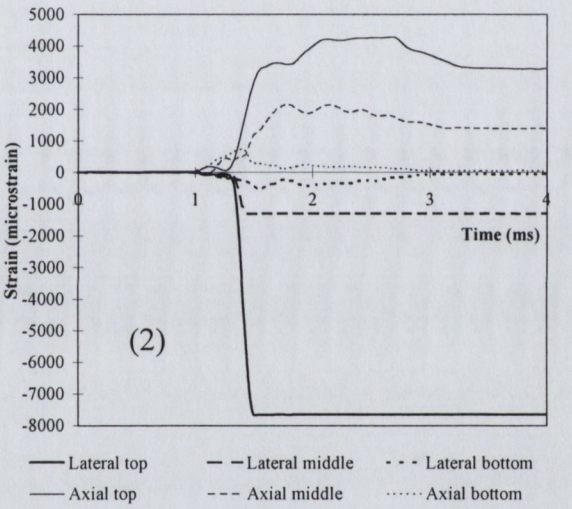


Figure A3.54 C(110)P (3.6)1a

(1) Loadcell response, (2) lateral strain gauge and (3) axial strain gauge response





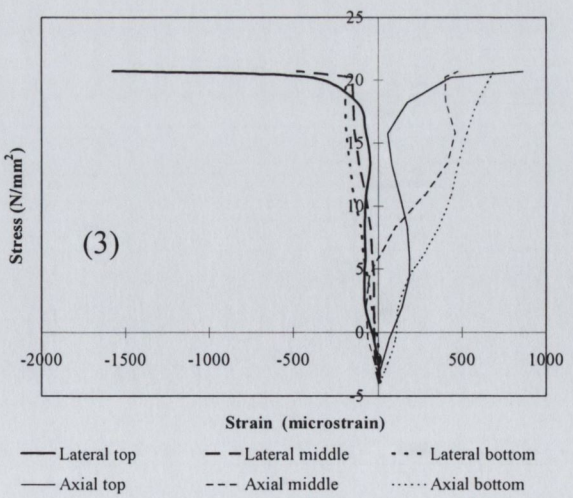


Figure A3.55 C(110)P (3.6)1b

(1) Loadcell response, (2) strain gauge response and (3) stress-strain response

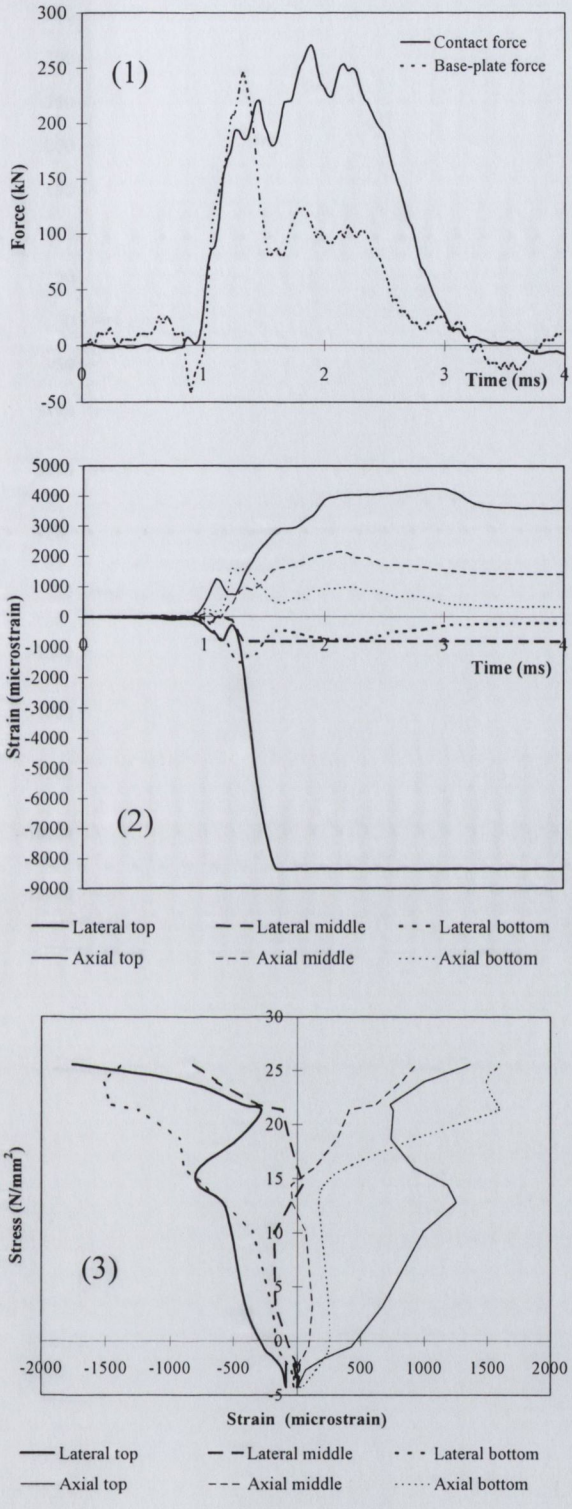


Figure A3.56 C(110)P (3.6)1c

(1) Loadcell response, (2) strain gauge response and (3) stress-strain response

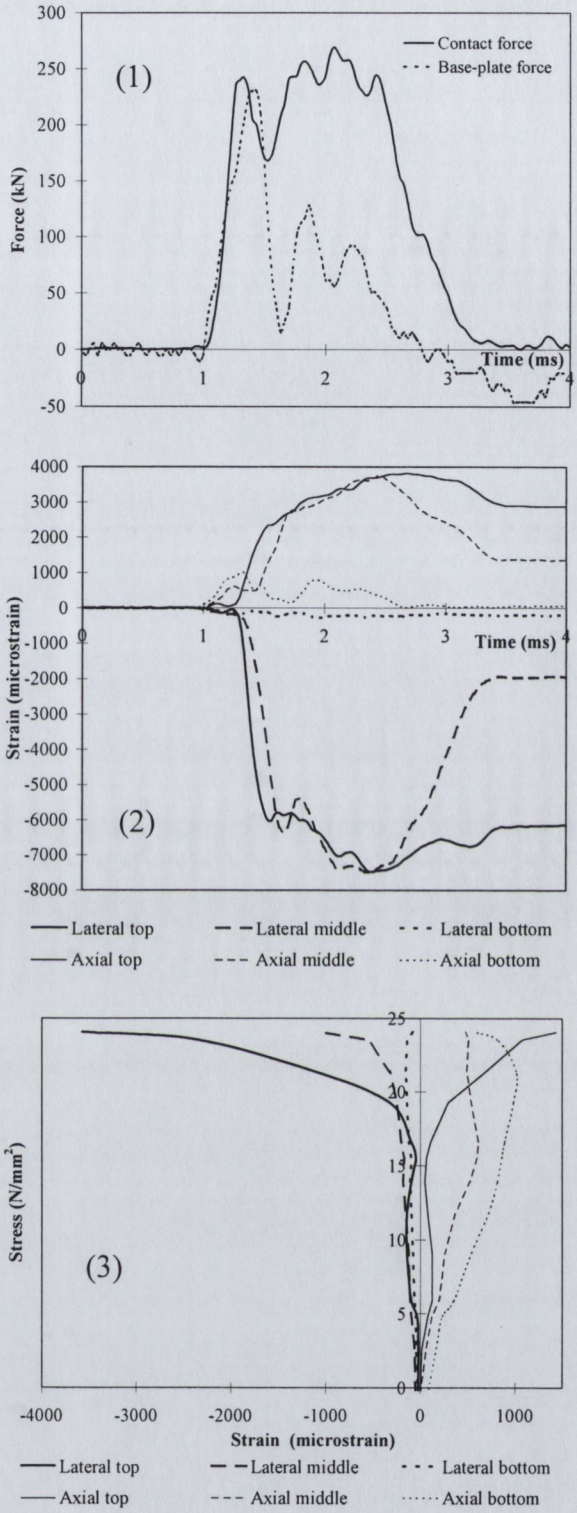


Figure A3.57 C(110)P (3.6)1d

(1) Loadcell response, (2) strain gauge response and (3) stress-strain response

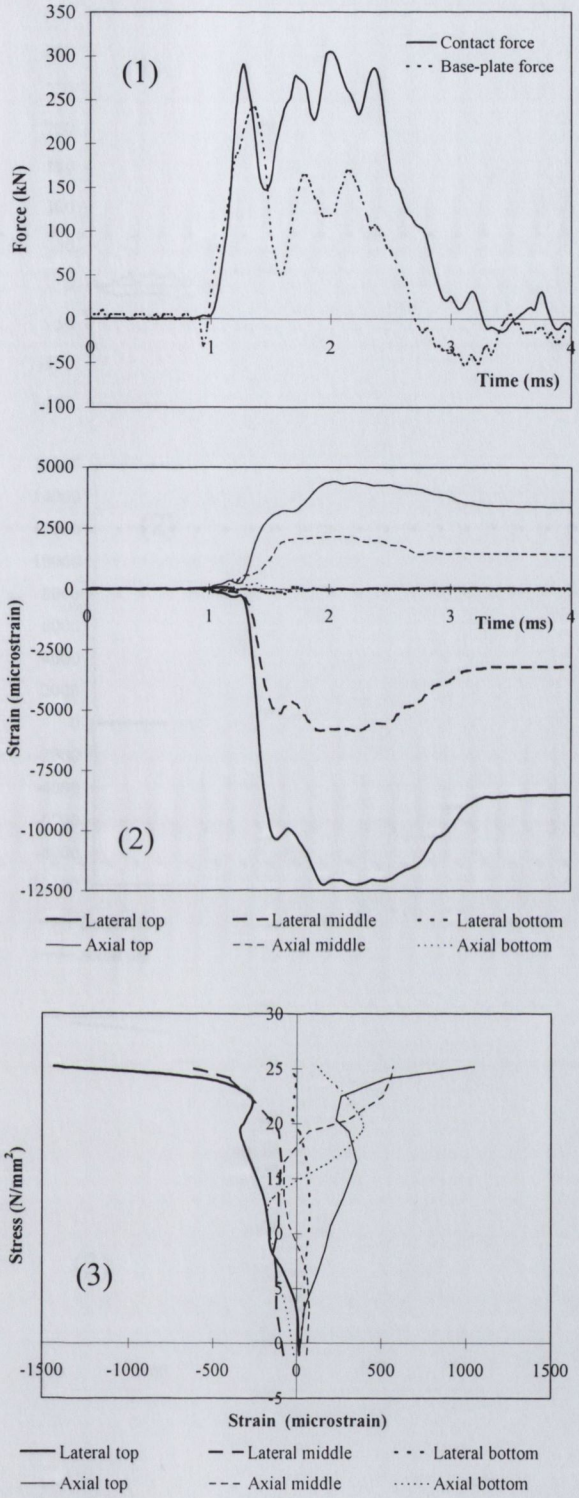


Figure A3.58 C(110)P (3.6)1e

(1) Loadcell response, (2) strain gauge response and (3) stress-strain response

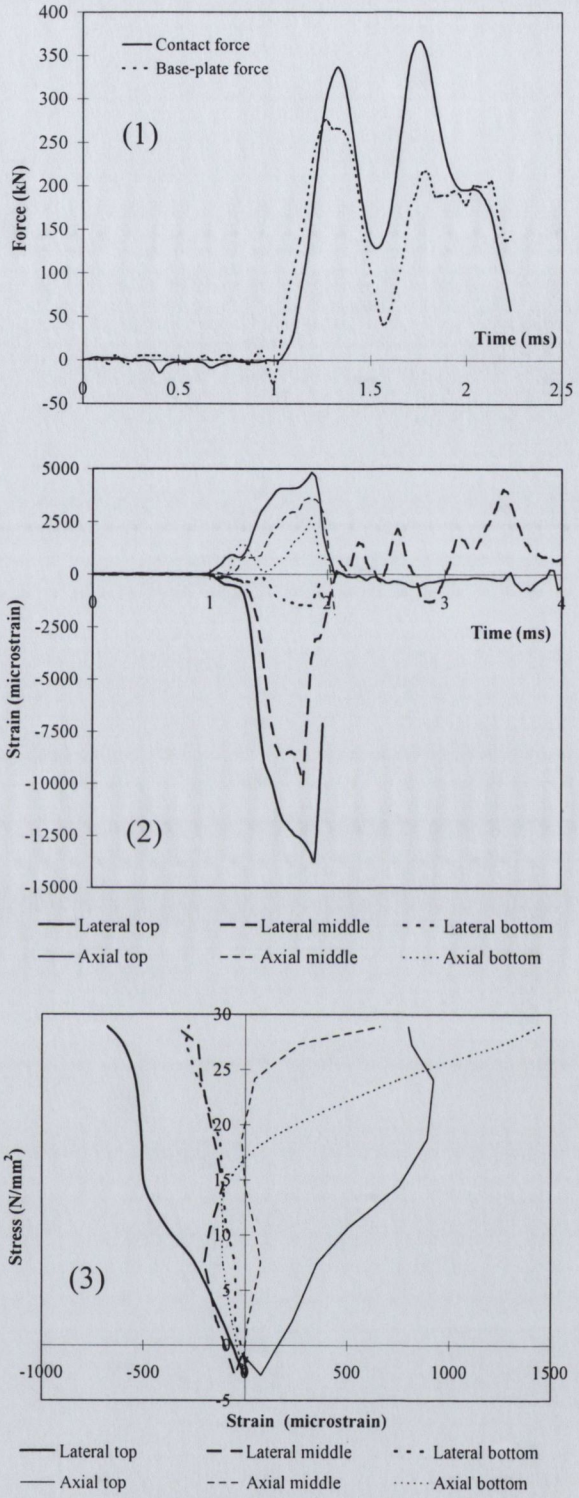
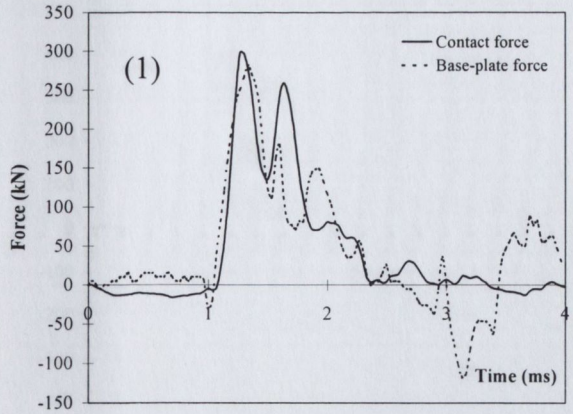
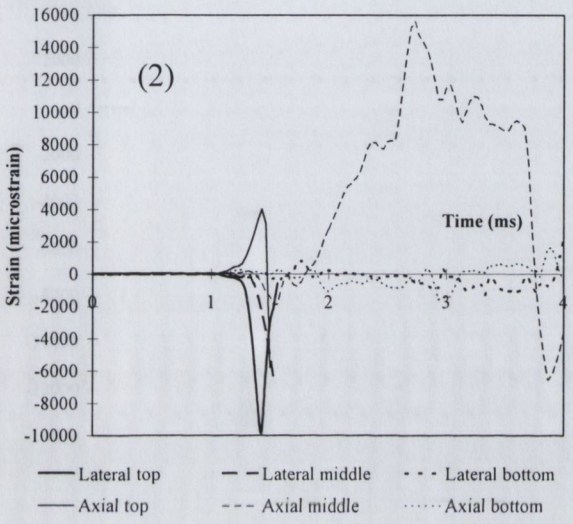


Figure A3.59 C(110)P (3.6)2a

(1) Loadcell response, (2) strain gauge response and (3) stress-strain response





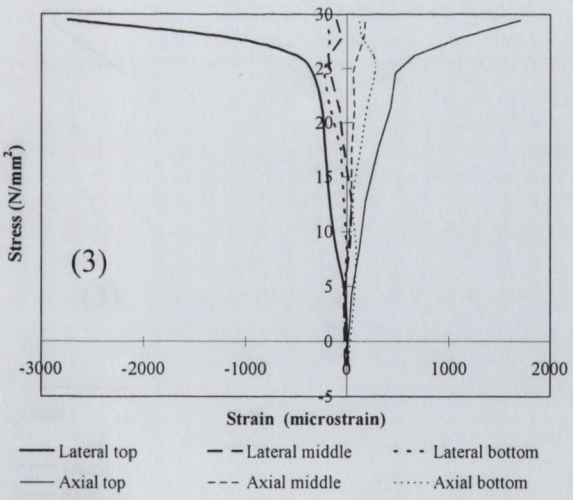
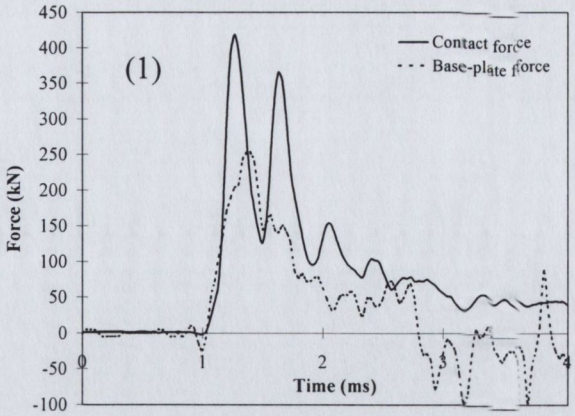
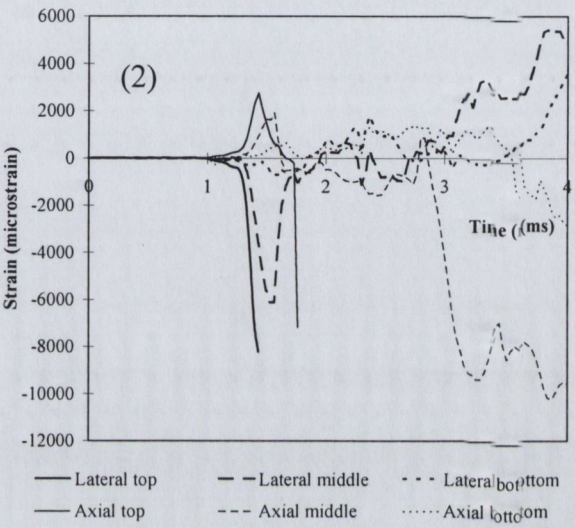


Figure A3.60 C(110)P (3.6)2b

(1) Loadcell response, (2) strain gauge response and (3) stress-strain response





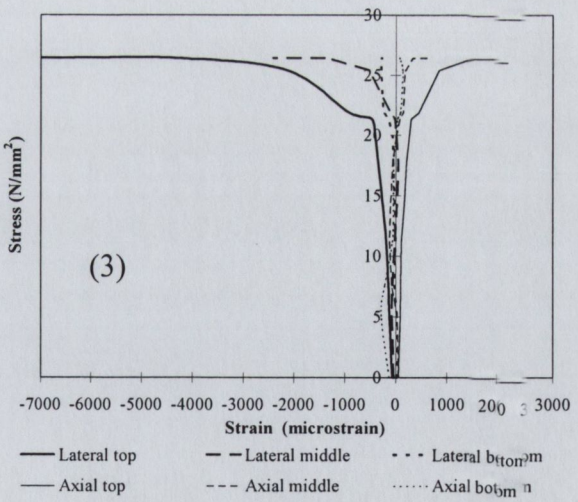


Figure A3.61 C(110)P (3.6)2c

(1) Loadcell response, (2) strain gauge response and (3) stress-strain response

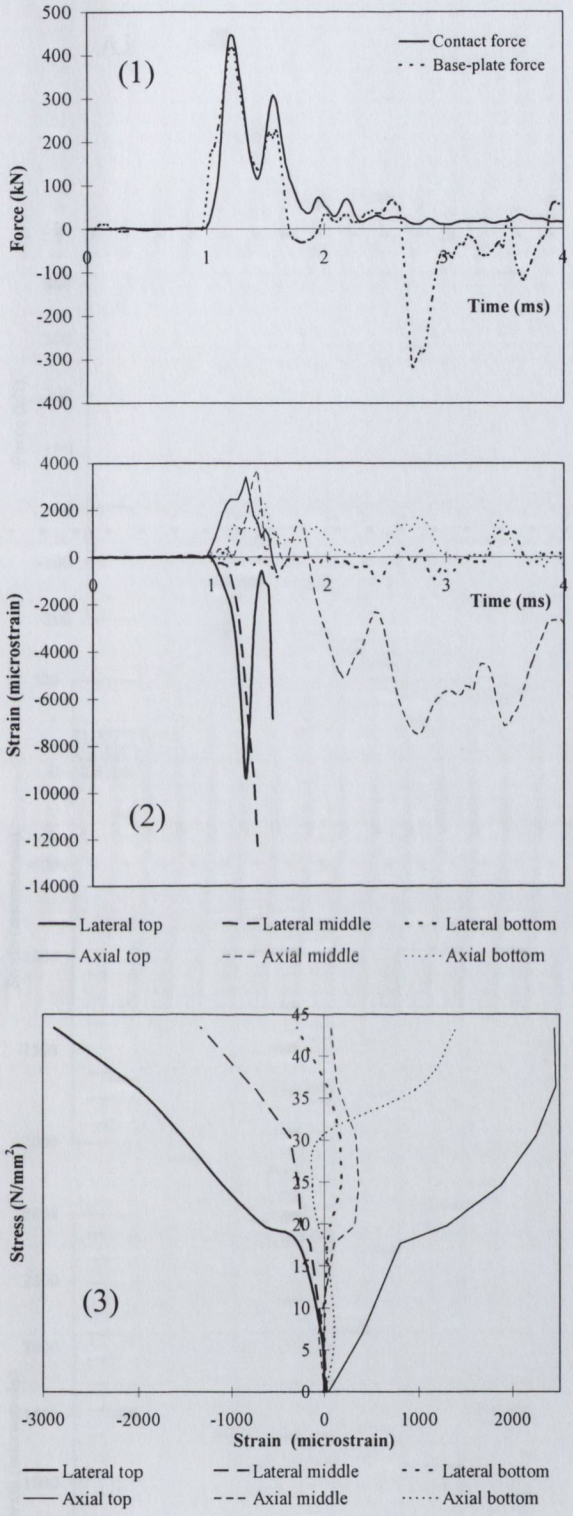


Figure A3.62 C(110)P (3.6)3a

(1) Loadcell response, (2) strain gauge response and (3) stress-strain response

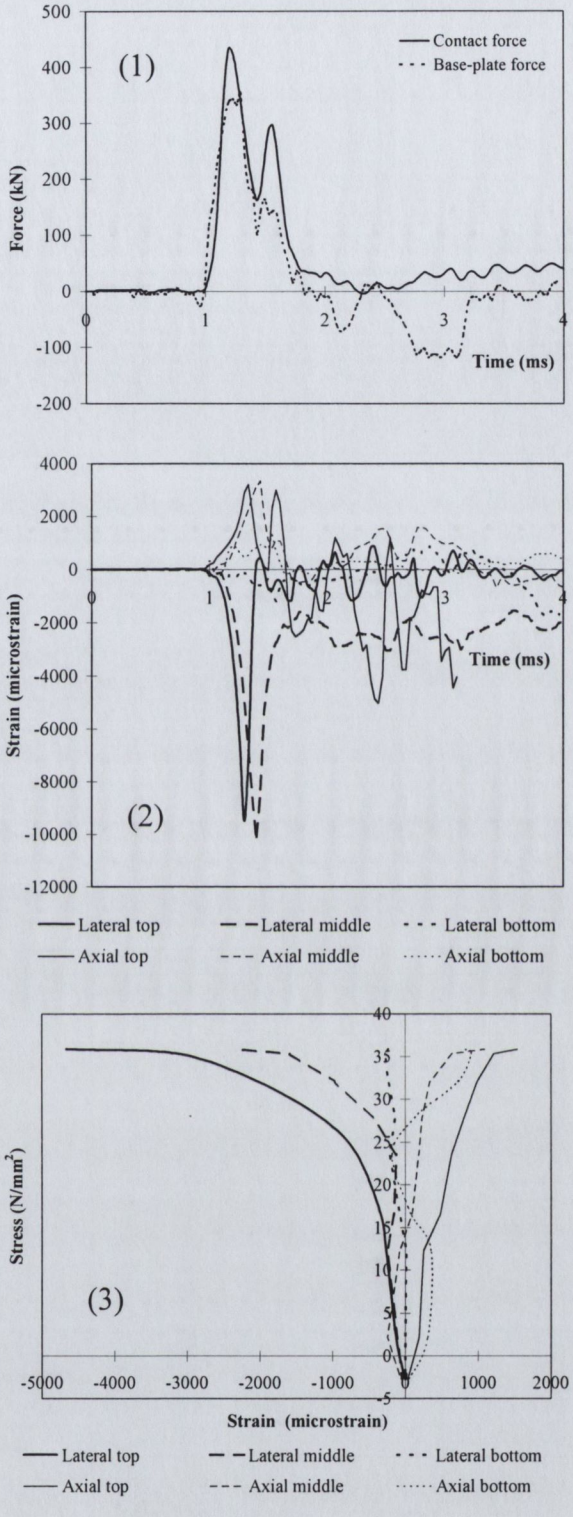


Figure A3.63 C(110)P (3.6)3b

(1) Loadcell response, (2) strain gauge response and (3) stress-strain response

APPENDIX 3.7. IMPACT RESPONSE OF SLEEVED CYLINDERS, 3.25 MM ALUMINIUM

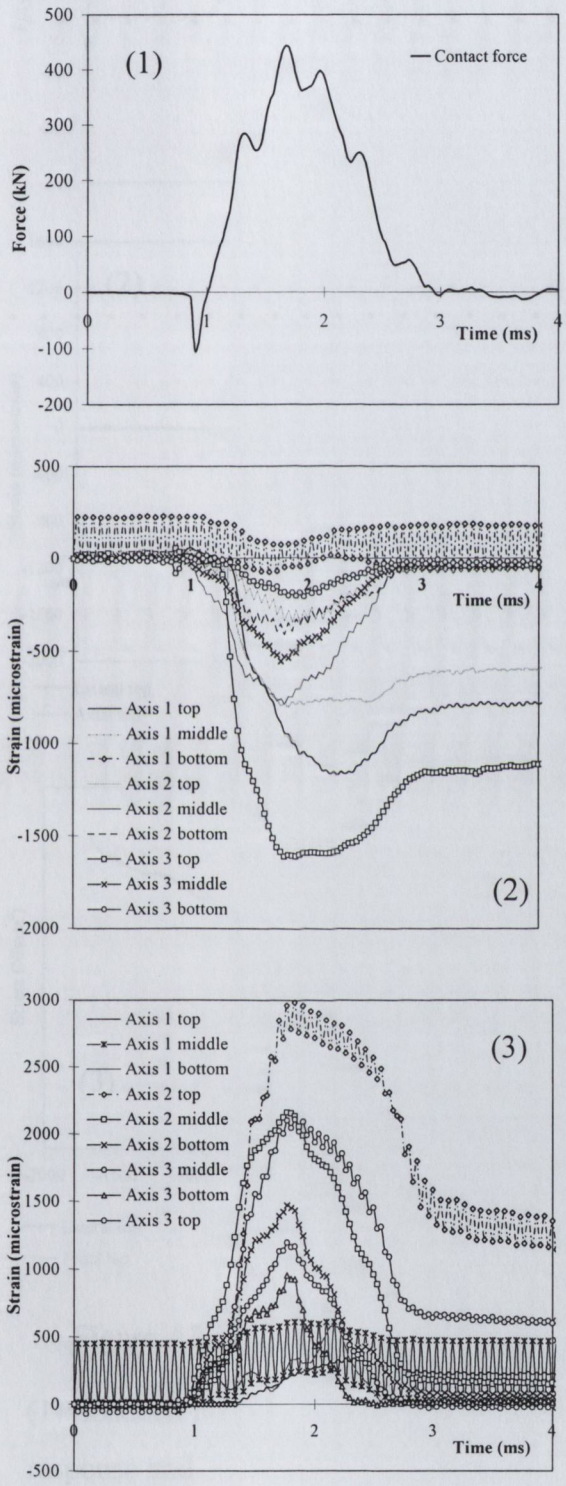


Figure A3.64 C(115)A (3.25)1a

(1) Loadcell response, (2) lateral strain gauge and (3) axial strain gauge response

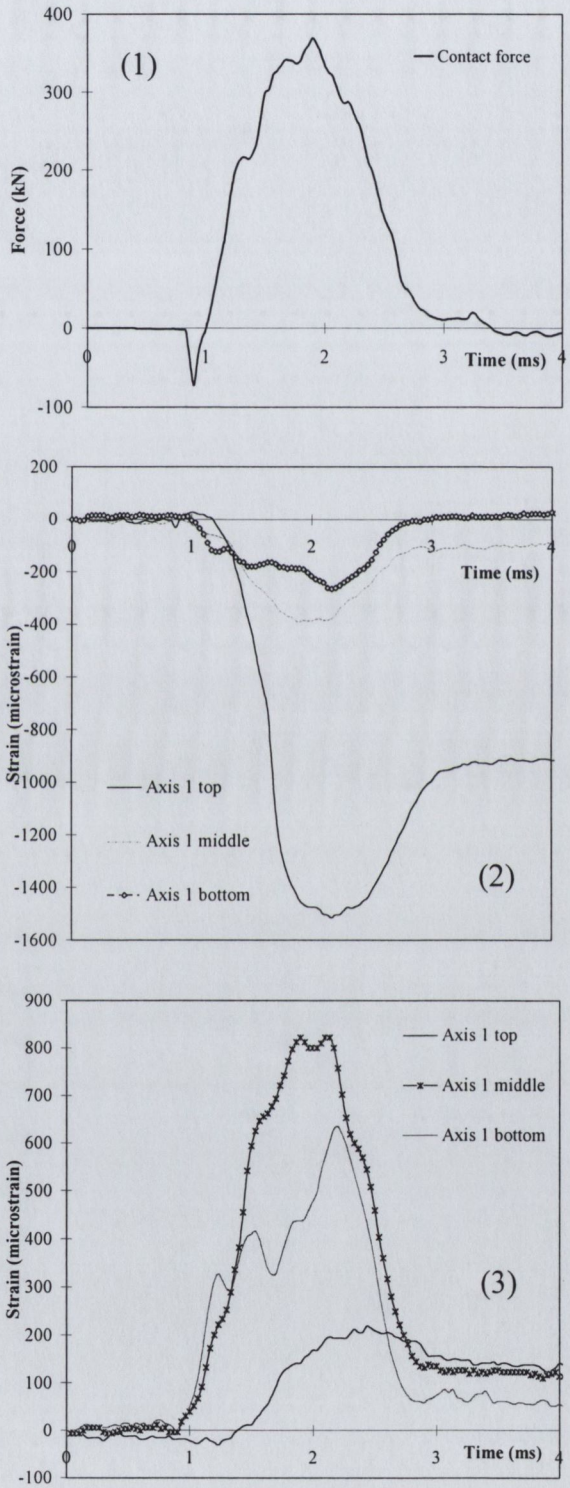


Figure A3.65 C(115)A (3.25)1b

(1) Loadcell response, (2) lateral strain gauge and (3) axial strain gauge response

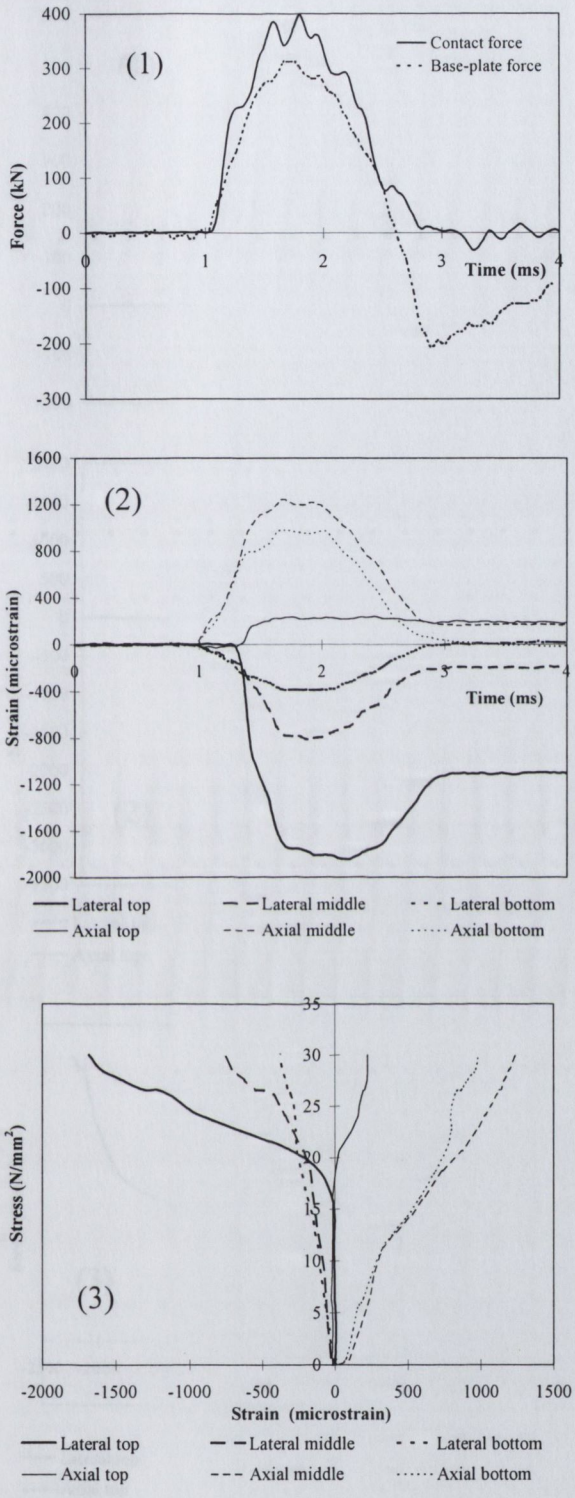


Figure A3.66 C(115)A (3.25)1c

(1) Loadcell response, (2) strain gauge response and (3) stress-strain response

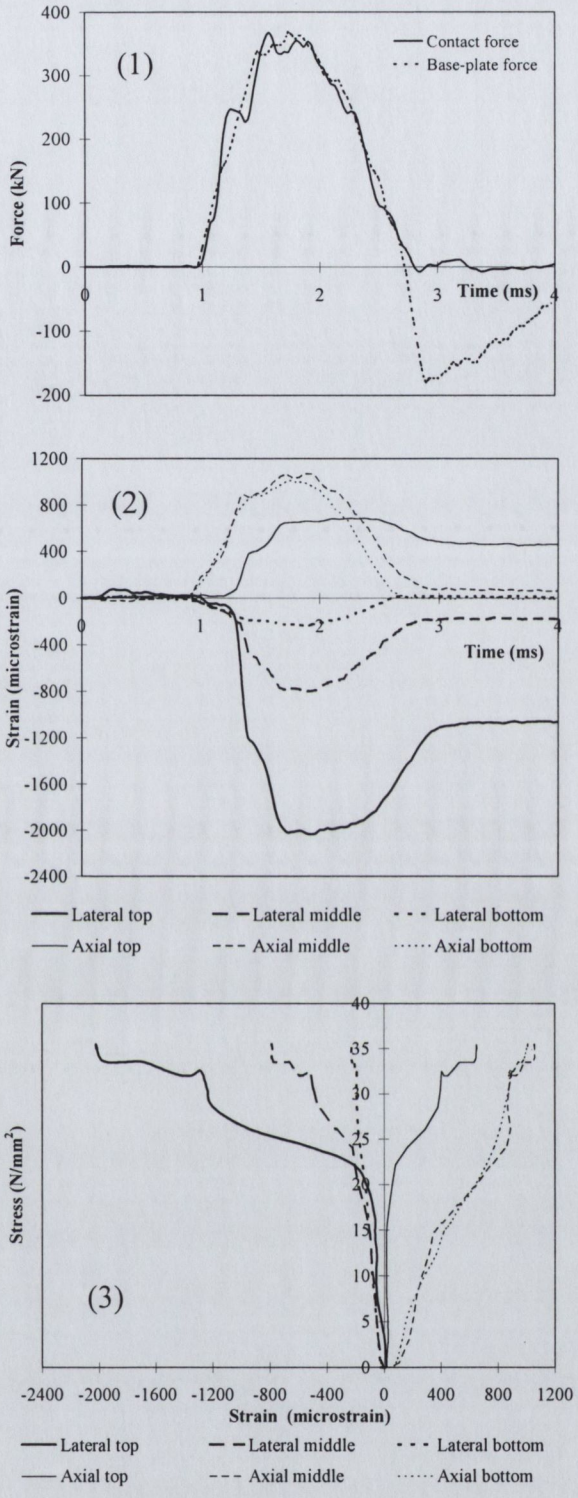


Figure A3.67 C(115)A (3.25)1d

(1) Loadcell response, (2) strain gauge response and (3) stress-strain response

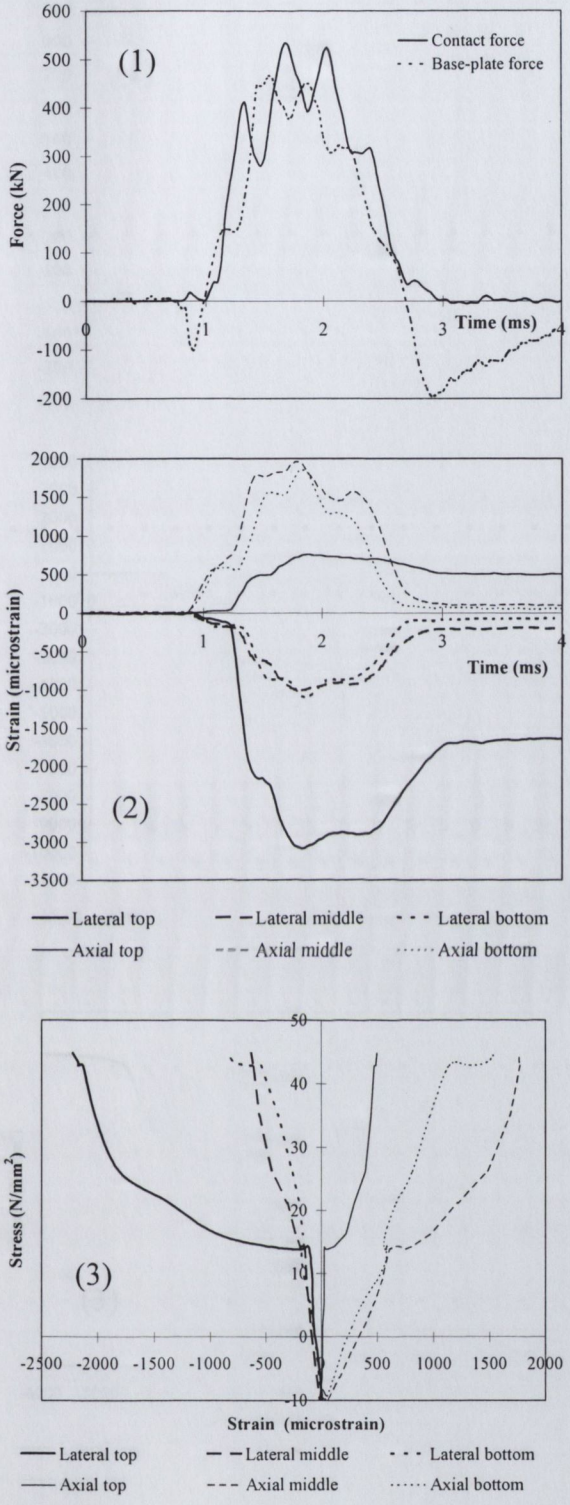


Figure A3.68 C(115)A (3.25)2a

(1) Loadcell response, (2) strain gauge response and (3) stress-strain response

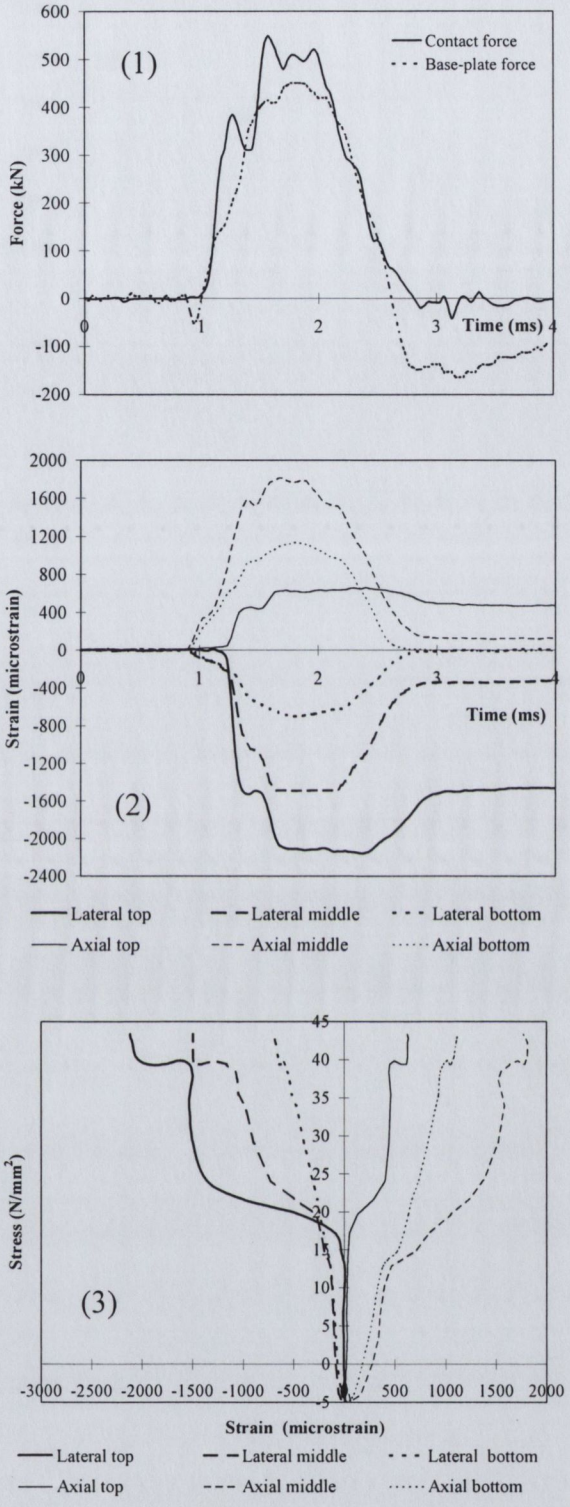


Figure A3.69 C(115)A (3.25)2b

(1) Loadcell response, (2) strain gauge response and (3) stress-strain response

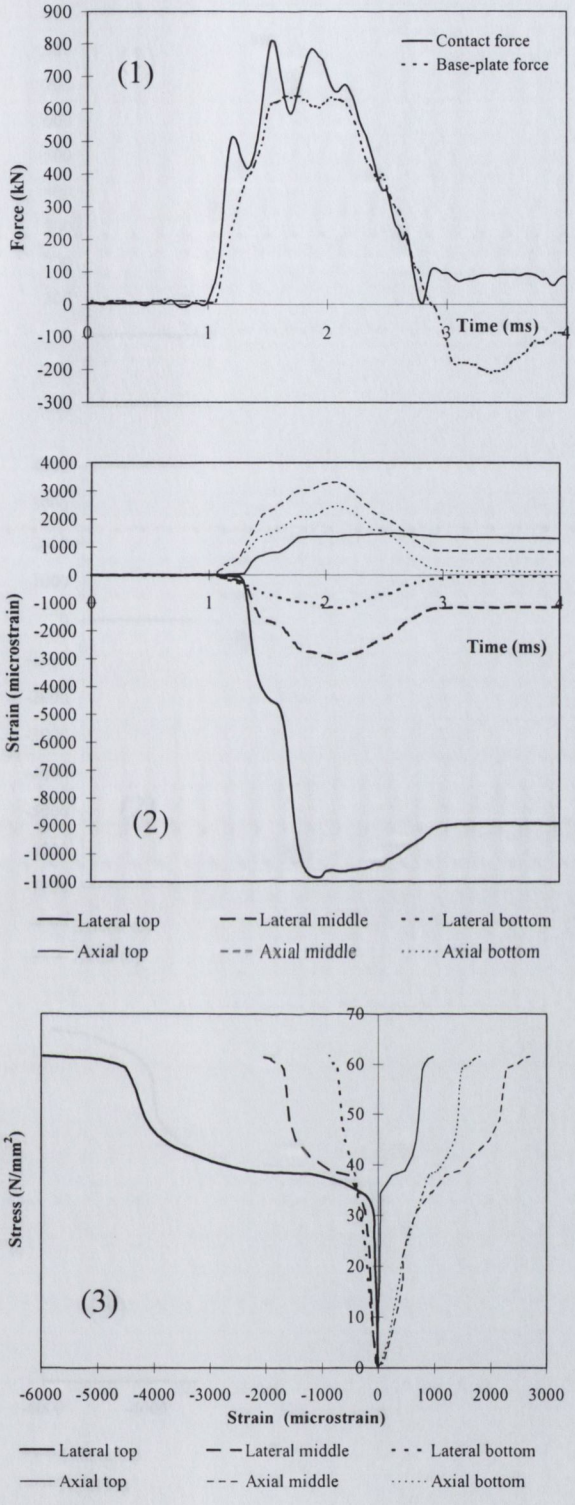


Figure A3.70 C(115)A (3.25)3a

(1) Loadcell response, (2) strain gauge response and (3) stress-strain response

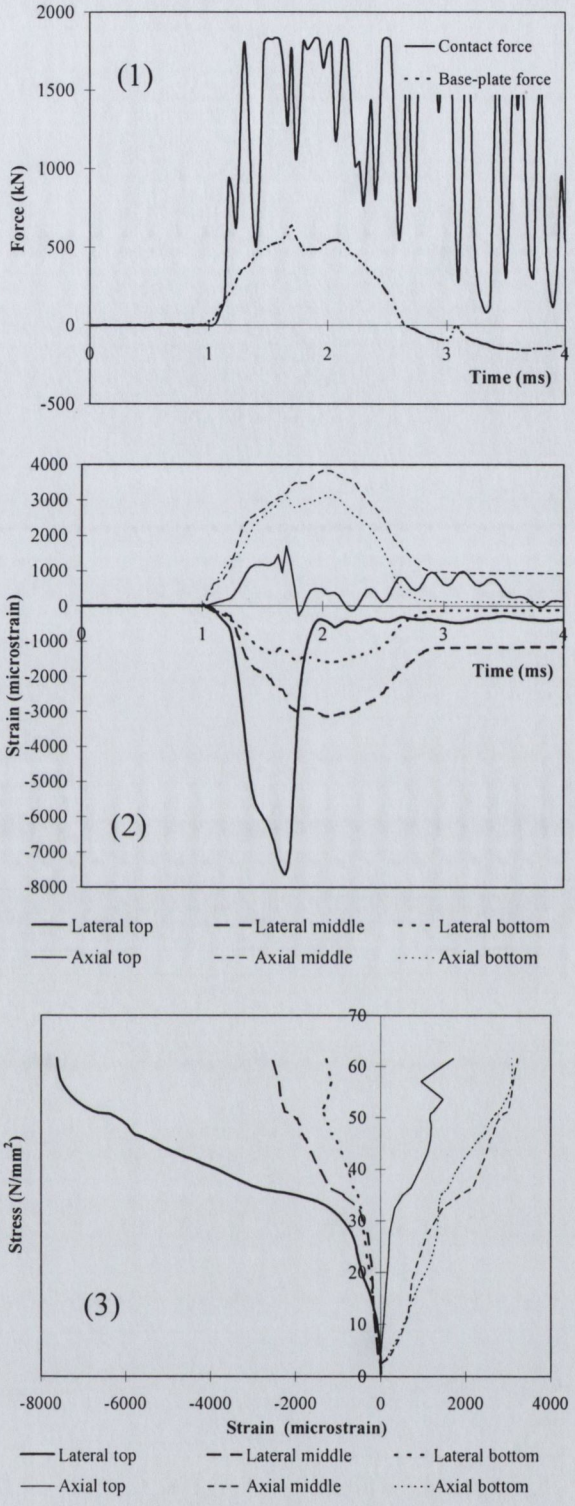


Figure A3.71 C(115)A (3.25)3b

(1) Loadcell response, (2) strain gauge response and (3) stress-strain response

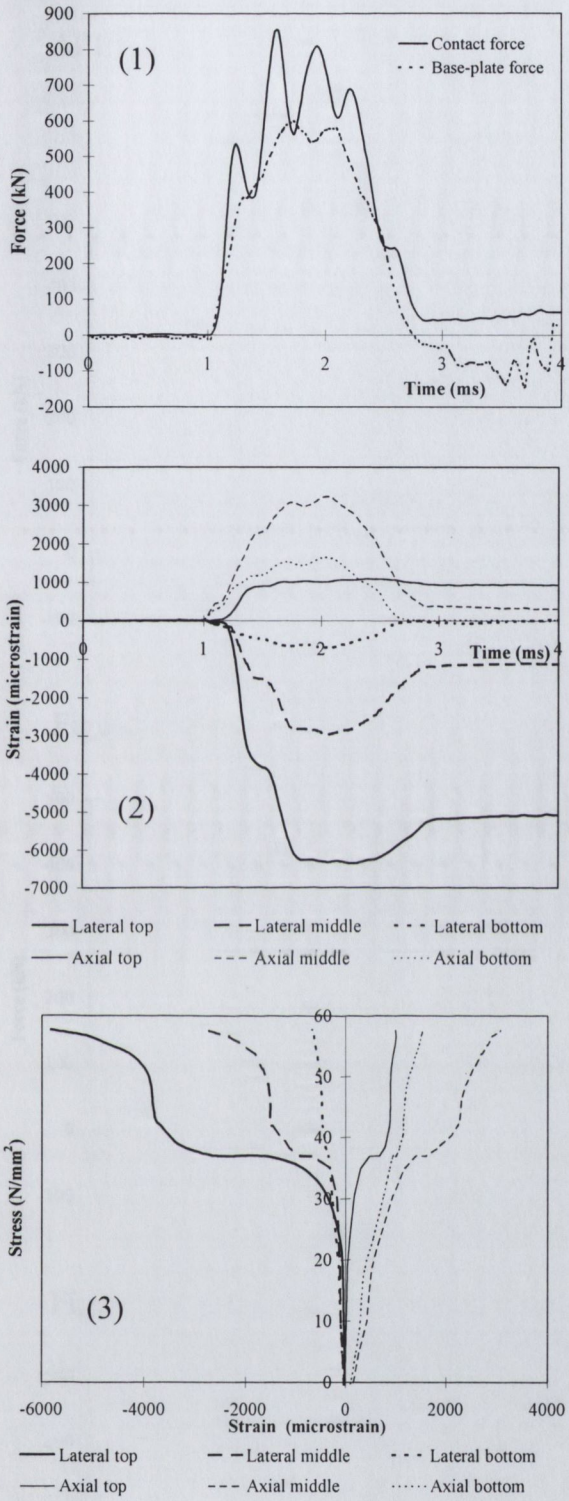


Figure A3.72 C(115)A (3.25)3c

(1) Loadcell response, (2) strain gauge response and (3) stress-strain response

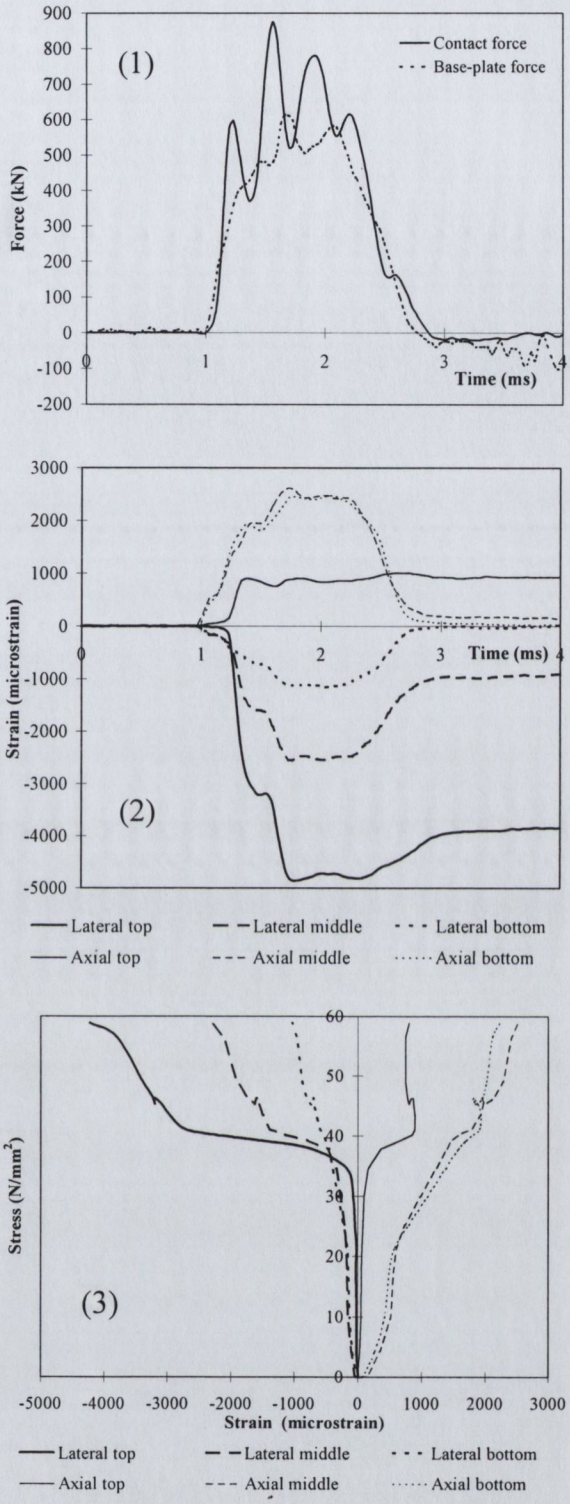


Figure A3.73 C(115)A (3.25)3d

(1) Loadcell response, (2) strain gauge response and (3) stress-strain response

APPENDIX 4.1. IMPACT RESPONSE OF LARGE DIAMETER SLEEVED CONCRETE CYLINDERS, STEEL, 3 MM THICK

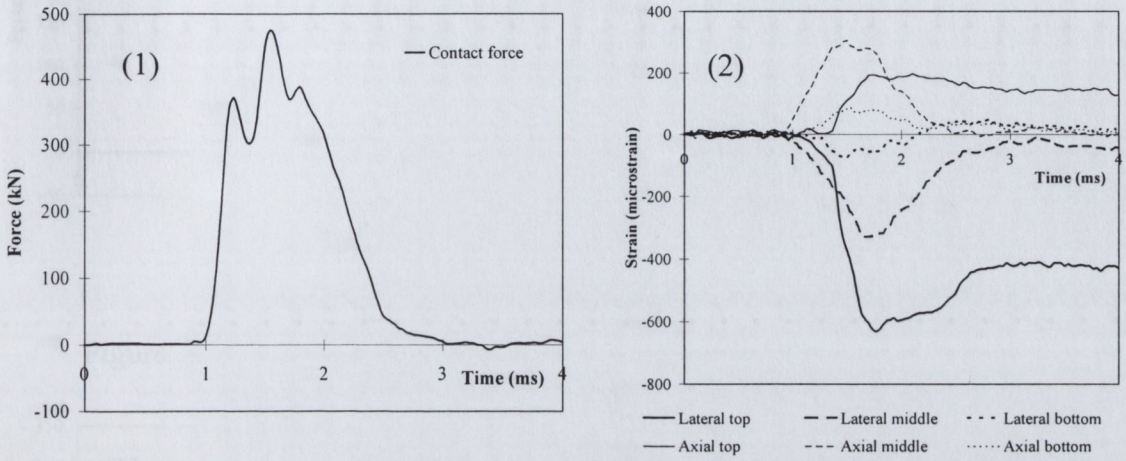


Figure A4.1 C(168)S (3)1a (1) Loadcell response and (2) strain gauge response

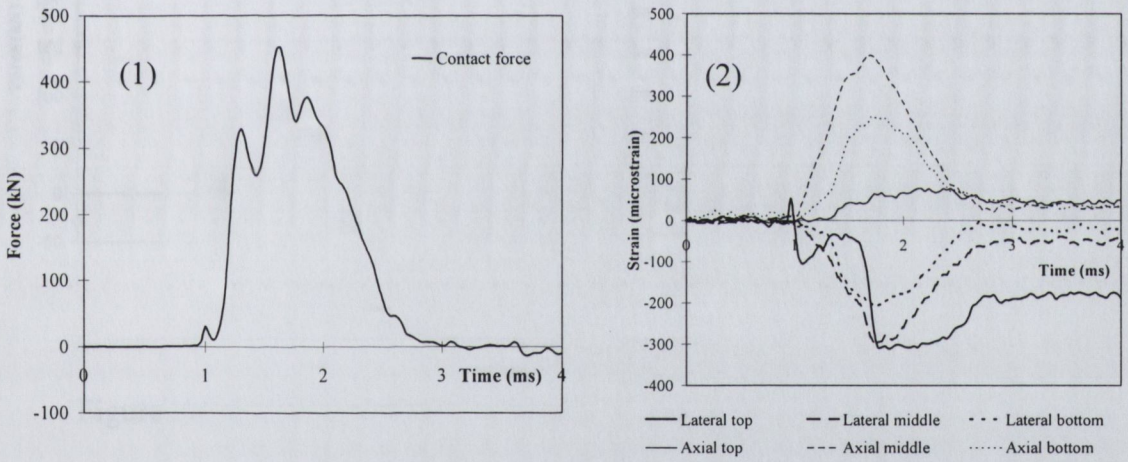


Figure A4.2 C(168)S (3)1b (1) Loadcell response and (2) strain gauge response

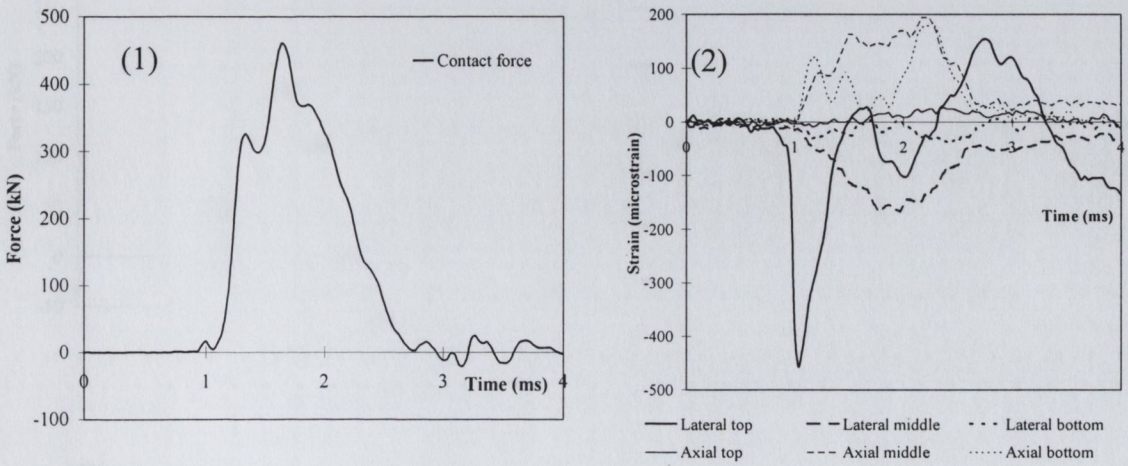


Figure A4.3 C(168)S (3)1c (1) Loadcell response and (2) strain gauge response

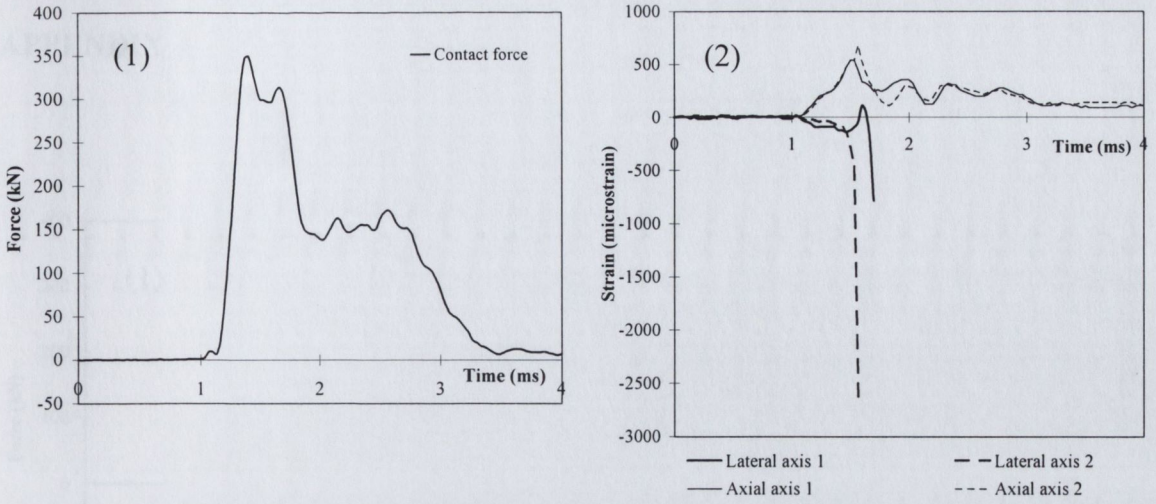


Figure A4.4 U(162)1a (1) Loadcell response and (2) strain gauge response

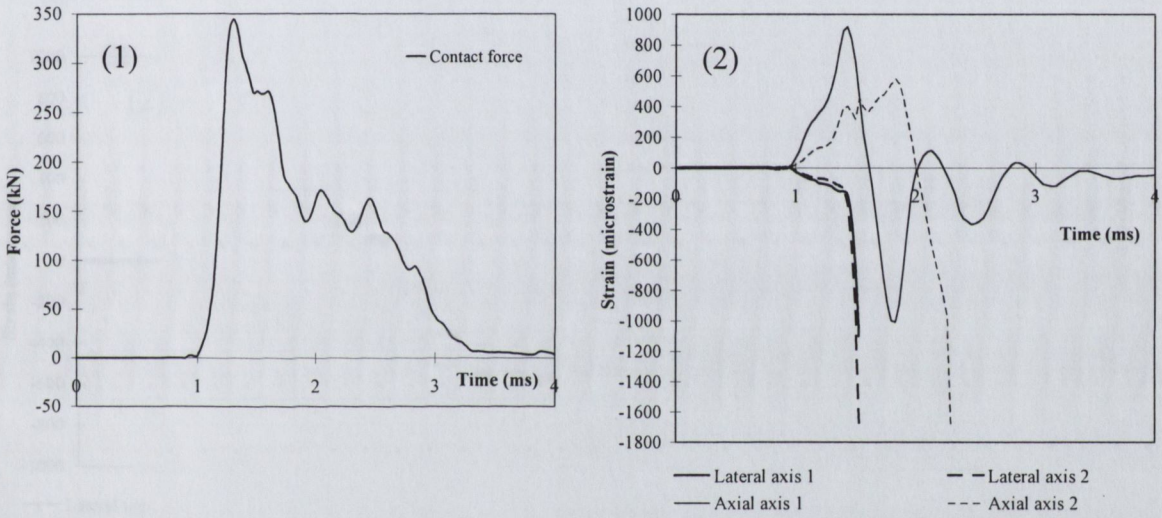


Figure A4.5 U(162)1b (1) Loadcell response and (2) strain gauge response

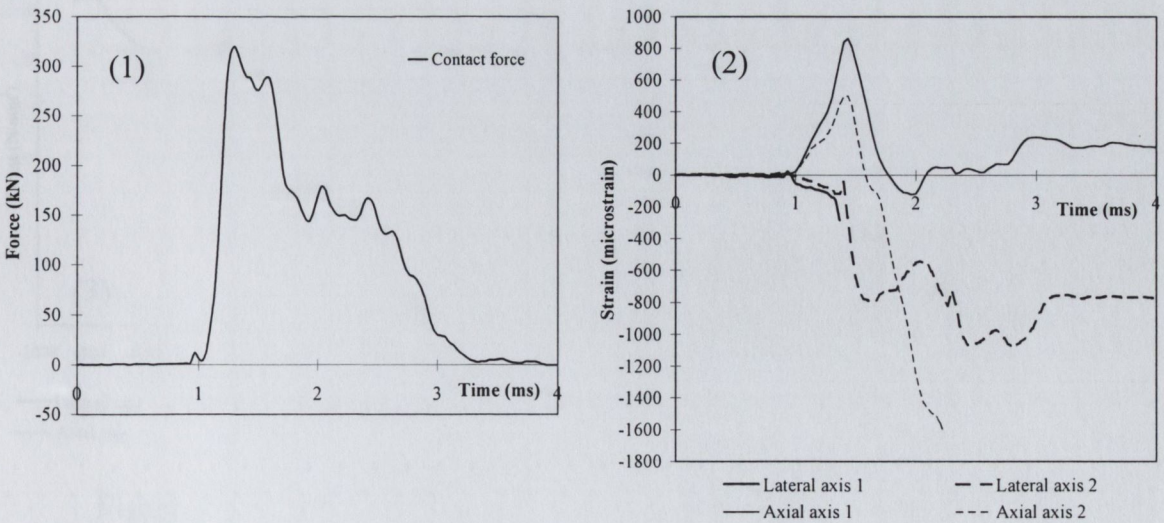


Figure A4.6 U(162)1c (1) Loadcell response and (2) strain gauge response

APPENDIX 4.2. IMPACT RESPONSE OF SLEEVED CONCRETE CYLINDERS, REDUCED LENGTH OF CONFINEMENT AT THE BASE

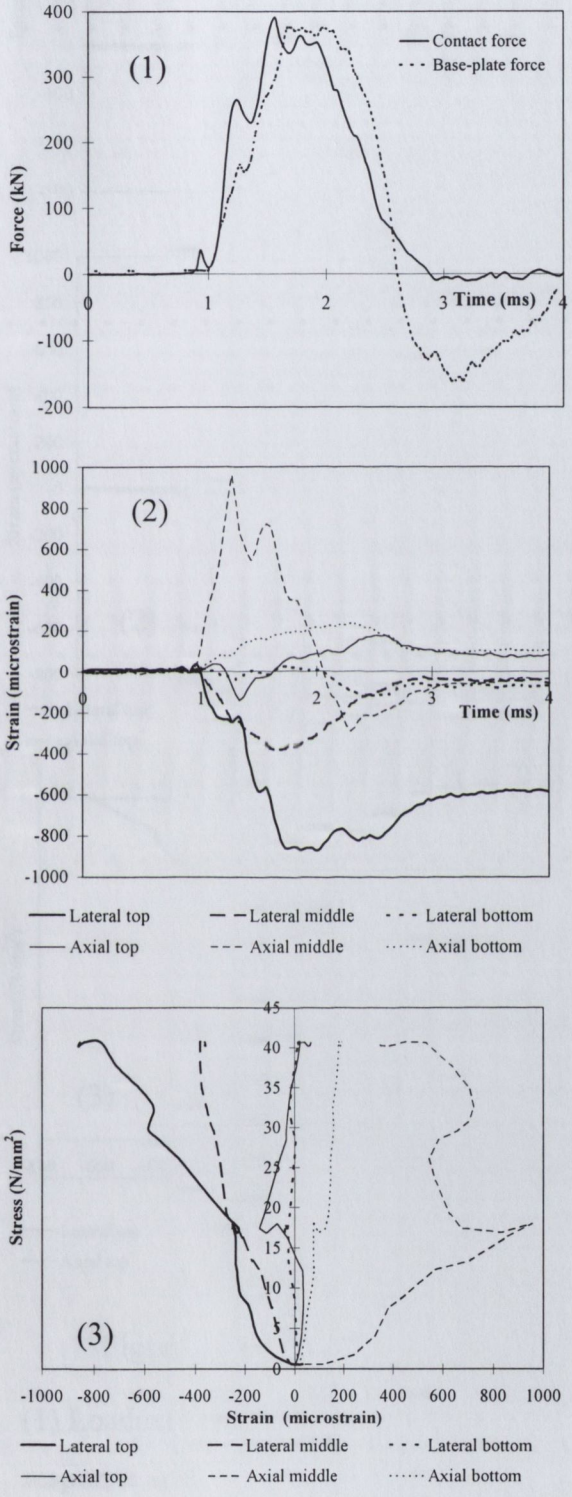


Figure A4.7 R(114)S (3)1a

(1) Loadcell response, (2) strain gauge response and (3) stress-strain response

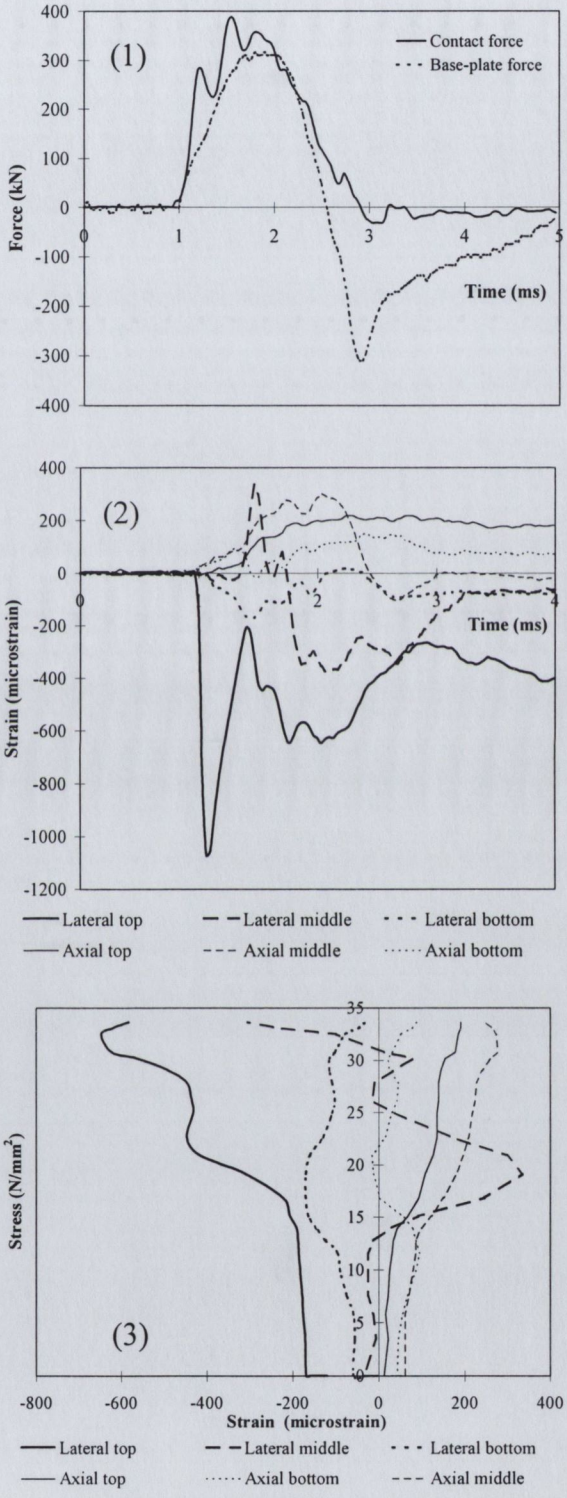


Figure A4.8 R(114)S (3)1b

(1) Loadcell response, (2) strain gauge response and (3) stress-strain response

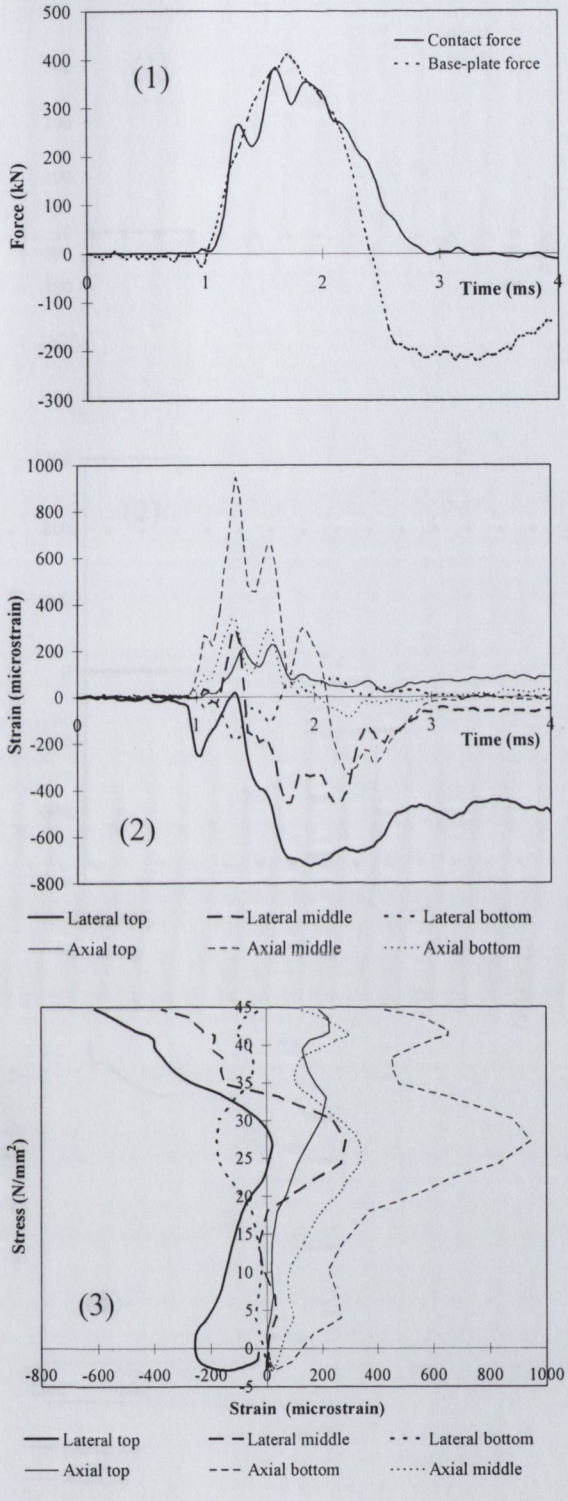


Figure A4.9 R(114)S (3)1c

(1) Loadcell response, (2) strain gauge response and (3) stress-strain response

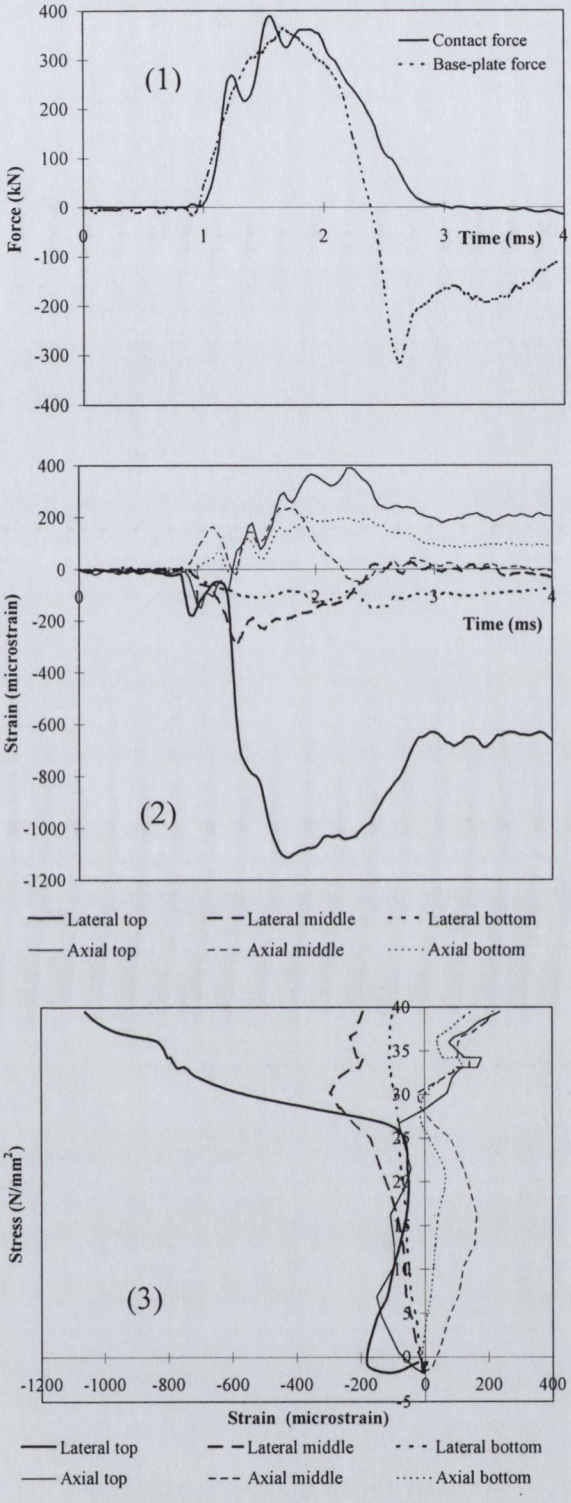


Figure A4.10 R(114)S (3)1d

(1) Loadcell response, (2) strain gauge response and (3) stress-strain response

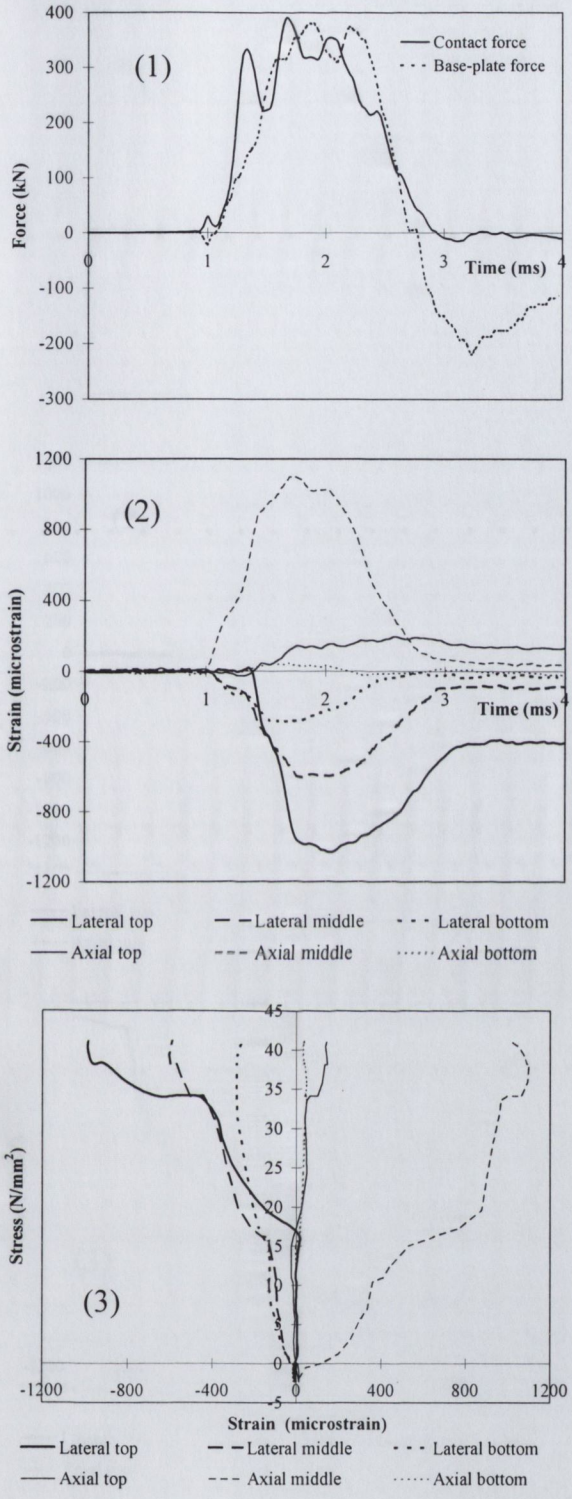


Figure A4.11 R(115)A (3.25)1a

(1) Loadcell response, (2) strain gauge response and (3) stress-strain response

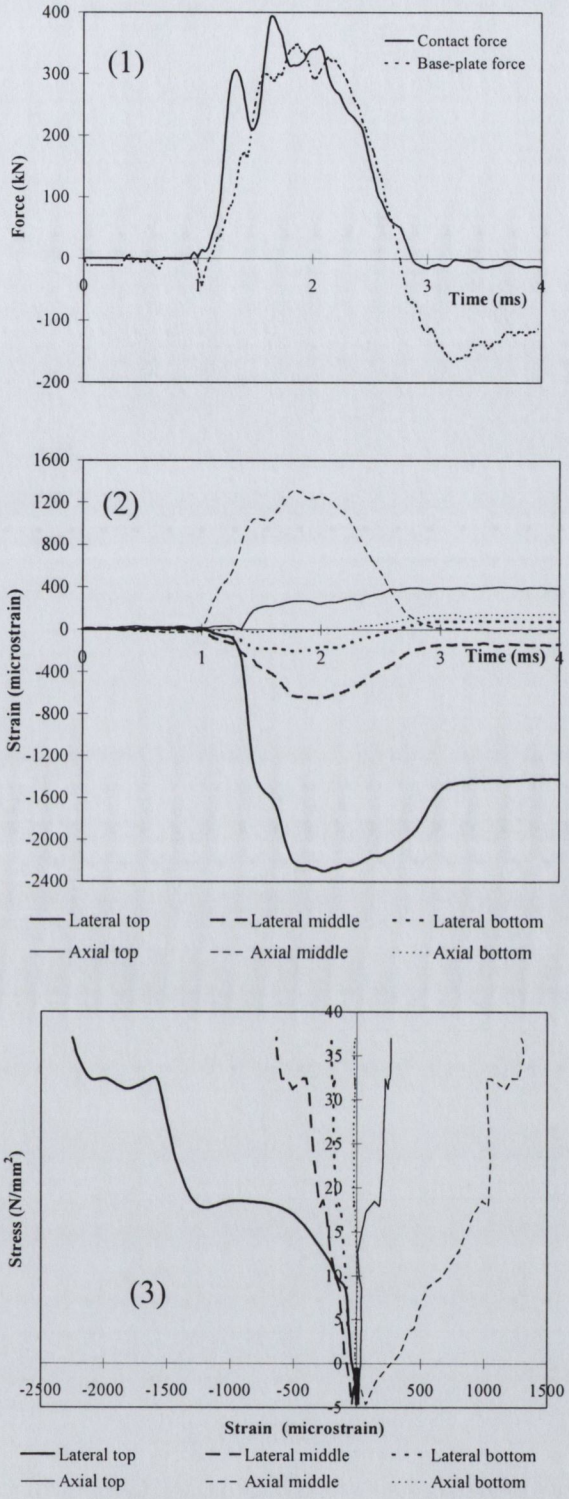


Figure A4.12 R(115)A (3.25)1b

(1) Loadcell response, (2) strain gauge response and (3) stress-strain response

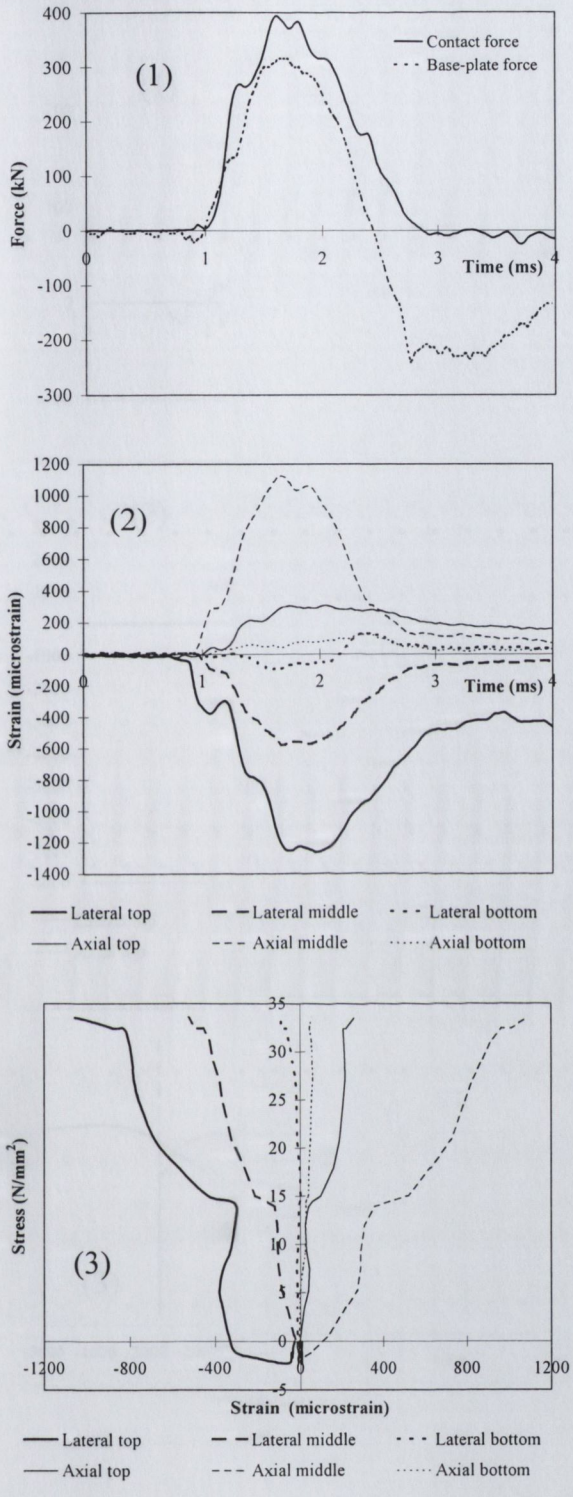


Figure A4.13 R(115)A (3.25)1c

(1) Loadcell response, (2) strain gauge response and (3) stress-strain response

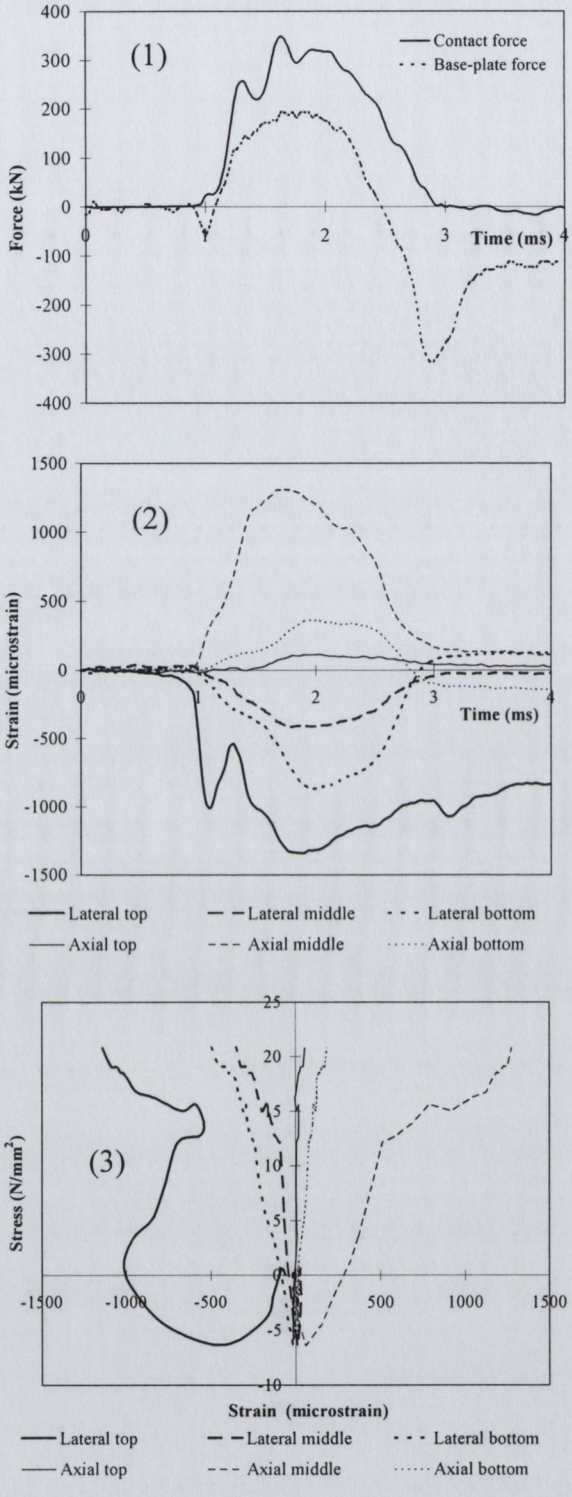


Figure A4.14 R(115)A (3.25)1d

(1) Loadcell response, (2) strain gauge response and (3) stress-strain response

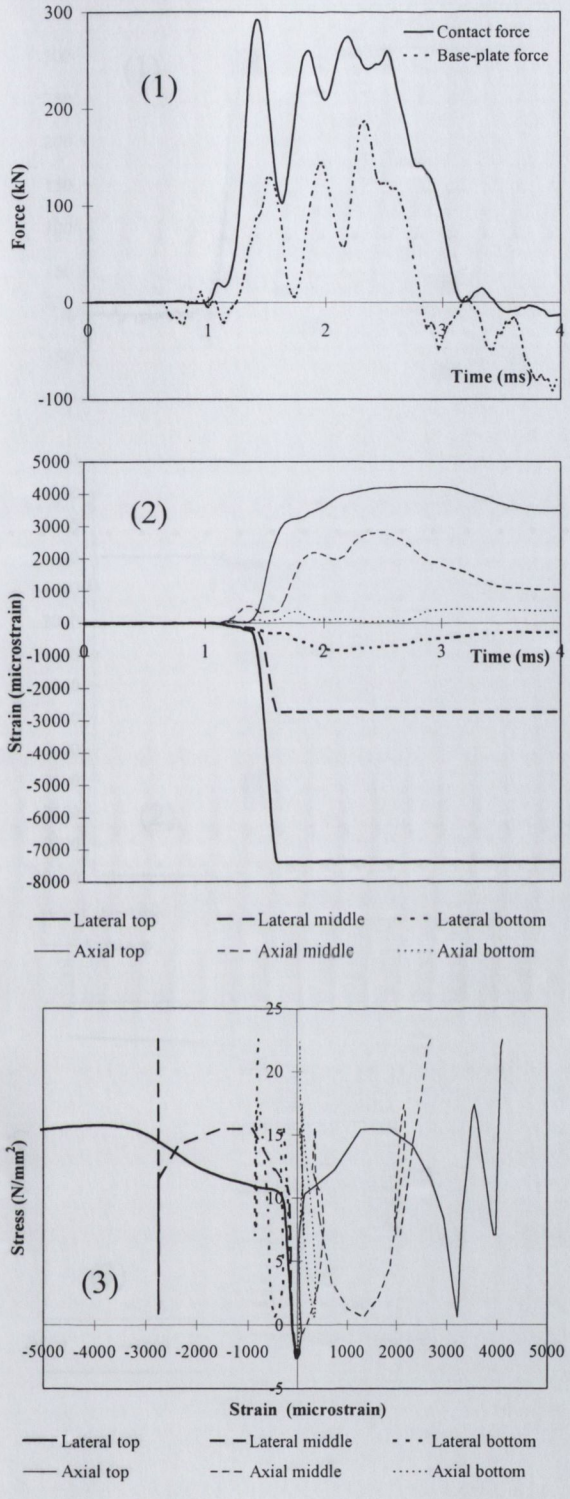


Figure A4.15 R(110)P (3.6)1a

(1) Loadcell response, (2) strain gauge response and (3) stress-strain response

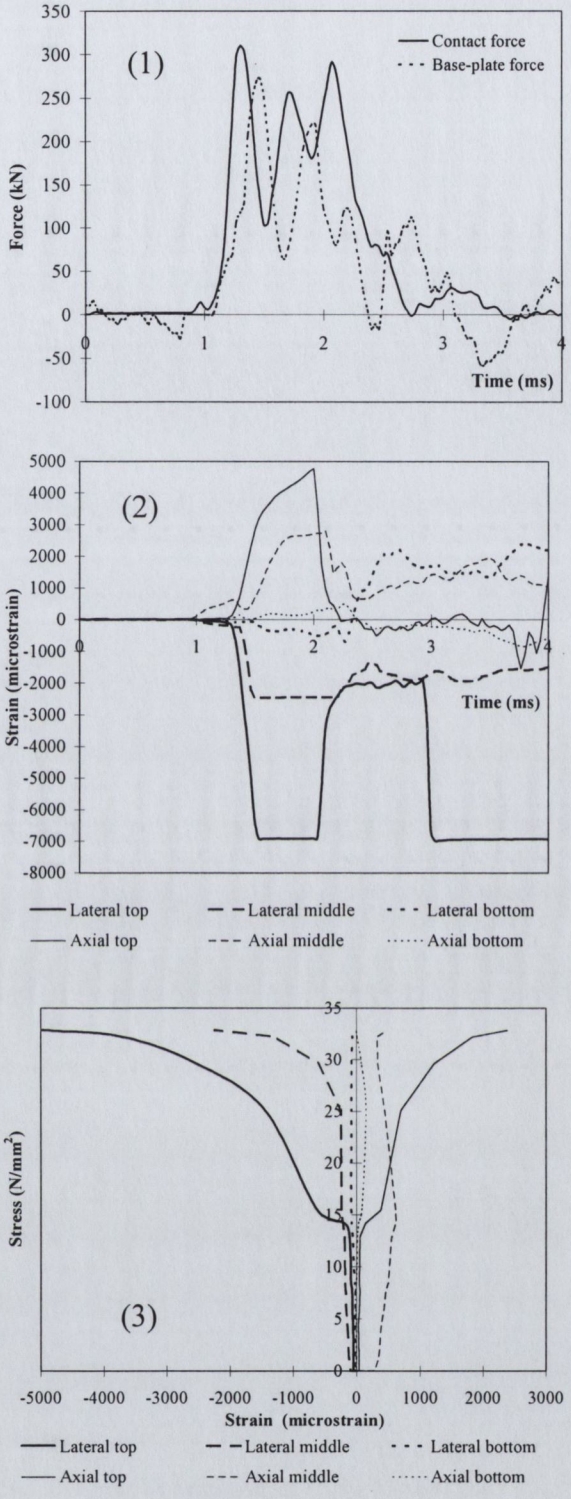


Figure A4.16 R(110)P (3.6)1b

(1) Loadcell response, (2) strain gauge response and (3) stress-strain response

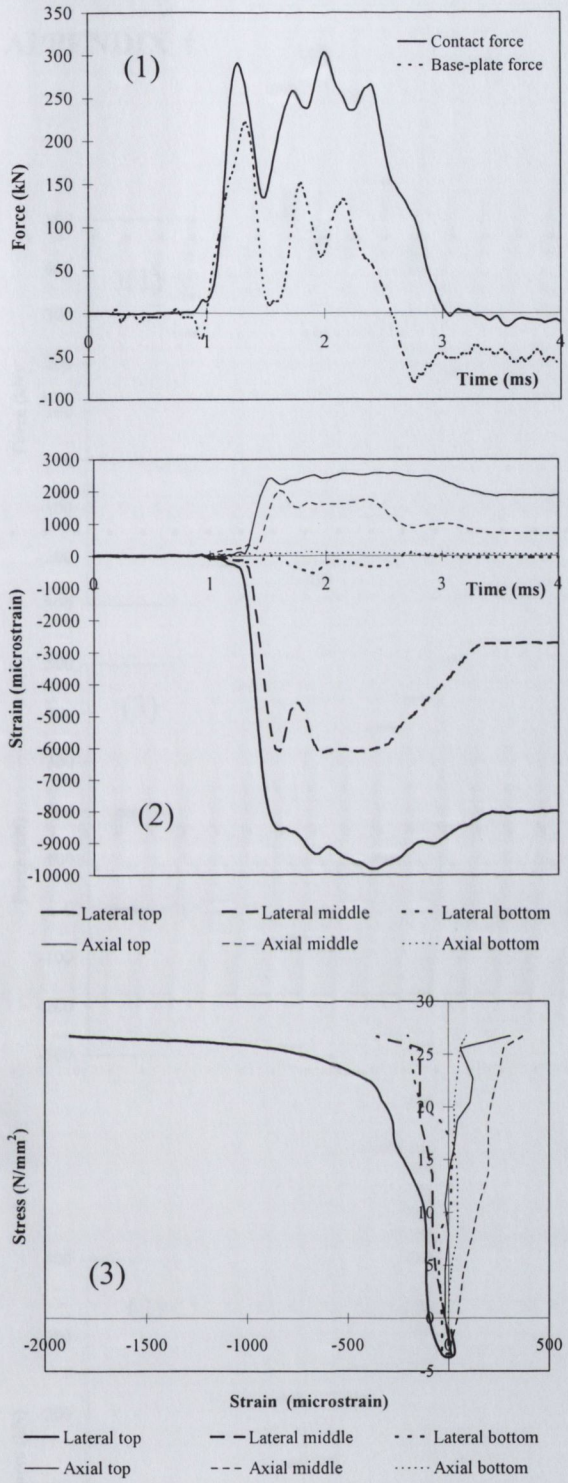


Figure A4.17 R(110)P (3.6)1c

(1) Loadcell response, (2) strain gauge response and (3) stress-strain response

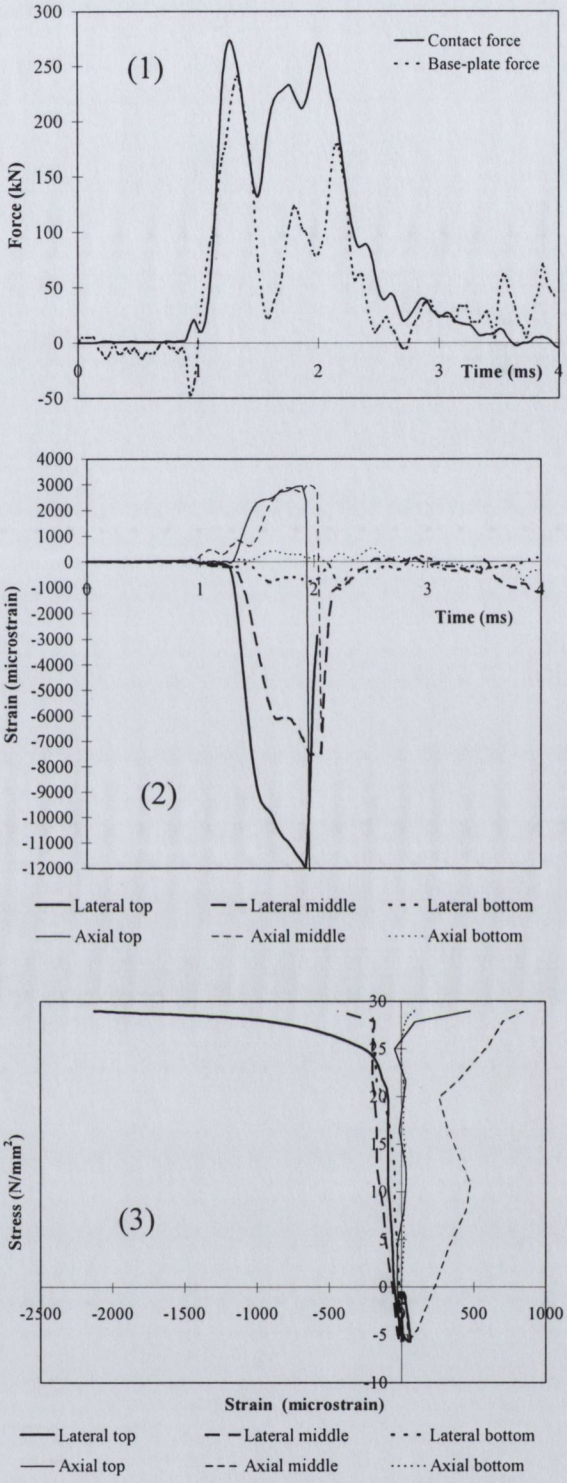


Figure A4.18 R(110)P (3.6)1d

(1) Loadcell response, (2) strain gauge response and (3) stress-strain response

APPENDIX 4.3. IMPACT RESPONSE OF SLEEVED CONCRETE CYLINDERS, REPEAT IMPACT TESTS

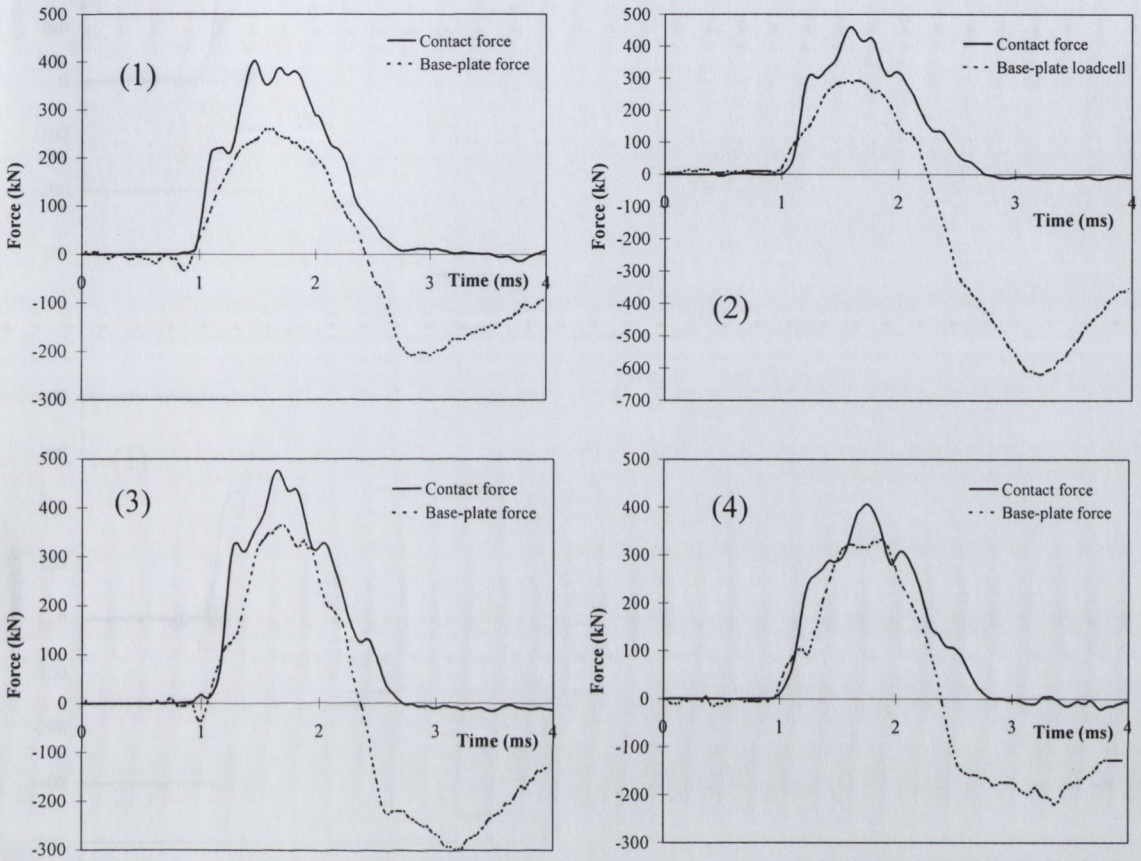
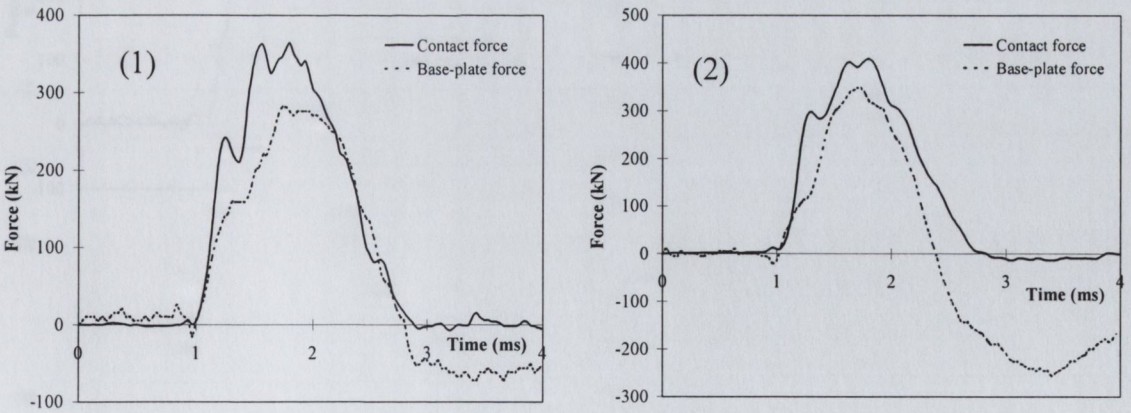


Figure A4.19 C(114)S (3)1d

Original test and repeats 2, 3 and 4



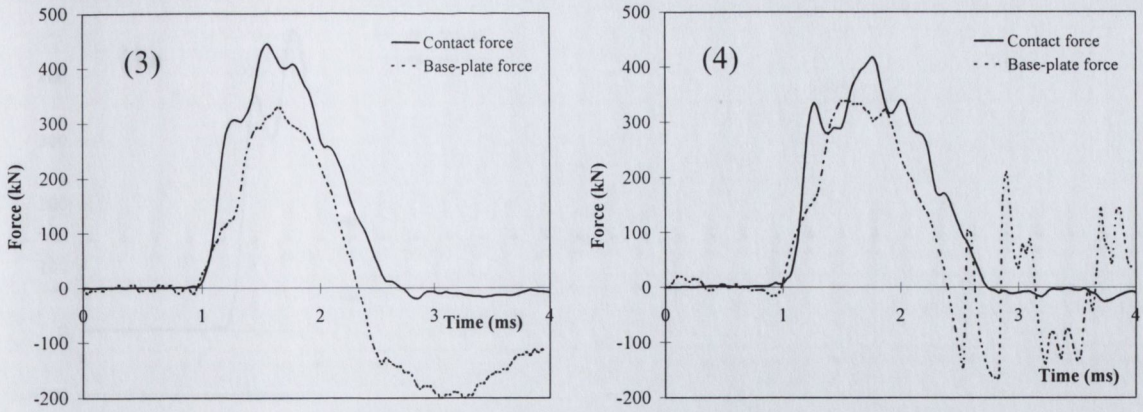


Figure A4.20 C(114)S (1.2)1d

Original test and repeats 2, 3 and 4

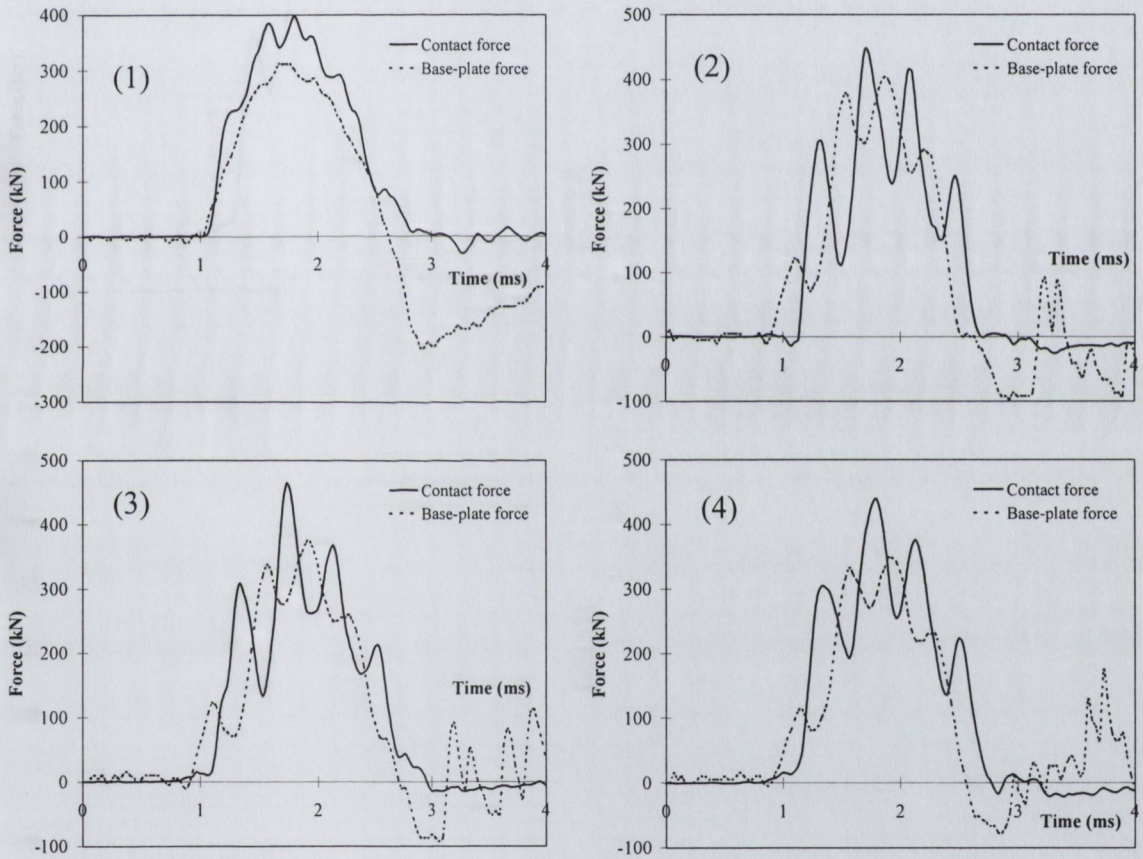


Figure A4.21 C(115)A (3.25)1c

Original test and repeats 2, 3 and 4

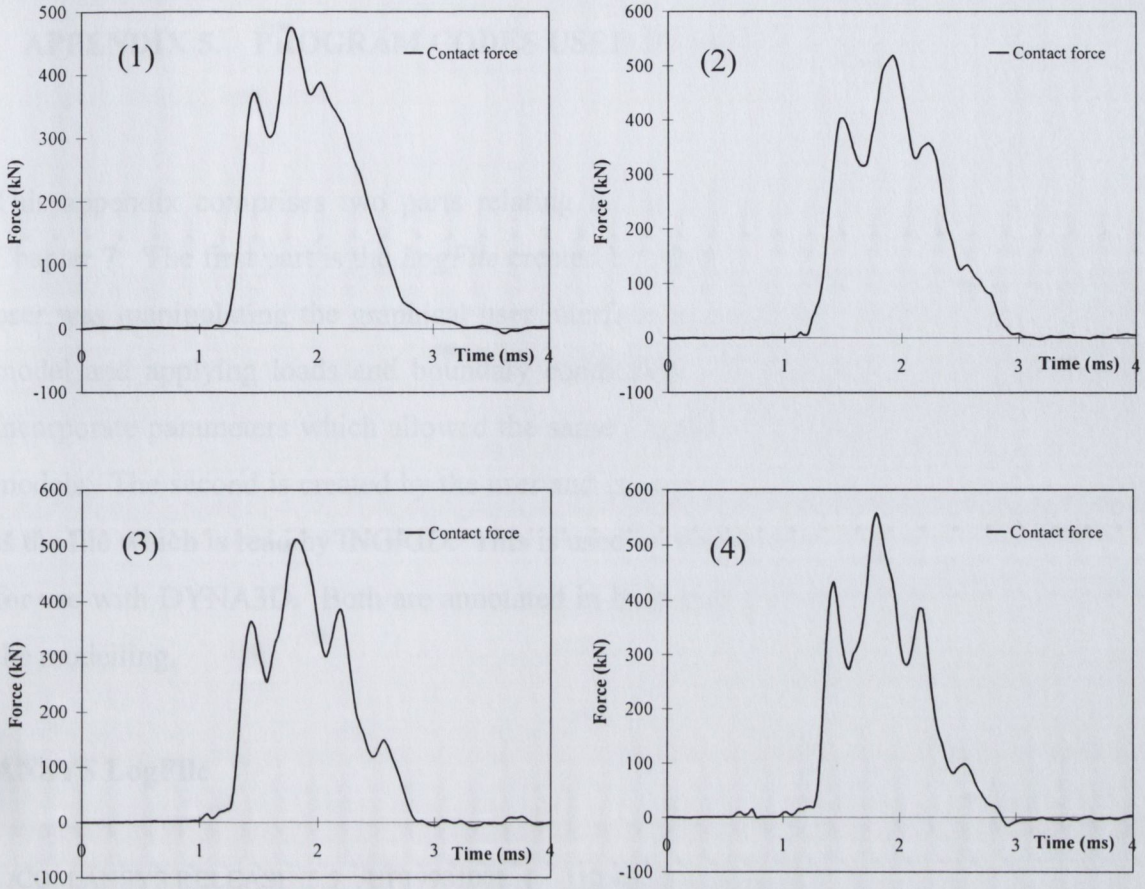


Figure A4.22 C(168)S (3)1a

Original test and repeats 2, 3 and 4

APPENDIX 5. PROGRAM CODES USED IN FINITE ELEMENT ANALYSIS

This appendix comprises two parts relating to the finite element analysis performed in Chapter 7. The first part is the *LogFile* created by ANSYS, in the background, whilst the user was manipulating the graphical user interface to create the 2-dimensional geometric model and applying loads and boundary conditions. The *Logfile* was then modified to incorporate parameters which allowed the same *Logfile* to be used to generate subsequent models. The second is created by the user and is used in the modelling with DYNA3D. It is the file which is read by INGRID. This is used by the program to create the control cards for use with DYNA3D. Both are annotated in bold italics to describe what occurs during the modelling.

ANSYS LogFile

```
! /COM,ANSYS RELEASE  5.5    UP19981001 .1      12:48:23    07/11/2000
!*
! This ANSYS Logfile has been edited to remove internal program calculations such as rotating and
! zooming in on the model. These modifications do not alter the core principles of the model.
!*
! Define variables in this Parameterised Model
kp1 = 54.15                    ! Width of concrete cylinder
th = 3                         ! Thickness of sleeve
es1 = 210000                   ! Young's modulus of sleeve
ros1 = 7800                    ! Density of sleeve
prsl = .3                      ! Poisson's ratio of sleeve
fric = .25                     ! Friction coefficient between concrete & sleeve
divs = 3                       ! Element divisions on sleeve thickness
pressure =120                  ! Pressure applied to concrete
!*
/NOPR
/PMETH,OFF
KEYW,PR_SET,1
KEYW,PR_STRUC,1                ! Use ANSYS Structural Edition
KEYW,PR_THERM,0
KEYW,PR_FLUID,0
KEYW,PR_ELMAG,0
KEYW,MAGNOD,0
KEYW,MAGEDG,0
KEYW,MAGHFE,0
KEYW,MAGELC,0
KEYW,PR_MULTI,0
KEYW,PR_CFD,0
/GO
!*
/PREP7                         ! Enter the ANSYS Pre-Processor
!*
ET,1,PLANE42                   ! Element Type 1 (Concrete) – 4 noded brick (Plane 42)
!*
```

```
ET,2,PLANE42            ! Element Type 2 (Sleeve) – 4 noded brick  (Plane 42)
!*
!*                      ! Set element options for element 1
KEYOPT,1,1,0
KEYOPT,1,2,0
KEYOPT,1,3,1            !  Defines that the element is axi-symmetric
KEYOPT,1,5,0
KEYOPT,1,6,0
!*                      ! Set element options for element 2
KEYOPT,2,1,0
KEYOPT,2,2,0
KEYOPT,2,3,1            !  Defines that the element is axi-symmetric
KEYOPT,2,5,0
KEYOPT,2,6,0
!*                      ! Set material properties for element 1
UIMP,1,EX, , ,40000,    ! Young's modulus of concrete
UIMP,1,DENS, , ,2400,   ! Density of concrete
UIMP,1,ALPX, , , ,
UIMP,1,REFT, , , ,
UIMP,1,NUXY, , ,.2,     ! Poisson's ratio of concrete
UIMP,1,PRXY, , , ,
UIMP,1,GXY, , , ,
UIMP,1,MU, , , ,
UIMP,1,DAMP, , , ,
UIMP,1,ENTH, , , ,
UIMP,1,HF, , , ,
UIMP,1,QRATE, , , ,
UIMP,1,VISC, , , ,
UIMP,1,SONC, , , ,
!*                      ! Set material properties for element 2
UIMP,2,EX, , ,esl,      ! Parameterised Young's modulus of sleeve
UIMP,2,DENS, , ,rosl,   ! Parameterised density of sleeve
UIMP,2,ALPX, , , ,
UIMP,2,REFT, , , ,
UIMP,2,NUXY, , ,prsl,   ! Parameterised Poisson's ratio of sleeve
UIMP,2,PRXY, , , ,
UIMP,2,GXY, , , ,
UIMP,2,MU, , , ,
UIMP,2,DAMP, , , ,
UIMP,2,ENTH, , , ,
UIMP,2,HF, , , ,
UIMP,2,QRATE, , , ,
UIMP,2,VISC, , , ,
UIMP,2,SONC, , , ,
!*                      ! Construct area of concrete rectangle using KeyPoints
FLST,3,5,8
FITEM,3,0,0,0           ! (x1,y1) = (0,0)
FITEM,3,kp1,0,0         ! (x2,y2) = (kp1,0) Use parameterised width of concrete
FITEM,3,kp1,200,0       ! (x3,y3) = (kp1,200) Use parameterised width of concrete
FITEM,3,0,200,0         ! (x4,y3) = (0,200)
A,P51X                  ! Generate area from KeyPoints
BLC4,kp1,0,th,200       ! Generate area of sleeve using parameterised width of sleeve
!*
                        ! Line sizing of all lines so as to have identical mesh in every model.
FLST,5,4,4,ORDE,4
FITEM,5,2
FITEM,5,5
FITEM,5,7
FITEM,5,9
CM,_Y,LINE
LSEL, , , ,P51X
```

```
!*
CM,_Y1,LINE
CMSEL,,_Y
LESIZE,_Y1, , ,40,1,          ! All vertical lines to contain 40 nodes
CMDEL,_Y
CMDEL,_Y1
!*
FLST,5,2,4,ORDE,2
FITEM,5,6
FITEM,5,8
CM,_Y,LINE
LSEL, , , ,P51X
!*
CM,_Y1,LINE
CMSEL,,_Y
LESIZE,_Y1, , ,divs,1,        ! Parameterised variable for sleeve to contain "divs" nodes
CMDEL,_Y
CMDEL,_Y1
!*
MSHAPE,0,2D                   ! Specify 2D Quadrilateral-shaped elements
MSHKEY,0                      ! Use free meshing – with previous line sizing enabled
!*
CM,_Y,AREA
ASEL, , , ,     1             ! Select concrete area
CM,_Y1,AREA
CHKMSH,'AREA'
CMSEL,S,_Y
!*
AMESH,_Y1                     ! Mesh concrete area
!*
CMDEL,_Y
CMDEL,_Y1
CMDEL,_Y2
!*
CM,_Y,AREA
ASEL, , , ,     2             ! Select sleeve area
CM,_Y1,AREA
CHKMSH,'AREA'
CMSEL,S,_Y
!*
AMESH,_Y1                     ! Mesh sleeve area
!*
CMDEL,_Y
CMDEL,_Y1
CMDEL,_Y2
!*
! Connect the concrete and sleeve using the ANSYS Contact Wizard.
! This will create  another two more element types the program needs for internal calculations.
! ANSYS sets up contact between adjacent nodes and then transforms this into contact between elements,
then lines, then areas.
! /COM, CONTACT PAIR CREATION - START
CM,_NODECM,NODE
CM,_ELEMCM,ELEM
CM,_LINECM,LINE
CM,_AREACM,AREA
! /GSAV,cwz,gsav,,temp         ! Save settings for future use after Contact has been generated
MP,MU,1,fric          ! Use Parameterised friction condition for friction between sleeve and concrete
MAT,1
R,3                           ! Real constant set 3 defines that these contact surfaces act together
REAL,3
ET,3,169                      ! Define new element type 3  (target element - Targe169)
```

```
ET,4,172                    ! Define new element type 4  (contact element - Conta172)
KEYOPT,4,9,0
!
LSEL,S,,,2                  ! Select line on concrete area adjacent to sleeve
CM,_TARGET,LINE             ! Define this as the  target line
TYPE,3
NSLL,S,1                    ! Select all nodes on selected line
ESLN,S,0                    ! Select all elements attached to selected nodes along targeted line
ESURF,ALL                   !Generate elements on surface of existing elements (towards sleeve)
!
LSEL,S,,,9                  ! Select line on sleeve area adjacent to concrete
CM,_CONTACT,LINE            ! Define this as the contact line
TYPE,4
NSLL,S,1                    ! Select all nodes on selected line
ESLN,S,0                    ! Select all elements attached to selected nodes along targeted line
ESURF,ALL                   !Generate elements on surface of existing elements (towards conc)
ALLSEL                      ! Select all nodes, elements, lines & areas
!*
! /GRES,cwz,gsav
! /COM, CONTACT PAIR CREATION - END
! EPLOT
FINISH                      ! Exit the ANSYS Pre-Processor
!*
/SOLU                 ! Enter the ANSYS Solver.  The model uses most of the defaults in ANSYS.
NLGEOM,1              ! Turn on large deformation effects in Solution due to the possible large strain
NROPT,AUTO, ,         ! Use the default Automatic Newton-Raphson Iterative Solver
LUMPM,0
EQSLV, , ,0,
PREC,0
PIVCHECK,1
SSTIF
PSTRES
TOFFST,0,
!*
FLST,2,2,4,ORDE,2
FITEM,2,1
FITEM,2,6
!*
/GO
DL,P51X, ,ALL,0             ! Constrain the model at the base  in the x & y-axes.
DL,      5, ,SYMM           ! apply symmetry boundary conditions along the left hand edge
FLST,2,1,4,ORDE,1
FITEM,2,4
/GO
!*
SFL,P51X,PRES,pressure,     ! Apply the parameterised pressure value on the concrete surface
!*
TIME,1
AUTOTS,-1                   ! Turn on automatic time stepping
NSUBST,10,10,5,1            ! Set up the number of substeps in the Solver
KBC,0
!*
TSRES,ERASE
! LGWRITE,confined,lgw,,COMMENT      ! Write this LogFile
```

INGRID input file

Test 1 t=3mm, v=6.3m/s (DYNA 3D)

c control part of the program

dn3d *c define the analysis as using the DYNA3D processor.*

term 1.6 *c define the length of time over which the program is to run (in milliseconds)*

plti 0.02 *c define the problem plotfile dump interval (in milliseconds)*

mat 1 1 *c material model 1 (elastic) - to be used for the elastic impactor and the steel sleeve*

ro 7.8e-6 *c density of the impactor*

e 210 *c Young's modulus of impactor*

pr 0.3 *c Poisson's ratio of impactor*

endmat *c end material definition*

mat 2 1 *c material model 2 (elastic) - to be used for the elastic target*

ro 2.4e-6 *c density of concrete*

e 40 *c Young's modulus of concrete*

pr 0.2 *c Poisson's ratio of concrete*

endmat *c end material definition*

plane 2 *c establish two planes of symmetry about the x and y axes*

0 0 0 0 -1 0 .0001 symm

0 0 0 -1 0 0 .0001 symm

si 1 sv; *c establish a sliding interface definition with voids for the impactor-concrete interface*

si 2 fric .25 sv; *c establish a sliding interface with voids and friction for the core-sleeve interface*

c ---------- create the impactor (1st part definition)

start *c start part definition*

1 3 5 6 7 8 9 10 11 13 15; *c define nodes in x direction*

1 3 5 6 7 8 9 10 11 13 15; *c define nodes in y direction*

1 10 19 20; *c define nodes in z direction This forms a rectangle*

-25 -25 -25 -16.6 -8.33 0 8.33 16.6 25 25 25 *c move x nodes, defined above, to particular locations*

-25 -25 -25 -16.6 -8.33 0 8.33 16.6 25 25 25 *c move y nodes, defined above, to particular locations*

0 455.1 760 795 *c move z nodes, defined above, to particular locations*

```
di 1 3 0 9 11; 1 3 0 9 11; 1 4;          c remove corners from the rectangle
a 1 1 1 11 11 4 3 75                     c rotate outermost nodes onto a circle with radius 75 mm
a 2 2 1 10 10 4 3 50                     c rotate 2nd group of nodes onto a circle with radius 50 mm
d 1 1 2 11 2 4                           c } remove nodes at the base of
d 1 1 2 2 11 4                           c } the cylinder to create the step of different diameters
d 10 1 2 11 11 4                         c } which gives impactor an approximate
d 1 10 2 11 11 4                         c } geometry but the correct mass
d 1 0 1 6 0 4                            c remove all nodes from half of the x direction (½ geom)
d 0 1 1 0 6 4                            c remove all nodes from half of the y direction (¼ geom)

velocity 0. 0. 6.3                       c give the impactor an initial velocity in the z direction
b 11 1 1 11 11 2  110000                 c establish boundary conditions to prevent wobble post impact
b 1 11 1 11 11 2  110000                 c establish boundary conditions to prevent wobble post impact
si 1 1 4 11 11 4 1 m                     c define a master sliding interface of type 1 at the base
mate 1                                   c give the impactor material properties number 1 above

end                                      c end part definition
```

c ----------define concrete core (2nd part definition)

```
start                                    c start part definition

1 2 3 4 5 6 7 8 9 10 11 12 13 14 15 16 17 18 19 20 21;
1 2 3 4 5 6 7 8 9 10 11 12 13 14 15 16 17 18 19 20 21;
1 20;
-25 -25 -25 -25 -25 -25 -20 -15 -10 -5 0 5 10 15 20 25 25 25 25 25 25
-25 -25 -25 -25 -25 -25 -20 -15 -10 -5 0 5 10 15 20 25 25 25 25 25 25
795.2 995.2                              c create geometry in a similar way to that described above by
                                         c defining nodes and moving them to particular locations

di 1 5 0 16 21; 1 5 0 16 21; 1 2;        c delete corners
a 1 1 1 21 21 2 3 54.15                  c rotate outermost nodes onto a circle with radius 54.15 mm
a 2 2 1 20 20 2 3 49.6                   c rotate 2nd group of nodes onto circle with radius 49.6mm
a 3 3 1 19 19 2 3 45.1                   c rotate 3rd group of nodes onto circle with radius 45.1 mm
a 4 4 1 18 18 2 3 40.5                   c rotate 4th group of nodes onto circle with radius 40.5 mm
a 5 5 1 17 17 2 3 36                     c rotate 5th group of nodes onto circle with radius 36 mm
d 1 0 1 11 0 2                           c remove all nodes from half of the x direction (½ geom)
d 0 1 1 0 11 2                           c remove all nodes from half of the y direction (¼ geom)
```

```
b 1 1 2 21 21 2  111111          c restrain the cylinder fully at the base
mate 2                           c give the concrete core material properties number 2 above
si+ 1 1 1 21 21 1 1 s 0 0 1      c define a slave sliding interface of type 1 at the top
si+ 11 21 1 21 21 2 2 s 1 0 0    c define a slave sliding interface of type 2 at the side (x)
si+ 21 11 1 21 21 2 2 s 0 1 0    c define a slave sliding interface of type 2 at the side (y)

end                              c end part definition
```

c ----------define sleeve (3rd part definition)

```
start                            c start part definition

1 2 3 4 5 6 7 8 9 10 11 12 13 14 15 16 17 18 19 20 21;
1 2 3 4 5 6 7 8 9 10 11 12 13 14 15 16 17 18 19 20 21;
1 20;
-25 -25 -25 -25 -25 -25 -20 -15 -10 -5 0 5 10 15 20 25 25 25 25 25 25
-25 -25 -25 -25 -25 -25 -20 -15 -10 -5 0 5 10 15 20 25 25 25 25 25 25
795.2 995.2                      c create geometry in a similar way to that described above
                                 c by defining nodes and moving them to particular locations

di 1 5 0 16 21; 1 5 0 16 21; 1 2;   c delete corners
a 1 1 1 21 21 2 3 57.15          c rotate outermost nodes onto a circle with radius 57.15 mm
a 2 2 1 20 20 2 3 55.65          c rotate 2nd group of nodes onto circle with radius 45.65mm
a 3 3 1 19 19 2 3 54.15          c rotate 3rd group of nodes onto circle with radius 54.15mm
d 11 11 1 19 19 2                c delete all nodes from the centre of cylinder to create sleeve
d 1 0 1 11 0 2                   c remove all nodes from half of the x direction(½ geom)
d 0 1 1 0 11 2                   c remove all nodes from half of the y direction (¼ geom)

b 1 1 2 21 21 2  111111          c restrain the sleeve fully at the base
mate 1                           c give the sleeve material properties number 1 above
si 11 19 1 19 19 2 2 m           c define a master sliding interface of type 2 at the side (x)
si 19 11 1 19 19 2 2 m           c define a master sliding interface of type 2 at the side (y)

end                              c end part definition
end                              c end INGRID file
```